The ear region of the Proboscidea (Afrotheria, Mammalia) : anatomy, function, evolution

Arnaud Schmitt

MUSEUM NATIONAL D'HISTOIRE NATURELLE

Ecole Doctorale Sciences de la Nature et de l'Homme – ED 227

Année 2016 **N° attribué par la bibliothèque**
|_|_|_|_|_|_|_|_|_|_|_|_|

THESE

Pour obtenir le grade de

DOCTEUR DU MUSEUM NATIONAL D'HISTOIRE NATURELLE

Spécialité : Paléontologie

Présentée et soutenue publiquement par

Arnaud Schmitt

Le 04 octobre 2016

La région de l'oreille osseuse chez les Proboscidea (Afrotheria, Mammalia) : anatomie, fonction, évolution

---

Sous la direction de **:**

M. Gheerbrant, Emmanuel, Directeur de Recherche

M. Tassy, Pascal, Professeur émérite

JURY :

M. Sánchez, Marcelo	**Professeur, Universität Zürich, Zürich (Suisse)**	**Rapporteur**
M. Seiffert, Erik	**Professeur, University of South California, Los Angeles (USA)**	**Rapporteur**
M. Antoine, Pierre-Olivier	**Professeur, Université de Montpellier 2, Montpellier (034)**	**Examinateur**
M. Billet, Guillaume	**Maître de conférences, Muséum national d'Histoire naturelle, Paris (075)**	**Examinateur**
M. David, Romain	**Docteur, Max Planck Institute for Evolutionary Anthropology, Leipzig (Allemagne)**	**Invité**
M. Gheerbrant, Emmanuel	**Directeur de Recherche, CNRS, Paris (075)**	**Directeur de thèse**
M. Tassy, Pascal	**Professeur émérite, Muséum national d'Histoire naturelle, Paris (075)**	**Directeur de thèse**

Remerciements

On pourrait penser qu'une thèse est un travail solitaire. Loin de là. Bien qu'il s'agisse d'un travail personnel qui nécessite d'être autonome, les trois ans passés à préparer ce diplôme m'ont donné l'opportunité d'échanger avec de nombreuses personnes. Personnes qui ont participé à faire de cette thèse ce qu'elle est aujourd'hui et que j'aimerais remercier.

Je tiens avant tout à remercier mes directeurs de thèse, au nombre de deux (ou trois) pour leur disponibilité et leur engagement et qui m'ont accompagné durablement tout au long de ce travail « mastodontesque » que peut représenter une thèse de doctorat.

A Emmanuel Gheerbrant, qui a le courage de m'encadrer depuis presque 5 ans déjà puisqu'il supervise mon travail depuis ma première année de Master.

A Pascal Tassy, véritable encyclopédie vivante des proboscidiens et qui a su toujours rester disponible malgré la distance.

A Romain David, qui n'est pas officiellement un directeur de cette thèse, mais qui s'est investi dans ce travail tout autant que les précédents, en me faisant découvrir le monde (magique) de la biomécanique des canaux semi-circulaires.

Je remercie également les autres personnes qui ont pu contribuer à améliorer ce travail. La recherche est une activité qui peut s'avérer bien solitaire, mais partager et échanger avec d'autres collègues est primordial pour faire mûrir un projet de recherche. Pour ces raisons, je tiens à remercier Guillaume Billet, Stéphane Peigné, Damien Germain, Maeva Orliac et plus particulièrement Pierre-Olivier Antoine et Sandrine Ladevèze qui ont accepté de faire partie de mon comité de thèse.

Une thèse qui porte sur les nouvelles techniques d'investigation CT scan ne pourrait pas voir le jour sans l'aide de personnes qui maîtrisent ces techniques et qui peuvent s'avérer d'une grande aide dans leur application aux fossiles. Je remercie ainsi Miguel Garcia Sanz, Florent Goussard, Patricia Wils, Gaël Clément et Antoine Balzeau.

Un grand merci également aux personnes qui sont là pour nous épauler, sans qui, avouons-le, nous ne pourrions pas faire grand-chose. Je remercie particulièrement Charlène Letenneur pour les très jolies illustrations anatomiques qu'elle a réalisées pour moi. Je remercie l'équipe administrative du laboratoire, Angelina Bastos, Suzy Colas et Mélinée Deretz, qui nous facilitent parfois grandement la vie. Je pense également aux préparateurs, Renaud Vacant et Colas Bouillet, qui ont assuré la préparation de certains de mes spécimens et à Vincent Pernègre, pour son aide dans la préparation des spécimens en vue de les scanner. Je pense également à Philippe Loubry qui a photographié le spécimen d'*Eritherium* figurant dans le manuscrit et Marie-Astrid Angel de la bibliothèque, toujours disponible si on en ressent le besoin.

Tout aussi important, il faut un matériel d'étude pour pouvoir développer un projet. Les spécimens étudiés dans cette thèse sont issus de collections réparties sur plusieurs continents. Ainsi, je tiens à remercier toutes les personnes qui m'ont permis d'accéder à ces spécimens afin de les étudier. Je pense à Christine Argot, pour les collections de paléontologie du Muséum, Joséphine Lesur, Aurélie Verguin, Marc Herbin, Eric Pellé et Jacques Cuisin, pour les collections d'anatomie comparée du Muséum, Pip Brewer, Dan Sykes et Farah Ahmed du Muséum de Londres, Reinhard Ziegler, pour les collections du Muséum de Stuttgart, Judith Galkin, Henry Tobin, Alana Gishlick, Ruth O'Leary, Morgan Hill et Meng Jin du Muséum de New York et Julien Benoit, Rodolphe Tabuce, Renaud Lebrun et Lionel Hautier de l'université de Montpellier 2. Parfois, les projets ne se concrétisent pas et certains spécimens demeurent hors de portée ou impossibles à scanner. Malgré tout, je remercie Gerard Weber et Ursula Göhlich respectivement de l'université et du Muséum de Vienne pour leur tentative de scanner un crâne de *Choerolophodon* pour mon projet. Je remercie également Erik Ekdale et Jeffrey Saunders qui m'ont mis sur la piste de pétreux isolés américains.

Si le Muséum fut ma maison pour la très grande majorité de ces 3 ans, je garderai toujours en mémoire mes séjours au Max Planck Institute for Evolutionary Anthropology de Leipzig, où j'ai résidé pendant de longues semaines très productives. Je remercie principalement, David Plotzki pour son efficacité à scanner de nombreux spécimens, Alexander Stoessel, pour sa participation aux aspects plus théoriques du sujet, Fred Spoor, qui m'a gentiment prêté du matériel d'étude et le directeur du département d'accueil, Jean-Jacques Hublin.

Balader une douzaine de crânes d'éléphants à travers le Jardin des Plantes, ce n'est pas une sinécure ! Je remercie toutes les personnes qui se sont montrées disponibles pour permettre la migration de ce troupeau singulier d'éléphants de la zoothèque vers le CT scan.

Ces trois années n'ont pas été consacrés uniquement à la recherche, puisque j'ai choisi d'effectuer des missions doctorales en parallèle de mon travail de thèse. Ce fut une expérience enrichissante, qui m'a permis de confirmer mon goût pour l'enseignement et qui m'a aussi permis de laisser libre court à ma créativité. Ainsi, j'aimerais tout d'abord remercier Emilie Detouillon, qui s'occupe bien de nous, doctorants missionnaires, en se montrant toujours disponible et ouverte aux nouvelles idées. Je remercie Véronique Barriel, avec qui j'ai eu le grand plaisir de participer à l'enseignement de l'UE de morphologie cladistique informatisée pendant trois années consécutives. J'en profite pour la remercier pour tout son soutien au cours des cinq dernières années passées en Master et en thèse au Muséum. Je remercie également l'équipe de l'UE d'illustration scientifique, Didier Geffard-Kuriyama, Jean-François Dejouannet et Bernard Duhem, avec qui ce fut un plaisir de travailler. Je tiens enfin à remercier Lauriane Cacheux, Sophie Fernandez et Laure Dassonville, avec qui j'ai pris plaisir à animer plusieurs ateliers pédagogiques destinés à des classes du secondaire.

Je tiens à remercier les ATM « Formes » et « Emergences », dont le financement a permis à ce projet de se développer et de s'étendre. Je remercie également la directrice de l'UMR 7207, Sylvie Crasquin, pour permettre aux doctorants d'effectuer leur thèse dans de bonnes conditions.

Je remercie également Erik Seiffert et Marcelo Sánchez qui ont accepté de faire partie de mon jury et de rapporter ce travail.

Ces trois années au Muséum m'ont également permis de tisser des liens avec d'autres doctorants ou anciens étudiants de la maison. Je pense à Malcolm, Laure, Fabrice, Maxime… Une pensée particulière pour Charlène, dont le sujet de thèse proche du mien nous a permis de beaucoup partager ces deux dernières années. Je garderai un très bon souvenir de notre séjour à Leipzig, de nos ateliers pédagogiques et de tout le soutien dont tu as pu faire preuve. Je remercie aussi Rémi et Claire, mes compagnons de galère depuis 5 ans, sans qui ma vie au muséum aurait franchement été moins chouette. Enfin, je remercie Alexandre, mon colocataire de bureau pour cette dernière année de thèse, qui a pu m'apporter tout son soutien et avec qui les discussions sont toujours aussi passionnantes.

Enfin, j'en profite pour remercier mes proches, qui, par leur soutien, m'ont permis d'être là où j'en suis. Je remercie bien sûr mes parents, qui ont toujours cru en moi et m'ont toujours appris à poursuivre mes rêves plutôt que de faire des compromis. Je remercie également mes sœurs, pour leur soutien sans faille tout au long de ces trois ans. Je remercie mes « invalides » de beaux-parents (ils comprendront), qui m'ont toujours ouvert leur porte quand j'en avais besoin au cours de ces trois ans. Une petite pensée pour Zaza, qui a toujours été une oreille attentive, particulièrement dans les moments de doute. Enfin, je ne pourrais jamais assez remercier Jérémy, qui m'a donné le courage d'aller au bout de ce projet de longue haleine.

Je m'excuse par avance de toutes les personnes que j'aurais pu oublier (il y en a forcément). La thèse c'est un peu comme une épreuve sportive ; un marathon qui finit par un sprint. A quelques mètres de la ligne d'arrivée, on n'a plus les idées très claires.

TABLE OF CONTENTS

INTRODUCTION

1. Context, concepts and objectives

The Proboscidea: a 60 million-year-old history

The Proboscidea Illiger, 1811 is the mammalian order that contains the elephants and their close relatives. The elephants are the largest extant terrestrial mammals and some recent studies on the size and body mass of extinct proboscideans consider that the largest terrestrial mammal in history was also a proboscidean (*Palaeoloxodon namadicus*, considered to have a shoulder height of 5 m and to weigh 22 t; Larramendi, in press.). There are only three extant representatives of the Proboscidea: the African bush elephant *Loxodonta africana,* Blumenbach, 1797, the African forest elephant *Loxodonta cyclotis,* Matschie, 1900, and the Asian elephant *Elephas maximus*, Linnaeus, 1758. However, they were much more diverse in the past. Their fossil record starts from the middle Paleocene and includes more than 180 known fossil species (Gheerbrant & Tassy, 2009), forming one of the most complete fossil sequences of a modern mammal order. During their 60 million-year-old long history, the proboscideans developed various adaptive morphotypes, from the likely semi-aquatic and tapir-like *Moeritherium* to the "shovel tusker" *Platybelodon*. To the present knowledge, the origin of the Proboscidea is deeply rooted in Africa. The first radiation of the proboscideans leads to the appearance of the Paleocene and early Eocene lophodont taxa (Gheerbrant & Tassy, 2009). The earliest-known proboscidean, *Eritherium azzouzorum* Gheerbrant, 2009 (Selandian, 60 Ma) has the size of a large hyrax and retains numerous paenungulate plesiomorphies (Gheerbrant, 2009). It was discovered in the Ouled Abdoun basin in Morocco that also yielded the more recent *Phosphatherium escuilliei* Gheerbrant, Sudre & Cappetta, 1996 (Ypresian, 55 Ma) which is slightly larger and more derived than *Eritherium* (Gheerbrant et al. 1996, 1998, 2005), and *Daouitherium rebouli* Gheerbrant and Sudre, 2002 (Middle Ypresian, ca. 53 Ma, Yans et al. 2014; Kocsis et al. 2014), which is much larger (80-170 kg; Gheerbrant et al. 2002). Several other large Eocene-Oligocene lophodont taxa were also uncovered in North Africa: *Numidotherium koholense*

Jaeger, 1986 (described in Mahboubi et al. 1986) from the midlle Eocene of El Kohol, Algeria; *Barytherium grave* Andrews, 1901 from the late Eocene and early Oligocene of the Fayum (Andrews, 1901; 1906), Egypt, and of Dor El Talah, Libya; and *Arcanotherium savagei* (Court 1995) from the late Eocene and early Oligocene of Dor El Talah (Court 1995, Delmer 2009), Libya. *Moeritherium* from the Eocene of North Africa, and peculiarly from the late Eocene to early Oligocene of the Fayum and Dor El Tahla (Andrews 1901, Tassy 1981), is more closely related to modern elephants than previously cited proboscideans. Indeed, it is the earliest known proboscidean with bunolophodont molars and with an undivided perilymphatic foramen (Gheerbrant & Tassy, 2009).

Even more closely related to modern proboscideans is the Neogene family of the Deinotheriidae that includes *Prodeinotherium* Ehik, 1930, *Deinotherium* Kaup, 1829 and probably *Chilgatherium* Sanders, Kappelman & Rasmussen, 2004. They display a posture similar to the modern elephants as well as remarkable dental autapomorphies such as the loss of the superior incisors, and the development of downward incurved inferior tusks (Gheerbrant & Tassy, 2009).

Table 1 : Simplified classification of the main proboscidean groups and taxa presented in the introduction, after Gheerbrant & Tassy (2009). '?' is for debated attributions. Not all proboscidean taxa are represented here.

Proboscidea
- *Eritherium*
- *Phosphatherium*
- *Daouitherium*
- *Numidotherium*
- *Arcanotherium*
- *Barytherium*
- *Moeritherium*
- **Deinotheriidae**
  - *?Chilgatherium*
  - *Prodeinotherium*
  - *Deinotherium*
- **Elephantiformes**
  - *Palaeomastodon, Phiomia*
  - **Elephantimorpha**
    - **Mammutida**
      - **Mammutidae**
        - *Eozygodon*
        - *Mammut*
        - *?Losodokodon*
        - *Zygolophodon*
        - *Sinomammut*
    - **Elephantida**
      - **Choerolophodontidae**
        - *Choerolophodon*
      - **Amebelodontidae**
        - *Platybelodon*
        - *Amebelodon*
      - **Gomphotheriidae**
        - *Gomphotherium*
        - *Cuvieronius*
        - *Stegomastodon*
        - *Anancus*
      - **Stegodontidae**
        - *Stegodon*
        - *Stegolophodon*
      - **Elephantidae**
        - *Loxodonta*
        - *Mammuthus*
        - *Elephas*
        - *Palaeoloxodon*

The Elephantiformes is a vast clade that contains all proboscideans that display the modern elephantine graviportal posture. The group originates in the early Oligocene of North Africa from genera like *Palaeomastodon* Andrews, 1901 and *Phiomia* Andrews & Beadnell, 1902 that were discovered initially in the Fayum Jebel Qatrani Formation.

Within the Elephantiformes, a major radiation occurs in the Neogene: the Elephantimorpha Tassy & Shoshani, 1997 (in Shoshani et al. 1998), from which originate the Mammutida Tassy & Shoshani, 1997 (in Shoshani et al. 1998) and the Elephantida Tassy & Shoshani, 1997 (in Shoshani et al. 1998). The Mammutida contains the Mammutidae Hay, 1922. This family includes the early Eocene *Eozygodon* Tassy & Pickford, 1983, the emblematic *Mammut americanum* Kerr, 1792, as well as *Zygolophodon* Vacek, 1877, probably *Losodokodon* Rasmussen & Gutiérrez, 2009 and the recently described new genus *Sinomammut* Mothé, 2016 from the Miocene of China (Mothé et al. 2016b). On the other hand, the Elephantida includes the paraphyletic group of gomphothers from which originate the Stegodontidae Osborn, 1918 and the family that contains the extant elephants (Elephantidae Gray, 1821). The gomphothers are generally classified in three families: the Choerolophodontidae that includes *Choerolophodon* Schlesinger, 1917, the Amebelodontidae (e.g. *Platybelodon* Borissiak, 1928 and *Amebelodon* Barbour, 1927) and the Gomphotheriidae (e.g. *Gomphotherium* Burmeister, 1837, *Anancus* Aymard, 1855 and American gomphothers such as *Stegomastodon* Pohlig, 1912 and *Cuvieronius* Osborn, 1923). On the other hand, the Stegodontidae includes *Stegodon* Falconer, 1847 and *Stegolophodon* Pohlig, 1888. Finally, the Elephantidae is the only family that still includes extant taxa (*Elephas* and *Loxodonta*). Among the elephantids are also found the mammoths *Mammuthus* Brookes, 1828, and *Palaeoloxodon* Matsumoto, 1924. A simplified classification of the proboscideans presented here is given in Table 1.

The Proboscidea among the Afrotheria

As previously said, the origin of the Proboscidea is deeply rooted in Africa. However, the African origin of the proboscideans is even earlier because they belong to a more inclusive clade of

mammals that originates from Africa: the Afrotheria. The Afrotheria is a major clade of placental mammals that was recently recognized and defined by molecular studies of extant species (Dejong et al. 1981; Stanhope et al. 1998). It includes the extant orders Afrosoricida Stanhope et al. 1998 (golden-moles and tenrecs), Tubulidentata Huxley, 1872 (aardvarks), Macroscelidea Butler, 1956 (elephant-shrews), Hyracoidea Huxley, 1869 (hyraxes), Sirenia Illiger, 1811 (sea-cows and dugongs) and the Proboscidea (Fig. 1). The interordinal relationships in the Afrotheria are still debated, although some afrotherian clades such as the Paenungulata (extant Hyracoidea, Sirenia, Proboscidea; Fig.1) are well supported.

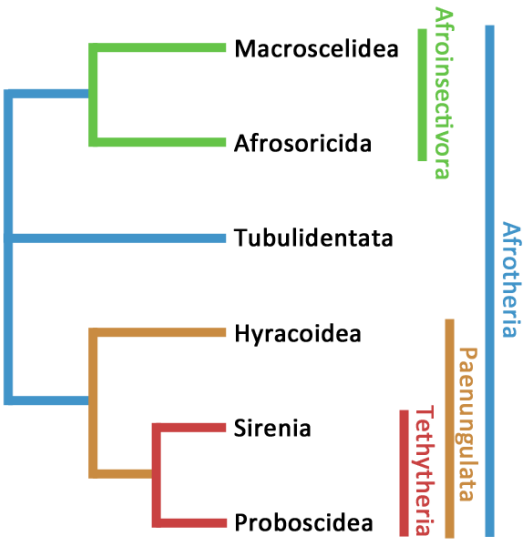

Figure 1 : A hypothesized tree of the Afrotheria, based on Seiffert (2007), except for the debated position of Tubulidentata, left at the base of the Afrotheria here.

Macroscelidea and Afrosoricida are generally found closely related, forming the Afroinsectivora (Springer et al. 2004; Seiffert, 2007). However, the clade is not found in some other studies (Stanhope et al. 1998; Seiffert et al. 2012). The most debated position is probably that of the Tubulidentata, which can be found as the sister-group of the Macroscelidea (Stanhope et al. 1998), as the sister group of the Afroinsectivora (Springer et al. 2004) or as the sister group of the Paeunungulata Simpson, 1945 (Seiffert, 2007; Seiffert et al. 2012). The grouping of the orders Hyracoidea, Sirenia and Proboscidea in a clade called Paenungulata is supported by morphological, molecular (Stanhope et al. 1998) and mixed data (Seiffert, 2007; Seiffert et al. 2012). The position of the Hyracoidea within the Paenungulata is also debated but it is commonly found as the sister-group of Tethytheria McKenna, 1975 which includes the orders Proboscidea and Sirenia (Fischer & Tassy, 1993; Seiffert, 2007). Entirely extinct orders are also generally believed to be afrotherians (e.g. Bibymalagasia) and even tethytheres (e.g. Embrithopoda). Proboscideans are therefore afrotherians, paenungulates and tethytheres.

Why studying the ear region of the Proboscidea?

In mammals, the ear region is mostly comprised of the petrosal which is a complex bone that exhibits many anatomical features. It is located on the ventral part of the skull, generally in contact with the occipital, squamosal and tympanic bones. The anatomy of this bone is commonly studied and compared within the Mammalia. It provides numerous characters that can be tested in phylogenetic analyses. The internal structures of the petrosal are especially crucial to infer functional capacities of extinct taxa. Indeed, the petrosal houses the bony labyrinth which contains the membranous labyrinth in life. This organ has two very important sensory functions: the audition and the detection of motion and spatial orientation. The perception of sound is made by the cochlear part of the labyrinth, whereas the vestibular part of the labyrinth allows the perception of motion and spatial orientation (Dercum, 1879).

The investigation of the petrosal and inner ear of proboscideans is of great interest. Indeed, the elephants display several peculiarities related to the ear region. First, they are among the few mammals that display a unique perilymphatic foramen. In the vast majority of mammals, this foramen only exists during the early ontogeny and it divides into the *fenestra cochleae* and the *aquaeductus cochleae*. However, the single opening is retained in only few extant taxa: elephants, sirenians (Fischer, 1990) and the gray whale *Eschrichtius robustus* (Geisler and Luo, 1996). The undivided perilymphatic foramen was first considered a synapormorphy of the Tethytheria (it is also found in *Arsinoitherium*, Court, 1990), but this hypothesis was challenged by later discoveries of divided foramens in early sirenians and proboscideans (Court & Jaeger, 1991).

The elephants are also among the few mammals that are able to hear infrasound (Payne et al 1986, Poole et al 1988). The study of the cochlear morphology of proboscideans is of great interest to trace back the evolutionary history of low frequency hearing in the Proboscidea.

Finally, some early representatives of the order, such as *Barytherium* and *Moeritherium*, are generally believed to be semi-aquatic (Liu et al. 2008), while others

such as *Numidotherium* exhibit adaptations to terrestrial life (Mahboubi et al. 2014). Studies of the early embryology of elephants suggests that the elephant's ancestors were aquatic (Gaeth et al. 1999), based on observation of the development of the nephrostomes. However, this can be due to the very long gestation of elephants (22 months; Sikes, 1971). The aquatic ancestry of proboscideans is still debated today and the study of the functional capacities of the vestibular system in the Proboscidea can provide new clues on their sensory perception of the environment.

The ear region of the Proboscidea in science: a 300-year history

The ear region of proboscideans has not been thoroughly studied in the past. However, it has been of very early interest in the scientific community, the earliest study focused on the subject that we could trace back being 300 years old. It consists of an anatomical description of the ear region of an extant elephant (Blair, 1717-1719). This study was published several years after Blair described the whole skeleton of the elephant in his *Osteographia Elephantina* (Blair, 1710-1712a; 1710-1712b) in which he describes the ear region only briefly. In the 1717-1719 publication, however, the general anatomy of the ear region is thoroughly described. The description is accompanied by an anatomical chart, but the illustrations seem not very accurate (Fig. 2A). For the next century, the subject seems to have been forsaken by the scientific community. The labyrinth of elephant was later reappraised by Fick (1844); however we could not have access to the publication. The next year, the labyrinth is compared to that of other mammals in a comprehensive comparative anatomy work (Hyrtl, 1845). More precise illustrations of the bony labyrinth and the ossicles are given (Fig. 2B). Twenty years later, the study of the bony labyrinth of *Deinotherium giganteum* is the first known attempt to describe the bony labyrinth of an extinct member of the Proboscidea (Claudius, 1865). The fossil labyrinth is compared with that of the extant Asian elephant as well as with other mammals using accurate anatomical drawings (Fig. 2C). This marks the end of the early studies on the bony labyrinth of proboscideans. Further publications of the second half of the 19th century and of the first half of the 20th century are focused on the external and middle ear.

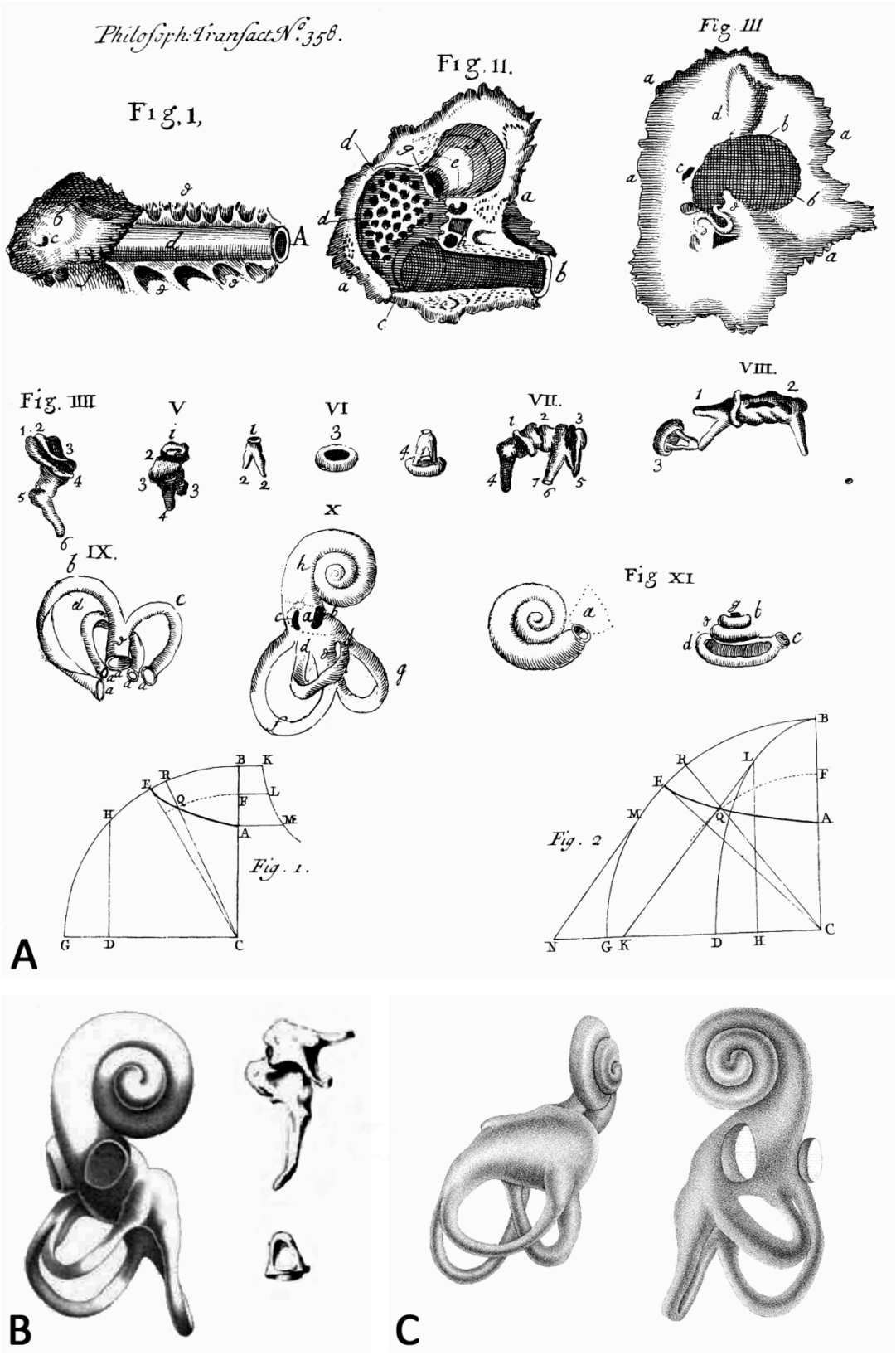

Figure 2 : Illustrations of the ear region of the Proboscidea in the early publications. **(A)** Anatomical chart of the ear region of an extant elephant given in Blair (1717-1719, Royal Society Publishing), **(B)** Illustration of the bony labyrinth of an African elephant given in Hyrtl (1845, Bavarian State Library), **(C)** Illustration of the bony labyrinth of the extinct proboscidean *Deinotherium giganteum* given in Claudius (1865).

In his work on the muscles and blood vessels of the Asian elephant head, Watson (1874) describes several soft structures linked to the ear region, such as the internal carotid artery or the muscles of the external ear. The bones of the ear region of the extant elephant are again described in three related publications (Buck, 1888; 1890; Richards, 1890). Several interesting considerations are made, but these studies lack proper illustrations of the petrosal. A few elements of the anatomical descriptions are addressed in Chapter II. Finally, a few details on the petrosal of a fetus of African elephant are given in Eales (1926). Except for the early description of the bony labyrinth of *Deinotherium giganteum* (Claudius, 1865), the ear region of extinct proboscideans has been investigated only recently. A natural endocast of the cochlea is briefly described in a *Moeritherium* skull from the Eocene of Libya (Tassy, 1981). The study of the petrosal ontogeny of elephants and sirenians reveals a shared peculiar feature of both mammalian orders: the undivided perilymphatic foramen retained in adult life. This is first hypothesized as a synapomorphy of the Tethytheria, especially as the embrithopod *Arsinoitherium* (an extinct relative of the tethytheres) displays the same characteristic (Court, 1990). However, investigations of the petrosal of the early proboscidean *Numidotherium* (Court & Jaeger, 1991) shows that this morphology is convergent, since the perilymphatic foramen is divided into the *fenestra cochleae* and the *aquaeductus cochleae* in *Numidotherium*. On the other hand, a later study of the bony labyrinth of *Numidotherium* suggests that they were not adapted to low frequency hearing as extant elephants (Court, 1992). The petrosal of *Moeritherium* is described for the first time by Court (1994). It displays the undivided perilymphatic foramen which challenged the phylogenetic position of *Moeritherium* admitted at that time, which was believed to be less derived than *Numidotherium*. Finally, the petrosal of *Gomphotherium angustidens* is described in details in Tassy (2013) with one of the only clear anatomical illustrations of a proboscidean petrosal.

The recent development of CT scan acquisition methods and their applications to paleontology pave the way to further investigations of the bony labyrinth of extinct taxa. The first attempt to use CT scanning method for the study of the petrosal of an extinct proboscidean dates

is very recent (*Elephas tiliensis* in Provatidis, 2011). However, the anatomy of the petrosal and the bony labyrinth was not thoroughly studied in this paper. On the other hand, the isolated petrosal of an unknown elephantimorph is investigated using CT scanning methods in Ekdale (2011). The bony labyrinth is reconstructed in 3D and meticulously described and the petrosal is well illustrated. The bony labyrinths and the petrosals of *Numidotherium* and *Moeritherium* were investigated by Benoit et al. (2013b) with good illustrations. Finally, the ear region of earliest known elephant relatives *Eritherium* and *Phosphatherium* were investigated with CT scan methods by Schmitt & Gheerbrant (2016). This paper is actually part of this PhD thesis, its unmodified version is presented in the Chapter I.

The development of new methods of investigation of the petrosal and the bony labyrinth of proboscideans hence opened new work perspectives on this complex yet critical anatomical region. However, there are still a lot of grey areas. Even though the elephants are emblematic extant animals, a modern comprehensive study of their petrosal and bony labyrinth has not been carried out yet. Detailed illustrations of the petrosal anatomy and 3D reconstructions of their bony labyrinth have not been published. The variability of this anatomical region has been studied in elephantimorphs (Ekdale, 2011), but it is still unknown in extant elephants. In addition, the petrosal and inner ear anatomy of the majority of extinct proboscideans has yet to be described.

Objectives

The main objective of this work is to account for the morphological diversity and evolution of the ear region within the Proboscidea, by taking advantage of the recently developed CT scanning methods applied in the field of paleontology. The study of the ear region of the two earliest known elephant relatives *Eritherium* and *Phosphatherium* (Schmitt & Gheerbrant, 2016) provides new data on the ancestral morphotype of this region for the Proboscidea and even for the Afrotheria. This published work is part of the PhD thesis and corresponds to the first chapter. The poorly known anatomy of the ear region of extant proboscideans is studied in Chapter II. The petrosals of several specimens belonging to the three extant species of elephants are

investigated with CT scanning methods. A richly illustrated comprehensive study of the region provides a reappraisal of the petrosal and bony labyrinth anatomy, as well as the first 3D reconstructed membranous labyrinth of an extant elephant. Study of several specimens helps to characterize the intraspecific variations of the bony labyrinth and the petrosal, which remains poorly known in mammals. The elucidation of these variations allows refining the comparison between fossil taxa and more importantly the definition of phylogenetic characters. The anatomy of the ear region of most extinct proboscideans remains unexplored; it is described in several extinct proboscideans in Chapter III. Comparisons of these taxa with other proboscideans and some other orders allow formalizing primary homologies of ear evolution. The morphological variation of the bony labyrinth is then investigated using geometric morphometrics in Chapter IV. This method allows quantifying morphological resemblances between taxa and investigating the effect of allometry on the bony labyrinth morphology of proboscideans. Moreover, this step is helpful in formalizing new primary homologies for the purpose of a phylogenetic analysis of the Proboscidea. The study of the evolution of the ear region characters within the Proboscidea (and to a lesser extent within the Afrotheria) is conducted in Chapter V, using cladistic methods. The functional capacities of the vestibular system of extant afrotherians are investigated using a very recent and original method (David et al. in press). Based on this new approach, the functional capacities of the semicircular system of extinct proboscideans are inferred. Finally, a preliminary study of the evolution of audition within proboscideans is conducted.

2. Material and methods

2.1. Material

As previously said, the main objective of this PhD thesis is to highlight the morphological variability of the petrosal and inner ear in Proboscidea. To do so, many proboscideans specimens and some outgroups were CT-scanned. Table 2 summarizes the scanned specimens in this study. Only classification details, the collection number and scanning properties are given. The material will be presented with more details in the next related chapters.

The earliest known proboscideans *Eritherium* and *Phosphatherium* were previously scanned and partially studied during my Master's thesis. A further presentation of these specimens is given in the "Material and methods" section of Chapter I.

Several skulls of extant elephants were also scanned in order to study the intraspecific variability of the ear region in Proboscidea. Further details about these specimens are given in the "Material and methods" section of Chapter II.

Finally, several fossil taxa of proboscideans and outgroups were scanned in order to study the evolution of this anatomical region. The subsequent material is presented in the "Material and methods" section of Chapter III.

As presented in Table 2, 19 different species belonging to 16 different genera of proboscideans were scanned during the PhD thesis.

Early representatives of proboscideans from the Paleocene (*Eritherium*) and Eocene (*Phosphatherium*, *Numidotherium* and *Moeritherium*) have been investigated. The Miocene Deinotheriidae *Prodeinotherium* was also studied which brings to five the number of non-elephantimorph proboscideans scanned for this work. Specimens of *Phiomia* (Natural History Museum of United Kingdom) and *Palaeomastodon* (AMNH.FM.13448, American Natural History Museum) that potentially bears at least one bony labyrinth were also identified during this study, but it was materially not possible to scan them. Concerning the elephantimorphs, two isolated petrosals of the mammutid *Mammut americanum* were scanned. The American gomphothers *Cuvieronius* and

Stegomastodon have been sampled as well. Other members of the paraphyletic gomphothers that were scanned include *Gomphotherium angustidens*, *Platybelodon grangeri* and *Anancus arvernensis*. One Stegodontidae, *Stegodon orientalis*, was sampled as well. As for the Elephantidae family, we obtained scans of specimens from both the African elephant species (*Loxodonta africana* and *Loxodonta cyclotis*), as well as from the Asian elephant (*Elephas maximus*). The mammoth species *Mammuthus primigenius* and *Mammuthus columbi* were investigated as well as a specimen of *Palaeoloxodon antiquus*.

Concerning the outgroups, the hyracoid *Procavia* and the elephant-shrew *Elephantulus* were scanned. These specimens have been prepared in order to preserve and study their membranous labyrinth in place within the bony labyrinth (more details in chapter VI). Two isolated petrosals of rhinocerotids previously thought to belong to *Prodeinotherium* were also investigated. The earliest afrotherian *Ocepeia* was segmented as well for comparisons. Finally, the isolated petrosal of an unpublished early Eocene new species of Embrithopoda from Morocco was scanned and segmented.

This list only describes specimens specifically scanned and segmented for this work. Comparisons with specimens from the literature were also conducted. These specimens and their bibliographical references are further presented in chapter V.

Table 2 : List of the taxa scanned during this PhD thesis with indications on their collection number, the location of where they were scanned, the model of the scanner and the resolution used during the acquisition. **AMNH** stands for American Museum of Natural History; **AST-RX** stands for Accès Scientifique à la Tomographie à Rayons X; **GEIT** stands for General Electronics Inspection Technologies; **MNHN** stands for Muséum national d'Histoire naturelle; **MPI-EVA** stands for Max Planck Institute for Evolutionary Anthropology; **NHMUK** stands for Natural History Museum of the United Kingdom.

Order	Genus	Species	Collection number	Scanning platform and scanner	Voxel size (µm)
Proboscidea	*Eritherium*	*azzouzorum*	PM88	AST-RX (MNHN) v¦tome¦x L240 (GEIT)	10.1
Proboscidea	*Phosphatherium*	*escuilliei*	PM17	AST-RX (MNHN) v¦tome¦x L240 (GEIT)	38.6
Proboscidea	*Elephas*	*maximus*	MNHN.ZM.AC.1904-273	AST-RX (MNHN) v¦tome¦x L240 (GEIT)	79.27(l) 73.26(r)
Proboscidea	*Elephas*	*maximus*	MNHN.ZM.AC.1941-209	AST-RX (MNHN) v¦tome¦x L240 (GEIT)	78.27
Proboscidea	*Elephas*	*maximus*	MNHN.ZM.AC.2008-81	AST-RX (MNHN) v¦tome¦x L240 (GEIT)	83.28

Proboscidea	*Elephas*	*maximus*	CEB150009	MPI-EVA (Leipzig) SkyScan1173	8.94
Proboscidea	*Loxodonta*	*africana*	MNHN.ZM.AC.1861-53	AST-RX (MNHN) v¦tome¦x L240 (GEIT)	79.27
Proboscidea	*Loxodonta*	*cyclotis*	MNHN.ZM.AC.1950-728	AST-RX (MNHN) v¦tome¦x L240 (GEIT)	94.27
Proboscidea	*Loxodonta*	*cyclotis*	MNHN.ZM.AC.1956-194	AST-RX (MNHN) v¦tome¦x L240 (GEIT)	81.74
Proboscidea	*Loxodonta*	*cyclotis*	MNHN.ZM.AC.1957-465	AST-RX (MNHN) v¦tome¦x L240 (GEIT)	89.07
Proboscidea	*Loxodonta*	*cyclotis*	MNHN.ZM.AC.1961-69	AST-RX (MNHN) v¦tome¦x L240 (GEIT)	56.51
Proboscidea	*Loxodonta*	*sp*	MNHN.ZM.AC.1932-523	AST-RX (MNHN) v¦tome¦x L240 (GEIT)	120.24
Proboscidea	*Loxodonta*	*sp*	MNHN.ZM.AC.2008-70	AST-RX (MNHN) v¦tome¦x L240 (GEIT)	67.90
Proboscidea	*Loxodonta*	*sp*	MNHN.ZM.AC.2008-71	AST-RX (MNHN) v¦tome¦x L240 (GEIT)	65.00(l)
Proboscidea	*Anancus*	*arvernensis*	NMNHS.FM2991A	AST-RX (MNHN) v¦tome¦x L240 (GEIT)	39.62
Proboscidea	*Anancus*	*arvernensis*	NMNHS.FM2991B	MPI-EVA (Leipzig) SkyScan1173	35.12
Proboscidea	*Anancus*	*arvernensis*	NMNHS.FM2991C	MPI-EVA (Leipzig) SkyScan1173	35.12
Proboscidea	*Anancus*	*arvernensis*	NMNHS.FM2991D	MPI-EVA (Leipzig) SkyScan1173	35.12
Proboscidea	*Anancus*	*arvernensis*	NMNHS.FM2991E	MPI-EVA (Leipzig) SkyScan1173	35.12
Proboscidea	*Anancus*	*arvernensis*	NMNHS.FM2991F	MPI-EVA (Leipzig) SkyScan1173	35.12
Proboscidea	*Anancus*	*arvernensis*	NMNHS.FM2991G	MPI-EVA (Leipzig) SkyScan1173	35.12
Proboscidea	*Cuvieronius*	*sp*	AMNH.FM.103247	AMNH	67.69
Proboscidea	*Gomphotherium*	*angustidens*	MNHN.F.SEP18	AST-RX (MNHN) v¦tome¦x L240 (GEIT)	119.2
Proboscidea	*Gomphotherium*	*angustidens*	MNHN.F.SEP38	AST-RX (MNHN) v¦tome¦x L240 (GEIT)	117.06
Proboscidea	*Gomphotherium*	*angustidens*	CBar coll. V2	MPI-EVA (Leipzig) SkyScan1173	31.89
Proboscidea	*Mammut*	*americanum*	AMNH.FM.14293A	AMNH	75.20
Proboscidea	*Mammut*	*americanum*	AMNH.FM.14293B	AMNH	88.30
Proboscidea	*Mammuthus*	*columbi*	AMNH.FM.144658	AMNH	89.61(r) 95.49(l)
Proboscidea	*Mammuthus*	*primigenius*	MNHN.F.1904-12	MPI-EVA (Leipzig) SkyScan1173	35.12
Proboscidea	*Moeritherium*	*lyonsi*	SMNS 47789-90	AST-RX (MNHN) v¦tome¦x L240 (GEIT)	41.93
Proboscidea	*Moeritherium*	*trigodon*	NHMUK 68436	AST-RX (MNHN) v¦tome¦x L240 (GEIT)	46.10
Proboscidea	*Numidotherium*	*koholense*	UOK5	AST-RX (MNHN) v¦tome¦x L240 (GEIT)	81.66
Proboscidea	*Palaeoloxodon*	*antiquus*	NHMUK.M82706	NHMUK	41.48
Proboscidea	*Platybelodon*	*grangeri*	AMNH.FM.26564	AMNH	95.49
Proboscidea	*Prodeinotherium*	*bavaricum*	MHNT.PAL.2013.01108E	AST-RX (MNHN) v¦tome¦x L240 (GEIT)	54.17
Proboscidea	*Stegodon*	*orientalis*	AMNH.FM.18632	AMNH	141.85
Proboscidea	*Stegomastodon*	*sp*	AMNH.FM.21807	AMNH	89.61(l) 102.72(r)
Hyracoidea	*Procavia*	*capensis*	CEB150012	MPI-EVA (Leipzig) SkyScan1173	8.22
Embrithopoda	*Nov. gen.*	*Nov. spec.*	PM53	AST-RX (MNHN) v¦tome¦x L240 (GEIT)	38.6
Perissodactyla	*Unknown*	*Unknown*	Beon 98 E1 3049	AST-RX (MNHN) v¦tome¦x L240 (GEIT)	88.67
Perissodactyla	*Unknown*	*Unknown*	MHNT.PAL.2013.01108A	AST-RX (MNHN) v¦tome¦x L240 (GEIT)	56.18
Macroscelidea	*Elephantulus*	*sp*	MNHN.ZM.AC.1930-92	MPI-EVA (Leipzig) SkyScan1173	7.86
Incerte saedis	*Ocepeia*	*daouiensis*	PM45	AST-RX (MNHN) v¦tome¦x L240 (GEIT)	25.5

2.2. Methods

CT scanning acquisitions and segmentation

The specimens were scanned with different microtomographs. Details about the location of the scanners, the models of the microtomographs and the different resolutions are given in Table 2. The petrosals and bony labyrinths were then segmented at the 3D imagery platform of MNHN using MIMICS INNOVATION SUITE software (Materialise, releases 16 and 17 depending on the specimen). Further details about the post-treatment of the 3D models for specific purposes will be explained in the "Material and methods" section of the related chapter (chapters IV and V mostly).

Petrosal and labyrinth measurements

Angle between the cerebral and cerebellar surfaces of the petrosal

The dorsal surface of the petrosal of the major part of the proboscideans (elephantimorphs) displays two well distinct surfaces: the cerebellar surface and the cerebral surface. The two surfaces are separated by a ridge called the *crista partis petrosa*. To calculate the angle between these surfaces, we orient the petrosal in posterior view. Then we trace a line starting from the *crista partis petrosa* and following the cerebellar surface and a line starting from the *crista partis petrosa* and following the cerebral surface (Fig. 3A). The angle between these two lines is then measured manually.

Stapedial ratio of the fenestra vestibuli

The stapedial ratio is calculated according to Segall (1970): r = L/w with L = length and w = width of the *fenestra vestibuli* (Fig. 3B). It expresses the general shape of the fenestra vestibuli. Specimens with high ratios tend to display a relatively oval *fenestra vestibuli* while specimens with low ratios generally display a rounder *fenestra vestibuli*.

Aspect ratio of the cochlea

The aspect ratio of the cochlea has been calculated using the same method described in Benoit et al. (2013b). The width of the cochlea is measured from the basal hook to the periphery of the cochlear canal in ventral view (Fig. 3C). The height of the cochlea is measured in profile view.

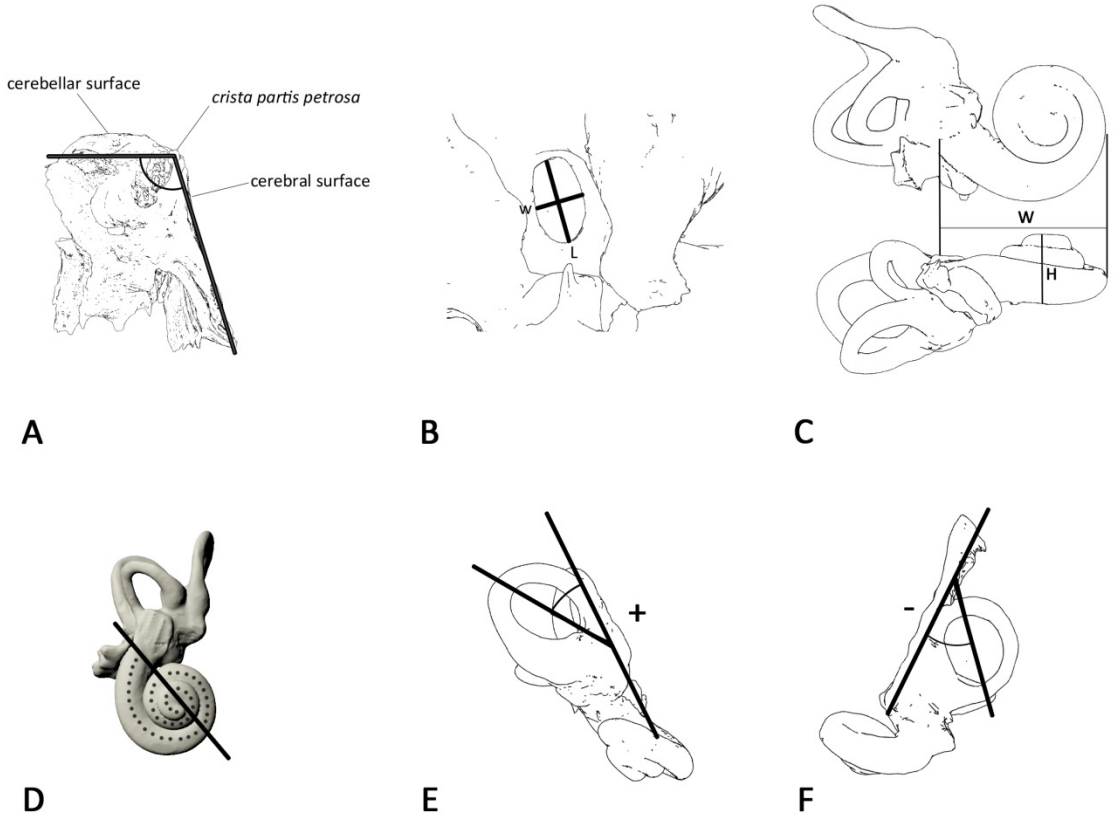

Figure 3 : Measurement protocols. Angle between the cerebellar and cerebral surfaces of the petrosal (A). Stapedial ratio (B) following Segall (1970); **w**=width, **L**=length. Cochlear aspect ratio (C) following Benoit et al. (2013b); **W**=width, **H**=height. Number of turns of the cochlea (D) following West (1985). Angle between the major axis of the semicircular canal and the *crus commune* (E and F).

Number of turns of the cochlea

The number of turns of the cochlea was calculated using the protocol of West (1985). A line is drawn between the basal hook of the cochlea and the modiolus (rotation axis of the cochlea; Fig. 3D). Then, the number of times that the cochlea crosses that line is counted as a half-turn and the total number of turns of the cochlea is calculated.

Angle between the major axis of the semicircular canals and the crus commune

This angle value can only be calculated for the vertical semicircular canals (anterior and posterior canals). It is pertinent only for canals exhibiting an oval overall shape. The specimen should be oriented so that its anatomical plane is the plane of the screen. A line is drawn following the major axis (greater radius) of the ellipse formed by the canal. Another

line is drawn following the axis of the *crus commune*. The angle between these two lines is then measured manually (Fig. 3E and 3F). If the line following the major axis of the canal crosses the line of the *crus commune* at the level of the crus basis, the value is considered to be positive (Fig. 3E). On the contrary, if the major axis of the canal crosses the line of the *crus commune* at the level of the crus apex, the value is considered to be negative (Fig. 3F).

Landmark protocol

The functional analysis of the semicircular canals requires a certain number of landmarks placed on the bony labyrinth. The landmarks are then used to calculate several measurements. Based on these measurements and measurements on the membranous labyrinth of closely related specimens (chapter VI), functional features can be inferred. Several portions of this PhD thesis are based on these landmarks. Indeed, we used the same landmark sets to conduct a geometric morphometrics analysis (chapter IV). On the other hand, we used several measurements of the bony labyrinth based on these landmarks and given by an ARIADNE add-on currently developed by Romain David to compare our specimens (chapter II and III). These compared measurements were sometimes used to create or recalibrate phylogenetic characters (chapter V). Some of the measurements used in chapters II and III have been obtained with these landmarks. Every complete (or almost complete) inner ear that has been segmented for this work has been landmarked following a modified version of the protocol presented in Gunz et al. (2012). This protocol consists of 13 landmark sets (Fig. 4A). The landmarks were placed on the specimens using the software AVIZO 7.1.1. The Auto-Skeleton tool was used to obtain the central streamlines of the semicircular canals.

First, an external set of landmarks for each semicircular canal is placed (Fig. 4B-D, black sets). The first landmark is a type-I landmark and it is located on the ventral part of the ampulla. It is centered on the symmetry axis of the canal and placed at the external level of the crista ampullaris (at this place, the *nervus ampullaris* usually enters the ampulla). Semi-landmarks are placed along the canal following its most external portion until its connection with the *crus commune*. Three of these sets are placed on the inner ear (one on each semicircular canal).

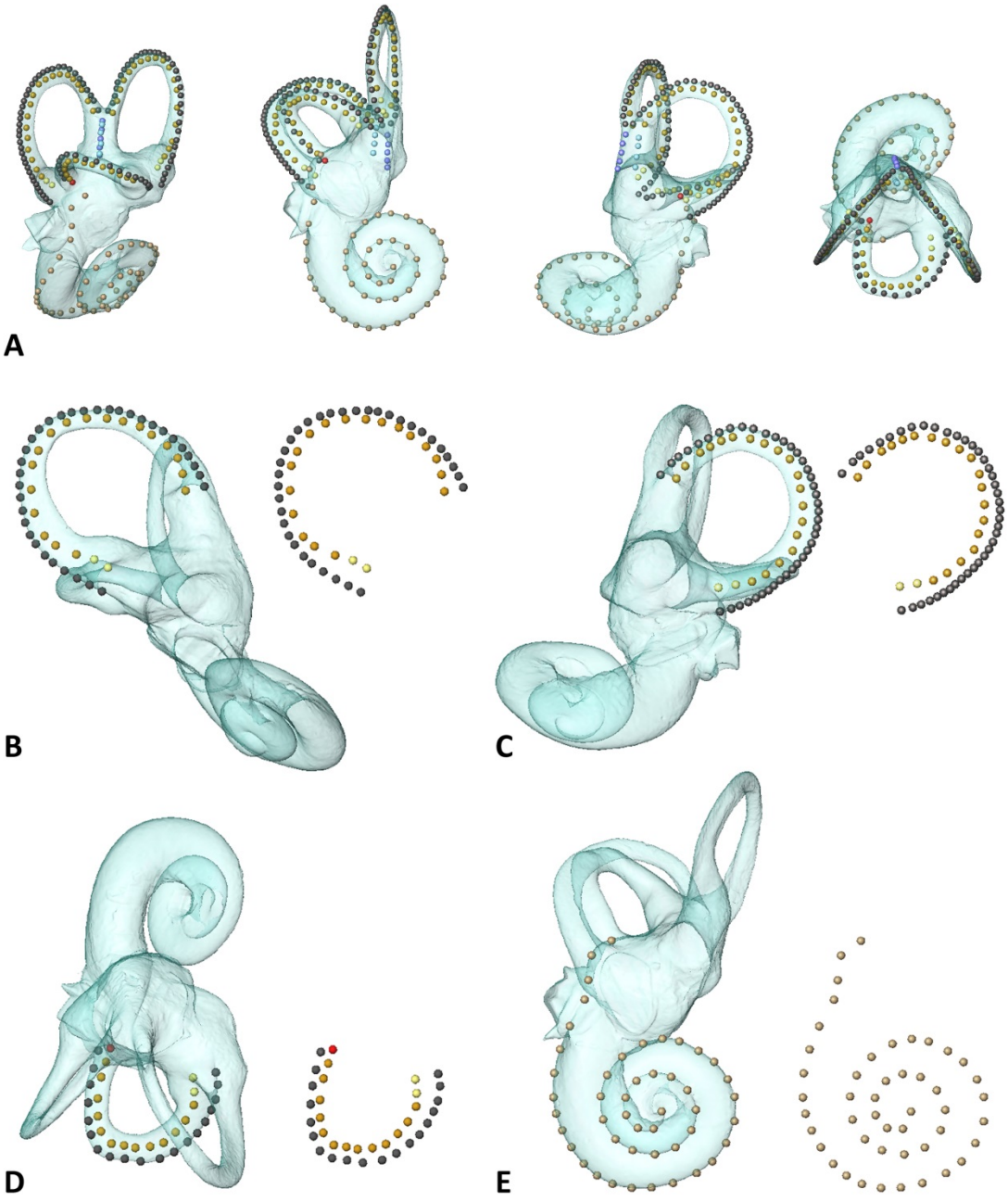

Figure 4 : Landmark sets visualized on the bony labyrinth of *Loxodonta* MNHN.ZM.AC.1861-53 in frontal, ventral, profile and dorsal view respectively (A). Detailed view of the landmark set of the anterior (B), posterior (C) and lateral (D) canals and of the cochlea (E). In **black**, external landmarks of the semicircular canals (3 sets in total); in **orange**, internal landmarks of the slender part of the semicircular canals (3 sets in total); in **yellow**, internal sets of the ampullae of the semicircular canals (3 sets in total); in **red**, internal set of the connection between the lateral canal and lateral utricle (1 set); in **grey-brown**, external set of the cochlea (1 set); in **dark blue**, external set of the *crus commune* (1 set); in **sky blue**, internal set of the *crus commune* (1 set).

An internal set is placed on the central streamline of each semi-circular canal (Fig. 4B-D, orange sets). It is entirely composed of semi-landmarks (the set is associated with other sets holding a type-I landmark during the geometric morphometrics analysis). The first landmark is placed at the intersection between the ampulla and the slender part of the canal. Then, landmarks are placed along the central streamline until reaching the intersection between the canal and the *crus commune*. Three of these sets are placed on the inner ear (one on each semicircular canal). Concerning the lateral canal, when it is partially fused with the posterior canal (partial or total '*crus commune secundaria'*), the last landmark is placed on the streamline before the canals begin to fuse. In this case, the last remaining landmarks are placed in the "slender-utricle intersection" set (next paragraph).

An internal set of landmarks is placed at the intersection between the lateral canal and the lateral utricle (Fig. 4D, red set). When the lateral and posterior canals are not fused, this set simply consists of a single type-I landmark placed at the junction of the lateral canal and the vestibule. When the lateral and posterior canals are fused, several landmarks are placed manually on the central streamline of the fused lateral canal and the last landmark is a type-I landmark placed at the junction of the lateral canal and the vestibule.

An internal set of landmarks is placed on the central streamline of the ampulla of each canal (Fig. 4B-D, yellow sets). The first landmark (type I) is placed at the level of the crista ampullaris on the central streamline. Semi-landmarks are then placed along the streamline until reaching the intersection with the semicircular canal. Three of these sets are placed on the inner ear (one on each semicircular canal).

An external landmarks set is placed along the *crus commune* (Fig. 4A, dark blue set). The first landmark is a type-I landmark and it is located at the reunion of the anterior and posterior canals streamline. Semi-landmarks are then placed along the *crus commune*, parallel to its long axis. The last placed landmark is also a type-I landmark and is placed at the basis of the crus.

An internal set is placed on the *crus commune* as well (Fig. 4A, sky blue set). The first landmark is a type-I landmark and is placed at the intersection of the anterior

and posterior canals streamline. Semi-landmarks are then placed on the central streamline. The last landmark (type I) is placed at the basis of the *crus commune*.

An external set of landmarks is placed on the cochlea (Fig. 4E, grey-brown set). The first landmark is a type-I landmark and it is located at the top of the *fenestra vestibuli.* Semi-landmarks are then placed along the external portion of the cochlea (which follows the basilar membrane). The last landmark is placed at the tip of the helecotrema and is a type-I landmark.

Volumes and landmark-based measurements

As previously said, the ARIADNE add-on currently developed by Romain David outputs several measurements of the bony labyrinths than can be helpful to compare specimens. Because these measurements were used in several following chapters of the thesis (comparative anatomy chapters II and III and phylogenetics chapter V), they are presented in this section.

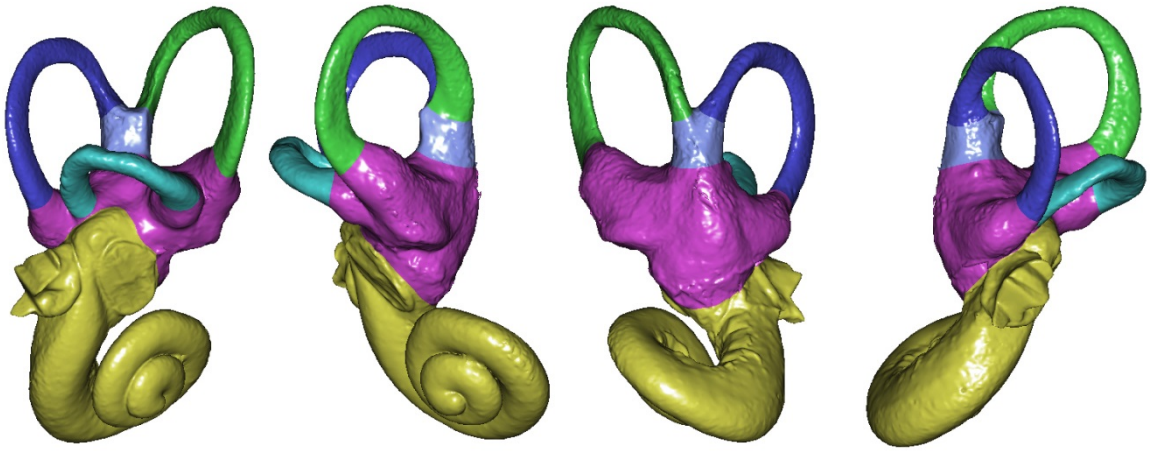

Figure 5 : 3D view of the bony labyrinth of *Loxodonta* MNHN.ZM.AC.1861-53 showing the different volumes obtained after the separation protocol. **Yellow**: cochlea, **purple**: vestibule, **green**: anterior semicircular canal, **dark blue**: posterior semicircular canal, **sky blue**: lateral semicircular canal, **grey-blue**: *crus commune*.

Volumes

The total volume of the bony labyrinth is directly given (in mm^3) by the ARIADNE add-on currently developed by Romain David. The volume of the cochlear part only is also available. The cochlea is separated from the vestibular part of the labyrinth at the beginning of the preparation protocol required for the software. The limit is drawn using the software GEOMAGICS Studio 2012 (Fig. 5). It is important to include the superior extremity of the cochlear canal as well as the *fenestra vestibuli* in the cochlear volume. On the other hand, the saccule must be included in the vestibule volume. During the comparison of the specimens, we essentially used the relative volume of the cochlea (cochlear volume / total volume * 100). It is very difficult to separate the cochlea from the vestibule in the same way. Hence, these values are somewhat approximate and cannot be used in proper statistical analysis. However, approximate relative volumes of the cochlea obtained with this protocol and given in the literature using other protocol can be compared within a certain range of precision.

Crus commune length, average section radius and average thickness ratio

The *crus commune* length is measured by the ARIADNE add-on currently in development. It simply consists of the sum of the distances between consecutive internal landmarks of the *crus commune*. The average section radius is given by the software as well. It is the mean of the *crus commune* radii taken at different sections of the *crus commune*. We used these two values to calculate the average thickness ratio (average section radius / *crus commune* length * 100). This ratio gives a quantitative value that expresses the global thickness of the *crus commune*. *Crus commune* with a high ratio tend to be thicker and stockier than *crus commune* with a low ratio.

Semicircular canals length, average section radius and thickness ratio

The semicircular canal length is measured by the ARIADNE add-on as well. It is the sum of the distances between consecutive landmarks of the whole canal. As for the anterior and posterior canals, the measurement starts at the first internal landmark of the ampulla (type-I landmark that represents the *crista ampullaris*) and ends at the level of the intersection of the two canals (first

internal landmark of the *crus commune*). For the lateral canal, the measurement starts at the first internal landmark of the ampulla and ends at the last landmark of the lateral canal / lateral utricle intersection set (red landmark in Fig. 4A and 4D). The average section radius is calculated in the same manner as for the *crus commune* average section radius. It only expresses the mean section radius of the slender part of the canal (green, dark blue and sky blue in Fig. 4). Indeed, the ampullae radii are not used to calculate this value. Using these two values given by the ARIADNE add-on, an average thickness ratio of each semicircular canal can be calculated (average section radius / semicircular canal length * 100). The mean of these three ratios expresses the global thickness of the semicircular canals quantitatively.

Radii of curvature

The radius of curvature of each semicircular canal is given directly by the ARIADNE add-on currently under development. For the vertical canals, it considers the torus that consists of the slender part, the *crus commune* and the part that connects the two structures. It then measures the average between the equivalent radius of the torus perimeter and the radius of the torus area. For the lateral canal, it considers only the slender part of the canal and the straight line that connects both extremities and then measures the average between the radius of the torus perimeter and the radius of the torus area.

Angle between the semicircular canals

The angles between the semicircular canals are given by the ARIADNE add-on under development. Measuring manually these angles can be tricky, because the semicircular canals are rarely perfectly planar. The software uses the landmarks to determine the functional plane of each semicircular canal. The angles are then compared between the functional planes of the canals.

CHAPTER I

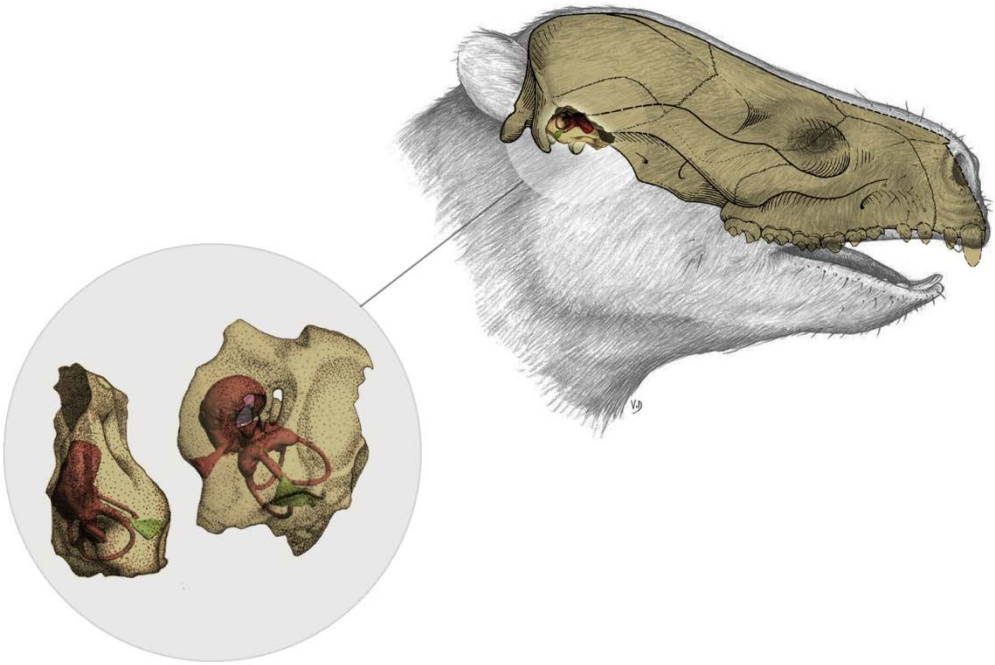

The ear region of earliest known elephant relatives: new light on the ancestral morphotype of proboscideans and afrotherians

1. Introduction

Today there are only three living species of proboscideans: the Asian elephant (*Elephas maximus*), the African bush elephant (*Loxodonta africana*) and the African forest elephant (*Loxodonta cyclotis*). The fossil diversity of this mammalian order is much greater: approximately 180 extinct species of proboscideans have been described (Gheerbrant & Tassy, 2009), with a rich evolutionary history dating as far back as 60 million years (Gheerbrant, 2009). The evolutionary history of the order Proboscidea is indeed one of the best documented among placentals, especially for its debut at the beginning of the Tertiary with the discovery of the remarkably primitive and early genera *Phosphatherium* and *Eritherium* (Gheerbrant et al. 2005; Gheerbrant, 2009). The early evolutionary sequence represented by *Eritherium*, *Phosphatherium, Daouitherium, Numidotherium, Barytherium, Moeritherium* and *Phiomia*, is the most completely known documentation of the emergence and initial radiation of an extant order of mammals at a remarkably and rarely preserved primitive stage, of one of the most specialized and popular mammals – the elephants.

In this work we describe and compare the middle and inner ear morphology of the petrosal of the earliest known proboscideans *Phosphatherium* and *Eritherium,* which were both found in the Ouled Abdoun Basin in Morocco, respectively in Selandian (60 Ma; Kocsis et al. 2014; Yans et al. 2014) and early Ypresian phosphate levels (55.5 Ma; Gheerbrant et al. 2003, 2005). The petrosal is a key anatomical region of the skull for the phylogenetic analysis of placental mammals, which is especially significant at high systematic ranks. It is useful for analysis of intra- and interordinal relationships of proboscideans, especially among the Afrotheria, which are at the heart of active researches in several disciplines such as palaeontology and molecular systematics and phylogeny.

The labyrinth anatomy remains poorly understood in placentals, and especially in Proboscidea. The middle ear anatomy of *Phosphatherium* has been partly described (Gheerbrant et al. 2005), but the petrosal of *Eritherium* and the

inner ear of *Phosphatherium* were entirely unknown before this work. Our study of the ear region of these two stem proboscideans was made with the help of CT scan method of examination. We compare the petrosal morphology of *Eritherium* and *Phosphatherium* with that of other proboscideans and to other afrotherians, and discuss their significance for augmenting knowledge about the evolution of the morphology of the middle and inner ear among proboscideans and especially for the characterization of the ancestral morphotype of the order.

2. Material and methods

2.1. Material studied

Eritherium azzouzorum from the Selandian of the Ouled Abdoun Basin (Morocco) is the only known species of the genus *Eritherium* and is the oldest known proboscidean. It is represented by some elements of the skull and most of the dentition (Gheerbrant, 2009; Gheerbrant et al. 2012). The isolated petrosal described in this study was mentioned by Gheerbrant et al. (2012), as specimen PM88, but was not described or illustrated. It is associated with other broken elements of the skull of the same individual, including maxillae, parietals and basicranium, all belonging to specimen PM88. It is a left petrosal covered by a thin pellicle of phosphatic matrix (Fig. I.1). The maxillae associated with the petrosal of specimen PM88 are confidently identified as *Eritherium azzouzorum* (see Gheerbrant et al. 2012, plate 2), and the size and aspect of the bone of the isolated petrosal indicate that they belong to the same individual. This petrosal is partly damaged by two fissures that run across its surface (one on the tympanic surface and one on the cerebellar surface).

Phosphatherium escuilliei was discovered in early Ypresian phosphate beds of the Ouled Abdoun Basin (Morocco) (Gheerbrant et al. 1996, 2003, 2005). Dental and cranial remains have been found, and a description and reconstruction of the whole skull was provided by Gheerbrant et al. (2005). It was based on the nearly complete skull specimens OCP DEK/GE 305 and MNHN.F.PM17. Here we investigate the detailed anatomy of the petrosal, including the inner ear, preserved in MNHN.F.PM17, with the help of CT scanning technology. The scanned specimen MNHN.F.PM17 is an incomplete

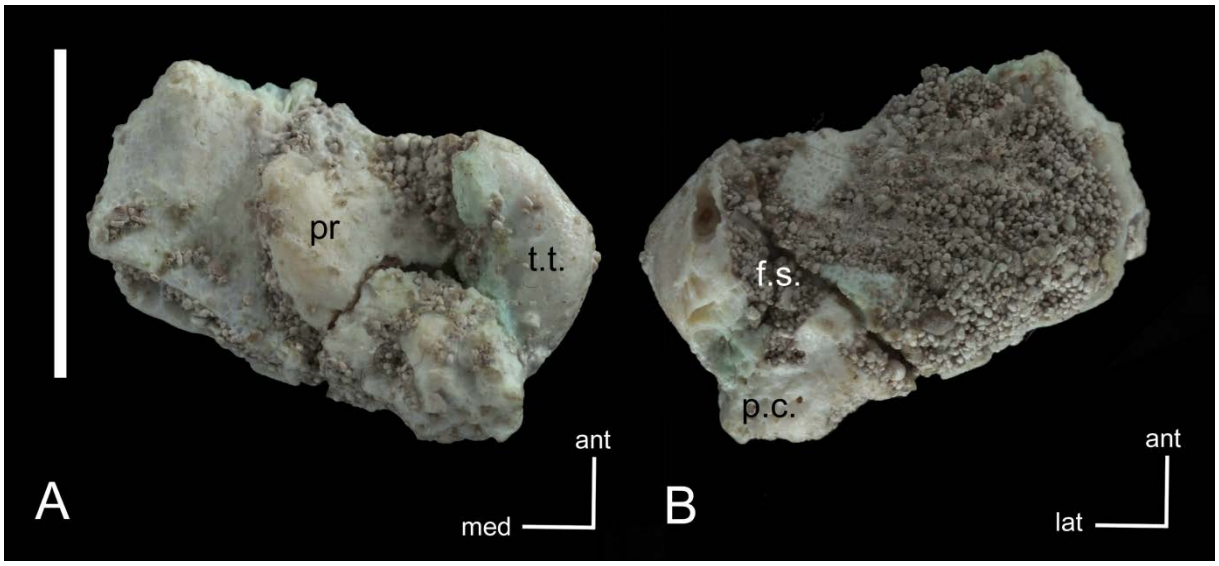

Figure I.1 : Photograph of the isolated petrosal of *Eritherium azzouzorum* PM88 (scale = 1 cm). (A) Ventrolateral view showing the tympanic surface of the petrosal: **pr** *promontorium*, **t.t.** *tegmen tympani*. (B) Dorsomedial view showing the cerebellar surface of the petrosal: **f.s.** location of the *fossa subarcuata*, **p.c.** *pars cochlearis*.

skull with both right and left petrosals preserved (Gheerbrant et al. 2005; Fig. I.3). However, the *promontorium* is damaged on both petrosals which prevented the reconstruction of the entire cochlea. In this work we reconstruct and describe mostly the right petrosal (and labyrinth) of MNHN.F.PM17, because it is the better preserved one. The right petrosal (the left is missing) of specimen OCP DEK/GE 305 of *Phosphatherium escuilliei* seems to be better preserved (Gheerbrant et al. 2005; Figs 1 and 2) with an undamaged *promontorium,* but this specimen housed in the OCP collection (Khouribga, Morocco) was not available for CT scanning.

2.2. CT scanning acquisition

The two studied specimens of *Eritherium* (PM88) and *Phosphatherium (*MNHN.F.PM17) were scanned at the AST-RX platform of the MNHN (Paris) using a v¦tome¦x L240 from GE Inspection Technologies CT scanner with a voxel size of 10.1 µm for PM88 (voltage: 150 kV, intensity: 270 µA) and 38.6 µm for MNHN.F.PM17 (voltage: 150 kV, intensity: 250 µA). The slices were treated with ImageJ to adjust the contrast and reduce the size of the data. 3D digital reconstructions of the petrosal and inner ear of both specimens were then done at the 3D imagery platform of the MNHN using MIMICS innovation suite software (Materialise®, release 16).

2.3. Measurements

Measurements (size and volume) of the semi-circular canals and the cochlea were obtained with the software mimics, following the methods explained in Benoit et al. (2013a). The number of turns of the cochlea was measured using the protocol of West (1985). The calculation of the radii of curvature of the semi-circular canals was done thanks to the Spoor–Zonneveld equation (Spoor & Zonneveld, 1998): 0.5 ($l + w$)/2 with l = length and w = width of the canals. The stapedial ratio was calculated according to Segall (1970): L/w with L = length and w = width of the *fenestra vestibuli*. The aspect ratio of the cochlea was calculated according to the formula found in Ekdale (2011): H/W with H = height and W = width of the cochlea.

2.4. Abbreviations

MNHN.F: Collections of the Museum National d'Histoire Naturelle (F: Paleontology), Paris, France.

OCP: Office Cherifien des Phosphates, Khouribga, Morocco.

OCP DEK/GE: Collections of the Office Cherifien des Phosphates, Khouribga, Morocco.

PM: phosphate of Morocco.

3. Systematic descriptions

3.1. *Eritherium azzouzorum* Gheerbrant, 2009

The left petrosal PM88 of *Eritherium azzouzorum* was found broken and isolated, but in association with several other skull fragments (Gheerbrant et al. 2012). It was oriented indirectly based on comparisons with the petrosals of *Protungulatum* (O'Leary, 2010) and *Ocepeia* (Gheerbrant et al. 2014).

Cerebellar surface

The cerebellar surface (dorsomedial view, Fig. I.2A) of the petrosal is smooth and carries two large openings: the internal acoustic meatus (*meatus acusticus internus*) and the subarcuate fossa (*fossa subarcuata*). These two openings are separated by a large and well-defined ridge called the *eminantia arcuata*. The subarcuate fossa is very deep and round, and does not carry a petromastoid canal. The internal acoustic meatus is oval and not well-defined. It is separated into two foramina of similar size (the *foramen acusticum inferius*, which contained the cranial nerve VIII and the *foramen acusticum superius*, which was

the exit point of the cranial nerve VII) by a rather narrow and well-defined *crista transversa*. Whereas the *foramen acusticum inferius* is round, the *foramen acusticum superius* is oval, with the major axis of the ellipse oriented antero-posteriorly. The surface around the internal acoustic meatus is relatively smooth. The prefacial commissure, located on the lateral part of the meatus, is large. The *foramen singulare* is visible and situated in the posterior part of the *foramen acusticum inferius*. It contained a portion of the cranial nerve VIII (*nervus ampullaris* posterior canal, Macrini et al. 2010) linked to the posterior ampulla of the vestibule. The *tractus spiralis foraminosus* is visible and consists of a perforated and spiralled surface related to the vestibulo-cochlear nerve (cranial nerve VIII) (O'Leary, 2010). A groove is visible on the anterior aspect of the *pars cochlearis*, oriented medially to the internal acoustic meatus. It extends from the anterior extremity of the petrosal to the posterior extremity of the internal acoustic meatus and preserves the track of the inferior petrosal sinus (Ladevèze et al. 2010), which drained the venous blood from brain (Cifelli, 1982). The cochlear canaliculus (*aquaeductus cochleae*) connects the perilymphatic space of the inner ear to the subarachnoid space of the endocranial cavity (Meng & Fox, 1995). In specimen PM88 of *Eritherium* it was likely located in the large fissure that runs across the petrosal, which renders observation and reconstruction difficult. However, despite the fact that this area is damaged by the fissure, we observed a foramen at the level of the jugular fossa (medial surface) that likely corresponds to the *cochlear canaliculus*. The *aquaeductus vestibuli* exits perpendicularly to the cerebellar surface and medially to the subarcuate fossa. The *tegmen tympani* is massive and carries two large grooves. The one that is the closest to the subarcuate fossa is probably the sigmoid sinus, observed in *Orthaspidotherium* (Ladevèze et al. 2010). The other one is probably the prootic sinus.

Tympanic surface

In ventrolateral view (Fig. I.2B), the *pars cochlearis* can be observed in the anteromedial side of the petrosal. It carries a hemi-ellipsoid and almost flat *promontorium* which contains the cochlea. The *promontorium* is crossed by a fissure, separating the anterior part from the posterior part that carries the *fenestra vestibuli* and the *fenestra cochleae*.

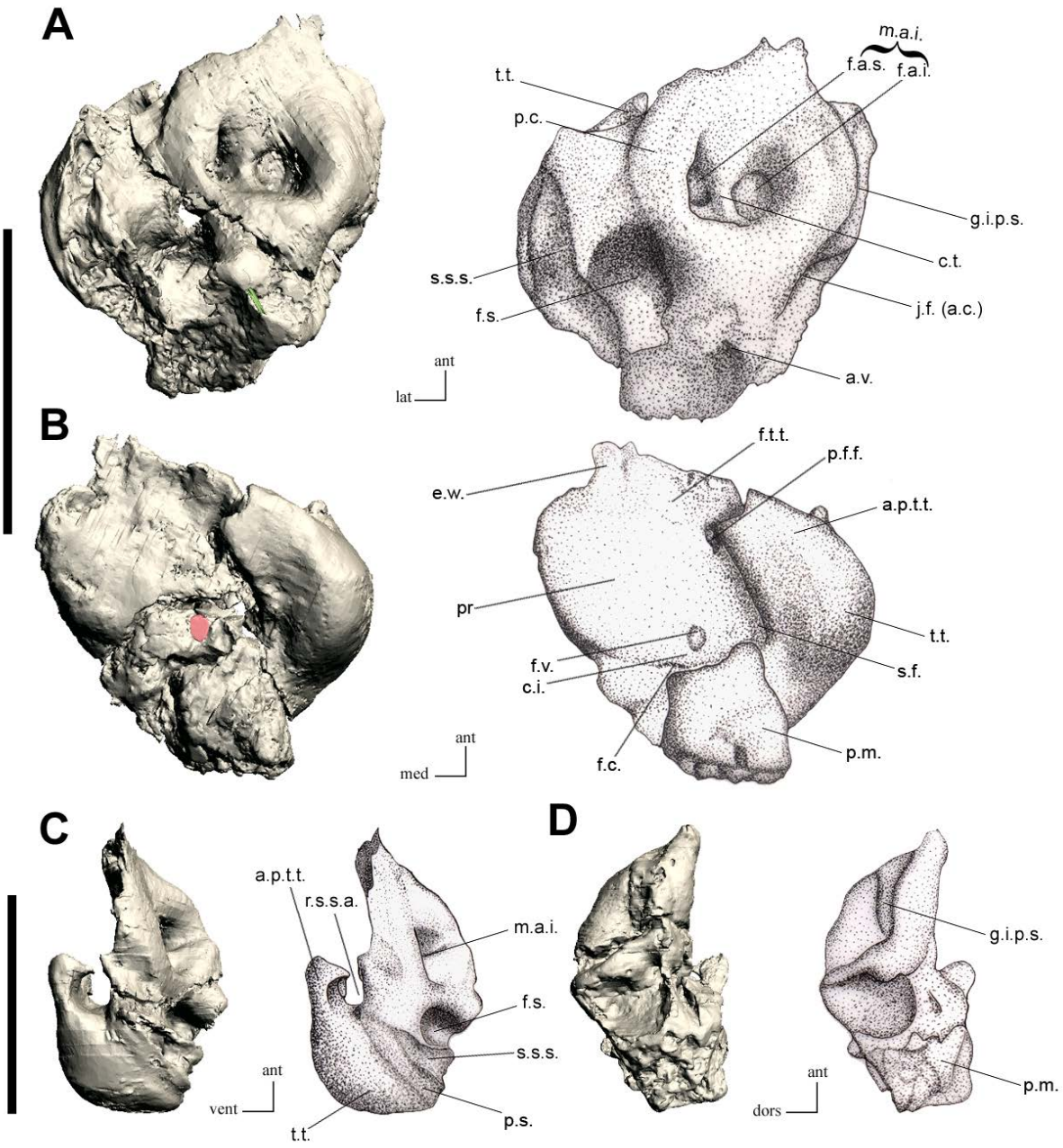

Figure I.2 : 3D reconstructions and annotated drawings of the left petrosal PM88 of *Eritherium* (scale = 1 cm) in cerebellar (A), tympanic (B), dorsolateral (C) and ventromedial (D) views: **a.p.t.t.** anterior part of the *tegmen tympani*, **a.v.** bony duct for the *aquaeductus vestibuli*, **c.i.** *crista interfenestralis*, **c.t.** *crista transversa*, **e.w.** epitympanic wing, **f.a.i.** *foramen acusticum inferius*, **f.a.s.** *foramen acusticum superius*, **f.c.** *fenestra cochleae*, **f.s.** *fossa subarcuata*, **f.t.t.** fossa for the *tensor tympani*, **f.v.** *fenestra vestibuli*, **j.f. (a.c.)** jugular fossa holding the *aquaeductus cochleae*, **g.i.p.s**. groove for the inferior petrosal sinus, **m.a.i.** *meatus acusticum internalis*, **p.c.** prefacial commissure, **p.f.f.** primary facial foramen, **p.m.** *pars mastoidea*, **p.s.** prootic sinus, **pr** *promontorium*, **r.s.s.a.** ramus superior for the stapedial artery, **s.f.** *sulcus facialis*, **s.s.s.** sinus for the sigmoid sinus, **t.t.** *tegmen tympani*.

The *fenestra vestibuli* is round (stapedial ratio = 1.57), whereas the *fenestra cochleae* is sub-rectangular. The *fenestra cochleae* continues to a surface called the postpromontorial tympanic sinus, which bears the medial part of the caudal tympanic process. The *fenestra cochleae* and *fenestra vestibuli* are about the same size, but the *fenestra vestibuli* is slightly wider. They are separated by quite a large and bulging *crista interfenestralis*. No sulcus can be observed on the surface of the *promontorium*. The *promontorium* carries an epitympanic wing, a narrow flange of bone that links it to the *tegmen tympani* and demarcates the limit of the *pars cochlearis*. The *pars canalicularis* borders the *pars cochlearis* on its lateral and posterior sides. The primary facial foramen (which is the exit point of the facial nerve from inside the petrosal) is visible, whereas the secondary facial foramen is not distinct because the bony roof which covers the geniculate ganglion is not preserved. However, since the primary facial foramen is located anteriorly to both fenestrae, the secondary facial foramen is also likely to be located anteriorly to the *fenestra vestibuli* and the *fenestra cochleae*. The fossa for the *tensor tympani* is visible in the anterior part of the petrosal, located anteromedially to the primary facial foramen. The fossa is quite large, oval, not very deep and partially crossed by a fissure. The facial sulcus is C-shaped and contained the facial nerve. It is laterally delimited by the *crista parotica*, which is an osseous ridge extending partially on top of the facial sulcus. A large but poorly defined fossa for the stapedial muscle is present medio-posteriorly to the *fenestra vestibuli*, under an osseous projection. The tip of this osseous ridge is generally referred to as the tympanohyal. The facial nerve probably followed the stapedial muscle fossa before exiting the petrosal through the stylomastoid notch located medio-posteriorly and bounded by the caudal tympanic process and the tympanohyal. The position of the *hiatus Fallopii* is not clear but we can infer its location from its continuity with the groove made by the facial nerve. It was probably located on the anterior part of the petrosal, but its exact position there is unknown. The broken anterior process of the *tegmen tympani* is extremely rounded and extends along the postero-lateral edge of the facial sulcus. The *tegmen tympani* displays two large incomplete ossified canals on its cerebellar surface. The first one is oriented laterally and probably corresponds to the passage of

the *ramus superior* for the stapedial artery. The second one is oriented anteriorly and might be the *ramus inferius* for the stapedial artery (Wible, 1983). On the posterior part of the petrosal, the *pars mastoidea* is square and prominent.

In dorso-lateral view (Fig. I.2C), the *tegmen tympani* is clearly visible. It is voluminous, bulging, triangular with rounded corners and carries a rather large anterior process. A laterally oriented large canal, which contained the *ramus superior* for the stapedial artery, is present in the anterior process of the *tegmen tympani*. Both sinuses described in the cerebellar surface (including the probable sinus for the sigmoid sinus) are also visible in this view.

In ventro-medial view (Fig. I.2D), the petrosal has a rather triangular shape (including the missing medial part of the *pars canalicularis*). The medial surface of the *pars cochlearis* is bulging, therefore the internal acoustic meatus is not visible in this view. However, the inferior petrosal sinus is clearly visible and extends from the anterior aspect of the *pars cochlearis* to the fissure. The *cochlear canaliculus*, which has been damaged by the fissure, cannot be described in this view.

The observation of *Eritherium* in tomographic section shows the presence of a well-developed pneumatization of its petrosal, with the presence of numerous and large osseous cells, especially inside the *tegmen tympani* (see Appendix 2, character 11).

Inner ear

The endocast of the bony labyrinth of *Eritherium* is reconstructed in Fig. I.3. The cochlea of *Eritherium* is partially broken and the number of turns is approximately 2 (720°). The total spiral length of the cochlea is 14.13 mm. In dorsal view, the first turn (basal turn) appears to be larger and overlaps the second turn (apical turn). In lateral view, the cochlea is flattened with an aspect ratio of 0.35. This morphology seems to be natural because no major distortion of the petrosal is visible. The *cochlear canaliculus* could not be reconstructed because it was located in the long fissure running through the petrosal, but it was probably present. The *fenestra cochleae* and the *cochlear canaliculus* are therefore most likely separated from each other and not merged in a common perilymphatic foramen. The *fenestra cochleae* is sub-rectangular, with rounded corners.

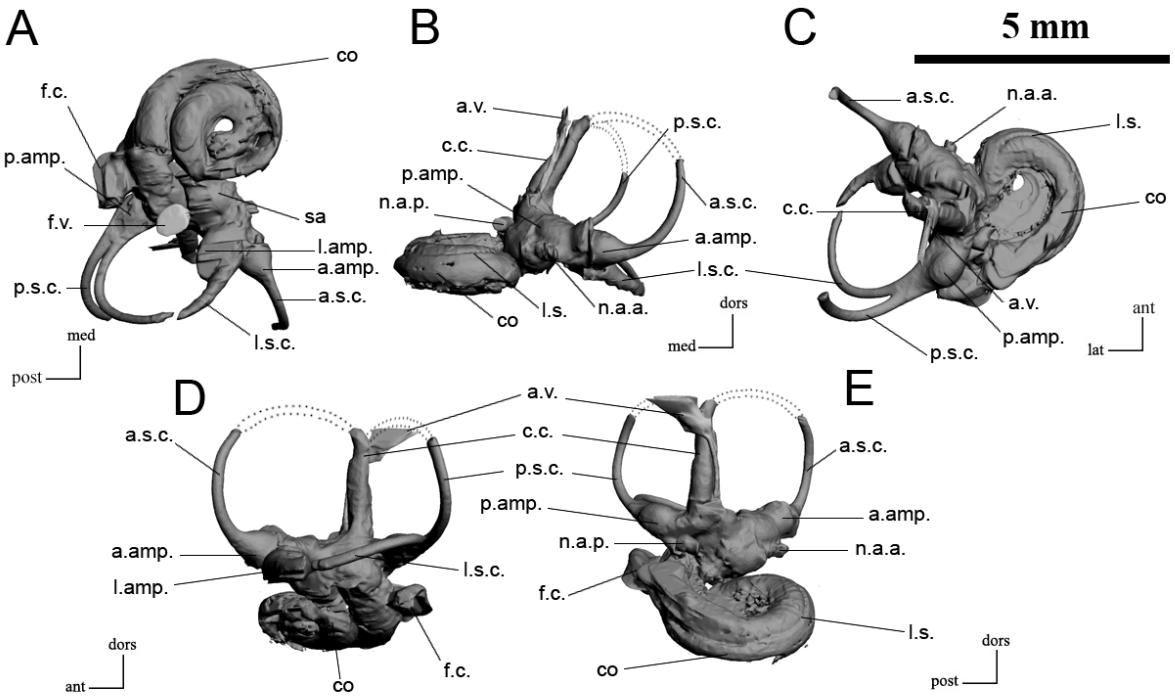

Figure I.3 : 3D reconstructions of the Eritherium bony labyrinth (scale = 5 mm) in ventral (A), posterior (B), dorsal (C), lateral (D) and medial (E) views: **a.amp.** anterior ampulla, **a.s.c.** anterior semicircular canal, **a.v.** *aquaeductus cochleae*, **c.c.** *crus commune*, **co.** cochlea, **f.c.** *fenestra cochleae*, **f.v.** *fenestra vestibuli*, **l.amp.** lateral ampulla, **l.s.** *lamina secundaria*, **l.s.c.** lateral semicircular canal, **n.a.a.** *nervus ampullaris anterior*, **n.a.p.** *nervus ampullaris posterior*, **p.amp**. posterior ampulla, **p.s.c.** posterior semicircular canal, **sa.** saccule.

The cochlear volume (Table I.1) is approximately 45% of the total volume of the inner ear. The cochlea of *Eritherium* being damaged (fractured but not distorted), the *scala tympani* and the *scala vestibuli* cannot be located on the slices. However, the *lamina secundaria* is visible on the reconstructed endocast of the cochlea; it covers at least three quarters of the first turn and its depth is approximately 0.1 mm.

The limits of the vestibule were not well defined on the slices of PM88, therefore the general aspect of the 3D modeling is imprecise and the length of the vestibule is overestimated. The other structures, however, are clearly visible. The canal for the *aquaeductus vestibuli,* which contained the endolymphatic sac and the endolymphatic canal, is trumpet-shaped and originates at the anterior level of the common crus basis. It extends dorsally along the common crus. The outlet of the different parts of the vestibulo-cochlear nerve (VIII) is also visible. The part of the nerve VIII that innervates the posterior semi-circular

canal (*nervus ampullaris posterior*) ends under the posterior ampulla and is parallel to the major axis of this ampulla. It originates from the *foramen singulare*, located in the anterior part of the *foramen acusticum inferius*. The part of nerve VIII that innervates the anterior semi-circular canal (*nervus ampullaris anterior*) ends under the anterior ampulla, perpendicularly to the major axis of this ampulla. It originates from a small foramen situated in the dorso-lateral part of the *foramen acusticum superius*.

Although the anterior and posterior semi-circular canals of *Eritherium* are incomplete (*pars canalicularis* damaged), some of their characters can be described. There is a common crus between the anterior and posterior semi-circular canals and its length is at least 2.26 mm. The lateral and posterior semi-circular canals are partially merged at the level of the posterior ampulla; however, they do not form a true secondary common crus because the lumen of the two canals is not fused, and the lateral canal enters directly into the vestibule. The ampullae are well defined and bulging. The cross-section of the canals is rather circular, without any flattening and the canals are particularly thin. The arcs of the posterior and anterior semi-circular canals have approximately the same radius of curvature (even though the anterior canal is slightly larger), whereas the lateral semi-circular canal is shorter than the other two. The lateral canal presents a moderate but distinct undulation. The angles between the semi-circular canals are close to 90°. The measurements of the inner ear are presented in Table I.1.

3.2. *Phosphatherium escuilliei* Gheerbrant et al. 1996

Cerebellar surface

On the cerebellar surface (dorsal view, Fig. I.4A), the subarcuate fossa and internal acoustic meatus are separated by a shallow *eminantia arcuata*. The internal acoustic meatus is rather large, ellipsoid and elongated antero-posteriorly. The subarcuate fossa – which was not visible without the CT scan because of the encrusting phosphate matrix – is larger than the internal acoustic meatus and of moderate depth, its outline forming an antero-posteriorly stretched-out ellipse. The subarcuate fossa of the other specimen of *Phosphatherium* (OCP DEK/GE 305) is described as deep in Gheerbrant et al. (2005) but it is in fact moderately deep in comparison with the

fossa in *Eritherium*. However, the depth of this fossa shows some intra-specific variability in *Phosphatherium escuilliei* because it is clearly deeper on OCP DEK/GE305 than on PM17. Compared with *Eritherium*, the subarcuate fossa of *Phosphatherium* is also longer in an antero-posterior position. The *foramen acusticum superius* is ellipsoid; its long axis is aligned with the long axis of the petrosal. Despite the area being broken, we estimate that the *foramen acusticum inferius* was round. These two foramina are delimited by a partially damaged, narrow and sharp *crista transversa*. The surface around the meatus is smooth and the *foramen singulare* pierces the *foramen acusticum inferius* in its posterior part, as in *Eritherium*. The *tractus spiralis foraminosus* is not visible because of the poor preservation of the *foramen acusticum inferius*. The vestibular aqueduct is located at the posterior extremity of the subarcuate fossa. It forms a large slit perpendicular to the long axis of the fossa.

Tympanic surface

In ventral view (tympanic surface of the petrosal, Fig. I.4B), the *promontorium* is bulging, hemi-ellipsoid and located on the medial part of the petrosal. It is damaged, which allows the observation of some internal characters of the cochleae. No sulcus is observable on the *promontorium*, which could be explained by the absence of these structures or the poor state of preservation of the *promontorium*. Lateral to the *promontorium*, the *fenestra vestibuli* opens ventro-laterally. It appears to be slightly oval but it is considered to be round with a stapedial ratio of 1.62 (stapedial ratio < 1.7; Benoit et al. 2013b). The *fenestra cochleae* is located posterior to the *promontorium*, and is oriented towards the posterior surface of the petrosal. It is sub-rectangular with rounded corners and is almost twice as large as the *fenestra vestibuli*, in contrast to *Eritherium*, which shows a *f. vestibuli* slightly larger than the *f. cochleae*. The fenestrae are separated by quite a large and flat *crista interfenestralis*. The secondary facial foramen, which corresponds to the exit of the facial nerve, is also visible. The facial sulcus that conveyed the facial nerve from the secondary facial foramen is C-shaped. The fossa for the stapedial muscle is present posterolateral to the *fenestra vestibuli* and is followed by the facial sulcus.

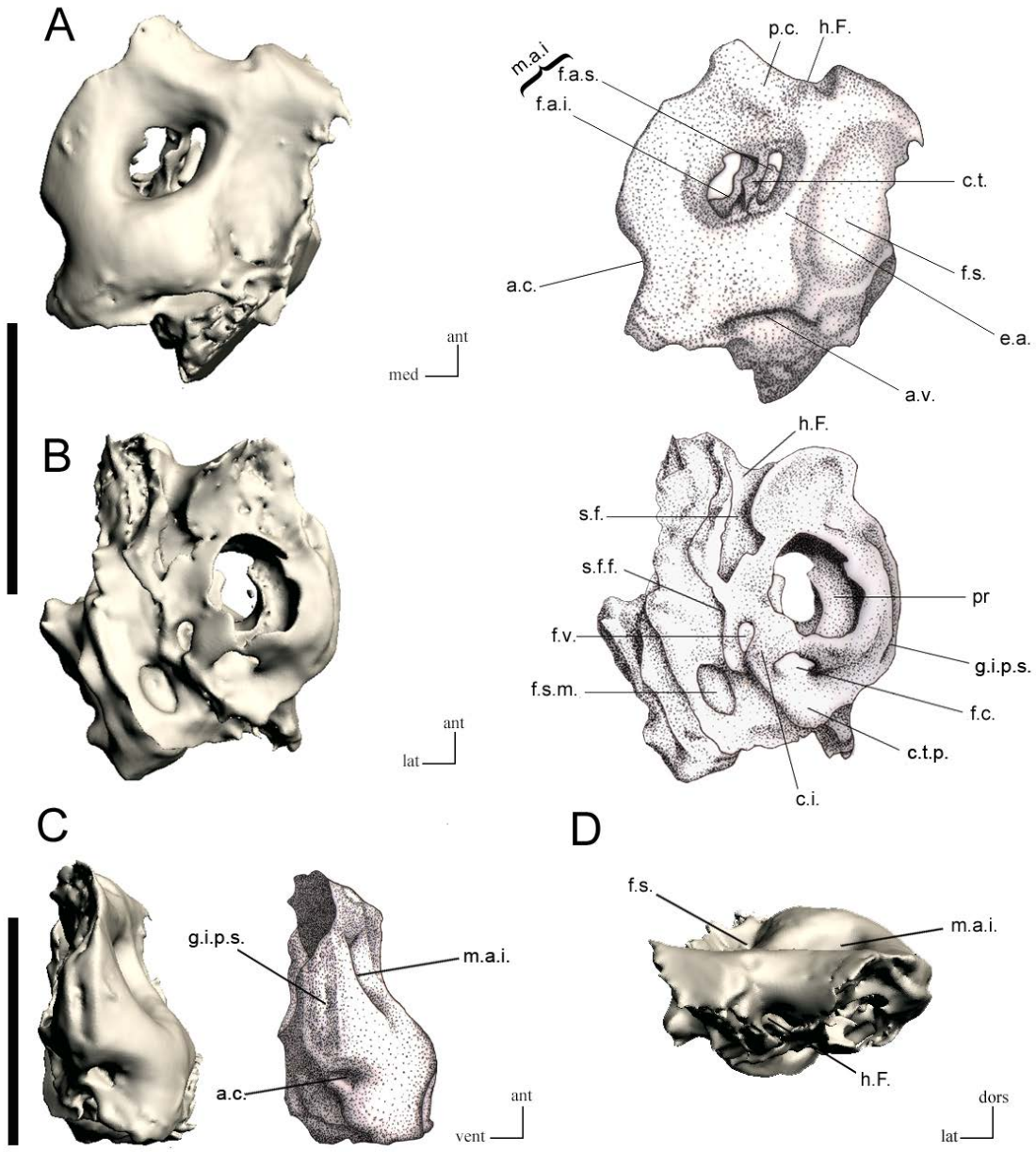

Figure I.4 : 3D reconstructions and annotated drawings of the right petrosal MNHN.F PM17 of *Phosphatherium* (scale = 5 mm) in cerebellar (A), tympanic (B), medial (C) and anterior (D) views: **a.c.** aquaeductus cochlea, **a.v.** bony duct for the *aquaeductus vestibuli*, **c.i.** *crista interfenestralis*, **c.t.** *crista transversa*, **e.a.** *eminantia arcuata*, **f.a.i.** *foramen acusticum inferius*, **f.a.s.** *foramen acusticum superius*, **f.c.** *fenestra cochleae*, **f.s.** *fossa subarcuata*, **f.v.** *fenestra vestibuli*, **g.i.p.s.** groove for the inferior petrosal sinus, **h.F.** *hiatus Fallopii*, **m.a.i.** *meatus acusticum internalis*, **p.c.** prefacial commissure, **pr.** *promontorium*, **s.f.** *sulcus facialis*, **s.f.f.** secondary facial foramen, **s.s.s.** sinus for the sigmoid sinus.

It is quite small compared with that of *Eritherium*, oval and clearly marked. The fallopian canal used to accommodate the great petrosal nerve which is a branch of the facial nerve (VII). This canal extends from the primary facial foramen to the anterior part of the petrosal and exits through the *hiatus Fallopii*. The modelling of the *tegmen tympani* could not be correctly obtained by segmentation, but it is clearly not inflated especially in comparison with *Eritherium*. The medial section of the caudal tympanic process is located under the *fenestra cochleae* and consists of a planar structure, without any ridge or inflation. The modelling of the mastoid region could not be correctly obtained by segmentation because of the poor contrast of the tomographic slices.

In medial view (Fig. I.4C), the cochlear canaliculus is located in the jugular fossa, on the posterior part of the petrosal. Its outline is sub-rectangular with rounded corners and it is postero-medially oriented. The rather deep groove for the inferior petrosal sinus crosses the medial surface of the petrosal antero-posteriorly and runs along the internal acoustic meatus.

In anterior view (Fig. I.4D), the *hiatus Fallopii* is ovoid and is completely bordered by an osseous wall, although it has been damaged in MNHN.F.PM17. The *hiatus Fallopii* is located on the ventral part, at the center of the petrosal. The petrosal shows no sign of pneumatization on the tomographic slices, in contrast to *Eritherium*.

Inner ear

The reconstructed endocast of the bony labyrinth of *Phosphatherium* is illustrated in Fig. I.5. The apical part of the cochlea of *Phosphatherium* is damaged on both right and left petrosals. Therefore, the precise number of turns of the cochleae is unknown. However, the cochlea shows at least one turn (> 360°), and we estimate that there were approximately two full turns. The *cochlear canaliculus* and the *fenestra cochleae* are not merged into a common perilymphatic foramen. The outline of the *fenestra cochleae* is rectangular with rounded corners. The cochlea is probably flattened in lateral view with an aspect ratio slightly superior to 0.41, although we cannot determine its precise height because the roof of the *promontorium* is broken.

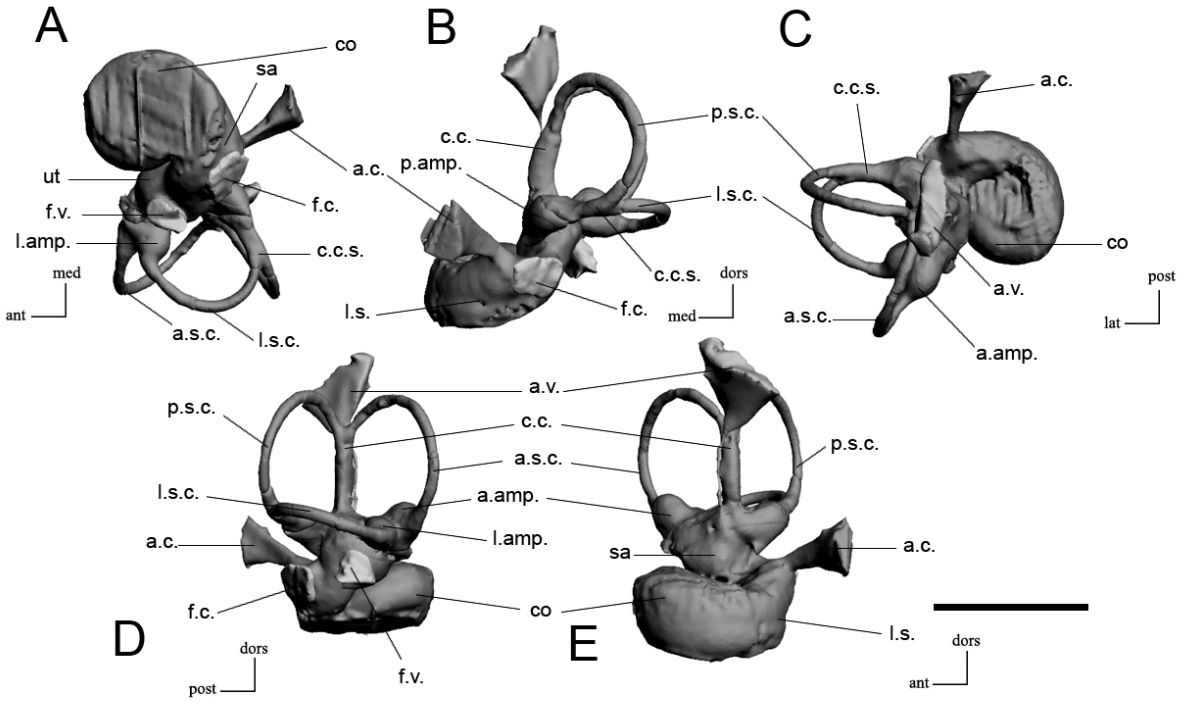

Figure I.5 : 3D reconstructions of the *Phosphatherium* bony labyrinth (scale = 5 mm) in ventral (A), posterior (B), dorsal (C), lateral (D) and medial (E) views: **a.amp.** anterior ampulla, **a.s.c.** anterior semicircular canal, **a.c.** *aquaeductus cochleae*, **a.v.** *aquaeductus vestibuli*, **c.c.** *crus commune*, **c.c.s.** *crus commune secundaria*, **co.** cochlea, **f.c.** *fenestra cochleae*, **f.v.** *fenestra vestibuli*, **l.amp**. lateral ampulla, **l.s.** *lamina secundaria*, **l.s.c.** lateral semicircular canal, **p.amp.** posterior ampulla, **p.s.c.** posterior semicircular canal, **sa.** saccule, **ut.** utricle.

The estimated cochlear volume (preserved part of the cochlea only) is approximately 25% of the total volume of the inner ear. However, the endocast of the cochlea being incomplete, its total and relative volume is probably higher. The *lamina secundaria* is visible on the endocast, although its contours are shallow. It is seen only in the first half turn of the cochlea and is 0.07 mm deep.

The *recessus ellipticus* and the *recessus sphericus*, which contained respectively the utricle and the saccule of the vestibule, are clearly defined and bulging. The vestibular aqueduct takes its origin medial to the common crus basis. It starts as a very thin canal and then expands at the level of the superior extremity of the common crus, hence displaying a 'trumpet' shape. It leads to a large, thin slit located on the posterior extremity of the subarcuate fossa.

The common crus between the anterior and posterior canals measures 2.57 mm, which is slightly longer than in *Eritherium*. The posterior and lateral

canals merge into a true secondary common crus at the level of the posterior ampulla. The ampullae are well defined and bulging. Each canal has a rather circular cross-section without any visible flattening. The canals are approximately the same size, although the lateral canal is slightly smaller (radius of curvature = 1.41) than the anterior canal (radii of curvature = 1.74) and the posterior canal radii of curvature = 1.66). Compared with *Eritherium*, the semi-circular canals are taller and do not present any clearly marked undulation. The lateral and posterior semi-circular canals form a right angle (91°), which is almost the case for the angle between the anterior and posterior canals (85°). In contrast, the angle between the lateral and the anterior semi-circular canals is clearly acute (76°).

Table I.1 : Measurements of the bony labyrinths of *Eritherium* and *Phosphatherium*. ? indicates unknown states.

	Eritherium	*Phosphatherium*
Stapedial ratio	1.57	1.62
Number of turns of the cochlea	2	>1
Length of the cochlea (mm)	14.13	?
Relative cochlear volume (%)	45	25
Cochlear aspect ratio	0.35	>0.41
***Lamina secundaria* depth (mm)**	0.1	0.07
Length of the *crus commune* (mm)	>2.26	2.57
Anterior canal radius of curvature	1.53	1.74
Lateral canal radius of curvature	1.36	1.41
Posterior canal radius of curvature	1.36	1.66
Angle between anterior and posterior canals (°)	92	91
Angle between anterior and lateral canals (°)	87	76
Angle between lateral and posterior canals (°)	90	85
Mean of the angles (°)	89.8	84

4. Discussion

4.1. Comparison of the petrosal morphology of *Eritherium* and *Phosphatherium*

Although *Eritherium* and *Phosphatherium* are both basal primitive Proboscidea, the anatomy of their ear regions differs markedly. They display differences in both middle and inner ear structures. The most remarkable difference is seen in the depth of the *fossa subarcuata*; *Eritherium* has an extremely deep fossa, whereas it is much more moderate in *Phosphatherium* (with some individual variation). In addition, the *fossa subarcuata* of *Phosphatherium* is larger and longer antero-posteriorly. The *tegmen tympani* of *Eritherium* is strongly inflated and displays an ossified canal for the ramus superior of the stapedial artery, whereas in *Phosphatherium* the *tegmen tympani* is not inflated, and it does not possess a canal for the superior ramus of the stapedial artery. The lateral and posterior semicircular canals of *Phosphatherium* are fully merged, thus forming a true *crus commune secundaria*, whereas they are only partly merged in *Eritherium*. In general, the semicircular canals in *Eritherium* are larger than those of *Phosphatherium*. The main features of both taxa are compared and summarized in greater detail in Table I.2.

We compared the petrosal and inner ear characters of *Eritherium* and *Phosphatherium* with other proboscideans and also among various afrotherians, placentals and primitive eutherians and therians (e.g. *zhelestids* and *Henkelotherium*), in order to assess their evolution and their significance and throw light on the ancestral morphotype of the order Proboscidea.

4.2. Cladistic analysis of petrosal and inner ear features of *Eritherium* and *Phosphatherium* among Proboscidea

The matrix analyzed here contains 18 petrosal characters seen in *Eritherium* and *Phosphatherium*. The definition of most of these characters follows Benoit et al. (2013a-c). Seven characters are not modified; eight characters come from the previously cited studies and were modified; two characters come from O'Leary (2010) and Wible et al. (2009) and were modified; one new character was defined and analyzed in this study. Numerous characters in Benoit et al. (2013a-c) are not retained here because they were constant among our sampled taxa.

Table I.2 : Comparisons of the main features of the ear region of *Eritherium* and *Phosphatherium.* ? is for unknown states.

	Eritherium	Phosphatherium
Fossa subarcuata	Very deep	Moderately deep but wider antero-posteriorly
Fenestra cochleae and cochlear aqueduct	Probably not merged into a unique perilymphatic foramen	Not merged into a unique perilymphatic foramen
Stapedial ratio	1.57	1.62
Size of the *fenestra vestibuli*	Large	Small
Promontorium shape	Rather flat	Bulging
Inflation of the *tegmen tympani*	Strong	Absent
Stapedial sulcus	Absent	Absent
Transpromontory sulcus	Absent	Absent
Superior ramus for the stapedial artery	Located in an ossified canal	Absent
Prootic sinus	Present	Absent
Pneumatization of the petrosal	Present	Absent
Cross-section of the semicircular canals	Round	Round
Crus commune secundaria	Partial	Present
Semicircular canal aspects	Slender	Slender
Cochlear aspect in profile	Planispiral	? (broken)
Number of turns of the cochlea	2	? (broken but >1)
Lamina secundaria	Present on the three quarters of the first turn	Present on the first half-turn but less deep

Among the 18 characters, two have more than two states ([1], [13]) and both of them were unordered. The detailed list of characters is available in Appendix 1. Illustrations of the characters are provided in Appendix 2. The matrix (Appendix 3) was analyzed with PAUP 3.1.1. (Swofford 1991), with a heuristic search and all characters were equally weighted.

A first exploratory cladistic analysis was extended to Proboscidea and other afrotherian fossil and extant taxa with the coding of petrosal features taken and completed mostly from Benoit et al. (2013b). The outgroups of Proboscidea that were included comprise Macroscelidea (represented by *Chambius*; Benoit et al. 2013c), Afrosoricida (represented by *Potamogale*; Wible et al. 2009; Benoit et al. 2015), Tubulidentata (represented by *Orycteropus*; Benoit et al. 2013b; Ekdale, 2013), the oldest-known Afrotherian *Ocepeia* (Gheerbrant et al. 2014), Hyracoidea (represented by *Procavia*; Benoit et al. 2013b; Ekdale, 2013), Embrithopoda (represented by *Arsinoitherium*; Court, 1990; Benoit et al. 2013b), Sirenia (represented by *Trichechus*; Benoit et al. 2013a; Ekdale, 2013), *Prorastomus* and the sirenian of Chambi (Benoit et al. 2013a), and non-Afrotherian placentals (represented by *Protungulatum*; Wible et al. 2009; O'Leary, 2010), *Diacodexis* (Orliac et al. 2012; Orliac & O'Leary, 2014) and *Dasypus* (Wible, 2010; Ekdale, 2013). *Henkelotherium* (Ruf et al. 2009) and zhelestids (Ekdale et al. 2004; Ekdale & Rowe, 2011; Ekdale, 2013) were used as therian and eutherian outgroups. However, this analysis showed a strong homoplasy among afrotherians (homoplasy index HI = 0.753) (Appendix 4), probably due to several convergences, as already discussed by Benoit et al. (2013b). The unresolved polytomy obtained in the consensus tree (see Appendix 4) does not allow us to discuss the distribution of the characters observed in *Phosphatherium* and *Eritherium* at an intra-ordinal level. The use of other members of Afrotheria or Placentalia as outgroups of Proboscidea in our analysis did not provide resolved topology at either inter- or intra-ordinal levels because of the high level of homoplasy.

Consequently, we developed and carried out a cladistic analysis of the petrosal features of *Phosphatherium* and *Eritherium* that is restricted to the Proboscidea. Because the petrosal and inner ear morphology remains poorly known among proboscideans, the analysis

was restricted to the few taxa where petrosal characters have been described: *Eritherium* and *Phosphatherium, Moeritherium* (Court, 1994), *Numidotherium* (Court & Jaeger, 1991; Court, 1992; Benoit et al. 2013b), *Gomphotherium* (Tassy, 2013) and Elephantidae (presumed petrosal of *Mammuthus* from Ekdale, 2011; inner ear of *Elephas* from Benoit et al. 2013b). *Zhelestids* (Ekdale et al. 2004; Ekdale & Rowe, 2011; Ekdale, 2013) and *Henkelotherium* (Ruf et al. 2009) were used as outgroup taxa, bringing to eight the total number of analyzed taxa.

It should be stressed that this is only a preliminary study, aiming at a first look at the distribution of the characters of *Phosphatherium* and *Eritherium* and of their significance for understanding the morphological evolution of the petrosal in Proboscidea. These characters should be later included in a larger matrix including other characters and extended to at least Afrotheria.

We obtained only one parsimonious tree with a length of 21 steps (Fig. I.6). The consistency index (CI) and retention index (RI) are high (CI = 0.905; RI = 0.833): The tree shows a very low level of homoplasy.

In this tree, it should be noted that the monophyly of the Proboscidea is not tested because the analysis does not include other taxa of the Paenungulata and Afrotheria. In such a restricted systematic context of analysis, the characters supporting the monophyly of the Proboscidea could also be synapomorphies of more inclusive groups within Afrotheria.

At the base of the Proboscidea in our tree, two synapomorphies are seen (Fig. I.6B), one being non-homoplastic. First, the transpromontorial sulcus is lost [8(0)] in Proboscidea. This is a homoplasy (CI = 0.5) because the character is reversed in *Numidotherium*, which shows a transpromontorial sulcus on its *promontorium* according to Benoit et al. (2013c). Another synapomorphy is the increase in the number of turns of the cochlea from less than one and a half turn [17(0)] to two turns or more [17(1)]. However, this feature may not be very significant because previous studies (Ekdale, 2013) showed that it varies intraspecifically.

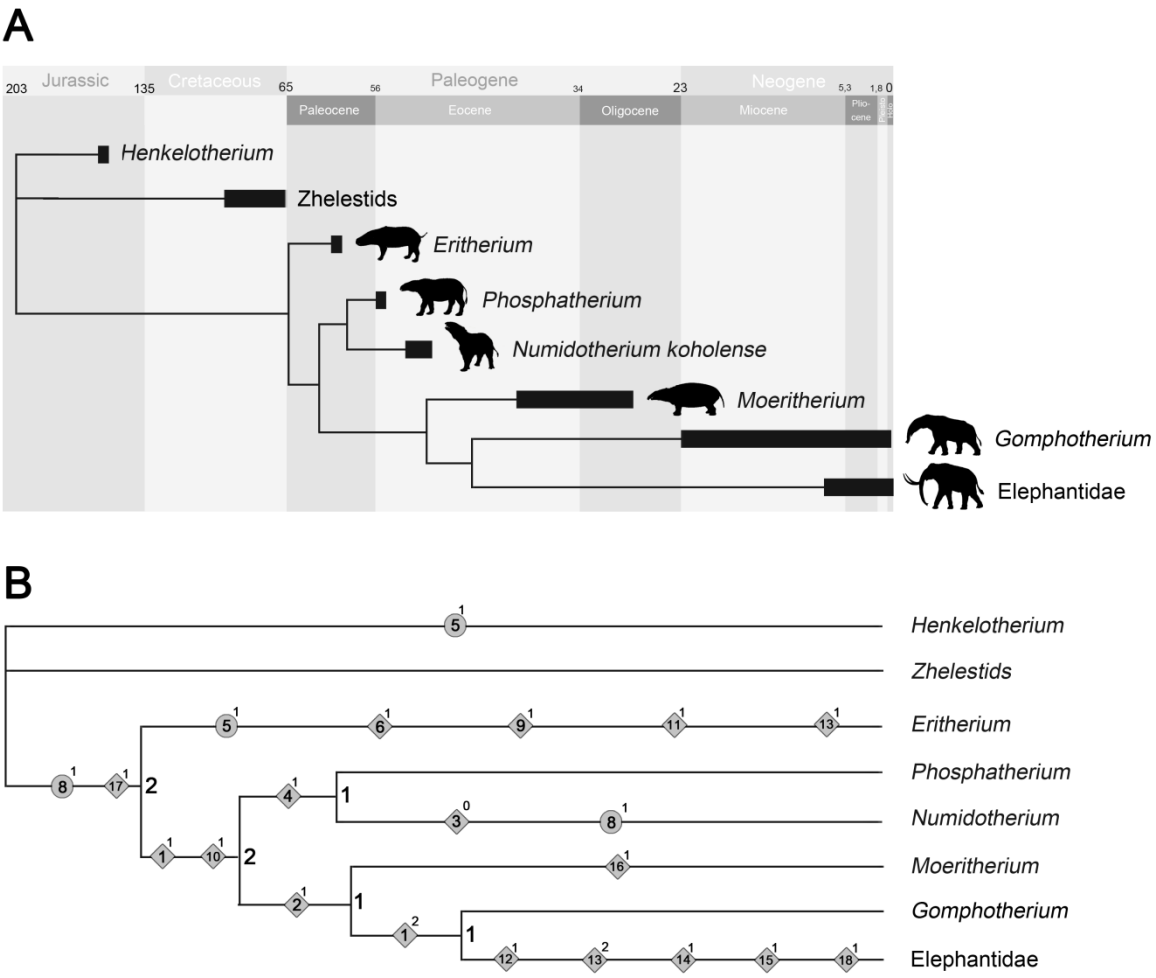

Figure I.6 : Results of the cladistic analysis of the petrosal features of *Eritherium* and *Phosphatherium* within Proboscidea: (A) phylogenetic tree replacing the taxa in temporal context; (B) most parsimonious cladogram obtained with our analysis. Length = 21 steps. Consistency index (CI) = 0.905. Homoplasy index (HI) = 0.095. Retention index (RI) = 0.833. Rescaled consistency index (RC) = 0.754. Numbers of non-homoplastic characters are represented with diamond symbols, and numbers of homoplastic characters are represented with circles. The state number is specified after the character number. Bremer indexes are indicated right to the nodes.

Eritherium has five autapomorphies, of which one is non-homoplastic. The *promontorium* becomes flat in *Eritherium* [5(1)]; however, the *promontorium* is also flat in *Henkelotherium* so this character is a convergence in our tree and is therefore homoplastic (CI = 0.500). Moreover, this character state has an ambiguous location. Indeed, we can assume that the state « flat » [5(1)] is plesiomorphic and the state « bulging » [5(0)] is apomorphic. In this case, the *promontorium* would be ancestrally flat and would become convergently bulging in zhelestids and the other proboscideans. Other

autapomorphies of *Eritherium* are non-homoplastic: the very inflated *tegmen tympani* [6(1)], the superior ramus of the stapedial artery included in an ossified canal [9(1)], the pneumatized *tegmen tympani* [11(1)] and the lateral and posterior semi-circular canals only partially merged [13(1)]. However, the pneumatization and the inflation of the *tegmen tympani* are present in the afrotherian *Ocepeia* (Gheerbrant et al. 2014), suggesting they might be plesiomorphic among Afrotheria.

Other proboscideans form a monophyletic group supported by two non-homoplastic synapomorphies: the *fossa subarcuata* becomes less deep [1(1)] and the prootic sinus is absent [10(1)]. The tree supports two clades of Proboscidea: (*Phosphatherium, Numidotherium*) and {*Moeritherium* [*Gomphotherium* (Elephantidae)]}. Previous analyses (Gheerbrant et al. 2005; Gheerbrant, 2009) show in contrast a stem successive sequential position of *Phosphatherium* and *Numidotherium* to other more derived proboscideans. However, the clade (*Phosphatherium, Numidotherium)* was also found by Benoit et al. (2013b) based only on petrosal and inner ear characters. The clade {*Moeritherium* [*Gomphotherium* (Elephantidae)]} is congruent with previous proboscidean phylogenies using other characters (e.g. Gheerbrant, 2009; Gheerbrant & Tassy, 2009).

The clade (*Phosphatherium*, *Numidotherium*) is supported by a small *fenestra vestibuli* [4(1)], a non-homoplastic synapomorphy. In Benoit et al. (2013b), this clade is supported by one non-homoplastic synapomorphy: the unfused posttympanic process and postglenoid process of the squamosal. However, this character is not used in our study because it cannot be observed on the isolated petrosal of *Eritherium,* and it is most probably a plesiomorphic trait known in many placentals and eutherians (Gheerbrant et al. 2005, 2014). *Phosphatherium* has no autapomorphy, whereas *Numidotherium* has two. One is non-homoplastic: the presence of a transpromontorial sulcus on the *promontorium* [8(0)] is only seen in *Numidotherium* among Proboscidea. In our tree the autapomorphic oval *fenestra vestibuli* [3(0)] in *Numidotherium* is a reversal with respect to the state at the base of Proboscidea [3(1)].

The clade {*Moeritherium* [*Gomphotherium* (Elephantidae)]} is supported in our analysis by six non-homoplastic synapomorphies. The cochlear aqueduct and the *fenestra*

cochleae are not separated, forming a unique perilymphatic foramen [2(1)]. This state has an unambiguous location, whereas the other synapomorphies are ambiguous probably because the inner ear characters are unknown in *Moeritherium* and *Gomphotherium*. The cross-section of the semi-circular canals is flattened [12(1)], there is no longer a fusion of the posterior and lateral semi-circular canals [13(1)], the aspect of the semi-circular canals is stocky [14(1)], the position of the lateral semi-circular canal is low [15(1)], and the *45uminaria secundaria* disappears [18(1)]. *Moeritherium* has a non-homoplastic autapomorphy: the cochlea has a rather conical aspect (aspect ratio > 0.65) [16(1)]. The clade (*Gomphotherium*, Elephantidae) is supported by one non-homoplastic synapomorphy: the superficial *fossa subarcuta* [1(2)].

4.3. Significance of *Phosphatherium* and *Eritherium* for understanding petrosal character evolution among Placentalia, Afrotheria and Proboscidea

Our cladistic analysis allows discussion of the distribution of petrosal and inner ear characters among the order Proboscidea. However, the absence in the analysis of other afrotherian and placental taxa prevents discussion of the synapomorphies of the ear region at the base of the clade Proboscidea and the evolution of these characters among Tethytheria, Paenungulata, Afrotheria and Eutheria. To assess the evolution of the characters seen in *Eritherium* and *Phosphatherium* at a higher level than Proboscidea, we compared some important features of the ear region among several other placentals and eutherians; this is summarized in Table I.3. Each order is represented by the closest representative to the ancestral morphotype of the group, i.e. its most primitive representative(s) for which petrosal features are known. The plesiomorphic states of characters among Xenarthra were determined based on the study of Billet et al. (2015). States of other taxa were taken from the references mentioned above (§4.2). This comparison is preliminary and should be tested further and developed in the future with extended cladistic analyses.

Fossa subarcuata

The *fossa subarcuata* is a depression on the cerebellar surface of the petrosal which houses the paraflocculus of the cerebellum (Cifelli, 1982). The great depth [1(0)] of the

subarcuate fossa seen in *Eritherium* (Appendix 2) is plesiomorphic within eutherians (MacIntyre, 1972). It is known for instance in non-placental eutherian mammals such as *Prokennalestes, Zalambdalestes* and *Maelestes* (Wible et al. 2001, 2004, 2009) and in early afrotherians such as *Ocepeia* (Gheerbrant et al. 2014). A synapomorphic moderate infilling [1(1)] of the fossa is observed in *Phosphatherium* (Appendix 2) and *Numidotherium,* whereas the infilling of the fossa becomes complete [1(2)] in the clade {*Moeritherium* [*Gomphotherium* (Elephantidae)]}. This progressive infilling of the fossa is a convergent trend in several afrotherian lineages such as macroscelideans, tubulidentates (Benoit et al. 2013c), embrithopods (Court, 1990) and sirenians (Benoit et al. 2013a).

Perilymphatic foramen

In most adult mammals, the *fenestra cochleae* and the *cochlear canaliculus* are two distinct openings. In the early stages of embryological development, however, the petrosal bears only one opening, the perilymphatic foramen. It divides later during the development as a separate *fenestra cochleae* and *cochlear canaliculus* (Fischer, 1990). These two foramina [2(0)] are present in early eutherians and almost all mammals (Table I.3), corresponding to a plesiomorphic state in placentals and afrotherians. Early afrotherians such as *Ocepeia* also display two separated foramina (Gheerbrant et al. 2014). In some afrotherians, however, the perilymphatic foramen is not divided and is retained at the adult stage. This is observed in extant sirenians and proboscideans, and in the embrithopod *Arsinoitherium* (Court, 1990; Fischer, 1990). This led to their grouping in the clade Tethytheria. However, later palaeontological discoveries showed that the non-division of the perilymphatic foramen [2(1)] is a convergent character. Indeed, early proboscideans such as *Phosphatherium* (Gheerbrant et al. 2005) and *Numidotherium* (Court & Jaeger, 1991) and early sirenians such as *Prorastomus* (Benoit et al. 2013a) have a separated perilymphatic foramen, forming a *fenestra cochleae* and a *cochlear canaliculus* [2(0)]. This is confirmed in this work for *Eritherium* and *Phosphatherium* (Appendix 2). Within Proboscidea the presence of a non-separated perilymphatic foramen is therefore likely a synapomorphy of the clade including *Moeritherium*, the Deinotheriidae and the Elephantidae.

Table I.3 : Comparison of some major described characters of the petrosal and inner ear of the early proboscideans *Eritherium* and *Phosphatherium* among eutherians and placentals, and inferred ancestral state optimization. Sources: Macroscelidea represented by *Chambius* (Benoit et al. 2013c), Afrosoricida represented by *Potamogale* (Wible et al. 2009; Benoit et al. 2015), Tubulidentata represented by *Orycteropus* (Benoit et al. 2013b; Ekdale, 2013), *Ocepeia* (Gheerbrant et al. 2014), Hyracoidea represented by *Procavia* (Benoit et al. 2013b; Ekdale, 2013), Embrithopoda represented by *Arsinoitherium* (Court, 1990; Benoit et al. 2013b), Sirenia represented by *Trichechus* (Benoit et al. 2013a; Ekdale, 2013), *Prorastomus* and the sirenian of Chambi (Benoit et al. 2013a), and non-afrotherian placentals represented by *Protungulatum* (Wible et al. 2009; O'Leary, 2010), *Diacodexis* (Orliac et al. 2012; Orliac & O'Leary, 2014) and *Dasypus* (Wible, 2010; Ekdale, 2013). The therians and eutherians *Henkelotherium* (Ruf et al. 2009), zhelestids (Ekdale et al. 2004; Ekdale & Rowe, 2011; Ekdale, 2013) and *Zalambdalestes* (Wible et al. 2009; Ekdale & Rowe,2011). In bold, ancestral states found in *Eritherium* and *Phosphatherium*.

	Fossa subarcuata (1)	Undivided perilymphatic foramen (2)	Shape of the *fenestra vestibuli* (3)	Size of the *fenestra vestibuli* (4)	*Crus commune secundaria* (13)	Thickness of the semicircular canals (14)	Number of turns of the cochlea (17)	*Lamina secundaria* (18)
Henkelotherium	Deep	Absent	Oval	Large	Present	Slender	<1.5	Present
Zalambdalestes	Deep	Absent	Oval	?	Present	Slender	<1.5	Present
Zhelestids	Deep	Absent	Variable	Large	Present	Slender	<1.5	Present
Xenarthra	Moderate	Absent	?	Large	Absent	Slender	>1.5	Present
Diacodexis	Deep	Absent	Oval	Large	Present	Slender	>1.5	Present
Protungulatum	Deep	Absent	Oval	Large	Present	?	?	?
Macroscelidea	Deep	Absent	Oval	Large	Present	Slender	>1.5	Present
Afrosoricida	Deep	Absent	Round	Large	Absent	Slender	>1.5	Present
Tubulidentata	Moderate	Absent	Round	?	Present	Slender	>1.5	Present
Ocepeia	Deep	Absent	Oval	Large	Partial	Slender	>1.5	Present
Hyracoidea	Moderate	Absent	Oval	Large	Absent	Slender	>1.5	Present
Embrithopoda	Superficial	Present	Round	?	Absent	Stocky	>1.5	Absent
Chambi sirenian	?	Absent	Oval	Large	Present	Slender	>1.5	Absent
Prorastomus	Superficial	Absent	Round	?	Absent	Slender	>1.5	Absent
Trichechus	Superficial	Present	Round	?	Absent	Slender	<1.5	Absent
Eritherium	**Deep**	**Absent**	Round	**Large**	Partial	**Slender**	>1.5	**Present**
Phosphatherium	Moderate	**Absent**	Round	Small	**Present**	**Slender**	?	**Present**
Elephantimorpha	Superficial	Present	Round	Large	Absent	Stocky	>1.5	Absent
Inferred ancestral state	**Deep**	**Absent**	**Oval**	**Large**	**Present**	**Slender**	**<1.5**	**Present**

Fenestra vestibuli

The *fenestra vestibuli* is the opening which bears the footplate of the stapes in life. The stapes touches the petrosal at the level of this opening and transmits the auditory message to the cochlea and the organ of Corti. The shape of the *fenestra vestibuli* varies between taxa and the stapedial ratio (Segall, 1970) yields a value for this shape variation. The *fenestra vestibuli* (Table I.3) seems to be primitively oval [3(0)] because many non-placental eutherians such as *Zalambdalestes* have an oval *fenestra vestibuli* (Wible et al. 2004). It is also oval in early afrotherians such as *Ocepeia* (Gheerbrant et al. 2014). This opening is generally round [3(1)] in Paenungulata but there are exceptions such as *Numidotherium* (Benoit et al. 2013b), the sirenian from Chambi (Benoit et al. 2013a) and some fossil elephantimorphs (Ekdale, 2011). The stapedial ratio was used as a character in several phylogenetic studies based on the petrosal anatomy (Benoit et al. 2013a-c). However, this ratio can be extremely variable in some taxa; for example, it varies from 1.4 to 2.1 in an elephantimorph sample bearing almost only *Mammuthus* (Ekdale, 2011) and potentially a few *Mammut* petrosals. This character is therefore questionable for taxonomic comparisons and phylogenetic studies, which might explain its homoplasy in our analysis (CI = 0.500). In the Proboscidea, the *fenestra vestibuli* seems to be primitively wide [4(0)] (Table I.3) and becomes small [4(1)] in *Numidotherium* and *Phosphatherium* (Appendix 2), resulting in the grouping of these two taxa as a clade. However, the size of the *fenestra vestibuli* is probably also variable, just like the stapedial ratio, and its phylogenetic significance is therefore questionable.

Crus commune secundaria

The fusion of the lateral and posterior canal (Table I.3) as a true *crus commune secundaria* [13(0)] seems to be plesiomorphic as it is found in many non-placental eutherian mammals such as *Zalambdalestes* and *Kulbeckia,* and even in dryolestids such as *Henkelotherium* (Ruf et al. 2009). In *Eritherium* (Appendix 2)*,* the canals are not fully merged but are partly fused [13(1)] as in *Ocepeia* (Gheerbrant et al. 2014); the fusion of the canals appears to be more advanced in *Eritherium* than in *Ocepeia* (Gheerbrant et al. 2014). In contrast, *Phosphatherium* and *Numidotherium* both display a true secondary common crus [13(0)]. Such is

also the case in early sirenians, including the unnamed taxon from Chambi described by Benoit et al. (2013a). We can thus infer that the plesiomorphic state for this character among tethytheres and probably Proboscidea is the likely presence of the *crus commune secundaria*. This feature, which is present in *Phosphatherium* (Appendix 2) and *Numidotherium*, tends to disappear convergently in *Eritherium* (autapomorphy) and Elephantidae. However, the canals are more separated in Elephantidae [13(2)] than in *Eritherium* [13(1)]. The exact evolution of this feature in the proboscideans remains poorly characterized because it is unknown in *Moeritherium*, Deinotheriidae and Mammutidae. The absence of a *crus commune secundaria* is common among modern placentals (Xenarthra, Afrosoricida, Hyracoidea, Sirenia, and the extinct Embrithopoda) and is very likely due to a convergent loss among various placental orders. The partial separation of the canals in *Ocepeia* is also a probable convergence within Paenungulata and Afrotheria.

Aspect of the semi-circular canals

The evolution of the thickness of the bony semi-circular canals seems to be quite simple (Table I.3). Most mammals display slender canals, especially Afrotheria. The semi-circular canals of *Ocepeia* are slender [14(0)] as in *Eritherium* and in *Phosphatherium* (Appendix 2). *Numidotherium* displays slender canals as well. Stocky canals [14(1)] seem to have appeared convergently in Embrithopoda and extant elephants. However, as for the secondary common crus, the exact appearance of this character state within the proboscidean tree is unknown because the information is lacking for several taxa.

Number of turns of the cochlea

The number of turns of the cochlea (Table I.3) has been used in several phylogenetic analyses (Ekdale, 2013). Almost every therian mammal possesses at least one full turn of the cochlea (Meng & Fox, 1995). The primitive state for Afrotheria seems to be a cochlea with at least two turns. Even the earliest known afrotherian, *Ocepeia,* has two full turns (Gheerbrant et al. 2014). Among afrotherians, only *Trichechus* shows a very small number of turns (inferior to 1.5 turns) which seems to be autapomorphic. All proboscideans studied with CT scan methods show at least one and a half turns (Ekdale, 2011; Benoit et al. 2013b).

The cochlea of *Eritherium* has two turns but that of *Phosphatherium* is damaged so the number of turns remains unknown (Appendix 2). *Numidotherium* displays the lowest number of turns among Proboscidea, 1.62 turns (Benoit et al. 2013b), and Elephantidae has at least two turns (Ekdale, 2011; Benoit et al. 2013b). However, it should be noted that the number of turns can vary within the same species (Ekdale, 2013), with a variability up to 360° (one full turn). Without a study of intra-specific variability of the inner ear of proboscideans and afrotherians, a difference of < 1 turn in the cochlear coiling seems to be of low significance for systematics and phylogeny.

Secondary bony lamina

The secondary bony lamina (or *lamina secundaria*) is primitively present in non-placental eutherian mammals [18(0)] (Table I.3). It is also present in early afrotherians such as *Ocepeia* (Gheerbrant et al. 2014) and is therefore the plesiomorphic state for this clade. Primitive proboscideans such as *Eritherium*, *Phosphatherium* and *Numidotherium* display a secondary bony lamina (Appendix 2) but this feature is absent in Elephantidae [18(1)]. The exact location of this state transformation within Proboscidea is ambiguous as the state is unknown in *Gomphotherium* and *Moeritherium*. This feature is also absent in *Tenrec*, but it is present in *Hemicentetes*. It is also absent in Sirenia and Embrithopoda. There are two equally parsimonious ways of explaining the transformation of this character within paenungulates. The first would be to consider the loss of the secondary bony lamina to be a synapomorphy of tethytherians. The *lamina secundaria* would reappear in Proboscidea and then be lost again in modern taxa. This seems very unlikely. Therefore we favoured the alternative, equally parsimonious hypothesis that implies a convergent loss of this feature in the three Tethytheria lineages and in some tenrecids such as *Tenrec*. The convergent loss in Embrithopoda and Proboscidea is suspected to be related to a convergent adaptation to low-frequency hearing (Benoit et al. 2013b).

5. Conclusion

The petrosal and inner ear anatomy of the two oldest-known proboscideans *Eritherium* and *Phosphatherium* provides key data concerning the ancestral morphotype of the order Proboscidea. It shows that the ancestral state of the ear region of Proboscidea was not specialized but was close to the generalized morphology of other paenungulates and afrotherians. Most of the features of the ancestral morphotype of Proboscidea illustrated by *Eritherium* and *Phosphatherium* are primitive, such as a deep *fossa subarcuata*, the absence of a perilymphatic foramen, the presence of a *crus commune secundaria*, slender semi-circular canals and the presence of the *lamina secundaria*. These features were inherited from Paenungulata, Afrotheria, and even Eutheria. More derived characters appeared later in proboscidean phylogeny.

The petrosal morphology of *Eritherium* is clearly more primitive than that of *Phosphatherium* and is closer to the basal afrotherian paenungulate *Ocepeia* in several symplesiomorphies such as the morphology of the *tegmen tympani* region, the extremely deep *fossa subarcuata* and an ossified canal for the superior ramus of the stapedial artery. These features are noticeably more derived in *Phosphatherium, Numidotherium* and other proboscideans. The undivided perilymphatic foramen was not present in early proboscideans. The partial fusion of the lateral and posterior semicircular canal is shared by *Eritherium* and *Ocepeia,* but it differs from the more fused canal which occurs in *Phosphatherium* and some other afrotherians, likely representing the ancestral state of proboscideans and other paenungulates; the condition in *Eritherium* and *Ocepeia* might correspond to early convergences within afrotherians. However, this character remains poorly known within proboscideans and afrotherians in general.

The early fossil record of the Proboscidea is one of the best among placental orders, and *Eritherium* and *Phosphatherium* are two of the earliest known and most primitive representatives of extant placental orders. Therefore, they provide new insights concerning the ancestral morphotype of petrosal anatomy not only of Proboscidea but also

at a supra-ordinal level among placentals (e.g. paenungulates and afrotherians). Previous studies showed important homoplasy in the ear region of Tethytheria (Benoit et al. 2013b), which is also supported by our analysis including Proboscidea and other eutherians. Here, the restriction of the analysis to Proboscidea provides a topology close to the consensual phylogenetic tree of Proboscidea, but most noticeably with low homoplasy indexes. This shows that the evolutionary modalities of the ear region characters differ according to the taxonomic level considered among Afrotheria. Multiple convergences between the different orders of Afrotheria and Paenungulata occurred and led to significant homoplasy. However, few convergences and reversals seem to have occurred at an intra-ordinal level, which would explain the low level of homoplasy found among Proboscidea.

This supports the view that the ancestral morphotypes of the different orders of at least Paenungulata were probably close to each other. Specializations occurred rapidly after the ordinal radiation. This is consistent with previous conclusions based on cranial and dental characters of *Eritherium*.

CHAPTER II

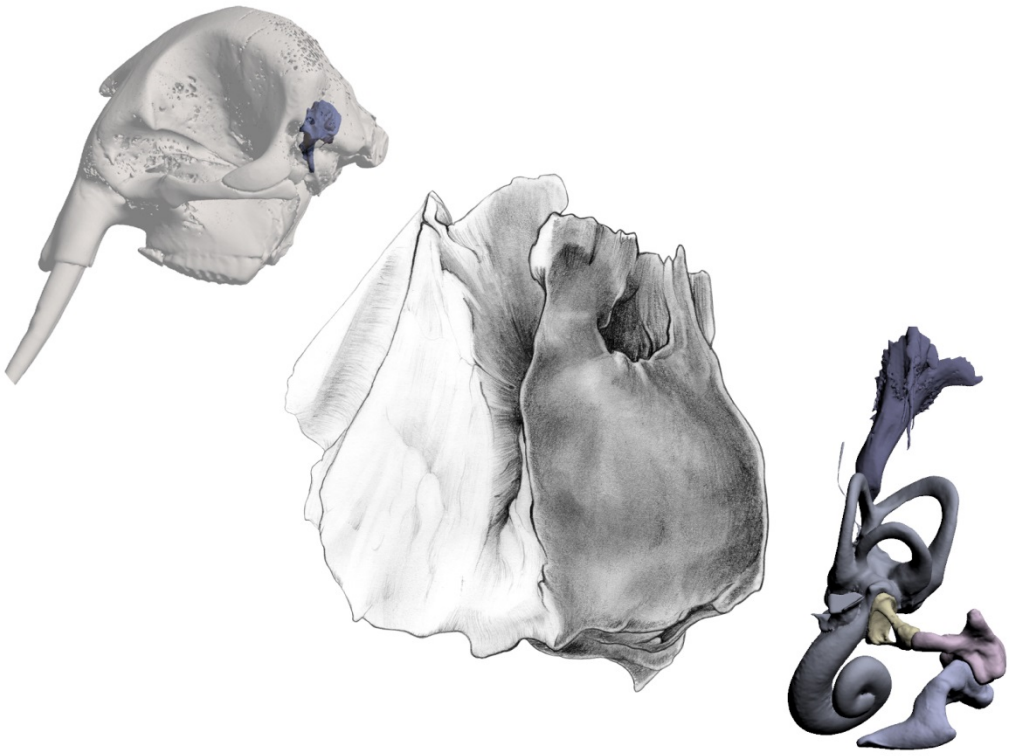

Petrosal and inner ear anatomy of extant elephants

1. Introduction

The petrosal of extant elephants is difficult to observe when it is still in connection within the skull. Indeed, it is located rather internally in the skull and it is covered by other bones when the skull is viewed ventrally. Isolated petrosals of extant elephants are rarely found in collections because this bone is fused with other bones of the skull. Nonetheless, the anatomy of the ear region of extant elephants has been investigated early in the past (Blair, 1717-1719; Hyrtl, 1845; Buck, 1888, 1890; Richards, 1890; Fischer, 1990). However, this anatomical region remains poorly illustrated in elephants. There are no complete illustrations of the petrosal anatomy in the literature. The bony labyrinth has been rapidly investigated in Benoit et al. (2013b) but a detailed study of these internal structures in extant elephants has yet to be conducted.

Studying the evolution of the ear region within the Proboscidea requires a good knowledge of this structure in extant taxa. Hence, we decided to focus this chapter on the anatomy of the petrosal and the bony labyrinth of extant elephants prior to discussing the ear region of fossil proboscideans in Chapter III. We took advantage of the relatively recent development of microtomographic CT data analyses in the field of anatomical investigations. The main objective is to provide the first comprehensive anatomical study of the ear region of extant elephants. The location of the petrosal within the skull and its position with respect to other bones is clarified. A detailed and richly illustrated anatomical description of the petrosal is given. 3D models of the bony labyrinth are segmented in high resolution. Finally, the first microtomographic 3D reconstruction of the membranous vestibular system of an elephant is carried out in this chapter.

The comprehensive study of the ear region in extant taxa provides primary and key comparative data for the anatomical descriptions of extinct taxa. The segmentation of the petrosal and bony labyrinth of several specimens of each extant species allows us to discuss intraspecific variations of this anatomical region as well. These considerations are useful because the descriptions of fossil taxa are generally based on one specimen. This is also helpful for a critical review of previously used phylogenetic characters and for the identification of new ones.

2. Material and methods

2.1. Material

The specimens of extant elephants used in this study are listed in Table II.1. In addition, we mention which side of the skull was scanned and segmented, as well as the ossicles that were found within the tympanic cavity.

Elephas

Four specimens of *Elephas maximus* have been studied. Among them, three skulls from the collections of the MNHN were CT-scanned. There are no isolated petrosals belonging to extant elephants in the MNHN collections which explains why we scanned these complete skulls. On the other hand, scanning petrosals still connected to the skull allows us to control the taxonomic assignment of the ear bone as it is not unusual for isolated bones to be incorrectly assigned in centuries-old collections. The major difficulty was to find specimens that could fit in the CT-scan. It is not possible to fit very large specimens in the scanning machine available at the MNHN and the greater the specimens the lower the resolution. Therefore, we chose skulls belonging to juveniles and young adults. The first skull MNHN.ZM.AC.1904-273 is a juvenile of which both bony ears were CT-scanned. However, the scanning of the left ear was unsuccessful so we could only segment the right ear. The second skull MNHN.ZM.AC.1941-209 is a juvenile (died at 5 years) which comes from Indochine. Only its left ear was scanned. Finally, the right side of the third skull (MNHN.ZM.AC.2008-81) was CT-scanned. There are no additional details about the age and provenance of this specimen in the MNHN collection database.

A fourth specimen CEB 150009 was studied. It consists of a newborn elephant that died following a cranial trauma at an early age (less than three months old). This elephant was a resident of the Leipzig zoo. The head was collected less than 48 hours after its death and preserved in Bouin solution. The ear region was then cut off for CT investigations. This allowed us to obtain a 3D model of the membranous structures of the labyrinth contained in the bony inner ear. Since this specimen was cut and the scan was only focused on the labyrinth, it was not possible to segment the petrosal for this specimen.

Loxodonta

Ten specimens of *Loxodonta* have been studied. Until recently, the two extant species *L. africana*, African savannah (or bush) elephant and *L. cyclotis*, African forest elephant, were considered sub-species of a single African elephant species: *Loxodonta africana.* However, two species of *Loxodonta* are recognized today (Frade, 1955). The majority of the studied specimens are labelled *Loxodonta africana* in the MNHN collection database without further details about the sub-species. Furthermore, species determination of African elephants based on skull observation is not easy. Therefore, it was difficult to assign the *Loxodonta* specimens to a definite species. Three specimens were left unassigned while others were assigned to a species based on details given by the collection database and their geographical provenance (when provided).

Amongst the ten studied specimens, eight skulls belong to the collections of the MNHN. As for the *Elephas* skulls, we chose to sample small skulls that could fit in the CT-scan. Hence we studied preferably juveniles and young adults.

The first skull MNHN.ZM.AC.1950-728 has been attributed to the species *Loxodonta cyclotis* based on the original labelling which assign this specimen to the invalid species *Loxodonta pumilio*. This invalid species refers to the African pygmy forest elephant which status has been debated. The species was abandoned after a molecular study highlighted the inclusion of the African pygmy elephants within a monophyletic group of forest elephants *sensu lato* (Debruyne *et al.* 2003). No other details were available on this specimen but its provenance (Gabon) is given in Debruyne *et al.* (2003). The right ear of this specimen was CT-scanned. Another skull from Cameroun and attributed to the invalid species *Loxodonta pumilio* MNHN.ZM.AC.1956-194 is reattributed to *Loxodonta cyclotis*. In addition to its right ear, the entire skull of this specimen was scanned. Given the great size of this skull, it needed several acquisitions to scan it completely. A third specimen MNHN.ZM.AC.1957-465, although not labelled *Loxodonta pumilio*, corresponds in the collection database to “éléphant nain du Gabon” (pygmy elephant from Gabon), that is the species *L. cyclotis*. Its left ear was CT-scanned. A fourth specimen MNHN.ZM.AC.1961-69 is attributed to *L. cyclotis* based on

geographical provenance details (Gabon) and its right ear was CT-scanned. Additional details inform us that this individual died at 15 days which explains its particularly small size. The fifth specimen MNHN.ZM.AC.1861-53 comes from Sudan and died at 8 years. It is assigned to *L. africana* based on geographical data.

The three other skulls were left unassigned to a *Loxodonta* species because we could not identify them without doubts. Hence we refer them to as *Loxodonta* sp. No details are given concerning the sixth specimen MNHN.ZM.AC.1932-523 which right ear was CT-scanned. The left ear of the seventh specimen MNHN.ZM.AC.2008-70, was CT-scanned but the inside of skull was shattered and only a small part of the petrosal was still present. Finally, both ears of MNHN.ZM.AC.2008-71 were CT-scanned in order to have at least one full set of ears of the same specimen to compare. Additional details from the MNHN collection database tell us that this specimen was a juvenile.

On the other hand, a left isolated petrosal of an African bush elephant (*Loxodonta africana)* had been CT-scanned several years ago for investigation. The microtomographic slices were used for measurements (Spoor et al. 2007) but the inner ear was never actually segmented. The microtomographic data was given to us by Fred Spoor and the specimen was added to the sample. It is from Kenya and and unarguably belongs to the species *Loxodonta africana*.

2.2. Methods

CT scanning and segmentation

The skulls were scanned at the AST-RX platform of the MNHN using a v¦tome¦x L240 from GE Inspection Technologies CT scanner. The voxel sizes of the different acquisitions are given in Table II.1. The segmentation of the petrosals and inner ears were then conducted at the 3D imagery platform of the MNHN using MIMICS INNOVATION SUITE software (Materialise®, release 18).

Membranous labyrinth

As mentioned above, the specimen CEB150009 still preserves its membranous structures (i.e. the membranous labyrinth). The head of this newborn elephant was collected by Romain David and Alexander Stoessel at the IWF in Berlin (2015). It was kept in Bouin solution for several weeks before extracting the petrous bone. Following the protocols described in David et al. (in press), the

petrosal was dehydrated in several baths of alcohol of various concentrations and was then stained in a phosphotungstic acid solution for several weeks before scanning. The scanning was done at the Max Planck Institute for evolutionary anthropology (Leipzig) using a SkyScan1173 with a resolution of 8.94 µm. The bony and membranous labyrinths were then segmented using the same software than for the other specimens.

Measurements

The measurement protocol for the bony ears of extant elephants is the same than for the fossil sample. A general paragraph explaining all the measurement is available in the main 'Material and methods' section of the thesis.

Table II.1 : Extant elephants taxa sample. 'L' is for left, 'R' is for right. 'Ossicles column' references the ossicles preserved in the middle ear. 'M' is for malleus, 'I' is for incus, 'S' is for stapes,'-' is for none. In the provenance column, '-' is for missing data.

Taxon	Specimen number	Side	Ossicles	Age	Provenance	Resolution (µm)
Elephas maximus	1904-273	R	M-I-S	Juv.	-	73.26
Elephas maximus	1941-209	L	I-S	5 yo	Ex-Indochina	78.27
Elephas maximus	2008-81	R	-	-	-	83.28
Elephas maximus	CEB 150009	R	M-I-S	<1yo	Leipzig zoo	8.93
Loxodonta sp.	1932-523	R	-	-	-	120.24
Loxodonta sp.	2008-70	L	-	-	-	67.90
Loxodonta sp.	2008-71	L-R	M-I-S	Juv.	-	65.00
Loxodonta africana	1861-53	R	-	8 yo	Sudan	79.27
Loxodonta africana	CEB130168	L	-	-	Kenya	45.99
Loxodonta cyclotis	1950-728	R	S	-	Gabon	94.27
Loxodonta cyclotis	1956-194	R	S	-	Cameroon	81.74
Loxodonta cyclotis	1957-465	L	-	-	Gabon	89.07
Loxodonta cyclotis	1961-69	R	-	<1yo	Gabon	56.51

3. Anatomical descriptions

3.1. The auditory region and its location in the skull

The auditory region consists, in elephants (and in mammals in general), of several bones located in the basicranial part of the skull (Fig II.2). In veterinary studies, the squamosal, petrosal and tympanic bones are considered to form a unique bone called the temporal. Hence, it is common to come across different nomenclature terms when talking about the petrosal. In Van Der Merwe et al. (1995) for instance, the petrosal of elephants is referred to as the petrous part (*pars petrosa*) of the temporal bone. Here, I will refer to the tympanic, petrosal and squamosal as distinct bones. The structures of the inner ear are contained in the petrosal. This bone is partially fused (medially and caudally) with the tympanic bone which forms the tympanic bulla and is in contact with the squamosal and the occipital. In addition, there are three small bones (actually the smallest bones in mammals) located in the tympanic cavity that form the auditory ossicles chain: the malleus, the incus and the stapes (which is in contact with the *fenestra vestibuli* of the petrosal).

The study of the auditory region of a complete elephant skull (especially the petrosal) is difficult because most of the structures are located in the endocranial part of the skull and therefore are not visible directly on the skull. In ventral view, the petrosal is only visible at the level of the stylomastoid foramen (that contains the facial nerve, VII) which is delimited by the tympanic and the petrosal in its most internal part, and by the occipital and the squamosal in its most external part. This is confirmed in Van Der Merwe et al. (1995). The petrosal is impossible to observe in this view because it is located under the tympanic. The tympanic is more or less bulbous in ventral view because of the tympanic bulla. The *canalis musculotubarius* leaves the tympanic antero-medially. This canal is for the Eustachian tube (Van Der Merwe et al. 1995). The tympanic bulla delimits medially the *canalis caroticus* with the occipital. Posteriorly, the occipital and the tympanic delimit the jugular foramen that opens ventrally and probably housed the hypoglossal nerve (XII). In the lateral part of the skull, the *processus retrotympanicus* and the *processus retro-articularis* of the squamosal form the external auditory

meatus which is the entry point of the external auditory canal and opens laterally. The notch located between the two processes is called the *incisura tympanica*. The external auditory canal is delimited by the squamosal for its most external part and then by the petrosal bone antero-dorsally and the tympanic bone postero-ventrally until it reaches the tympanic cavity of the middle ear. In one specimen (*Elephas* MNHN.ZM.AC.1941-209), I was able to reconstruct a thin empty tubular structure located inside the external auditory meatus (Fig. II.1).

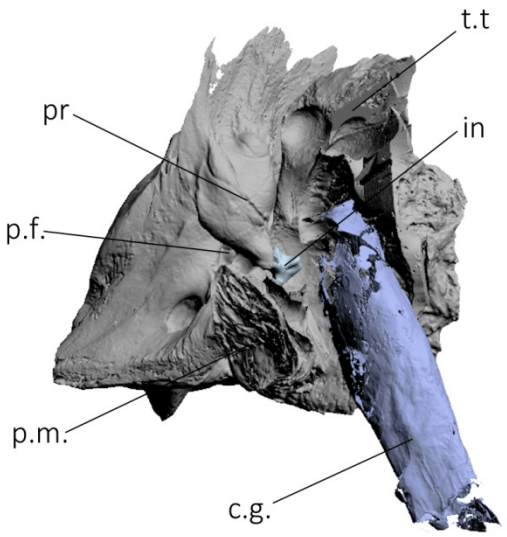

Figure II.1 : 3D reconstruction of the petrosal of *Elephas* specimen MNHN.ZM.AC.1941-209 and its probable cartilaginous gutter. Legends: **c.g.** cartilaginous gutter?, **in** incus, **p.f.** perilymphatic foramen, **p.m.** *pars mastoidea*, **pr** *promontorium*, **t.t.** *tegmen tympani*

This structure ends in the tympanic cavity near the approximate location of the tympanic membrane in life and is less dense than the bone in the microtomographic slices. Its cross-section is oval and its width increase towards the tympanic cavity (around 16 mm at the external extremity and more than 21 mm at the tympanic extremity). Its shape more or less mimics the shape of the external auditory canal but it is narrower. This could be the cartilaginous gutters of the external auditory canal described in Buck (1888, 1890).

The microtomographic study of an adult skull of *Loxodonta* permitted us to dissect the skull virtually. Hence I segmented only the ventral part of the skull which allowed us to observe the inside of the endocranial cavity. In dorsal view, the petrosal is visible. It is in contact with the squamosal laterally, the occipital posteriorly and the tympanic antero-medially. The petrosal is partially fused with the tympanic anteriorly.

In most mammals, the petrosal is visible in lateral view between the squamosal and the occipital. The region of the petrosal that extends externally is the *pars mastoidea*. However, in extant elephants (and in most of extinct proboscideans) the *pars mastoidea* is reduced and is not visible at the surface of the skull in lateral view. This condition is called amastoidy.

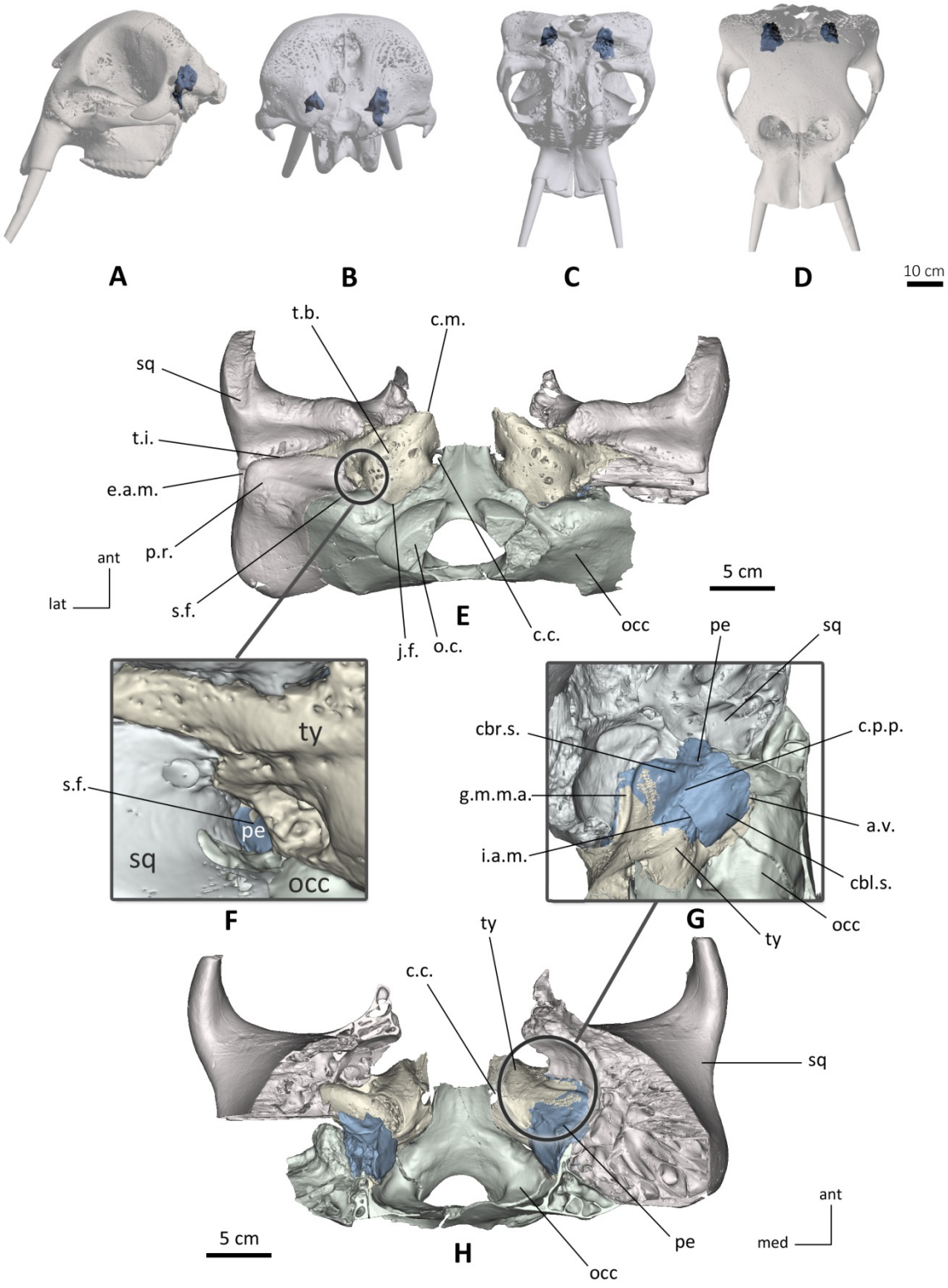

Figure II.2 : Position of the petrosal (blue) in the skull of *L. cyclotis* 1956-194 in lateral (A), caudal (B), ventral (C) and antero-dorsal (D) views. Virtual dissections of the basicranium in ventral view (E) with a focus on the stylomastoid foramen (F) and in antero-dorsal view (H) with a focus on the petrosal (G). Legends: **a.v.** *aquaeductus vestibuli*, **c.c.** *canalis caroticus*, **c.m.** *canalis musculotubarius*, **c.p.p.** *crista partis petrosa*, **cbl.s.** cerebellar surface of the petrosal, **cbr.s.** cerebral surface of the petrosal, **e.a.m.** external auditory meatus, **g.m.m.a.** groove for the middle meningeal artery, **i.a.m.** internal auditory meatus, **j.f.** jugular foramen, **o.c.** occipital condyle, **occ** occipital, **pe** petrosal, **p.r.** *processus retrotympanicus*, **s.f.** stylomastoid foramen, **sq** squamosal, **t.b.** tympanic bulla, **t.i.** tympanic incisura, **ty** tympanic.

3.2. Petrosal

The following section focuses on the anatomical description of the extant elephants petrosal. Detailed anatomical drawings of one petrosal of *Elephas* (MNHN.ZM.AC.2008-81) and one petrosal of *Loxodonta* (MNHN.ZM.AC.1957-465) in ventral and dorsal views are given in Fig. II.3 and II.4 respectively. They allow observing the general morphology of the extant elephants petrosal. On the other hand, less detailed anatomical charts representing the petrosal in tympanic, medial, cerebral and cerebellar views are given for each studied specimen (Fig. II.12-20). These charts are more schematic and allow observing the several variations observed within the sample.

In dorsal view, the petrosal displays two surfaces separated by a ridge called the *crista partis petrosa*: the cerebellar surface that bears the internal acoustic meatus and the subarcuate fossa, and the cerebral surface that displays a deep vascular groove. These surfaces form an obtuse angle of roughly 110°. Contrary to the observation made by Tassy (2013), the *crista partis petrosa* appears less sharp in extant elephants than in *Gomphotherium angustidens*.

Cerebellar surface

The cerebellar surface of the petrosal is more or less flat. In cerebellar view, the petrosal appears rectangular and elongated antero-posteriorly. In most mammals, the *subarcuate fossa* is a rather deep depression that houses the paraflocullus part of the cerebellum. In extant elephants, however, this fossa is so much shallow that one cannot really tell if it is present. In *Elephas* MNHN.ZM.AC.1904-273, the cerebellar surface is slightly convex while it is rather concave in the other two *Elephas* specimens. In *Loxodonta*, it is always slightly convex. In the anterior part of the petrosal and visible in cerebellar view is the internal auditory meatus. This opening is the point of entry of the VIIth and VIIIth nerves into the petrosal. It opens anteriorly, parallel to the cerebellar surface. It begins as a unique opening but it rapidly bifurcates internally, the passage for the VIIth nerve being located medially and the passage for the VIIIth nerve laterally. The VIIIth nerve bifurcates rapidly as well into the vestibular (located at the center of the meatus) and cochlear (located in the lateral portion of the meatus) nerves. The internal auditory meatus is partially broken in *Loxodonta* specimens MNHN.ZM.AC.1932-523 and

MNHN.ZM.AC.1956-194, displaying a rather slit-like shape. Anteriorly to the internal auditory meatus lies a thin bony flange known as the epitympanic wing. This structure is fragile and is sometimes broken (*Loxodonta* MNHN.ZM.AC.1956-194, 1932-523). On the cerebellar surface lies the vestibular aqueduct (*aquaeductus vestibuli*) which contained the endolymphatic duct in life. It overhangs the occipital and tympanic bones and has the shape of a thin slit that opens postero-ventrally in the *L. cylotis* specimen MNHN.ZM.AC.1956-194. However, the morphology of the *aquaeductus vestibuli* varies among specimens. In cerebellar view, it always has the shape of a slit, but in posterior view, it has a quite circular opening in all *Elephas* specimens and in *L. cyclotis* MNHN.ZM.AC.1961-69. In the other specimens of extant elephants, the *aquaeductus vestibuli* has the shape of a slit even in posterior view. The slit is quite small in *L. cyclotis* MNHN.ZM.AC.1961-69 while it is extremely large in *L. africana* MNHN.ZM.AC.1861-53. In the latter specimen, the *aquaeductus vestibuli* overhangs a large flat surface belonging to the petrosal while it overhangs directly the tympanic and occipital bones in the other specimens. This opening generally opens in the postero-ventral corner of the petrosal but it displays a more posterior orientation in *Elephas* specimens and *L. cyclotis* MNHN.ZM.AC.1961-69. Hence the *aquaeductus vestibuli* appears more centered in the latter specimens in posterior view.

Cerebral surface

The cerebral surface consists mostly of a very large *tegmen tympani*. The *tegmen tympani* is in contact with the squamosal posteriorly and ventrally and it is partially fused with the tympanic anteriorly. Its overall surface is flat in general. In *Elephas* MNHN.ZM.AC.1941-209, it displays a small convexity in its center while it is slightly concave in the other *Elephas* specimen MNHN.ZM.AC.2008-81. A deep vascular groove runs along the ventral suture with the squamosal. It is oriented antero-posteriorly and the trajectory is straight in MNHN.ZM.AC.1941-209 and 2008-81 but it is slightly curved in MNHN.ZM.AC.1904-273. The groove appears larger in MNHN.ZM.AC.2008-81. This groove probably housed the middle meningeal artery or the carotid artery which both converge into the same foramen (Tassy, 2013). There is a thin separation with the cerebellar surface at the anterior level of the *crista partis petrosa*.

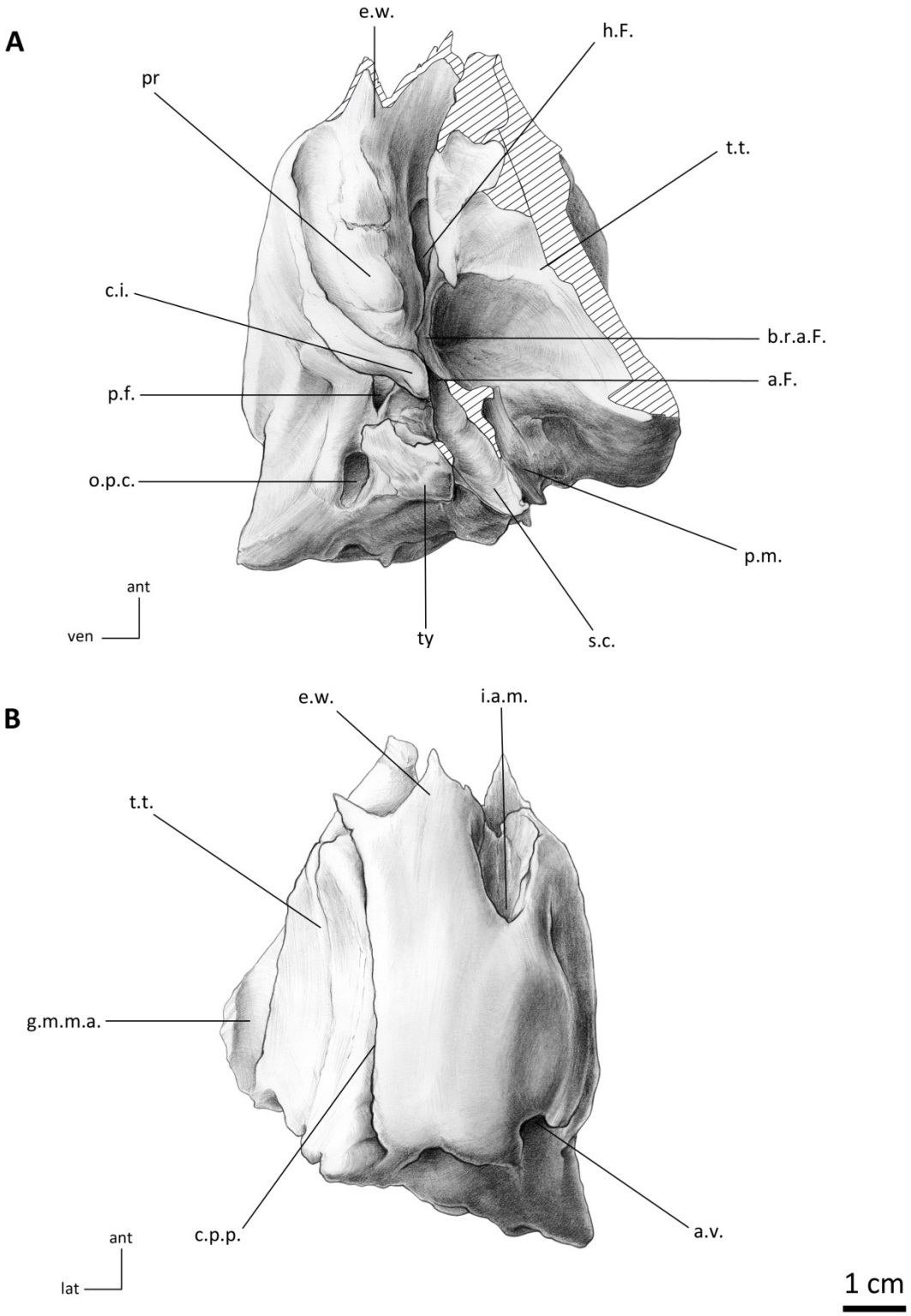

Figure II.3 : Petrosal of *Elephas* MNHN.ZM.AC.2008-81 in ventral (A) and dorsal (B) views (mirrored). Illustrations by Charlène Letenneur (MNHN, CR2P). Legends: **a.F.** *aquaeductus Fallopii*, **a.v.** *aquaeductus vestibuli*, **b.r.a.F.** bony roof over the *aquaeductus Fallopii*, **c.i.** *crista interfenestralis*, **c.p.p.** *crista partis petrosa*, **e.w.** epitympanic wing, **g.m.m.a.** groove for the middle meningeal artery, **h.F.** *hiatus Fallopii*, **i.a.m.** internal auditory meatus, **o.p.c.** opening of a pneumatic cell, **p.f.** perilymphatic foramen, **p.m.** *pars mastoidea,* **pr** *promontorium*, **s.c.** stylomastoid canal, **t.t.** *tegmen tympani*, **ty** tympanohyal.

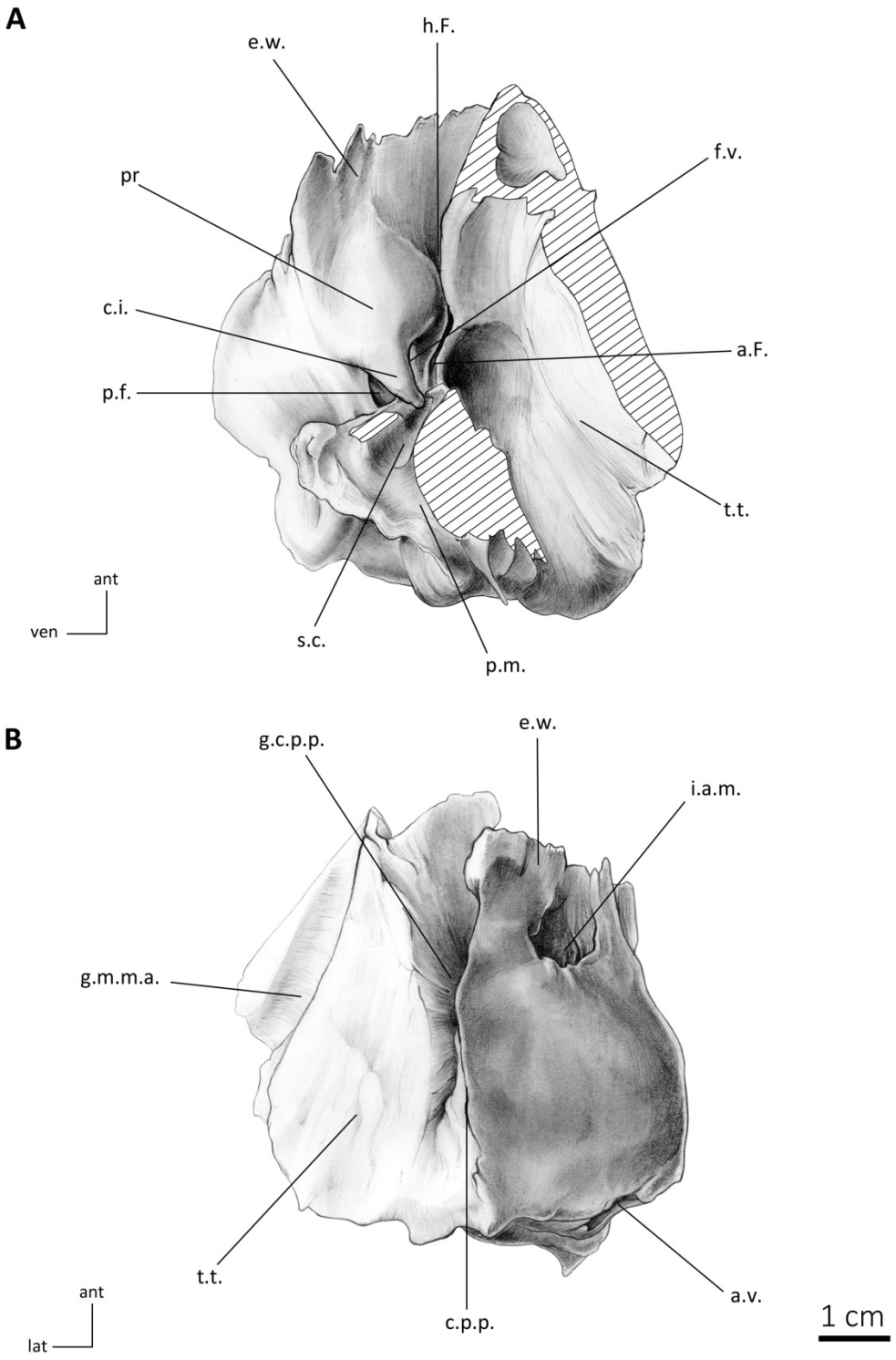

Figure II.4 : Petrosal of *L. cyclotis* MNHN.ZM.AC.1957-465 in ventral (A) and dorsal (B) views. Illustrations by Charlène Letenneur (MNHN, CR2P). Legends: **a.F.** *aquaeductus Fallopii*, **a.v.** *aquaeductus vestibuli*, **c.i.** *crista interfenestralis*, **c.p.p.** *crista partis petrosa*, **e.w.** epitympanic wing, **g.c.p.p.** groove under the *crista partis petrosa*, **g.m.m.a.** groove for the middle meningeal artery, **h.F.** *hiatus Fallopii*, **i.a.m.** internal auditory meatus, **o.p.c.** opening of a pneumatic cell, **p.f.** perilymphatic foramen, **p.m.** *pars mastoidea,* **pr** *promontorium*, **s.c.** stylomastoid canal, **t.t.** *tegmen tympani*.

In MNHN.ZM.AC.2008-81 this separation seems to follow the ridge entirely but a closer investigation of the microtomographic slices reveals that this is caused by a fissure. The cerebral surface displays really narrower and shallower grooves as well in most of the specimens. One groove is slightly more marked and has a trajectory more or less parallel to the groove for the middle meningeal artery. It is closer to the *crista partis petrosa*, hence we assume that it could be the groove for the superior petrosal sinus.

Tympanic surface

In tympanic view, the petrosal is covered by the tympanic on the skull. A bone to bone segmentation allowed us to separate the tympanic from the petrosal in order to visualize only the latter. The lateral part of the petrosal consists of the large and flat *tegmen tympani*. It is bound laterally to the squamosal and fused antero-medially to the tympanic. The postero-lateral part of the *tegmen tympani* forms the most inner part of the external auditory canal with the tympanic. This canal ends in the tympanic cavity delimited by the tympanic bone. This cavity contains the ossicles. On the medial part of the petrosal lies the bulbous *promontorium* that is oriented medio-laterally and has the overall shape of a teardrop. This structure houses the cochlea and displays two openings.

The most anterior opening is the *fenestra vestibuli*. It is generally oval and houses the footplate of the stapes when the ossicles are still connected to the skull. The average value for the stapedial ratio in extant elephants is 1.7. The ratio varies slightly between 1.6 and 1.8 (see Table II.2 below). Illustrations of the *fenestrae vestibuli* are given in Fig. II.5.

Table II.3: Stapedial ratio of extant elephants

Taxon	Specimen	Ratio
Elephas	1904-273	1.8
Elephas	1941-209	1.7
Elephas	2008-81	1.6
Elephas	CEB 150009	-
Loxodonta	1861-53	1.6
Loxodonta	1932-523	1.7
Loxodonta	1950-278	1.8
Loxodonta	1956-194	-
Loxodonta	1957-465	1.7
Loxodonta	1961-69	1.7
Loxodonta	2008-71L	1.7
Loxodonta	2008-71R	1.7
Loxodonta	CEB130168	1.7

The *fenestrae* of *Elephas* specimen 1904-273 and *Loxodonta* specimen 1950-278 are slightly more oval than the other specimens (ratio of 1.8). In contrast, the *fenestra vestibuli* of *Elephas* specimen 2008-81 and *Loxodonta* specimen 1861-53 are slightly rounder (ratio of 1.6).

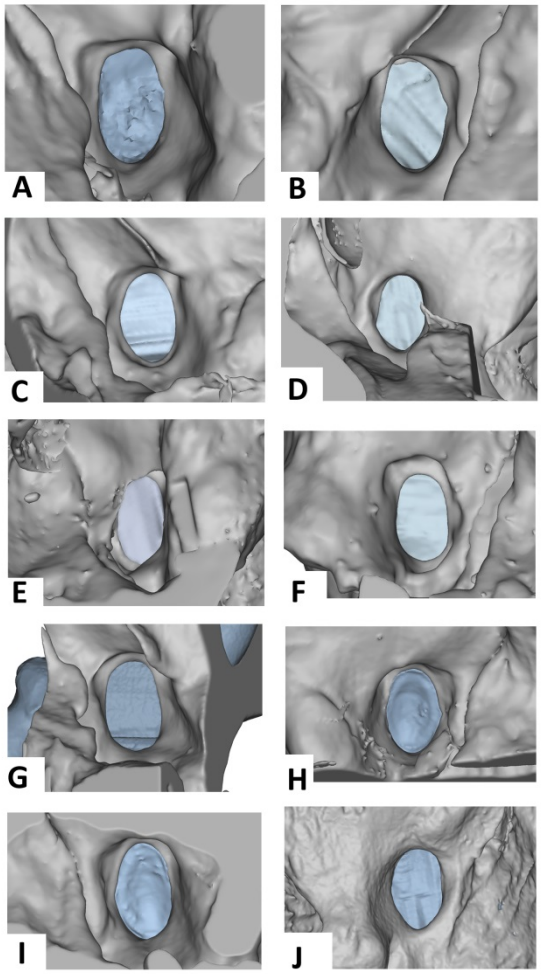

Figure II.5 : *Fenestrae vestibuli* of *Elephas* specimens 1904-273 (A), 1941-209 (B) and 2008-81 (C) and *Loxodonta* specimens 1861-53 (D), 1950-278 (E), 1957-465 (F), 1961-69 (G), 2008-71 left (H), 2008-71 right (I) and CEB130168 (J).

The *fenestra vestibuli* opens over the *aquaeductus Fallopii* (or Fallopian canal) that contained the facial nerve in life. This canal is the continuity of the stylomastoid canal and is located lateral to the *promontorium*. It conducts the facial nerve from the *hiatus Fallopii* which is its exit point. It also communicates anteriorly with the internal auditory meatus. The canal is formed ventrally by the medial and lateral walls of the floor as in the elephantimorph petrosals described in Ekdale (2011). The junction of the walls is visible in every specimen and looks like a fissure. The junction (near the *pars mastoidea*) is quite loose in the posterior part of the canal resulting in a posteriorly opened canal. This condition has already been described in some of the elephantimorphs studied in Ekdale (2011) but this feature was subject to variability. It appears that extant elephants display only the posteriorly opened condition. As we will discuss later, this opened part of the facial canal may house the geniculate ganglion.

The second opening of the *promontorium* is the perilymphatic foramen which is more posterior and opens medially. This is a paedogenetic character because the perilymphatic canal separates in two (the *fenestra cochleae* and the *canaliculus cochleae*) during the development of most mammals; however, the single opening is retained in elephants

and extant sirenians (Fischer, 1990). The perilymphatic foramen is irregular in shape and is always somewhat oblong. The *fenestra vestibuli* and the perilymphatic foramen are separated by a rather large ridge called the *crista interfenestralis*.

Ventrally to the *promontorium* lies a large process which is the *pars mastoidea* of the petrosal. The presence of the *pars mastoidea* in elephants has been somewhat controversial. According to Köstlin (1844) there is no *pars mastoidea* at all in elephants. However, this portion of the petrosal has been observed by Flower (1885) which remarks its small size compared to most mammals and its absence on the surface of the skull. This part of the petrosal was neglected by Buck (1888 and 1890) because of strict dissection restrictions about the specimens. Those restrictions were nevertheless lifted afterwards which allowed Richards (1890) to complete the anatomical description of this region. Richards agreed with the observation made by Flower and pursued a further investigation of the area. He noted the presence of small pneumatic cells contained in the mastoid portion (*pars mastoidea*) which did not communicate with the pneumatic cells of the mastoid process of the occipital and assumed that these cells belongs to the petrosal and precisely to the mastoid portion described by Flower. However, some doubts remained as the mastoid portion of the petrosal is fused with the tympanic at this level. To sum up, Köstlin (1844) assumes that there is no mastoid portion of the petrosal at all in elephant skulls (hence this region would belong to another bone) while Flower (1885) and Richards (1890) assumes that the observed process is a relatively small (compared to other mammals) mastoid portion of the petrosal. Our virtual dissection tips the scales in favor of Flower and Richards hypothesis. I was able to reconstruct the pneumatic cells which are clearly contained in the petrosal and do not connect with the pneumatic cells of the tympanic. Hence, I assume that the most posterior part of the process is clearly part of the petrosal (and referred it to as the *pars mastoidea*) while the anterior part is part of the tympanic. The pneumatic cells contained in the *pars mastoidea* are represented in Figure II.6. Their number and shape vary significantly between specimens.

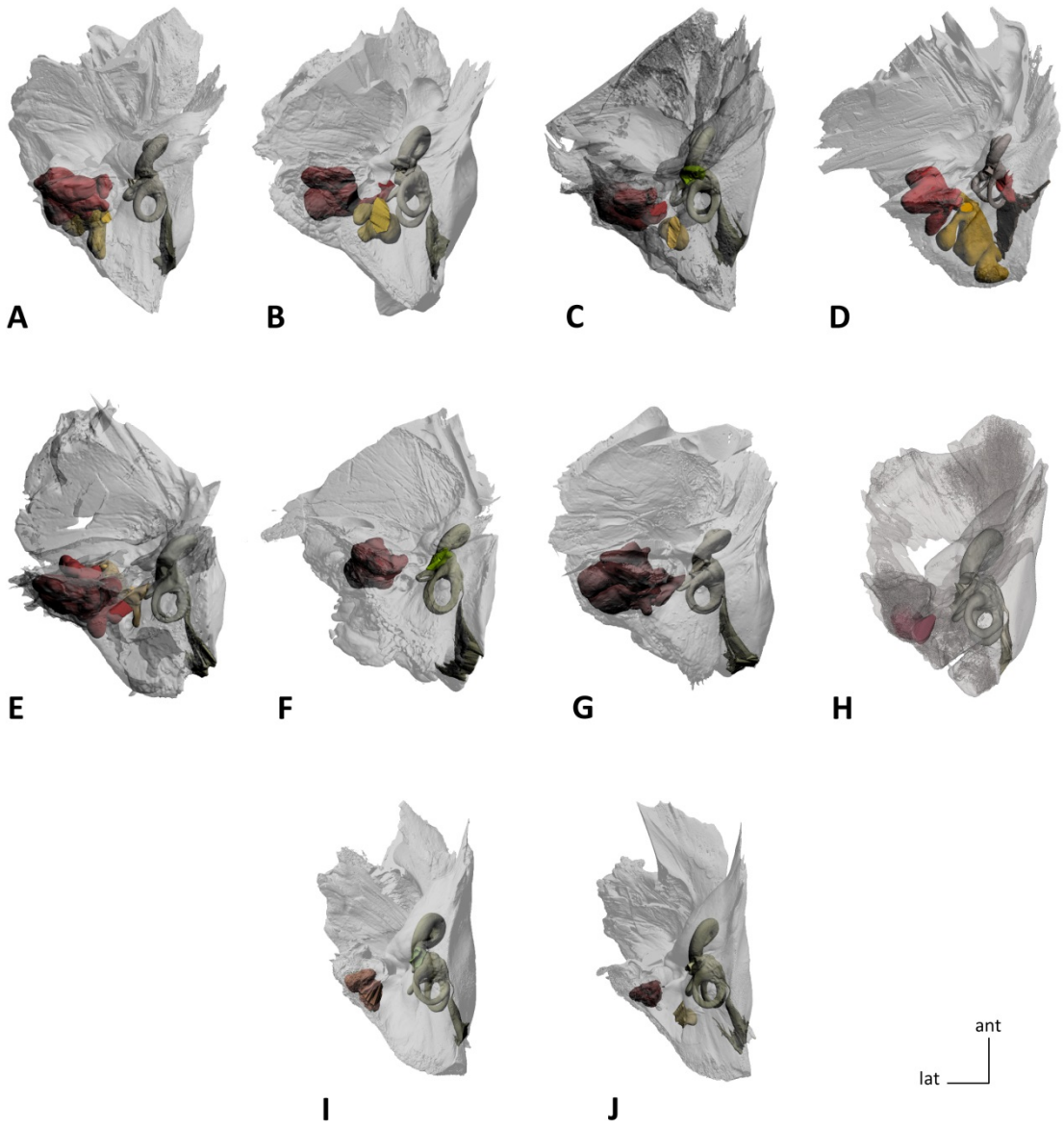

Figure II.6 : Pneumatic cells of the *pars mastoidea* viewed in transparency, in medial view, in *Elephas* specimens MNHN.ZM.AC.1904-273 (A), 1941-209 mirrored (B), 2008-81 (C), *L. africana* specimen MNHN.ZM.AC.1861-53 (D), *Loxodonta* sp specimens MNHN.ZM.AC.1932-523 (E), 2008-71 left mirrored (I) and 2008-71 right (J) and *L. cyclotis* specimens MNHN.ZM.AC.1956-194 (F), 1957-765 mirrored (G) and 1961-69 (H). The cells are in red and yellow. Cells with the same color appear to be homologous.

Generally, there are one or two independent cells contained strictly in the *pars mastoidea* whereas Richards (1890) assumes that the *pars mastoidea* contains one network of communicating cells. In some specimens, there is another cell contained more posteriorly in the petrosal. These cells open in the secondary tympanic cavity near the fossa for the stapedius muscle. They do not open at the level of the ossicles in our specimens, which corroborates the observations made by Richards (1890). These pneumatic cells may play the role of the mastoid antrum which receives and amplify sonic waves, but this is has yet to be demonstrated.

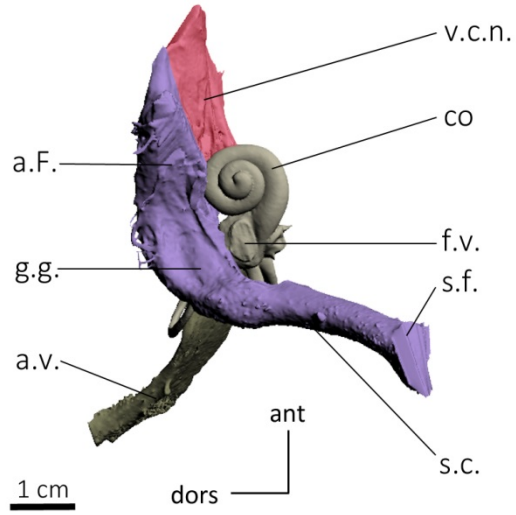

Figure II.7 : Reconstruction of the course of the facial nerve (violet) in *L. africana* 1861-53 using bony canals. **a.F.** *aquaeductus Fallopii*, **a.v.** *aquaeductus vestibuli*, **co** cochlea, **f.v.** *fenestra vestibuli*, **g.g.** geniculate ganglion, **s.c.** stylomastoid canal, **s.f.** stylomastoid foramen, **v.c.n.** vestibulo-cochleae nerve.

The *pars mastoidea* contains the stylomastoid canal that continues its course through the stylomastoid foramen and which houses the facial nerve in life. The *pars mastoidea* contributes to the posterior roof of the canal while the anterior roof is delimited by the tympanic. In life, the facial nerve originates "from the dorsal aspect of the facial nuclear complex, travels dorsally to the roof of the caudal aspect of the pons, bends laterally over the *abducens nucleus* to form the facial colliculus, and then extends ventrally to exit at the pontomedullary junction ventral to the vestibulocochlear nerve" (Maseko et al. 2013). It was possible to reconstruct the course of the facial nerve in the auditory region (Fig. II.7). The nerve enters the petrosal through the *hiatus Fallopii* and runs inside the Fallopian canal. It passes close to the *fenestra vestibuli* and widens where the roof of the Fallopian canal is open. This is probably the location of the geniculate ganglion. The further course of the facial nerve deviates laterally and enters the *pars mastoidea* of the petrosal via the stylomastoid canal. It then exits the skull through the stylomastoid foramen.

Close to the *crista interfenestralis* on its posteromedial side is the tympanohyal which is part of the *pars mastoidea*. It has the aspect of a rather sharp ridge that overhangs the canal for the facial nerve. Laterally to the perilymphatic foramen lies a deep fossa that housed the stapedius muscle. This muscle is attached to the stapes and permits its movements. The fossa communicates with the area where the stapes is located in life through a foramen called the stapedial foramen. Ekdale (2011) highlighted a variation of the stapedial foramen in petrosals of elephantimorphs and I observe a variation of this area as well in extant elephants. In some specimens, the tympanohyal and the *crista interfenestralis* are in contact thus delimiting a true stapedial foramen (Elephas 1904-273, *Loxodonta* 1956-194 and in both ears of 2008-71, Fig. II.8A). However, the tympanohyal is located somewhat more distant from the *crista interfenestralis* in other specimens.

In *Loxodonta* specimens 1961-69 and 1950-278 and *Elephas* specimens 1941-209 and 2008-81, the tympanohyal and the *crista interfenestralis* are not strictly in contact (but extremely close), thus the stapedial foramen is not fully delimited (Fig. II.8B).

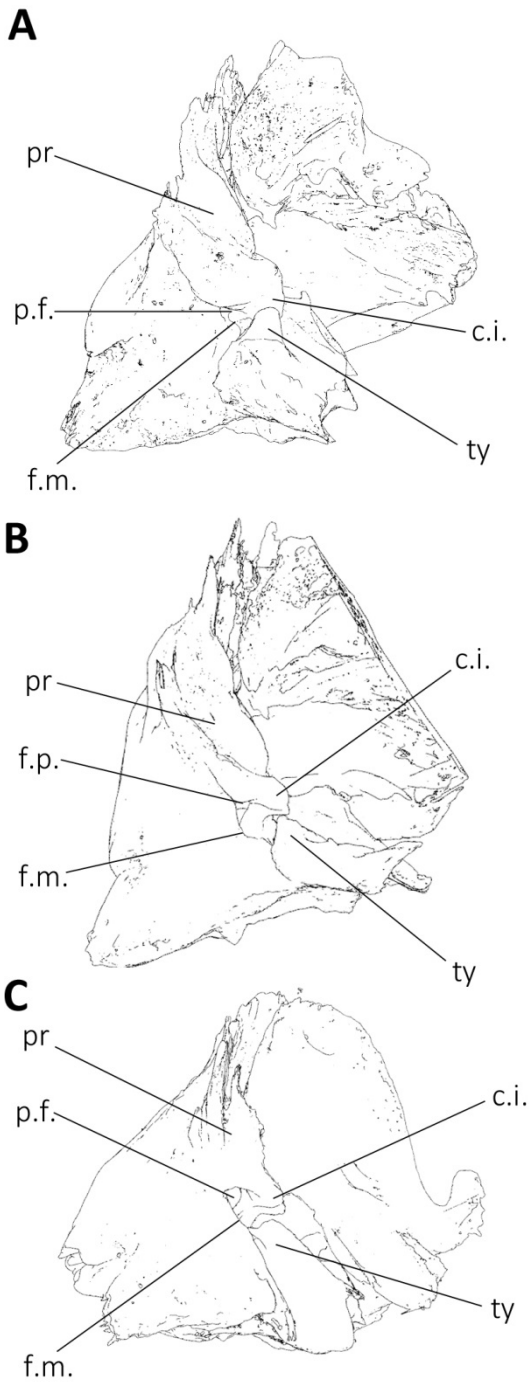

Figure II.8 : Variations of the stapedial foramen: (A) fully delimited (*Elephas* 1904-273), (B) partially delimited (*Elephas* 2008-81) and (C) poorly delimited (*L. cyclotis* 1957-465). **Legends: c.i.** *crista interfenestralis*, **f.m.** fossa for the stapedius muscle, **p.f.** perilymphatic foramen, **pr** *promontorium*, **ty** tympanohyal.

Moreover, in *Loxodonta* specimens 1957-465 and 1932-523, the tympanohyal is even more distant from the *crista interfenestralis*, the stapedial foramen being really poorly delimited (Fig. II.8C).

In the medial part of the *promontorium* lies the epitympanic wing which consists of a very thin bony flange. The medial part of the *promontorium* is in contact with the tympanic but not fused. In several specimens, a groove separates the *promontorium* in two clear and bulbous structures. The most anterior part houses the cochlea and is really bulbous while the most posterior is thick and elongated and consists of a bulge which is the extension of the *crista interfenestralis* (Fig. II.9B). This condition is seen in all the three *Elephas* specimens but it is less marked in specimen MNHN.ZM.AC.1941-209. In *Loxodonta*, only MNHN.ZM.AC.1961-69 displays these features.

In several specimens (*Elephas* MNHN.ZM.AC.2008-81, *Loxodonta* MNHN.ZM.AC.1932-523, 1861-53, 1950-728 and CEB130168) the portion of the petrosal located medially to the *promontorium* is inflated.

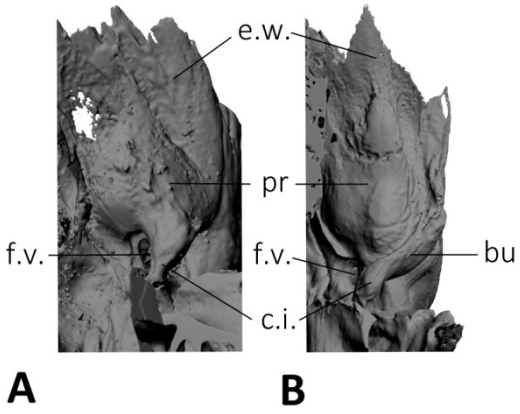

Figure II.9 : Ventral view of the petrosal. *Promontorium* without the posterior bulge (**A**, *L. cyclotis* MNHN.ZM.AC.1957-465) and *promontorium* with the posterior bulge (**B**, *Elephas* MNHN.ZM.AC.2008-81). Legends: **bu** posterior bulge, **c.i.** *crista interfenestralis*, **e.w.** epitympanic wing, **f.v.** *fenestra vestibuli*, **pr** *promontorium*.

In 1861-53, there is a cavity located near the inflation. In *Loxodonta* 2008-71 (left and right side) the inflation is extreme and displays a bean-shaped protuberance. The protuberance is present in *Loxodonta* 1956-194 and 1950-278 but is less developed than in 2008-71. The investigation of the protuberance through the microtomographic slices reveals no peculiar internal structure.

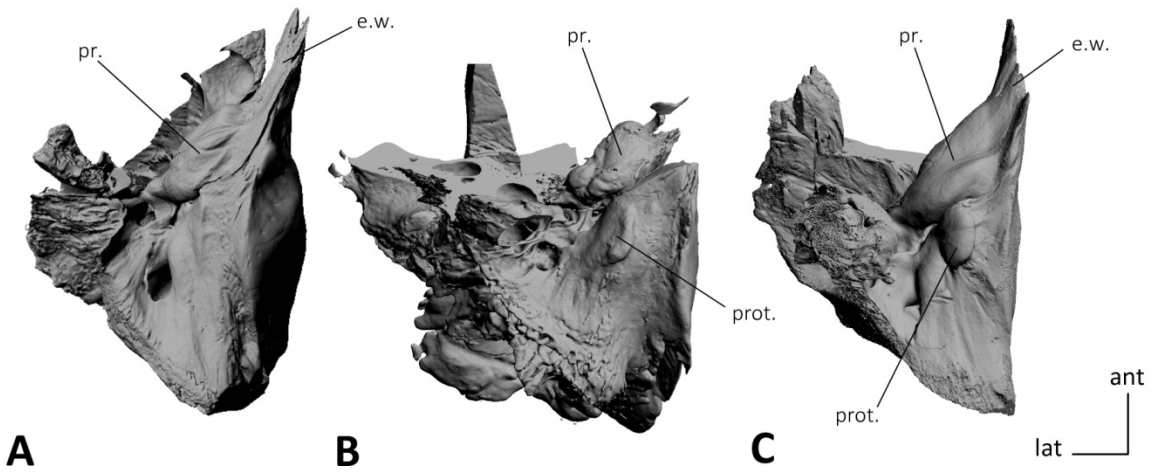

Figure II.10 : Variations of the protuberance located closely to the *promontorium* in medial view. (A) No protuberance (*Elephas* MNHN.ZM.AC.1941-209), (B) slight protuberance (*L. cyclotis* MNHN.ZM.AC.1956-194), (C) very inflated protuberance (*Loxodonta* sp MNHN.ZM.AC.2008-71, right ear). Legends: **e.w.** epitympanic wing, **pr** *promontorium*, **prot** protuberance.

3.3. Ossicles

Some ossicles are still present in the skull of several extant elephants studied (Table II.1). Three specimens preserve the complete ossicular chain. In both ears of *Loxodonta* sp MNHN.ZM.AC.2008-71, the ossicles are even in connection (Fig. II.11A). The malleus is the most lateral ossicles and its manubrium attaches the tympanic membrane in life. It is articulated with the incus at the level of the articular surface. The short process of the incus is lodged in a shallow depression located on the surface of the petrosal: the *fossa incudis* (Fig. II.11B). The incus is articulated with the stapes whose footplate occupies the *fenestra vestibuli*.

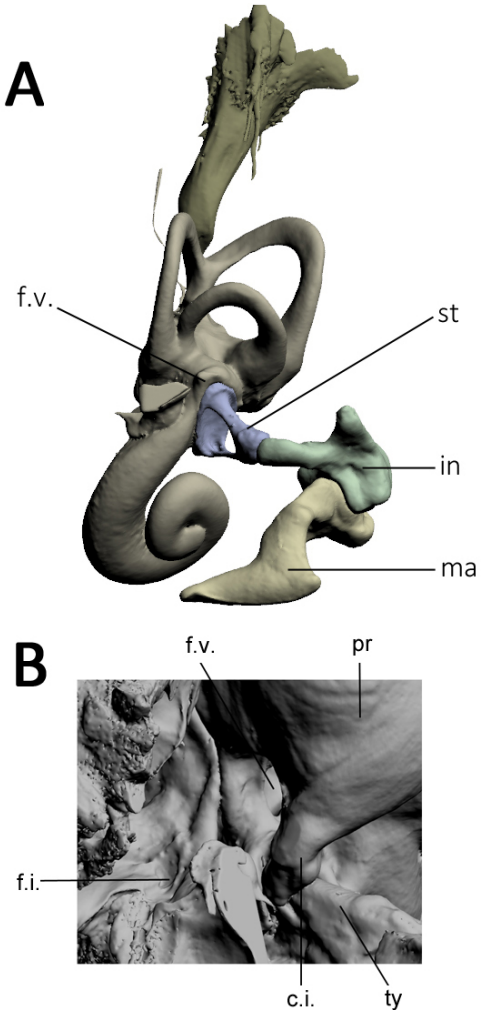

Figure II.11 : Complete ossicular chain of an African elephant (A) and articulation region of the ossicles (B). **c.i.** *crista interfenestralis*, **f.i.** *fossa incudis*, **f.v.** *fenestra vestibuli*, **in** incus, **ma** malleus, **pr** *promontorium*, **st** stapes, **ty** tympanohyal.

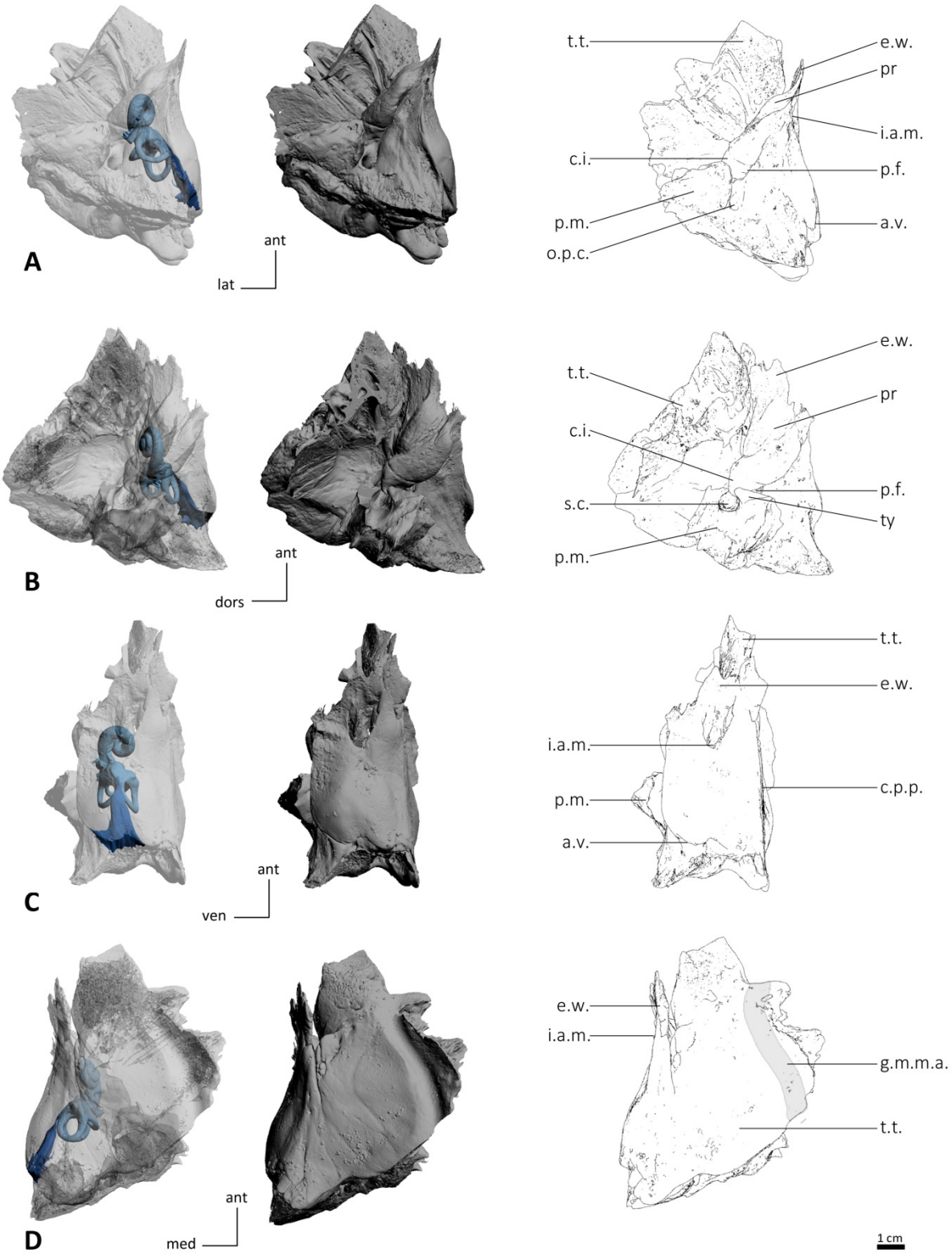

Figure II.12 : 3D models and drawings of the right petrosal of *Elephas maximus* MNHN.ZM.AC.1904-273 in medial (A), tympanic (B), cerebellar (C) and cerebral (D) views. Legends: **a.v.** *aquaeductus vestibuli*, **c.i.** *crista interfenestralis*, **c.p.p.** *crista partis petrosa*, **e.w**. epitympanic wing, **g.m.m.a.** groove for the middle meningeal artery, **i.a.m.** internal auditory meatus, **o.p.c.** opening of a pneumatic cell, **p.f.** perilymphatic foramen, **p.m.** *pars mastoidea*, **pr** *promontorium*, **s.c.** stylomastoid canal, **t.t.** *tegmen tympani,* **ty** tympanohyal

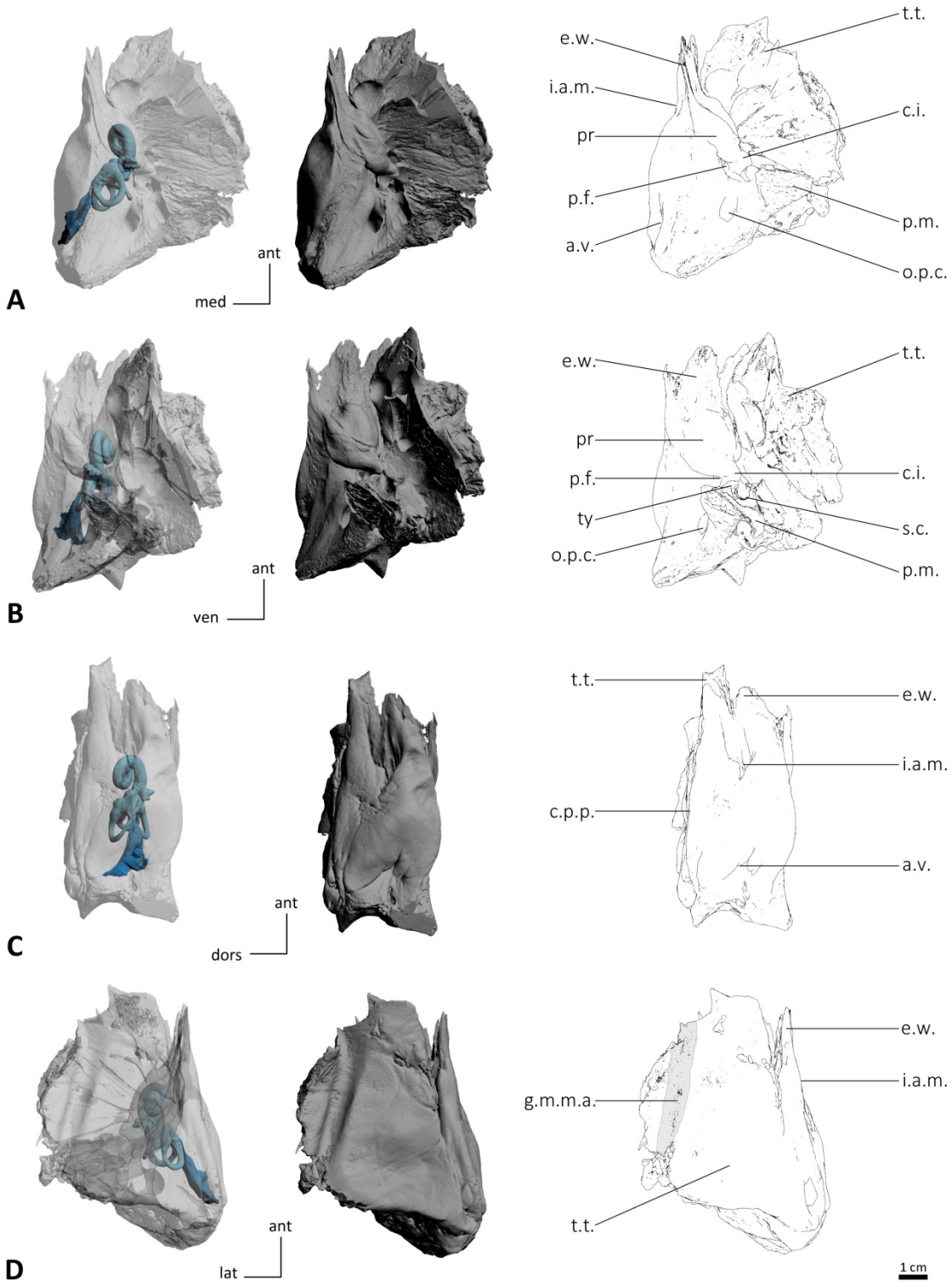

Figure II.13 : 3D models and drawings of the left petrosal of *Elephas maximus* MNHN.ZM.AC.1941-209 in medial (A), tympanic (B), cerebellar (C) and cerebral (D) views. Legends: **a.v.** *aquaeductus vestibuli*, **c.i.** *crista interfenestralis*, **c.p.p.** *crista partis petrosa*, **e.w**. epitympanic wing, **g.m.m.a.** groove for the middle meningeal artery, **i.a.m.** internal auditory meatus, **o.p.c.** opening of a pneumatic cell, **p.f.** perilymphatic foramen, **p.m.** *pars mastoidea*, **pr** *promontorium*, **s.c.** stylomastoid canal, **t.t.** *tegmen tympani,* **ty** tympanohyal

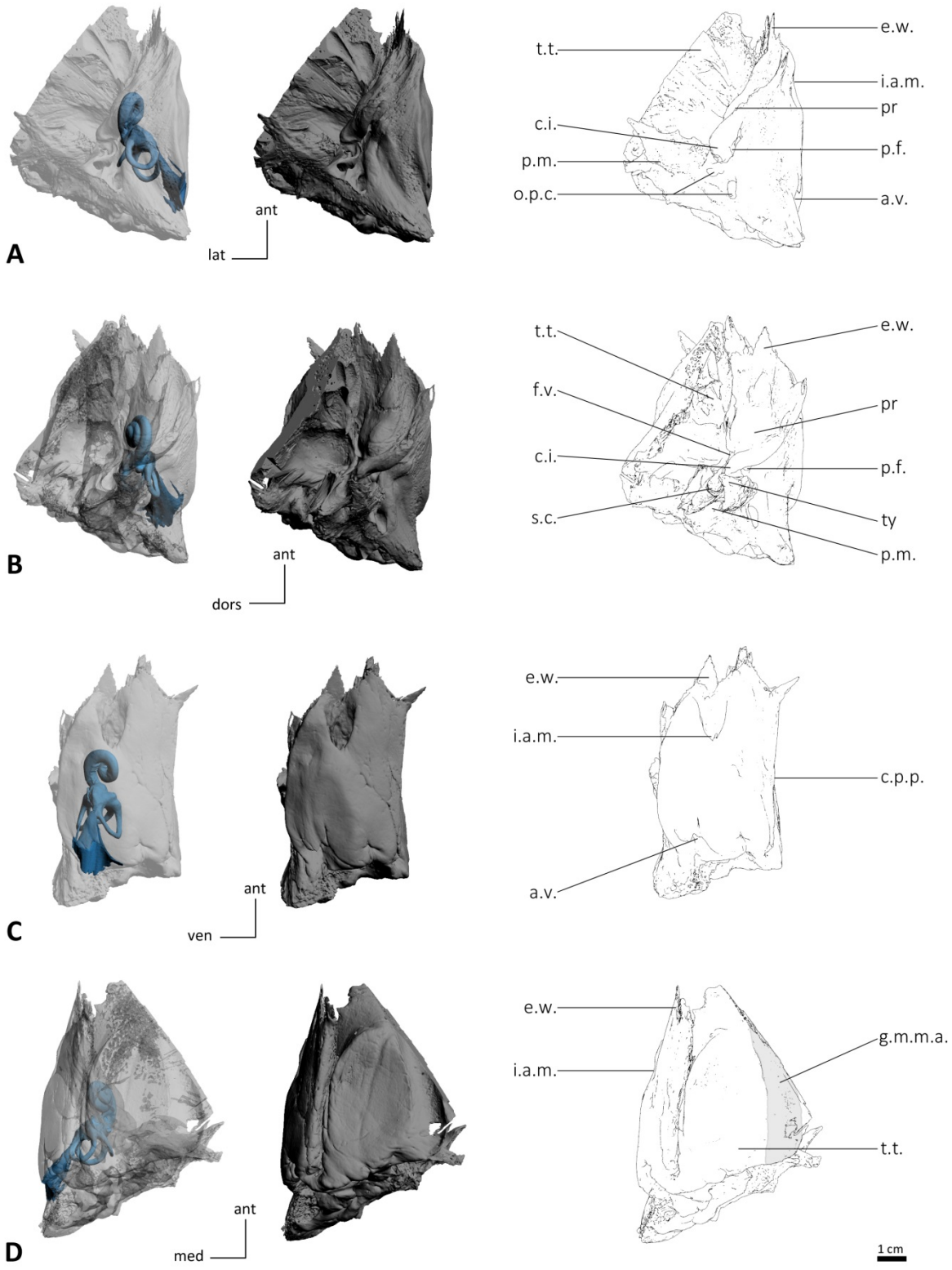

Figure II.14 : 3D models and drawings of the right petrosal of *Elephas maximus* MNHN.ZM.AC.2008-81 in medial (A), tympanic (B), cerebellar (C) and cerebral (D) views. Legends: **a.v.** *aquaeductus vestibuli*, **c.i.** *crista interfenestralis*, **c.p.p.** *crista partis petrosa*, **e.w**. epitympanic wing, **f.v.** *fenestra vestibuli*, **g.m.m.a.** groove for the middle meningeal artery, **i.a.m.** internal auditory meatus, **o.p.c.** opening of a pneumatic cell, **p.f.** perilymphatic foramen, **p.m.** *pars mastoidea*, **pr** *promontorium*, **s.c.** stylomastoid canal, **t.t.** *tegmen tympani,* **ty** tympanohyal

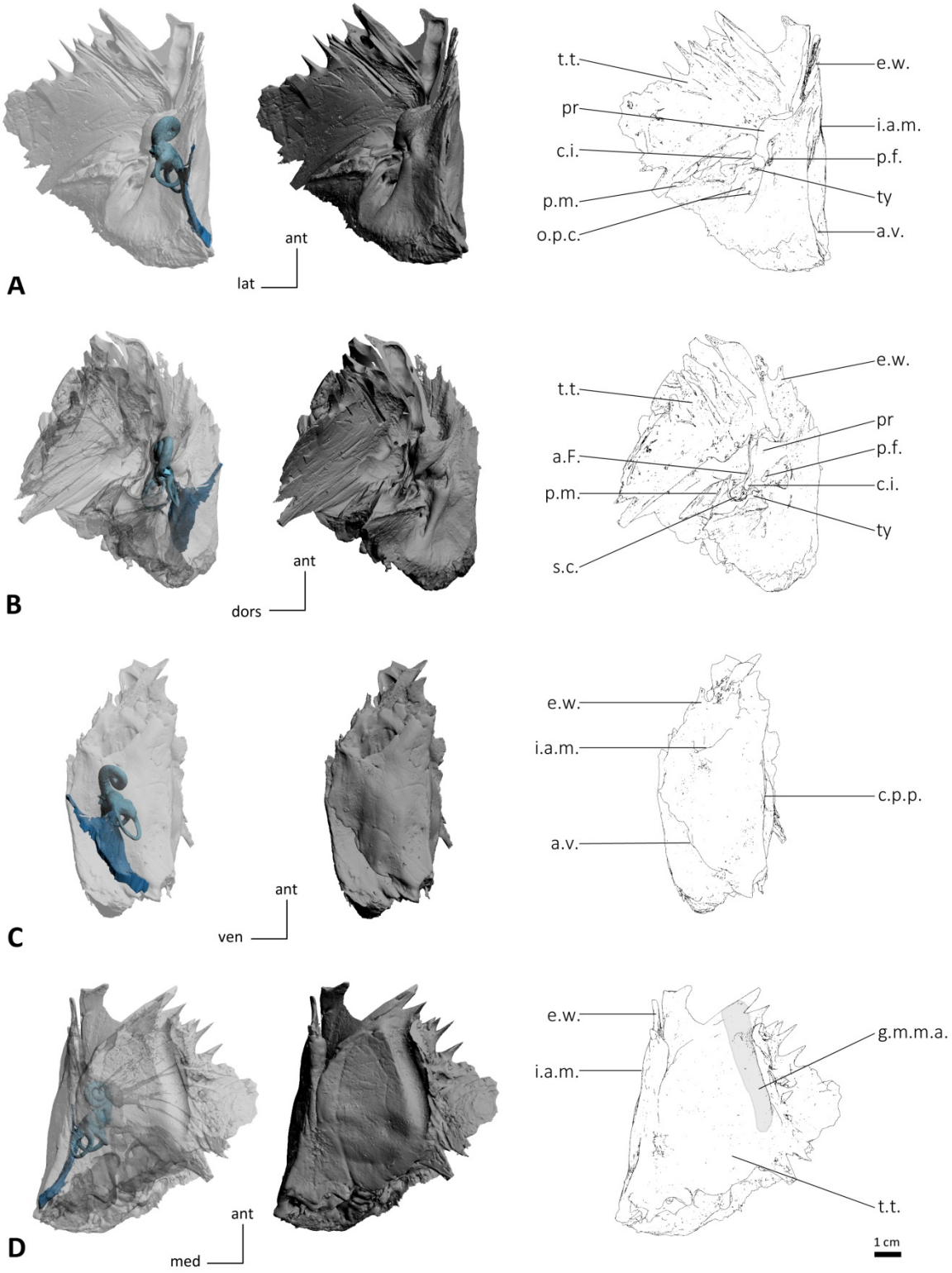

Figure II.15 - 3D models and drawings of the right petrosal of *Loxodonta africana* MNHN.ZM.AC.1861-53 in tympanic (A), medial (B), cerebellar (C) and cerebral (D) views. **Legends: a.F.** *aquaeductus Fallopii*, **a.v.** *aquaeductus vestibuli*, **c.i.** *crista interfenestralis*, c.p.p. *crista partis petrosa*, **e.w**. epitympanic wing, **g.m.m.a.** groove for the middle meningeal artery, **i.a.m.** internal auditory meatus, **o.p.c.** opening for a pneumatic cell, **p.f.** perilymphatic foramen, **p.m.** *pars mastoidea*, **pr** *promontorium*, **s.c.** stylomastoid canal, **t.t.** *tegmen tympani,* **ty** tympanohyal.

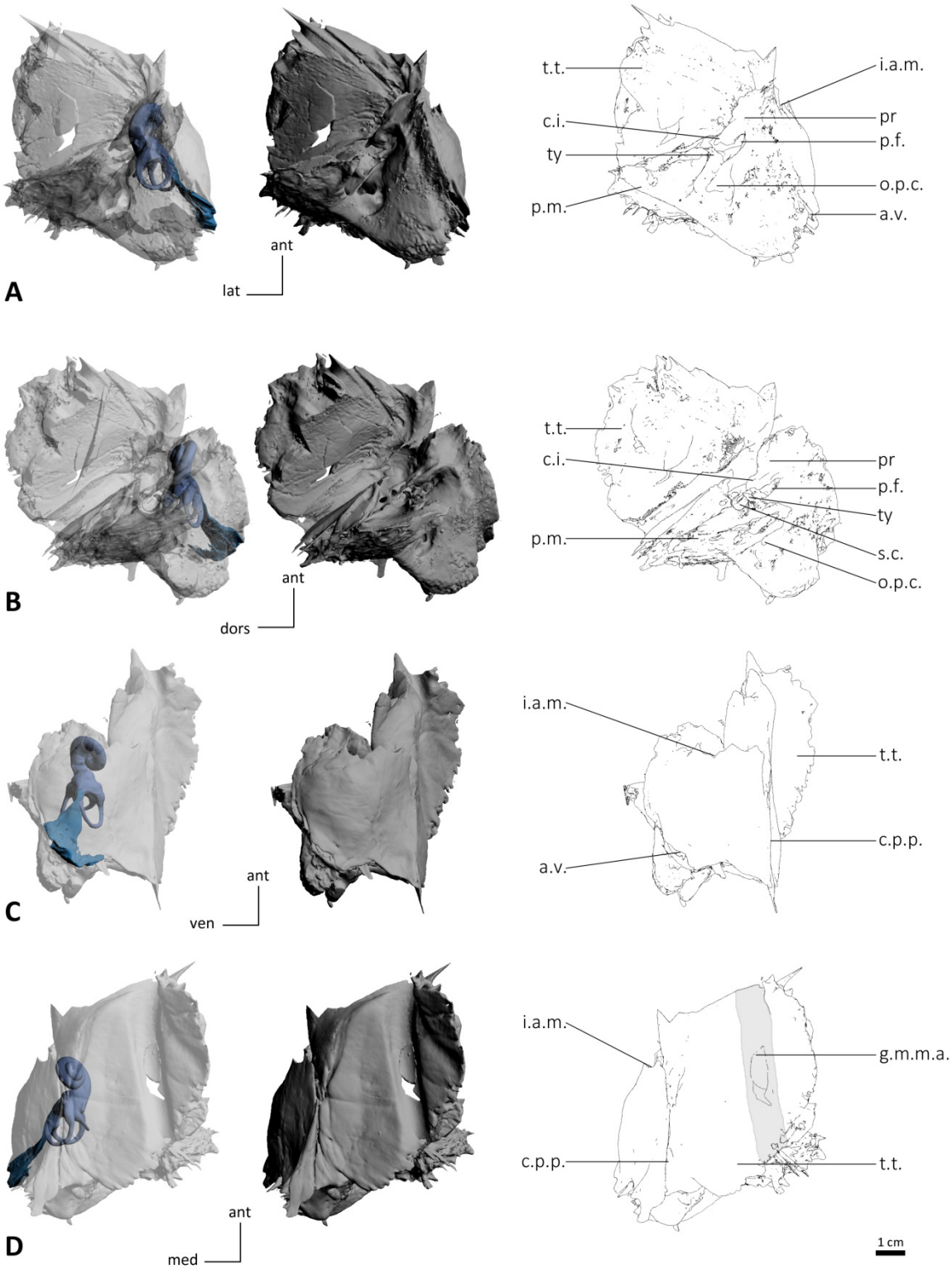

Figure II.16 : 3D models and drawings of the right petrosal of *Loxodonta sp.* MNHN.ZM.AC.1932-523 in tympanic (A), medial (B), cerebellar (C) and cerebral (D) views. **Legends: a.v.** *aquaeductus vestibuli*, **c.i.** *crista interfenestralis*, **c.p.p.** *crista partis petrosa*, **g.m.m.a.** groove for the middle meningeal artery, **i.a.m.** internal auditory meatus, **o.p.c.** opening of a pneumatic cell, **p.f.** perilymphatic foramen, **p.m.** *pars mastoidea*, **pr** *promontorium*, **s.c.** stylomastoid canal, **t.t.** *tegmen tympani,* **ty** tympanohyal.

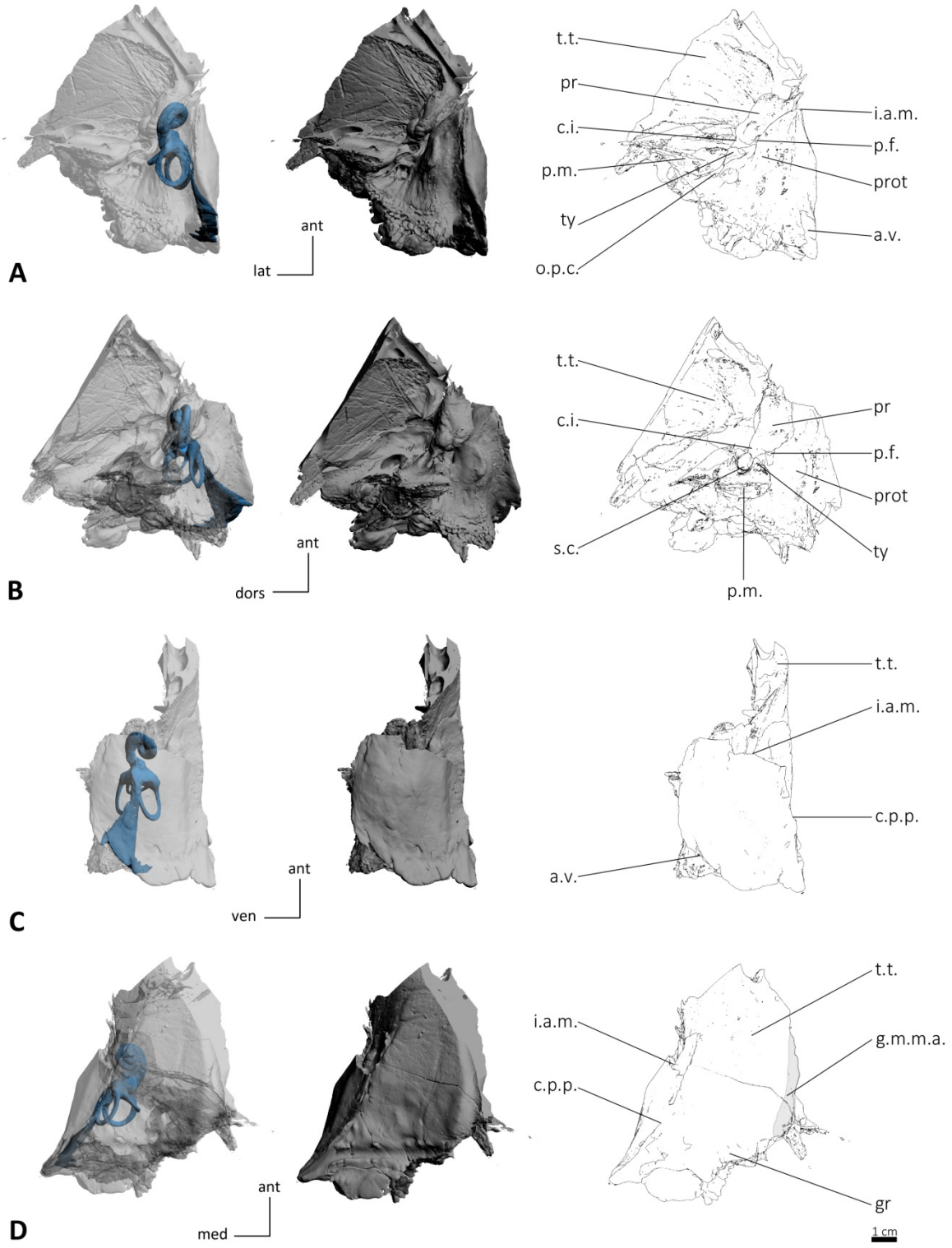

Figure II.17 : 3D models and drawings of the right petrosal of *Loxodonta cyclotis* MNHN.ZM.AC.1956-194 in tympanic (A), medial (B), cerebellar (C) and cerebral (D) views. **Legends: a.v.** *aquaeductus vestibuli*, **c.i.** *crista interfenestralis*, **c.p.p.** *crista partis petrosa*, **g.m.m.a.** groove for the middle meningeal artery, **gr** cerebral groove, **i.a.m.** internal auditory meatus, **o.p.c.** opening of a pneumatic cell, **p.f.** perilymphatic foramen, **p.m.** *pars mastoidea*, **pr** *promontorium*, **prot** protuberance, **s.c.** stylomastoid canal, **t.t.** *tegmen tympani,* **ty** tympanohyal.

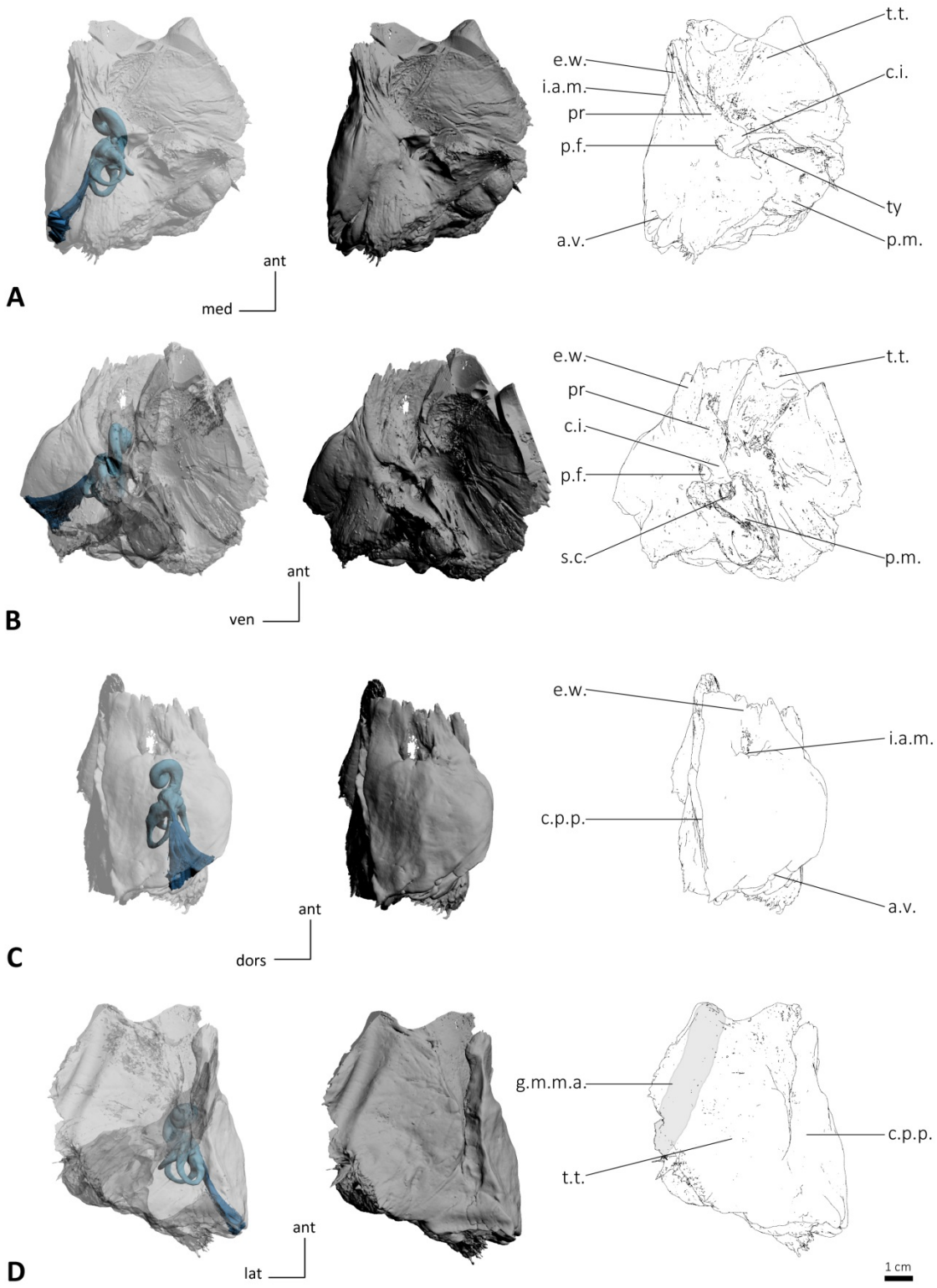

Figure II.18 : 3D models and drawings of the left petrosal of *Loxodonta cyclotis* MNHN.ZM.AC.1957-465 in tympanic (A), medial (B), cerebellar (C) and cerebral (D) views. **Legends: a.v.** *aquaeductus vestibuli*, **c.i.** *crista interfenestralis*, **c.p.p.** *crista partis petrosa*, **e.w**. epitympanic wing, **g.m.m.a.** groove for the middle meningeal artery, **i.a.m.** internal auditory meatus, **p.f.** perilymphatic foramen, **p.m.** *pars mastoidea*, **pr** *promontorium*, **s.c.** stylomastoid canal, **t.t.** *tegmen tympani,* **ty** tympanohyal

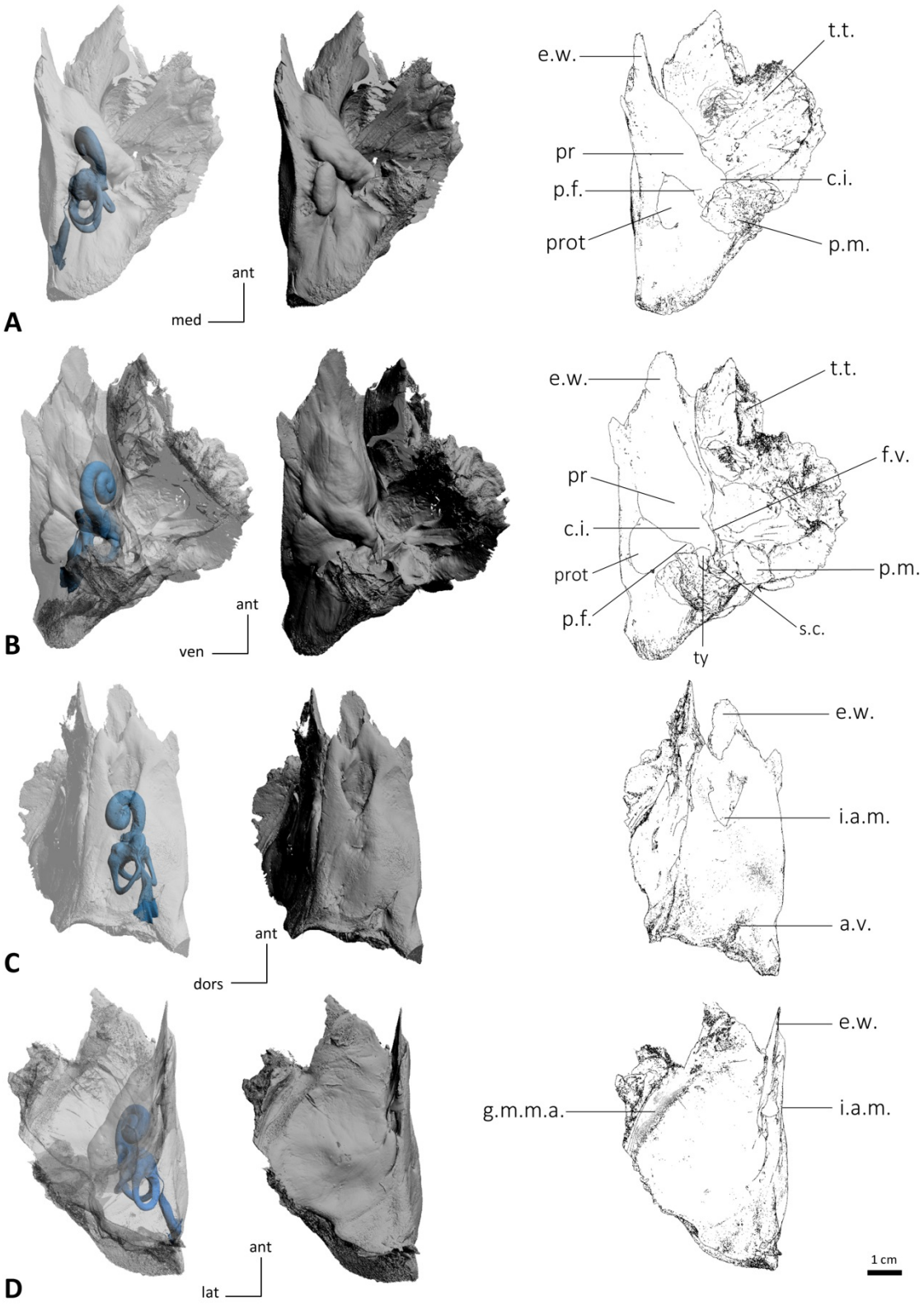

Figure II.19 : 3D models and drawings of the left petrosal of *Loxodonta sp.* MNHN.ZM.AC.2008-71 in tympanic (A), medial (B), cerebellar (C) and cerebral (D) views. **Legends: a.v.** *aquaeductus vestibuli*, **c.i.** *crista interfenestralis*, **e.w**. epitympanic wing, **f.v.** *fenestra vestibuli*, **g.m.m.a.** groove for the middle meningeal artery, **i.a.m.** internal auditory meatus, **p.f.** perilymphatic foramen, **p.m.** *pars mastoidea*, **pr** *promontorium*, **prot** protuberance, **s.c.** stylomastoid canal, **t.t.** *tegmen tympani,* **ty** tympanohyal

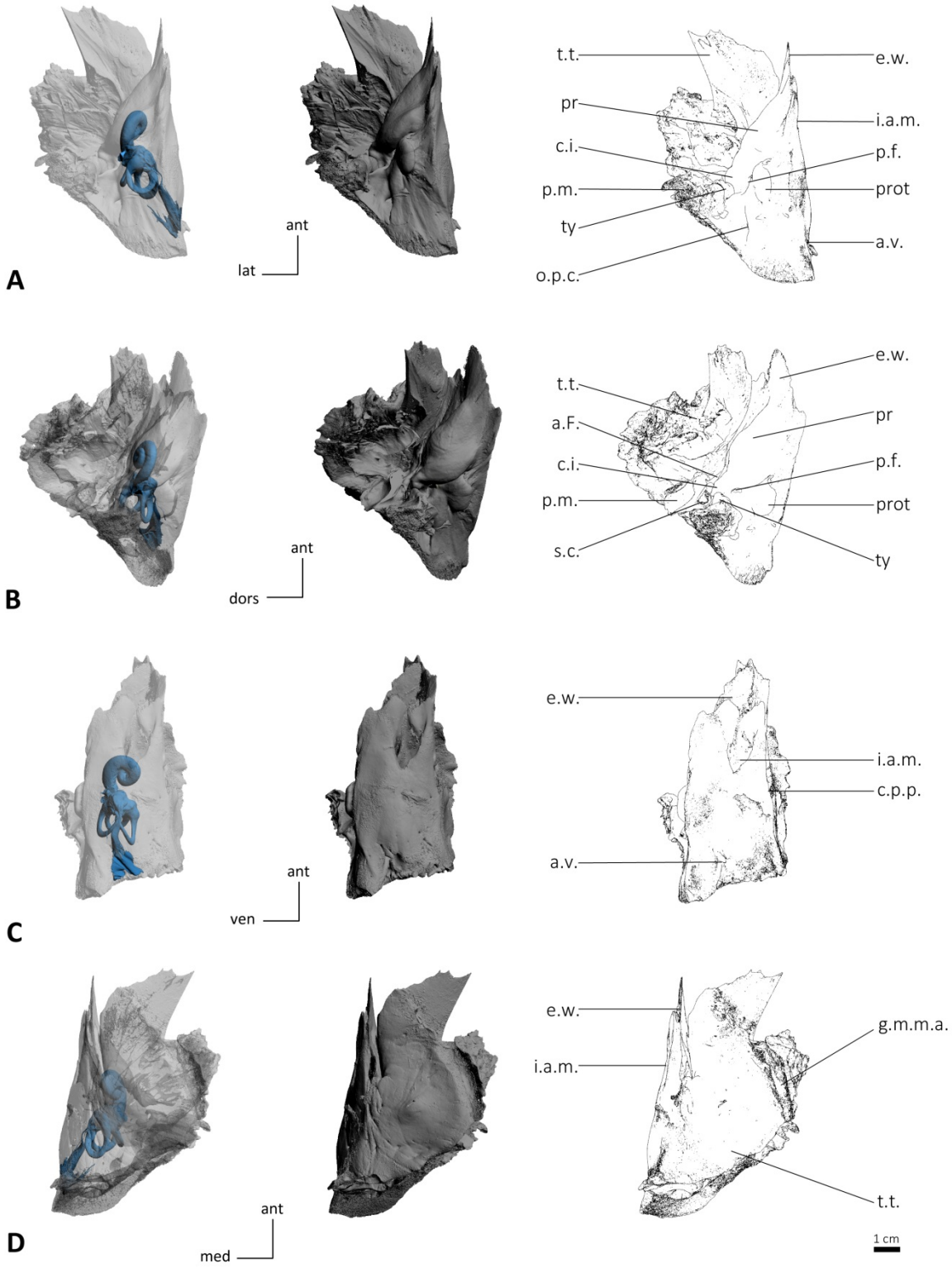

Figure II.20 : 3D models and drawings of the right petrosal of *Loxodonta sp.* MNHN.ZM.AC.2008-71 in tympanic (A), medial (B), cerebellar (C) and cerebral (D) views. Legends: **a.F.** *aquaeductus Fallopii*, **a.v.** *aquaeductus vestibuli*, **c.i.** *crista interfenestralis*, **c.p.p.** *crista partis petrosa*, **e.w**. epitympanic wing, **g.m.m.a.** groove for the middle meningeal artery, **i.a.m.** internal auditory meatus, **o.p.c.** opening of a pneumatic cell, **p.f.** perilymphatic foramen, **p.m.** *pars mastoidea*, **pr** *promontorium*, **prot** protuberance, **s.c.** stylomastoid canal, **t.t.** *tegmen tympani*, **ty** tympanohyal

3.4. Labyrinth

Reconstructed bony labyrinths of extant elephants are illustrated in Fig II.21-25.

3.4.1. *Loxodonta* sp.

Nine specimens of *Loxodonta* were CT-scanned. On one of the nine specimens of *Loxodonta* that were CT-scanned (MNHN.ZM.AC.2008-70), the petrosal is shattered and only a small part of the semicircular canals could be segmented. For each specimen, only one ear was CT-scanned except for MNHN.ZM.AC.2008-71 which both left and right ears were investigated.

Vestibular bony labyrinth

Ampullae

The ampullae of *Loxodonta* are less defined than in most other mammals. While there is a clear demarcation between the ampullar and slender part of the semicircular canals in most mammals, the demarcation is less marked in extant elephants especially when viewed in profile. This feature was already noticed by Benoit et al. (2013b). Some *Loxodonta* specimens display ossification irregularities on their ampullae. The lateral ampulla of the right ear of *Loxodonta* sp MNHN.ZM.AC.2008-71 displays a small protuberance on its vestibular part. This irregularity is not found in the left ear of the same individual. However, a similar structure is visible in *L. cyclotis* MNHN.ZM.AC.1956-194 but it is even less defined. On the other hand, *Loxodonta* sp MNHN.ZM.AC.1932-523 and *L. cyclotis* MNHN.ZM.AC.1957-465 display shallow ridges on each ampulla. They are more defined in MNHN.ZM.AC.1932-523. In this specimen they seem to follow the continuity of the slender part of the canals and continue their course on the vestibule onto the *crus commune*. The lateral and anterior ridges meet at the base of the *crus commune*. A similar ridge is present in *L. cyclotis* MNHN.ZM.AC.1950-728 but only on the anterior ampulla.

Crus commune

The aspect of the *crus commune* varies between specimens of *Loxodonta.* Some specimens display a short and stocky *crus commune* (MNHN.ZM.AC.1861-53, 1956-194, 1957-465, 1961-69, CEB130168) while it is more elongated in other specimens (MNHN.ZM.AC.1932-523, 1950-728, both ears of 2008-71). There is no particular basal thickening of the *crus commune* except for *L. cyclotis* MNHN.ZM.AC.1961-

69 and *Loxodonta* sp 2008-71. Some *Loxodonta* specimens display ossification irregularities on their *crus commune*.

L. africana MNHN.ZM.AC.1861-53 displays a bump at the junction of the posterior and anterior canal ridges. It is located on the anterior side of the crus. *Loxodonta* sp MNHN.ZM.AC.1932-523 displays a vertical ridge on the *crus commune* located in the continuation of the posterior canal ridge. It is associated with a bump below the level of the anterior and posterior canals meeting. There are two ridges on the *crus commune* of *L. cyclotis* MNHN.ZM.AC.1956-194, one in the continuation of the anterior canal ridge and the other in the continuation of the posterior canal ridge. The latter is associated with a bump while another bump is present on the central part of the *crus commune*. Both ridges are very lateral compared to the other specimens ridges. There is a thin salient ridge at the basis of the *crus commune* of *L. cyclotis* MNHN.ZM.AC.1961-69. The left *crus commune* of MNHN.ZM.AC.2008-71 displays a sharp ridge in the continuation of the posterior canal ridge. The right ear of this specimen is different as the *crus commune* is smoother. CEB130168 displays a shallow vertical ridge on its *crus commune*. The average section radii of the *crus commune* of the different *Loxodonta* specimens are given in Table II.3. The radius is particularly large in MNHN.ZM.AC.1957-465 (1.94 mm). In contrast, this value is particularly low in MNHN.ZM.AC.2008-71 (1.13 mm). The values for the *crus commune* length are given in Table II.3. Using these two values, a thickness ratio of the *crus commune* can be calculated. The specimen with the higher ratio (and therefore the thicker *crus commune*) is MNHN.ZM.AC.1957-465 (40.15). MNHN.ZM.AC.1961-69 and CEB130168 also display thick *crus commune* (ratio: respectively 31.33 and 37.23). This is visible directly on the 3D model but the thickness ratio values allow us to quantify and compare the thickness of the *crus commune* of the different specimens. In most specimens, the anterior and posterior semicircular canals meet quite high (approximately at three quarters of the height of the anterior canal). However, the canals meet quite low (approximately at the mid-height of the anterior canal) in MNHN.ZM.AC.1861-53, 1956-194 and CEB130168. The *crus commune* is not inclined in all examined specimens.

Semicircular canals

The anterior semicircular canal is oval in every specimen of *Loxodonta*. The major axis of the canal forms an angle of 40.8° (in average) with the *crus commune*. These values can vary between 32° (CEB130168) and 48° (MNHN.ZM.AC.1961-69). The central streamline length of this semicircular canal varies as well. While the average value is around 25.56 mm, it can vary from 22.30 mm (MNHN.ZM.AC.1961-69) to 31.98 mm (MNHN.ZM.AC.1956-194). The same can be said for the average section radius with values as low as 0.69 mm (MNHN.ZM.AC.1932-523) to values up to 1.06 mm (MNHN.ZM.AC.1961-69). Hence the average thickness ratio is not constant among *Loxodonta* specimens and can be either low (MNHN.ZM.AC.1861-53, 1932-523, 1956-194 and CEB130168 with respective ratios of 2.91, 2.78, 2.63 and 2.88) or higher (MNHN.ZM.AC.1950-728, 1957-465, 1961-69 and 2008-71 with respective ratios of 3.53, 3.75, 4.73 and 3.94). The radii of curvature of the anterior canal of the different specimens vary as well. Most of the specimens have a radius between 5 and 5.8, but MNHN.ZM.AC.1956-194 displays a particularly large radius of curvature of 6.87. The mean value for the anterior canal of *Loxodonta* is 5.67.

The posterior semicircular canal is round in every specimen of *Loxodonta*, but it is more oval in MNHN.ZM.AC.1956-194. The central streamline length of this semicircular canal can vary. The average value is 23.69 mm which is shorter than the anterior canal, and it can vary from 20.61 mm (MNHN.ZM.AC.1961-69) to 29.92 mm (MNHN.ZM.AC.1956-194). The average section radius varies as well with values as low as 0.74 mm (MNHN.ZM.AC.1932-523) to values up to 1.06 mm (MNHN.ZM.AC.1961-69) which is close to the values for the anterior canal. The average thickness ratio varies as well. MNHN.ZM.AC.1956-194 displays a particularly low ratio (2.60) while MNHN.ZM.AC.1961-69 displays the highest value (5.15). The radius of curvature of the posterior canal varies a little less than the radius of the anterior canal. MNHN.ZM.AC.1961-69 displays the lower value (4.78) and MNHN.ZM.AC.1956-194 the higher value (6.25). The mean value for the posterior canal of *Loxodonta* is 5.28.

The overall shape of the lateral semicircular canal is variable between the *Loxodonta* specimens. It is round in MNHN.ZM.AC.1861-53, 1961-69, CEB130168 and MNHN.ZM.AC.1950-728 (particularly in the latter), but it appears

more oval in the other specimens. However the difference is slight and this feature can be interpreted differently among observers. The length of the central streamline of this canal varies less than the previous ones (20.50 to 24.07 mm with a mean value of 21.88 mm). The lateral canal is always the canal with the shortest central streamline value except for MNHN.ZM.AC.2008-71 for which the value is more or less the same as for the other canal. The average section radius varies as well with values as low as 0.67 mm (MNHN.ZM.AC.1932-523) to values up to 0.97 mm (MNHN.ZM.AC.1861-53). Hence the thickness ratio is not constant among *Loxodonta* specimens. It can vary from 3.00 (MNHN.ZM.AC.1956-194) to 4.63 (MNHN.ZM.AC.1861-53). The radius of curvature of this canal does not vary greatly (from 3.15 to 3.73) with a mean value of 3.50.

There are differences between the angle values between semicircular canals of the specimens of *Loxodonta*. There is a difference of more than 12° in the values for the angle between the anterior and posterior canals (from 70.9° in MNHN.ZM.AC.1932-523 up to 84.8° in CEB130168). The difference is 20° in the values for the angle between the anterior and lateral canals (from 59.8° in MNHN.ZM.AC.2008-71 up to 80.0° in MNHN.ZM.AC.1957-465). Finally, there is a difference of almost 16° in the value for the angle between the posterior and lateral canals (from 78.0° in CEB130168 to 93.8° in MNHN.ZM.AC.1956-194). However, despite a certain variability of angle values, some features are quite constant. First, the angle between the lateral and posterior canals is always the largest one except for CEB130168 (this angle value is the same as the anterior-posterior canals angle value in MNHN.ZM.AC.1961-69). This angle tends to be right or almost right with values mostly between 85° and 95°. On the other hand, the angle between the anterior and lateral canals tends to be the smallest one except for MNHN.ZM.AC.1957-465 and MNHN.ZM.AC.1932-523. This angle is always acute and never attains values higher than 80°.

If we compare the radii of curvature, we can first observe a few constant features despite the variability of measurements. The lateral canal is always clearly smaller (mean value of 3.50) than the anterior and posterior canals. The smaller size of the lateral canal is well distinct on the reconstruction. The anterior canal has always a larger radius of curvature (mean value of 5.67) than the

posterior canal (mean value of 5.28) but the difference is lower. The anterior canal apex is located higher than the posterior one. However, this feature is less marked in MNHN.ZM.AC.1950-728. The thickness of the semicircular canals is average to high, depending on the specimens. These observations are confirmed by the values of the average thickness ratio. The average specimens (MNHN.ZM.AC.1861-53, 1932-523, 1956-194 and CEB130168) display rather lower values (3.57, 3.02, 2.74 and 3.28 respectively) than the thicker specimens (MNHN.ZM.AC.1950-728, 1957-465, 1961-69 and 2008-71) that display higher values for this ratio (3.69, 4.01, 4.77 and 3.90). It should be noted that MNHN.ZM.AC.1956-194 is particularly thin compared to the other *Loxodonta* specimens and has a low thickness ratio. All three semicircular canals of *Loxodonta* are flattened in every specimen. This is especially well-marked in MNHN.ZM.AC.1861-53, 1950-728 and 1957-465, and even more in 1956-194. The point of entry of the lateral canal inside the vestibule is located at a low position, near the posterior ampulla. The posterior and lateral semicircular canals are not fused at all. Of all the *Loxodonta* specimens, only MNHN.ZM.AC.1961-69 does not display any ridges on its semicircular canals. Other specimens display a ridge on both the anterior and posterior canals, with exception of MNHN.ZM.AC.1950-728 that has no clear posterior ridge. Usually, all three semicircular canals of *Loxodonta* specimens display an undulation, but there are some exceptions. In MNHN.ZM.AC.1861-53, only the lateral canal is clearly undulated while it is the opposite for MNHN.ZM.AC.1932-523 and MNHN.ZM.AC.1950-728. In CEB130168, only the anterior canal displays a marked undulation.

Cochlear bony labyrinth

The number of turns of the cochlea is not a constant feature amongst studied specimens of *Loxodonta*. MNHN.ZM.AC.1957-465, 1956-194 and 1961-69 display the greatest value which is 2.625 (945°). In MNHN.ZM.AC.1861-53, the cochlea has 2.375 turns (855°) while MNHN.ZM.AC.1932-523 and 1950-728 display only 2.25 turns (810°). Even lower is the number of turns of the cochlea of CEB130168 which is only 2 full turns (720°). But the most peculiar values are unarguably those of MNHN.ZM.AC.2008-71. This is the only *Loxodonta* specimen for which both ears were investigated. The left ear has a low number of turns (two full

turns) but the value remains close to the other specimens. However the right ear displays a strikingly low number of turns (1.625; 585°). Not only is it an unexpected value compared to the other specimens, the difference of value between the left and right ears of the same specimen is extremely high (almost a half turn). This means that this individual heard the sounds differently between its left and right ears. This condition is probably pathological.

In ventral view, the modiolus of both specimens is completely overlapped by the apical turn and there is no visible gap except in CEB130168 which displays a small apical lacuna. The basal turn of the cochlea is only partially overlapped by the apical turn and is still visible in ventral view. The *lamina secundaria* is absent in all specimens. The volume of the cochlea represents roughly between 40% and 50% of the total volume of the bony labyrinth. The average value of the cochlear volume of the *Loxodonta* specimens is 539.6 mm^3. The specimen MNHN.ZM.AC.1956-194 shows a cochlea with a particularly low volume (442 mm^3; 39.5%). On the other hand, MNHN.ZM.AC.1961-69 displays a cochlea that has a particularly high volume (626 mm^3; 48.3%). It is interesting to note that both specimens share the same number of turns (2.625) which is the maximum for *Loxodonta*. Hence a great number of turns does not imply a high cochlear volume.

In profile view, the cochlea of *Loxodonta* is rather planispiral with an average aspect ratio of 0.39 (Table II.4). This ratio varies among *Loxodonta* specimens, with both ears of MNHN.ZM.AC.2008-71 displaying low ratios (left: 0.34, right: 0.30), and MNHN.ZM.AC.1861-53 displaying the highest ratio (0.45). The low ratio seems to depend of the number of turns, since the two cochleae with the lowest number of turns display the lower ratios (especially the right ear of MNHN.ZM.AC.2008-71).

3.4.2. *Elephas maximus*

Four specimens of *Elephas* were studied including one petrosal removed from a fresh cadaver and still preserving the membranous labyrinth. For each specimen, only one ear was CT-scanned.

Vestibular bony labyrinth

Ampullae

The ampullae of *Elephas* are poorly defined compared to most other mammals. As in *Loxodonta*, the

demarcation between the slender part of the canal and the ampulla is less marked in extant elephants especially viewed in profile. Two specimens do not display irregularities on their ampullae (MNHN.ZM.AC.1941-209 and MNHN.ZM.AC.2008-81). The anterior ampulla of MNHN.ZM.AC.1904-273 displays a sharp ridge originating from the inner trajectory of the canal while CEB150009 displays a ridge on its lateral ampulla.

Crus commune

The *crus commune* is stocky in all the specimens of *Elephas*. There is a basal thickening of the *crus commune* (the basis is clearly thicker than for *Loxodonta*). Some *Elephas* specimens display ossification irregularities on their *crus commune*. This is not the case for CEB150009 and MNHN.ZM.AC.1941-209. MNHN.ZM.AC.1904-273 displays a depression at the base of the *crus commune* on the side of the anterior canal. On the other hand, MNHN.ZM.AC.2008-81 displays a thin sharp ridge at the base of the *crus commune* originating from the center and heading towards the anterior canal. *Elephas* specimens display close values for the average section radius of the *crus commune* (from 1.20 mm in MNHN.ZM.AC.1941-209 to 1.51 mm in MNHN.ZM.AC.1904-273). In contrast, the length of this structure is more variable,

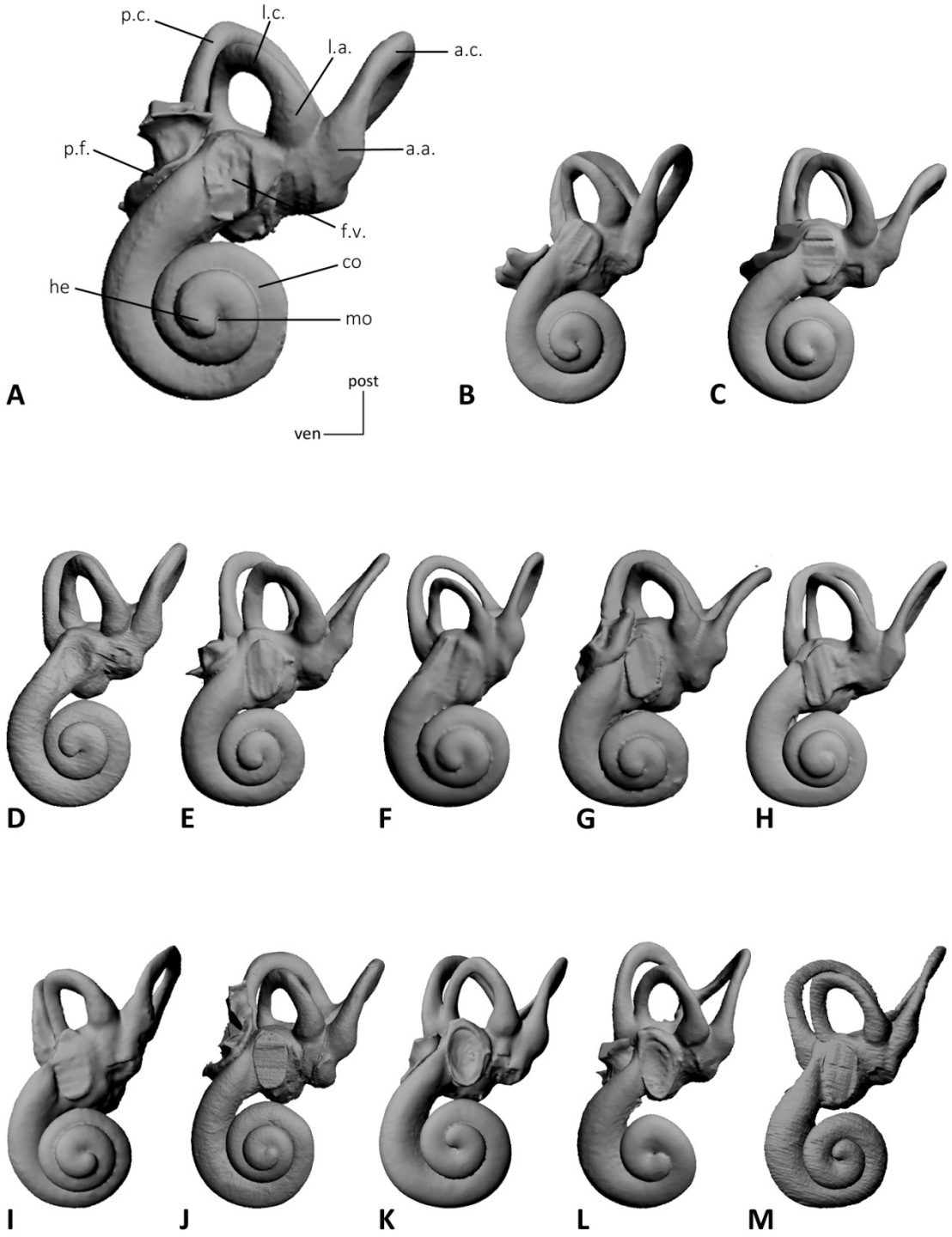

Figure II.21 : Comparative chart representing the 3D reconstructions of the bony labyrinths of extant elephants in ventral view. ***Elephas* specimens:** MNHN.ZM.AC.1904-273 (**A**), 1941-209 (**B**), 2008-81 (**C**) and CEB 150009 (**D**). ***Loxodonta* specimens:** MNHN.ZM.AC.1861-53 (**E**), 1932-523 (**F**), 1950-278 (**G**), 1956-194 (**H**), 1957-465 (**I**), 1961-69 (**J**), 2008-71 left ear (**K**), 2008-71 right ear (**L**) and CEB130168 (**M**). Legends: **a.a.** anterior ampulla, **a.c.** anterior semicircular canal, **co** cochlea, **f.v.** *fenestra vestibuli*, **he** helicotrema**, l.a.** lateral ampulla, **l.c.** lateral semicircular canal, **mo** modiolus, **p.c.** posterior semicircular canal, **p.f.** perilymphatic foramen.

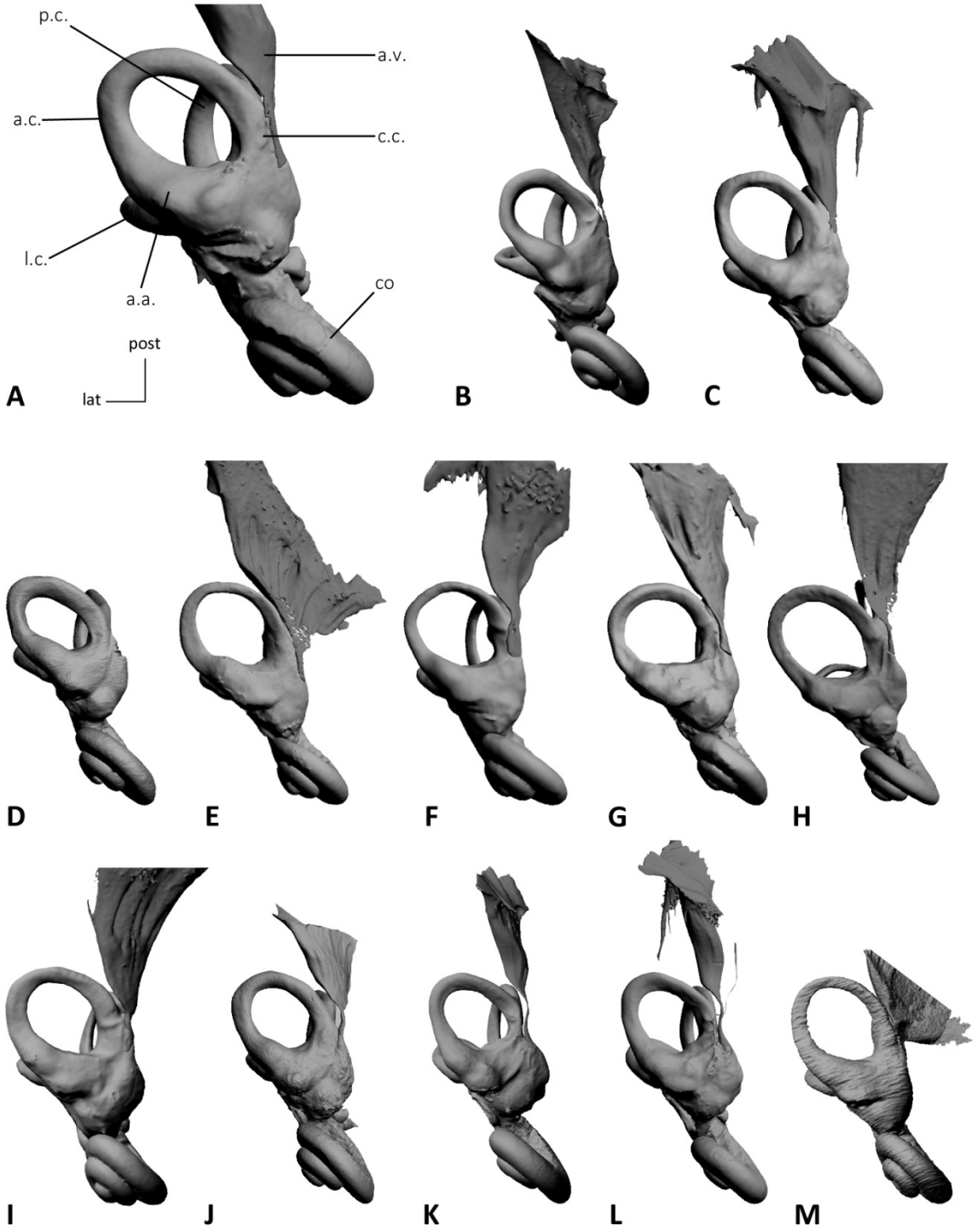

Figure II.22 : Comparative chart representing the 3D reconstructions of the bony labyrinths of extant elephants in the plane of the anterior canal. ***Elephas* specimens:** MNHN.ZM.AC.1904-273 (**A**), 1941-209 (**B**), 2008-81 (**C**) and CEB 150009 (**D**). ***Loxodonta* specimens:** MNHN.ZM.AC.1861-53 (**E**), 1932-523 (**F**), 1950-278 (**G**), 1956-194 (**H**), 1957-465 (**I**), 1961-69 (**J**), 2008-71 left ear (**K**), 2008-71 right ear (**L**) and CEB130168 (**M**). Legends: **a.a.** anterior ampulla, **a.c.** anterior semicircular canal, **a.v.** *aquaeductus vestibuli*, **c.c.** *crus commune*, **co** cochlea, **l.c.** lateral semicircular canal, **p.c.** posterior semicircular canal

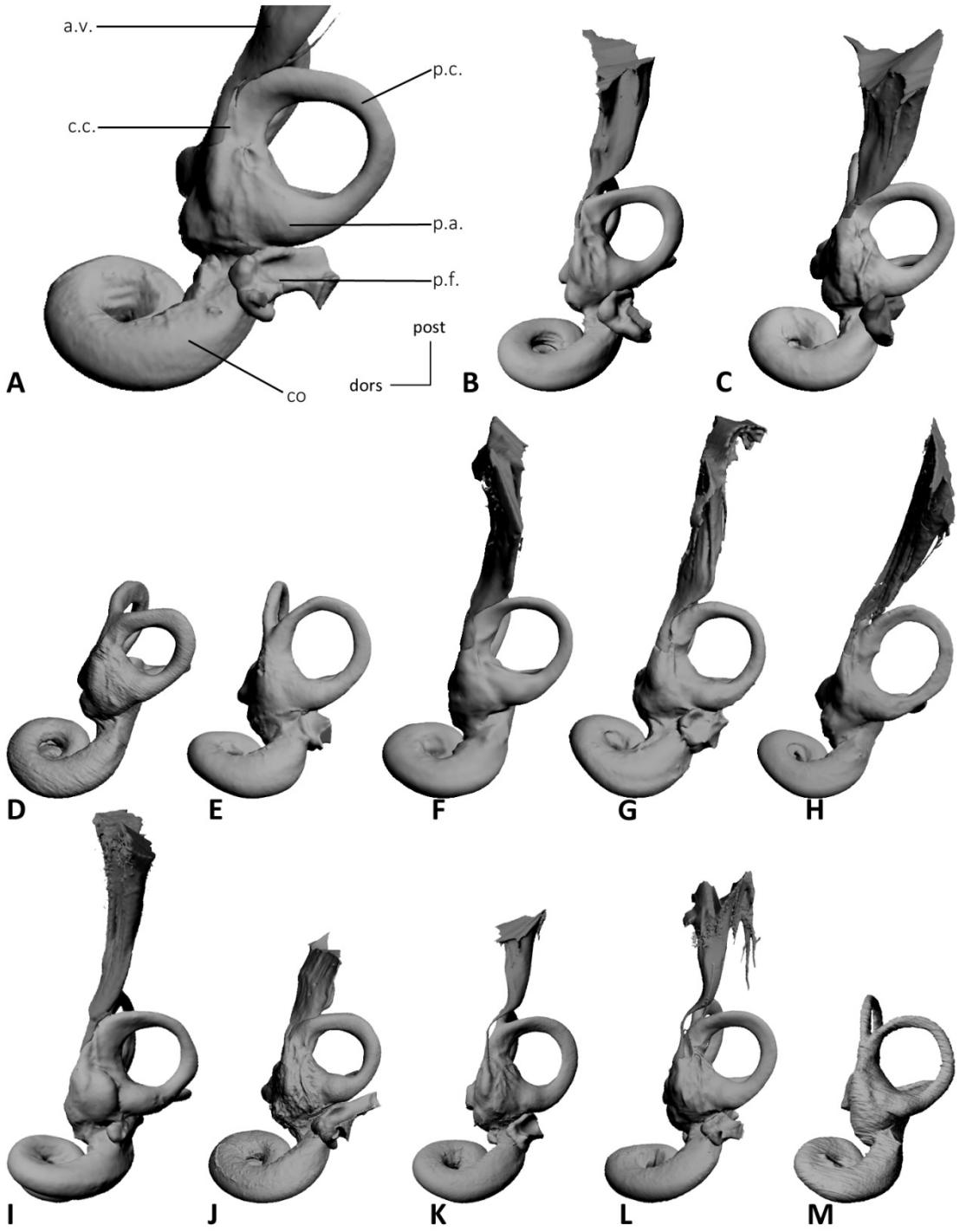

Figure II.23 : Comparative chart representing the 3D reconstructions of the bony labyrinths of extant elephants viewed in the plane of the posterior canal. ***Elephas* specimens:** MNHN.ZM.AC.1904-273 (**A**), 1941-209 (**B**), 2008-81 (**C**) and CEB 150009 (**D**). ***Loxodonta* specimens:** MNHN.ZM.AC.1861-53 (**E**), 1932-523 (**F**), 1950-278 (**G**), 1956-194 (**H**), 1957-465 (**I**), 1961-69 (**J**), 2008-71 left ear (**K**), 2008-71 right ear (**L**) and CEB130168 (**M**). **Legends: a.v.** *aquaeductus vestibuli*, **c.c.** *crus commune*, **co** cochlea, **p.a.** posterior ampulla, **p.c.** posterior semicircular canal, **p.f.** perilymphatic foramen.

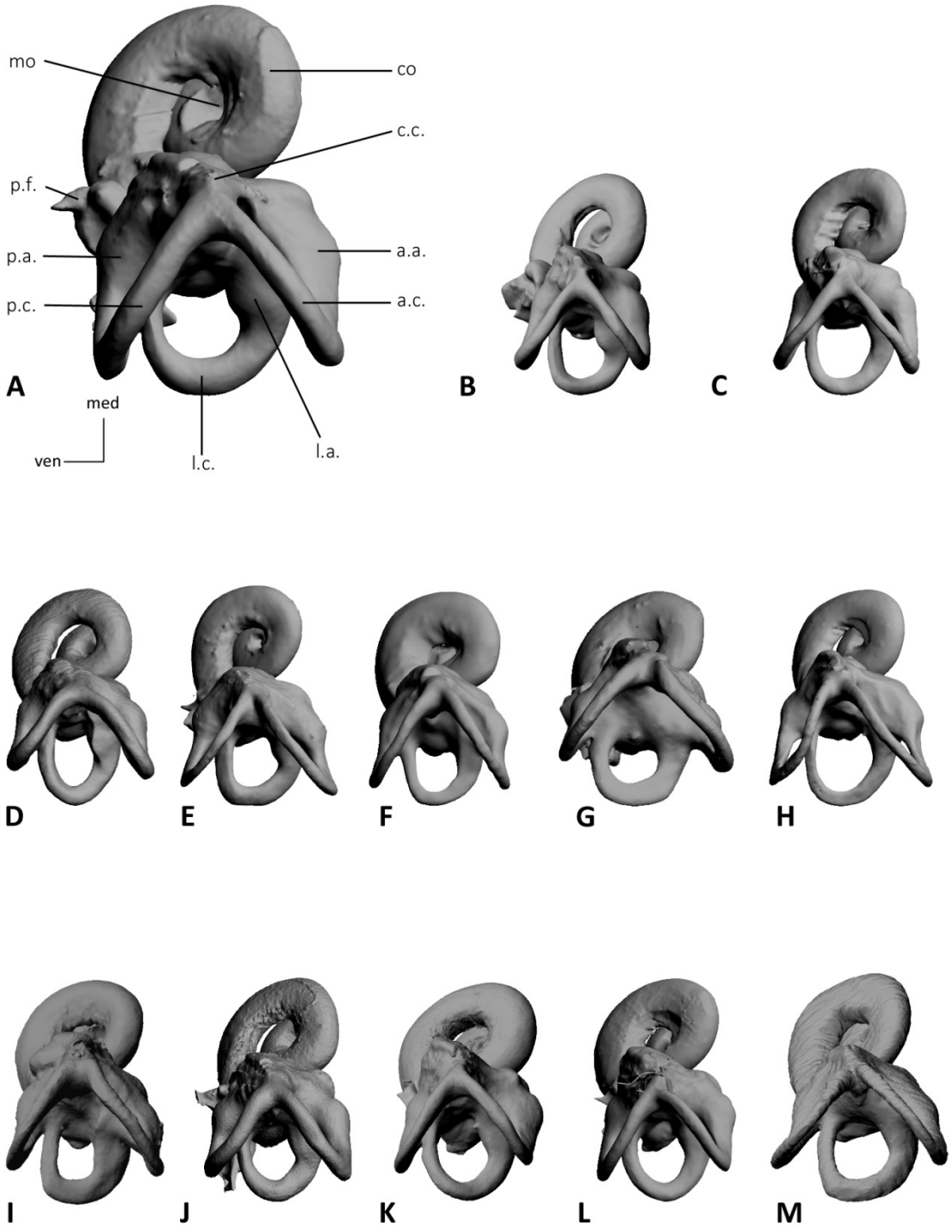

Figure II.24 : Comparative chart representing the 3D reconstructions of the bony labyrinths of extant elephants viewed in the plane of the lateral canal. ***Elephas* specimens:** MNHN.ZM.AC.1904-273 (**A**), 1941-209 (**B**), 2008-81 (**C**) and CEB 150009 (**D**). ***Loxodonta* specimens:** MNHN.ZM.AC.1861-53 (**E**), 1932-523 (**F**), 1950-278 (**G**), 1956-194 (**H**), 1957-465 (**I**), 1961-69 (**J**), 2008-71 left ear (**K**), 2008-71 right ear (**L**) and CEB130168 (**M**). **Legends: a.a.** anterior ampulla, **a.c.** anterior semicircular canal, **c.c.** *crus commune*, **co** cochlea, **l.a.** lateral ampulla, **l.c.** lateral semicircular canal, **mo** modiolus, **p.a.** posterior ampulla, **p.c.** posterior semicircular canal, **p.f.** perilymphatic foramen.

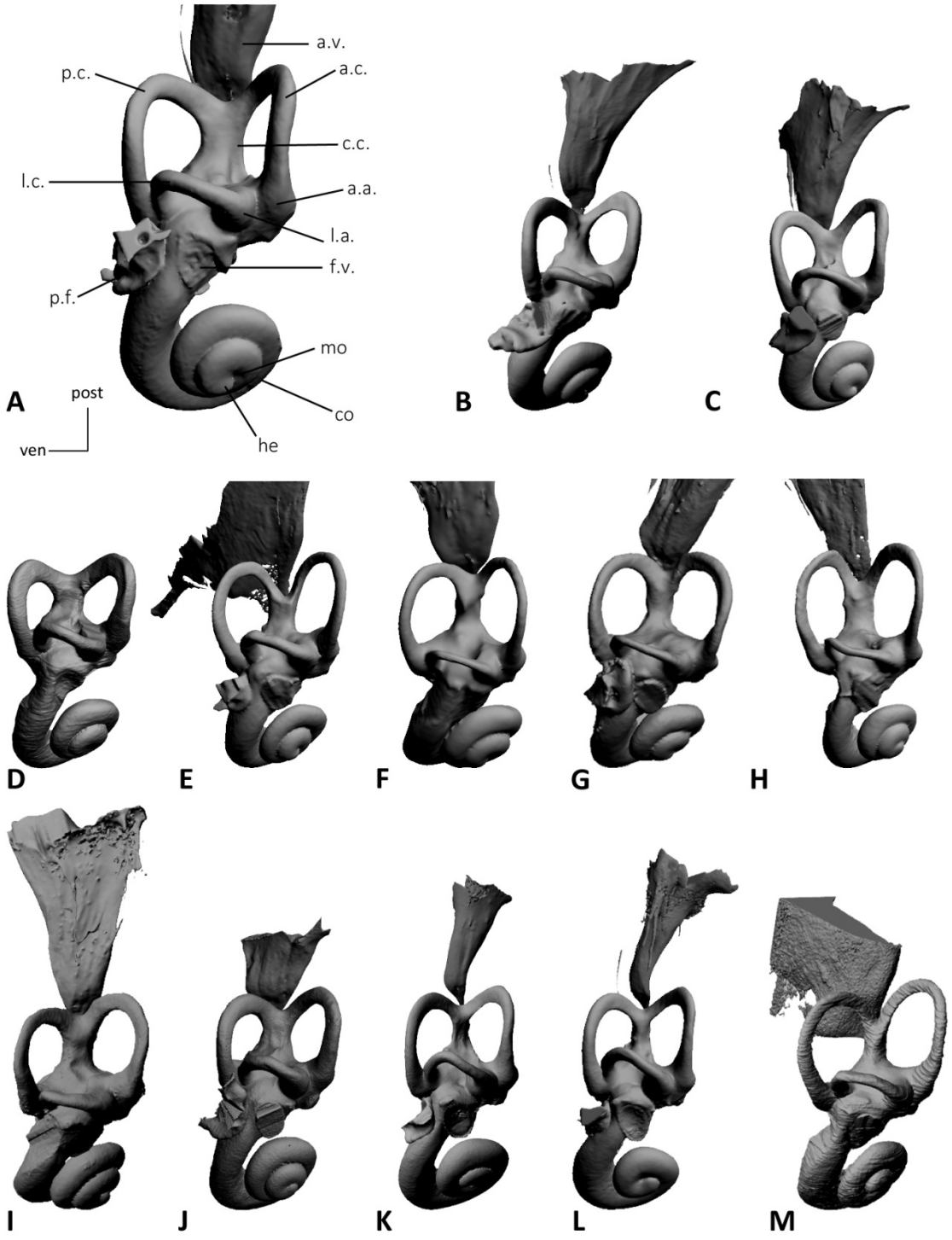

Figure II.25 : Comparative chart representing the 3D reconstructions of the bony labyrinths of extant elephants in frontal view. ***Elephas* specimens:** MNHN.ZM.AC.1904-273 (**A**), 1941-209 (**B**), 2008-81 (**C**) and CEB 150009 (**D**). ***Loxodonta* specimens:** MNHN.ZM.AC.1861-53 (**E**), 1932-523 (**F**), 1950-278 (**G**), 1956-194 (**H**), 1957-465 (**I**), 1961-69 (**J**), 2008-71 left ear (**K**), 2008-71 right ear (**L**) and CEB130168 (**M**). Legends: **a.a.** anterior ampulla, **a.c.** anterior semicircular canal, **a.v.** *aquaeductus vestibuli*, **c.c.** *crus commune*, **co** cochlea, **f.v.** *fenestra vestibuli*, **he** helicotrema, **l.a.** lateral ampulla, **l.c.** lateral semicircular canal, **mo** modiolus, **p.c.** posterior semicircular canal, **p.f.** perilymphatic foramen.

with specimens displaying a shorter *crus commune* (CEB 150009 and MNHN.ZM.AC.1941-209 with respective lengths of 3.07 mm and 5.58 mm) and the other specimens displaying longer values for this structure (6.53 mm and 7.11 mm in MNHN.ZM.AC.2008-81 and MNHN.ZM.AC.1904-273 respectively). CEB 150009 has the thickest *crus commune*, with a thickness ratio of 49.20. In MNHN.ZM.AC.1904-273 and MNHN.ZM.AC.1941-209, the anterior and posterior semicircular canals meet quite high (approximately at three quarters of the height of the anterior canal). However the canals meet quite low (approximately at the mid-height of the anterior canal) in MNHN.ZM.AC.2008-81 and CEB 150009. The *crus commune* is not inclined on any specimen.

Semicircular canals

The anterior semicircular canal is oval in every specimen of *Elephas*. The oval shape of this canal is particularly well-marked in CEB150009. The major axis of the canal forms an angle of 39.5° (in average) with the *crus commune*. Most specimens display values slightly greater than 40° (41° in MNHN.ZM.AC.1941-209 and MNHN.ZM.AC.1904-273 and 46° in CEB 150009), but MNHN.ZM.AC.2008-81 is different with a smaller angle (30°). The central streamline length of the anterior canal is similar among all specimens (around 23 mm), except for MNHN.ZM.AC.2008-81 which is longer (26.66 mm). The average section radius is variable (from 0.91 mm in MNHN.ZM.AC.2008-81 to 1.16 mm in CEB 150009). Hence, the average thickness ratio is not constant among the specimens. CEB150009 has a particularly thick anterior canal (ratio of 4.93) while MNHN.ZM.AC.2008-81 has a thinner anterior canal (ratio of 3.43). The anterior canals of MNHN.ZM.AC.1941-209 and MNHN.ZM.AC.1904-273 are average. In *Elephas*, the radius of curvature of the anterior canal is more or less the same among specimens. The mean value for the anterior canal of *Elephas* is 5.36.

The posterior semicircular canal is round in every specimen of *Elephas*. The values of the central streamline length for the posterior canal are comparable to those of the anterior canal. However, this canal is shorter than the anterior canal in MNHN.ZM.AC.2008-81 (24.56 mm) and CEB150009 (21.01 mm). The average section radius varies as well but less so than for the anterior canal (from 0.96 mm in MNHN.ZM.AC.2008-81 to 1.15 mm in CEB150009). CEB 150009 also displays the

thickest posterior canal (average thickness ratio of 5.46) and MNHN.ZM.AC.2008-81 displays the thinnest posterior canal (ratio of 3.91). The radius of curvature of the posterior canal of CEB150009 is particularly small (4.65) while it is large in MNHN.ZM.AC.2008-81 (5.60). The average value for the posterior canal is 5.17.

The overall shape of the lateral semicircular canal varies among *Elephas* specimens. It is round in MNHN.ZM.AC.1904-273, while it is oval in the three other studied specimens. The oval condition is especially marked in CEB 150009. The length of the central streamline of this canal varies greatly between 20.33 mm (MNHN.ZM.AC.1904-273) and 26.07 mm (MNHN.ZM.AC.2008-81). The length values for this canal are comparable to the values for the other canals. However, the average section radius is always smaller for this canal than for the other two. The radius of curvature of this canal is particularly small in MNHN.ZM.AC.1904-273 (3.16). MNHN.ZM.AC.2008-81 displays the greater radius (4.06). The mean value for the lateral canal is 3.60.

The angles between the semicircular canals are not constant in *Elephas*. There is a difference of roughly 6° in the values for the angle between the anterior and posterior canals (from 72.6° in MNHN.ZM.AC.1904-273 up to 78.9° in CEB 150009). The difference is around 8° for the angle values between the anterior and lateral canals (from 67.9° in CEB 150009 up to 75.7° in MNHN.ZM.AC.1904-273). The variability is lower (around 6°) for the angle values between the posterior and lateral canals (from 83.2° in MNHN.ZM.AC.1941-209 up to and 88.8° in MNHN.ZM.AC.1904-273). The angle between the lateral and posterior canals is always the greatest one. It tends to be almost right with an average value of 85.9°. The angles between the anterior and lateral canals and between the anterior and posterior canals have more similar values and are always acute. They are roughly the same in MNHN.ZM.AC.1904-273, 1941-209 and 2008-81, while it varies more in CEB 150009 which has a much greater angle between the anterior and posterior canals (78.9°) than between the anterior and lateral canals (67.9°). In general, the radius of curvature is always the greatest in the anterior canal in *Elephas*. However, in MNHN.ZM.AC.1941-209, the posterior canal has a greater radius of curvature. On the other hand, the lateral canal is always and by far the smallest one with an average value of 3.60 (the average value is

5.36 for the anterior canal and 5.17 for the posterior canal). The anterior canal apex is always located higher than the posterior one. The global thickness of the semicircular canals varies slightly in *Elephas* specimens. The canals of CEB 150009 are particularly thick (the average thickness ratio of the three canals is 4.86), while those of MNHN.ZM.AC.1941-209 and 1904-273 are also thick but more average (respective ratios of 4.13 and 4.64). In contrast, the canals of MNHN.ZM.AC.2008-81 are thinner (ratio of 3.52) compared to the other *Elephas* specimens. All three semicircular canals are flattened among *Elephas* specimens. It is particularly marked in MNHN.ZM.AC.2008-81. The point of entry of the lateral canal inside the vestibule is located at a low position, near the posterior ampulla as in *Loxodonta*. CEB 150009 does not display clear ridges on the slender part of its semicircular canals. In MNHN.ZM.AC.2008-81 there are sharp posterior and anterior ridges. In MNHN.ZM.AC.1941-209, there is a very sharp ridge on the anterior canal and a shallower one on the lateral canal, while only a sharp anterior ridge is found in MNHN.ZM.AC.1904-273. In CEB 150009, MNHN.ZM.AC.1941-209 and 1904-273, the three semicircular canals are well undulated. However, in MNHN.ZM.AC.2008-81, the lateral canal undulation is moderate, while the anterior canal undulation is particularly developed.

Cochlear bony labyrinth

There is a small variability in the number of turns of the cochlea amongst the four studied specimens of *Elephas*. In MNHN.ZM.AC.1904-273, 1941-209 and 2008-81, the number of turns is 2.375 (855°) but it is a little less in CEB 150009 (2.25; 810°). In ventral view, the modiolus of both specimens is completely overlapped by the apical turn and there is no visible apical lacuna. The basal turn of the cochlea is only partially overlapped by the apical turn and is still visible in ventral view. The *lamina secundaria* is absent in every specimen. The volume of the cochlea represents roughly 50% of the total volume of the bony labyrinth in each specimen except CEB 150009 which displays lower values (43.5%). This can be partially explained by the particularly voluminous semicircular canals of this specimen but the cochlear volume of this specimen is also strikingly small compared to the other specimens (518 mm^3). This could also be explained by the smaller number of turns of this specimen. The

average value for the cochlear volume in *Elephas* is 597.2 mm^3. As in *Loxodonta*, the cochlea appears planispiral in profile view, with an average aspect ratio of 0.39.

Membranous vestibular labyrinth

The complete membranous labyrinth is preserved in *Elephas* specimen CEB150009. However, only the upper (vestibular) part is discussed here. The remaining part of the membranous labyrinth (cochlear duct, cochlear *scalae*, saccule, innervation, vascularization…) has yet to be segmented and will be described in a separate work. The membranous vestibular system of *Elephas* is compared here with the afrotherians *Procavia* and *Elephantulus*, for which both ears were segmented in this study.

In general, the semicircular ducts of *Elephas* are much thinner than the bony canals with respect to *Elephantulus* and *Procavia* (Fig. II.26). In the latter, the membranous ducts fill the bony canals almost entirely while in *Elephas* the ducts represent only a small part of the bony volume. This could suggest that large mammals tend to have a membranous labyrinth relatively less voluminous than the bony labyrinth. The difference between the bony labyrinth volume and the effective endolymphatic volume of the membranous labyrinth in *Elephas* is very important to point out on the studies of the functional capacities of extinct proboscideans (Chapter VI). Indeed, calculations of the endolymphatic fluid motion are highly biased if the volume of the bony labyrinth is used instead of the volume of the membranous labyrinth.

On the other hand, the semicircular ducts are always located in the most peripheral part of the bony canals in all three specimens. The ossifications irregularities of the bony labyrinth previously described in this chapter do not appear to result from irregularities located on the membranous labyrinth. For instance, the lateral bony ampulla of *Elephas* exhibits a very salient ridge but there are no irregularities at this location on the lateral membranous ampulla.

In a view in the plane of the anterior semicircular duct (Fig. II.27), the shape formed by the latter is oval. However, it appears less oval than the anterior semicircular canal in which it is contained. Its great axis is oriented slightly differently than that of the bony canal and it forms a lower angle with the *crus commune* than in *Procavia*, which great axis forms an

almost right angle with the *crus commune*. As in the bony labyrinth, its apex is located higher than that of the posterior duct.

The slender part of the anterior duct is particularly thin compared to the bony canals. Its length represents approximately two thirds of the total length of the anterior duct. Its cross-section is circular contrary to the flattened cross-section of the bony ducts. The thickness of the slender part of the anterior duct is rather constant along the duct except at the level of its connection with the *crus commune* and at the level of its connection with the anterior ampulla where the slender part of the duct progressively thickens. This results in a lesser defined ampulla in *Elephas* than in *Procavia* and *Elephantulus* which do not exhibit such thickening at this location. Hence, the thickening of the canals resulting in poorly defined bony ampullae in the bony labyrinth of extant elephants is a feature also observed in the membranous labyrinth, but to a lesser extent. The slender anterior duct enters almost parallel to the great axis of the anterior ampulla, contrary to *Procavia* and *Elephantulus* in which the duct enters the ampulla more ventrally (especially in *Procavia*). On the other hand, the angle formed by the slender anterior duct and the *crus commune* at the level of their connection is similar to that of *Procavia* and *Elephantulus*.

The *crus commune* length represents only a small part of the total anterior semicircular duct length (one sixth at most). This differs from *Procavia* and *Elephantulus* which *crus commune* represents around one fourth of the total length of the anterior duct. It does not exhibit a particular curving in any of the sampled afrotherians. Its cross-section is thicker (approximately twice) than that of the slender duct. From the apex to the base of the crus, the area of the cross-section increases. In parallel, the cross-section of the *crus commune* changes from an oval form (close to the apex) to a rounder form (close to the base). The distal part of the *crus commune* is connected slightly obliquely to the proximal part of the common utricle. This utricular section is the part where the streamlines of all three semicircular ducts meet. It is strikingly thick in elephants compared to *Procavia* and *Elephantulus*, and even to mammals in general (pers. comm. Romain David 2016).

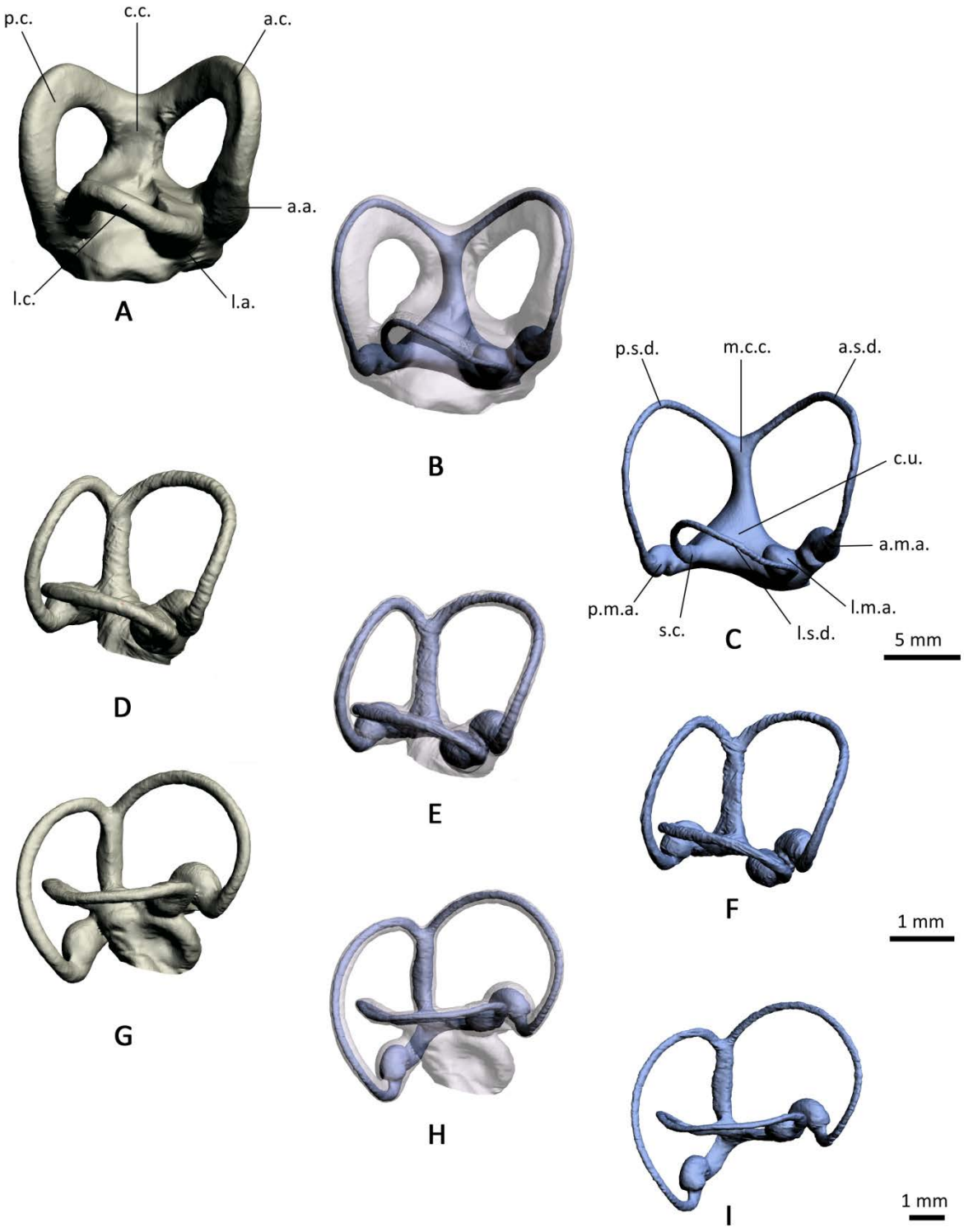

Figure II.26 : Bony (A,D,G), membranous (C, E, H) and both (C,F,I) labyrinths of *Elephas* (A-C) compared with those of *Elephantulus* (D-F) and *Procavia* (G-I) in frontal view. Legends: **a.a.** anterior ampulla, **a.c.** anterior semicircular canal, **a.m.a.** anterior membranous ampulla, **a.s.d.** anterior semicircular duct, **c.c.** *crus commune*, **c.u.** common utricle, **l.a.** lateral ampulla, **l.c.** lateral semicircular canal, **l.m.a.** lateral membranous ampulla, **l.s.d.** lateral semicircular duct, **m.c.c.** membranous *crus commune*, **p.c.** posterior semicircular canal, **p.m.a.** posterior membranous ampulla, **p.s.d.** posterior semicircular duct, **s.c.** simple crus.

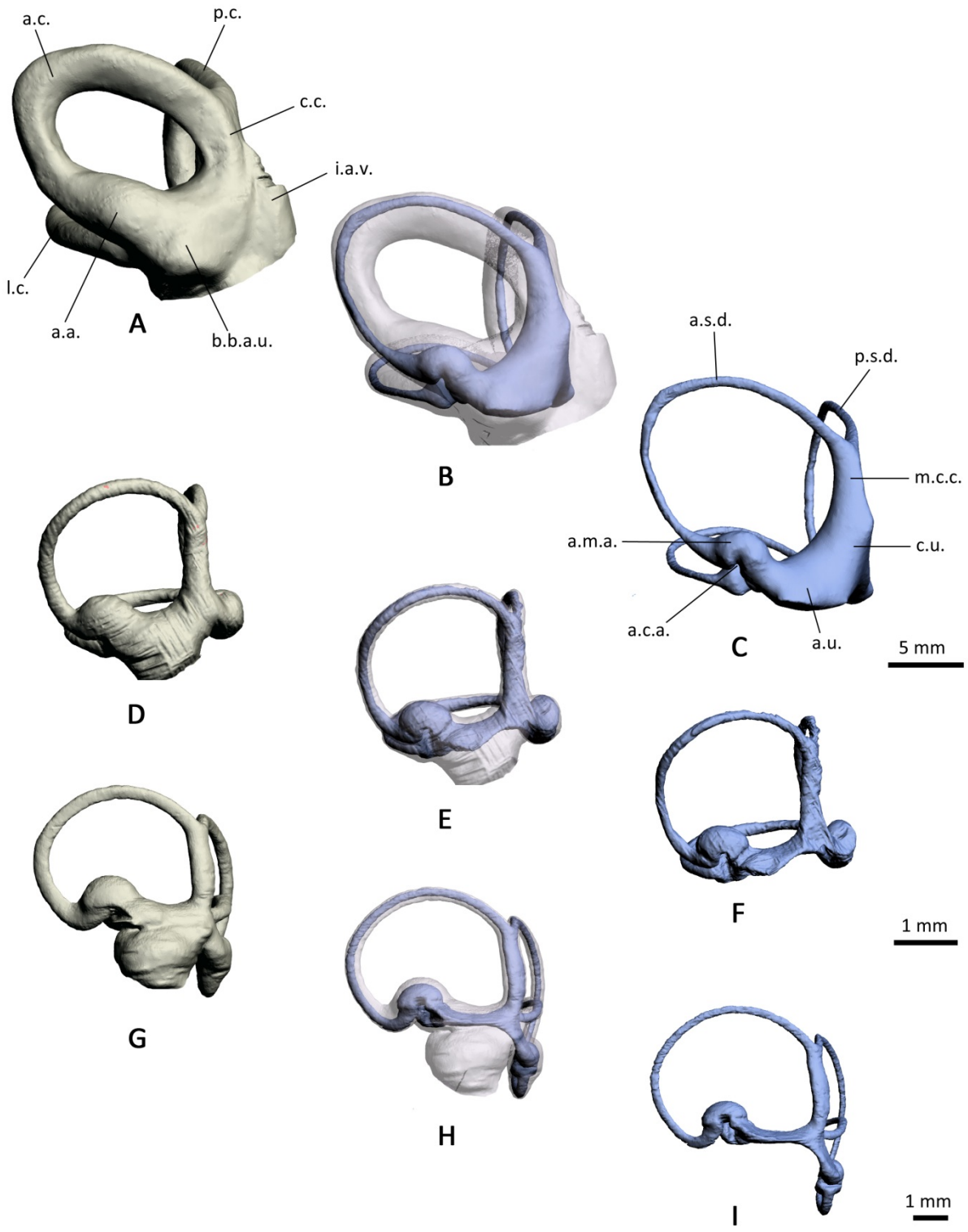

Figure II.27 : Bony (A,D,G), membranous (C, E, H) and both (C,F,I) labyrinths of *Elephas* (A-C) compared with those of *Elephantulus* (D-F) and *Procavia* (G-I) in the plane of the anterior semicircular canal. Legends: **a.a.** anterior ampulla, **a.c.** anterior semicircular canal, **a.c.a.** anterior crista ampullaris, **a.m.a.** anterior membranous ampulla, **a.s.d.** anterior semicircular duct, **a.u.** anterior utricle, **b.b.a.u.** bony bulge for the anterior utricle, **c.c.** *crus commune*, **c.u.** common utricle, **i.a.v.** insertion of the *aquaeductus vestibuli*, **l.c.** lateral semicircular canal, **m.c.c.** membranous *crus commune*, **p.c.** posterior semicircular canal, **p.s.d.** posterior semicircular duct.

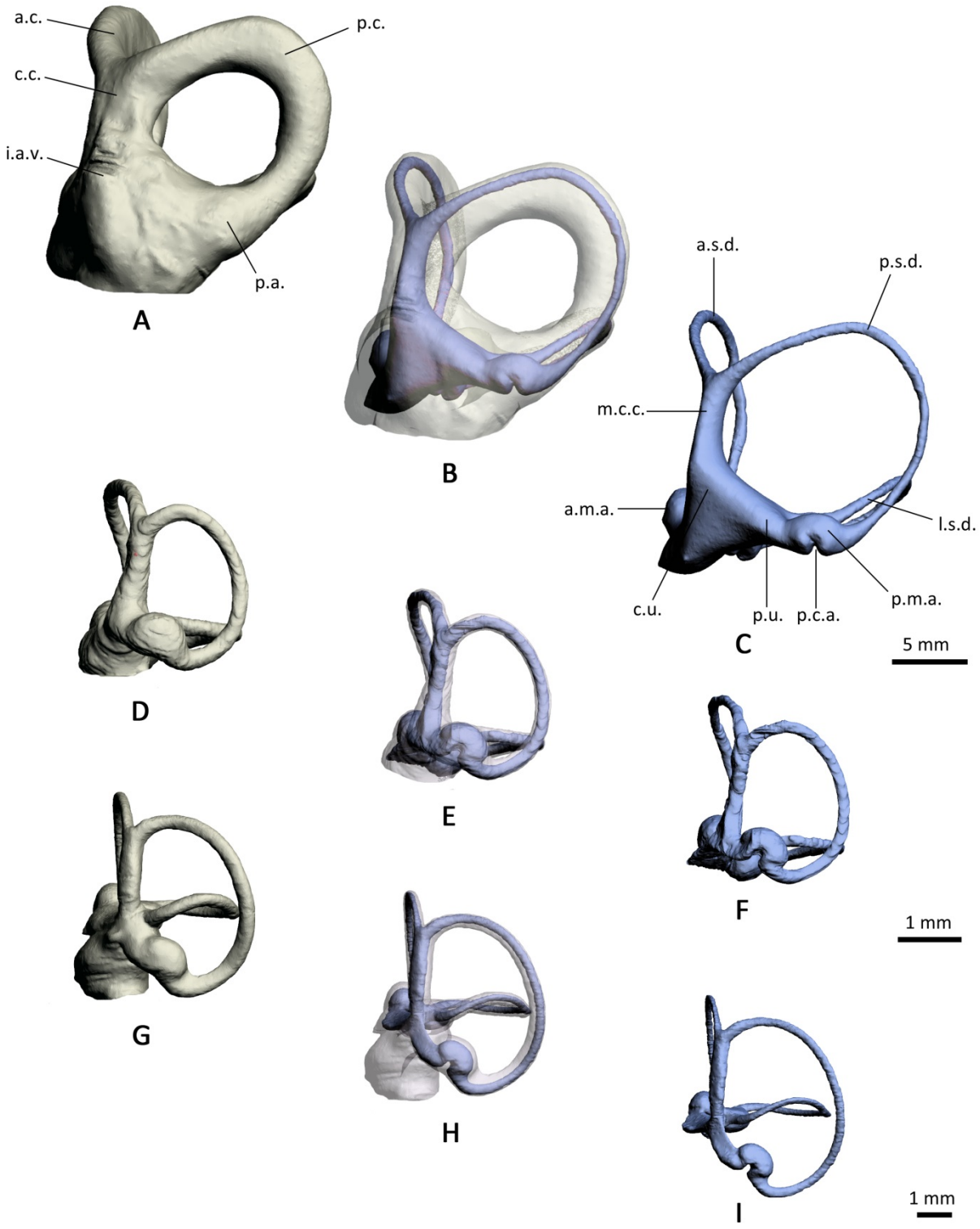

Figure II.28 : Bony (A,D,G), membranous (C, E, H) and both (C,F,I) labyrinths of *Elephas* (A-C) compared with those of *Elephantulus* (D-F) and *Procavia* (G-I) in the plane of the posterior semicircular canal. Legends: **a.c.** anterior semicircular canal, **a.m.a.** anterior membranous ampulla, **a.s.d.** anterior semicircular duct, **c.c.** *crus commune*, **c.u.** common utricle, **i.a.v.** insertion of the *aquaeductus vestibuli*, **l.s.d.** lateral semicircular duct, **m.c.c.** membranous *crus commune*, **p.a.** posterior ampulla, **p.c.** posterior semicircular canal, **p.c.a.** posterior *crista ampullaris*, **p.m.a.** posterior membranous ampulla, **p.s.d.** posterior semicircular duct, **p.u.** posterior utricle.

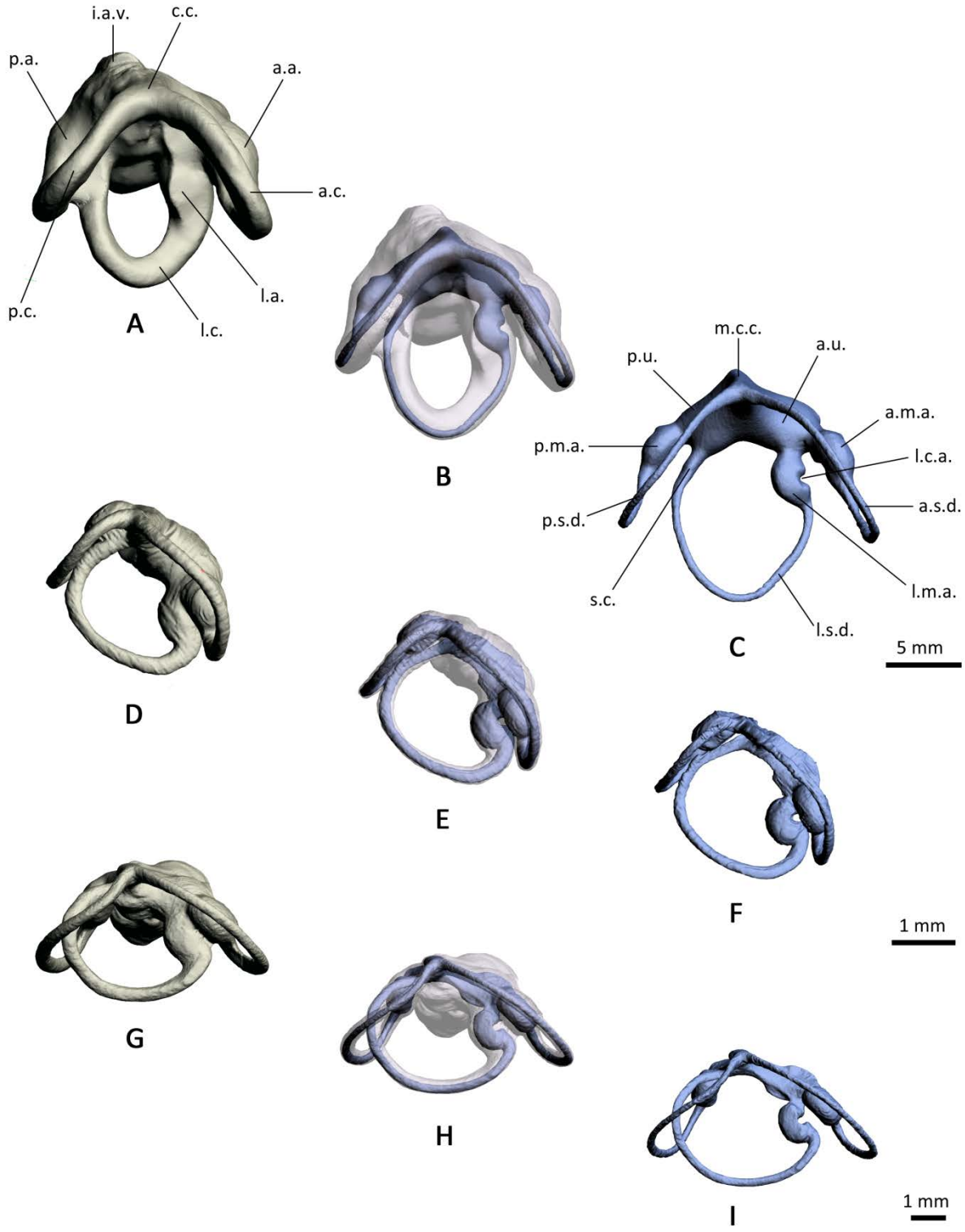

Figure II.29 : Bony (A,D,G), membranous (C, E, H) and both (C,F,I) labyrinths of *Elephas* (A-C) compared with those of *Elephantulus* (D-F) and *Procavia* (G-I) in the plane of the lateral semicircular canal. Legends: **a.a.** anterior ampulla, **a.c.** anterior semicircular canal, **a.m.a.** anterior membranous ampulla, **a.s.d.** anterior semicircular duct, **a.u.** anterior utricle, **c.c.** *crus commune*, **i.a.v.** insertion of the *aquaeductus vestibuli*, **l.a.** lateral ampulla, **l.c.** lateral semicircular canal, **l.c.a.** lateral crista ampullaris, **l.m.a.** lateral membranous ampulla, **l.s.d.** lateral semicircular duct, **m.c.c.** membranous *crus commune*, **p.a.** posterior ampulla, **p.c.** posterior semicircular canal, **p.m.a.** posterior membranous ampulla, **p.s.d.** posterior semicircular duct, **p.u.** posterior utricle, **s.c.** simple crus.

The anterior utricle is also very prominent in *Elephas* compared to *Procavia* and *Elephantulus*. Its thickness decreases from the common utricle to the connection with the anterior and lateral ampullae contrary to the other sampled afrotherians which display an enlargement of the anterior utricle in the ampullar part. The cross-section is triangular in the common utricle part and progressively takes a rounder form in the ampullar part. This contrasts with the shape of the cross-section in *Procavia* and *Elephantulus* which is flattened. An enlarged ridge runs along the external part of the anterior utricle as in *Procavia* and *Elephantulus*. It is very prominent to the point of leaving a trace on the bony labyrinth. Indeed, there is prominent bony bulge at this level that clearly houses this membranous structure (Fig. II.27A, **b.b.a.u.** bony bulge for the anterior utricle).

The anterior ampulla connects with the anterior utricle in a smoother manner than in *Procavia* and *Elephantulus,* in which (particularly in *Procavia*) the anterior utricle enters the anterior ampulla more ventrally. The anterior ampulla is clearly bulbous but the connection points with the anterior utricle and the anterior slender duct thickens progressively. The *crista ampullaris* is clearly visible in the reconstruction. It consists of a very marked ridge located at the center of the ampulla. It has the shape of a semi-catenoid when viewed from the top. The *crista ampullaris* concentrates hair cells which ciliae are embed in a more or less rigid – though deformable – structure called the cupula. The relative size of the *crista ampullaris* is similar to that of *Procavia* and *Elephantulus* and none of the three sampled afrotherians display an *eminentia cruciata*, which is a *crista ampullaris* that has the shape of a cross when viewed ventrally (Igarashi and Yoshinobu, 1966).

In a view in the plane of the posterior semicircular duct (Fig. II.28), the shape formed by the latter is rounder than for the anterior duct, with a slightly flat portion at the connection between the *crus commune* and the slender part. It contrasts with the very oval posterior ducts of *Procavia* and *Elephantulus*. In these taxa, the great axis of the duct is almost parallel to the *crus commune* while it forms a rather right angle in *Elephas*.

The length of the slender part of the posterior duct represents approximately two thirds of the total length of the entire duct (as for the anterior duct). Its cross-section is circular as well. The posterior

duct exhibits the same features as the anterior duct in terms of thickness, including the less defined ampulla. The slender posterior duct enters the anterior ampulla with a similar angle to that of the anterior duct which contrasts with *Procavia* and *Elephantulus*. Conversely, the angle formed by the slender anterior duct and the *crus commune* at the level of their connection is similar to that of *Procavia* and *Elephantulus*.

The posterior utricle is very thick in *Elephas* compared to *Procavia* and *Elephantulus*. Its relative length is similar to that of *Procavia* - though slightly longer – but it contrasts with the particularly small length of *Elephantulus*. Its thickness decreases from the common utricle to the connection with the posterior ampulla. In *Procavia* and *Elephantulus*, the thickness is constant. The cross-section is quadrangular in the common utricle part and progressively takes a flattened oval form in the ampullar part. In the other afrotherians, the posterior utricle is very flattened. In *Procavia*, the posterior utricle is inclined and extends ventrally to the *crus commune*.

The streamline at the level of the connection between the posterior ampulla connects and the posterior utricle is straight. This contrasts with *Procavia* and *Elephantulus* in which the posterior utricle enters the posterior ampulla more ventrally. In *Procavia*, the posterior ampulla is inclined. Thus, a significant part of the posterior duct is located lower than the plane defined by the lateral duct, a condition not developed in *Elephas* and present but less marked in *Elephantulus*. The posterior ampulla is slightly smaller than the two other ampullae. The *crista ampullaris* is clearly visible in the reconstruction as well. The relative size of the *crista ampullaris* is similar to that of *Procavia* and *Elephantulus* and none of the three sampled afrotherians display an *eminentia cruciata*.

In a view in the plane of the lateral semicircular duct (Fig. II.29), the shape formed by the latter is oval, as for *Procavia* and *Elephantulus*. In *Elephas*, the great axis of the duct forms an almost right angle with the axis formed by the utricle while it is rather parallel in *Procavia* and *Elephantulus*. As for the bony canals, the area enclosed by the lateral duct is smaller than that of the anterior and posterior ducts.

The length of the slender part of the lateral duct represents approximately two thirds of the total length of the entire duct (as for the other ducts) and its cross-

section is circular. The trajectory of the slender lateral duct is slightly curved. The connection between the slender duct and the ampulla is less thick than in the anterior and posterior duct. Therefore, the lateral membranous ampulla is better defined than the other two. The lateral slender duct never crosses the plane defined by the posterior duct in *Elephas*. In *Elephantulus*, the lateral duct extends towards the posterior duct and slightly crosses its plane. In *Procavia*, the extension is even more pronounced and the lateral duct clearly defines the plane defined by the posterior duct.

Distally, the lateral slender duct thickens very progressively to form the simple crus. The bulge is similar to that of the anterior and posterior ducts in terms of thickness. In *Elephas*, the bulge enters the common utricle almost horizontally and at a very low position compared to the posterior ampulla. This confirms the observations made on the bony labyrinth of elephants and will be addressed in the next chapters as well. In *Elephantulus*, the simple crus enters the common utricle horizontally as well but the connection is located higher in the vestibule with respect to the posterior ampulla. In *Procavia*, the simple crus enters the common utricle very high and with an oblique trajectory.

The lateral ampulla is very similar to the anterior ampulla. The streamline of the lateral duct from the anterior utricle to the lateral ampulla is very smooth. Conversely, the anterior utricle enters the lateral ampulla orthogonally in *Procavia* and *Elephantulus*. In a view perpendicular to the anterior duct, the ampullae form an angle of almost 90° with each other in *Elephas*, *Elephantulus* and *Procavia*. The *crista ampullaris* does not exhibit an *eminentia crucita*.

4. Discussion

4.1. Intraspecific variability

The study of several specimens belonging to the same genus and sometimes to the same species allows us to point out the intrageneric and intraspecific variability of the ear region of proboscideans. These observations are a good way to evaluate the characters that could be used for phylogenetic analyses. Indeed, the number of phylogenetic analyses using inner ear characters of fossil taxa is growing but the intraspecific (or at least intrageneric) variability of such characters have not been much investigated, especially within the Proboscidea. In Ekdale (2011) - the first study focused on the variability of ear region characters in proboscideans - only external petrosal characters have been investigated since only one specimen has been CT-scanned. The study of several specimens of *Elephas* and *Loxodonta* allows us to discuss the intra-specific and intrageneric variability of the inner ear among proboscidean representatives. Measurements are presented in Tables II.3 and II.4.

First, the numerous ossification irregularities (ridges and bumps) observed in several bony labyrinths of extant elephants display a high level of intraspecific variability. They can be found on the ampullae, the *crus commune*, semicircular canals and sometimes in the vestibule. These features seem to develop more or less randomly. They have been described in other taxa than proboscideans; for instance *Arsinoitherium* (this study). Our first hypothesis was that these ridges could be grooves that contained blood vessels in life. However, in CEB150009 - in which the blood vessels are preserved – the ridges do not seem to contain any soft structures. The origin and function of these ossification irregularities remains mysterious.

Whereas it is clearly stocky in every studied specimen belonging to the genus *Elephas*, the *crus commune* appears more elongated in some of the *Loxodonta* specimens. It cannot be an interspecific variation due to the presence of two species in the *Loxodonta* studied sample because the specimens confidently assigned to the species *L. cyclotis* display both morphologies: the *crus commune* is elongated in MNHN.ZM.AC.1950-728, but stocky in 1956-194, 1957-465 and 1961-69. Hence, the stocky or elongated aspect of the *crus commune* is an intraspecific

variable character not pertinent for phylogenetic analyses.

The location of the meeting of the anterior and posterior canals is also subject to intraspecific variability. In most specimens of *Loxodonta*, the two canals meet quite high (at approximately three quarters of the height of the anterior canal), but the meeting point can be at a low position in some of the specimens of *L. africana* and *L. cyclotis* (MNHN.ZM.AC.1861-53, 1956-194 and CEB130168). An intraspecific variation of this character is also found in *Elephas maximus* which displays two specimens with a high meeting point of the two canals (MNHN.ZM.AC.1904-273 and 1941-209) and two with a rather low meeting point (MNHN.ZM.AC.2008-81 and CEB 150009). The usefulness of these two character states for phylogenetic analysis is therefore questionable.

The overall shape of the lateral semicircular canal differs between specimens of the same genus and even between specimens of the same species. In *Elephas*, it is round for every specimen except MNHN.ZM.AC.1904-273. In L. cyclotis, half of the specimens displays a round lateral canal while the other half displays an oval canal. The shape of this canal is therefore variable and should not be used in phylogenetic analysis. However, the shape of the two other semicircular canals is constant in extant elephants (the anterior canal is oval and the posterior canal is round in all studied specimens).

The angle formed between the major axis of the anterior semicircular canal and the axis of the *crus commune* is not constant among specimens of the same genus or of the same species. In *Elephas maximus*, both MNHN.ZM.AC.1904-273 and 1941-209 display an angle of 41°, but MNHN.ZM.AC.2008-81 has a more acute angle of 30°. In *Loxodonta*, this value varies between 32° and 48° (*L. africana*: from 32° to 37°; *L. cyclotis*: from 40° to 48°). Even though this feature is somewhat variable, we can notice that the major axis is always oriented in the same direction.

Table II.3 : Measurements of the semicircular canals of extant elephants

	Crus commune length (mm)	*Crus commune* section radius (mm)	*Crus commune* thickness ratio	ASC length (mm)	PSC length (mm)	LSC length (mm)	SCC average thickness ratio	Angle ASC-PSC (°)	Angle ASC-LSC (°)	Angle PSC-LSC (°)	ASC radius of curvature	PSC radius of curvature	LSC radius of curvature
***Elephas* 1904-273**	7.11	1.51	21.19	22.45	22.44	20.33	4.64	72.6	75.7	88.8	5.25	5.20	3.16
***Elephas* 1941-209**	5.58	1.20	21.53	22.79	22.49	23.06	4.13	76.5	74.2	83.2	5.19	5.23	3.52
***Elephas* 2008-81**	6.53	1.48	22.62	26.66	24.56	26.07	3.52	76.6	75.0	85.8	5.97	5.60	4.06
***Elephas* CEB150009**	3.07	1.51	49.20	23.47	21.01	24.10	4.86	78.9	67.9	85.7	5.04	4.65	3.65
***Loxodonta* 1932-523**	5.47	1.38	25.26	24.99	23.65	21.26	3.02	70.9	72.4	85.8	5.66	5.37	3.21
***Loxodonta* 2008-71**	5.63	1.13	20.09	22.49	22.31	22.54	3.90	75.9	59.8	83.5	5.18	5.14	3.56
***L. africana* 1861-53**	5.50	1.82	27.27	27.42	24.36	21.04	3.57	81.1	73.8	82.2	5.86	5.25	3.54
***L. africana* CEB130168**	4.05	1.51	37.23	27.44	25.40	24.07	3.28	84.8	72.7	78.0	5.80	5.55	3.72
***L. cyclotis* 1950-728**	5.89	1.64	27.87	23.85	21.40	21.06	3.69	83.3	72.3	88.5	5.41	4.91	3.35
***L. cyclotis* 1956-194**	5.37	1.57	29.20	31.98	29.92	23.44	2.74	76.7	72.9	93.8	6.87	6.25	4.09
***L. cyclotis* 1957-465**	4.84	1.94	40.15	23.99	21.88	20.50	4.01	74.7	80.0	85.0	5.48	4.98	3.15
***L. cyclotis* 1961-69**	4.46	1.40	31.33	22.30	20.61	21.16	4.77	80.9	68.1	80.6	5.06	4.78	3.37

The angle between the anterior and posterior semicircular canals varies between the species. In *Elephas maximus*, the variation is minimal (from 72.6° to 78.9°) but it is more pronounced in *Loxodonta*. Indeed there are specimens displaying very acute canals (*Loxodonta sp.* MNHN.ZM.AC.1932-523 with 70.9°) while other specimens display larger angles (*L. africana* CEB130168 with 84.8° and *L. cyclotis* MNHN.ZM.AC.1950-728 with 83.3°). The variation is also found at the intra-specific level in *L. cyclotis*. The same can be said concerning the angle between the anterior and lateral canals. The variability is less pronounced in *Elephas* (from 67.9° to 74.2°) than in *Loxodonta* (from Loxodonta *sp.* MNHN.ZM.AC.2008-71 with 59.8° to *L. cyclotis* MNHN.ZM.AC.1957-465 with 80°). The variation is also found at the intra-specific level in *L. cyclotis*. Finally, the angle between the posterior and lateral canals seems to follow the same pattern of variation. It is more or less constant in *Elephas maximus* (from 83.2° to 88.8°), while it varies greatly in *Loxodonta* (it varies from 80.6° to 93.8° in *L. cyclotis*). It should be also noted that the measurements of these angle values are difficult to take because the canals do not always form a regular plane (they actually rarely do so). Measuring these angles manually is tricky, and it can lead to inter-users variability. We tried to address this problem by using only angle values taken between the functional planes of the canals. These planes were calculated with an ARIADNE add-on, based on central streamline landmarks that we placed on the specimens. Hence, our values can somewhat differ with values taken manually and we have to be cautious when comparing these calculated values with manually taken measurements. Every angle values used during this study were obtained using the same protocol.

When viewed in cross-section, the semicircular canals of extant elephants are always flattened. However, the degree of flattening is variable. In our *Elephas maximus* sample, the canals of MNHN.ZM.AC.2008-81 are more flattened than in the other specimens. Concerning *Loxodonta*, the anterior and posterior canals are more flattened in *Loxodonta* sp. MNHN.ZM.AC.1861-53. In *L. cyclotis* MNHN.ZM.AC.1950-728 and 1957-465 all three canals appear slightly more flattened. Finally, in *L. cyclotis* MNHN.ZM.AC.1956-194, the flattening of the canals is extremely marked especially in the anterior and posterior canals. This is

the highest degree of flattening observed in our sample.

Another feature showing a small variability is the thickness of the canals. The semicircular canals of extant elephants are thicker than most mammals. However, the thickness is more or less pronounced between specimens of the same genus and sometime of the same species. In *Loxodonta cyclotis*, some specimens display really thick canals (MNHN.ZM.AC.1961-69 and 1957-465 for instance). The thickness of the canals can also be investigated through continuous values thanks to the average thickness ratio. However, it should be noted that this ratio is calculated using the average section radius of the canal and the length of the central streamline. These measures can be slightly different depending on where the user decides to separate the slender part of the canal from the ampulla. Moreover, the ampullae in extant elephants are less defined than in most mammals which contribute to increase the variability of the delimitation.

In most specimens, the semicircular canals of extant elephants display an undulation. However, in some specimens, one or several canals lack distinct undulations. For instance the anterior and posterior canals are not clearly undulated in *L. africana* MNHN.ZM.AC.1861-53. In *Loxodonta* sp. MNHN.ZM.AC.1932-523, *E. maximus* 2008-81 and *L. cyclotis* 1950-728, the lateral canal is not undulated either. For these reasons, this character will be excluded from the phylogenetic analysis.

The radii of curvature display some variability in *Elephas* and in *Loxodonta*. In general, the radii of *Elephas* are less variable than the radii of *Loxodonta*. This may be explained by a more restricted data sample for *Elephas* (4 specimens) than for *Loxodonta* (8 specimens) and the fact that there are two species of *Loxodonta* in our sample. The radius of curvature of the anterior is the least variable in *Elephas* (variance of 0.02) while it is the most variable in *Loxodonta* (variance of 0.34). Indeed there is a difference of almost 1.8 between the largest and smallest radius in *Loxodonta cyclotis*. The radius of the posterior canal is less variable than the anterior in *Loxodonta* (variance of 0.22) but it is more variable in *Elephas* (variance of 0.16). Finally, the radius of the lateral canal is the least variable in *Loxodonta* (variance of 0.09) and it is even less variable than the radius of *Elephas* (variance of 0.14). The variability of the radii of curvature should be taken into account if one wants to use

these measurements in a phylogenetic analysis. It would be wrong to separate the character states in the middle of the values range of the same species (which can attain 1.8 in *Loxodonta cyclotis*). Hence one must watch out for this when defining character states about the radii of curvature.

Table II.4 : Measurements of the bony cochlea of extant elephants

Specimen	Number of turns	Coiling (°)	Length (mm)	Aspect ratio
***Elephas* 1904-273**	2.375	855	74.13	0.38
***Elephas* 1941-209**	2.375	855	80.46	0.38
***Elephas* 2008-81**	2.375	855	80.28	0.43
***Elephas* CEB 150009**	2.25	810	73.11	0.36
***Loxodonta sp* 1932-523**	2.25	810	77.13	0.41
Loxodonta sp* 2008-71 *(average)	*1.81*	*653*	*67.92*	*0.32*
Left ear	2	720	73.61	0.34
Right ear	1.625	585	62.18	0.30
***Loxodonta africana* 1861-53**	2.375	855	71.54	0.45
***Loxodonta africana* CEB130168**	2	720	70.84	0.37
***Loxodonta cyclotis* 1950-728**	2.25	810	69.16	0.40
***Loxodonta cyclotis* 1956-194**	2.625	945	74.16	0.40
***Loxodonta cyclotis* 1957-465**	2.625	945	79.03	0.44
***Loxodonta cyclotis* 1961-69**	2.625	945	81.55	0.44

The number of turns of the cochlea is not a fully constant feature in extant elephants. It varies slightly in *Elephas*: MNHN.ZM.AC.2008-81, 1904-273 and 1941-209 display 2.375 turns (855°) but CEB 150009 displays a little less (2.25 turns; 810°). There is more variation in *Loxodonta*. The greatest number of turns is 2.625 (*L. cyclotis:* MNHN.ZM.AC.1956-194, 1957-465 and 1961-69). *Loxodonta* sp. MNHN.ZM.AC.2008-71 displays the smallest number of turns with two (720°) in the left ear and 1.625 (585°) in the right ear. The difference between the left and right ear of this specimen is discussed below (§ 4.2, Intra individual variability). *L. africana* CEB130168 displays a particularly small number of turns as well (two full turns). Hence the variability within one proboscidean species can extend to one full turn. This high degree of variability has to be taken into account while defining phylogenetic characters states. On the other hand, every specimen of *Elephas* and every specimen of *Loxodonta* lacks an apical lacuna except for *L. africana* CEB130168. This character is then also variable intra-specifically and should be used cautiously in phylogenetic analyses. In contrast, the relative volume of the cochlea seems to be quite constant in extant elephants. It is always around 50% of the total volume of labyrinth except for specimens of *L. cyclotis* MNHN.ZM.AC.1956-194 and MNHN.ZM.AC.1957-465 which display a relative volume of respectively 39.5% and 43.4%. This can be explained by the particularly high development of the semicircular canals in these two specimens. The aspect ratio of the cochlea can also vary greatly among the same genus. The cochlea of the left ear of *Loxodonta* sp. MNHN.AC.ZM.2008-71 displays an aspect ratio of 0.30 while it is 0.45 in *Loxodonta* africana MNHN.AC.ZM.1961-53. This is likely to be caused by the smaller number of turns of MNHN.AC.ZM.2008-71. However, values for the ratio are always between 0.30 and 0.45 in extant elephants and using this ratio in phylogenetic analyses remains possible if this variability is kept in mind during the definition of the characters states. In conclusion, in our studied elephant sample the petrosal and especially the bony labyrinth display a strong morphological variability, and especially a strong intraspecific variability. This variability is further investigated statistically in Chapter IV.

4.2. Intra-individual variability

The most spectacular example of variability that we observed among extant elephants is the difference of number of turns of the cochlea between two ears of the same *Loxodonta* specimen (MNHN.ZM.AC.2008-71). The left ear has 2 turns (Fig II.21K) while the right ear has 1.625 turns (Fig II.21L) which makes a difference of almost half a turn between two ears of the same individual. This condition must have been pathological as the individual was probably not hearing the same frequencies between its two ears. Our taxa sample does not allow us to analyze this condition statistically as both ears were sampled for only five proboscidean specimens (*Phosphatherium* PM17, *Gomphotherium* MNHN.F.SEP38, *Stegodon* FM18632, *Mammuthus* FM144658 and this specimen). The difference of number of turns between the two ears has been observed only in the *Loxodonta* specimen. However, we cannot know if this condition is rare or common among proboscideans.

4.3. Constant similarities between *Elephas* and *Loxodonta*

As we discussed earlier, there are no significant morphological differences between the petrosal of *Elephas* and of *Loxodonta*. Both genera display similar morphologies.

Concerning the bony labyrinth, in both genera, the anterior canal is always oval and the posterior always round. The lateral canal is always the smallest one which can be seen on the reconstruction as well as in the radii of curvature. The entry point of the lateral canal into the vestibule is located at the same level which is low and close to the posterior ampulla. The secondary bony lamina is absent in both genera. The average values of the radii of curvature are quite similar between *Elephas* and *Loxodonta* (respectively 5.4 and 5.7 for the anterior canal, 5.2 and 5.3 for the posterior canal and 3.6 and 3.5 for the lateral canal). The average relative volume of the cochlea is the same between *Elephas* and *Loxodonta* (respectively 47.7% and 47%). The cochleae of both genera share similar mean aspect ratios (0.39 in both *Loxodonta* and *Elephas*). The *crus commune* average thickness ratio is similar between *Elephas* (mean value of 28.6) and *Loxodonta* (mean value of 30.2).

4.4. Differences between *Elephas* and *Loxodonta*

Even though the bony labyrinths of *Elephas* and *Loxodonta* share a lot of common characteristics, there are some differences between the two genera. The *crus commune* is always stocky in *Elephas*, while it is variable in *Loxodonta.* Both specimens of *L. africana* display a stocky crus but there is some variability in the four specimens of *L. cyclotis*. The mean central streamline lengths of the anterior canal of *Elephas* and *Loxodonta* are similar but it tends to be longer in *Loxodonta* (25.56 mm opposed to 23.84 mm in *Elephas*). The same can be said for the mean central streamline length of the posterior canal (23.69 mm in *Loxodonta* opposed to 22.62 mm in *Elephas*). The values for the angles between canals are more constant in *Elephas*. Indeed the variances for the angle values in *Loxodonta* are 18.90 (ASC-PSC angle), 28.57 (ASC-LSC angle) and 26.48 (LSC-PSC angle) whereas they are respectively 6.90, 25.45 and 9.18 in *Elephas*. This difference of variability could be explained by the presence of two species among the *Loxodonta* sample while there is only one species in the *Elephas* sample. Moreover, there are only four *Elephas* specimens while there are eight *Loxodonta* specimens. The greater number of *Loxodonta* specimens could be the reason of the greater variance in this genus as well. The variability set aside, the mean values for each angle is very similar between *Loxodonta* and *Elephas* (respectively 78.7° and 76.1° for the ASC-PSC angle, 71.5° and 73.21° for the ASC-LSC angle and 84.7° and 85.9° for the LSC-PSC angle). In contrast, the mean value for the average thickness ratio is quite different between the two genera. The semicircular canals of *Elephas* tend to be thicker than those of *Loxodonta* (respective ratios of 4.29 and 3.62). The number of turns of the cochlea is also more variable in *Loxodonta*. The variance for this genus is 0.11 while it is 0.003 for *Elephas*. In addition to the reasons depicted earlier that could explained greater level of variance among *Loxodonta*, the pathological small number of turns in the right ear of MNHN.ZM.AC.2008-71 participates in the increase of variability in this genus. Hence, the average number of turns of the cochlea is higher in *Elephas* (2.34) than in *Loxodonta* (2.26). On the other hand, the total volume of the labyrinth is greater in *Elephas* (mean of 1250 mm^3) than in *Loxodonta* (mean of 1148 mm^3).

4.5. Differences between the two African species

A major part of our observations is the difficulty to discriminate petrosal and inner ears of *Elephas* and *Loxodonta*. Both genera seem to display similar ear regions. Moreover, the intra-specific variability of the inner ear is rather strong and it appears to be really difficult to discriminate the two genera using anatomical observations and basic linear measurements. Incidentally, it seems rather impossible to discriminate the two species of *Loxodonta* using only anatomical characters, especially given the taxonomic proximity of these two species (and difficulty to distinguish their skulls). An attempt will be made to discriminate both *Loxodonta* species and the two genera using a geometric morphometrics approach based on 3D labyrinth landmarks in Chapter IV.

5. Conclusions

We provide here the first comprehensive study of the ear region of extant elephants using CT scan methods. The anatomy of the petrosal and the bony labyrinth is thoroughly investigated and compared between the three extant species. Moreover, the membranous semicircular duct system of an extant elephant is here reconstructed in 3D for the first time using CT scan methods. The semicircular ducts of *Elephas* are strikingly thin compared to its semicircular canals. This contrasts with other afrotherians described here (*Elephantulus* and *Procavia*), whose semicircular ducts and canals have approximately the same thickness.

Comparisons of petrosals from the three extant species show that it is difficult to determine specific anatomical features that can discriminate the petrosal and bony labyrinth of the Asian and African elephants.

Comparisons of petrosals and bony labyrinths of several specimens of the same species show some level of intra-specific variability and even intra-individual variability (number of turns of the cochlea). The investigation of the variability allows refining the definition of petrosal and labyrinth phylogenetic characters.

In perspective, the ontogenetic variability of the petrosal and inner ear characters should be investigated in the future. The taxa sample is here too restricted to conduct such study and the precise age is unavailable for most specimens.

CHAPTER III

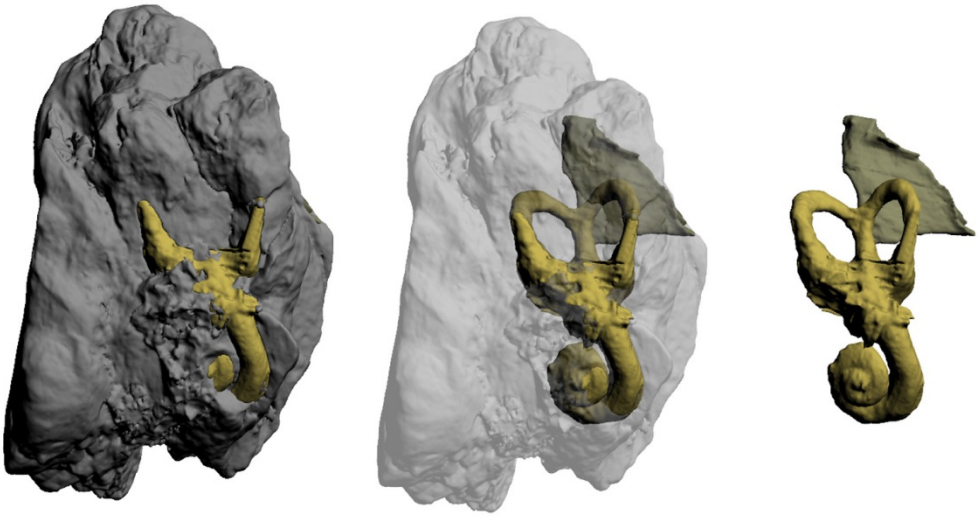

Anatomy of the ear region of fossil proboscideans: comparisons with extant elephants and close relatives

1. Introduction

The first chapter focuses on the two earliest-known elephant relatives (*Eritherium*, 60 Myo and *Phosphatherium*, 55 Myo) and helps characterizing the ancestral morphotype of Proboscidea and Afrotheria. The second chapter focuses on the ear region of extant elephants and provides some information about its variability at low taxonomic level. Even though the inner ear of other proboscidean fossils has already been investigated (*Numidotherium* and *Moeritherium* in Court, 1992 and Benoit et al. 2013b; an unknown elephantimorph in Ekdale, 2011), we lack information about the inner ear anatomy of most proboscidean lineages. Indeed, the Proboscidea is a diversified order that contains over 170 extinct species with very different morphologies. This clade is surprisingly well-documented, with known fossil covering almost its entire range of existence and found in every continent except Antarctica and Australia. The objective of Chapter III is to study the anatomy of the petrosal and inner ear of several fossil proboscideans in the perspective of tracing the evolution of this complex anatomical region in Proboscidea. To do so, we sampled proboscidean petrosals from several European and international institutions. They cover most proboscidean lineages: Deinotheriidae, Mammutidae, Gomphotheriidae, Amebelodontidae, Stegodontidae and even fossil Elephantidae. The detailed taxonomic sample is given in the next section ('Material and methods'). On the other hand, the ear region of an unpublished early embrithopod (from the Ouled Abdoun basin, Morocco) has been investigated as well during this work and used for comparisons. A more detailed anatomical study of the early afrotherian *Ocepeia daouiensis* (Gheerbrant et al. 2014) was also performed in this chapter. The final objective of this chapter is to compare the morphology of the newly investigated taxa with previously documented taxa in order to establish new primary homologies to be tested in a cladistic analysis (Chapter V).

2. Material and methods

2.1. Taxa sample

2.1.1. Non-proboscideans

Ocepeia

The petrosals of an *Ocepeia daouiensis* Gheerbrant & Sudre, 2001 skull (PM45) were investigated. The specimen is of Selandian age (ca. 59-60 Ma) and comes from the Sidi Chennane quarries (Ouled Abdoun basin, Morocco). Both petrosals were scanned in Gheerbrant et al. (2014) and the bony labyrinths are reappraised here.

Early Moroccan embrithopod

The fragmentary petrosal PM53 was found associated with several other diagnostic cranial fragments of the same individual which documents a new primitive embrithopod. This material was found in early Ypresian phosphates beds of the Ouled Abdoun basin, Morocco (Gheerbrant et al 2003), and it is currently under study (in progress, E. Gheerbrant pers. comm. 2016). Only a very small part of the cochlea is preserved, the slender semicircular canals are quite complete (only a part of the lateral canal is broken) and the area of the vestibule is damaged.

2.1.2. Proboscideans

Numidotherium

Numidotherium koholense Jaeger, 1986 was described by Mahboubi et al. (1984, 1986) from the late early Eocene of El Kohol in Algeria. Two specimens of *N. koholense* were investigated during this PhD thesis. First, the microtomographic slices of the unreferenced isolated petrosal described in Court & Jaeger (1991) and segmented in Benoit et al. (2013b) have been reinvestigated. As this specimen was described in details in previous publications we only used it for comparisons with other proboscideans. We applied the same measuring protocol using 3D landmarks to this specimen for adequate comparisons. We then CT-scanned the ear region of another specimen (UOK5) of *N. koholense* that consists of a mineralized and almost complete skull.

Moeritherium

Three specimens of *Moeritherium* C.W. Andrews, 1901 have been studied. First, the rather complete skull MNHN.F.LBE1 displaying the natural endocast of the bony labyrinth was investigated. This skull was found by Arambourg and Magnier (1961) in the Eocene deposits of Dor el Talha (Libya). It

has been attributed to the species *Moeritherium lyonsi* Andrews, 1901 but this determination is doubtful so we will refer to it as *Moeritherium cf. lyonsi*. Some features of the cochlea and the semi-circular canals can be seen with the naked eye on this specimen. However, the high degree of mineralization prevented us from any further CT scan acquisition which would have allowed us to access the other half of its bony labyrinth. Secondly, an isolated petrosal of *Moeritherium trigodon* Andrews, 1904 (SMNS 47789-90) has been CT-scanned. It belongs to the collections of the Natural History Museum of London (NHMUK 68436) and has been found in the Idam Unit of Dor el Talha (Libya) (Wight, 1980). It has been described in a previous work (Court, 1994). Although this specimen is also highly mineralized, the X-rays of the CT-scanner were able to pass through. However, the microtomographic slices are poorly contrasted and the segmentation was extremely difficult. Hence the 3D model is imprecise and some features are really difficult to describe properly. Finally, the third specimen also belongs to the species *Moeritherium lyonsi*. It belongs to the Stuttgart Museum für Naturkunde (SMNS 47789-90) and consists of a part of the basicranium still bearing a fraction of the petrosal. This specimen is extremely incomplete but in contrast with other studied specimens (MNHN.F.LBE1, NHMUK 68436) of *Moeritherium*, it shows a particularly low level of mineralization. Unfortunately, the CT-scan acquisition showed that only a small part of the semicircular canals is preserved in this specimen. The cochlea and vestibule are completely missing.

Prodeinotherium

Three specimens attributed to *Prodeinotherium bavaricum* von Meyer, 1831 were studied. They all belong to the collections of the Muséum d'Histoire Naturelle de Toulouse and are labelled MHNT.PAL.2013.01108A and 01108E and Beon 98 E1 3049. They consist of fragmentary parts of the basicranium found in Montréal-du-Gers (France).

Mammut

Two petrosals of *Mammut americanum* Kerr, 1792 were studied. They both belong to the collections of the AMNH and are numbered FM14293. However, they have a very different aspect and color. Even though they are left and right petrosals, they belong from different individuals. This is confirmed with the segmentation, showing different

semicircular canals morphologies. Hence, we chose to number them FM14293A (left petrosal) and FM14293B (right petrosal) to distinguish them. The cochlear part of FM14293-A is preserved, however the petrosal was cut off at the level of the cochlea a few years ago for investigation. Therefore, the bony cochlea can be seen with naked eye on the specimen. On the other hand, the cochlear part of FM14293-B is completely missing.

Gomphotherium

Three specimens of *Gomphotherium angustidens* Burmeister, 1837 were studied. First two basicrania from the collections of the Muséum National d'Histoire Naturelle (MNHN) – one male (MNHN.F.SEP38) and one female (MNHN.F.SEP18) - were CT scanned with access to both left and right ears. They come from the Miocene fossil deposit of En-Péjouan located on the territory of Simmore (Gers, France). Both petrosals and inner ear of MNHN.F.SEP38 were segmented. However, poor contrasting resulting from a strong mineralization of MNHN.F.SEP18 prevented us from obtaining a clear virtual cast. Therefore only part of the inner ears of this specimen was segmented and the petrosals were left unstudied. An isolated petrosal of a juvenile *Gomphotherium angustidens* from the collections of the Muséum d'Histoire Naturelle de Toulouse (CBar coll V. 2) was also CT scanned. It comes from a Miocene fossil deposit located in Castelnau-Barbarens (Gers, France) and it was entirely segmented (petrosal and inner ear).

Cuvieronius

An isolated petrosal of *Cuvieronius* sp. Osborn, 1923 (FM103247) was studied. It belongs to the collections of the AMNH and has not been attributed to any species of *Cuvieronius*. The specimen has been excavated in the Matthews Wash Locality, Graham County, Arizona (USA). Its cochlear part is broken but the specimen shows a low degree of mineralization so the segmentation of the semicircular canals was rather easy.

Stegomastodon

Two isolated petrosals of *Stegomastodon sp.* Pohlig, 1912 were studied. They both belong to the collections of the AMNH and have specimen number FM21807. They have been excavated in the Curtis Ranch locality, Cochise County, Arizona (USA). The first specimen numbered here FM21807-A is a left petrosal. It is quite

damaged and the bony labyrinth is not entirely preserved. The labyrinth has been filled with sediments during the fossilization before the petrosal was broken. Therefore, a natural endocast of a part of the cochlea and a part of the anterior and posterior semicircular canals shows on the tympanic surface of the petrosal. The lateral semicircular canal is completely missing. The second specimen FM21807-B lacks the cochlear part but all three canals are preserved.

Platybelodon

First, a skull of *Platybelodon grangeri* Osborn, 1929 (26564 824+, AMNH collections) has been CT-scanned. It comes from the Platybelodon Quarry locality that belongs to the Tung Gur formation deposits (Mongolia) of Pliocene age. This specimen is damaged, distorted and mineralized. It was not possible to identify its inner ears on the microtomographic slices. Therefore a cranial fragment belonging to the same specimen and associated with a sedimentary matrix was CT-scanned. It was suspected to be an isolated petrosal, which was confirmed by the study of the microtomographic slices despite the high degree of mineralization.

Anancus

Seven isolated petrosals of *Anancus arvernensis* Croizet & Jobert, 1828 from the Pliocene fossil deposit of Dorkovo (Pazardjik, Bulgaria) have been sampled. They all belong to the National Museum of Natural History of Sofia (they are labelled NMNHS.FM2991A to G). Each of these specimens was CT-scanned and the inner ears have been segmented successfully.

Stegodon

The left and right petrosals of the quite complete skull FM18632 (collections of the AMNH) of a juvenile *Stegodon orientalis* Owen, 1870 were studied. The specimen was excavated in Wan-hsien, Sze-chuan (China). The specimen is quite mineralized but it was possible to segment both ears. The cochlear part of the petrosal has been preserved in both ears.

Mammuthus

The isolated petrosal MNHN.F.1904-12 of *Mammuthus primigenius* Blumenbach, 1799 from a Pleistocene site of Mont-Dol (Britany, France) was CT scanned. In addition, the left and right petrosals of specimen FM 144658 of *Mammuthus columbi* Falconer, 1857 from the collection of the American

Museum of Natural History were studied. The cochlear part of the petrosal was missing in both of them but their vestibular part has been successfully segmented.

Palaeoloxodon

The isolated left petrosal of specimen M82706 of *Palaeoloxodon antiquus* Falconer & Cautley 1847 was studied. It belongs to the collections of the Natural History Museum of London (NHMUK). This specimen comes from the Pleistocene deposits of the Sandy Lane Quarry (Essex, United Kingdom). It is a rather complete individual which skull is broken in many fragments. Amongst the skull fragments, a single broken petrosal which cochlear part was missing was identified. This fragment was CT-scanned and the semicircular canals were segmented.

2.2. Methods

The specimens were CT-scanned in different facilities presented in the main 'Material and methods' section of the thesis (see Table III.2). Resolutions of the scans are also given in this table. The petrosal and bony labyrinths were then segmented using MIMICS Research 16 and 17. Anatomical descriptions were performed based on the 3D models obtained after segmentation. On the other hand, quantitative measurements were taken on the specimens for comparisons as well.

3. Systematic descriptions

3.1. Outgroups

3.1.1. *Ocepeia daouiensis*

The whole basicranium of *Ocepeia daouiensis* has been CT-scanned and it is still bearing both petrosals. While the petrosal is damaged in the mastoid region, the part containing the inner ear is well preserved. Since there are no significant differences between the left and the right ear, the measurements given below are an average of the left and right ears measurements. Only the bony labyrinth of *Ocepeia* will be discussed, as the petrosal was already detailed in Gheerbrant et al. (2014). The total volume of the inner ear of *Ocepeia* is 17.53 mm^3 (Table III.1).

Vestibular bony labyrinth

Ampullae

The ampullae of *Ocepeia* are well-defined and inflated (Fig III.1). They are smooth and display no ridges.

Crus commune

The *crus commune* is elongated and displays no marked basal thickening. It is smooth and displays no ridges. The average section radius of the *crus commune* of *Ocepeia* is small (0.30 mm) and its length is approximately 1.75 mm. Therefore, the crus commune thickness ratio is low (17.35). The anterior and posterior semicircular canals meet high (at 75% of the height of the anterior canal) and the *crus commune* is not inclined.

Semicircular canals

The anterior semicircular canal is round. The central streamline length of this canal is 6.87 mm (Table III.2) and its average section radius is 0.15 mm. Therefore, the thickness ratio of this canal is 2.22 making it quite slender. The anterior canal is the biggest in *Ocepeia* (the radius of curvature is 1.64).

The posterior semicircular canal is round. The central streamline length is similar to the value found for the anterior canal although slightly longer (7.49 mm). The average section radius is very similar to the anterior one (0.16 mm). Hence the thickness ratio of the posterior canal (2.18) is very close to the ratio of the anterior canal (2.22). The radius of curvature of the posterior canal is 1.55.

The lateral semicircular canal is oval. The estimated length of the central streamline and the average section radius are similar to the other canals. The thickness ratio is slightly lower (2.04) for the lateral canal than for the anterior and posterior canals.

Table III.1 : Measurements of the bony labyrinth in fossil proboscideans and outgroups. **ASC**: anterior semicircular canal, **LSC**: lateral semicircular canal, **PSC**: posterior semicircular canal, **SCC**: semicircular canals, **?**: missing data, **e**: estimated.

	Volume				Cochlea			*Crus commune*			Angles between the SCC		
	Bony labyrinth volume (mm^3)	Cochlea volume(mm^3)	Relative volume of the cochlea (%)	Stapedial ratio	Number of turns of the cochlea	Aspect ratio of the cochlea	Length of the cochlea (mm)	*Crus commune* length (mm)	*Crus commune* average section radius (mm)	*Crus commune* average thickness ratio	Angle between the ASC and the PSC (°)	Angle between the ASC and the LSC (°)	Angle between the LSC and the PSC (°)
***Ocepeia daouiensis* PM45**	17.5	11.7	66	2.05	2.13	0.72	19.2	1.75	0.30	17.4	91.6	80.1	87.8
Embrithopoda PM53	?	?	?	?	?	?	?	3.92	0.53	13.7	86.0	83.4	98.6
Unknown rhinocerotid 2013.01108A	401.3	229.2	57	?	2	0.33	50.6	4.02	1.12	27.8	94.4	76.1	98.9
Unknown rhinocerotid Beon 98 E1 3049	?	?	?	?	?	?	?	4.33	1.08	24.9	91.0	73.9	95.0
***Anancus arvernensis* NMNHS.FM2991A**	934.6	468.3	50	1.7	2.5	0.43	72.3	5.11	1.06	20.8	90.5	58.2	77.6
***Anancus arvernensis* NMNHS.FM2991B**	?	?	?	?	?	?	?	6.70	1.34	20.1	81.0	58.9	78.0
***Anancus arvernensis* NMNHS.FM2991C**	957.5e	442.2e	46e	1.6	2.5	0.41	?	3.28	1.32	40.4	79.8	63.8	81.3
***Anancus arvernensis* NMNHS.FM2991D**	1151e	539.3e	47e	1.7	2.5	0.37	78e	4.58	1.64	35.8	92.4	70.4	81.2
***Anancus arvernensis* NMNHS.FM2991E**	1440.5	701.8	49	1.6	2.5	0.37	80.1	6.39	1.38	21.7	87.5	70.4	87.9
***Anancus arvernensis* NMNHS.FM2991F**	1215e	502.1e	41e	1.8	2.5	0.47	78e	7.23	1.33	18.4	88.6	68.9	80.5
***Anancus arvernensis* NMNHS.FM2991G**	933.9e	394.1e	42e	1.6	>2.5	0.45	73e	6.04	1.23	20.3	78.5	64.6	79.7
***Cuvieronius sp* FM103247**	?	?	?	?	?	?	?	9.52	1.65	17.4	82.1	77.4	85.5

***Gomphotherium angustidens* CBar coll. V2**	988.3	497.0	50	1.5	2.63	0.47	90.1	8.73	1.24	14.2	79.2	67.8	85.3
***Gomphotherium angustidens* SEP38**	814.4	400.2	49	1.5	2.38	0.47	69.3	6.82	1.27	18.7	85.7	72.8	91.1
***Mammut americanum* FM14293A**	936.3	343.1	37e	?	2.38	0.44	68.0	7.74	1.18	15.2	86.5	68.8	81.4
***Mammut americanum* FM14293B**	?	?	?	?	?	?	?	7.21	1.55	21.6	80.5	65.1	80.9
***Mammuthus columbi* FM144658**	?	?	?	?	?	?	?	5.23	1.41	27	76.6	73.3	87.2
***Mammuthus primigenius* MNHN.F.1904-12**	1131	480.1	42	?	2.25	0.46	67.6	5.57	1.42	25.5	68.6	71.4	88.0
***Moeritherium* 68436**	?	?	?	?	1.5e	?	?	?	?	?	?	?	?
***Numidotherium koholense* UOK5**	84.4	35.1	42	?	1.5	0.48	27.1	4.50	0.67	14.9	78.0	75.5	96.1
***Palaeoloxodon antiquus* M82706**	?	?	?	?	?	?	?	6.35	1.41	22.2	77.1	76.2	92.6
***Platybelodon grangeri* 26564 (824+)**	854.5	373.8	44	?	2	0.41	56.8	4.20	1.17	27.9	73.9	67.4	98.8
***Prodeinotherium bavaricum* 2013.01108E**	674.4	322.1	48e	?	2.25	0.29	?	5.91	1.26	21.4	77.2	67.6	90.7
***Stegodon orientalis* FM18632**	1117.5	507.8	45	?	2	0.50	68.7	5.34	1.37	25.7	108	74.9	94.0
***Stegomastodon sp* FM21807**	?	530	?	?	2	0.45	65.8	6.67	1.29	19.4	96.6	?	?

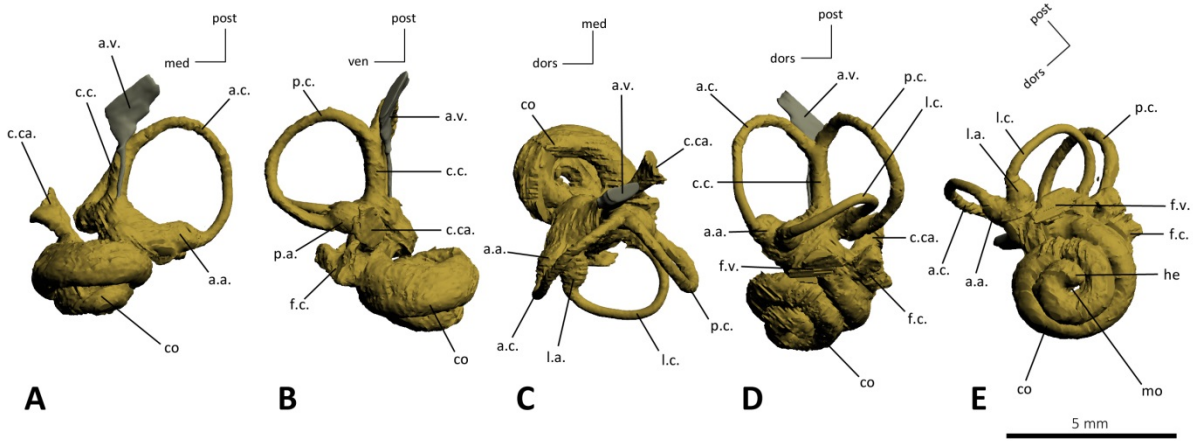

Figure III.1 : 3D reconstructed model of the left bony labyrinth of *Ocepeia daouiensis* PM45 in anterior canal (A), posterior canal (B), lateral canal (C), frontal (D) and cochlear (E) views. Legends: **a.a.** anterior ampulla, **a.c.** anterior semicircular canal, **a.v.** *aquaeductus vestibuli*, **c.c.** *crus commune*, **c.ca.** cochlear canaliculus, co cochlea, **f.c.** *fenestra cochleae*, **f.v.** *fenestra vestibuli*, **he** helicotrema, **l.a.** lateral ampulla, l.c. lateral semicircular canal, **mo** *modiolus*, **p.a.** posterior ampulla, **p.c.** posterior semicircular canal.

Table III.2 : Measurements of the semicircular canals in fossil proboscideans and outgroups

	Radius of curvature			Length (mm)			Average section radius (mm)			Average thickness ratio			
	ASC	PSC	LSC	ASC	PSC	LSC	ASC	PSC	LSC	ASC	PSC	LSC	Global thickness ratio
Ocepeia daouiensis	1.64	1.55	1.24	6.87	7.49	6.79	0.15	0.16	0.14	2.22	2.18	2.04	2.15
Unnamed Embrithopoda	3.26	3.13	2.3e	12.6	13.4	11e	0.22	0.21	0.12	1.72	1.57	1.1e	1.46
Rhinocerotid 2013.01108A	4.13	3.98	3.44	17.4	19.2	18.5	0.42	0.45	0.44	2.39	2.36	2.37	2.37
Rhinocerotid Beon 98 E1 3049	4.19	3.94	3.26	17.5	18.6	17.4	0.54	0.51	0.64	3.09	2.76	3.66	3.17
Anancus arvernensis **NMNHS.FM2991A**	5.02	4.79	3.19	22.7	20.9	20.3	0.70	0.70	0.74	3.09	3.37	3.63	3.36
Anancus arvernensis **NMNHS.FM2991B**	5.91	5.63	4.06	25.4	23.9	24.4	0.58	0.64	0.66	2.29	2.66	2.72	2.56
Anancus arvernensis **NMNHS.FM2991C**	5.15	4.89	3.39	23.8	21.5	21.7	0.76	0.74	0.78	3.18	3.43	3.58	3.40
Anancus arvernensis **NMNHS.FM2991D**	5.24	5.39	3.39	23.5	24.1	21.7	0.79	0.82	0.84	3.36	3.40	3.86	3.54
Anancus arvernensis **NMNHS.FM2991E**	5.52	5.37	3.54	24.3	23.0	21.8	0.91	0.92	1.06	3.75	3.99	4.87	4.20
Anancus arvernensis **NMNHS.FM2991F**	5.68	5.67	3.92	24.6	25	23.6	0.83	0.78	0.83	3.39	3.10	3.50	3.33
Anancus arvernensis **NMNHS.FM2991G**	5.33	5.67	3.58	23.2	25.8	22.2	0.79	0.70	0.79	3.39	2.70	3.56	3.21
Cuvieronius sp **FM103247**	6.18	6.06	3.57	25.0	25.4	21.4	0.85	0.86	0.89	3.41	3.37	4.18	3.65
Gomphotherium angustidens **CBar coll. V2**	5.26	5.56	3.71	20.4	23.2	22.2	0.77	0.76	0.78	3.78	3.26	3.50	3.51
Gomphotherium angustidens **SEP38**	5.45	5.11	3.36	22.8	21.6	19.1	0.64	0.71	0.78	2.82	3.29	4.09	3.40
Mammut americanum **FM14293A**	6.33	6.09	3.82	28.8	25.5	24.1	0.95	0.95	0.92	3.30	3.70	3.82	3.61
Mammut americanum **FM14293B**	5.43	5.68	2.96	23.6	23.8	18.4	1.01	1.04	0.87	4.30	4.33	4.74	4.47
Mammuthus columbi **FM144658**	5.71	4.84	3.08	25.9	21.2	21.3	1.10	1.2	0.99	4.24	5.65	4.65	4.85
Mammuthus primigenius **MNHN.F.1904-12**	5.80	5.53	2.92	26.8	25.3	19.7	0.88	1.01	0.93	3.28	3.99	4.69	3.99

***Numidotherium koholense* UOK5**	3.52	3.28	2.56	13.9	14.7	13.9	0.34	0.30	0.28	2.47	2.03	1.99	2.16
***Palaeoloxodon antiquus* M82706**	5.87	5.14	3.93	26.2	22.2	24.1	0.92	0.93	0.91	3.51	4.18	3.78	3.82
***Platybelodon grangeri* 26564**	5.16	4.89	3.54	22.0	22.0	22	0.81	0.65	0.68	3.69	2.93	3.11	3.25
***Prodeinotherium bavaricum* 2013.01108E**	5.60	5.01	3.98	24.7	22.5	22.7	0.69	0.69	0.59	2.79	3.06	2.62	2.82
***Stegodon orientalis* FM18632**	5.36	7.48	3.27	23.7	23.4	15.2	0.83	0.82	0.77	3.51	3.51	5.10	4.04
***Stegomastodon sp* FM21807**	4.91	5.30	?	19.4	22.5	?	1.32	1.18	?	6.8	5.24	?	6.02

The radius of curvature of the lateral canal is 1.24.

The angle between the anterior and posterior canals and the angle between the lateral and posterior canals are more or less right (respectively 91.5° and 87.8°). The angle between the anterior and lateral canals is smaller (80.1°). The radius of curvature of the lateral canal is smaller than those of the anterior and posterior canals. The anterior canal is the largest one and the posterior canal has a medium radius of curvature.

The smaller size of the lateral canal is obvious on the reconstruction (Fig III.1C and III1.D). The anterior canal apex is located slightly higher than the posterior canal apex. The semicircular canals of *Ocepeia* are noticeably thin with an average thickness ratio of 2.15. In cross-section, the canals appear to have a rather circular shape. The slender part of the lateral semicircular canal is connected to the vestibule at a quite high position. There is indeed a partial fusion of the bony lateral canal with the posterior ampulla. All three semicircular canals display a slight undulation. No ridges were observed on the semicircular canals.

Cochlear bony labyrinth

The number of turns of the cochlea is 2.125 (765°). In ventral view (Fig III.1E), the axis for the modiolus is very loose and there is a marked visible lacuna. The basal turn of the cochlea is only partially overlapped by the apical turn and is still visible in ventral view. The *lamina secundaria* is present on the first half-turn and is shallow. The volume of the cochlea is 11.65 mm^3 which represents around two thirds of the total volume of the bony labyrinth.

3.1.2. Unnamed *Embrithopoda* from the Ypresian of Morocco

The isolated petrosal of a yet unpublished representative of the order Embrithopoda (collection number PM53) has been CT-scanned and described for comparisons with proboscideans. Only a fragment of this petrosal has been preserved (the cochlea is almost completely broken) hence the total volume of its inner ear remains unknown.

Petrosal

The petrosal is very incomplete and damaged. In cerebellar view, the internal auditory meatus is shattered but its outline is still observable (Fig III.2B). It has the shape of a latero-medially elongated ellipse. The outline of the foramen acusticum inferior and superior is not visible as both structures are not preserved. The meatus is bordered by a thick prefacial commissure. The subarcuate fossa is located postero-laterally to the meatus and is moderately deep and broken. The *aquaeductus vestibuli* has the shape of a thin slit that opens in the lateral side of the petrosal. No other anatomical features can be seen in the other views.

Vestibular bony labyrinth

Ampullae

The ampullae of PM53 are well-defined and inflated (Fig III.2). They are smooth and display neither ridges nor bumps.

Crus commune

The *crus commune* is elongated and displays no marked basal thickening. It is smooth and displays no ridges. The average section radius of the *crus commune* of PM53 is 0.53 mm and its length is approximately 3.92 mm. Therefore PM53 has the *crus commune* with the lowest thickness ratio of our sample (13.63). The anterior and posterior semicircular canals meet very high (at more than 85% of the anterior canal height) and the *crus commune* is not inclined.

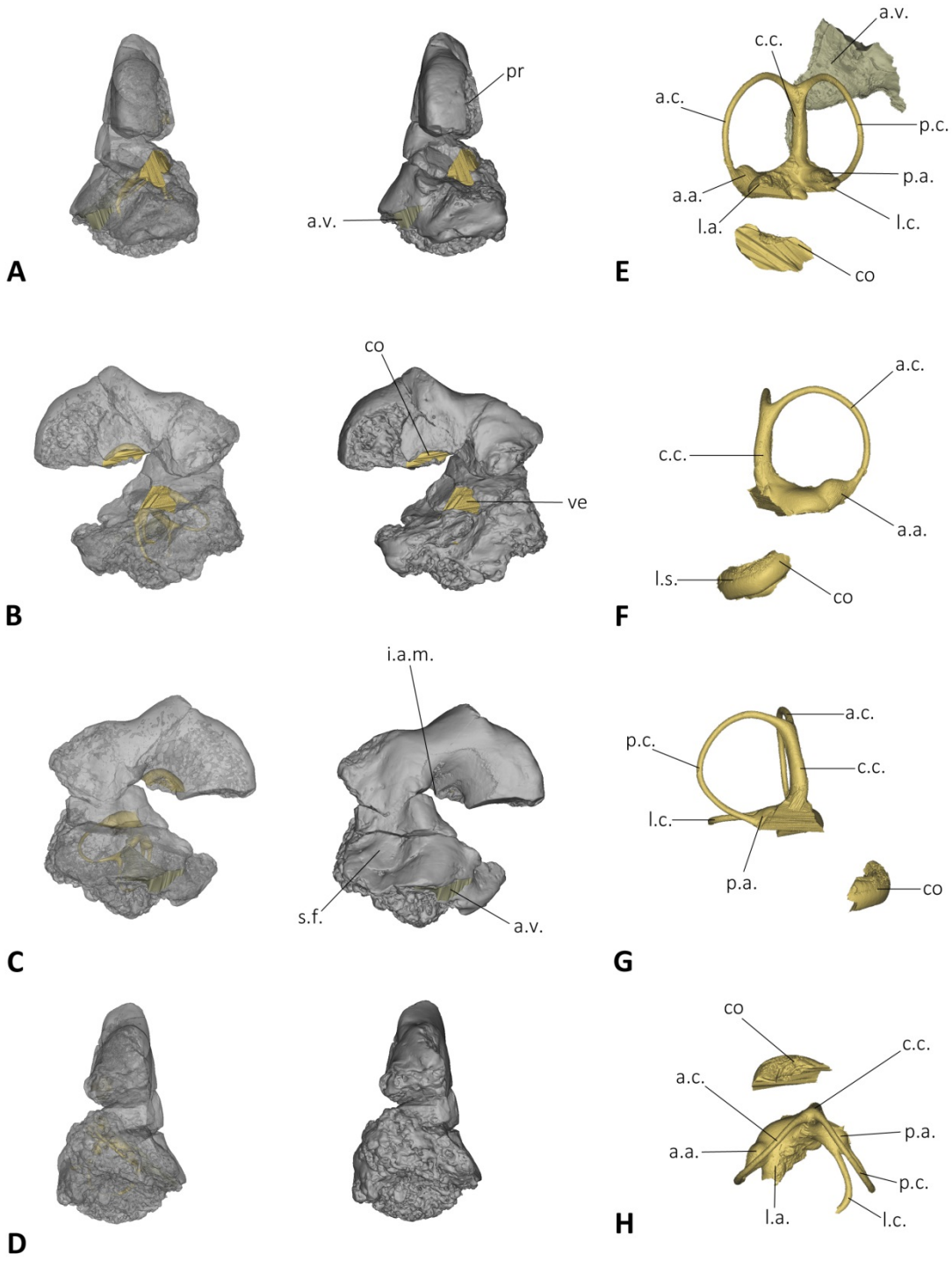

Figure III.2 : Reconstructed 3D model of the petrosal (A-D) and bony labyrinth (E-H) of PM53. (A) Medial view (B) Tympanic view (C) Cerebellar view (D) Lateral view (E) Frontal view (F) Anterior canal view (G) Posterior canal view (H) Lateral canal view. Legends: **a.a.** anterior ampulla, **a.c.** anterior semicircular canal, **a.v.** *aquaeductus vestibuli*, **c.c.** crus commune, **co** cochlea, **i.a.m.** internal auditory meatus, **l.a.** lateral ampulla, **l.c.** lateral semicircular canal, **l.s.** *lamina secundaria*, **p.a.** posterior ampulla, **p.c.** posterior semicircular canal, **pr** *promontorium*, **s.f.** subarcuate fossa, **ve** vestibule

Semicircular canals

The anterior semicircular canal is round. The central streamline length of this canal is 12.63 mm and its average section radius is 0.22 mm. Therefore, the thickness ratio of this canal is 1.72, making it very slender. The anterior canal is the largest in PM53 and its radius of curvature is 3.26.

The posterior semicircular canal is round. The central streamline length of the posterior canal is 13.38 mm which is longer than the value found for the anterior canal. The average section radius of the posterior canal is very similar to the anterior one (0.21 mm). Hence the thickness ratio of the posterior canal (1.57) is very close to the ratio of the anterior canal. The radius of curvature of the posterior canal is similar to the radius of the anterior canal but slightly smaller (3.13).

The lateral semicircular canal is incomplete because the petrosal is broken at this level but it seems to be oval. The estimated length of the central streamline of the lateral canal is 10.96 mm but this is an approximation. The average section radius of the lateral canal is lower than the other canals (0.12 mm). Hence the thickness ratio is clearly lower (1.08) for the lateral canal than for the anterior and posterior canals. The estimated radius of curvature of the lateral canal is 2.29.

The angles between semicircular canals are always around 90°. The highest angle between canals in PM53 is between the lateral and posterior canals (98.6°) which is very large. The angle between the anterior and lateral canals is the lowest and is (83.4°) while the angle between the anterior and posterior canals is in the middle range (86°). The radius of curvature of the lateral canal is smaller (2.29) than those of the anterior (3.26) and posterior canals (3.13). The smaller size of the lateral canal is obvious on the reconstruction. The anterior canal apex is located roughly at the same level than the posterior canal apex. In PM53, the canals are really thin. The average thickness ratio of the semicircular canals is 1.46, which is the lowest observed ratio of our sample. In cross-section, the canals appear to be circular with no particular flattening. The slender part of the lateral semicircular canal is connected to the vestibule at a quite high position. This is illustrated by a partial fusion of the bony lateral canal with the posterior ampulla, as in *Ocepeia*. No ridges nor marked undulations were observed on the semicircular canals.

Cochlear bony labyrinth

Little can be described about the cochlea of this specimen because only a small fraction of this region is preserved. The number of turns is unknown but it displays more than one and a half turn. Indeed, traces of a second cochlear turn have been reconstructed but we cannot know if this second turn is complete. The *lamina secundaria* is present in PM53 as it is preserved on the part of the first turn that we were able to reconstruct.

3.2. Proboscideans

3.2.1. *Numidotherium koholense*

The petrosal and bony labyrinth of *Numidotherium* have already been described in the literature. In Court & Jaeger (1991), the petrosal bone is studied and compared with other tethytheres. In Court (1992), a natural cast of a left cochlea is described. Finally, the first study of the labyrinth of *Numidotherium* using microtomographic methods is carried out by Benoit et al. (2013b). However, the bony labyrinth of *Numidotherium* has never been fully segmented as the specimen studied by Benoit et al. is incomplete. Here we will describe the first complete 3D model of a bony labyrinth of *Numidotherium* and compare it with the other studied specimens. The specimen studied is a rather complete skull belonging to a *Numidotherium koholense* specimen (UOK5). Given the large size of the skull, the ear region was scanned at a rather low resolution (81.66 µm). Moreover, the advanced mineralization of the specimen leads to a poor contrast in the microtomographic slices obtained after reconstruction. Hence, the segmentation might be slightly imprecise, especially concerning the thickness of the various labyrinth structures. The numerical values concerning average section radii, given by the ARIADNE add-on that is currently developed by Romain David, have, for instance, to be taken with caution.

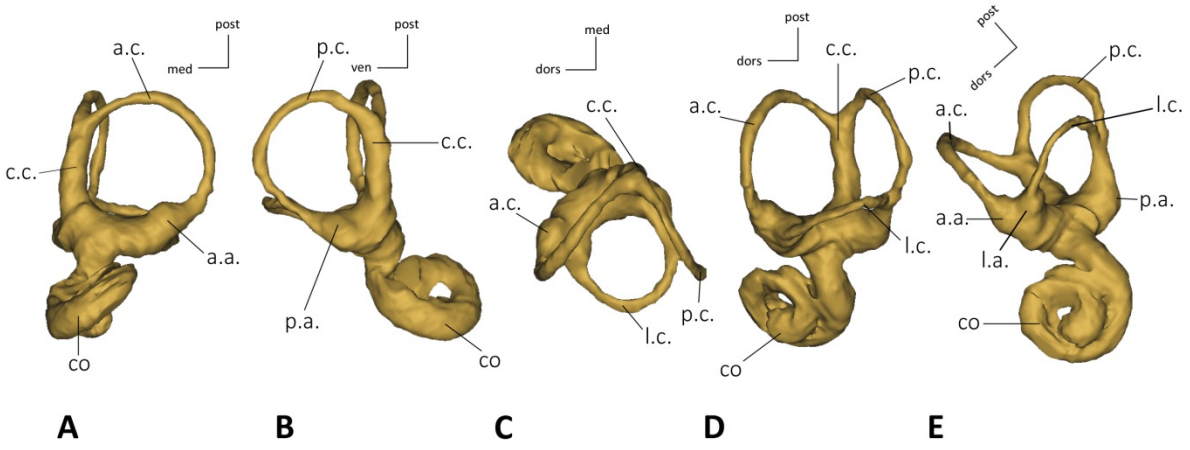

Figure III.3 : Reconstructed 3D model of the bony labyrinth of *Numidotherium koholense* UOK5 in anterior canal (A), posterior canal (B), lateral canal (C), frontal (D) and cochlear (E) views. Legends: **a.a.** anterior ampulla, **a.c.** anterior semicircular canal, **c.c.** *crus commune*, **co** cochlea, **l.a.** lateral ampulla, **l.c.** lateral semicircular canal, **p.a.** posterior ampulla, **p.c.** posterior semicircular canal.

Vestibular bony labyrinth

Ampullae

The ampullae are well marked as in the unlabeled specimen studied in Benoit et al. (2013b). There are no ridges observed on the ampullae (Fig III.3).

Crus commune

The *crus commune* is elongated with no marked basal thickening. It does not display any ossification irregularities as in some specimens of extant elephants. The *crus commune* is thin with an aspect ratio of 14.96. Its central streamline length is 4.5 mm and its average section radius 0.67 mm. The anterior and posterior canals meet quite high (approximately 75% of the height of the anterior canal) and the *crus commune* is not inclined as in the specimen described in Benoit et al. (2013b).

Semicircular canals

The anterior semicircular canal is round. The central streamline length of this canal is 13.89 mm and its average section radius is 0.34 mm. Therefore, the thickness ratio of this canal is 2.47. The length that we found is longer than the measure given by Benoit et al. (2013b) (12.17 mm) for the other specimen. However, this could be due to the difference of protocol used to calculate the length. The anterior canal is the largest canal with a radius of curvature of 3.52. Again, the radius of curvature is larger in our specimen but this could be explained by the difference of measurement protocol that we used. Indeed, the development of the software ARIADNE shows that classical

measurements of the radius of curvature tend to underestimate this value.

The posterior semicircular canal is slightly oval but less clearly than in the unlabeled specimen described in Benoit et al. (2013b). The major axis of the canal forms an angle of 22° with the *crus commune.* A similar value is found in the other specimen (25°). The central streamline length of the posterior canal is 14.79 mm which is slightly longer than for the anterior canal. This is close to the estimated value given in Benoit et al. (2013b). Hence we support their assumption that the posterior canal is longer than the anterior canal. The average section radius of the posterior canal is slightly smaller than the anterior one (0.30 mm). Hence the thickness ratio of the posterior canal (2.02) is smaller than the ratio of the anterior canal. The estimated radius of curvature of the posterior canal is slightly smaller than the radius of the anterior canal (3.28). This is very close to the estimated value (3.21) given by Benoit et al. (2013b).

The lateral semicircular canal is round in this specimen and the unlabeled specimen described by Benoit et al. (2013b). The central streamline length of this canal (13.89 mm) is identical to the anterior canal length. In the specimen described in Benoit et al. (2013b), the lateral canal was too damaged to estimate its length. The average section radius of the lateral canal is close to that of the other canals (0.29 mm) and the thickness ratio (1.99) is close to the ratio of the anterior canal. The radius of curvature of the lateral canal is clearly the smallest with a value of 2.56. It is slightly larger than the measurement estimated by Benoit et al. (2013b) for the other specimen (2.46) but nonetheless very close.

The functional planes of the anterior and posterior canals form an angle of 78.23°. This value is close to the angle measured by Benoit et al. (2013b) on the unlabeled specimen (75°). The angle between the anterior and lateral canals is similar but slightly more acute (75.5°). This differs with the estimation given by Benoit et al. (2013b) which is more obtuse (82°) than for the anterior canal. However, the value found for the angle between the posterior and lateral canals (96°) supports the estimation given by Benoit et al. (2013b) for the other specimen which indicates a larger value for this angle (92°). It appears that this angle is clearly more obtuse in both specimens. In UOK5 and the unlabeled specimen, we find the same pattern of

radii of curvature. The anterior and the posterior canals have quite similar radii while the lateral canal is clearly smaller. The anterior canal is always slightly bigger than the posterior canal, a condition even more marked within our study (there is a difference of 0.23 between the two radii while the difference is only of 0.06 in Benoit et al. 2013b). As it is pointed out in their study, the lateral canal is the smallest one but it is proportionally larger than the lateral canal of extant elephants that display a relatively smaller canal. The anterior canal apex is located slightly higher than the posterior canal apex. As observed in Benoit et al. (2013b), the canals are more slender than the canals of *Moeritherium* and Elephantimorpha. It is approximately as thick as the canals of *Phosphatherium* and thicker than the canals of *Eritherium*. These observations are confirmed by the values of the average thickness ratio (2.16 in *Numidotherium*, 2.09 in *Phosphatherium*, 1.07 in *Eritherium*). The anterior and posterior canals appear to be circular in cross-section. The lateral canal seems to be slightly flattened but this could be due to the imprecise segmentation. The slender part of the lateral semicircular canal is connected to the vestibule at a quite high position. As a result, there is a partial fusion of the bony lateral canal with the posterior canal and ampulla. This structure is generally referred to as secondary common crus. However, contrary to the *crus commune*, the membranous lateral and posterior ducts are never fused together (Gray, 1907, 1908; David, 2011). The fusion occurring in the secondary common crus is only a character of the ossification resulting from the proximity of the posterior and lateral canals. This proximity can be caused by several factors (expansion of the lateral canal, of the posterior canal…) and therefore its homology between taxa is not verified. No ridges were observed on the specimen UOK5 nor on the unlabeled specimen studied in Benoit et al. (2013b). The anterior canal displays an undulation contrary to the other two canals.

Cochlear bony labyrinth

The cochlear bony labyrinth of *Numidotherium* was previously described by Court (1992) and Benoit et al. (2013b). Here, we will compare the endocast of UOK5 with the cochlea of the previously published specimens. The cochlea completes only one and a half turns (Fig III.3E) as the specimen described by Court (1992), while the unlabeled specimen described by Benoit et al. (2013b)

completes 1.62 turns. The aspect ratio is 0.48 which is close to the values calculated for the other specimens (0.52 in Court, 1992; 0.51 in Benoit et al. 2013b). The cochlear coiling is indeed rather planar. The helecotrema is quite large and our specimen bears a small apical lacuna as the unlabeled specimen described in Benoit et al. (2013b). There are no traces of a *lamina secundaria* on this specimen and on the specimen described by Benoit et al. (2013b). However, this structure is clearly present in the specimen described by Court (1992). We can assume that the poor resolution prevents us from observing the furrow for the *lamina secundaria*. The cochlear volume (35.06 mm^3) represents around 42% of the total volume of the bony labyrinth which is close to the values found by Benoit et al. (2013b) for the unlabeled specimen (44%).

3.2.2. *Moeritherium lyonsi*

The periotic of *Moeritherium* was already described in Court (1994) using a specimen from the collection of the London Natural History Museum (NHMUK 68436). The inner ear was partially described in Tassy (1981) in a specimen that bears a partial natural cast of the labyrinth. We tried to scan this specimen but it was too dense to obtain legible tomographies. On the other hand, the specimen described by Court (1994) has been CT-scanned successfully. However, the bony labyrinth is not complete and it is filled with sediment. The specimen is also highly mineralized which prevented from recovering a clear 3D model. Hence, the obtained 3D model is not well detailed and not suitable to any geometric morphometric analysis. Secondly, a basicranium of *Moeritherium lyonsi* from the Stuttgart Museum für Naturkunde (SMNS 47789-90) has been CT-scanned. Contrary to the London specimen, the Stuttgart specimen is not mineralized and the labyrinth remains unfilled. However, only fragments of two semicircular canals are preserved. In this section, we nonetheless present the few anatomical features of the labyrinth that are observed in both specimens and we compare them based on previous descriptions.

Vestibular bony labyrinth

Ampullae

It is difficult to judge of the ampullae definition in specimen NHMUK 68436 given the poor quality of the reconstruction but they seem to be quite well-defined (Fig III.4), by contrast to modern elephants which display poorly defined ampullae.

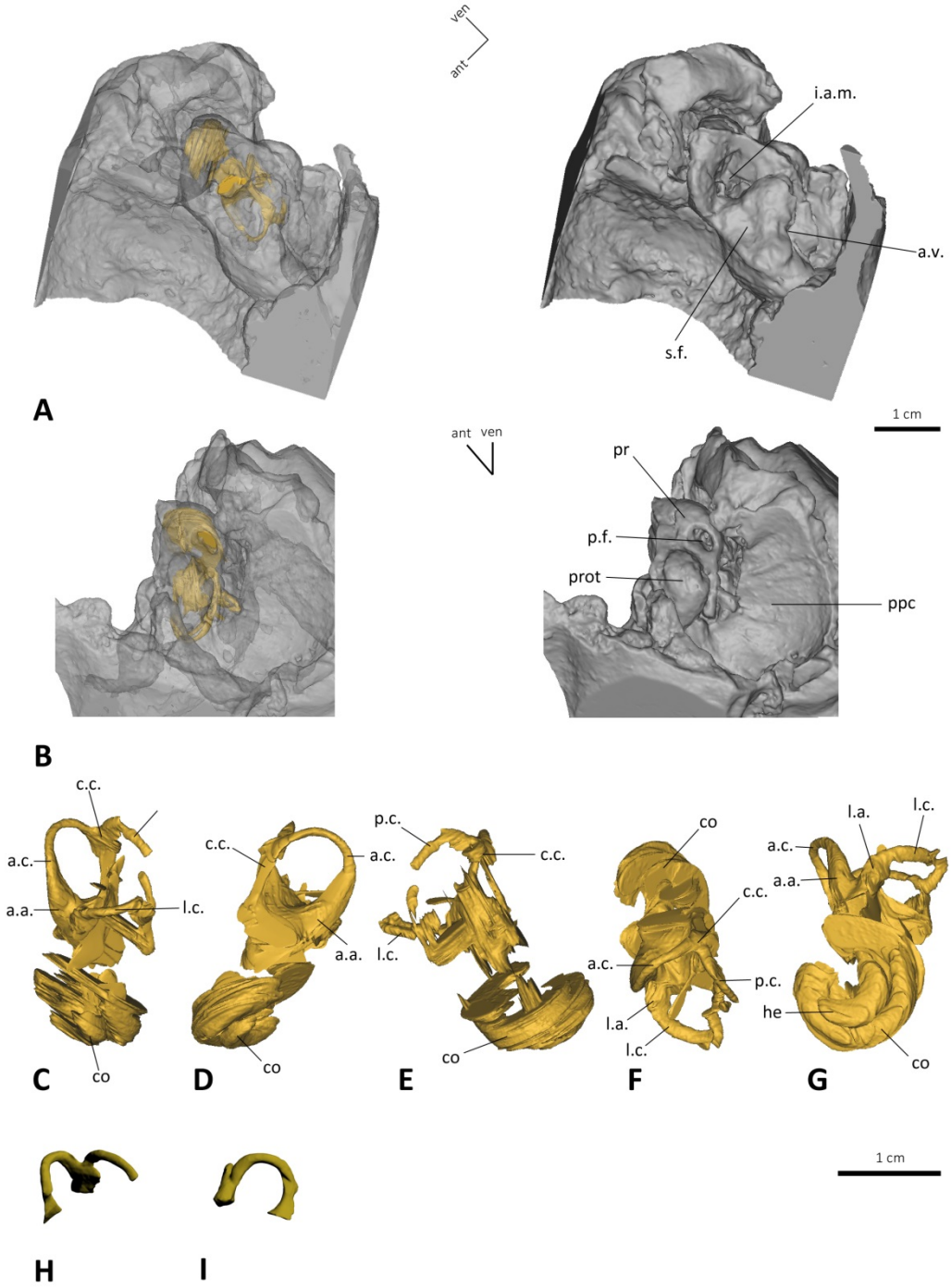

Figure III.4 : Reconstructed 3D models of the petrosal of *Moeritherium* 68436 in cerebellar (A) and posteromedial (B) views. Reconstructed 3D models of the bony labyrinths of specimen 68436 in frontal (C), anterior canal (D), posterior canal (E), lateral canal (F) and cochlear (G) views and of specimen SMNS 47789-90 in frontal (H) and anterior canal (I) views. Legends: **a.a.** anterior ampulla, **a.c.** anterior semicircular canal, **a.v.** *aquaeductus vestibuli*, **c.c.** *crus commune*, **co** cochlea, **he** helicotrema, **i.a.m.** internal auditory meatus, **l.a.** lateral ampulla, **l.c.** lateral semicircular canal, **p.c.** posterior semicircular canal, **p.f.** perilymphatic foramen, **ppc** posterior paratympanic cavity, **pr** *promontorium*, **prot** protuberance, **s.f.** location of the subarcuate fossa.

The poor resolution of the CT scans prevents us from discussing the eventual ossification irregularities of the ampullae. The ampullae are not preserved at all in SMNS 47789-90.

Crus commune

The crus commune, although not fully reconstructed, appears to be elongated in 68436. It is only partially preserved in SMNS 47789-90 and we cannot see if it is elongated or stocky in this specimen. It is difficult to evaluate the presence of a basal thickening as well as ossification irregularities in 68436. It was not possible to landmark these specimens and the reconstructions are too poor to evaluate the average section radius. Hence, there are no quantitative values available for the crus commune. The anterior and posterior canals meet quite high (more than 75% the height of the anterior canal) in both specimens. The crus commune does not seem inclined.

Semicircular canals

No quantitative values (length, average section radius) are available for the semicircular canals. The anterior semicircular canal seems oval and the major axis of the canal forms an angle of 30° with the *crus commune* in specimen NHMUK 68436. The posterior semicircular canal seems to be oval but its reconstruction is very imprecise. The shape of the lateral canal is also difficult to evaluate. The canals of SMNS 47789-90 are too incomplete to determine their shape. In cross-section, the canals of *Moeritherium* appear slightly flattened in 68436, but circular in SMNS 47789-90. The anterior canal apex seems to be located slightly higher than the posterior apex in 68436, but they seem to have the same height in SMNS 47789-90. It is difficult to evaluate the entry point of the lateral canal into the vestibule in specimen NHMUK 68436. Hence, we do not know if there is a fusion with the posterior ampulla. The lateral canal is not preserved at all in SMNS 47789-90.

Cochlear bony labyrinth

The cochlear part and the area of the vestibule are not preserved at all in SMNS 47789-90. The cochlea is not well preserved as well. It completes at least one and a half turns in specimen NHMUK 68436 (Fig III.4G). In the specimen described in Tassy (1981), the cochlea completes 2.25 turns. There could be an apical lacuna in specimen NHMUK 68436 but it is hard to tell. In all cases, the modiolus is rather loose. The poor contrast prevents us from observing the presence of a *lamina secundaria.*

3.2.3. *Prodeinotherium bavaricum*

Three isolated basicranial regions referred to *Prodeinotherium bavaricum* were CT-scanned. However, once the segmentations carried out, we observed that two specimens display very similar bony labyrinths (MHNT.PAL.2013.01108A and Beon 98 E1 3049) while the third one (MHNT.PAL.2013.01108E) displays a very different morphology. The three specimens were found in Montréal-du-Gers, a locality that yielded very few large mammals. All the proboscidean teeth excavated belong to the *Prodeinotherium bavaricum* species except for very rare teeth belonging to *Gomphotherium* (pers. comm. Pascal Tassy 2016) On the other hand, the only other large mammals found in the site are rhinocerotids. Thanks to comparisons with other 3D models and petrosals (pers. comm. Maëva Orliac and Pierre-Olivier Antoine, 2016) we assume that the two similar ears (MHNT.PAL.2013.01108A and Beon 98 E1 3049) are certainly rhinocerotids and do not belong to the species *Prodeinotherium bavaricum* as previously stated. Given the taxonomic sample found in Montréal-du-Gers, the third petrosal (MHNT.PAL.2013.01108E) likely belongs to *Prodeinotherium bavaricum*. Nevertheless, there still could be a very small chance that this specimen belongs to *Gomphotherium*. In all cases the three specimens will be described and compared in this section. Comparisons with other proboscideans will be carried out later in this chapter in order to test our taxonomic assignment. Moreover, the bony labyrinth of *Deinotherium giganteum* (another Deinotheriidae) was investigated in Claudius (1865). Comparisons with this specimen will allow us to compare our sample with the only-known described bony labyrinth of a Deinotheriidae. However, it is to note that this paper is ancient and the given anatomical details are different to what is described nowadays in anatomical investigations of the bony labyrinth. Most of the comparisons made with the *Deinotherium* specimen are based on the illustrations given by the author.

Petrosal

The petrosal of the only specimen that is probably a *Prodeinotherium* (MHNT.PAL.2013.01108E) is quite damaged. Its morphology is very close to the morphology of extant elephants, with the dorsal view separated in two different surfaces (the cerebellar and cerebral surfaces). The cerebellar surface is shattered as well as the internal auditory

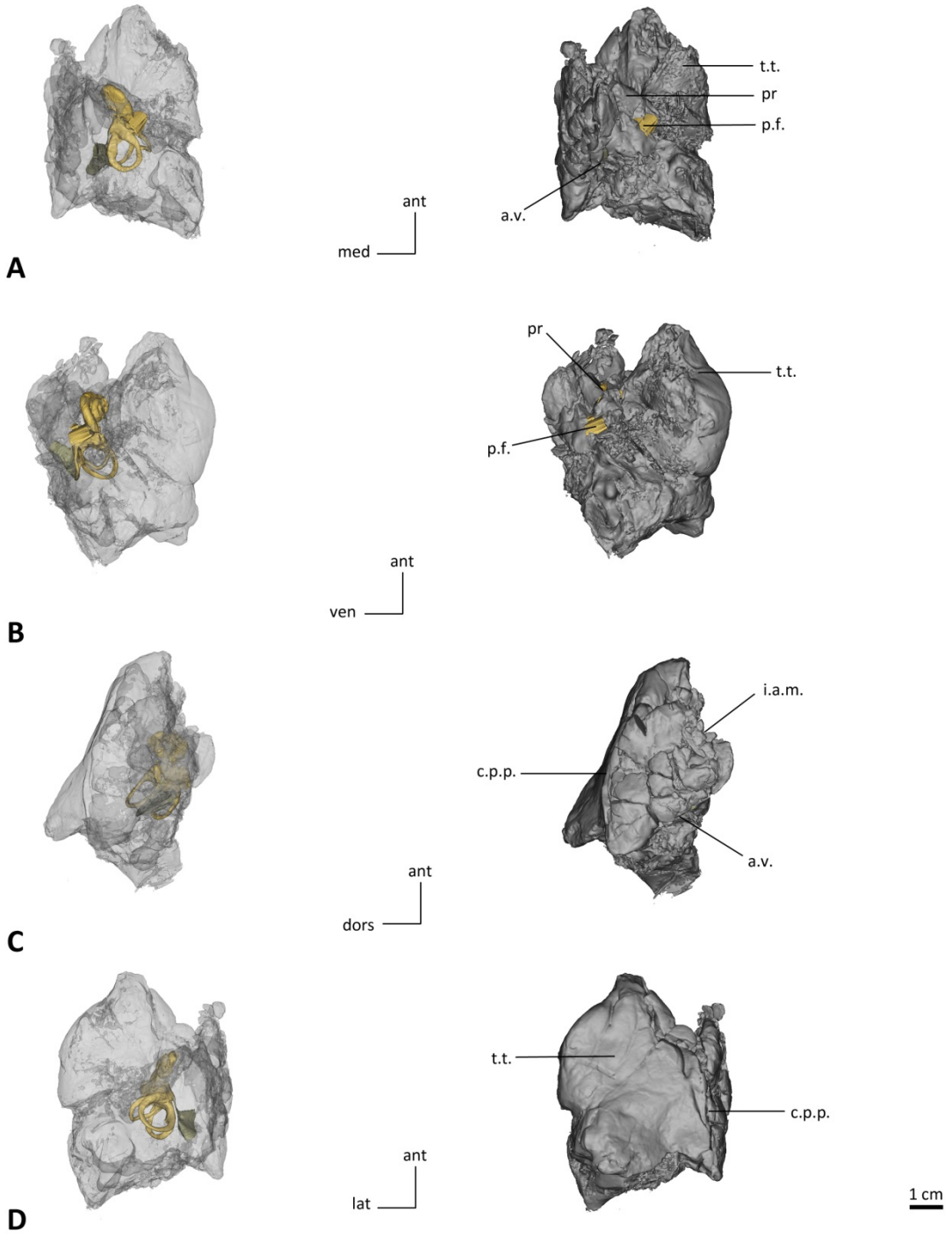

Figure III.5 : Reconstructed 3D models of the petrosal of *Prodeinotherium bavaricum* MHNT.PAL.2013.01108E in medial (A), tympanic (B), cerebellar (C) and cerebral (D) views. Legends: **a.v.** *aquaeductus vestibuli*, **c.p.p.** *crista partis petrosa*, **i.a.m.** internal auditory meatus, **p.f**. location of the perilymphatic foramen, **pr** *promontorium*, **t.t.** *tegmen tympani*.

meatus (Fig III.5). Given the morphology of this specimen, the internal auditory meatus is very probably oriented antero-posteriorly as in extant elephants. The vestibular aqueduct has the shape of a thin slit and is located postero-ventrally. The *crista partis petrosa* is not sharp. There is no trace of a subarcuate fossa. The cerebral surface consists mostly of the *tegmen tympani*. The groove for the middle meningeal artery is not visible. In tympanic view, the *tegmen tympani* appears shorter and more bulbous than in elephantimorphs. The *promontorium* is damaged but it appears to be moderately bulbous. The *fenestra vestibuli* is not preserved (if so, it is heavily broken). The perilymphatic foramen is broken as well but its location is still visible on the reconstruction (Fig III.6A and 6B). There is no trace of a cochlear canaliculus, hence the unique perilymphatic foramen seems to be retained during ontogeny as in extant elephants (Fischer, 1990). In contrary, there is a cochlear canaliculus well distinct from the *fenestra cochleae* in the specimen secondarily referred to a member of the rhinocerotids (MHNT.PAL.2013.01108A, Fig III.6F to J). We assume that the third specimen (Beon 98 E1 3049) certainly displays the same morphology as MHNT.PAL.2013.01108A since they seem to belong to the same species.

Inner ear

The bony labyrinths of MHNT.PAL.2013.01108E and MHNT.PAL.2013.01108A are more or less complete although the cochlea of MHNT.PAL.2013.01108E is partially shattered. On the other hand, the cochlea is not preserved at all in Beon 98 E1 3049 which makes it impossible for us to calculate the total volume of its bony labyrinth. The total volume is around 674 mm^3 in MHNT.PAL.2013.01108E and 401 mm^3 in MHNT.PAL.2013.01108A.

Vestibular bony labyrinth

Ampullae

The ampullae of specimen MHNT.PAL.2013.01108E are poorly defined while they are rather well defined in rhinocerotids MHNT.PAL.2013.01108A and Beon 98 E1 3049. MHNT.PAL.2013.01108E displays a small bump on its lateral ampulla (Fig III.6). In contrast, no ossification irregularities are found in specimens MHNT.PAL.2013.01108A and Beon 98 E1 3049.

Crus commune

The *crus commune* is quite slender and elongated in all the studied specimens. It never displays a clear basal thickening. The *crus commune* is smooth in MHNT.PAL.2013.01108A and Beon 98 E1 3049. On the contrary, the *crus commune* of MHNT.PAL.2013.01108E displays extreme ossification irregularities. There is a bump at the intersection of the anterior and posterior canals. A very sharp and salient ridge originates from this bump and runs across the *crus commune* to the insertion of the lateral canal into the vestibule. The average section radius of the *crus commune* is very similar in MHNT.PAL.2013.01108A and Beon 98 E1 3049 (respectively 1.12 mm and 1.08 mm) but it is slightly larger in MHNT.PAL.2013.01108E (1.26 mm). The same can be said about the length. MHNT.PAL.2013.01108A and Beon 98 E1 3049 share similar values (4.02 mm and 4.33 mm respectively) but it is clearly longer in MHNT.PAL.2013.01108E (5.91 mm). Therefore the *crus commune* is slightly more slender in MHNT.PAL.2013.01108E than in the other two specimens. This is confirmed by the values of the average thickness ratio (Table III.1). The anterior and posterior canals meet quite high (approximately 75% of the height of the anterior canal in MHNT.PAL.2013.01108A and Beon 98 E1 3049 and two thirds of the height of the anterior canal in MHNT.PAL.2013.01108E). The *crus commune* is not inclined in MHNT.PAL.2013.01108A and Beon 98 E1 3049, while it is slightly inclined towards the anterior semicircular canal in MHNT.PAL.2013.01108E.

Semicircular canals

The anterior semicircular canal is oval in all the studied specimens. In MHNT.PAL.2013.01108E, the major axis of the canal forms an angle of 47° with the *crus commune.* In contrast, the angle is smaller in MHNT.PAL.2013.01108A and Beon 98 E1 3049 (36° in both specimens). The length of the anterior canal is very similar in MHNT.PAL.2013.01108A and Beon 98 E1 3049 (17.42 mm and 17.45 mm respectively) but is clearly longer in MHNT.PAL.2013.01108E (24.73 mm). The average section radius and the average thickness ratio values of the anterior canal are given in Table III.2. The radius of curvature of the anterior canal is similar in MHNT.PAL.2013.01108A and Beon 98 E1 3049 (4.13 and 4.19 respectively) while it is much larger in MHNT.PAL.2013.01108E (5.60).

The posterior semicircular canal is round in MHNT.PAL.2013.01108E but more oval in MHNT.PAL.2013.01108A and Beon 98 E1 3049 where their major axis both form an angle of 31 ° with the *crus commune*. Again, the central streamline length of this canal is similar in MHNT.PAL.2013.01108A and Beon 98 E1 3049 (respectively 19.21 mm and 18.63 mm) but longer in MHNT.PAL.2013.01108E (22.52 mm). The average section radius and the average thickness ratio values of the posterior canal are given in Table III.2. As for the anterior canal, the values of the radius of curvature of the posterior canal are close in MHNT.PAL.2013.01108A and Beon 98 E1 3049 (3.98 and 3.94 respectively) while it is much larger in MHNT.PAL.2013.01108E (5.01).

The lateral semicircular canal is oval in MHNT.PAL.2013.01108E while it is rounder in MHNT.PAL.2013.01108A and Beon 98 E1 3049. As for the anterior and posterior canals, the central streamline length is similar between specimens MHNT.PAL.2013.01108A and Beon 98 E1 3049 (respectively 18.47 mm and 17.40 mm) while it is longer in MHNT.PAL.2013.01108E (22.67 mm). The average section radius and the average thickness ratio values of the lateral canal are given in Table III.2. Again, the radius of curvature of this canal is similar in MHNT.PAL.2013.01108A and Beon 98 E1 3049 (3.44 and 3.26 respectively) while it is larger in MHNT.PAL.2013.01108E (3.98).

The angle between the anterior and posterior semicircular canals is similar and almost right in MHNT.PAL.2013.01108A (94.41°) and Beon 98 E1 3049 (90.95°) with a difference of less than 4°. However, it is much more acute in MHNT.PAL.2013.01108E (77.16°). The angle between the anterior and lateral canals is however acute in all three specimens. Nevertheless, specimens MHNT.PAL.2013.01108A and Beon 98 E1 3049 again display a larger angle (respectively 76.10° and 73.92°) than MHNT.PAL.2013.01108E (67.60°). Finally, the angle between the posterior and lateral canals displays more similar values among the three studied specimens. However specimens MHNT.PAL.2013.01108A and Beon 98 E1 3049 still display similar larger angles (respectively 98.9° and 95°) than MHNT.PAL.2013.01108E (90.7°). If we compare these angles with one

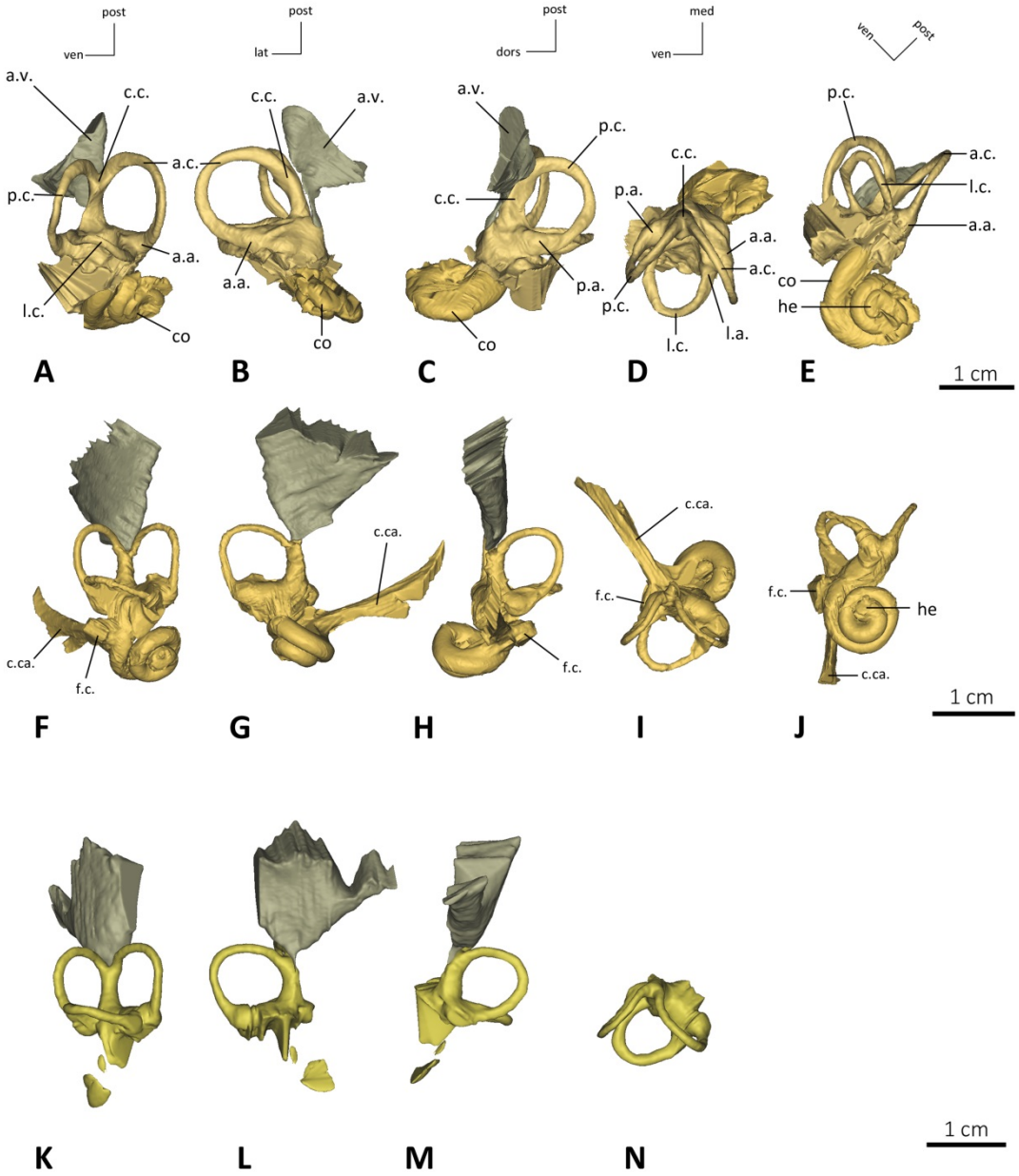

Figure III.6 : 3D reconstructed models of the bony labyrinths of *Prodeinotherium bavaricum* MHNT.PAL.2013.01108E (A-E) and unknown rhinocerotids isolated petrosals previously assigned to *Prodeinotherium* MHNT.PAL.2013.01108A (F-J) and Beon 98 E1 3049 (K-N) in frontal (A, F, K), anterior canal (B, G, L), posterior canal (C, H, M), lateral canal (D, I, N) and cochlear (E, J) views. Legends: **a.a.** anterior ampulla, **a.c.** anterior semicircular canal, **a.v.** *aquaeductus vestibuli*, **c.c.** *crus commune*, **c.ca.** cochlear canaliculus, **co** cochlea, **f.c.** *fenestra cochleae*, **he** helicotrema, **l.a.** lateral ampulla, **l.c.** lateral semicircular canal, **p.a.** posterior ampulla, **p.c.** posterior semicircular canal.

another, we find out that the specimens display more or less the same pattern. The largest angle is always the one between the posterior and lateral canals. It is a right angle in MHNT.PAL.2013.01108E and a more obtuse angle in MHNT.PAL.2013.01108A and Beon 98 E1 3049. The angle between the anterior and posterior canals is always in the middle range. However, while it is rather right and slightly smaller than the angle between the lateral and posterior canals in MHNT.PAL.2013.01108A and Beon 98 E1 3049 (difference of 4-5°), it is acute and very much smaller than the previous angle in MHNT.PAL.2013.01108E (difference of almost 13°). Finally, the angle between the anterior and lateral canal is always the smallest angle. It is more acute in MHNT.PAL.2013.01108E than in the other two specimens. However, if we compare to the other angles, the difference between this angle and the other angles is greater in MHNT.PAL.2013.01108A and Beon 98 E1 3049 (difference of around 17° with the angle between the anterior and posterior canals) than in MHNT.PAL.2013.01108E (difference of around 10° with the angle between the anterior and posterior canals). Regarding the radii of curvature, in all the specimens the canal with the greater radius is the anterior canal, then comes the posterior canal and the smallest one is always the lateral canal. However, the radii of curvature of MHNT.PAL.2013.01108A and Beon 98 E1 3049 are very similar to one another, while the radii of MHNT.PAL.2013.01108E are always much larger (Table III.2). On the other hand, and even though the lateral is always the smallest one, it is relatively smaller compared to the anterior and posterior in MHNT.PAL.2013.01108E. This is confirmed by the radii of curvature values. In MHNT.PAL.2013.01108A and Beon 98 E1 3049, the apex of the posterior and anterior canals are located at the same height while the anterior canal apex is located clearly higher than the posterior one in MHNT.PAL.2013.01108E. In terms of thickness, the semicircular canals are in the mean range compared to extant elephants, but thicker than earliest known proboscideans such as *Eritherium* and *Phosphatherium*. In cross-section, the canals of MHNT.PAL.2013.01108E appear clearly flattened. However, they are rather circular in MHNT.PAL.2013.01108A and Beon 98 E1 3049. The slender part of the lateral semicircular canal enters the vestibule in a somewhat high position in all three specimens. In MHNT.PAL.2013.01108E, the entry point is

markedly distant from the posterior ampulla. Therefore, the lateral and posterior bony canals are never fused. The same conformation is seen in the illustration of the specimen studied by Claudius (1864) which supports our taxonomic assignment. In contrast, in MHNT.PAL.2013.01108A and Beon 98 E1 3049, the entry point is quite close to the posterior ampulla. Hence, the lateral bony canal is fused with the posterior ampulla and with the slender part of the posterior canal. There are no marked ridges on the semicircular canals of any of the studied specimens. In MHNT.PAL.2013.01108A and Beon 98 E1 3049, the anterior and posterior canals are slightly undulated while the lateral canal seems quite straight. In MHNT.PAL.2013.01108E, the anterior canal is slightly undulated as well. However, the posterior and lateral canals display extreme undulations (especially the lateral one).

Cochlear bony labyrinth

The cochlea of Beon 98 E1 3049 is not preserved at all. In MHNT.PAL.2013.01108A, it is well preserved and in MHNT.PAL.2013.01108E, the cochlea was quite shattered but we were able to segment it more or less completely. It completes two full turns (720°) in MHNT.PAL.2013.01108A (Fig III.6E) and 2.25 turns (810°) in MHNT.PAL.2013.01108E (Fig III.6J). We estimate the number of turns of the specimen studied by Claudius (1864) to be 2.25 as in MHNT.PAL.2013.01108E which supports our taxonomic assignment. In ventral view, the modiolus is slightly loose in MHNT.PAL.2013.01108E and displays a small apical lacuna. This is not the case in MHNT.PAL.2013.01108A. The *lamina secundaria* is absent in both specimens. The relative volume of the cochlea (57%) is higher in the rhinocerotid specimen (MHNT.PAL.2013.01108A) than in the *Prodeinotherium* specimen (2013.01108E).

3.2.4. *Mammut americanum*

Petrosal

Two specimens of *Mammut americanum* from the AMNH were CT-scanned. On the first specimen (FM14293-A), a part of the petrosal has been cut off at the level of the cochlea a few years ago for investigation. On the second specimen (FM14293-B), the cochlear part of the petrosal is completely missing. Hence the total volume of the bony labyrinth is unknown for both specimens. However,

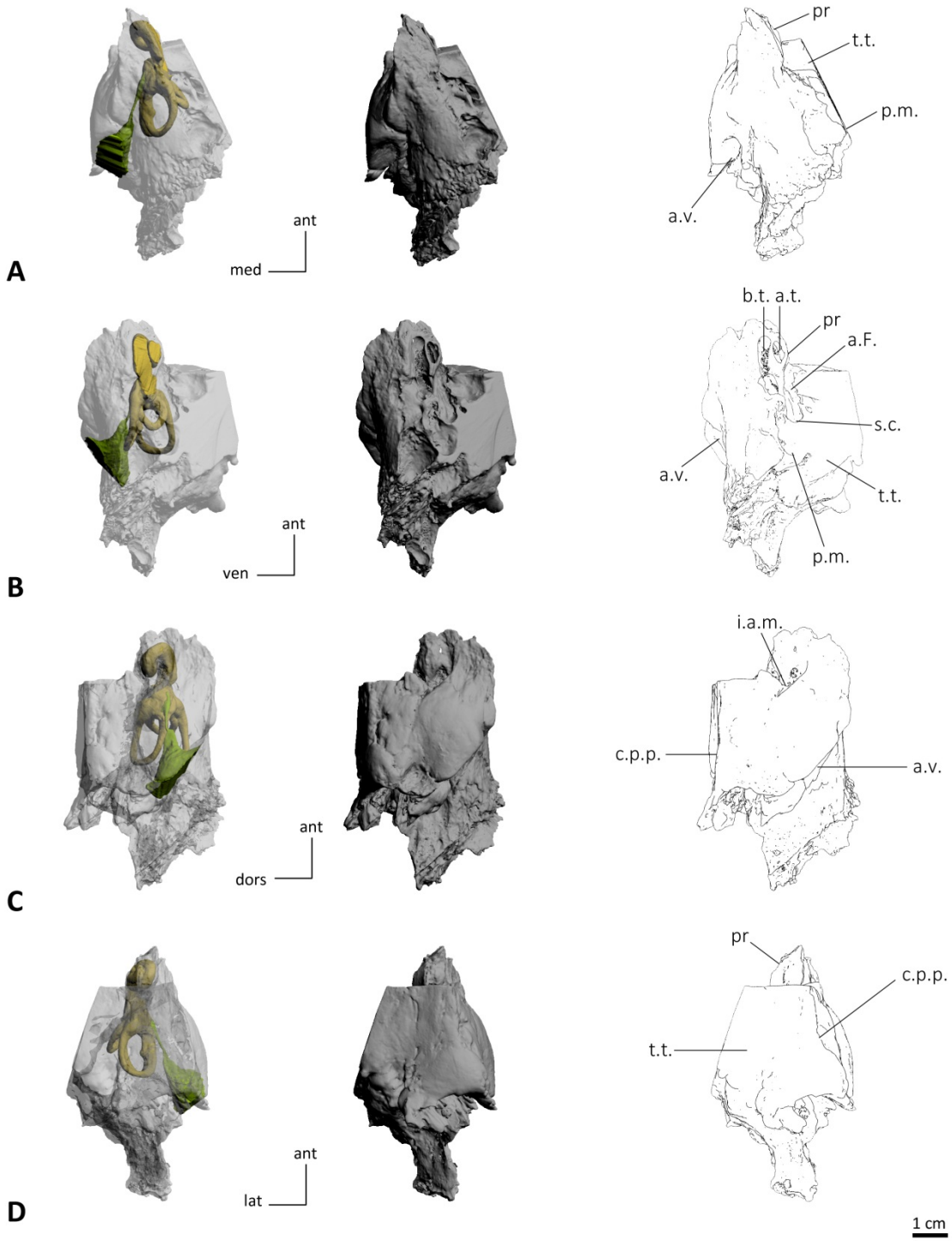

Figure III.7 : 3D reconstructed models and drawings of the petrosal of *Mammut americanum* FM14293A in medial (A), tympanic (B), cerebellar (C) and cerebral (D) views. Legends: **a.F.** *aquaeductus Fallopii*, **a.t.** apical turn of the cochlea, **a.v.** *aquaeductus vestibuli*, **b.t.** basal turn of the cochlea, **c.p.p.** *crista partis petrosa*, **i.a.m.** internal auditory meatus, **p.m.** *pars mastoidea*, **pr** *promontorium*, **s.c.** stylomastoid canal (part of), **t.t.** *tegmen tympani*.

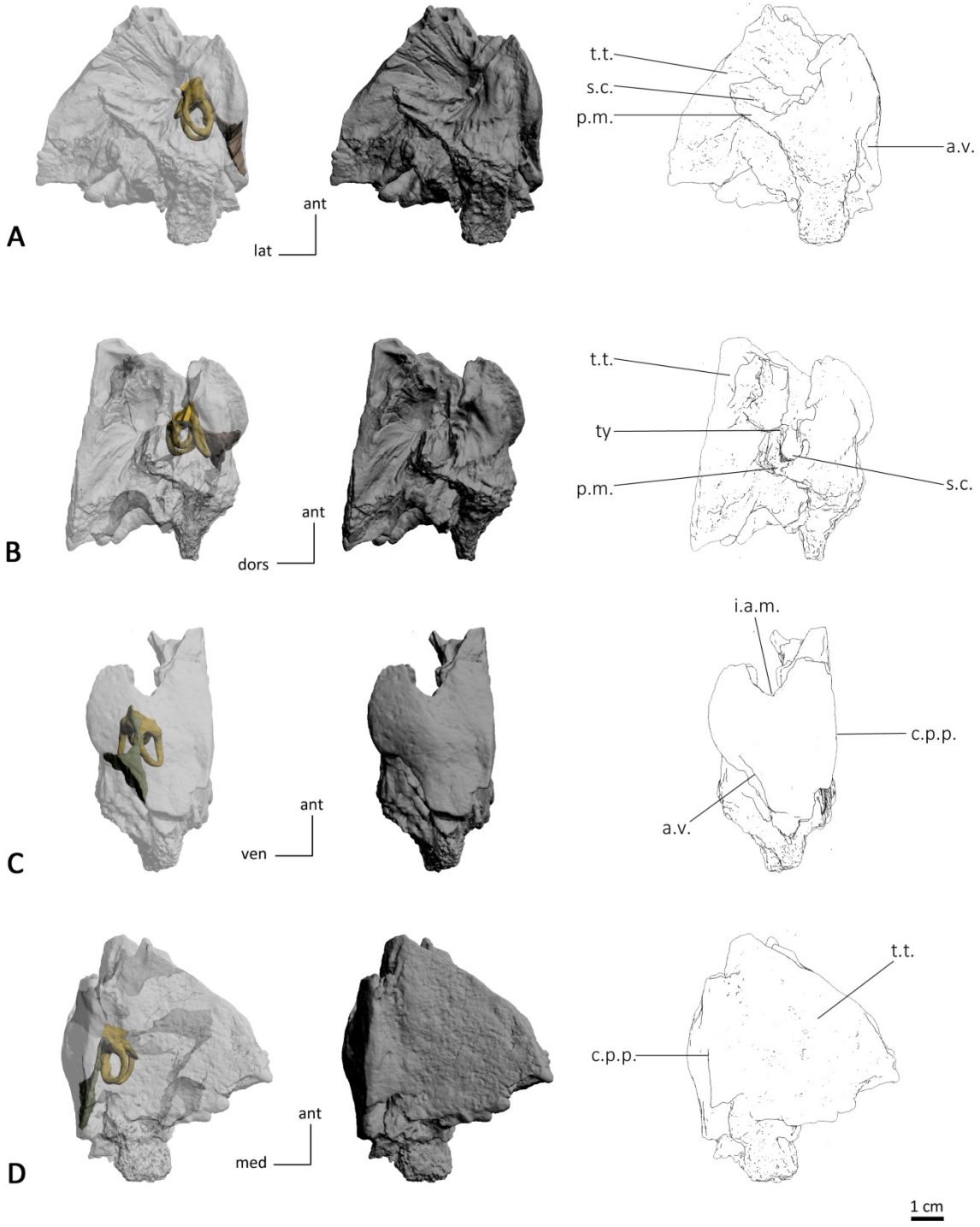

Figure III.8 : 3D reconstructed models and drawings of the petrosal of *Mammut americanum* FM14293B in medial (A), tympanic (B), cerebellar (C) and cerebral (D) views. Legends: **a.v.** *aquaeductus vestibuli*, **c.p.p.** *crista partis petrosa*, **i.a.m.** internal auditory meatus, **p.m.** *pars mastoidea*, **pr** *promontorium*, **s.c.** stylomastoid canal (part of), **t.t.** *tegmen tympani*, **ty** tympanohyal.

the bone fragment collected on FM14293-A is minor. Therefore we can infer that the approximated total volume of the bony labyrinth of FM14393-A is slightly over 936.25 mm^3. In cerebellar view, the petrosal is elongated antero-posteriorly but less than in extant elephants. The *aquaeductus vestibuli* is oriented in the same way and exits postero-ventrally in both specimens. It has the aspect of a slit in FM14293B but the opening is rounder in FM14293A, especially in posterior view. The cerebellar surface is rather flat in FM14293A but it is slightly convex in FM14293B. There is no trace of a subarcuate fossa. The *crista partis petrosa* is well defined in FM14293B but it is blunter in FM14293A. The internal auditory meatus is partially damaged in FM14293B but more preserved in FM14293A. It is oriented antero-posteriorly, as in extant elephants. The epitympanic wing, if present, is broken in both specimens. The angle between the cerebral and cerebellar surfaces of the petrosal is right in both specimens (93°).

In cerebral view (Fig III.7A and III.8A), the *tegmen tympani* is broken anteriorly in FM14293B and it has been cut off anteriorly and laterally. There is no trace of the middle meningeal artery in both ears. It could be absent in life or not preserved in the studied specimens as the *tegmen tympani* is incomplete in both of them.

In tympanic view (Fig III.7B and III.8B), specimen FM14293B is more complete than FM14293A. The *promontorium* is only partially preserved in both specimens but the *crista interfenestralis* is broken. The unique perilymphatic foramen that generally divides into the f*enestra cochleae* and cochlear canaliculus in mammals is retained in *Mammut* as in extant elephants. Only part of the *fenestra vestibuli* is preserved (in FM14293B). It is impossible to calculate the stapedial ratio. The *pars mastoidea* is partially preserved in in FM14293B with the stylomastoid canal still visible. In in FM14293A, the *pars mastoidea* is broken but the imprint of at least one pneumatic cavity is visible on the 3D model. The tympanohyal is broken in both specimens. The *aquaeductus Fallopii* is deep and the bony roof that covers it is broken in both specimens.

Inner ear

Vestibular bony labyrinth

Ampullae

Compared to other mammals, the ampullae of *Mammut* appear less defined. It is a common feature shared by every

studied elephantimorphs. There is no clear ampullar ridge on FM14393-B, but on FM14393-A, both anterior and lateral semicircular canal ampullae display a ridge. The anterior one is superficial but the lateral one is associated with a small bulge (Fig III.9).

Crus commune

The *crus commune* is elongated and displays no marked basal thickening. In FM14393-A, a vertical ridge runs on the *crus commune* in the extension of the posterior semicircular canal ridge associated with a well-marked bulge. In FM14393-B, the vertical ridge is present as well as a less pointy bulge. The average section radius of the *crus commune* of *Mammut* is 1.18 in FM14393-A and 1.55 mm in FM14393-B. The length of the *crus commune* is approximately 7.74 in FM14393-A and 7.21 mm in FM14393-B. Therefore the specimens have a *crus commune* with a thickness ratio of 15.24 (FM14393-A) and 21.55 (FM14393-B). In FM14393-A, the anterior and posterior semicircular canals meet quite low (approximately at the mid-height of the anterior canal) while they meet higher in FM14393-B (approximately at two thirds of the height of the anterior canal). The *crus commune* is not inclined on both specimens.

Semicircular canals

The anterior semicircular canal is oval in both FM14293-A and FM14293-B. While the major axis of the canal forms an angle of 27° with the *crus commune* in FM14293-A, it forms an even bigger angle in FM14293-B (36°). The anterior semicircular canal appears more slender in FM14293-A than in FM14293-B. Indeed the central streamline of the anterior canal is longer in FM14293-A (28.81 mm) than in FM14293-B (23.58 mm). The average section radius of the anterior canal of *Mammut* is 0.95 mm in FM14393-A and 1.01 mm in FM14393-B. Therefore, the thickness ratio of this canal is 3.30 in FM14393-A and 4.30 in FM14393-B. The anterior canal radius of curvature is 6.33 in FM14293-A and 5.43 in FM14293-B.

The posterior semicircular canal is oval in both FM14293-A and FM14293-B. The major axis of the canal forms an angle of 5° with the *crus commune* in both specimens which is clearly less than the angle of the anterior canal. The central streamline length of the posterior canal is 25.54 mm in FM14293-A and 23.79 mm in FM14293-B.

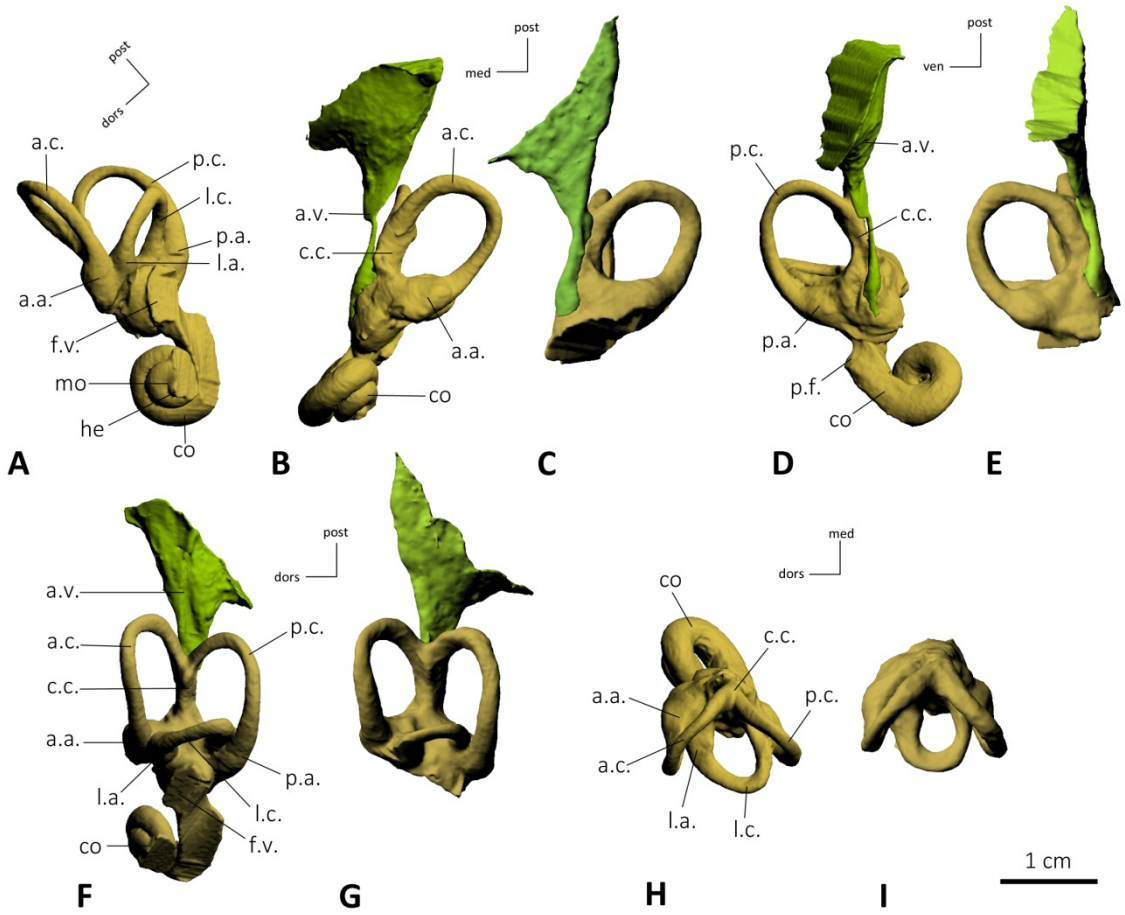

Figure III.9 : 3D reconstructed models of the bony labyrinths of *Mammut americanum* FM14293A (A,B,D,F,H) and FM14293B (C,E,G,I) in cochlear (A), anterior canal (B-C), posterior canal (D-E), frontal (F-G) and lateral canal (H-I) views. Legends: **a.a.** anterior ampulla, **a.c.** anterior semicircular canal, **a.v.** *aquaeductus vestibuli*, **c.c.** *crus commune*, **c.ca.** cochlear canaliculus, **co** cochlea, **f.c.** *fenestra cochleae*, **f.v.** *fenestra vestibuli*, **he** helicotrema, **l.a.** lateral ampulla, **l.c.** lateral semicircular canal, **mo** modiolus, **p.a.** posterior ampulla, **p.c.** posterior semicircular canal, **p.f.** perilymphatic foramen.

While the value is very similar with the anterior canal value in FM14293-B, there is a difference of more than 3 mm in FM14293-A. The average section radius of the posterior canal is very similar to the anterior one (0.95 mm in FM14393-A and 1.04 mm in FM14393-B). The thickness ratio of this canal is very close to the anterior ratio in FM14293-B (4.36) and slightly higher in FM14393-A (3.70). The radius of curvature of the posterior canal is greater 6.09 in FM14293-A (6.09) than in FM14293-B (5.68).

The lateral semicircular canal is clearly oval in FM14293-A but it is more round in FM14293-B. The central streamline of the lateral canal is shorter compared to the other semicircular canals (24.13 mm in FM14293-A and 18.37 mm in FM14293-B). The average section radius of the lateral canal is lower than in other canals (0.92 mm in FM14393-A and 0.87

mm in FM14393-B). The thickness ratio of this canal is higher than the ratio of the anterior and posterior canals (3.82 in FM14393-A and 4.74 in FM14393-B). The radius of curvature of the lateral canal is 3.82 in FM14293-A and 2.96 in FM14293-B.

The angles between semicircular canals are more or less similar in FM14393-A and FM14393-B, but the intraspecific variability can reach a difference of more than 5°. In both specimens, the angle between the anterior and posterior canals (86.5° in FM14393-A and 80.5° in FM14393-B) and the angle between the posterior and lateral canals (81.4° in FM14393-A and 80.9° in FM14393-B) are similar and larger than the angle between the anterior and the lateral canal (68.8° in FM14393-A and 65.1° in FM14393-B). The radii of curvature of FM14393-A canals are always larger than those of FM14393-B which is probably due to a difference of size between the specimens. Moreover, the lateral canal is always smaller (3.82 in FM14393-A and 2.96 in FM14393-B) than the anterior and posterior canals which tend to have quite similar radii of curvature (respectively 6.33 and 5.43 in FM14393-A and 6.09 and 5.68 in FM14393-B). The smaller size of the lateral canal is obvious even on the reconstruction. The radius of the anterior canal is higher than the posterior canal radius in FM14393-A. This feature is clearly visible and marked in the reconstruction of FM14393-A. Furthermore the anterior canal apex is located higher than the posterior one which could explain the larger radii values. This feature is present in both specimens but it is clearly more pronounced in FM14393-A. In terms of thickness, the semicircular canals of *Mammut* are rather average but the canals of FM14393-B are slightly thicker (average thickness ratio = 4.47) than those of FM14393-A (average thickness ratio = 3.61). In cross-section, the canals appear to be flattened but less than extant elephants. In FM14393-B, the posterior semicircular canal does not display a marked flattening. The slender part of the lateral semicircular canal is connected to the vestibule at a high position. No ridges were observed on the semicircular canals of FM14393-B but the anterior and posterior canals of FM14393-A each display a ridge near the *crus commune*. All the canals of FM14393-A displays a slight undulation. In FM14393-B, only the anterior and posterior canals display one.

Cochlear bony labyrinth

The cochlea is completely missing in FM14293-B. The cochlea of the other specimen (FM14293-A) is only partially broken and the number of turns is 2.375 (855°). In ventral view, the modiolus is completely overlapped by the apical turn and there is no visible gap. The basal turn of the cochlea is only partially overlapped by the apical turn and is still visible in ventral view. The *lamina secundaria* is absent. The volume of the cochlea (343 mm^3) represents 37% of the total volume of the bony labyrinth but this value is slightly underestimated given the broken part.

3.2.5. *Gomphotherium angustidens*

Three specimens of *Gomphotherium angustidens* were CT-scanned. First, the basicranial region of MNHN skull specimens SEP18 and SEP38 was scanned. The contrast and resolution of the microtomographic sections obtained for SEP18 were so poor that the inner ears of this specimen could not be segmented. On the contrary, both inner ears of SEP38 were complete and contrasted enough to be segmented. However, the resolution was not good because of the great size of the specimen. Hence, an isolated petrosal of another specimen of *Gomphotherium angustidens* from the collections of the Natural History Museum of Toulouse (Cbar coll.V 2) was scanned and entirely segmented.

Petrosal

The petrosal of *Gomphotherium* was previously described by Tassy (2013) so we will not describe it in details here. The petrosal is very similar to the petrosal of extant elephants (Fig III.10 and III.11), with the dorsal part consisting of two surfaces. Contrary to the description of Tassy (2013), we found that the *crista partis petrosa* is very sharp in SEP38. However it is blunt in Cbar coll.V 2 in which the *tegmen tympani* is broken. The groove for the middle meningeal artery is deep and it meanders upon the surface of the *tegmen tympani* in SEP38. The cerebellar surface that normally bears the subarcuate fossa is slightly convex in SEP38 and concave in Cbar coll.V 2. The internal auditory meatus is oriented anteriorly as every other studied elephantimorphs. The vestibular aqueduct is oriented postero-ventrally in SEP38 and has the aspect of a thin slit. However, it is oriented posteriorly in Cbar coll.V 2 and has a rounder shaper. In posterior view, the vestibular aqueduct is clearly ventral in SEP38 but more centered in Cbar coll.V 2. The stapedial ratio is 1.5 for both specimens.

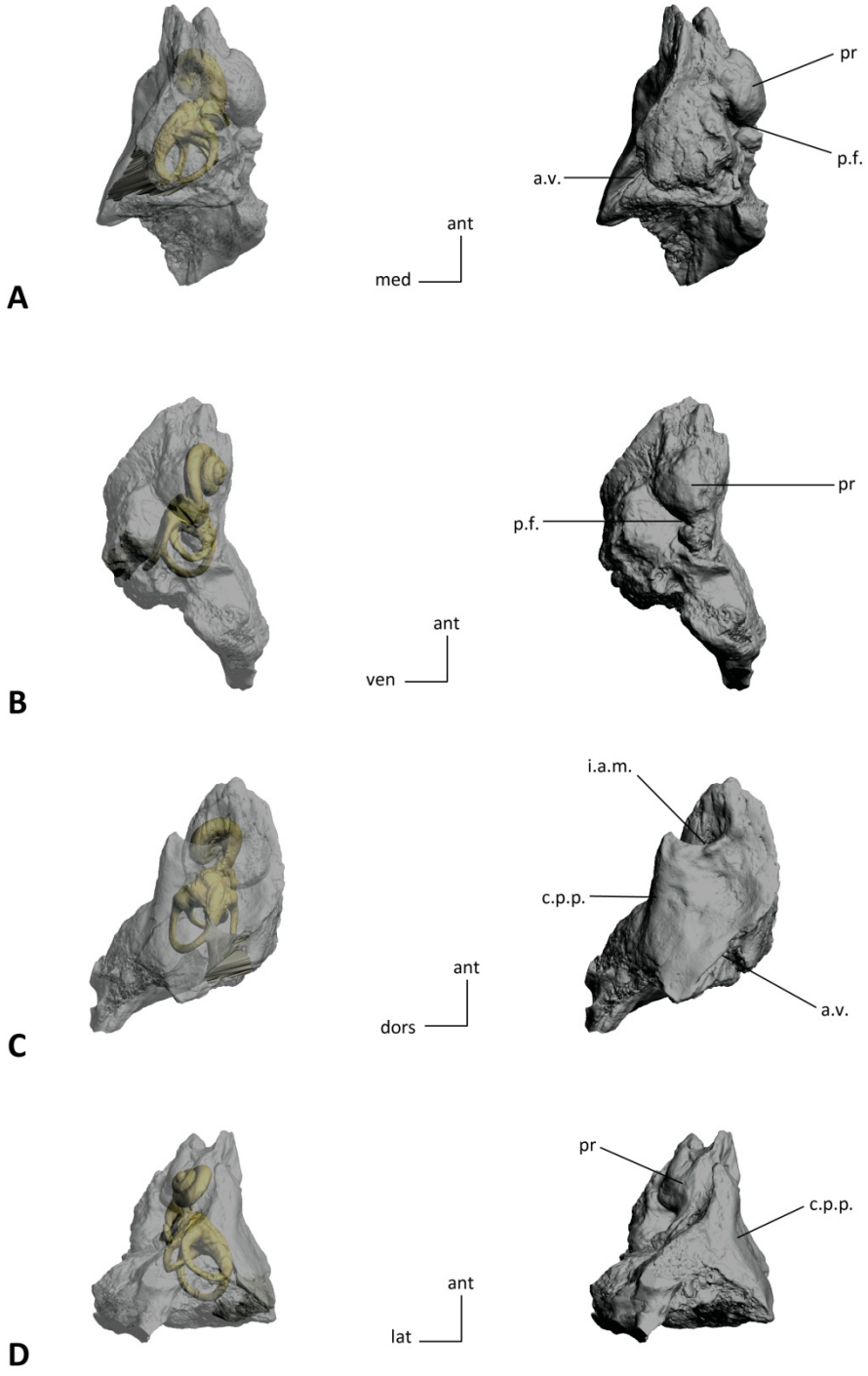

Figure III.10 : 3D reconstructed models of the petrosal of *Gomphotherium angustidens* CBar coll. V2 in medial (A), tympanic (B), cerebellar (C) and cerebral (D) views. Legends: **a.v.** *aquaeductus vestibuli*, **c.p.p.** *crista partis petrosa*, **i.a.m.** internal auditory meatus, **p.f.** perilymphatic foramen, **pr** *promontorium*, **t.t.** *tegmen tympani*.

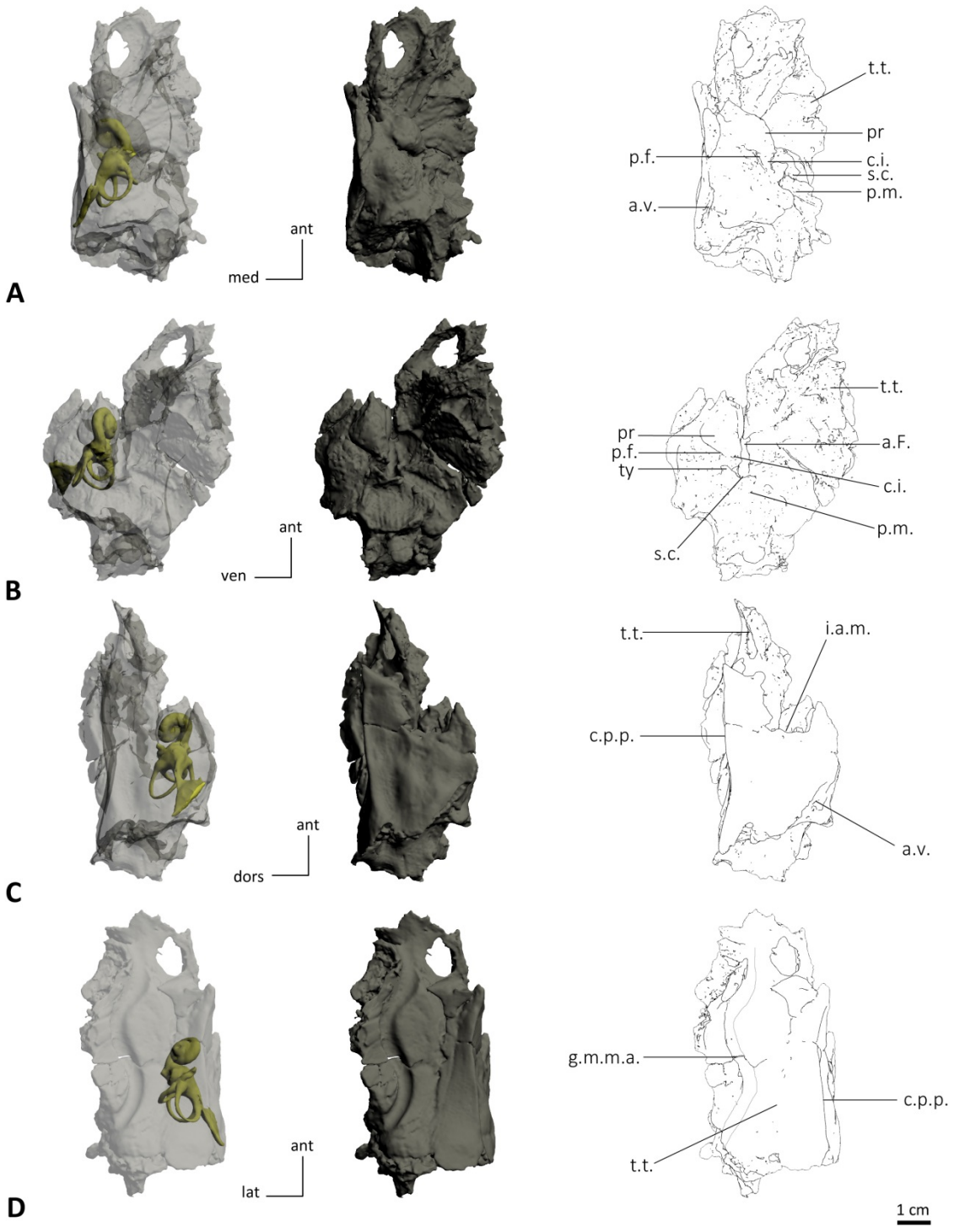

Figure 11 : 3D reconstructed models and drawings of the petrosal of *Gomphotherium angustidens* MNHN.F.SEP38 in medial (A), tympanic (B), cerebellar (C) and cerebral (D) views. Legends: **a.F.** *aquaeductus Fallopii*, **a.v.** *aquaeductus vestibuli*, **c.i.** *crista interfenestralis*, **c.p.p.** *crista partis petrosa*, **g.m.m.a.** groove for the middle meningeal artery, **i.a.m.** internal auditory meatus, **p.f.** perilymphatic foramen, **p.m.** *pars mastoidea*, **pr** *promontorium*, **s.c.** stylomastoid canal (part of), **t.t.** *tegmen tympani*, **ty** tympanohyal.

Inner ear

The total volume of the inner ear is 814 mm^3 in MNHN.F.SEP38 (average value of the left and right inner ears) and 988 mm^3 for Cbar coll.V 2.

Vestibular bony labyrinth

Ampullae

The ampullae of *Gomphotherium angustidens* appear less defined like most proboscideans. There is no clear ampullar ridge on any studied specimens (Fig III.12).

Crus commune

The *crus commune* is elongated in all studied specimens of *Gomphotherium*. There is a huge basal thickening of the *crus commune* on both specimens giving it a pyramidal shape. This feature is slightly more pronounced in Cbar coll.V 2. The *crus commune* is quite smooth in all specimens and it does not display any bulge and ridges. The average section radius of the *crus commune* of *Gomphotherium* is 1.24 mm in MNHN.F.SEP38 and 1.27 mm in Cbar coll.V 2. The length of the *crus commune* is approximately 6.82 mm in MNHN.F.SEP38 and 8.73 mm in Cbar coll.V 2. Therefore the specimen MNHN.F.SEP38 has a *crus commune* with a higher thickness ratio of (18.66) than the *crus commune* of Cbar coll.V 2 (14.25). In both specimens, the anterior and posterior semicircular canals meet quite high, approximately at two third of the height of the anterior canal. The *crus commune* is not inclined in any specimen of *Gomphotherium angustidens*.

Semicircular canals

The anterior semicircular canal is oval in MNHN.F.SEP38 right and left ears but quite round in Cbar coll.V 2. The major axis of the canal forms an angle of 33° with the *crus commune* in both ears of MNHN.F.SEP38. The anterior semicircular canal appears more slender in MNHN.F.SEP38 than in Cbar coll.V 2. Indeed the central streamline of the anterior canal is longer in MNHN.F.SEP38 (22.80 mm) than in Cbar coll.V 2 (20.43 mm). The average section radius of the anterior canal is 0.64 mm in MNHN.F.SEP38 and 0.77 mm in Cbar coll.V 2. Therefore, the thickness ratio of this canal is 2.82 in MNHN.F.SEP38 and 3.78 in Cbar coll.V 2. The radii of curvature of the anterior canal are very similar in both specimens (5.45 in MNHN.F.SEP38 and 5.26 in Cbar coll.V 2).

The posterior semicircular canal is oval in both MNHN.F.SEP38 and Cbar coll.V 2. The major axis of the canal forms an angle of -21° with the *crus commune* in MNHN.F.SEP38 but this value

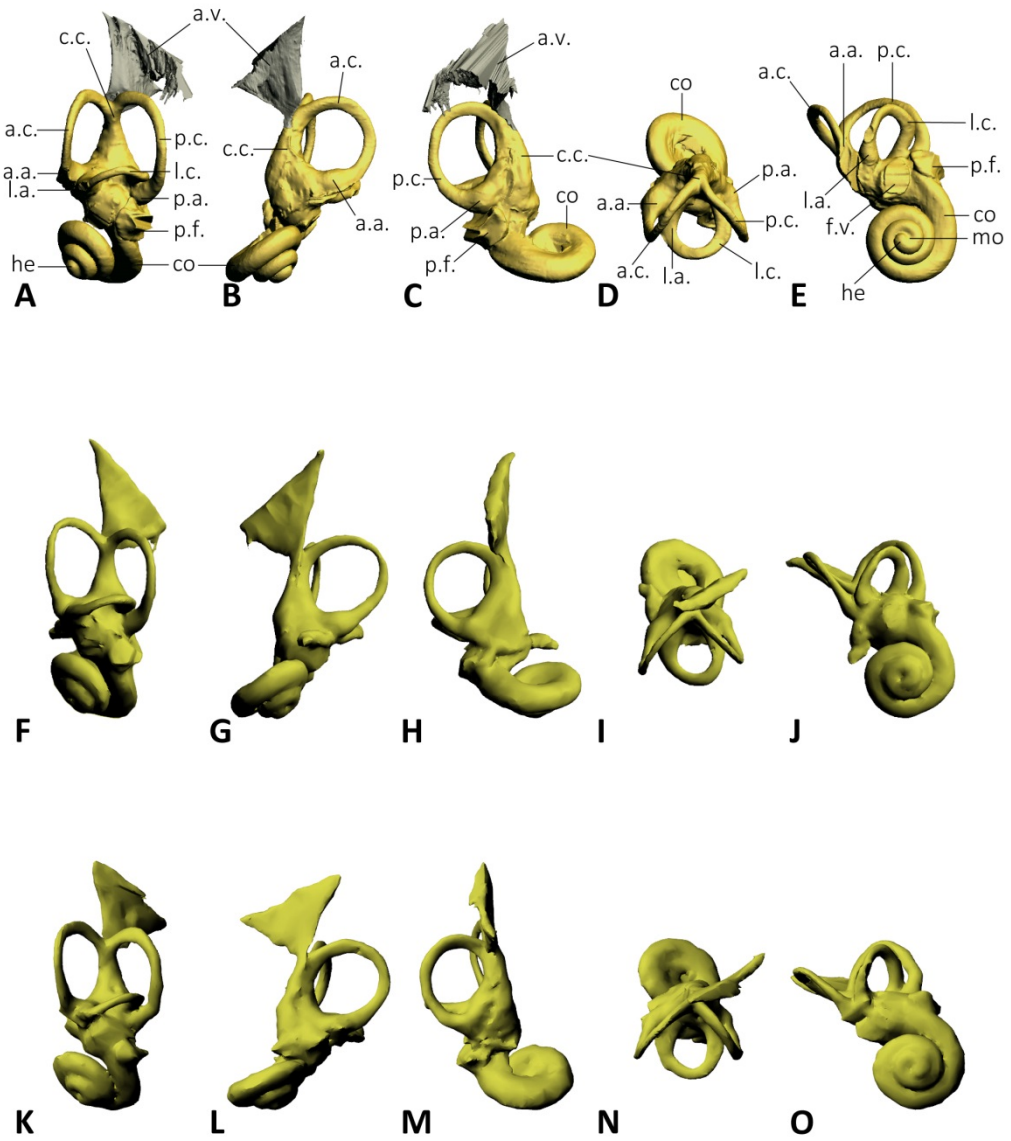

Figure III.12 : 3D reconstructed models of the bony labyrinths of *Gomphotherium angustidens* specimens CBar coll. V2 (A-E) and MNHN.F.SEP38 left (F-J) and right (K-O, mirrored) sides in frontal (A,F,K), anterior canal (B,G,L), posterior canal (C,H,M), lateral canal (D,I,N) and cochlear (E,J,O) views. Legends: **a.a.** anterior ampulla, **a.c.** anterior semicircular canal, **a.v.** *aquaeductus vestibuli*, **c.c.** *crus commune*, **co** cochlea, **f.v.** *fenestra vestibuli*, **he** helicotrema, **l.a.** lateral ampulla, **l.c.** lateral semicircular canal, **mo** modiolus, **p.a.** posterior ampulla, **p.c.** posterior semicircular canal, **p.f.** perilymphatic foramen.

is higher in Cbar coll.V 2 (-29°). It is important to note that the orientation of the major axis is reversed compared to the anterior in both specimens (hence the negative values). The central streamline length of the posterior canal is 21.61 mm in MNHN.F.SEP38 and 23.24 mm in Cbar coll.V 2. While the value is very similar with the anterior canal value in MNHN.F.SEP38, there is a difference of almost 3 mm in Cbar coll.V 2. The average section radius of the posterior canal is similar to the anterior one (0.71 mm in MNHN.F.SEP38 and 0.76 mm in Cbar coll.V 2). Values for the posterior thickness ratio are almost exactly the same in both specimens (3.29 in MNHN.F.SEP38 and 3.26 in Cbar coll.V 2). Compared to the anterior canal, the posterior canal is thicker in MNHN.F.SEP38 but more slender in Cbar coll.V 2. The radius of curvature of the posterior canal is 5.11 in MNHN.F.SEP38 and 5.56 in Cbar coll.V 2.

The lateral semicircular canal is clearly oval in Cbar coll.V 2 but it is rounder in MNHN.F.SEP38. The length of the central streamline of the lateral canal is slightly shorter in MNHN.F.SEP38 (19.11 mm) than in Cbar coll.V 2 (22.24 mm). Compared to the other semicircular canals, the lateral canal is the shortest in MNHN.F.SEP38 but it is approximately as long as the other canals in Cbar coll.V 2. Both specimens share the same value of the average section radius for the lateral canal (0.78 mm in both MNHN.F.SEP38 and Cbar coll.V 2). The average section radius of the lateral canal is similar to the values of the other canals in Cbar coll.V 2 but it is clearly higher than the two other canals in MNHN.F.SEP38. In MNHN.F.SEP38, the thickness ratio of this canal (4.09) is clearly higher than the ratio of the anterior and posterior canals while it is more or less similar to the other two canals in the other specimen (3.50 in Cbar coll.V 2). Moreover, the lateral canal of MNHN.F.SEP38 is slightly thicker than the lateral canal of Cbar coll.V 2. The radius of curvature of the lateral canal is 3.36 in MNHN.F.SEP38 and 3.71 in Cbar coll.V 2.

There are differences between the angle values of the two specimens of *Gomphotherium angustidens*. There is a difference of more than 6° in the value of the angle between the anterior and posterior canals (79.2° in Cbar coll.V 2 and 85.7° in MNHN.F.SEP38). There is a difference of 5° in the value of the angle between the anterior and lateral canals (67.8° in Cbar coll.V 2 and 72.8° in MNHN.F.SEP38). Finally, there is a difference of almost 6° in the value of the

angle between the posterior and lateral canals (85.3° in Cbar coll.V 2 and 91.1° in MNHN.F.SEP38). In both specimens, the highest angle is between the lateral and posterior canals while the smallest angle is between the anterior and lateral canals. If we compare the radii of curvature we can first observe that the lateral canal is always smaller (3.36 in MNHN.F.SEP38 and 3.71 in Cbar coll.V 2) than the anterior and posterior canals which tend to share quite similar radii of curvature (respectively 5.45 and 5.11 in MNHN.F.SEP38 and 5.26 and 5.46 in Cbar coll.V 2). The smaller size of the lateral canal is marked and obvious on the reconstruction. The anterior canal apex is located slightly higher than the posterior one in both specimens (but is more pronounced in MNHN.F.SEP38). In general, the thickness of the semicircular canals of *Gomphotherium* is on the middle range compared to other proboscideans, but it is thicker than most mammals. Those of Cbar coll.V 2 are slightly thicker (average thickness ratio = 3.51) than those of MNHN.F.SEP38 (average thickness ratio = 3.40). In cross-section, the canals appear flattened. The slender part of the lateral semicircular canal is connected to the vestibule at a high position. No ridges are observed on the semicircular canals. In Cbar coll.V 2, each canal displays an undulation while only the anterior and posterior canals display one in SEP38.

Cochlear bony labyrinth

The number of turns of the cochlea is not constant amongst studied specimens of *Gomphotherium angustidens*. The specimen CBar coll.V 2 shows 2.625 turns (945°) whereas both ears of SEP38 have 2.375 turns (855°) which makes a difference of a quarter turn. In ventral view, the modiolus of both specimens is completely overlapped by the apical turn and there is no visible gap. The basal turn of the cochlea is only partially overlapped by the apical turn and is still visible in ventral view. The *lamina secundaria* is absent on both specimens. The cochlear volume (497 mm^3 in Cbar coll.V2 and 400 mm^3 in SEP38) represents around 50% of the total bony labyrinth volume in both specimens.

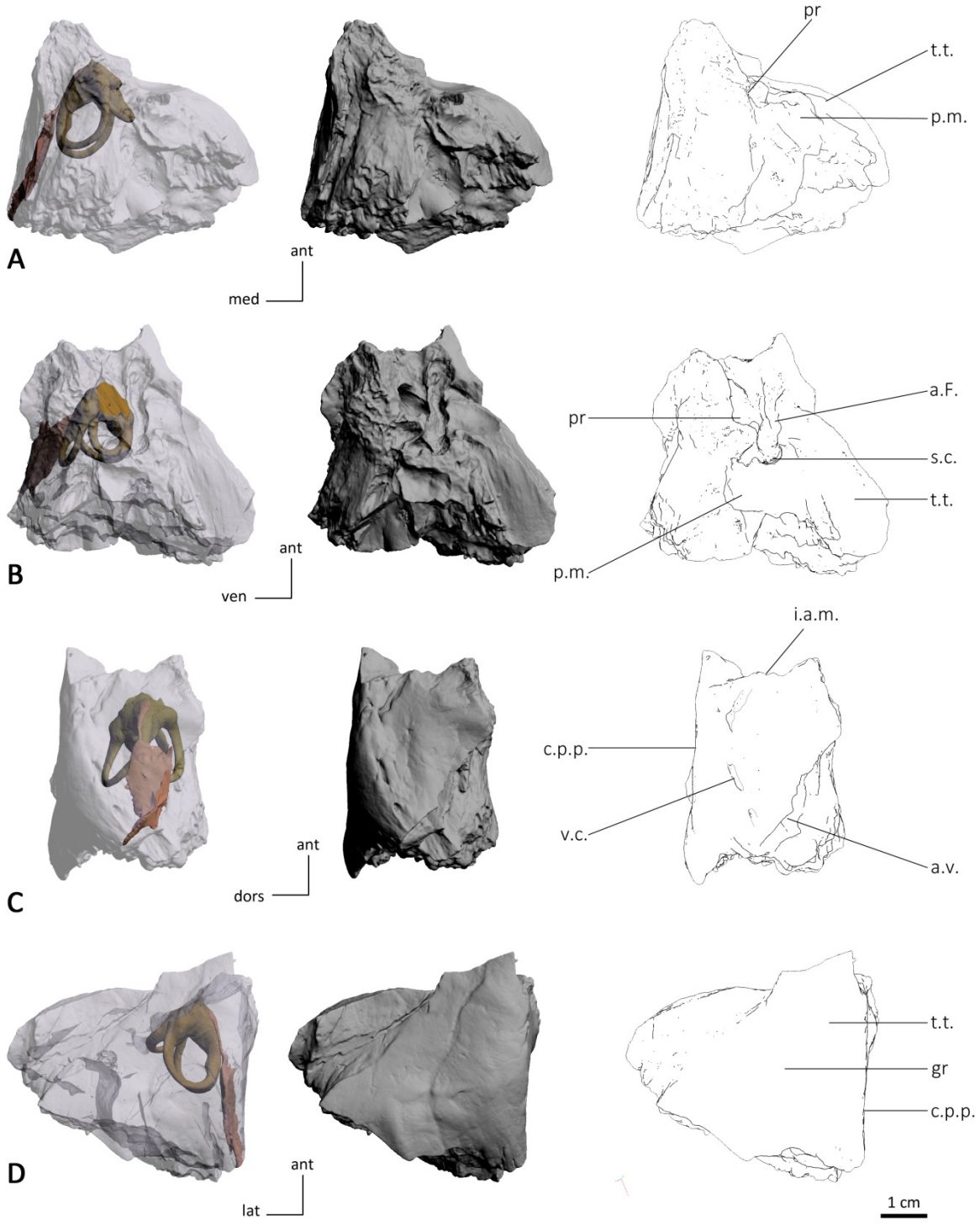

Figure III.13 : 3D reconstructed models and drawings of the petrosal of *Cuvieronius sp.* FM103247 in medial (A), tympanic (B), cerebellar (C) and cerebral (D) views. Legends: **a.F.** *aquaeductus Fallopii*, **a.v.** *aquaeductus vestibuli*, **c.p.p.** *crista partis petrosa*, **gr** groove of the cerebral surface, **i.a.m.** internal auditory meatus, **p.m.** *pars mastoidea* (broken), **pr** *promontorium*, **s.c.** stylomastoid canal (part of), **t.t.** *tegmen tympani*, **v.c.** vascular canal.

3.2.6. *Cuvieronius sp.*

Petrosal

The overall aspect of the petrosal is similar to the elephantimorphs in general (Fig III.13). In cerebellar view, the *aquaeductus vestibuli* has the aspect of a thin slit and is located in the posterior part of the petrosal. It is, however, more centered than in most extant elephants. The region bearing the internal auditory meatus is broken but its location is clearly visible. It is oriented antero-posteriorly. The epitympanic wing is completely broken. There is no trace of a subarcuate fossa and the *crista partis petrosa* is very blunt. Along the crista runs a semi-enclosed vascular canal (v.c. in Fig III.13C). It is distinct on the petrosals in some parts but it is totally enclosed in others. This canal probably housed a blood vessel but it seems to exist only in *Cuvieronius,* as it has not been described in any other examined proboscideans. The angle between the cerebellar and cerebral surface of the petrosal is right (90°). In cerebral view, the *tegmen tympani* is rather well preserved, but its anterior part is broken. There is a thin and shallow groove running almost parallel to the *crista partis petrosa* that probably housed the superior petrosal sinus. A larger groove lies in the posterior part of the *tegmen tympani*. This is probably the groove for the middle meningeal artery but this feature is not well defined. In tympanic view, the petrosal is quite damaged. The *promontorium* is completely broken making the observation of the fenestrae impossible. The *aquaeductus Fallopii* is preserved. It consists of a deep sulcus which presents the same location and orientation as in extant elephants. The sulcus is not covered by a bony roof but it could have been broken after the death of the animal. The fossa for the stapedius muscle is well preserved and lies medial to the *aquaeductus Fallopii* (at the supposed level of the perilymphatic foramen). Between the fossa and the *aquaeductus Fallopii* lies a deep cavity that is probably a broken pneumatic cell of the *pars mastoidea*. In this view, it is clear that the anterior part of the *tegmen tympani* is missing.

Inner ear

Since the cochlear part of the petrosal is broken on the scanned *Cuvieronius* specimen, the cochlear part of the bony labyrinth could not be segmented. Hence the total volume of the bony labyrinth is unknown.

Vestibular bony labyrinth

Ampullae

The ampullae of *Cuvieronius* appear less defined like most modern proboscideans. The ampulla of the lateral semicircular canal shows a bump on its common part with the anterior semicircular canal ampulla (Fig III.14).

Crus commune

The *crus commune* is elongated (not stocky as in *Elephas* 1904-273 for example) and displays a slight basal thickening. A bump is located on the posterior part of the *crus commune* near the insertion of the lateral semicircular canal into the vestibule. The average section radius of the *crus commune* of *Cuvieronius* is 1.65 mm and its length is approximately 9.52 mm. Therefore the specimen of *Cuvieronius* has a *crus commune* with a thickness ratio of 17.39. The anterior and posterior semicircular canals meet quite high (approximately at 75% of the height of the anterior canal) and the *crus commune* is slightly inclined towards the anterior canal.

Semicircular canals

The anterior semicircular canal is oval. Its major axis forms an angle of 28° with the *crus commune*. The central streamline length of the anterior canal is 25.02 mm and the average section radius is 0.85 mm. Therefore, the thickness ratio of this canal is 3.41. Its radius of curvature is particularly large (6.18).

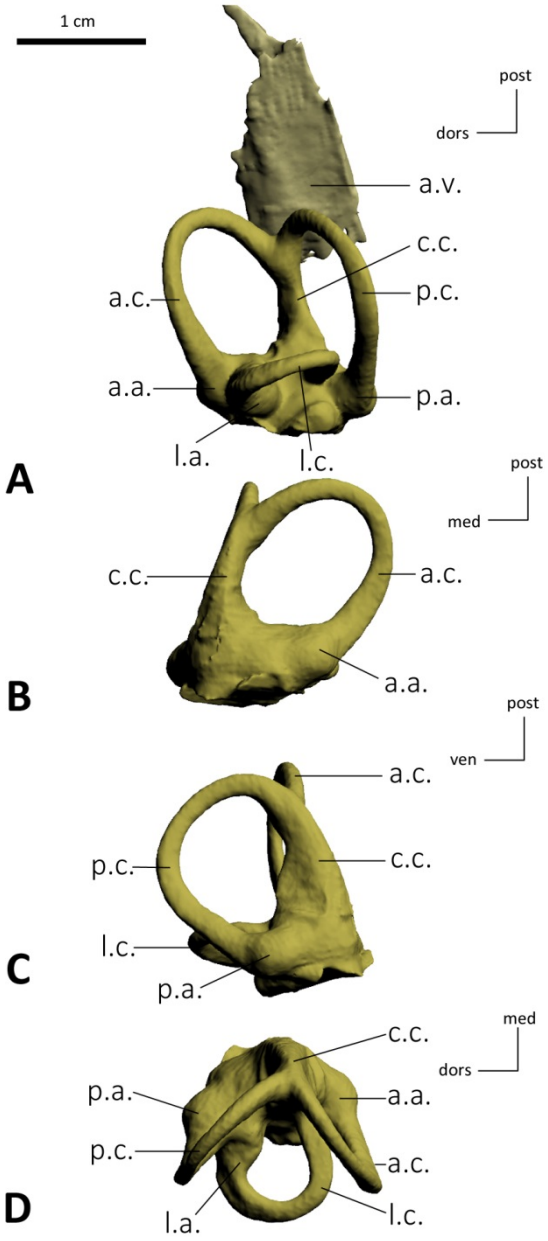

Figure III.14 : 3D reconstructed model of the bony labyrinth of *Cuvieronius sp.* FM103247 in frontal (A), anterior canal (B), posterior canal (C) and lateral canal (D) views. Legends: **a.a.** anterior ampulla, **a.c.** anterior semicircular canal, **a.v.** *aquaeductus vestibuli*, **c.c.** *crus commune*, **l.a.** lateral ampulla, **l.c.** lateral semicircular canal, **p.a.** posterior ampulla, **p.c.** posterior semicircular canal

The posterior semicircular canal is oval. The major axis of the canal forms an angle of -17° with the *crus commune.* It is important to note that the orientation of the major axis is reversed compared to the anterior canal (hence the negative values). The central streamline length of the posterior canal is 25.38 mm which is very similar to the value found for the anterior canal. The average section radius of the posterior canal is also very similar to the anterior one (0.86 mm). Hence, the thickness ratio of the posterior canal (3.37) is very close to the ratio of the anterior canal. The radius of curvature of the posterior canal is also large (6.06).

The lateral semicircular canal is also oval. The length of the central streamline is shorter than the two other canals (21.37 mm). In contrast, the average section radius of the lateral canal is slightly higher than the other canals (0.89 mm). Hence the thickness ratio is higher (4.18) for the lateral canal than for the anterior and posterior canals. The radius of curvature of the lateral canal is 3.57.

The largest angle between the canals in *Cuvieronius* is between the lateral and posterior canals (85.5°) while the smallest angle is between the anterior and lateral canals (77.4°). The angle between the anterior and posterior canals is on the middle range (82.2°). If we compare the radii of curvature we can observe that the lateral canal is clearly smaller (3.57) than the anterior and posterior canals which tend to share quite similar radii of curvature (respectively 6.18 and 6.06). The smaller size of the lateral canal can be observed directly on the reconstruction. The anterior canal apex is located higher than the posterior canal apex. In *Cuvieronius*, the thickness of the canals is in the middle range compared to other proboscideans (but stockier than most mammals) with an average thickness ratio of 3.65. In cross-section, the canals appear flattened. The slender part of the lateral semicircular canal is connected to the vestibule at a high position and distant from the posterior ampulla. No ridges were observed on the semicircular canals. Only the anterior canal displays an undulation.

3.2.7. *Stegomastodon sp*

Two isolated petrosals of *Stegomastodon sp*. supposedly belonging to the same specimen (FM21807) were scanned. The left ear preserves the cochlea but not the lateral canal as seen in the petrosal description. The right ear does not preserve the cochlea but preserves all the semicircular canals. However, the right semicircular canals are extremely inflated and the right petrosal seems to have undergone major taphonomic transformations. Given these details, we cannot give a precise value of the total volume of the bony labyrinth of *Stegomastodon*.

Petrosal

The overall aspect of the petrosal is very similar to the petrosal of other elephantimorphs (Fig III.15 and III.16). In cerebellar view, the subarcuate fossa is completely absent in the right ear and the area where it should be located is even slightly convex. In the left petrosal, this area is slightly concave and it could be the trace of a very shallow subarcuate fossa. In both ears, the *aquaeductus vestibuli* has the shape of an elongated slit located in the posteromedial corner of the petrosal. The *crista partis petrosa* is sharper in the right ear than in the left ear but both cristae are less sharp than *Gomphotherium* or even extant elephants. The angle between the cerebral and the cerebellar surfaces of the petrosal is right in the left ear (90°) and slightly more obtuse in the right ear (95°). The internal auditory meatus is preserved in both ears. It is located antero-posteriorly as in every studied elephantimorphs. In cerebral view, the *tegmen tympani* is incomplete in the left ear. A shallow groove is visible on this surface. It runs parallel to the *crista partis petrosa* and is located quite close to this ridge. This could be the groove for the middle meningeal artery but in this case, its proximity with the crista is unusual. Hence, it could be alternatively the groove for the superior petrosal sinus. In the right ear, the *tegmen tympani* is better preserved. There is a shallow groove, distant from the *crista partis petrosa* and with a bow-shaped trajectory. This is certainly the groove for the middle meningeal artery. Compared to the groove seen in the left ear, it is really more distant from the *crista partis petrosa* which supports the previous hypothesis that the groove on the left petrosal is not for the middle meningeal artery. However, such groove, parallel and close to the *crista partis petrosa*, is not seen in the right ear. In tympanic view, the left ear is extremely

damaged. The *pars mastoidea* is completely broken and there is no trace of the *aquaeductus Fallopii*. The *promontorium* is almost completely broken as well as the fenestrae. The petrosal is so damaged that most of the inner ear is directly observable. The labyrinth was filled with sediment before the destruction of this part of the petrosal. Hence, the natural endocast of the labyrinth is distinct on the surface (Fig III.15B). The posterior and anterior ampullae are distinguishable as well as parts of the cochlea. The petrosal is however broken at the level of the *fenestra vestibuli* and the perilymphatic foramen making these two structures impossible to observe. However, since there is no trace of a cochlear canaliculus, the perilymphatic foramen is certainly retained in *Stegomastodon*.

Inner ear

Vestibular bony labyrinth

Ampullae

The ampullae of *Stegomastodon* appear poorly defined as in most modern proboscideans. There is no clear ampullar ridge on any of the ears (Fig III.17). However this feature is impossible to observe in the right ear given their condition.

Crus commune

The *crus commune* is elongated in the left ear but appears stockier in the right one; this can be due to the conditions of preservation of the right petrosal. There is no marked basal thickening at the basis of the *crus commune*. The *crus commune* is quite smooth and does not display any bulge and ridges. The average section radius of the *crus commune* of *Stegomastodon* is 1.66 mm. The values given are only from the left ear which is the only one well-preserved. The length of the *crus commune* is approximately 7.25 mm. Therefore this specimen has a *crus commune* with a thickness ratio of 32.33. In both ears, the anterior and posterior semicircular canals meet quite high, approximately at three quarters of the height of the anterior canal. The *crus commune* is not inclined.

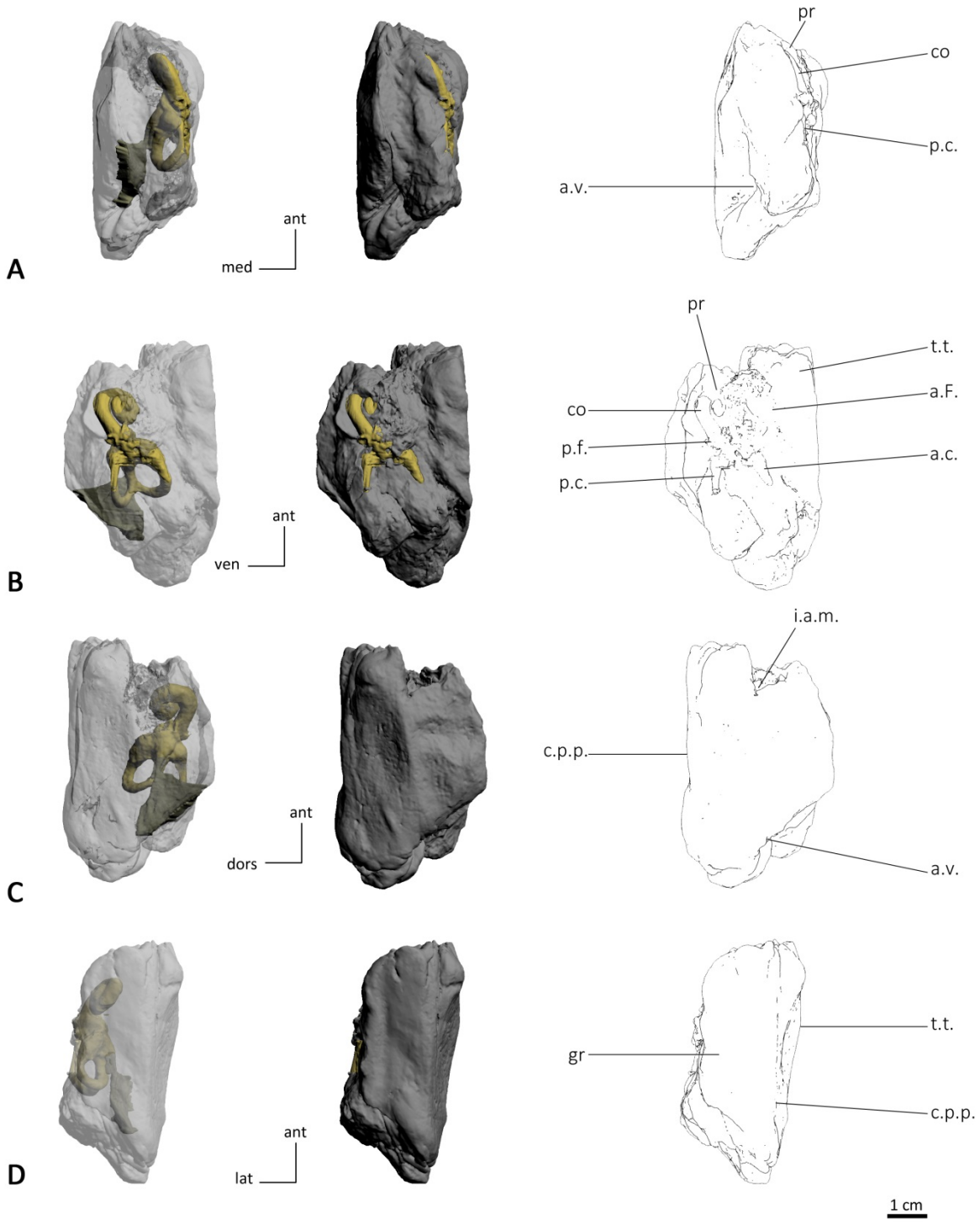

Figure III.15 : 3D reconstructed models and drawings of the left petrosal of *Stegomastodon sp.* FM21807 in medial (A), tympanic (B), cerebellar (C) and cerebral (D) views. Legends: **a.c.** natural cast of the anterior semicircular canal, **a.F.** *aquaeductus Fallopii* (location), **a.v.** *aquaeductus vestibuli*, **c.p.p.** *crista partis petrosa*, **co** natural cast of the cochlea, **gr** groove of the cerebral surface, **i.a.m.** internal auditory meatus, **p.c.** natural cast of the posterior semicircular canal, **p.f.** perilymphatic foramen, **p.m.** *pars mastoidea* (broken), **pr** *promontorium*, **s.c.** stylomastoid canal (part of), **t.t.** *tegmen tympani* (broken), **v.c.** vascular canal.

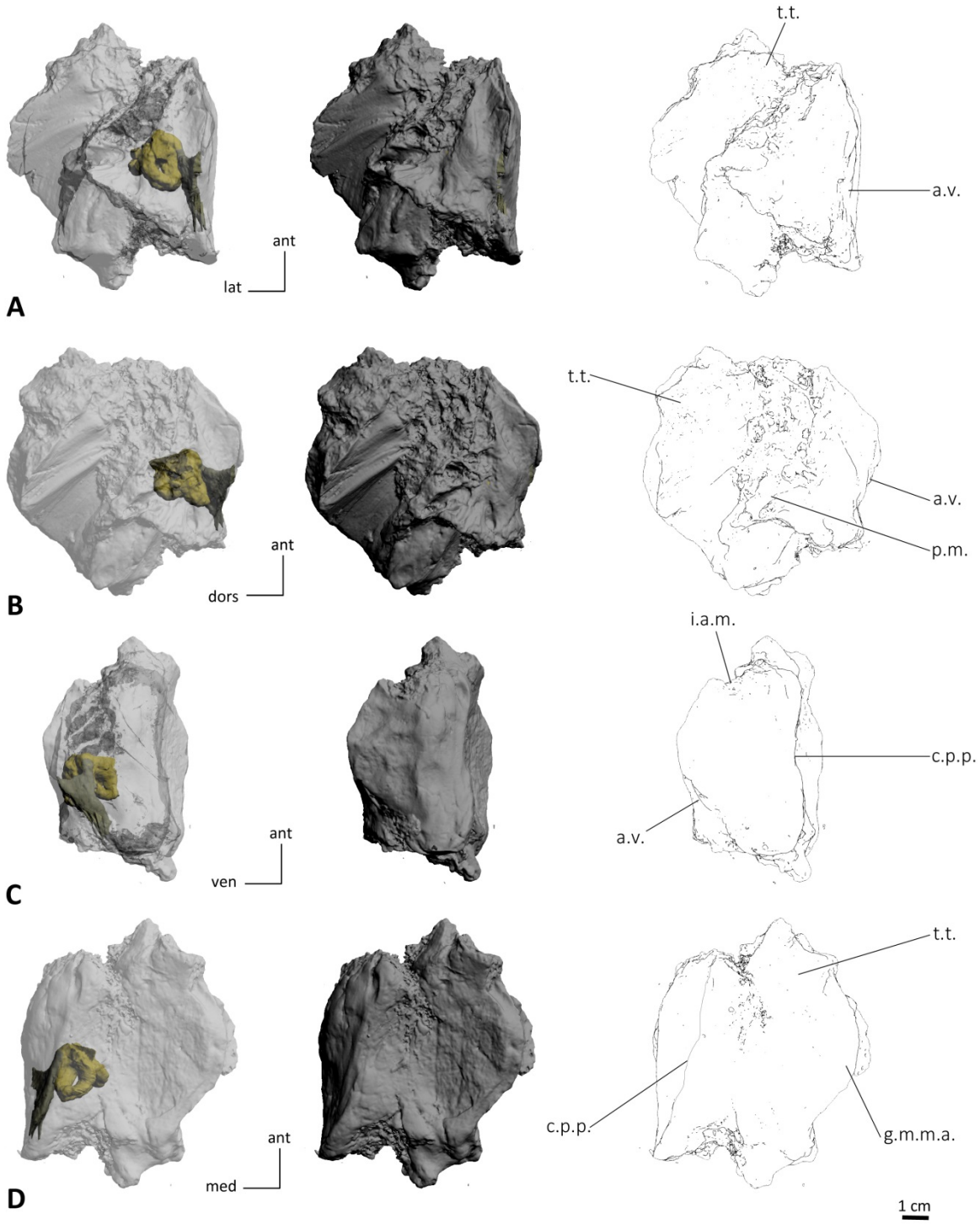

Figure 16 : 3D reconstructed models and drawings of the right petrosal of *Stegomastodon sp.* FM21807 in medial (A), tympanic (B), cerebellar (C) and cerebral (D) views. Legends: **a.v.** *aquaeductus vestibuli*, **c.p.p.** *crista partis petrosa*, **g.m.m.a.** groove for the middle meningeal artery, **i.a.m.** internal auditory meatus, **p.f.** perilymphatic foramen, **p.m.** *pars mastoidea* (broken), **pr** *promontorium*, **t.t.** *tegmen tympani* (broken).

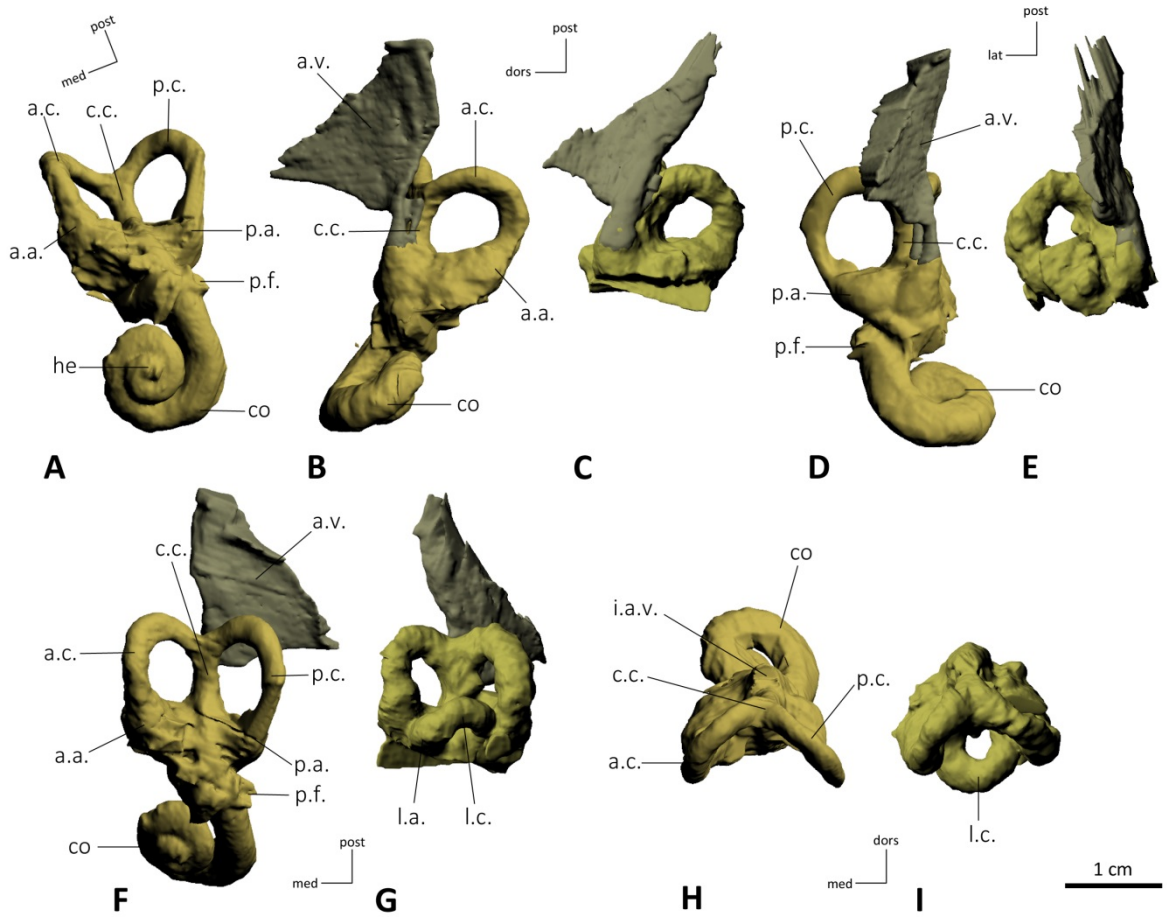

Figure 17 : 3D reconstructed models of the left (A,B,D,F,H) and right (C,E,G,I, mirrored) bony labyrinths of *Stegomastodon sp.* FM103247 in cochlear (A), anterior canal (B,C), posterior canal (D,E), frontal (F,G) and lateral canal (H,I) views. Legends: **a.a.** anterior ampulla, **a.c.** anterior semicircular canal, **a.v.** *aquaeductus vestibuli*, **c.c.** *crus commune*, **co** cochlea, **he** helicotrema, **i.a.v.** insertion of the *aquaeductus vestibuli*, **l.a.** lateral ampulla, **l.c.** lateral semicircular canal, **p.a.** posterior ampulla, **p.c.** posterior semicircular canal, **p.f.** perilymphatic foramen

Semicircular canals

The anterior semicircular canal is oval in both right and left ears of FM21807. The major axis of the canal forms an angle of 48° with the *crus commune* in the left ear but the angle is lower in the right ear (31°). Because of the swollen aspect of the right ear canals that does not seem to be natural, their measurements and thickness will not be discussed. On the other hand, the left ear seems well-preserved. The average section radius of its anterior canal is 1.32 mm and its central streamline length is 19.39 mm so this canal has a 6.80 thickness ratio. Its radius of curvature is 4.91.

The posterior semicircular canal is partially broken in the left ear. It is rather round in the right ear but oval in the left one, with the major axis of the canal forming an angle of -13° with the *crus*

commune. The central streamline length of the posterior canal is 22.28 mm for the left ear which is longer than the anterior canal. The average section radius of the posterior canal is slightly smaller than the anterior one (1.18 mm) which can be due to the missing part of the slender canal. The posterior thickness ratio is lower than for the anterior ratio (5.29). Its radius of curvature is larger than for the anterior canal (5.3).

The lateral semicircular canal is completely broken in the left ear and it is round in the right ear. The swollen condition of the right ear and the missing canal of the left ear prevent us from discussing this canal measurements and thickness.

The only angle value available for *Stegomastodon* is the angle between the anterior and posterior canals as the lateral canal is not preserved in the left ear and the canals are too swollen in the right ear. This angle is obtuse (96.6°) and one of the largest angles observed in proboscideans for these canals. The apex of the anterior canal extends at the same height as for the posterior canal in both ears. The semicircular canals of *Stegomastodon* are markedly thick compared to other proboscideans (and other mammals). The general thickness ratio of the left ear is 6.05 which is the highest ratio encountered in proboscideans. The swollen canals of the right ear are even thicker but this condition is probably caused by taphonomic processes. In cross-section, the canals are flattened. The entry point of the lateral canal in the vestibule is not visible in the left ear because the lateral canal is not preserved. It is difficult to observe in the right ear because of the swollen aspect of the canals but it seems to enter the vestibule in a somewhat high position. There is a slight fusion between the lateral and posterior canals at the level of the posterior ampulla but this could be due to the swollen aspect of the canals. There is no trace of ridges on the canals of *Stegomastodon*. In both ears, the semicircular canals display undulations.

Cochlear bony labyrinth

The cochlear part is only preserved in the left ear. The cochlea displays 2 turns (720°) and a length of 65.8 mm. In ventral view, the modiolus is completely overlapped by the apical turn and there is no visible apical lacuna. The basal turn of the cochlea is only partially overlapped by the apical turn and is still visible in ventral view. The *lamina secundaria* is absent. The cochlea is planispiral with an aspect ratio of 0.45.

3.2.8. *Platybelodon grangeri*

Petrosal

The contrast of the microtomographic slices for this specimen was particularly poor. The inner ear is filled with sediment that has grey values similar to the bone. Therefore, the 3D model obtained after segmentation is a bit imprecise. Moreover, it was not possible to segment the petrosal as its limits with other bones and sediment were not visible. The only visible parts of the petrosal are the external ones which consist of parts of the cerebral and cerebellar surfaces. The angle between the cerebral and cerebellar surfaces is obtuse (105°). In cerebral view, a shallow groove is visible and is probably the groove for the middle meningeal artery. It is more or less parallel to the *crista partis petrosa* which is sharp. In cerebellar view, no structures are really recognizable. There is no trace of a subarcuate fossa and the internal auditory meatus is not visible.

Vestibular bony labyrinth

Ampullae

The ampullae of *Platybelodon* are poorly defined (Fig III.18). The poor level of contrast and therefore the rather imprecise segmentation of the labyrinth prevents us from observing the presence of ridges on the ampullae.

Crus commune

The *crus commune* is stocky and displays a marked basal thickening. However, it is not pyramidal as in *Gomphotherium*. Again, the poor level of contrast prevents us from observing the potential ridges of the *crus commune*. In addition, numerical values like the average section radius have to be taken with caution as the segmentation of this specimen is imprecise. With all these factors in mind, we can continue the description of the bony labyrinth of *Platybelodon*. The average section radius of the crus commune is 1.17 mm and its length is 4.20, which gives a quite high average thickness ratio (27.92). The anterior and posterior semicircular canals meet quite low (approximately at the mid-height of the anterior canal) and the *crus commune* is not inclined.

Semicircular canals

The overall shape of anterior semicircular canal is oval. The major axis of this canal forms an angle of 30° with the *crus commune*. The central streamline length is 22.02 mm and the average section radius of the canal is 0.81 mm. Therefore, the average thickness ratio of

the canal is 3.69. The radius of curvature of the anterior canal is 5.16.

On the contrary, the posterior semicircular canal is round. Its central streamline length is basically the same as the anterior canal (22.00 mm) but its average section radius is lower (0.65 mm) which gives the posterior semicircular canal of *Platybelodon* a lower average thickness ratio than its anterior canal (2.93). However it is hard to see a difference of thickness between this canal and the anterior canal.

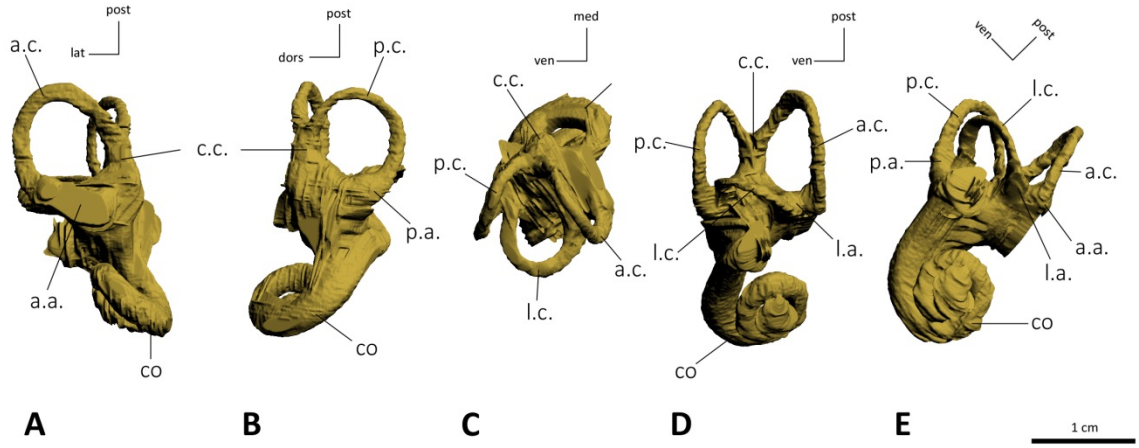

Figure III.18 : 3D reconstructed models of the left bony labyrinth of *Platybelodon grangeri* 26564 (824+) in anterior canal (A), posterior canal (B), lateral canal (C), frontal (D) and cochlear (E) views. Legends: **a.a.** anterior ampulla, **a.c.** anterior semicircular canal, **c.c.** *crus commune*, **co** cochlea, **l.a.** lateral ampulla, **l.c.** lateral semicircular canal, **p.a.** posterior ampulla, **p.c.** posterior semicircular canal

Nevertheless, the anterior canal seems larger than the posterior canal at the level of its connection with the *crus commune*. This feature might be due to the imprecise segmentation of the bony labyrinth. The radius of curvature for this canal is 4.89.

The lateral canal is oval and shares a very similar central streamline length value as the other canals (21.97 mm). The average section radius is close to the radius of the posterior canal (0.68 mm) as well as the average thickness ratio (3.11). The radius of curvature of the lateral is 3.54.

The angle between the posterior and lateral semicircular canals is obtuse and particularly large in *Platybelodon* (98.8°). The two other angles are acute and clearly smaller. The smallest of the angle is the angle between the anterior and lateral canals (67.4°), the angle between the anterior and posterior canals being larger (73.9°). The radii of curvature of the anterior and posterior canals are

larger (respectively 5.16 and 4.89) than the radius of the lateral canal (3.54). Indeed, the lateral canal appears smaller on the reconstruction. The anterior canal apex is located slightly higher than the posterior canal apex. Compared to other proboscideans, the semicircular canals of *Platybelodon* display an average thickness (ratio = 3.25). The semicircular canals are flattened, especially the lateral canal. The slender part of the lateral semicircular canal is connected to the vestibule at a high position. No ridges were observed on the semicircular canals but the imprecise segmentation does not allow us to verify these features. Only the anterior and posterior canals display an undulation.

Cochlear bony labyrinth

The cochlear canal was particularly difficult to segment given the very poor contrast in this part of the petrosal. The cochlea displays around two turns (720°) but the count can be imprecise because we failed to clearly isolate the cochlear apex during the segmentation. The cochlear length is around 57 mm but this value is imprecise given the difficulties we met to segment the cochlea. Additionally, it is hard to define whether the modiolus displays an apical lacuna or not. It seems nevertheless that this feature is absent. The basal turn of the cochlea is only partially overlapped by the apical turn and is still visible in ventral view. There is no trace of a *lamina secundaria*. The cochlear volume (373.8 mm^3) represents around 44% of the total volume of the bony labyrinth. The cochlea is planispiral with an aspect ratio of 0.41.

3.2.9. *Anancus arvernensis*

Petrosal (Fig III.19-25)

The petrosal of *Anancus* is similar to that of extant elephants. The bone is elongated anteroposteriorly. In dorsal view, the petrosal consists of two surfaces (the cerebral and cerebellar surfaces) that form an angle of 98° (mean). The values are given in Table III.3. The standard deviation for the angle value is 6.47.

Table III.3 : Angle between the cerebral and cerebellar surfaces and stapedial ratio of *Anancus arvernensis*. "?" is for missing data.

	Angle between surfaces	Stapedial ratio
NMNHS.FM2991A	110°	1.7
NMNHS.FM2991B	100°	?
NMNHS.FM2991C	95°	1.6
NMNHS.FM2991D	100°	1.7
NMNHS.FM2991E	90°	1.6
NMNHS.FM2991F	90°	1.8
NMNHS.FM2991G	100°	1.6

The subarcuate fossa is absent, however the cerebellar surface of the petrosal is slightly convex except for NMNHS.FM2991B in which it is completely flat. The internal auditory meatus is oriented antero-posteriorly as in extant elephants. The *crista partis petrosa* is blunt in general but it is sharper in specimens NMNHS.FM2991C, F and G. In cerebral view, the middle meningeal artery leaves a deep groove on the surface of the *tegmen tympani*. This feature is visible in every specimen except for NMNHS.FM2991E, F and G in which the *tegmen tympani* is broken.

In tympanic view, the unique perilymphatic foramen is retained during ontogeny, therefore, the cochlear canaliculus is absent. The *promontorium* is bulbous and exhibits a very thick *crista interfenestralis*. The *fenestra vestibuli* is oval. Its stapedial ratio varies around 1.7 (Table III.3). A lateral protuberance (like in some extant elephants specimens) is present near the perilymphatic foramen in several specimens (NMNHS.FM2991A, B, C and G). The fragile mastoid process is broken in all of the studied specimens. However, in some specimens such as NMNHS.FM2991A, C, E and G, the trace of the mastoid pneumatic cells is still visible on the petrosal. The *aquaeductus Fallopii* is also preserved in several specimens. It is not covered by bone roofs as in extant elephants, however these structures could have been lost during the taphonomic process.

Vestibular bony labyrinth (Fig III.26-30)

Ampullae

As in all proboscideans except the earliest ones such as *Eritherium* and *Phosphatherium*, the ampullae of *Anancus* appear less defined. On NMNHS.FM2991B a sharp ampullar ridge is visible on the lateral canal. It extends from the basis to the apical part of the lateral ampulla. The ampullar ridge maximum height is located at the center of the ampulla; it has the shape of a flattened bump. Although no other specimen displays such type of ridge, some of them show a slight ridge on their lateral ampulla. It is the case of NMNHS.FM2991A, NMNHS.FM2991C, NMNHS.FM2991D and NMNHS.FM2991G. At the limit between the posterior ampulla and the vestibule, there is a highly marked bulge in NMNHS.FM2991F. It is small but high and has the appearance of a wart. This feature is only seen in NMNHS.FM2991F so it is an intra-specific variable character as the other ridges and bulges.

Crus commune

The *crus commune* of *Anancus* is elongated in all specimens and never displays a strong basal thickening. Some specimens of *Anancus* display a more or less sharp ridge on their *crus commune*. This feature is not visible on all specimens of *Anancus* and it takes different shapes from specimen to specimen. In NMNHS.FM2991A, the ridge is rather clearly less marked in this specimen. In NMNHS.FM2991C, no ridge is visible on the *crus commune*. NMNHS.FM2991D displays a ridge similar to the one of NMNHS.FM2991A but clearly less sharp. In NMNHS.FM2991E the ridge is present and extends only from the posterior canal to the basis of the *crus commune*. The ridge is absent in NMNHS.FM2991F. The thickness of the *crus commune* is variable. It is particularly thin in NMNHS.FM2991B, NMNHS.FM2991F and NMNHS.FM2991G sharp and extends from the posterior canal to the basis of the lateral canal ampulla. This structure creates two slightly concave planes on either sides of the ridge. In NMNHS.FM2991B, a ridge extends on the *crus commune* from the posterior semicircular canal to a bulge on the vestibule. A similar morphology is found in NMNHS.FM2991G but the ridge is

with respective thickness ratios of 20.05, 18.42 and 20.33. In NMNHS.FM2991A, the anterior and posterior semicircular canals meet quite low (approximately at the mid-height of the anterior canal) while they meet higher in the other specimens (approximately at two thirds of the height of the anterior canal). The *crus commune* is slightly inclined in NMNHS.FM2991A but the angle of inclination is even higher in NMNHS.FM2991B. The crus commune is vertical in the other specimens.

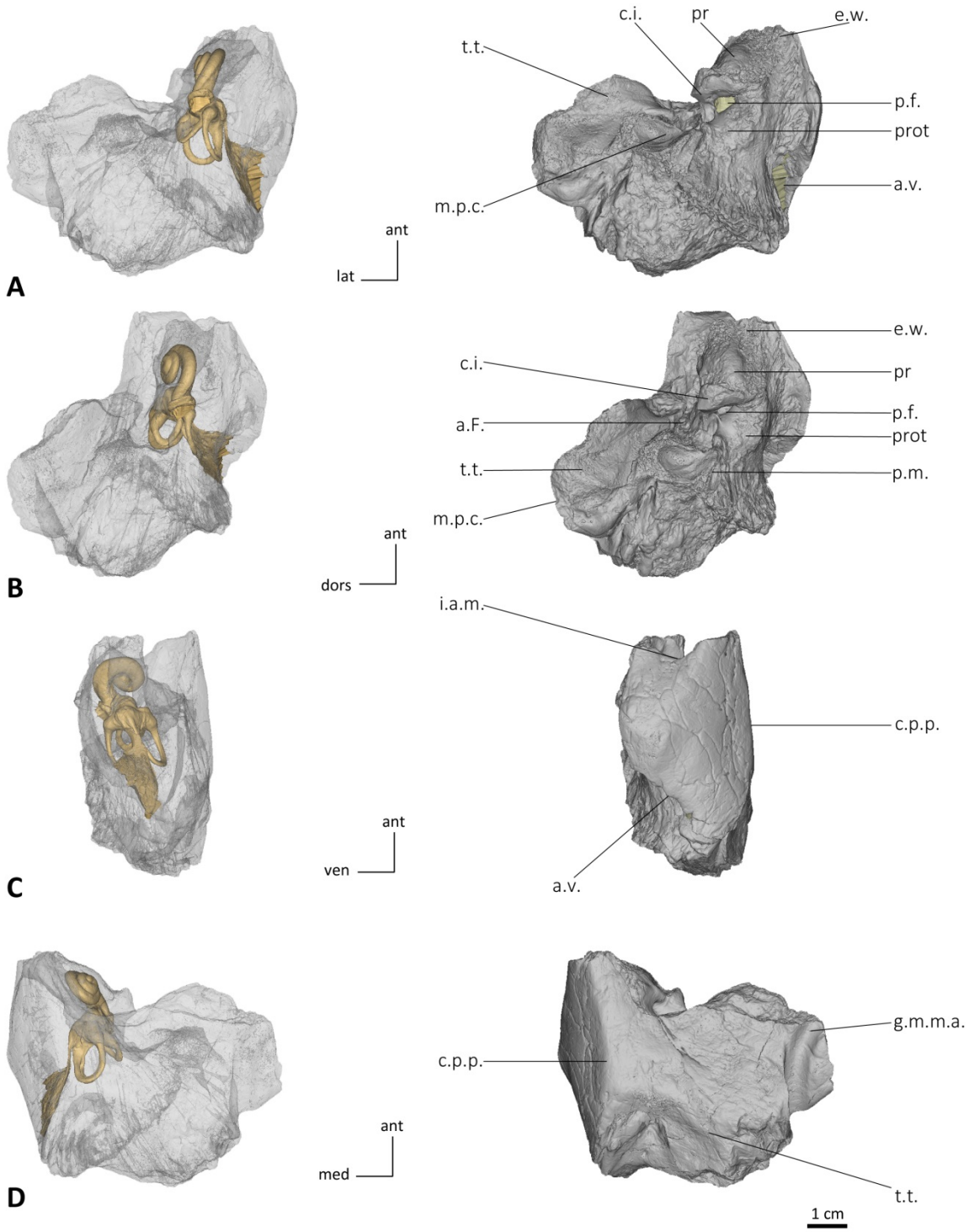

Figure III.19 : 3D reconstructed models of the petrosal of *Anancus arvernensis* NMNHS.FM2991A in medial (A), tympanic (B), cerebellar (C) and cerebral (D) views. Legends: **a.F.** *aquaeductus Fallopii*, **a.v.** *aquaeductus vestibuli*, **c.i.** *crista interfenestralis*, **c.p.p.** *crista partis petrosa*, **e.w.** epitympanic wing, **g.m.m.a.** groove for the middle meningeal artery, **i.a.m.** internal auditory meatus, **m.p.c.** mastoid pneumatic cell (broken), **p.f.** perilymphatic foramen, **p.m.** *pars mastoidea* (broken), **pr** *promontorium*, **prot** protuberance, **t.t.** *tegmen tympani*

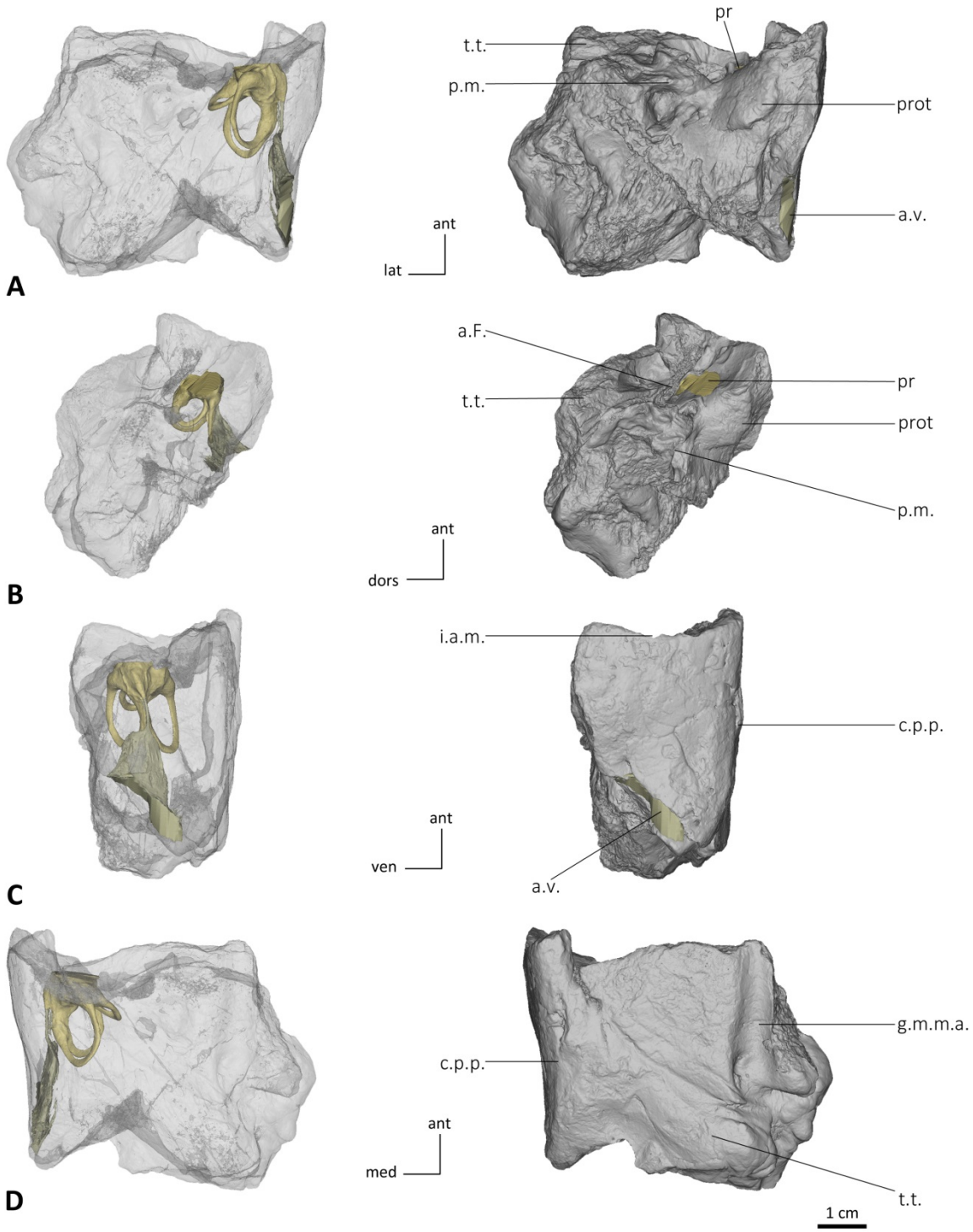

Figure III.20 : 3D reconstructed models of the petrosal of *Anancus arvernensis* NMNHS.FM2991B in medial (A), tympanic (B), cerebellar (C) and cerebral (D) views. Legends: **a.F.** *aquaeductus Fallopii*, **a.v.** *aquaeductus vestibuli*, **c.p.p.** *crista partis petrosa*, **g.m.m.a.** groove for the middle meningeal artery, **i.a.m.** internal auditory meatus, **p.m.** *pars mastoidea* (broken), **pr** *promontorium*, **prot** protuberance, **t.t.** *tegmen tympani*

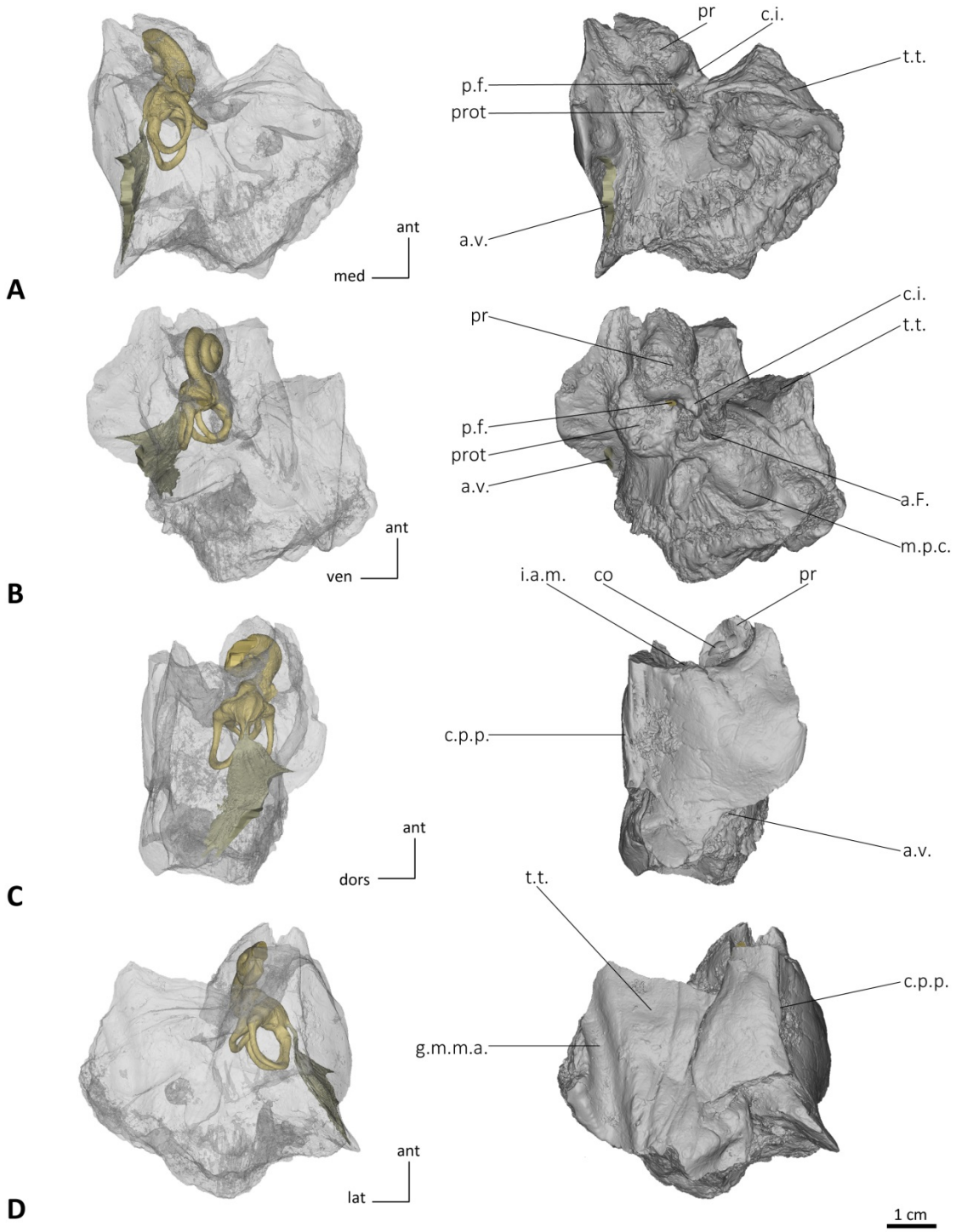

Figure III.21 : 3D reconstructed models of the petrosal of *Anancus arvernensis* NMNHS.FM2991C in medial (A), tympanic (B), cerebellar (C) and cerebral (D) views. Legends: **a.F.** *aquaeductus Fallopii*, **a.v.** *aquaeductus vestibuli*, **c.i.** *crista interfenestralis*, **c.p.p.** *crista partis petrosa*, **co** cochlea, **g.m.m.a.** groove for the middle meningeal artery, **i.a.m.** internal auditory meatus, **m.p.c.** mastoid pneumatic cell (broken), **p.f.** perilymphatic foramen, **pr** *promontorium* (broken), **prot** protuberance, **t.t.** *tegmen tympani* (broken).

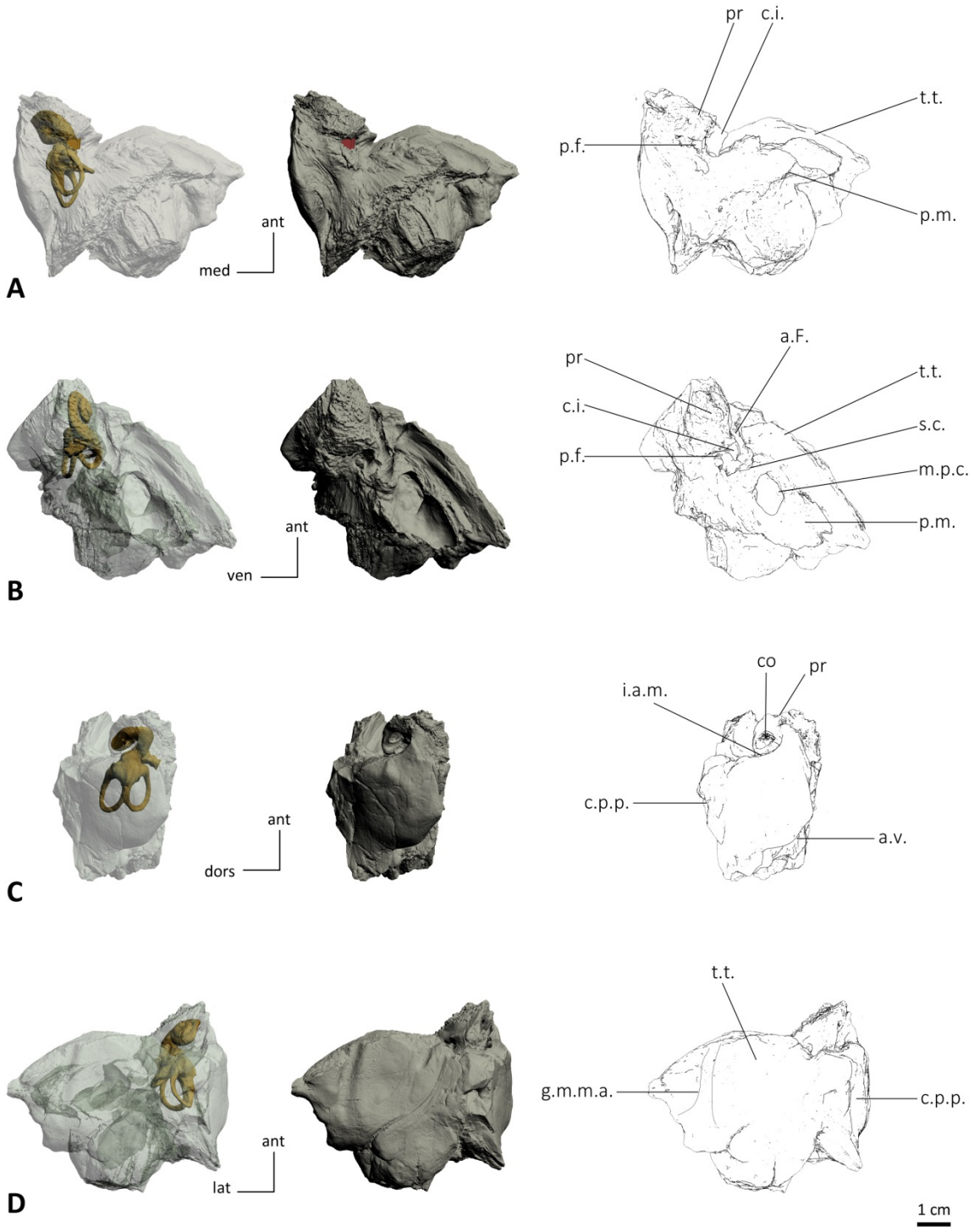

Figure III.22 : 3D reconstructed models and drawings of the petrosal of *Anancus arvernensis* NMNHS.FM2991D in medial (A), tympanic (B), cerebellar (C) and cerebral (D) views. Legends: **a.F.** *aquaeductus Fallopii*, **a.v.** *aquaeductus vestibuli*, **c.i.** *crista interfenestralis*, **c.p.p.** *crista partis petrosa*, **co** cochlea, **g.m.m.a.** groove for the middle meningeal artery, **i.a.m.** internal auditory meatus, **m.p.c.** mastoid pneumatic cell (broken), **p.f.** perilymphatic foramen, **p.m.** *pars mastoidea* (broken), **pr** *promontorium* (broken), **prot** protuberance, **s.c.** stylomastoid canal, **t.t.** *tegmen tympani*

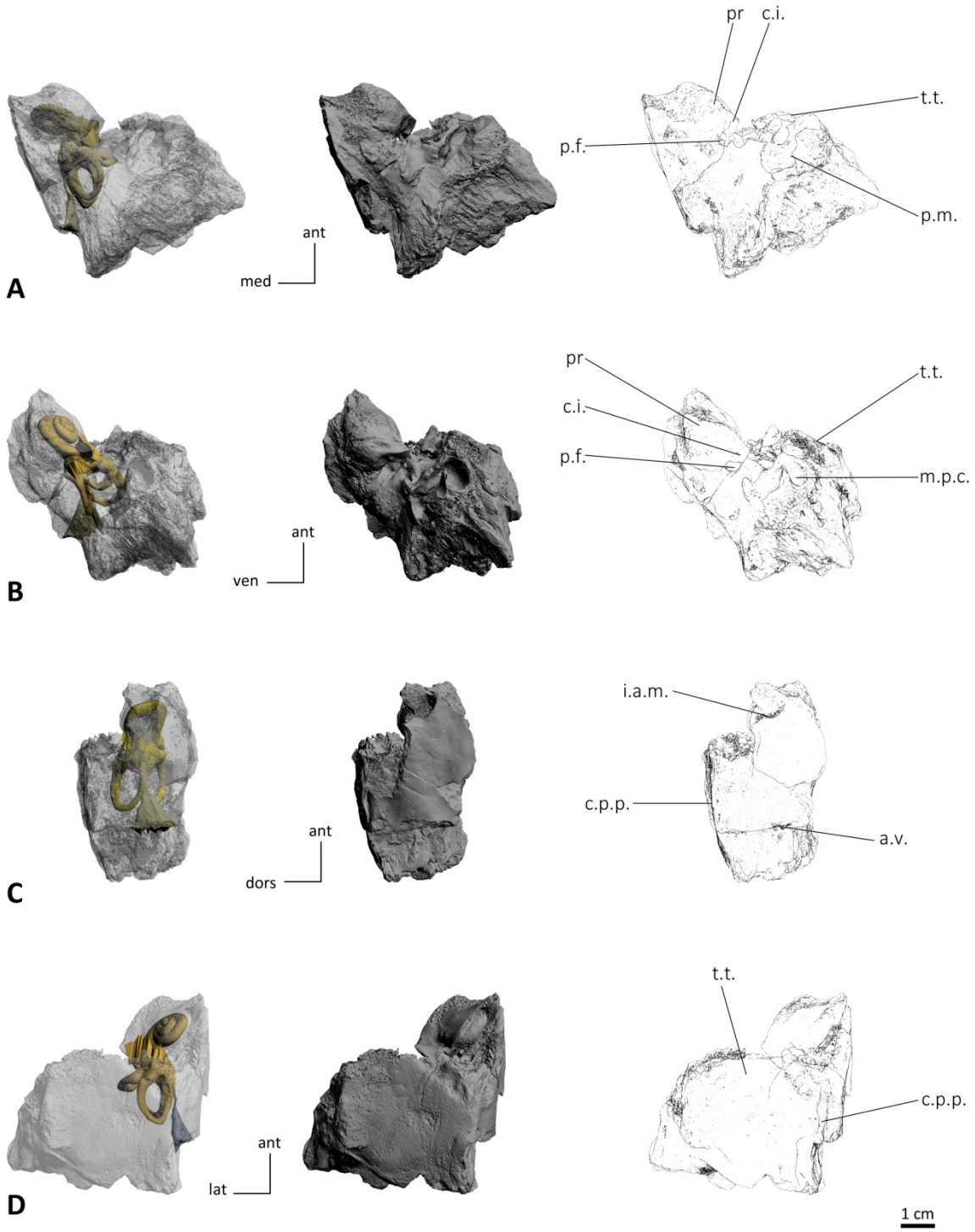

Figure III.23 : 3D reconstructed models and drawings of the petrosal of *Anancus arvernensis* NMNHS.FM2991E in medial (A), tympanic (B), cerebellar (C) and cerebral (D) views. Legends: **a.v.** *aquaeductus vestibuli*, **c.i.** *crista interfenestralis*, **c.p.p.** *crista partis petrosa*, **i.a.m.** internal auditory meatus, **m.p.c.** mastoid pneumatic cell (broken), **p.f.** perilymphatic foramen, **p.m.** *pars mastoidea* (broken), **pr** *promontorium*, **t.t.** *tegmen tympani*

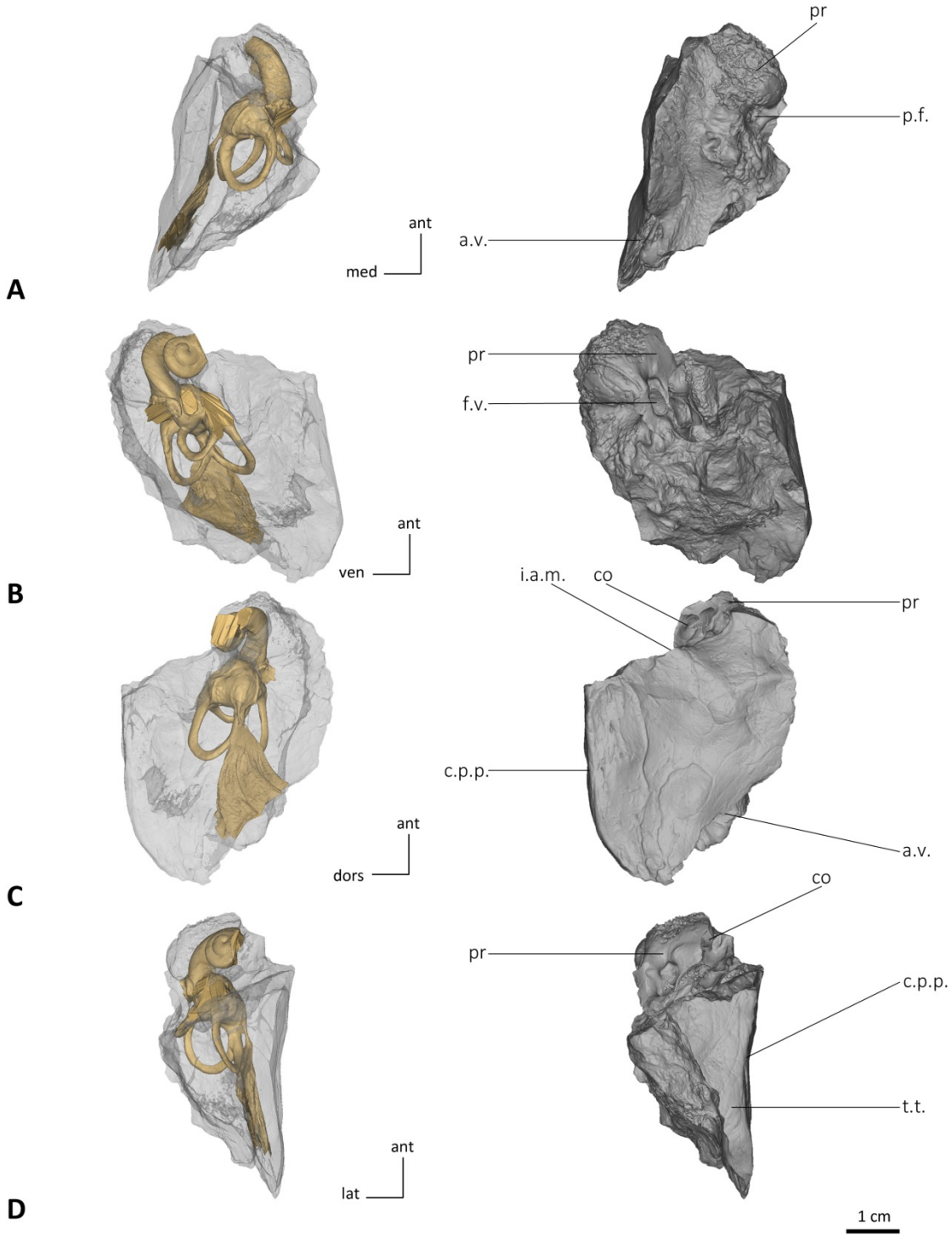

Figure III.24 : 3D reconstructed models of the petrosal of *Anancus arvernensis* NMNHS.FM2991F in medial (A), tympanic (B), cerebellar (C) and cerebral (D) views. Legends: **a.v.** *aquaeductus vestibuli*, **c.i.** *crista interfenestralis*, **c.p.p.** *crista partis petrosa*, **co** cochlea, **f.v.** *fenestra vestibuli*, **i.a.m.** internal auditory meatus, **p.f.** perilymphatic foramen, **pr** *promontorium* (broken), **t.t.** *tegmen tympani*

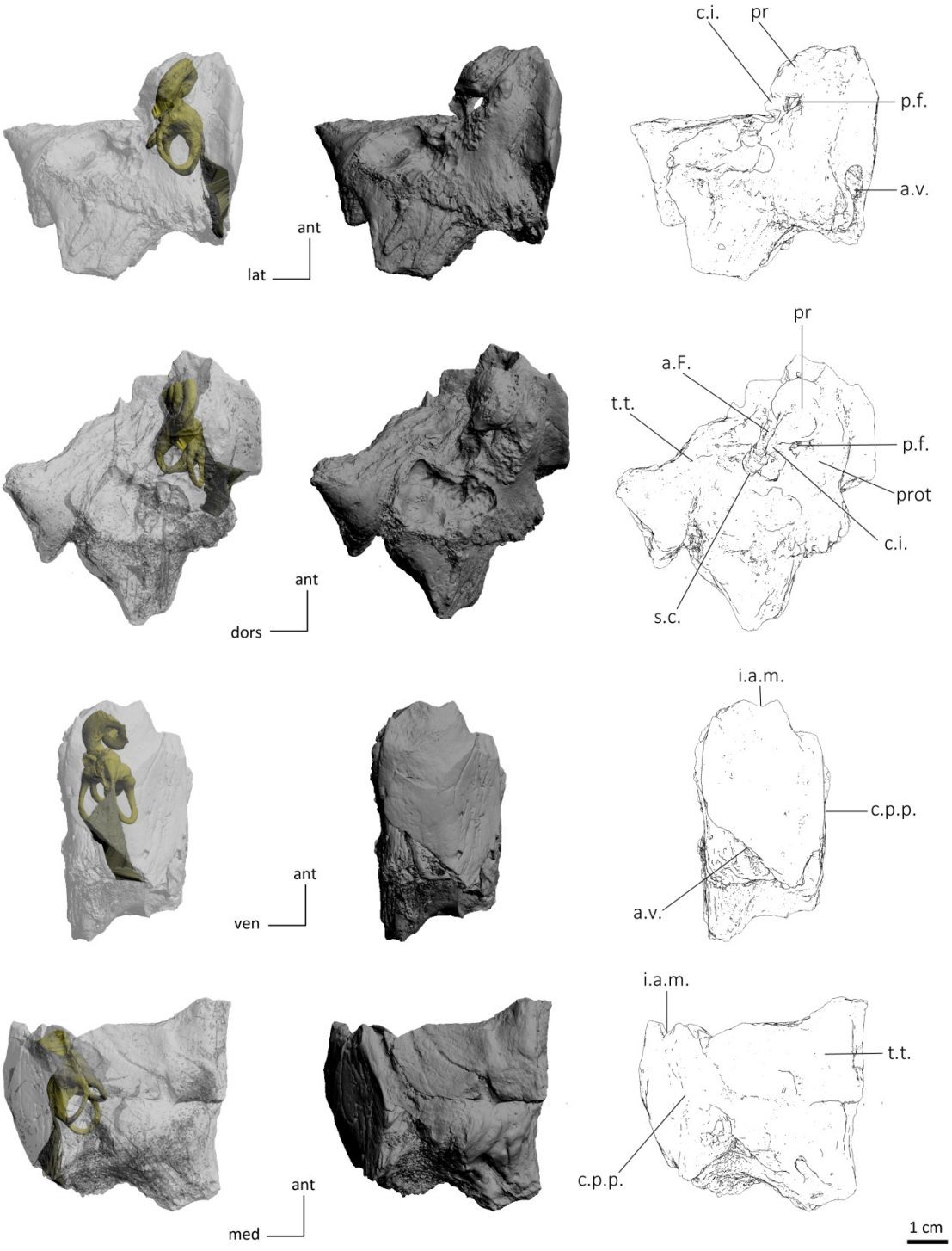

Figure III.25 : 3D reconstructed models and drawings of the petrosal of *Anancus arvernensis* NMNHS.FM2991G in medial (A), tympanic (B), cerebellar (C) and cerebral (D) views. Legends: **a.F.** *aquaeductus Fallopii*, **a.v.** *aquaeductus vestibuli*, **c.i.** *crista interfenestralis*, **c.p.p.** *crista partis petrosa*, **i.a.m.** internal auditory meatus, **m.p.c.** mastoid pneumatic cell (broken), **p.f.** perilymphatic foramen, **p.m.** *pars mastoidea* (broken), **pr** *promontorium* (broken), **prot** protuberance, **s.c.** stylomastoid canal, **t.t.** *tegmen tympani* (broken)

thickness of the *crus commune* is variable. It is particularly thin in NMNHS.FM2991B, NMNHS.FM2991F and NMNHS.FM2991G with respective thickness ratios of 20.05, 18.42 and 20.33. In NMNHS.FM2991A, the anterior and posterior semicircular canals meet quite low (approximately at the mid-height of the anterior canal) while they meet higher in the other specimens (approximately at two thirds of the height of the anterior canal). The *crus commune* is slightly inclined in NMNHS.FM2991A but the angle of inclination is even higher in NMNHS.FM2991B. The *crus commune* is vertical in the other specimens.

Semicircular canals

The anterior semicircular canal is oval in all specimens of *Anancus*, however the angle formed by the major axis of the canal and the *crus commune* vary among specimens. Three specimens display a very low angle (NMNHS.FM2991A, NMNHS.FM2991D and NMNHS.FM2991E with respective angle values of 14°, 10° and 11°). The major axis of the anterior canals of NMNHS.FM2991B and NMNHS.FM2991C forms an angle of respectively 23° and 24° with the *crus commune*. The values are even higher in NMNHS.FM2991F and NMNHS.FM2991G (32° and 38° respectively). The mean central streamline length is 23.90 mm (with a variation up to 1.5 mm, depending on the specimen) with NMNHS.FM2991B displaying the longest streamline (25.35 mm). The average section radius is 0.77 mm (mean). Every specimen displays a value close to the average except for NMNHS.FM2991B and NMNHS.FM2991E which have respectively very low (0.58 mm) and high (0.91 mm) values. Hence NMNHS.FM2991B has a particularly low thickness ratio compared to the other specimens (2.29). The relative slenderness of this specimen is distinct on the reconstruction. Other specimens have more or less similar thickness ratio values (3.09 to 3.75) with NMNHS.FM2991E displaying the higher ratio (3.78). The relative high thickness of this specimen is obvious on the 3D model. The average anterior thickness ratio of all seven specimens of *Anancus* is 3.21. The radius of curvature of the anterior canal is 5.41 on average. This value varies from 5.02 (NMNHS.FM2991A) to 5.91 (NMNHS.FM2991B).

The posterior semicircular canal is also oval in all specimens of *Anancus*, however it is slightly more rounded in NMNHS.FM2991C and NMNHS.FM2991G. The angle formed by the major axis of the canal and the *crus commune* varies among specimens but less than the anterior canal

angle values. Two specimens display posterior canals with a major axis parallel to the *crus commune* (NMNHS.FM2991A and NMNHS.FM2991B). The angle values of the other specimens are low, between -10° and -18° (see Table III.2). The main difference with the anterior canal is that the orientation of the major axis of the canal is reversed (hence the negative values). Indeed, the major axis of the anterior canals is inclined toward the base of the *crus commune* while it is inclined toward the apex of the *crus commune* for posterior canals. The mean central streamline length is 23.46 mm (with a variation up to 2.3 mm, depending on the specimen) which is very similar to the anterior canal. The average section radius is 0.76 mm (mean) like the anterior canal. Every specimen displays a value close to the mean except for NMNHS.FM2991B and NMNHS.FM2991E which have respectively very low (0.64 mm) and high (0.92 mm) values. Hence NMNHS.FM2991B has a particularly low posterior thickness ratio compared to the other specimens (2.66) although this is less marked than for its anterior canal (2.29). NMNHS.FM2991G also displays a low posterior thickness ratio (2.70) due to its high streamline length value (25.80 mm). The relative slenderness of the posterior canal of these specimens is distinct on the reconstruction. In the NMNHS.FM2991G specimen case, the posterior canal seems really thinner than the anterior one on the reconstruction. Other specimens have more or less similar thickness ratio values (3.10 to 3.99) with NMNHS.FM2991E displaying the higher ratio again (3.99). The relative high thickness of the posterior canal of this specimen is obvious on the 3D model. The average posterior thickness ratio of all seven specimens of *Anancus* is 3.24 (roughly the same value as for the anterior canal). The mean radius of curvature of the anterior canal is 5.35. This value varies from 4.79 (NMNHS.FM2991A) to 5.67 (NMNHS.FM2991F and NMNHS.FM2991G).

The lateral semicircular canal is oval in all specimens of *Anancus*. The mean central streamline length is 22.24 mm (with a variation up to 2.2 mm depending on the specimen) which is slightly lower than the anterior and posterior canals. The average section radius is 0.81 mm (mean) which is slightly higher than the other canals. Every specimen displays a value around the

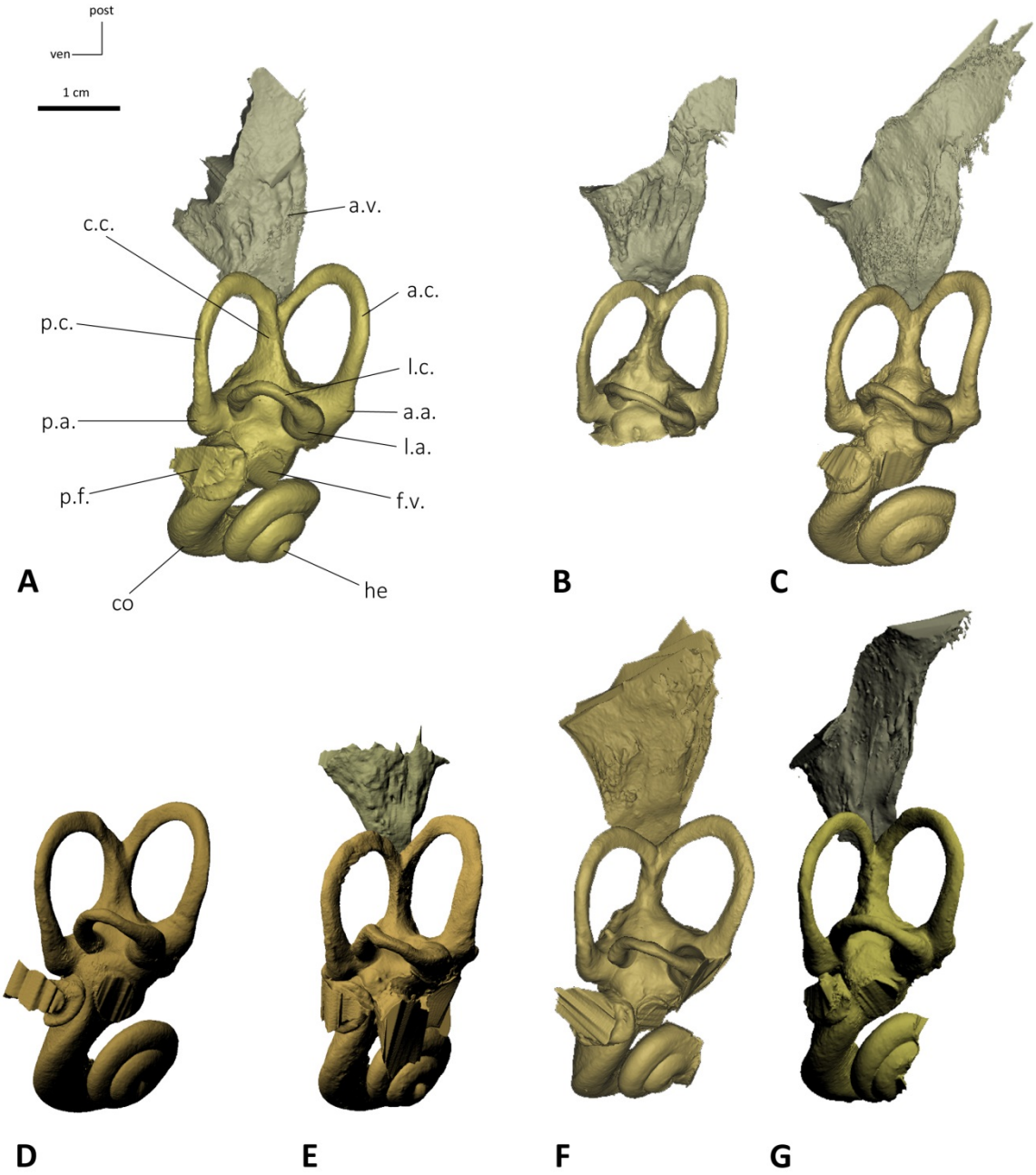

Figure III.26 : 3D reconstructed models of the bony labyrinths of *Anancus arvernensis* specimens NMNHS.FM2991A (A), NMNHS.FM2991B (B), NMNHS.FM2991C (C), NMNHS.FM2991D (D), NMNHS.FM2991E (E), NMNHS.FM2991F (F) and NMNHS.FM2991G (G) in frontal view. Legends: **a.a.** anterior ampulla, **a.c.** anterior semicircular canal, **a.v.** *aquaeductus vestibuli*, **c.c.** *crus commune*, **co** cochlea, **f.v.** *fenestra vestibuli*, **he** helicotrema, **l.a.** lateral ampulla, **l.c.** lateral semicircular canal, **p.a.** posterior ampulla, **p.c.** posterior semicircular canal, **p.f.** perilymphatic foramen.

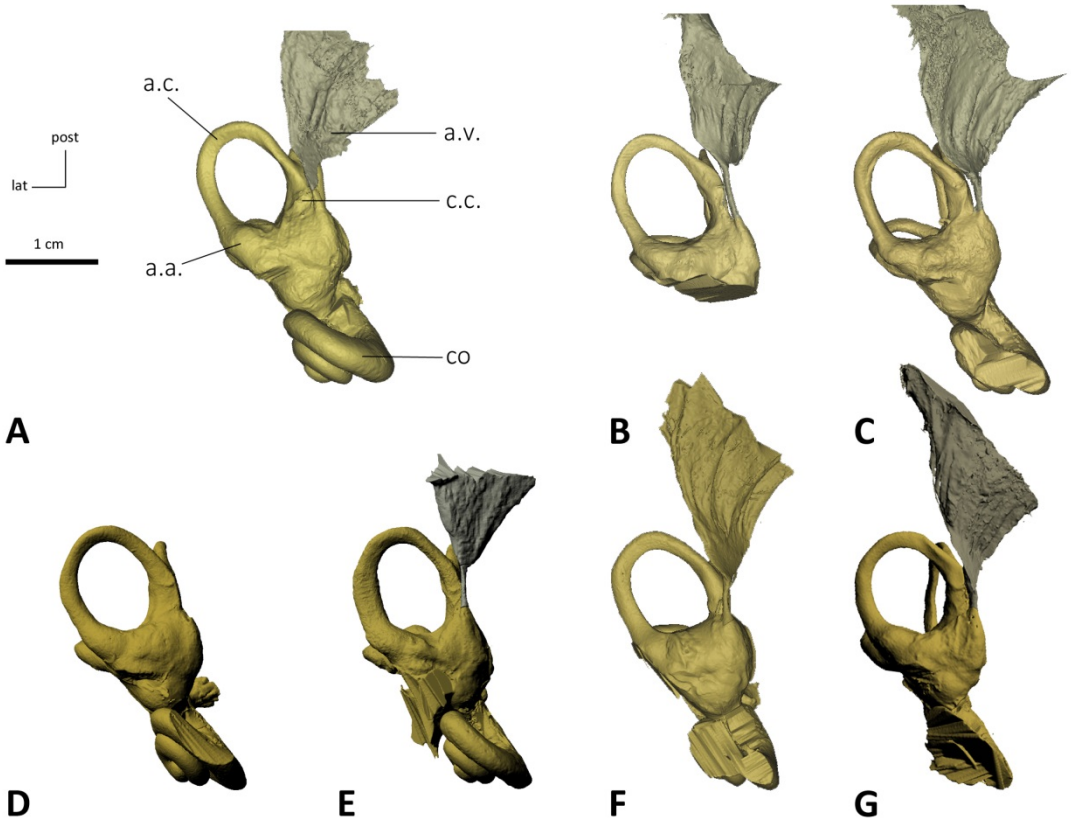

Figure III.27 : 3D reconstructed models of the bony labyrinths of *Anancus arvernensis* specimens NMNHS.FM2991A (A), NMNHS.FM2991B (B), NMNHS.FM2991C (C), NMNHS.FM2991D (D), NMNHS.FM2991E (E), NMNHS.FM2991F (F) and NMNHS.FM2991G (G) in anterior canal view. Legends: **a.a.** anterior ampulla, **a.c.** anterior semicircular canal, **a.v.** *aquaeductus vestibuli*, **c.c.** *crus commune*, **co** cochlea.

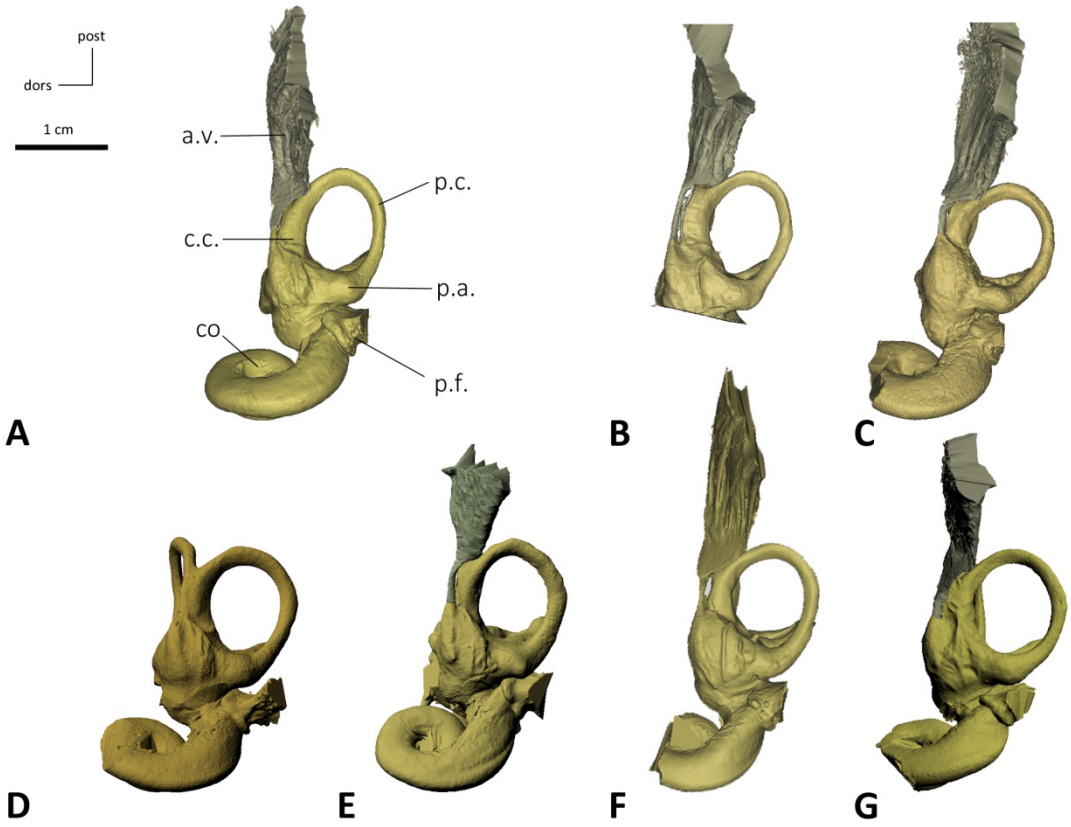

Figure III.28 : 3D reconstructed models of the bony labyrinths of *Anancus arvernensis* specimens NMNHS.FM2991A (A), NMNHS.FM2991B (B), NMNHS.FM2991C (C), NMNHS.FM2991D (D), NMNHS.FM2991E (E), NMNHS.FM2991F (F) and NMNHS.FM2991G (G) in posterior canal view. Legends: **a.v.** *aquaeductus vestibuli*, **c.c.** *crus commune*, **co** cochlea, **p.a.** posterior ampulla, **p.c.** posterior semicircular canal, **p.f.** perilymphatic foramen.

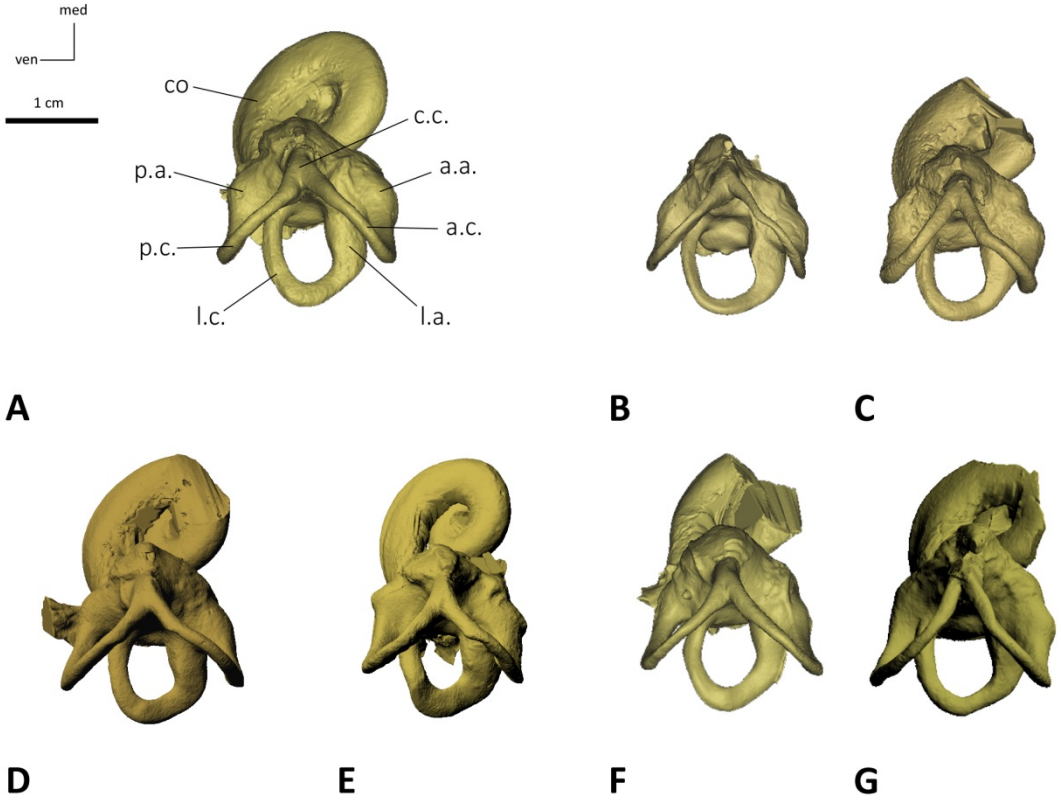

Figure III.29 : 3D reconstructed models of the bony labyrinths of *Anancus arvernensis* specimens NMNHS.FM2991A (A), NMNHS.FM2991B (B), NMNHS.FM2991C (C), NMNHS.FM2991D (D), NMNHS.FM2991E (E), NMNHS.FM2991F (F) and NMNHS.FM2991G (G) in lateral canal view. Legends: **a.a.** anterior ampulla, **a.c.** anterior semicircular canal, **c.c.** *crus commune*, **co** cochlea, **l.a.** lateral ampulla, **l.c.** lateral semicircular canal, **p.a.** posterior ampulla, **p.c.** posterior semicircular canal.

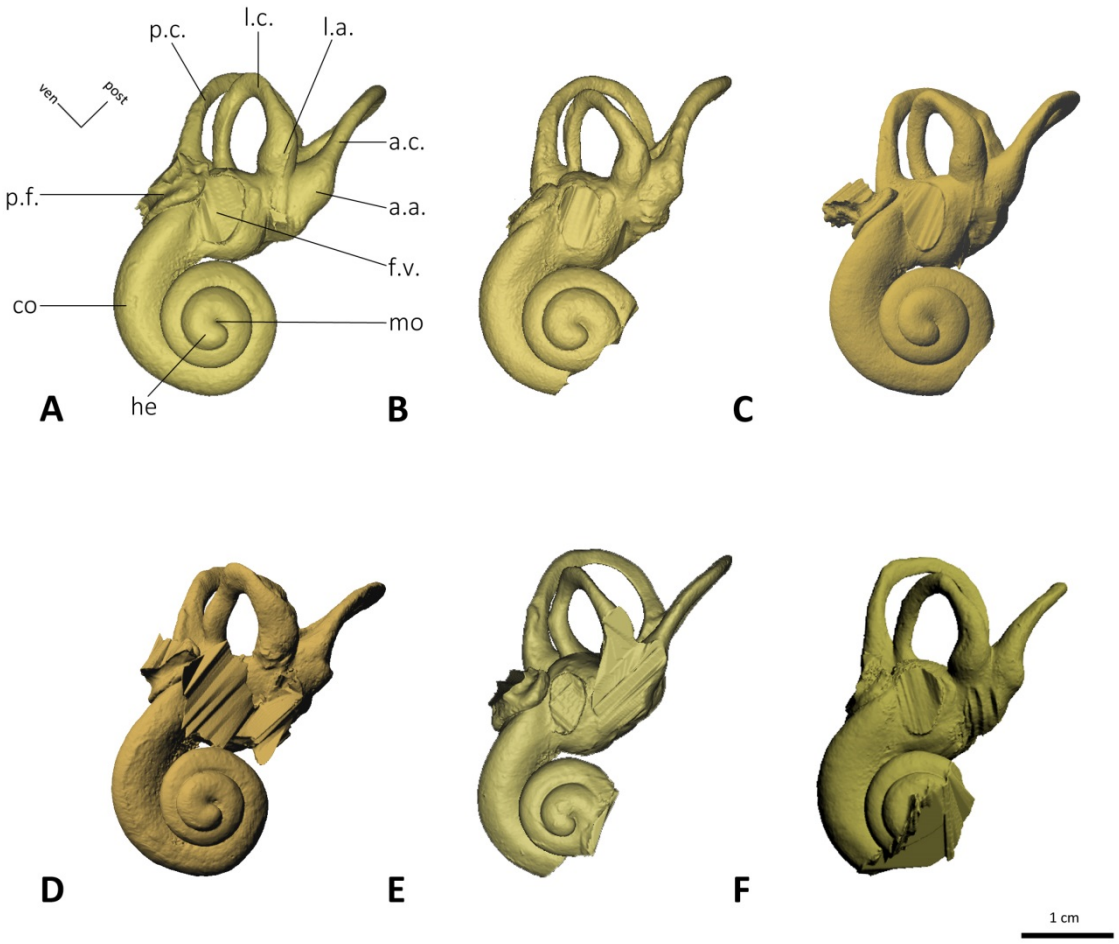

Figure III.30 : 3D reconstructed models of the bony labyrinths of *Anancus arvernensis* specimens NMNHS.FM2991A (A), NMNHS.FM2991C (B), NMNHS.FM2991D (C), NMNHS.FM2991E (D), NMNHS.FM2991F (E) and NMNHS.FM2991G (F) in cochlear view. Legends: **a.a.** anterior ampulla, **a.c.** anterior semicircular canal, **co** cochlea, **f.v.** *fenestra vestibuli*, **he** helicotrema, **l.a.** lateral ampulla, **l.c.** lateral semicircular canal, **mo** modiolus, **p.c.** posterior semicircular canal, **p.f.** perilymphatic foramen.

average except for NMNHS.FM2991B and NMNHS.FM2991E which have respectively very low (0.66 mm) and high (1.06 mm) values. Hence NMNHS.FM2991B has a particularly low posterior thickness ratio compared to the other specimens (2.72) although this is less marked than for its anterior canal (2.25). The relative slenderness of the lateral canal of this specimen is distinct on the reconstruction. In contrast NMNHS.FM2991E has a particularly high lateral thickness ratio (4.87). Other specimens have more or less similar thickness ratio values (3.50 to 3.86). The average lateral thickness ratio of all seven specimens of *Anancus* is 3.67 (which is slightly higher than the two other canals). The radius of curvature of the anterior canal is 3.58 on average. This value varies from 3.19 (NMNHS.FM2991A) to 4.06 (NMNHS.FM2991B).

The angle between the anterior and lateral canals is always the lowest in *Anancus* specimens. It is always acute and varies from particularly low values (58.20° and 58.9° in NMNHS.FM2991A and NMNHS.FM2991B respectively) to higher values (70.4° in NMNHS.FM2991D and NMNHS.FM2991E). The angle between the lateral and posterior canals oscillates between acute values (the lowest angle being 77.6° in NMNHS.FM2991A) and almost right values (87.9° in NMNHS.FM2991E). It is the same for the angle between the anterior and posterior canals (between 78.5° in NMNHS.FM2991G and 92.40 in NMNHS.FM2991D). In some specimens, the largest angle is the one between the anterior and posterior canals (NMNHS.FM2991A, NMNHS.FM2991B, NMNHS.FM2991D and NMNHS.FM2991F) while it is the opposite in others (NMNHS.FM2991C, NMNHS.FM2991E and NMNHS.FM2991G). If we compare the radii of curvature we can observe that the lateral canal is always smaller than the anterior and posterior canals, which tend to share more similar radii of curvature (see Table III.2). However, the radius of curvature of the anterior canal is always larger than for the posterior canal, except for NMNHS.FM2991D and NMNHS.FM2991G. The anterior canal apex is located higher than the posterior canal apex. In NMNHS.FM2991G, this feature is present but less marked. In *Anancus*, the thickness of the canals is average compared to other proboscideans (but stockier than most mammals) with an average thickness ratio of 3.37 (mean value). NMNHS.FM2991B and NMNHS.FM2991E display respectively particularly thinner (average thickness

ratio = 2.56) and stockier (average thickness ratio = 4.20) canals than the other specimens. In cross-section, the canals appear flattened. In NMNHS.FM2991C, they are a little more circular while the flattening is more pronounced in NMNHS.FM2991B and at the level of the anterior canal of NMNHS.FM2991E. The slender part of the lateral semicircular canal is connected to the vestibule at a high position and clearly distant from the posterior ampulla. NMNHS.FM2991A and NMNHS.FM2991D display no ridges on their canals. NMNHS.FM2991C and NMNHS.FM2991E have a ridge on their anterior and posterior canals while NMNHS.FM2991F and NMNHS.FM2991G have a ridge only on their posterior and anterior canal respectively. In NMNHS.FM2991B, all three canals have a ridge along the inner trajectory of each canal. The lateral canal displays a second ridge which is quite small and gives the impression that a small part of the canal has been folded. It is located on the trough of the ventral part of the canal. No other specimen displays this type of ridge. Every canal of every specimen displays at least a small undulation except for the lateral canal of NMNHS.FM2991G. The undulation is particularly well marked on the lateral canals of NMNHS.FM2991E and NMNHS.FM2991F and on the anterior canal of NMNHS.FM2991C.

Cochlear bony labyrinth

The number of turns of the cochlea of *Anancus arvernensis* seems to be constant. Indeed, each of the five specimens whose cochlea is well preserved (NMNHS.FM2991A, NMNHS.FM2991C, NMNHS.FM2991D, NMNHS.FM2991E, NMNHS.FM2991F) shows the same number of two and a half turns (900°). One specimen does not preserve the cochlea at all (NMNHS.FM2991B) and the last specimen is broken at the level of the cochlea which makes impossible to count the number of turns precisely (NMNHS.FM2991G). However, there is no doubt that this specimen displays at least two and a half turns. Only three specimens have a fully preserved cochlea (NMNHS.FM2991A, NMNHS.FM2991D, NMNHS.FM2991E). The precise length of the cochlea of these specimens is given in Table III.1. While the cochleae of NMNHS.FM2991D and NMNHS.FM2991E have almost the same length (around 79 mm), the cochlea of NMNHS.FM2991A is slightly shorter (around 72 mm). In ventral view, the

modiolus of all specimens is completely overlapped by the apical turn and there is no visible gap. The basal turn of the cochlea is only partially overlapped by the apical turn and is still visible in ventral view. The *lamina secundaria* is absent in all specimens.

3.2.10. *Stegodon orientalis*

Only one specimen of the genus *Stegodon* was CT-scanned (FM18632) and it consists of a juvenile skull bearing both the right and left petrosals. Even though the specimen is mineralized, both inner ears were segmented. The total volume of a *Stegodon* inner ear is 1117 mm^3.

Petrosal (Fig III.31)

The petrosals of *Stegodon* are more or less complete and still attached to the skull. Due to the large size of the specimen, the voxel size is great (141.85 µm) and the resolution is therefore low. This and the advanced mineralization of the specimen contribute to the poor contrast of the microtomographic sections, making the distinction between the petrosal and the tympanic very difficult. Hence, the *pars mastoidea* and the *tegmen tympani* were not fully segmented at the level of their connection with the tympanic. In general, the petrosal of *Stegodon* is similar to the petrosal of extant elephants. In cerebellar view, the *aquaeductus vestibuli* is oriented in the same way but it is smaller. Antero-laterally to the *aquaeductus vestibuli*, the cerebellar surface is very bulbous. The surface located antero-laterally to that bulbous structure is slightly concave and could be a shallow subarcuate fossa. The *crista partis petrosa* is blunt. The internal auditory meatus is filled with sediments and was difficult to segment but its opening on the cerebellar surface is distinct. It is oriented antero-posteriorly as in the other elephantimorphs. The epitympanic wing is preserved and very thin. The angle between the cerebral and cerebellar surfaces of the petrosal is more acute than in extant elephants (85°). In cerebral view, the *tegmen tympani* is not fully segmented but the groove for the middle meningeal artery is visible. It is narrower and shallower than in extant elephants. In tympanic view, the *promontorium* is completely preserved and very prominent. It does not display the “two-parts” morphology seen in some extant elephants. The poor contrast prevents from segmenting the *aquaeductus Fallopii*. The *crista interfenestralis* is preserved and thick. I was not able to segment the *pars*

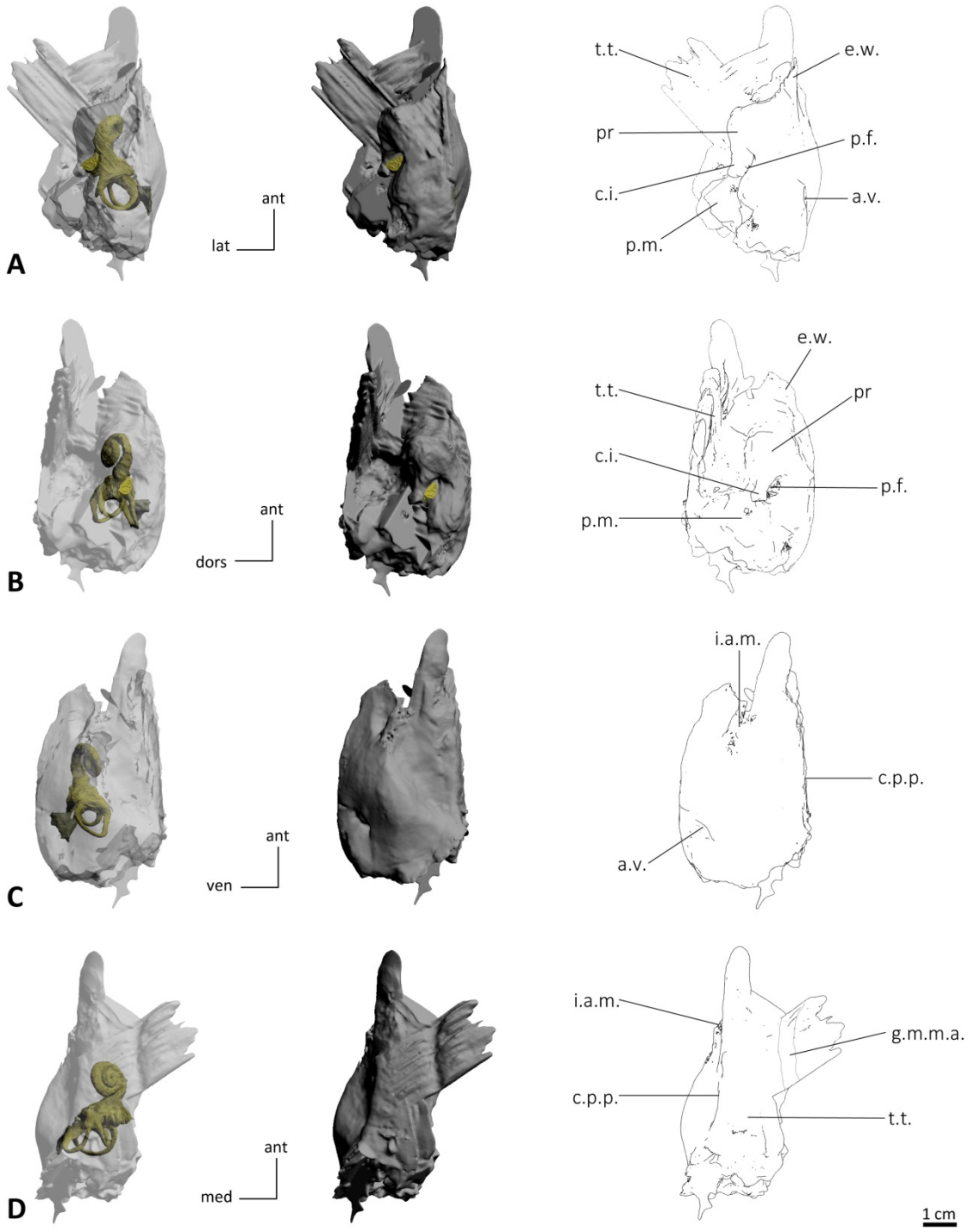

Figure III.31 : 3D reconstructed models and drawings of the right petrosal of *Stegodon orientalis* FM18632 in medial (A), tympanic (B), cerebellar (C) and cerebral (D) views. Legends: **a.v.** *aquaeductus vestibuli*, **c.i.** *crista interfenestralis*, **c.p.p.** *crista partis petrosa*, **co** cochlea, **f.v.** *fenestra vestibuli*, **i.a.m.** internal auditory meatus, **p.f.** perilymphatic foramen, **p.m.** *pars mastoidea* (broken), **pr** *promontorium*, **t.t.** *tegmen tympani* (partially reconstructed)

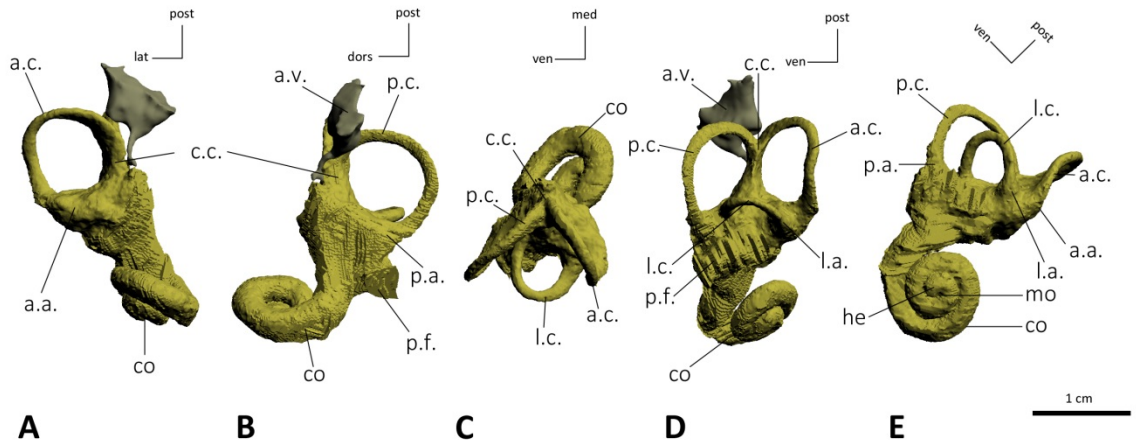

Figure III.32 : 3D reconstructed models of the right bony labyrinth of *Stegodon orientalis* FM18632 in anterior canal (A), posterior canal (B), lateral canal (C), frontal (D) and cochlear (E) views. Legends: **a.a.** anterior ampulla, **a.c.** anterior semicircular canal, **a.v.** *aquaeductus vestibuli*, **c.c.** *crus commune*, **co** cochlea, **he** helicotrema, **l.a.** lateral ampulla, **l.c.** lateral semicircular canal, **mo** modiolus, **p.a.** posterior ampulla, **p.c.** posterior semicircular canal, **p.f.** perilymphatic foramen.

mastoidea, hence the tympanohyal and the stapedial foramen are not observable and the stapedial foramen is not visible. Moreover, it was not possible to segment the pneumatic cavities usually contained in the *pars mastoidea*. The fusion between the *fenestra cochleae* and the cochlear canaliculus into a perilymphatic foramen is retained in *Stegodon* as well. The *fenestra vestibuli* is not well visible on the 3D model because of the poor contrast.

Vestibular bony labyrinth (Fig III.32)

Ampullae

The ampullae of both ears of the *Stegodon* specimen appear poorly defined. While the left inner ear of FM18632 displays no ridges on its ampullae, there is a rather sharp ridge on the anterior ampullae of the right ear.

Crus commune

The *crus commune* is elongated and displays a rather marked basal thickening. In the left ear, a poorly defined vertical ridge runs on the *crus commune* in the extension of the anterior semicircular canal ridge. In the right ear, the vertical ridge is present as well but is clearly sharper. The average section radius of the *crus commune* of *Stegodon* is 1.37 mm. The length of the *crus commune* is approximately 5.34 mm. Therefore *Stegodon* has a *crus commune* with a thickness ratio of 25.72 which is on the middle range for proboscideans. In both ears, the anterior and posterior semicircular canals meet quite high (at

least 75% of the height of the anterior canal). The *crus commune* is slightly inclined toward the anterior canal in both ears.

Semicircular canals

The anterior semicircular canal is oval in both ears of FM18632. The major axis of the canal forms an angle of 19° with the *crus commune* in the right ear while it is parallel in the left ear. The central streamline of the anterior canal has a length of 23.66 mm. The average section radius of this canal is 0.83 mm. Therefore, the thickness ratio is 3.51. The radius of curvature of the anterior canal is 5.36.

The posterior semicircular canal is oval in both ears of FM18632. The major axis of the canal forms an angle of -19° with the *crus commune* in the left ear but this value is slightly lower in the right ear (-13°). It is important to point out that the orientation of the major axis is reversed compared to the anterior in both ears (hence the negative values). The central streamline length of the posterior canal is 23.38 mm which is very similar with the anterior canal value. The average section radius of the posterior canal is also very similar to the anterior one (0.82 mm). Therefore, the value for the thickness ratio is the same as for the anterior canal (3.51). The radius of curvature of the posterior canal is 7.48 which is very large.

The lateral semicircular canal is quite round in both ears of FM18632. Compared to the other semicircular canals, the lateral canal is the shortest with a length of 15.17 mm. The average section radius for the lateral canal is slightly lower (0.77 mm) than the other canals as well. The thickness ratio of this canal (5.1) is clearly higher than that for the anterior and posterior canals, even though it is not noticeable on the reconstruction. The radius of curvature of the lateral canal is 3.27.

The angle between the anterior and posterior canals and the angle between the posterior and lateral canals are particularly large (respectively 107.6° and 94°). In contrast, the angle between the anterior and lateral canals is clearly lower (74.9°). The lateral canal is clearly smaller (radius of 3.27) than the anterior and posterior canals. The smaller size of the lateral canal is extremely marked and visible on the reconstruction. The posterior canal is the largest one with a radius of curvature of 7.48 (radius of curvature of the anterior canal: 5.36). The anterior canal apex is located slightly higher than the posterior one in both ears.

In *Stegodon*, the degree of thickness of the semicircular canals is high compared to other proboscideans and mammals (average thickness ratio = 4.04). The canals are flattened in cross-section and the slender part of the lateral canal enters the vestibule at a quite high position, distant to the posterior ampulla. Hence there is no fusion between the lateral and posterior canals. There is a ridge on the anterior and posterior canals of both ears, the anterior ridge being particularly sharp. All the canals display an undulation but the anterior canal is clearly more undulated than the others.

Cochlear bony labyrinth (Fig III.32)

The cochlear part is fully preserved in both ears of the studied specimen of *Stegodon orientalis* (FM18632). The cochlea displays 2 turns (720°) and a length of 68.7 mm. In ventral view, the modiolus is slightly loose and we can see a gap there. The basal turn of the cochlea is only partially overlapped by the apical turn and is still visible in ventral view. The *lamina secundaria* is absent. The cochlear volume (508 mm^3) represents around 45% of the total volume of the bony labyrinth. The aspect ratio of the cochlea is 0.5, making it more conical than in extant elephants.

3.2.11. *Mammuthus*

Two species of *Mammuthus* have been studied. First, the right isolated petrosal bone of *Mammuthus primigenius* (MNHN.F.1904-12) has been scanned and segmented. This specimen displays a complete inner ear even though the cochlear part is a little damaged. The total volume of the *Mammuthus primigenius* inner ear is around 1131 mm^3. Secondly, two isolated petrosals (left and right) of the same specimen of a *Mammuthus columbi* (FM 144658) have been scanned and segmented. However, the cochlear part is broken on both petrosals; hence the total volume of the inner ear is unknown for this species.

Petrosal (Fig III.33-34)

The overall aspect of the petrosal is very similar as the petrosal of extant elephants. In cerebellar view, the subarcuate fossa is absent. While the area surrounding the *aquaeductus vestibuli* is slightly convex in *Mammuthus columbi*, it is concave is *Mammuthus primigenius*. In both species, the *aquaeductus vestibuli* has the shape of an elongated slit located in the posteromedial corner of the petrosal. In *Mammuthus primigenius*, the slit is somewhat covered by the cerebellar surface of the petrosal. The *crista partis*

petrosa is blunt in every specimen of *Mammuthus*. The angle between the cerebral and the cerebellar surfaces of the petrosal is obtuse in both species, but it is larger in *M. primigenius* (112°) than in *M. columbi* (101° for the right ear, 103° for the left ear). While the internal auditory meatus is completely broken in *Mammuthus columbi*, it is better preserved in *Mammuthus primigenius*. It is oriented antero-posteriorly as in extant elephants. In cerebral view, *the tegmen tympani* is pretty shattered in *M. columbi*. The groove for the middle meningeal artery is not visible in both left and right ears but a thin groove runs across the cerebral surface parallel to the *crista partis petrosa*. In *M. primigenius*, the *tegmen tympani* is better preserved. The groove for the middle meningeal artery is visible and located on the ventral part of the surface which is connected in life with the squamosal bone. The groove is thinner and shallower than in extant elephants. In tympanic view, the petrosal of *M. primigenius* is better preserved than the petrosal of *M. columbi*. In the latter, the *promontorium* is damaged in both ears preventing any observation of the *fenestra vestibuli* and the perilymphatic foramen. These structures are preserved in *M. primigenius*. The *promontorium* is bulbous and displays a secondary bulging structure as in every *Elephas* and some *Loxodonta* specimen. The *fenestra vestibuli* is damaged, but it appears oval. The perilymphatic foramen is preserved and similar to the foramen of extant elephants. The *crista interfenestralis* is thick but the tympanohyal is not preserved hence the condition of the stapedial foramen remains unknown. The *pars mastoidea* is almost completely damaged in both species. Only the imprints of the tympanic cavities contained in the *pars mastoidea* are visible (particularly in the right ear of *M. columbi*). The roof of the *aquaeductus Fallopii* is partially broken in both ears of *M. columbi,* giving it the aspect of a groove. However, it seems to display the posteriorly opened condition seen in extant elephants. In *M. primigenius*, the roof is preserved and covers the whole canal except for its region close to the *crista interfenestralis* (posteriorly opened condition). On the flange of bone forming the roof of the canal, the fossa incudis is clearly visible in *M. primigenius*. A similar fossa is visible in the right ear of *M. columbi* but it is shallower and less marked.

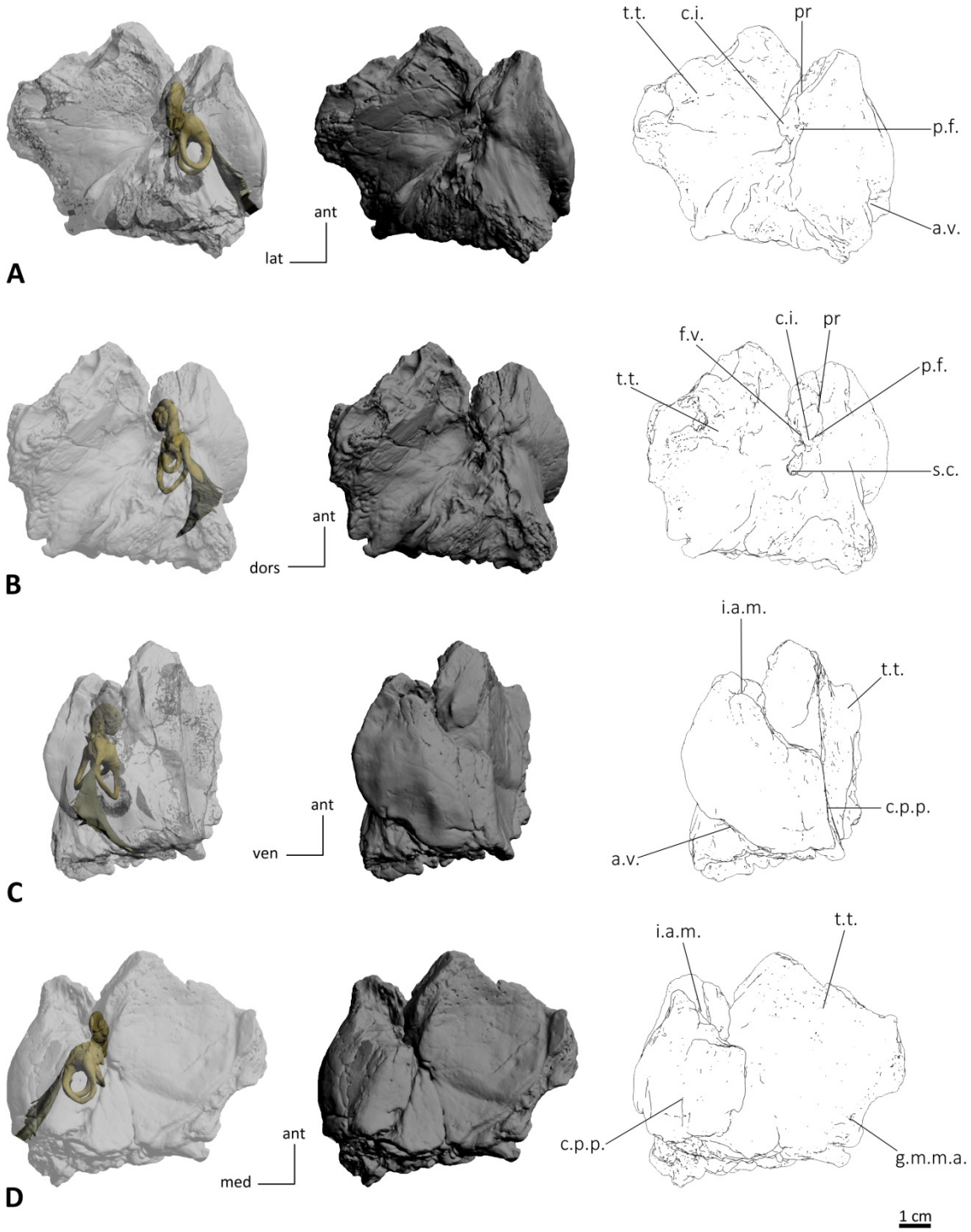

Figure III.33 : 3D reconstructed models of the right petrosal of *Mammuthus primigenius* MNHN.F.1904-12 in medial (A), tympanic (B), cerebellar (C) and cerebral (D) views. Legends: **a.v.** *aquaeductus vestibuli*, **c.i.** *crista interfenestralis*, **c.p.p.** *crista partis petrosa*, **f.v.** *fenestra vestibuli*, **g.m.m.a.** groove for the middle meningeal artery, **i.a.m.** internal auditory meatus (broken), **p.f.** perilymphatic foramen, **pr** *promontorium* (broken), **s.c.** stylomastoid canal, **t.t.** *tegmen tympani*

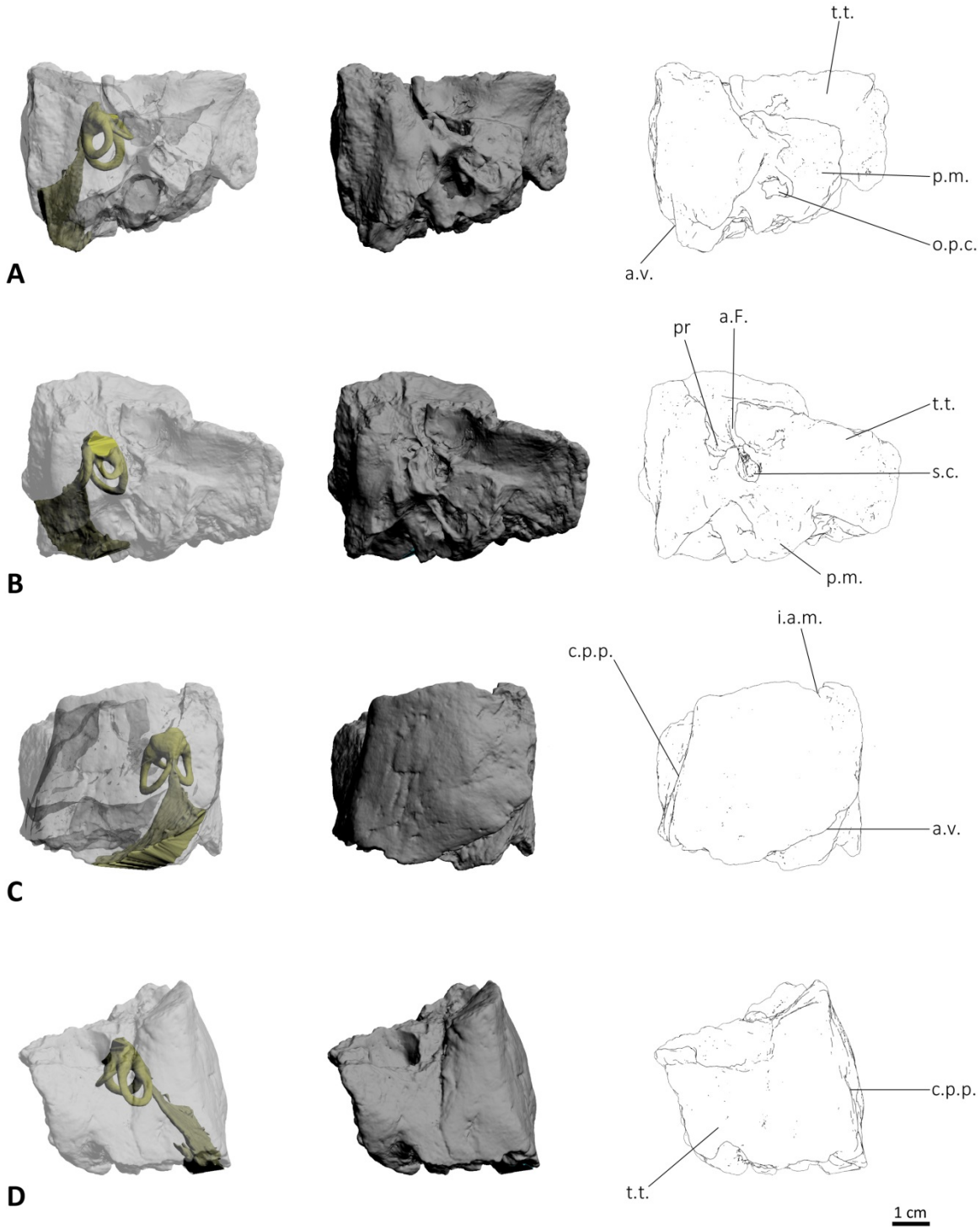

Figure III.34 : 3D reconstructed models of the left petrosal of *Mammuthus columbi* FM144658 in medial (A), tympanic (B), cerebellar (C) and cerebral (D) views. Legends: **a.F.** *aqueductus Fallopii*, **a.v.** *aquaeductus vestibuli*, **c.p.p.** *crista partis petrosa*, **i.a.m.** internal auditory meatus (broken), **o.p.c.** opening for the pneumatic cell, **p.m.** *pars mastoidea* (broken), **pr** location of the broken *promontorium*, **s.c.** stylomastoid canal, **t.t.** *tegmen tympani* (broken)

Vestibular bony labyrinth (Fig III.35)

Ampullae

The ampullae of both species of *Mammuthus* appear poorly defined. The ampullae of both ears of *Mammuthus columbi* (FM 144658) display neither ridges nor bulges. However both the anterior and lateral ampullae of the right ear of *Mammuthus primigenius* (MNHN.F.1904-12) display sharp ridges (one on each ampulla) that meet at the intersection of the two ampullae.

Crus commune

The *crus commune* is stocky in both taxa, with a slight basal thickening. It is smooth in *Mammuthus columbi* but displays a horizontal bulge in the extension of the posterior semicircular canal ridge. The average section radius of the *crus commune* of *Mammuthus columbi* is 1.41 mm (right: 1.38 mm, left: 1.43 mm). It is slightly larger in *Mammuthus primigenius* (1.42 mm). The average length of the *crus commune* is 5.24 mm in *Mammuthus columbi* (right: 5.64 mm, left: 4.83 mm) and it is also higher in *Mammuthus primigenius* (5.57 mm). *M. columbi* displays a stockier crus commune with a thickness ratio of 27.04 (right: 24.52, left: 29.57) compared to *M. primigenius* (thickness ratio of 25.45). In both specimens, the anterior and posterior semicircular canals meet quite low, approximately at the mid-height of the anterior canal. The *crus commune* is not tilted in any specimen.

Semicircular canals

The anterior semicircular canal is oval in both studied species of *Mammuthus*. The major axis of the canal forms an angle of 42° with the *crus commune* in both ears of the *Mammuthus columbi* specimen while the angle is higher in the *Mammuthus primigenius* specimen (52°). The anterior semicircular canal appears slightly more slender in *Mammuthus primigenius* than in *Mammuthus columbi*. This is supported by the thickness ratio values of the specimens. The central streamline of the anterior canal is very similar in *Mammuthus columbi* (25.95 mm) and *Mammuthus primigenius* (26.22 mm). The average section radius of the anterior canal is however slightly higher in *Mammuthus columbi* (1.10 mm) than in *Mammuthus primigenius* (0.88 mm). Therefore, the thickness ratio of this canal is 4.24 in *M. columbi* and 3.28 in *M. primigenius*. The radii of curvature of the anterior canal are very similar in both species (5.71 in *M. columbi* and 5.80 in *M. primigenius*).

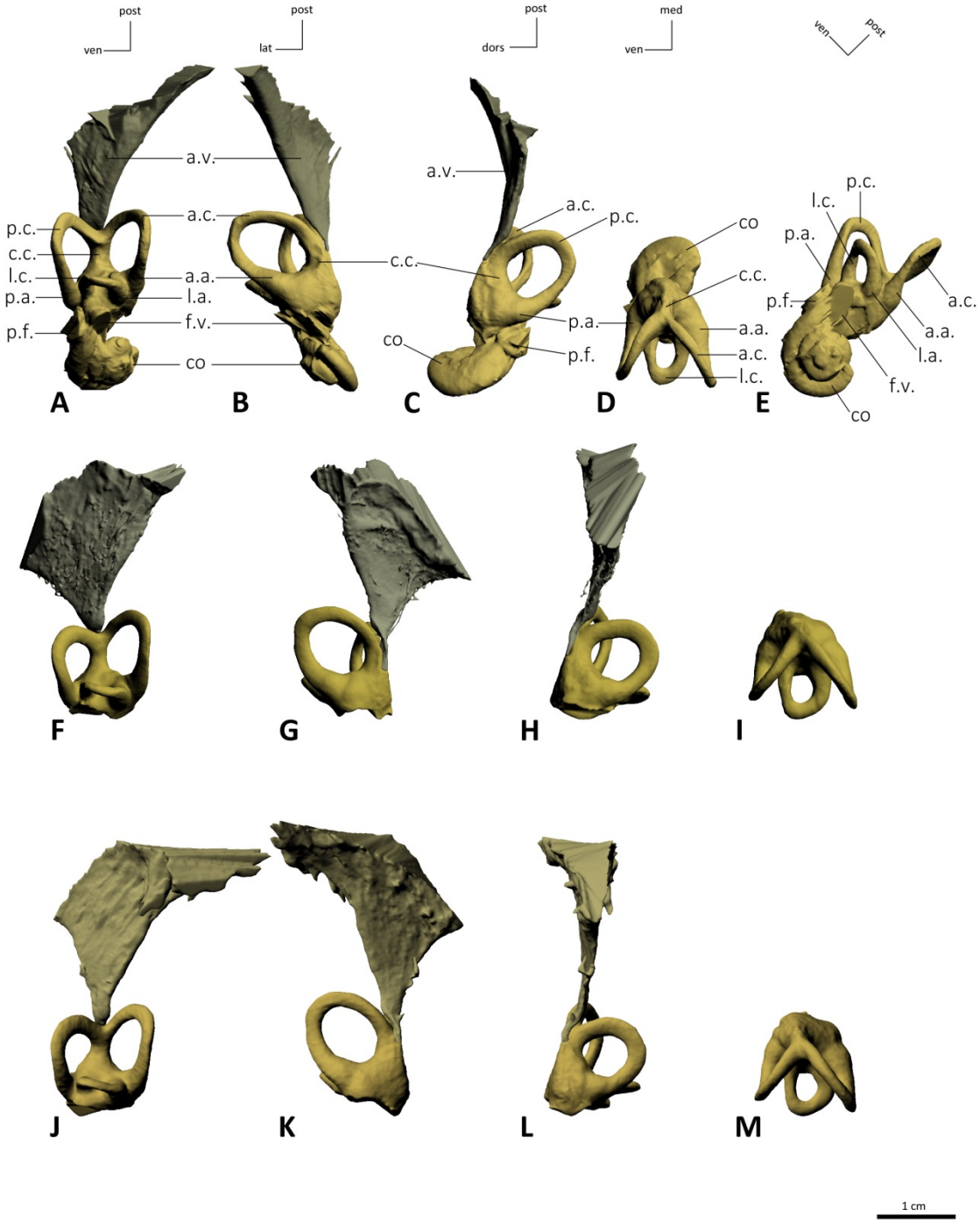

Figure III.35 : 3D reconstructed models of the bony labyrinths of *Mammuthus primigenius* MNHN.F.1904-12 (A-E) and *Mammuthus columbi* FM144658, right (F-I) and left (J-M, mirrored) in frontal (A,F,J), anterior canal (B,G,K), posterior canal (C,H,L), lateral canal (D,I,M) and cochlear (E) views. Legends: **a.a.** anterior ampulla, **a.c.** anterior semicircular canal, **a.v.** *aquaeductus vestibuli*, **c.c.** *crus commune*, **co** cochlea, **f.v.** *fenestra vestibuli*, **l.a.** lateral ampulla, **l.c.** lateral semicircular canal, **p.a.** posterior ampulla, **p.c.** posterior semicircular canal, **p.f.** perilymphatic foramen.

The posterior semicircular canal is round in both ears of *M. columbi* but oval in *M. primigenius*. The major axis of the canal forms an angle of 28° with the *crus commune* in *M. primigenius,* which is smaller than the anterior canal angle. The central streamline length of the posterior canal is 21.20 mm in *M. columbi* (right: 21.09 mm, left: 21.30 mm) and 25.25 mm in *M. primigenius*. While the value is very similar to that of the anterior canal in *M. primigenius*, there is a difference of almost 5 mm in *M. columbi*. The average section radius of the posterior canal is slightly higher than the anterior one (1.20 mm in *M. columbi* and 1.01 mm in *M. primigenius*). The values for the posterior thickness ratio are higher in *M. columbi* (5.65) than in *M. primigenius* (3.99) which means that the posterior canal is thicker in *M. columbi*. Compared to the anterior canal, the posterior canal is thicker in both specimens. The radius of curvature of the posterior canal is 4.84 in *M. columbi* (same value in both ears) and 5.53 in *M. primigenius*.

The lateral semicircular canal is oval in *M. columbi* and *M. primigenius*. The length of the central streamline of the lateral canal is slightly shorter in *M. primigenius* (19.74 mm) than in *M. columbi* (21.33 mm). Compared to the other semicircular canals, the lateral canal is clearly the shortest in *M. primigenius* but it is approximately as long as the posterior canal in *M. columbi*. Both specimens have a similar value of the average section radius for the lateral canal (0.99 mm in *M. columbi* and 0.93 mm in *M. primigenius*). In both specimens, the thickness ratio of this canal is more or less similar (4.65 in *M. columbi* and 4.69 in *M. primigenius*). Hence, the lateral canal is the thickest in *M. primigenius* while it is the posterior canal in *M. columbi*. The radius of curvature of the lateral canal is 3.12 in *M. columbi* (right: 3.08, left: 3.16) and 2.92 in *M. primigenius* which is similar.

Comparison of the angle values of canals between the left and right inner ears of the same specimen of *M. columbi* shows a small variability. There is a difference of 2.8° in the value of the angle between the anterior and lateral canals (71.9° in the right ear and 74.7° in the left ear). There is a difference of more than 4° in the value of the angle between the posterior and lateral canals (89° in the right ear and 85.4° in the left ear). In contrast, the values for the angle between the anterior and posterior canals are very similar (77.5° for the right ear and 75.7° for the left ear). Compared to *M. columbi*,

M. primigenius display similar values for the angle between the posterior and lateral canals (88.0°) and for the angle between the anterior and lateral canals (71.4°). However, the angle between the anterior and posterior canals is clearly lower in *M. primigenius* (68.6°) than in *M. columbi*. Finally, the angle with the highest value is the angle between the posterior and lateral canals in both specimens. Comparison of the radii of curvature shows that the lateral canal is always clearly smaller (2.92 in *M. primigenius* and 3.12 in average in *M. columbi*) than the anterior and posterior canals. The smaller size of the lateral canal is well distinct on the reconstruction. Moreover the anterior canal is always the largest canal; this is a feature more pronounced in *M. columbi* than in *M. primigenius*. Indeed, the anterior canal apex is located higher than the posterior one in both specimens, but it is more pronounced in *M. columbi*. In general, the semicircular canals of *M. columbi* are slightly thicker (average thickness ratio = 4.85) than those of *M. primigenius* (average thickness ratio = 3.99). The semicircular canals of *Mammuthus* are thick in general compared to other proboscideans (and other mammals). In cross-section, the canals are flattened. The slender part of the lateral canal enters the vestibule at a low position, which seems to be generalized among Elephantidae. There is no fusion between the lateral and posterior canals. The labyrinths of *M. columbi* do not display any ridge on their canals, while each canal of *M*. *primigenius* displays one (the lateral one being very shallow). In both species, all three semicircular canals display an undulation.

Cochlear bony labyrinth (Fig III.35)

The cochlear part of the petrosal is not preserved in both ears of the *Mammuthus columbi* specimen studied. However, it is fully preserved in the specimen of *Mammuthus primigenius* (MNHN.F.1904-12). The cochlea displays 2.25 turns (810°) and a length of almost 68 mm. In ventral view, the modiolus is completely overlapped by the apical turn and there is no visible gap. The basal turn of the cochlea is only partially overlapped by the apical turn and is still visible in ventral view. The *lamina secundaria* is absent. The cochlear volume (480 mm^3) represents around 42% of the total volume of the bony labyrinth. The cochlea is planispiral in profile view but a little less than extant elephants as its cochlear aspect ratio (0.46) is higher than any *Loxodonta* and *Elephas* specimens.

3.2.12. *Palaeoloxodon antiquus*

Since the cochlear part of the petrosal is missing on the scanned *Palaeoloxodon* specimen, the cochlear part of the bony labyrinth could not be segmented, therefore the total volume of the bony labyrinth is unknown.

Petrosal (Fig III.37)

The petrosal of *Palaeoloxodon* is very similar to the other Elephantidae petrosals (*Elephas, Mammuthus, Loxodonta*). In cerebellar view, the opening for the vestibular aqueduct has the shape of a very long fissure located in the posteromedial part of the petrosal. As in the *Loxodonta* specimen MNHN.AC.ZM.1861-53 and *Cuvieronius*, the surface surrounding the exit of the vestibular aqueduct is wide. There is no trace of a marked subarcuate fossa but the area surrounding the aqueduct is slightly concave. The *crista partis petrosa* is rather blunt and clearly less sharp than in *Gomphotherium angustidens*. The internal auditory meatus is broken but it is oriented antero-posteriorly as in the other elephantimorphs. The epitympanic wing (if present in life) is broken. In cerebral view, the *tegmen tympani* is broken in its anterior part. The groove for the middle meningeal artery is present but it is shallower and relatively smaller than in extant elephants. In tympanic view, the *promontorium* is completely broken. Hence the cochlea, the internal auditory meatus, the *fenestra vestibuli*, the perilymphatic foramen and the *crista interfenestralis* are not preserved at all in the studied specimen. The *aquaeductus Fallopii* is present and has the same orientation than in extant elephants. However, the thin bony roof covering this canal is broken, giving the structure the aspect of a sulcus. The *pars mastoidea* is partially preserved as well as the stylomastoid canal. However, the tympanohyal is completely broken as well as the pneumatic cavities contained in the *pars mastoidea*.

Vestibular bony labyrinth (Fig III.36)

Ampullae

The ampullae of *Palaeoloxodon* appear poorly defined. The posterior ampulla displays no ridge but there is some relief on the other two ampullae. The lateral ampulla carries a ridge along with a big bump. The ridge extends on the vestibule. A rather shallow ridge extends from the anterior ampulla to the vestibule. Both ridges (lateral and anterior) seem to converge and join at the base of the *crus commune*.

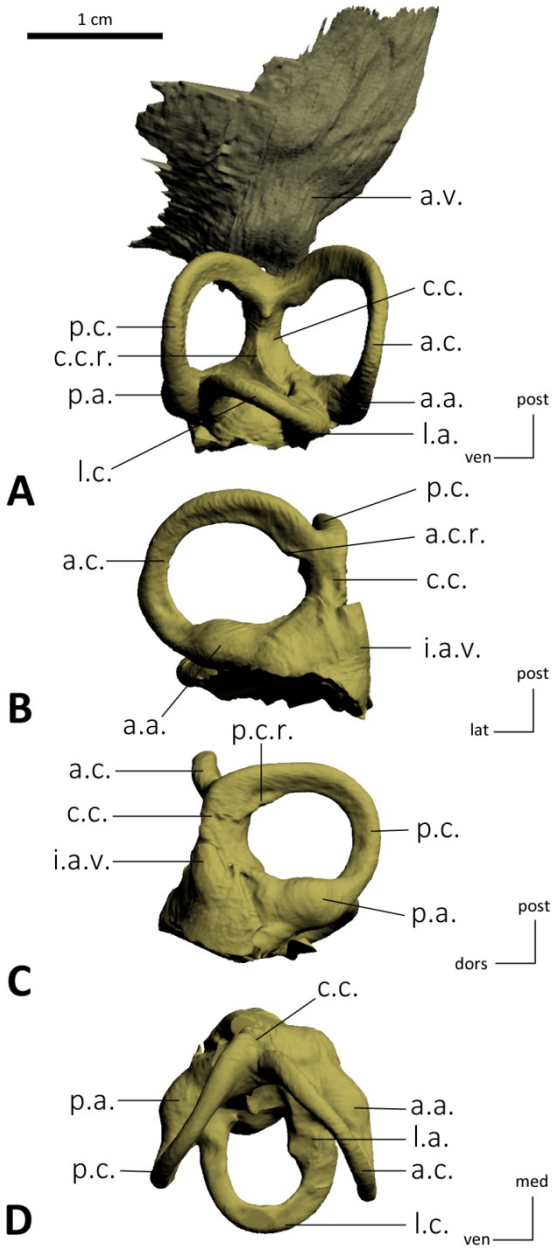

Figure III.36 : 3D reconstructed models of the left bony labyrinth of *Palaeoloxodon antiquus* M82706 (mirrored) in frontal (A), anterior canal (B), posterior canal (C) and lateral canal (D) views. Legends: **a.a.** anterior ampulla, **a.c.** anterior semicircular canal, **a.c.r.** anterior canal ridge, **a.v.** *aquaeductus vestibuli*, **c.c.** *crus commune*, **c.c.r.** *crus commune* ridge, **i.a.v.** insertion of the *aquaeductus vestibuli*, **l.a.** lateral ampulla, **l.c.** lateral semicircular canal, **p.a.** posterior ampulla, **p.c.** posterior semicircular canal, **p.c.r.** posterior canal ridge.

Crus commune

The *crus commune* is quite stocky and displays a slight basal thickening. A sharp ridge runs vertically across the *crus commune*. There is a big bulge at the beginning of the ridge located slightly under the meeting point of the anterior and posterior canals. The ridge extends from this bulge to the base of the lateral ampulla with a marked peaked structure at the level of the *crus commune* base. The ridge on the *crus commune* of *Palaeoloxodon* is probably the most prominent among proboscideans. The average section radius of the *crus commune* of *Palaeoloxodon* is 1.41 mm and its length 6.35 mm. Therefore *Palaeoloxodon* has a *crus commune* with a thickness ratio of 22.24. The anterior and posterior semicircular canals meet quite high (at least 75% of the height of the anterior canal). The *crus commune* is not inclined in the studied specimen.

Semicircular canals

The anterior semicircular canal is oval. Its major axis forms an angle of 87° with the *crus commune*. The central streamline length of the anterior canal is 26.23 mm and the average section radius is 0.92 mm. Therefore, the thickness ratio of this canal is 3.51. Its radius of curvature is 5.87.

The posterior semicircular canal is quite round. The central streamline length of the posterior is markedly shorter than for the anterior canal (22.24 mm). The average section radius of the posterior canal is in contrast very similar to the anterior one (0.93 mm). Hence the thickness ratio of the posterior canal (4.18) is higher than the ratio of the anterior canal (3.50). This difference of thickness between the two canals is hardly visible on the reconstruction. The radius of curvature of the posterior canal is 5.14.

The lateral semicircular canal is oval but definitely rounder than the anterior canal. The central streamline length of the lateral canal (27.20 mm) is higher than the posterior canal but lower than for the anterior canal. The average section radius of the lateral canal is very similar to that of the other canals (0.91 mm). The thickness ratio is similar (3.78) to that of the other canals. The radius of curvature of the lateral canal is 3.93.

The highest angle between canals in *Palaeoloxodon* is between the lateral and posterior canals (92.6°). The angle between the anterior and lateral canals and the angle between the anterior and posterior canals are roughly the same and more acute than the previous angle (respectively 77.1° and 76.2°). In terms of radii of curvature, the lateral canal is clearly smaller (3.93) than the anterior and posterior canals (respectively 5.87 and 5.14). The greater canal is the anterior canal which is elongated horizontally (the major axis of the canal and the *crus commune* are almost right-angled with a value of 87°). The smaller size of the lateral canal is distinct on the reconstruction. The anterior canal apex is located slightly higher than the posterior canal apex. In *Palaeoloxodon*, the thickness of the semicircular canals is medium to large, with an average thickness ratio of 3.82. The canals are flattened in cross-section. The slender part of the lateral canal connects with the vestibule in a somewhat low position, as for other Elephantidae, near the location where the posterior ampulla becomes the slender part of the posterior canal. There is no fusion between the lateral and posterior canals. The anterior canal displays two ridges: one following the inner trajectory of the canal from the *crus commune* and the other at the level of the meeting point with the posterior canal. The lateral and posterior canals display only a ridge following the inner trajectory of the canal from the *crus commune*. Each canal is undulated but the anterior one displays a particularly marked undulation.

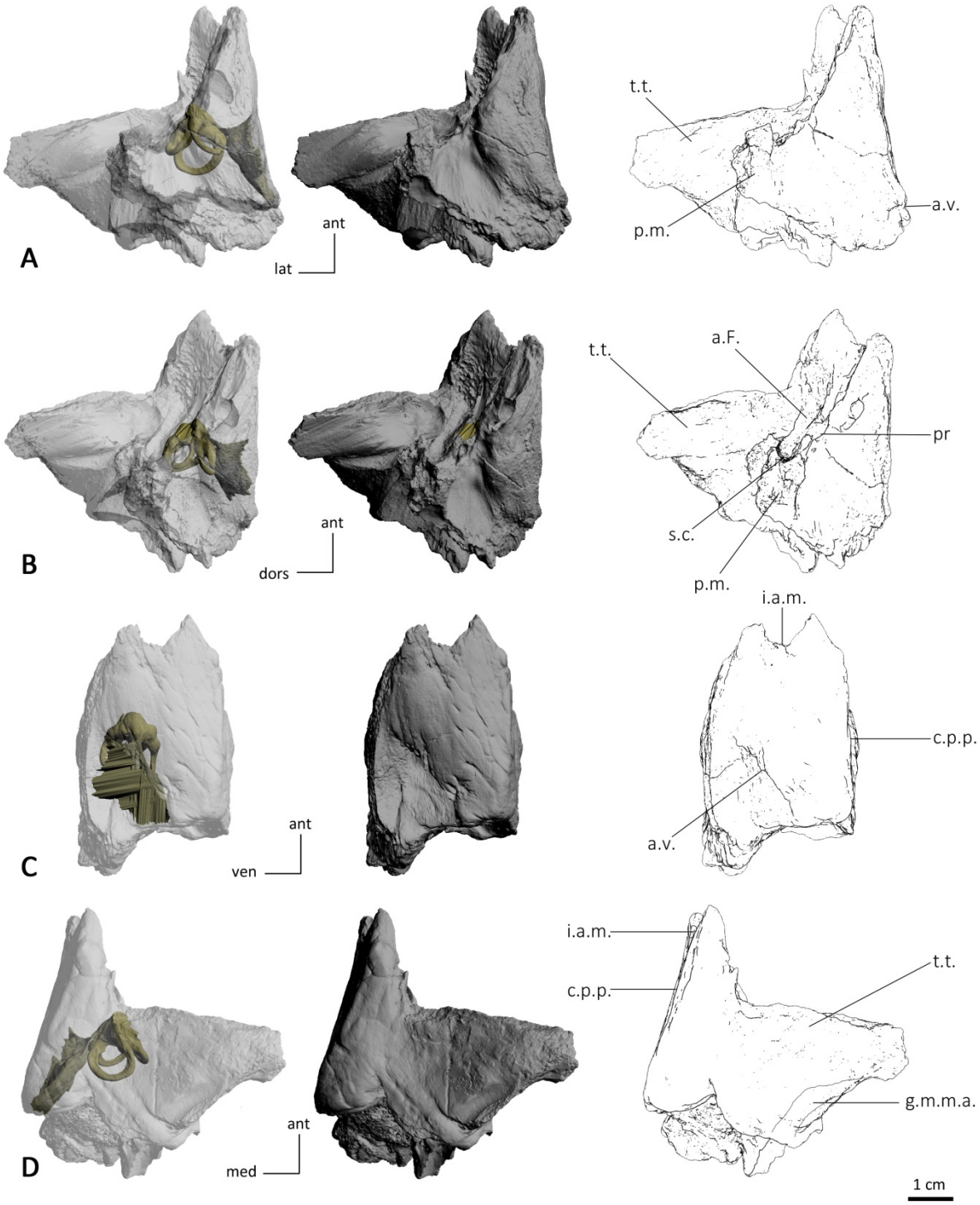

Figure 37 : 3D reconstructed models of the left petrosal of *Palaeoloxodon antiquus* M82706 (mirrored) in medial (A), tympanic (B), cerebellar (C) and cerebral (D) views. Legends: **a.F.** *aquaeductus Fallopii*, **a.v.** *aquaeductus vestibuli*, **c.p.p.** *crista partis petrosa*, **g.m.m.a.** groove for the middle meningeal artery, **i.a.m.** internal auditory meatus (broken), **p.m.** *pars mastoidea* (broken), **pr** *promontorium* (broken), **s.c.** stylomastoid canal, **t.t.** *tegmen tympani* (broken)

4. Comparisons

Comparative charts in different views are given in Appendices 5-10.

4.1. Petrosal

Subarcuate fossa

The subarcuate fossa is a depression that holds a paraflocculus lobe of the cerebellum in life. Its depth and even its presence is variable among mammals. The fossa is very deep in non-placental eutherian mammals such as the zhelestidae *Kulbeckia* (Ekdale et al. 2004). It seems to be the general condition of mammals. The early afrotherian *Ocepeia* exhibits a very deep and conical subarcuate fossa (Gheerbrant et al. 2014). In proboscideans, the early *Eritherium* displays a very deep fossa as well but its shape is somewhat different from that of *Ocepeia* as it is more spherical. *Phosphatherium*, on the other hand, exhibits a shallow fossa. *Moeritherium* and later proboscideans have completely lost the subarcuate fossa. A shallow depression might be retained in some proboscidean taxa such as *Moeritherium* (Court, 1994) but the region that usually holds the fossa is sometimes slightly convex (*Mammut, Stegomastodon, Anancus, Loxodonta*). The reduction and/or loss of the subarcuate fossa is by far not restricted to the proboscideans. The early embrithopod (PM53) displays a shallow subarcuate fossa while the fossa is absent in *Arsinoitherium*. The fossa is also absent in extant sirenians and *Prorastomus* (Benoit et al. 2013a). Most hyracoids such as *Procavia, Seggeurius, Titanohyrax, Microhyrax, Heterohyra, Dendrohyrax and Helioseus*) retain the subarcuate fossa, although it is shallow.

Internal auditory meatus

The internal auditory meatus is a structure that houses the *foramen acusticum superius* (cranial nerve VII) and the *foramen acusticum inferius* (cranial nerve VIII). While the meatus is oriented dorsomedially in other mammals, it opens anteriorly in all examined elephantimorphs. By contrast, early proboscideans such as *Eritherium, Phosphatherium, Numidotherium* and *Moeritherium* exhibit a dorsomedially oriented meatus. The structure is broken in *Prodeinotherium bavaricum* but given the morphology of the petrosal, the meatus was certainly oriented antero-posteriorly as in modern proboscideans.

Tegmen tympani

In *Ocepeia daouiensis* (Gheerbrant et al. 2014) and *Eritherium azzouzorum* (chapter I, Schmitt & Gheerbrant, 2016), the *tegmen tympani* exhibits a very similar structure. It is more or less kidney-shaped and highly inflated. The anterior part of the *tegmen tympani* is perforated by a large bony canal that most probably corresponds to the passage of the *ramus superior* for the stapedial artery. Among the outgroups, the *tegmen tympani* is not developed (if present) in the unpublished Moroccan embrithopod PM53. In *Arsinoitherium*, it is inflated but it does not form a cerebral surface as in modern elephants (Court, 1990; Benoit et al. 2013b). The inflated *tegmen tympani* found in *Ocepeia daouiensis*, *Eritherium azzouzorum* and in several other afrotherian clades is probably an afrotherian plesiomorphy (chapter I, Schmitt & Gheerbrant, 2016). In *Phosphatherium escuilliei*, the *tegmen tympani* region was difficult to reconstruct due to the poor contrast of the microtomographic slices (chapter I, Schmitt & Gheerbrant, 2016). The *tegmen tympani* of *Numidotherium koholense* displays a different structure (Benoit et al. 2013b). It is quite inflated (but less than in *Eritherium* and *Ocepeia*) but it forms a flat surface dorsally (cerebral surface). The petrosal of *Prodeinotherium bavaricum* is similar. It is inflated, and more than in *Numidotherium*, but it forms a very large and flat cerebral surface; this results in a dorsal petrosal aspect similar to those of modern elephants, with two large surfaces, the cerebellar and cerebral surfaces. In *Mammut americanum*, the *tegmen tympani* is large, flat and not inflated, as in modern elephants. On its dorsal surface runs a deep groove for the middle meningeal artery. This *tegmen tympani* morphology is observed in all other studied elephantimorphs.

Stapedial ratio

The stapedial ratio of the *fenestra vestibuli* is a variable character in proboscideans. In *Anancus arvernensis*, for example, it varies between 1.6 and 1.8. In *Elephas maximus*, it varies between 1.52 and 1.83. In Ekdale (2011), the ratio varies between 1.4 and 2.1 within the elephantimorphs sample (57 isolated petrosals) found in Friesenhahn Cave. The variability is also observed in other afrotherian taxa. In Benoit et al. (2015), the stapedial ratio measured in *Orycteropus afer* varies between 1.28 and 1.80. In *Potamogale velox*, it varies

between 1.32 and 1.93. Additionally, the distribution of this character among our taxa sample does not allow us to clearly separate several morphological groups based on the stapedial ratio values (see Fig. III.38). Indeed, the values form a continuum which is more or less contained within the variation range observed in the Friesenhahn elephantimorphs. Therefore, we decided to exclude this character from the phylogenetic analysis.

Perilymphatic foramen

The paedomorphic retention of a unique perilymphatic foramen during ontogeny instead of a separated *fenestra cochleae* and cochlear canaliculus is a derived feature seen in extant elephants. Such a unique perilymphatic foramen is retained in *Moeritherium*, *Prodeinotherium* and every studied elephantimorphs. Among fossil proboscideans, only *Eritherium*, *Phosphatherium* and *Numidotherium* display separated fenestrae. The separated condition is plesiomorphic as it is shared by almost every mammals including non-placentals. However, the unique perilymphatic foramen is retained in several other lineages. In Embrithopoda, the massive *Arsinoitherium* displays a unique perilymphatic foramen (Court, 1990), but this character is impossible to observe in the early embrithopod PM53, as it is broken at the level of the vestibule.

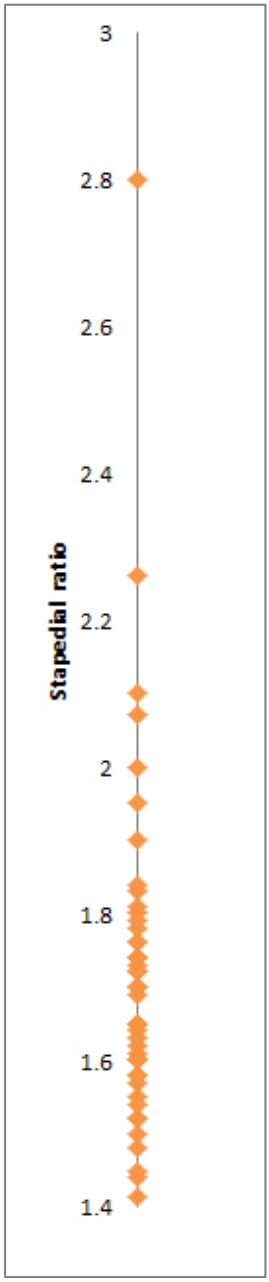

Figure III.38 : Distribution of the stapedial ratio values within proboscideans and some outgroups. Values are summarized in Appendix 11.

In Sirenia, the perilymphatic foramen is present only in extant genera (*Dugong, Trichechus*) but the foramen is separated in early sirenians such as *Prorastomus* and the specimen from Chambi (Benoit et al. 2013a). Finally, the unique perilymphatic foramen is also present in the gray whale *Eschrichtius robustus* (Geisler and Luo, 1996). As far as we know, no other mammal taxa than those cited here display this feature.

4.2. Inner ear

Definition of the ampullae

The ampulla of a semicircular canal is the usually inflated transition region that connects the slender part with the vestibule. In life, this is where the ampulla of the semicircular duct is located. This membranous structure holds many crucial structures for the detection of the angular accelerations such as the crista and the cupula. The bony ampulla consists of a bulging structure connected to the vestibule and to the slender part of the semicircular canal. The anterior and lateral ampullae are located close to each other while the posterior ampulla is generally close to point of entry of the slender part of the lateral canal into the vestibule. The definition of the ampullae (their identification from the slender part of the canal and the vestibule) is however variable. In embrithopods (*Arsinoitherium* and Embrithopoda PM53) the ampullae are well defined and bulbous. This is generally the case in all non-proboscidean placental taxa that we used for comparisons; *Ocepeia* (Gheerbrant et al. 2014), *Seggeurius* (Benoit et al. 2015), *Procavia*, *Prorastomus* and the sirenian from Chambi (Benoit et al. 2013a) and *Elephantulus*. In the earliest-known proboscideans (*Eritherium*, *Phosphatherium* and *Numidotherium*), the ampullae are well-defined as well. In contrast, the ampullae appear poorly defined in all the other studied proboscideans. The less defined bony ampullae house less defined membranous ampullae in *Elephas* CEB150009 (see chapter II). This suggests that the membranous ampullae of most proboscideans also display this condition. This character does not display intraspecific variability and is quite clear to define. Therefore it is included in our cladistic analysis.

Overall shape of the *crus commune*

The overall shape of the *crus commune* (slender or stockier) is rather variable. It seems to be always elongated and slender in non-proboscidean taxa that

were compared. It is also the case in non-Elephantida proboscideans (*Eritherium, Phosphatherium, Numidotherium, Moeritherium, Prodeinotherium, Mammut*). However, the *crus commune* is stocky in several Elephantida representatives (*Platybelodon*, *Mammuthus*, *Palaeoloxodon* and some specimens of *Elephas* and *Loxodonta*) while it is elongated in others (*Stegodon*, *Stegomastodon*, *Anancus* and some specimens of *Elephas* and *Loxodonta*). These two states of crus morphology could be significant phylogenetically; however the study of several specimens of extant elephants showed that this character is also variable at intra-generic and intra-specific levels. Hence, we decided not to include this character in the phylogenetic analysis performed in Chapter V.

Meeting point of the anterior and posterior canals

The height of the meeting point of the anterior and posterior canals is variable. It can be high (at the three quarters of the height of the anterior canal) or quite low (at about the mid-height of the anterior canal). A first hypothesis would be to assume that this is entirely linked to the *crus commune* overall shape character. It would be logical to assume that specimens with an elongated *crus commune* would display a quite high meeting point of the two canals (and vice versa). However, specimens that display an elongated crus do not necessarily display a high meeting point of the two canals. This is the case in *Anancus* (NMNHS.FM2991A) which displays a low meeting point. In contrast, specimens that display a stocky *crus commune* may display a high meeting point. This is the case in *Elephas* specimens MNHN.AC.ZM.1904-273 and MNHN.AC.ZM.1941-209, Loxodonta specimens MNHN.AC.ZM.1957-465 and MNHN.AC.ZM.1961-69 and *Palaeoloxodon*. This character is also variable intra-specifically as it varies among *Elephas*, *Loxodonta* and *Anancus* specimens. However, we included this character in our phylogenetic analysis to further test its significance.

Thickness ratio of the *crus commune*

The thickness ratio of the *crus commune* is based on two measurements given by the ARIADNE add-on using 3D landmarks (the average section radius of the *crus commune* and the length of the *crus commune*). Hence, it was possible to obtain this ratio only for specimens that

were segmented and landmarked in this work. The distribution of this ratio among our taxonomic sample is given in Fig III.39. We observe at least three groups: specimens with a ratio inferior to 15, specimens with ratios between 15 and 32 and specimens with ratios over 32. Evidently, this distribution is biased by the large proportion of proboscideans in our taxonomic sample and this does not represent what the distribution must be in mammals in general. However, studying the distribution of this ratio can be useful to compare proboscideans and some extra-groups in order to create new phylogenetic characters. The ratio is variable intra-specifically, especially for great values (it varies between 18.4 and 40.4 in Anancus for example). The third group with specimens with ratios over 32 is entirely composed of species for which we have several specimens. Hence, it does not seem pertinent to separate specimens with a ratio over 32 from the specimens with a ratio between 15 and 32. However, the distinction of specimens under and over ratio of 15 is interesting as it implies very few polymorphism (only *Gomphotherium* displays ratios ranging over and under 15). Early proboscideans such as *Eritherium, Phosphatherium* and *Numidotherium* display low ratios, i.e., a slender *crus commune*, while more recent proboscideans tends to display larger ratios. The two studied embrithopods *Arsinoitherium* and the unpublished Moroccan species (PM53) display low ratios as well. We further tested this character in our phylogenetic analysis (see chapter V).

Basal thickening of the *crus commune*

The basal thickening of the *crus commune* is a somewhat difficult character to study as it is quite variable and continuous. Most specimens display a slight basal thickening to no basal thickening at all. However, all *Gomphotherium* specimens studied display a characteristic form of basal thickening. The *crus commune* is extremely large at its basis and it progressively shrinks towards the meeting point of the anterior and posterior semicircular canals. The *crus commune* hence displays a characteristic pyramidal shape that was only observed in *Gomphotherium* specimens. In this regard, the pyramidal shape seems to be a good diagnostic character of *Gomphotherium*.

Inclination of the *crus commune*

In general, the *crus commune* is completely straight in mammals.

However, we identified several specimens displaying a rather inclined *crus commune*. The inclination is always towards the anterior semicircular canal in our sample.

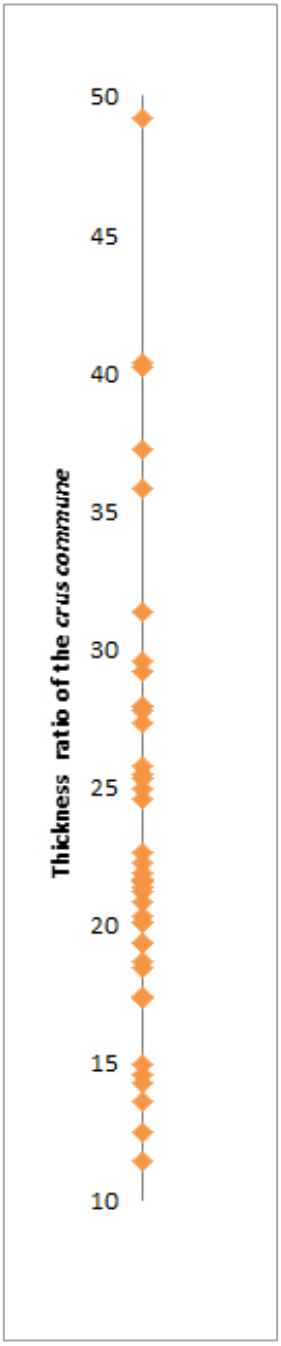

Figure III.39 : Distribution of the *crus commune* thickness ratio within proboscideans and some outgroups. Values are summarized in Appendix 12.

This contrasts with the posterior inclination seen in *Protungulatum* (Orliac & O'Leary, 2016). There is a slight inclination in the two ears of *Mammuthus columbi* and *Stegodon*, in the specimen referred to *Prodeinotherium* (MHNT.PAL.2013.01108E) and in a specimen of *Anancus* (NMNHS.FM2991A). Additionally, *Anancus* NMNHS.FM2991B displays a particularly marked inclination. The inclination does not seem to be caused by a taphonomic process as it is observed in both right and left ears in *Mammuthus columbi* and *Stegodon*. However, it seems to be variable inside the same species as it is not seen in some *Anancus* specimens.

Overall shape of the anterior canal

In early proboscideans such as *Eritherium*, *Phosphatherium* and *Numidotherium*, the anterior canal is quite round. It is oval in all other proboscideans, with the exception of one of the *Gomphotherium* specimens (CBar coll. V2). Regarding non-proboscidean taxa, the canal is very round in both studied embrithopods (*Arsinoitherium* and Embrithopoda PM53) and in both ears of the early afrotherian *Ocepeia*. It appears round as well in both *Prorastomus* and the sirenian from Chambi (Benoit et al. 2013a)

as well as in the fossil hyracoid *Seggeurius* (Benoit et al. 2016). However, it is oval in *Tenrec*. Even though there is some variability in *Gomphotherium*, the character seems quite constant intra-specifically. Therefore, it is be interesting to include this character in a cladistics analysis.

Overall shape of the posterior canal

The posterior canal is round in all our studied specimens of *Elephantidae* (*Elephas*, *Mammuthus*, *Palaeoloxodon* and *Loxodonta*), except for the specimen of *Mammuthus primigenius*. It is also round in *Platybelodon* and in the specimen referred to *Prodeinotherium* (MHNT.PAL.2013.01108E). It is round as well in the early proboscideans (*Eritherium*, *Phosphatherium* and *Numidotherium*) and in the early afrotherian *Ocepeia*. It is oval in all other proboscidean that we studied and in our sampled outgroups taxa, except for the unpublished Moroccan embrithopod. As for the anterior canal overall shape, this character does not seem to be subject to a strong intra-specific variability. However, the shape of this canal is different between the two *Mammuthus* species (oval in *M. primigenius* and round in *M. columbi*).

Overall shape of the lateral canal

As seen in chapter II, the overall shape of the lateral is more variable than for the other canals. Half the *Loxodonta cyclotis* specimens display a round canal while it is more oval in the other half. The character is also variable among *Elephas maximus* specimens. It is constant in *Anancus arvernensis*, but it show variations in other fossil species. In *Gomphotherium angustidens*, the canal is more oval in MNHN.F.SEP38 than in CBar coll V2. It is rounder in *Mammut americanum* specimen FM14293B than in FM14293A. In general, the lateral canal is oval in proboscideans at the exceptions of some *Elephas* and *Loxodonta* specimens, *Numidotherium* and *Stegodon* which display round canals. Given the intraspecific variability of the character, it is not included in our phylogenetic analysis.

Relative size of the canals

The radii of curvature of the semicircular canals are size-related characters. Larger mammals tend to display larger radii. Hence, it is not pertinent to discuss the radii separately among proboscideans. However, the discussion of the relative sizes of the

canals seems to be relevant. Comparison of the radii of curvature shows that the vertical canals (the anterior and posterior canals) always display similar values while the lateral canal is smaller. However, the relative size of the lateral canal compared to the other two is variable. We established a ratio to compare the relative size of the lateral canals among our specimens and other mammals: r = lateral radius/[(anterior radius + posterior radius)/2]*100. It gives the relative size of the lateral canal in percentage compared to the mean of the vertical canals radii. The distribution of this ratio is given in Fig. III.40. Given the distribution, we decided to separate specimens in three groups with three distinct states: those with a lateral canal approximately as large or larger than the vertical canals (ratio over 83%), those with an average size of the lateral canal (ratio between 72% and 83%) and those with relatively small lateral canals (ratio under 72%). The character is constant intra-specifically, except for *Elephas maximus* which shows specimens with average and small canals. Early proboscideans such as *Eritherium, Phosphatherium, Numidotherium* and *Prodeinotherium* display average lateral canals. All studied later proboscideans display relatively small lateral canals, with the exceptions of *Palaeoloxodon* and some *Elephas maximus* specimens (CEB150009 and MNHN.F.2008-81) that display average canals.

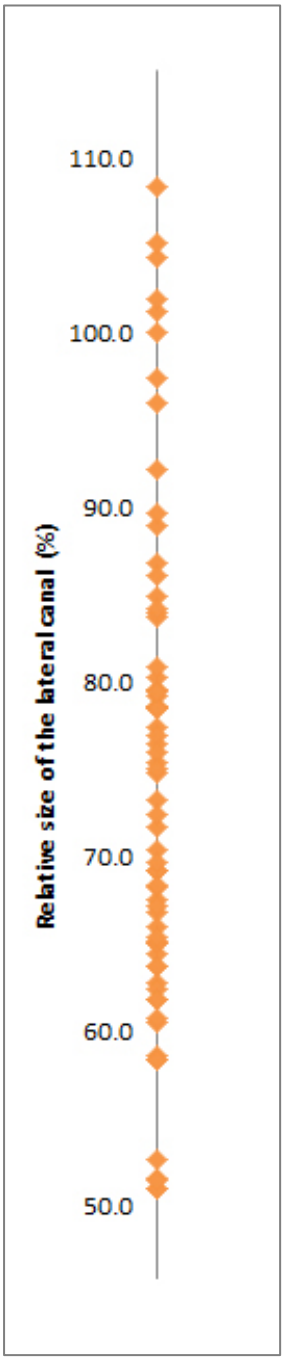

Figure III.40 : Distribution of the ratio measuring the relative size of the lateral canals compared to the mean of the vertical canals in percentage (based on radii of curvature values). Values are summarized in Appendix 13.

The elephantimorph described in Ekdale (2011) also displays a relatively small lateral canal. Both the two studied embrithopods (*Arsinoitherium* and PM53) display average canals, as well as *Ocepeia*. The sirenians (*Prorastomus*, *Dugong*, the sirenian from Chambi) display particularly large lateral canals, with the exception of *Trichechus* which displays more average canals. The character will be used in our phylogenetic analysis.

Apical extension of the anterior and posterior canals

The relative height of the apical part of the anterior and posterior semicircular canals varies among proboscideans. In the early representatives of the order (*Phosphatherium, Numidotherium, Moeritherium* and *Prodeinotherium*), the apexes of these two canals reach the same height. The apical part of these canals is not preserved in the single studied petrosal of *Eritherium*. In contrast, the anterior canal apex extends always higher than the posterior one in other later proboscidean taxa, except for *Stegomastodon*. The relative height of extension is variable, from slightly higher apexes (as in *Anancus* NMNHS.FM2991B for instance) to very much higher apexes (as in *Loxodonta* MNHN.AC.ZM.1957-465 or *Mammuthus columbi*).

Angles between the semicircular canals

The angles between the semicircular canals are not all pertinent to use for a phylogenetic analysis given our sample. First, the different angle values are variable among specimens of the same species. The angle between the anterior and posterior semicircular canals varies between 78.5° and 92.4° in *Anancus arvernensis* (variance: 31.33). In *Elephas maximus* and *Loxodonta cyclotis*, the range of variation of this angle is lower (respectively 6.83° and 15.28°). In *Anancus*, the variance for the angle between the anterior and lateral canals is lower (26.43), while it is greater in *Elephas maximus* (12.86) and *Loxodonta cyclotis* (24.36). Finally, the variance is small for the angle between the lateral and posterior canals in *Anancus* (11.7) and *Elephas* (5.25), while it is greater in *Loxodonta cyclotis* (31.15) with a difference of more than 13° between the same angle values in different specimens of the same species. The value itself is variable and it can be quite difficult to manage in a phylogenetic analysis. For instance, if we observe the distribution of

the angle values between the anterior and posterior canals among our specimens (Fig III.41), we can see that the values form a continuum with the exception of one particularly large angle in *Stegodon orientalis* (107.6°). It is very difficult to define the character states based on such a sample. There is a small gap around 89° but the *Anancus arvernensis* specimens exhibit values between 78.5° and 90.5°. Given the variability of these angle values, it is difficult and not pertinent to define in our sample a character "angle between the anterior and posterior canals". Concerning the angle between the anterior and lateral canals, the distribution is a little less continuous. The values between 58° and 59° form a distinct group but these include *Anancus* specimens that can also exhibit values up to 70.4°. There is another gap between values under 77.4° and values superior to 80°. In our sample, species with multiple specimens only display values inferior to 77.4°. The definition of a phylogenetic character with states separated by this gap can be interesting. Finally, the angle between the posterior and lateral canals does not seem pertinent to keep in our analysis. The variance is very strong in *Loxodonta cyclotis* (31.15). Moreover, the distribution is very narrow and continuous and the major part of the range of values of our sample is contained in the range of values of *Loxodonta cyclotis*.

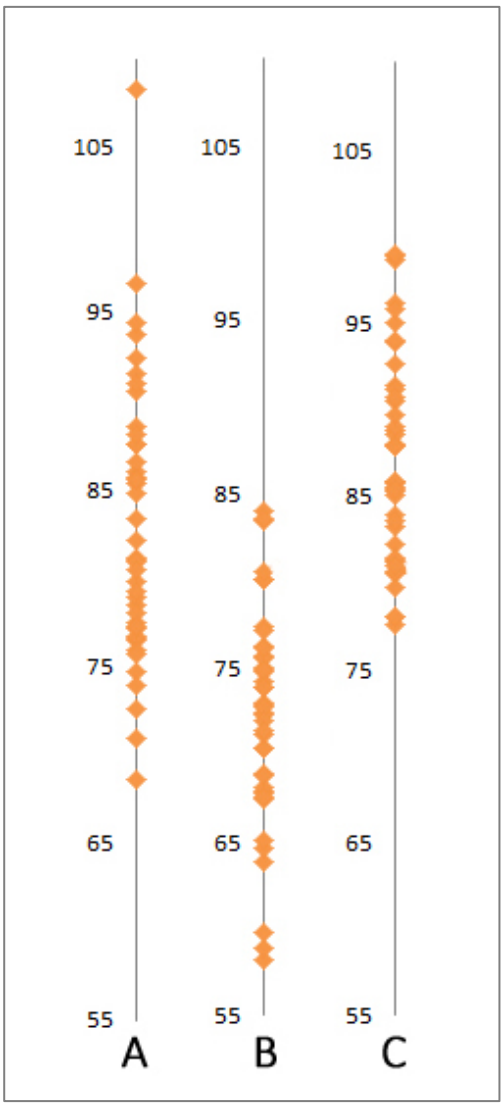

Figure III.41 : Distribution of the angles between the anterior and posterior (A), anterior and lateral (B) and posterior and lateral (C) semicircular canals among our sample. Values are summarized in Appendix 14.

Therefore, regarding the independent angle values, only the angle between the anterior and lateral semicircular canals seems to show significant interspecific variations that can be used as a

phylogenetic character. Other features concerning angles can be studied, for example the relative sizes of the angles. In most taxa, the most acute angle is between the anterior and lateral semicircular canals. There are a few exceptions. The smallest angle of one specimen of *Elephas maximus* (MNHN.AC.ZM.1904-273) is between the anterior and posterior canals. In *Loxodonta*, two specimens (MNHN.AC.ZM.1932-523 and 1957-465) display the same distribution as MNHN.AC.ZM.1904-273. Finally, the same is found in the specimen of *Mammuthus primigenius.* On the other hand, the most obtuse angle is generally between the posterior and lateral angles. However, this character is more variable. In *Anancus*, only half of the specimens display such distribution. Two specimens of *Loxodonta* (LoxodontaFred, MNHN.AC.ZM.1861-53) exhibit a greater angle between the anterior and posterior canals. The latter angle is the greatest in *Arsinoitherium, Eritherium, Stegodon, Ocepeia*, the rhincerotid Beon 98 E1 3049 and one specimen of *Mammut americanum* (FM14293-A).

Flattening of the canals

In most mammals, the cross-section of the semicircular canals is circular and the canals have a cylindrical shape. The early proboscideans (*Eritherium, Phosphatherium, Numidotherium*, *Moeritherium* and *Prodeinotherium*) display such canal morphologies. The same condition is found in *Ocepeia* and sirenians (Benoit et al. 2013a). However, all the other later proboscideans studied here display flattened semicircular canals. In addition, the same morphology was described by Benoit et al. (2013b) in the anterior and posterior canals of the embrithopod *Arsinoitherium*. However, the earlier Moroccan embrithopod PM53 does not display flattened canals.

General thickness of the canals

The semicircular canal thickness is variable among mammals and particularly among afrotherians and proboscideans. This feature can be assessed by the naked eye but we used a more quantitative approach by using the average thickness ratio. As explained in the Material and Methods section, this ratio is the mean of the thickness ratio of each semicircular canal. The individual value is calculated in as following: average section radius /

semicircular canal length * 100. The values of the global thickness ratio are given in Table III.2 (beginning of chapter III). The distribution of the global thickness ratio of the semicircular canals is given in Fig. III.42. Early proboscideans tend to display more slender semicircular canals than modern proboscideans. *Eritherium* exhibits the most slender semicircular canals (ratio of 1.08). *Phosphatherium* and *Numidotherium* canals are slightly thicker (respectively 2.24 and 2.16) but still relatively slender compared to modern proboscideans. The value is not available for *Moeritherium*. The specimen referred to *Prodeinotherium* exhibits thicker canals (2.82) but they are still less thick than modern proboscideans. Elephantimorphs always display ratios over 3.00 and up to 4.86 with one exception being a specimen of *Loxodonta* (MNHN.AC.ZM.1956-194) with a ratio of 2.74. It appears that the semicircular canals of proboscideans are primitively slender. They tend to become progressively thicker in modern taxa. The group that includes the most recent common ancestor of *Prodeinotherium* and elephantimorphs contains only taxa with a ratio over 2.7. Some extant specimens display ratios up to 4.86 (ElephasMemb). There is some intraspecific variability among *Anancus, Loxodonta* and *Elephas* specimens. The *Loxodonta* specimens display the greater variance (0.40) but the specimens compared are not all from the same species. Within *Loxodonta cyclotis* specimens, the variance is even greater (0.70).

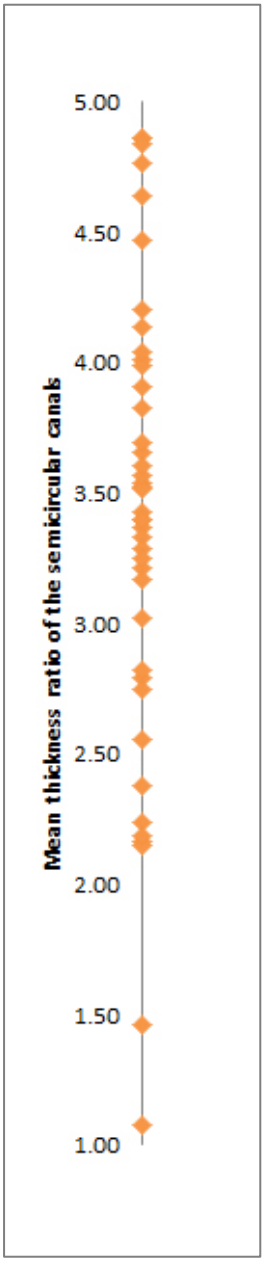

Figure III.42 : Distribution of the global thickness ratio of the semicircular canals among proboscideans and some outgroups. Values are summarized in Appendix 15.

The variance is smaller in *Elephas maximus* (0.35) and even smaller in *Anancus* specimens (0.24). However, such values are to be taken with caution because of our very small sample. Concerning the outgroups, the earliest known afrotherian *Ocepeia daouiensis* exhibits a small ratio (therefore slender semicircular canals) which is close to the ratios of *Numidotherium* and *Phosphatherium* (2.15). The early sirenian from Chambi displays slender canals as well (2.18). In embrithopods, the unpublished early specimen has very thin canals (1.46) while *Arsinoitherium* displays canals as thick as modern elephants (3.42). *Elephantulus* is in the middle range (2.79). This character seems interesting to keep for our phylogenetic analysis. Placing the states limit at 3 seems to discriminate well early proboscideans from elephantimorphs. Moreover, except for one *Loxodonta* specimen that displays a ratio of 3.02 (MNHN.AC.ZM.1932-523), there is a considerable gap in the distributions of the ratio between values under 2.82 and values over 3.21.

Insertion point of the lateral canal into the vestibule

The point of entry of the lateral canal into the vestibule is not subject to intraspecific variability. It is strictly constant in specimens belonging to the same genus or species. In the early afrotherian *Ocepeia*, it enters the vestibule at a quite high position and close to the posterior ampulla. This condition is found in the early sirenians *Prorastomus* and the sirenian from Chambi as well. Moreover, the early proboscideans *Eritherium*, *Phosphatherium*, *Numidotherium* and *Prodeinotherium* share the same morphology. In *Cuvieronius*, *Gomphotherium*, *Mammut*, *Stegodon, Anancus* and the specimen referred to *Prodeinotherium* (MHNT.PAL.2013.01108E), the lateral canal enters the vestibule at a high position as well, but the point of entry is distant from the posterior ampulla. In all the specimens of *Loxodonta*, *Elephas*, *Mammuthus* and *Palaeoloxodon*, the lateral canal enters the vestibule quite low. Given its regularity among specimens of the same species and its easily defined states, this character is interesting for a phylogenetic analysis.

Fusion of the lateral and posterior canals

When close to each other, the lateral and posterior bony semicircular canals can be fully or partially fused. The total fusion is often called *crus commune*

secundaria or secondary common crus in the literature. We find the term to be confusing because this structure differs from the "primary" *crus commune* (between the anterior and posterior canals). While the membranous ducts of the anterior and posterior canals are fused within the *crus commune*, the membranous ducts of the posterior and lateral canals are never fused at the level of the *crus commune secundaria* (Gray, 1907, 1908; David, 2011). The first *crus commune* observed in the bony labyrinth is linked to a functional feature which is the presence of the membranous *crus commune* between the anterior and posterior membranous ducts. However, the *crus commune secundaria* is merely an ossification artefact linked to the location of the lateral canal relative to the posterior canal. In early proboscideans such as *Eritherium*, *Phosphatherium* and *Numidotherium*, both the ampulla and the slender part of the posterior canal are in contact with the lateral canal. In *Eritherium*, only a small part of the posterior bony slender canal is fused with the lateral while large parts of the slender canals are fused in *Phosphatherium* and *Numidotherium* forming what is usually called the *crus commune secundaria*. The morphology observed in *Eritherium* can also be found in some specimens of *Elephas* (MNHN.AC.ZM.1904-273 and 2008-81) and *Loxodonta* (MNHN.AC.ZM.2008-71). The lateral bony canal is fused with the posterior ampulla only in our embrithopods sample (Embrithopoda PM53 and *Arsinoitherium*), in *Mammut, Ocepeia, Palaeoloxodon, Platybelodon, Prorastomus* and some specimens of *Loxodonta* (MNHN.AC.ZM.1961-69 for instance). The lateral canal is completely independent from the posterior canal in *Anancus, Cuvieronius, Gomphotherium,* some *Loxodonta* specimens, *Procavia, Prodeinotherium, Stegodon* and *Tenrec*.

Number of turns of the cochlea

Most proboscideans display a cochlea with a least two full turns. The notable exceptions are *Numidotherium* (1.5 or 1.62 depending on the specimen) and the right ear of *Loxodonta* specimen MNHN.ZM.AC.2008-71 which displays 1.625 turns. However, as mentioned in chapter II, the number of turns is extremely variable intra-specifically. The difference can be up to one full turn between two different specimens of *Loxodonta* (from 1.625 turns to 2.625*)*. The number of turns of the cochlea can vary even within the same specimen:

MNHN.ZM.AC.2008-71 displays a left ear with two turns while its right ear displays 1.625 turns. Such as intraspecific variation seems to weaken the pertinence of this character for a phylogenetic analysis. The distribution of the number of turns of the cochlea among our taxa sample and other afrotherians (see Fig III.43) is indeed irrelevant to discriminate groups in this range. However, there is a clear separation between specimens with a very high level of coiling (more than 3.3 turns) and those with a lower level of coiling (less than 2.63 turns). This separation would allow us to maintain this character in our phylogenetic analysis while taking into account the intraspecific variability.

Relative volume of the cochlea

The relative volume of the cochlea has to been taken with caution because it depends on the protocol used to separate the cochlear canal from the vestibular part of the bony labyrinth. We used the protocol detailed in the main 'Material & Method' section of the thesis. However, according to the specimen, the separation of the cochlear part can be slightly different. Hence the given values for the relative cochlear volume are estimations. On the other hand, some values that we use for comparisons come from different authors which separation protocols might be different. In summary, it is possible to compare the relative volumes but only at a certain level of precision. Nevertheless, this value is not accessible for several specimens as many fossil proboscideans that we sampled do not preserve the cochlea.

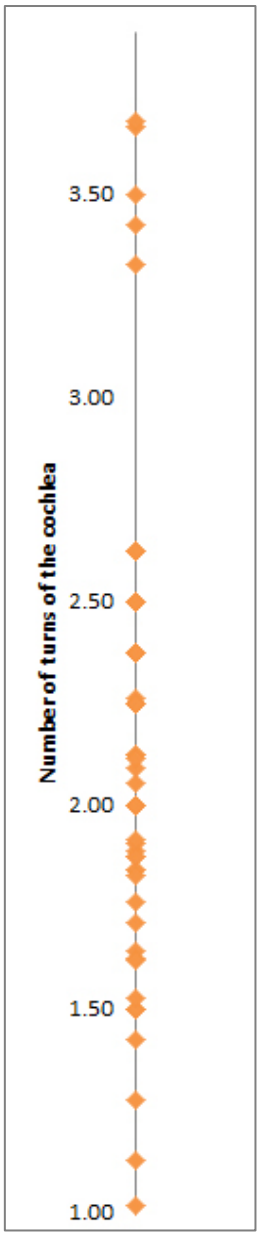

Figure III.43 : Distribution of the number of turns of the cochlea within proboscideans and some outgroups. Values are summarized in Appendix 16.

In the early afrotherian *Ocepeia*, the cochlea represents around two thirds of the total volume of the bony labyrinth. The value is similar in *Phosphatherium* (69%), but it is less voluminous in *Eritherium* (around 50%). *Numidotherium* displays a relatively smaller cochlea (42% in our study, 44% in the specimen described in Benoit et al. 2013b). Most of the other proboscideans display values around 50% (Fig III.44) but there are a few exceptions. *Platybelodon*, *Mammuthus primigenius* and two *Loxodonta cyclotis* specimens (MNHN.AC.ZM.1956-194 and MNHN.AC.ZM.1957-465) display smaller cochleae (respective relative volume of 43.7%, 42.5%, 39.5% and 43.4%). With the exception of *Phosphatherium*, the proboscideans do not display cochleae with a relative volume significantly greater than 50%.

Aspect ratio of the cochlea

The protocol used to calculate the aspect ratio of the cochlea is the same used in the literature. Therefore, our ratios are fully comparable with ratios obtained from different authors. The distribution of the ratios among our taxa sample and some outgroups (Fig. III.45) shows roughly two groups: those with a ratio inferior to 0.6 and those with a ratio superior to 0.6. Hence, the coding proposed in Benoit et al. (2013b) is pertinent and we will use this character with the same states in our phylogenetic analysis (chapter V). A cochlea with a high aspect ratio seems to be plesiomorphic among afrotherians. Ocepeia has a rather

high aspect ratio (0.72). However, the aspect ratio is low (always inferior to 0.6) in all studied proboscideans preserving the cochlea fully.

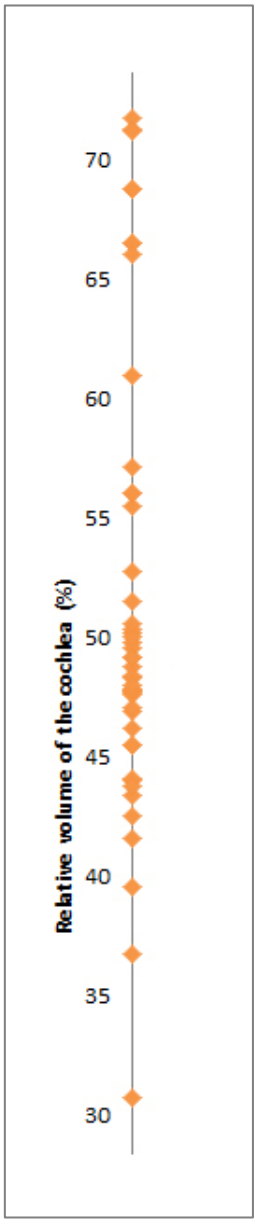

Figure III.44: Distribution of the relative volume of the cochlea within proboscideans (in %). Values are summarized in Appendix 17.

Apical lacuna

The presence of the apical lacuna is not a constant character. It is variable in *Loxodonta* as only one specimen displays one (CEB130168). A small apical lacuna is also seen in both ears of *Stegodon*, two *Numidotherium* specimens (UOK5 and the unlabeled specimens described in Benoit et al. (2013b) but not in the specimen described in Court, 1992), the specimen referred to *Prodeinotherium* (MHNT.PAL.2013.01108E) and one specimen of *Moeritherium* (68436). In *Ocepeia*, a small apical lacuna is present in both ears (Gheerbrant et al. 2014).

Lamina secundaria

The secondary bony lamina (or *lamina secundaria*) is a structure that excavates the external part of the cochlear canal. It marks the separation between the *scala tympani* and the *scala vestibuli*. It is present in the cochlea of most mammals, but it is absent in most of the proboscidean studied here. In fact, among proboscideans, only the early representatives such as *Eritherium*, *Phosphatherium* and *Numidotherium* display a secondary bony lamina. In *Phosphatherium*, it is extremely shallow and in *Numidotherium*, it has only been observed in the specimen described in Court, 1992. Its absence in UOK5 and in the unlabeled specimen segmented in Benoit et al. (2013b) can either be

explained by the poor resolution of the microtomographic slices in both studies or by an intraspecific variability of this character. The other proboscideans lack a *lamina secundaria*.

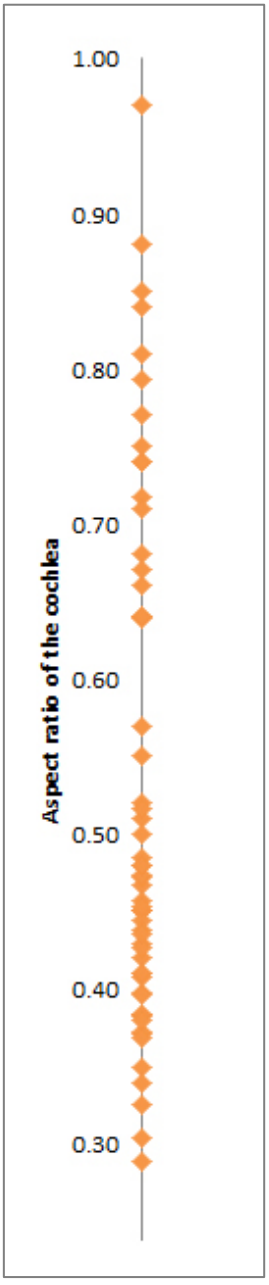

Figure III.45: Distribution of the cochlear aspect ratio within proboscideans and some outgroups. Values are summarized in Appendix 18.

This structure is also missing in extant and extinct sirenians such as the sirenian from Chambi and *Prorastomus* (Benoit et al. 2013a) and the extant species *Trichechus manatus* (Ekdale, 2013). It is present in the early afrotherian *Ocepeia* (Gheerbrant et al. 2014) and in the hyracoids *Seggeurius* and *Procavia* (Benoit et al. 2016). It is present in the unpublished Embrithopoda PM53, but it is absent in *Arsinoitherium*.

Vestibulo-cochlear angle

The protocol used to measure the vestibulo-cochlear angle comes from Benoit et al. (2013b). The angle between the *crus commune* and the plane defined by the first turn of the cochlea is measured. The distribution of this angle among our taxa sample and some outgroups (Fig. III.46) shows a gap between specimens with an acute or right angle (*Elephantulus*, *Tenrec*) and the other specimens. On the other hand, a smaller gap is visible between 140° and 144°, which allows defining a second (angle comprised between 90° and 142°) and third group (angle superior to 142°). This definition allows minimizing the polymorphism when this feature is used as a phylogenetic character. All specimens of *Anancus* and *Elephas* display an angle superior to 146° (see Appendix 19).

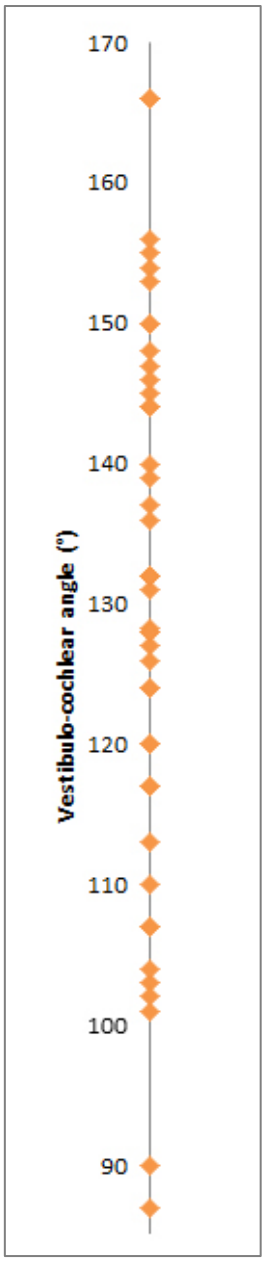

Figure III.46 : Distribution of the vestibulo-cochlear angle within proboscideans and some outgroups. Values are summarized in Appendix 19.

Mammut americanum exhibits a large angle as well (153°). While most *Loxodonta* specimens display a lower angle, the right ear of MNHN.AC.ZM.2008-71 and 1961-69 exhibit larger angles (144° and 145° respectively).

5. Conclusion

The observations confirm the presence of intra-specific variability of certain characters of the petrosal and the inner, already described in extant elephants in Chapter II. Almost the entire interspecific variation of the stapedial ratio of proboscideans is contained within the variation range of *Elephas*. The inclination of the *crus commune* varies within *Anancus arvernensis*. The shape of the lateral canal is also variable intra-specifically. The number of turns varies greatly in Loxodonta and the presence of an apical lacuna seems variable intra-specifically as well. In order to minimize polymorphisms within our data, we decided not to include such characters in the phylogenetic analysis performed in Chapter V.

Conversely, comparisons of the petrosal and inner ear of extinct and extant proboscideans and afrotherians confirm the importance of some characters. The subarcuate fossa depth seems rather constant intra-specifically but varies greatly within proboscideans and afrotherians. The *tegmen tympani* displays a characteristic shape in some taxa. The study of the perilymphatic foramen remains of great interest. Among others, the flattening of the canals, the relative volume and aspect ratio of the cochlea, the presence (or absence) of the *lamina secundaria* and the vestibulo-cochlear angle appear to be quite constant intra-specifically, but they vary within the Proboscidea and seem therefore interesting to include in the phylogenetic analysis.

On the other hand, some new characters are defined based on comparisons. The orientation of the internal auditory meatus (anterior or dorsal) is a striking feature that seems to have been neglected in previous comparisons. Investigations of the bony labyrinth of proboscideans allow observing new interesting features: the definition of the ampullae, the basal thickening of the *crus commune*, the apical extension of the anterior canal or the position of the lateral canal insertion into the vestibule with respect to the posterior ampulla. Some features are also reappraised using quantitative ratios: *crus commune* thickness ratio, relative size of the lateral canal and semicircular canal thickness ratio. These characters are to be included in a cladistic analysis to test the phylogenetic message that they carry.

CHAPTER IV

Geometric morphometrics study of the bony labyrinth of proboscideans and afrotherians using 3D semi-landmarks

1. Introduction

This chapter uses multivariate geometric morphometrics and 3D landmarks for the study of the distribution our sampled specimens within the morphospace. Morphologically similar specimens are gathered, while morphologically different specimens tend to be distant within the morphospace. The method also allows representing the morphological trend along the axes and it helps to identify those features of the bony labyrinth which define some group of specimens. This chapter IV investigates the morphological variability of the bony labyrinth of proboscideans, with three major questions:

1. Is it possible to discriminate the proboscideans from the other afrotherians based on the morphology of their bony labyrinth? If this is the case, what features characterize proboscideans?

2. Within the Proboscidea, is it possible to discriminate some main supported monophyletic groups such as the Elephantimorpha and the Elephantidae? If this is the case, what are the characteristics of those groups?

3. Among the extant elephants, is it possible to discriminate the bony labyrinth of the Asian elephants (*Elephas*) from that of the African elephants (*Loxodonta*)? If possible, what are the differences between the two genera?

Each of these questions corresponds to a different set of analyses in sections 3.1., 3.2., 3.3. from the 'Results' section. This study is also developed to help defining the different degrees of morphological resemblance within Proboscidea. These resemblances are helpful in formalizing new primary homologies in view of a phylogenetic analysis of the Proboscidea.

2. Material and methods

2.1. Taxa sample

In this chapter, we investigated the significance of the morphology at three distinct systematics levels, involving three distinct taxa samples: 1) analysis including specimens of afrotherians; 2) analysis restricted to proboscidean taxa; 3) analysis including only extant proboscideans. Although most of our specimens preserve the cochlea, there are several fossils in our taxa sample for which we do not have cochlear landmarks. In order to include these taxa in our study of the cochlea, we performed two analyses for each investigated question: one with cochlear landmarks and one without cochlear landmarks. Therefore, we conducted six different analyses:

- A1, analysis of the whole labyrinth including all afrotherian specimens preserving the cochlea;
- A2, analysis restricted to the semicircular canals and therefore including all afrotherian specimens;
- P1, analysis of the whole labyrinth of all proboscidean specimens that preserve the cochlea;
- P2, analysis restricted to the semicircular canals that includes all the proboscideans ;
- E1, analysis of the whole labyrinth of all extant elephants;
- E2, analysis restricted to the semicircular canals of extant elephants.

The composition of each data sample is summarized in Table IV.1.

Table IV.1 : Composition of the data sample of the different geometric morphometrics analyses conducted during this chapter

Taxa	A1	A2	P1	P2	E1	E2
Anancus arvernensis NMNHS.FM2991A	X	X	X	X		
Anancus arvernensis NMNHS.FM2991B		X		X		
Anancus arvernensis NMNHS.FM2991C		X		X		
Anancus arvernensis NMNHS.FM2991D	X	X	X	X		
Anancus arvernensis NMNHS.FM2991E	X	X	X	X		
Anancus arvernensis NMNHS.FM2991F	X	X	X	X		
Anancus arvernensis NMNHS.FM2991G		X		X		

Arsinoitherium zitteli BMNH 8800		X				
Chambi sirenian CBI-1-542	X	X				
Cuvieronius sp.		X		X		
Elephantulus sp.	X	X				
Elephas maximus MNHN.AC.ZM.1904-273	X	X	X	X	X	X
Elephas maximus MNHN.AC.ZM.1941-209	X	X	X	X	X	X
Elephas maximus MNHN.AC.ZM.2008-81	X	X	X	X	X	X
Elephas maximus	X	X	X	X	X	X
Embrithopoda PM53		X				
Eritherium azzouzorum PM88	X	X	X	X		
Gomphotherium angustidens CBar coll. V2	X	X	X	X		
Gomphotherium angustidens MNHN.F.SEP38	X	X	X	X		
Loxodonta africana MNHN.AC.ZM.1861-53	X	X	X	X	X	X
Loxodonta africana	X	X	X	X	X	X
Loxodonta cyclotis MNHN.AC.ZM.1950-728	X	X	X	X	X	X
Loxodonta cyclotis MNHN.AC.ZM.1956-194	X	X	X	X	X	X
Loxodonta cyclotis MNHN.AC.ZM.1957-465	X	X	X	X	X	X
Loxodonta cyclotis MNHN.AC.ZM.1961-69	X	X	X	X	X	X
Loxodonta sp. MNHN.AC.ZM.1932-523	X	X	X	X	X	X
Loxodonta sp. MNHN.AC.ZM.2008-71	X	X	X	X	X	X
Mammut americanum FM14293A	X	X	X	X		
Mammut americanum FM14293B		X		X		
Mammuthus primigenius MNHN.F.1904-12	X	X	X	X		
Mammuthus columbi FM144658 (left)		X		X		
Mammuthus columbi FM144658 (right)		X		X		
Numidotherium koholense UOK5	X	X	X	X		
Ocepeia daouiensis PM45	X	X				
Palaeoloxodon antiquus M82706		X		X		
Phosphatherium escuilliei PM17		X		X		
Platybelodon grangeri 26564 (824+)	X	X	X	X		
Procavia capensis	X	X				
Prodeinotherium bavaricum MHNT.PAL.2013.01108E		X		X		
Prorastomus sirenoides BMNH44897	X	X				
Stegodon orientalis FM18632	X	X	X	X		
Tenrec sp.	X	X				
Total	**30**	**42**	**24**	**34**	**12**	**12**

It should be noted that the systematic sampling is not fully homogeneous in our study. For instance, only a small part of our sample contains non-proboscidean afrotherians (8 specimens in total against 34 proboscideans). Some lineages of afrotherians are not sampled (Tubulidentata, Chrysochloridae) and we did not have time to include the extant members of Sirenia (only two fossil specimens are included in our sample). This study is preliminary and based on the data that were possible to get during the PhD thesis. We expect to extend the sampling and the study in the future.

2.2. Methods

Data preparation

The specimens were segmented using the same software (MIMICS innovation suite software Materialise®, releases 16 and 17) and same protocol. A manual segmentation (not using thresholds) was preferred to minimize the problems linked to differential segmentation. The raw 3D models of bony labyrinths were exported as it is, without smoothing or reduction. The specimens were then prepared in GEOMAGICS Studio 2012 following the same protocol for each 3D model (decimation, smoothing, spikes removal and repair). This allows minimizing the effect of differential smoothing that could introduce a bias in the analysis. Landmarks were then placed using AVIZO with the protocol described in the introduction of the thesis. This protocol was originally used in order to conduct functional inferences with the software ARIADNE (chapter VI) and it does not require having landmark sets that contain the same number of landmarks (for example, the cochlear set of landmarks can contain 48 landmarks in one specimen and 51 in another one). However, the software that we used to conduct the geometric morphometrics analyses (MORPHOTOOLS) requires equally composed landmark sets. Hence, we used the software MATHEMATICA to resample our landmark sets.

Analyses

The landmark sets were then analyzed with the interactive software package MORPHOTOOLS (Specht, 2007; Specht et al. 2007; Lebrun, 2008; Lebrun et al. 2010). First, we applied a sliding semilandmark algorithm given by the software until stable mean shape was obtained. This step allows removing information derived from the arbitrary spacing of semilandmarks along these curves (Billet et al. 2015, Gunz et al. 2012).

Procrustes superimposition is then performed on the landmarks set and we used principal component analysis (PCA) on Procrustes coordinates to analyze the shape variability of the bony labyrinth. Deformations of the bony labyrinth among the PC axes were visualized with MORPHOTOOLS. The PC scores were exported and we used the software R (R Development Core Team, 2008) to visualize the distribution of specimens within the morphospace.

Regressions

While the analyses presented in this chapter were performed on the bony labyrinth shape, which is supposedly free of size, size can still influence the results we get via allometry. To investigate allometry, phylogenetic generalized least squared regressions were performed between the three first PC scores of the first four analyses (A1, A2, P1 and P2) and the logarithm of body mass. To do so, we used estimates of the body mass found in the literature as well as a hypothetic phylogenetic tree representing the relationships between the taxa used in the geometric morphometrics analysis. Details are given in Appendix 20 and 21. Phylogenetic regressions were used to account for the non-independency of the data, arising from the shared evolutionary history of the species. The topology of this tree, as well as the divergence dates mainly come from Tassy (pers. comm. 2016). Regressions were not performed for analyses E1 and E2 (extant elephants), because of the lack of species.

3. Results

3.1. Analysis of the Afrotheria

3.1.1. Analysis A1 of the whole labyrinth

The results of the PCA performed on the whole labyrinth are given in Fig IV.4. The first three axes of the PCA explain 67.8% (PC1: 31.8%, PC2: 23.5%, PC3: 12.5%) of the total variation of the labyrinth morphology.

Deformations

PC1 (31.8%)

The deformations of the bony labyrinth along the first axis (PC1 which explains 31.8% of the total variation) are given in Fig IV.1 in several views.

Towards negative values, the angle between the cochlea and the lateral canal tends to be more acute (Fig IV.1A). The cochlea is smaller with less turns. The anterior canal tends to be rounder. The lateral canal tends to be larger and rounder. It expands towards the posterior canal and the utricular end of the slender lateral canal is located higher with respect to the posterior ampulla. The angle between the anterior and posterior canals and the angle between the posterior and lateral canals tend to be more obtuse.

Towards positive values, the angle between the cochlea and the lateral canal is a little more obtuse. The cochlea tends to be larger, with a second turn more developed. The anterior canal tends to be more oval while the lateral canal tends to be smaller and more oval. The angle between the anterior and posterior canals and the angle between the posterior and lateral canals tend to be more acute.

PC2 (23.5%)

The deformations of the bony labyrinth along the second axis (PC2 which explains 23.5% of the total variation) are given in Fig IV.2 in several views.

Towards the negative values, the three semicircular canals show a more oval shape. The angle between the anterior and posterior canals tends to be more acute. The cochlea displays less turns and is more tightly coiled.

Conversely, the three semicircular canals tend to display a rounder shape towards positive values. The angle between the anterior and posterior canals is more obtuse and the cochlea displays a larger number of turns and is less tightly coiled.

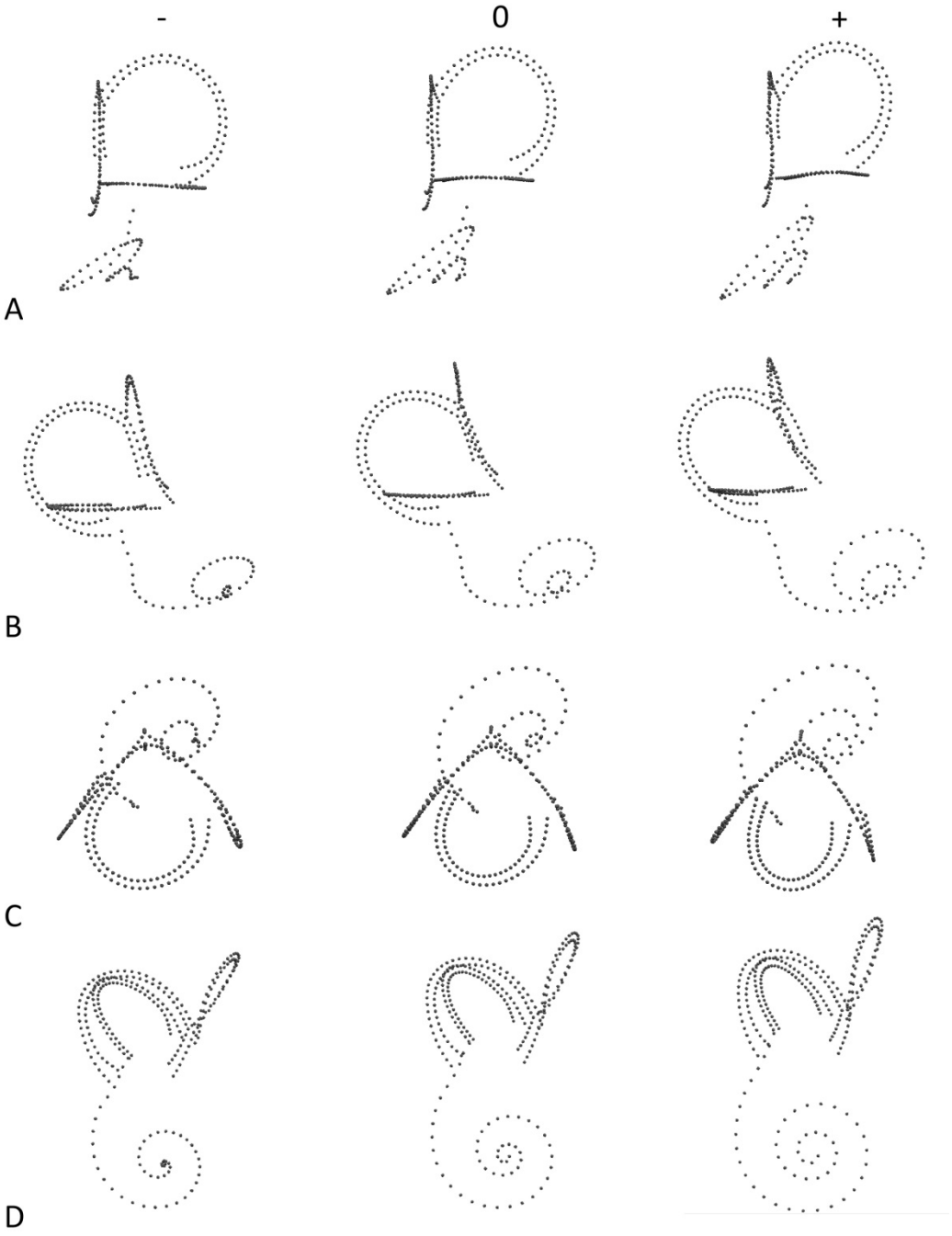

Figure IV.1 : Deformations along the first axis of the analysis (PC1, 31.8%) conducted on the whole labyrinth of Afrotheria (A1) in the view showing the plane of the anterior (A), posterior (B) and lateral (C) canals and the cochlea (D). "-" represents the extreme shape towards the negative extremity of the axis, "+" the extreme shape towards the positive extremity of the axis and "0" the mean shape on this axis.

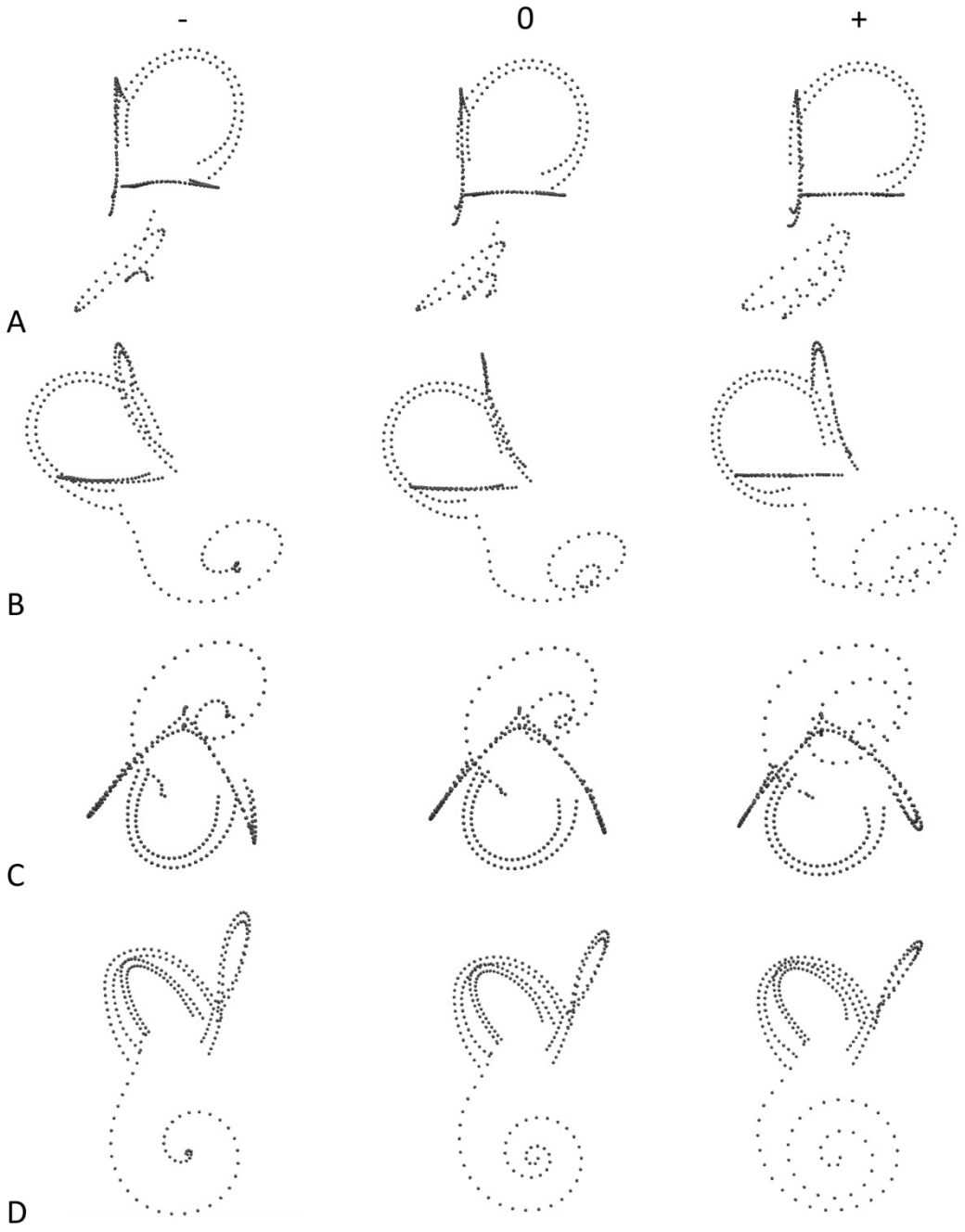

Figure IV.2 : Deformations along the second axis of the analysis (PC2, 23.5%) conducted on the whole labyrinth of Afrotheria (A1) in the view showing the plane of the anterior (A), posterior (B) and lateral (C) canals and the cochlea (D). "-" represents the extreme shape towards the negative extremity of the axis, "+" the extreme shape towards the positive extremity of the axis and "0" the mean shape on this axis.

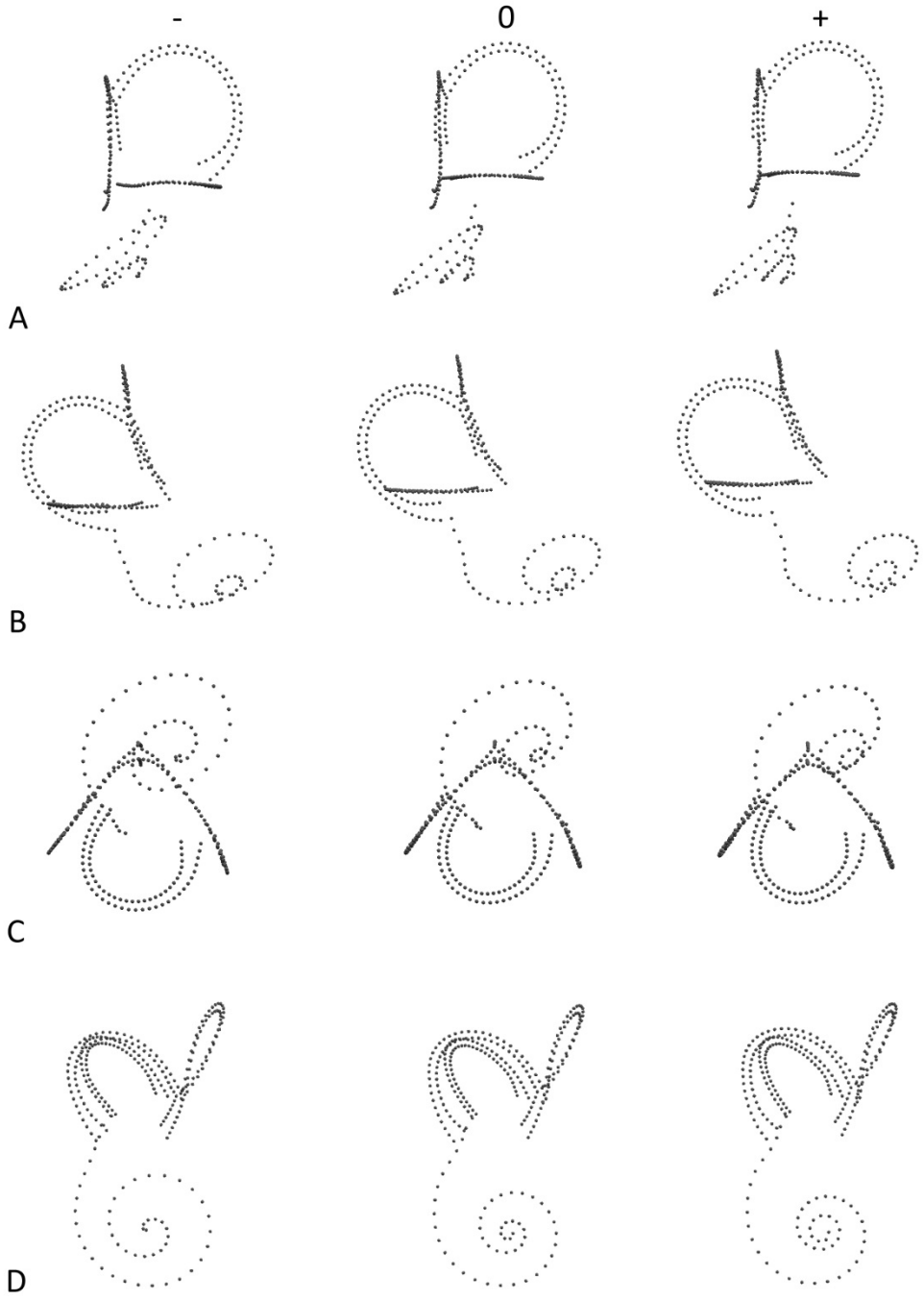

Figure IV.3 : Deformations along the third axis of the analysis (PC3, 12.5%) conducted on the whole labyrinth of Afrotheria (A1) in the view showing the plane of the anterior (A), posterior (B) and lateral (C) canals and the cochlea (D). "-" represents the extreme shape towards the negative extremity of the axis, "+" the extreme shape towards the positive extremity of the axis and "0" the mean shape on this axis.

PC3 (12.5%)

The deformations of the bony labyrinth along the third axis (PC3 which explains 12.5% of the total variation) are given in Fig IV.3 in several views.

Towards negative values, the utricular end of the slender lateral canal tends to be more distant from the posterior ampulla. The ratio between the radius of the apical turn of the cochlea and the basal turn is higher (the apical turn is larger than towards positive values). On the other hand, the axis of rotation of the apical turn is located close to the axis of rotation of the basal turn.

Conversely, towards positive values, the utricular end of the slender lateral canal tends to be located closer to the posterior ampulla. The radius of the apical turn of the cochlea is smaller especially compared to the radius of the basal turn. There is a shift of the axis of rotation of the apical turn with respect to the axis of rotation of the basal turn (the axis of rotation are not located at the same place).

Clusters

The proboscidean cluster overlaps with the cluster including the other afrotherians (Fig IV.4). However, it is important to note that only the early proboscideans (*Eritherium* and *Numidotherium*) overlap with the non-proboscidean afrotherians, the elephantimorphs being clearly separated. Their separation is mostly explained by PC1 (31.8%, towards the positive values) which correlates with a larger cochlea bearing a more developed apical turn. The cochlea also tends to form a more obtuse angle with the lateral canal towards this extremity. Among non-proboscidean afrotherians, *Procavia* displays a rather extreme morphology (very negative along PC1 and very positive along PC2 and PC3). This correlates with a small and tightly coiled cochlea. The particularly high number of turns of the specimen (3.5) does not seem to influence strongly the morphospace. In fact, the number of turns is a difficult feature to analyze through geometric morphometrics (pers. comm. Philipp Gunz 2016). *Numidotherium* and *Prorastomus* plot close to each other. This is not a surprise given the similarities seen in both specimens such as a loose cochlea that displays 1.5 turns. Other afrotherians (*Eritherium*, the sirenian from Chambi, *Ocepeia*, *Tenrec* and *Elephantulus*) plot more or less together.

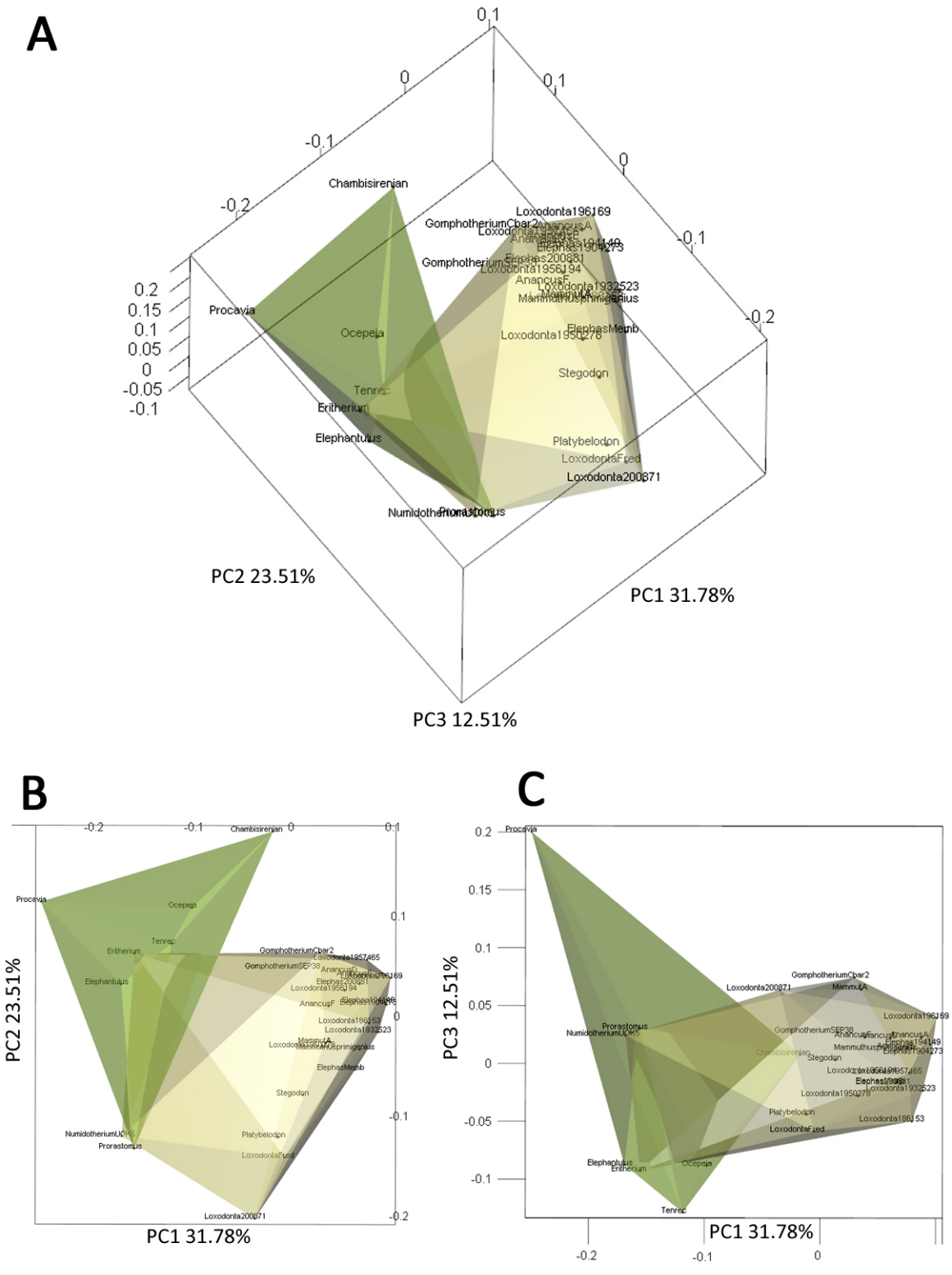

Figure IV.4 : Shape differentiation of the whole bony labyrinth of afrotherians (analysis **A1**). A) 3D Morphospace in the view best illustrating the two clusters. B) Principal components 1 and 2 and C) principal components 1 and 3. **Green cluster:** non-proboscideans. **Grey cluster:** proboscideans.

3.1.2. Analysis A2 restricted to the semicircular canals

Results of the PCA performed only on the semicircular canals are given in Fig IV.8. Restricting the study to the semicircular canals allows to add specimens of taxa lacking the cochlea (not preserved or broken: *Arsinoitherium, Cuvieronius, Mammuthus columbi, Palaeoloxodon, Prodeinotherium*…). The first three axes of the PCA explain 64.6% (PC1: 40.6%, PC2: 15.5%, PC3: 8.5%) of the total variation of the labyrinth morphology.

Deformations

PC1 (40.6%)

The deformations of the bony labyrinth along the first axis (PC1 which explains 40.6% of the total variation) are given in Fig IV.5 in several views.

Towards the negative values, specimens clearly have more slender canals. The lateral canal tends to increase in relative size. It tends to be more developed towards the posterior semicircular canal to the extent of crossing the plane defined by this canal. Additionally, the point of entry of the lateral canal into the vestibule is closer to the *crus commune* and clearly higher than in the mean shape of the labyrinth. *The crus commune* also tends to be more elongated towards negative values of the first axis. The angle between the anterior and posterior canals and the angle between the anterior and lateral canals clearly tend to increase and be obtuse. The posterior canal tends to be more oval and slightly smaller. Finally, the shape of the anterior semicircular canal is modified. More precisely, the major axis of the anterior canal forms a very different angle with the *crus commune*. If we follow the nomenclature used in chapter II and III, the angle tends to be negative in specimens located towards the negative values of this axis while this angle is positive otherwise. In any case, the anterior canal tends to be rounder in this end of the axis.

Specimens that display positive values along the first axis tend to have slightly thicker canals. The angle between the anterior and posterior semicircular canals tends to be more acute. The lateral semicircular canal tends to be slightly more oval and its point of entry into the vestibule is somewhat lower on this side of the axis. The *crus commune* tends to be slightly stockier as well.

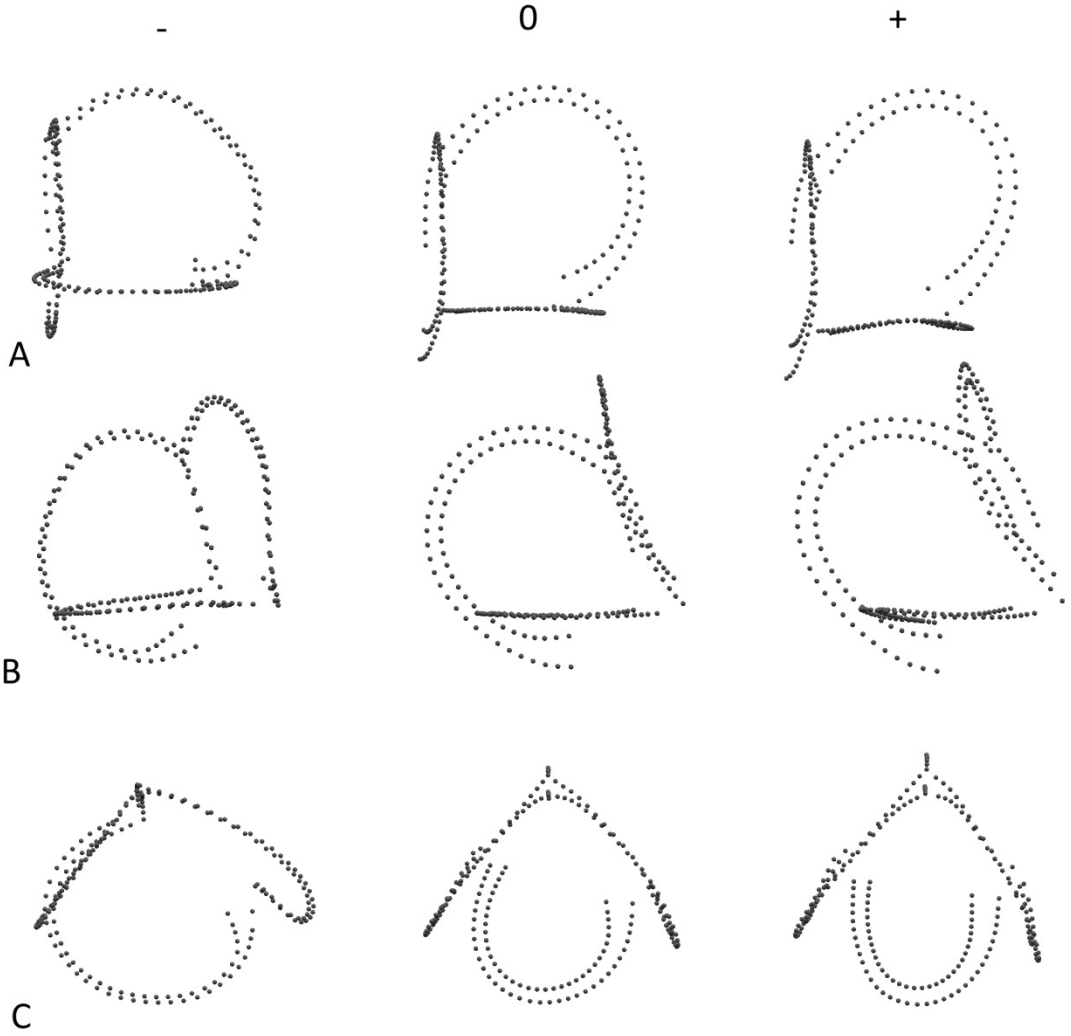

Figure IV.5 : Deformations along the first axis of the analysis (PC1, 40.6%) restricted to the semicircular canals of Afrotheria (A2) in the view showing the plane of the anterior (A), posterior (B) and lateral (C) canals. "-" represents the extreme shape towards the negative extremity of the axis, "+" the extreme shape towards the positive extremity of the axis and "0" the mean shape on this axis.

PC2 (15.5%)

The deformations of the bony labyrinth along the second axis (PC2 which explains 15.5% of the total variation) are given in Fig IV.6 in several views.

Specimens with negative values along the second axis exhibit a particularly obtuse angle between the posterior and lateral canals. The same can be said about the angle between the anterior and lateral canals although this is less marked. The posterior canal tends to be smaller. In contrary, the lateral canal tends to increase in relative size. The point of entry of the lateral canal into the vestibule tends to be lower.

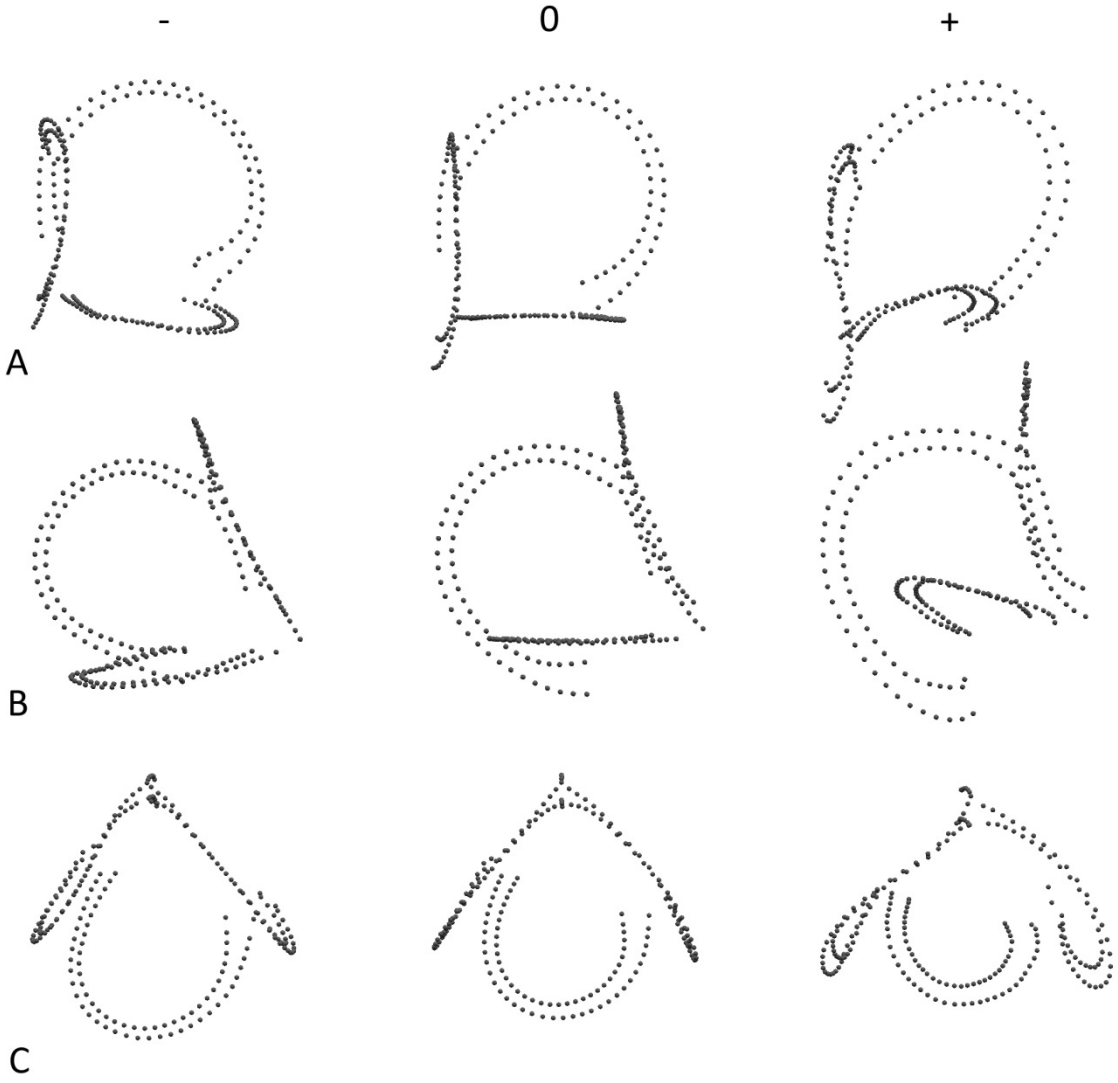

Figure IV.6 : Deformations along the second axis of the analysis (PC2, 15.5%) restricted to the semicircular canals of Afrotheria (A2) in the view showing the plane of the anterior (A), posterior (B) and lateral (C) canals. "-" represents the extreme shape towards the negative extremity of the axis, "+" the extreme shape towards the positive extremity of the axis and "0" the mean shape on this axis.

Towards the positive values, the angle between the anterior and lateral canals and the angle between the posterior and lateral canals tend to decrease and to be clearly more acute. The posterior canal increases in size and the anterior canal is somewhat more oval. Both anterior and posterior canals tend to display more undulations (this is more distinct in the posterior canal). The relative size of the lateral canal tends to decrease towards the positive values of this axis. The point of entry of the lateral canal into the vestibule is located very high in such specimens.

PC3 (8.5%)

The deformations of the bony labyrinth along the third axis (PC2 which explains 8.5% of the total variation) are given in Fig IV.7 in several views.

Towards the negative values, the anterior and posterior canals increase in size and are more oval. The angle between the anterior and lateral canals is slightly more acute.

Towards the positive values, the anterior and posterior canals tend to decrease in size and to be rounder.

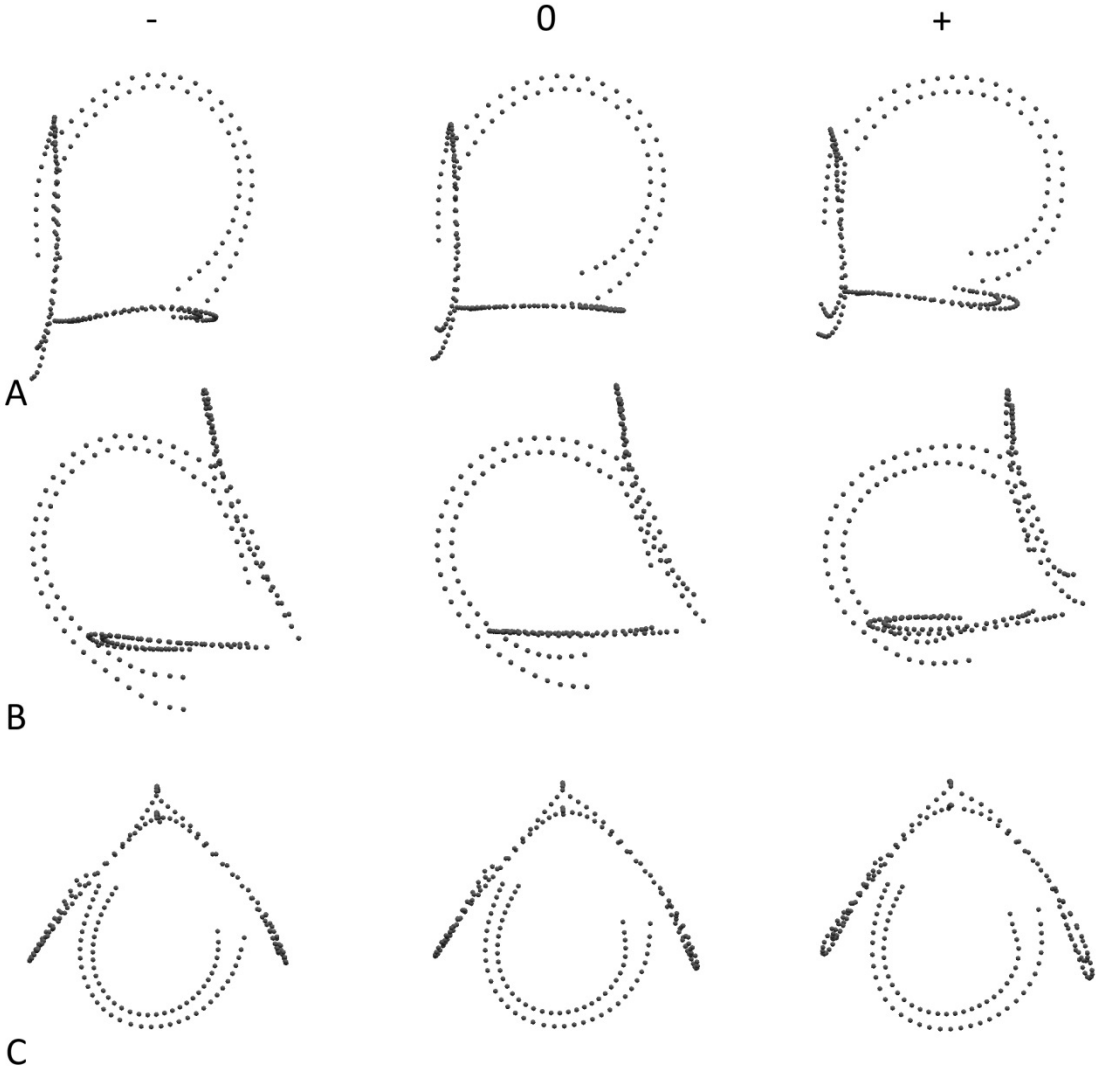

Figure IV.7 : Deformations along the third axis of the analysis (PC3, 8.5%) restricted to the semicircular canals of Afrotheria (A2) in the view showing the plane of the anterior (A), posterior (B) and lateral (C) canals. "-" represents the extreme shape towards the negative extremity of the axis, "+" the extreme shape towards the positive extremity of the axis and "0" the mean shape on this axis.

Clusters

Results of the PCA restricted on the semicircular canals of Afrotheria are given in Fig IV.8 below. The cluster containing all proboscideans (brown) and the cluster containing all non-proboscideans (green) afrotherians exhibit a small overlap. However, only the early proboscideans (*Eritherium, Phosphatherium, Numidotherium*) overlap with the non-proboscidean afrotherian taxa. Elephantimorphs and *Prodeinotherium* are well distinguished with respect to the other specimens and they form a distinct cluster (red). The first axis best discriminates the proboscideans from other afrotherians (PC1; 40.6%). Elephantimorphs and *Prodeinotherium* are located at the positive extremity of the axis which corresponds to a trend with slightly thicker canals. This trait separates them from the non-proboscidean afrotherians and early proboscideans. Moreover, elephantimorphs and *Prodeinotherium* display relatively smaller, more oval lateral canals which point of entry into the vestibule is situated lower with respect to the posterior ampulla. Their vertical canals are more oval as well. Finally, the *crus commune* is relatively shorter and stockier in modern proboscideans. Conversely, most outgroups and early proboscideans display relatively intermediate values along the first axis. They tend to have round canals. The point of entry of the lateral canal into the vestibule is located higher than in the modern proboscideans. Among non-proboscidean afrotherians, *Procavia capensis* exhibits an extreme morphology. It is very distant from other specimens and this disparity seems to be explained at least by the first three axes. *Procavia* displays extremely negative values for PC1 and extremely positive values for PC2 and PC3 (see previous section “Deformations”). This is explained by a very different morphology of this species and other Procaviidae (Benoit, 2013). *Procavia* displays very slender canals and the lateral canal increases in relative size towards the posterior semicircular canal to the extent of crossing the plane defined by this canal. The point of entry of the lateral canal into the vestibule is located markedly higher and closer to the *crus commune* than in other examined specimens. The second axis does not separate well proboscideans from outgroups. However, a combination of the first and second axis discriminates several outgroups. As mentioned earlier, *Procavia* displays an extreme morphology. On the other hand, the two studied sirenians

(*Prorastomus* and the sirenian from Chambi, Benoit et al. 2013a) differ from the other afrotherians along the second axis, displaying more negative values. This correlates with a particularly large lateral canal and a particularly small posterior canal. *Ocepeia*, *Tenrec* and both embrithopods (PM53 and *Arsinoitherium*) are morphologically similar regarding the semicircular canals. They are also similar to the early proboscideans (*Eritherium*, *Phosphatherium* and *Numidotherium*) with which they overlap. *Elephantulus*, however, seems to differ along the second axis and displays more positive values.

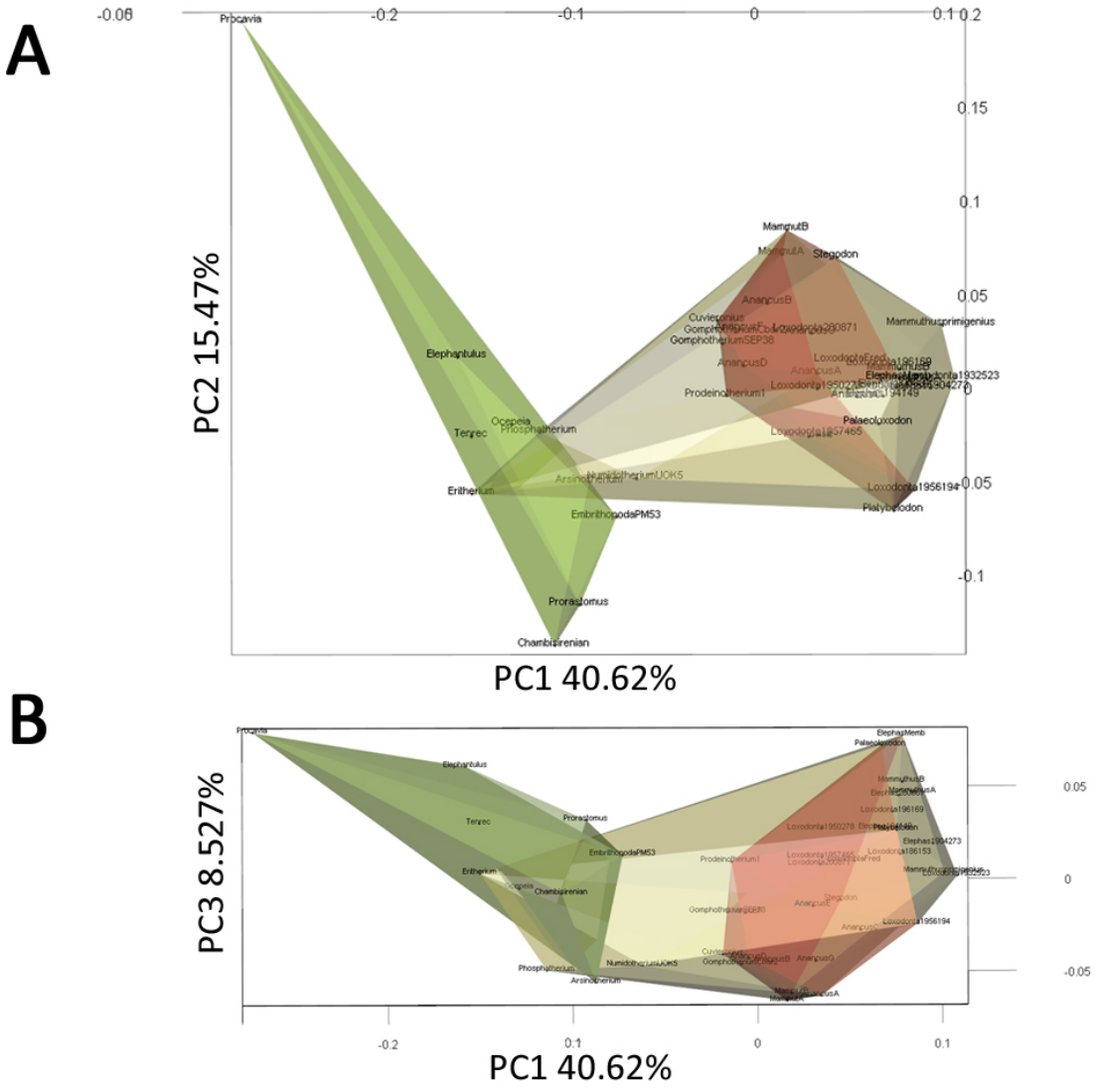

Figure IV.8 : Shape differentiation of the semicircular canals of afrotherians (analysis **A2**). A) 3D Morphospace in the view best illustrating the three clusters. B) Principal components 1 and 2 and C) principal components 1 and 3. **Green cluster:** non-proboscideans. **Grey cluster:** proboscideans. **Red cluster**: Elephantimorpha + *Prodeinotherium.*

3.2. Analysis of the Proboscidea

3.2.1. Analysis P1 of the whole labyrinth

Results of the PCA performed on the whole labyrinth are given in Fig IV.12. The first three axes of the PCA explain 67.4% (PC1: 36.6%, PC2: 19.8%, PC3: 11%) of the total variation of the labyrinth morphology.

Deformations

PC1 (36.6%)

The deformations of the bony labyrinth along the first axis (PC1 which explains 36.6% of the total variation) are given in Fig IV.9 in several views.

This axis seems to be controlled by the cochlear morphology only. The cochlea is more tightly coiled towards the negative values while it is less coiled towards the positive values. On the other hand, the number of turns appears to decrease towards the negative values. The angle between the cochlea and the lateral canal decreases towards the negative values and it increases towards the positive values.

PC2 (19.8%)

The deformations of the bony labyrinth along the second axis (PC2 which explains 19.8% of the total variation) are given in Fig IV.10 in several views.

The cochlea is less coiled towards negative values while it is more tightly coiled towards positive values. The axis of rotation of the apical turn is displaced with respect to the axis of rotation of the basal turn towards positive values. The anterior canal is rounder towards negative values and the semicircular canals are more slender. The lateral canal also tends to increase and to expand toward the posterior canal. The posterior canal displays an apical expansion towards negative values as well. The *crus commune* shape is also affected along this axis. It is more elongated towards the negative extremity of the axis while it is shorter and stockier towards its positive extremity. Finally, the angle between the anterior and posterior canals increases towards negative values.

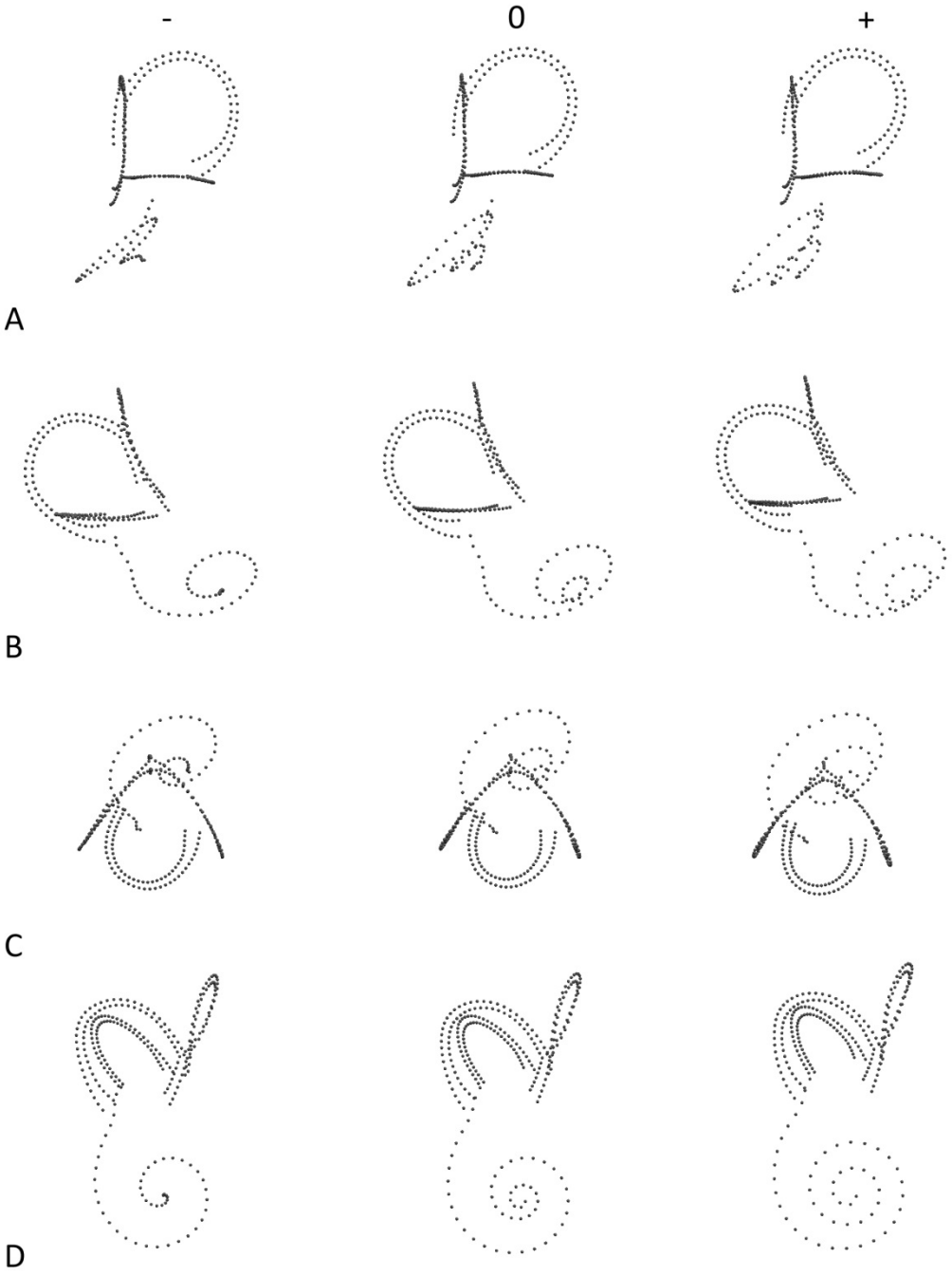

Figure IV.9 : Deformations along the first axis of the analysis (PC1, 36.6%) restricted to Proboscidea (P1) in the view showing the plane of the anterior (A), posterior (B) and lateral (C) canals and the cochlea (D). "-" represents the extreme shape towards the negative extremity of the axis, "+" the extreme shape towards the positive extremity of the axis and "0" the mean shape on this axis.

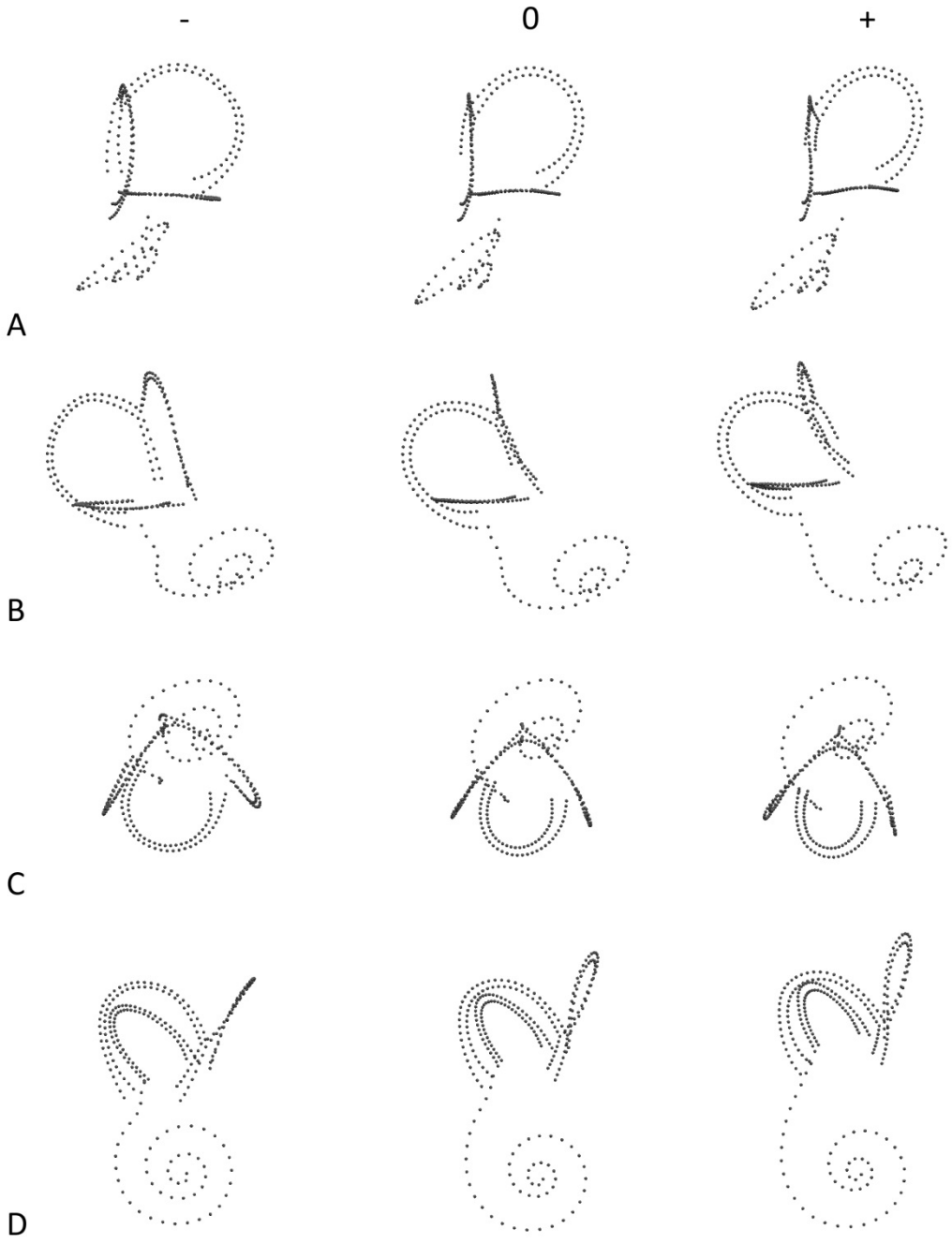

Figure IV.10 : Deformations along the second axis of the analysis (PC2, 19.8%) restricted to Proboscidea (P1) in the view showing the plane of the anterior (A), posterior (B) and lateral (C) canals and the cochlea (D). "-" represents the extreme shape towards the negative extremity of the axis, "+" the extreme shape towards the positive extremity of the axis and "0" the mean shape on this axis.

PC3 (11%)

The deformations of the bony labyrinth along the third axis (PC3 which explains 11% of the total variation) are given in Fig IV.11 in several views.

The third PC is explained by a combination of both the canals and the cochlear features. First, the anterior canal is rounder towards positive values along this axis. The angle formed by the major axis of the oval posterior canal and the crus commune changes along this axis as well. It is more acute towards negative values and more obtuse towards positive values. The zone of insertion of the lateral canal into the vestibule is closer to the posterior ampulla towards the negative extremity of the axis while the opposite is observed towards the positive extremity of PC3. Finally, the cochlea is more tightly coiled towards negative values and looser towards positive values.

Clusters

While the elephantimorphs are well distinct from early proboscideans within the morphospace (especially along PC1 and PC2), the Elephantidae family does not form a clear cluster that separates them from other elephantimorphs based on cochlear and canals landmarks (Fig IV.12). This is mostly explained by the location of CEB130168 and MNHN.AC.ZM.2008-71 within the morphospace. MNHN.AC.ZM.2008-71 is located towards the negative values of PC1. Indeed, as observed in Chapter III, this specimen displays a particularly low number of turns (1.5) which is a feature controlled by PC1. This explains its location and its proximity along this axis to *Numidotherium,* which displays a cochlea with 1.5 turns as well. However, *Numidotherium* and MNHN.AC.ZM.2008-71 are very distant from each other along PC2. CEB130168 and *Platybelodon* are also close within the morphospace (especially along PC1) likely based on their shared number of turns of the cochlea (2 turns). *Eritherium* is located roughly at the same level as *Platybelodon* and CEB130168 along PC1, however, it is very distant from those two along PC2. *Anancus* specimens are close within the morphospace but they are included within the Elephantidae cluster as well as *Stegodon*. Specimens with a large number of turns (*Anancus*, *Loxodonta* specimens MNHN.AC.ZM.1961-69, 1956-194, 1957-465) are located towards the positive extremity of PC1. Both *Gomphotherium* specimens plot together along PC1 and PC2.

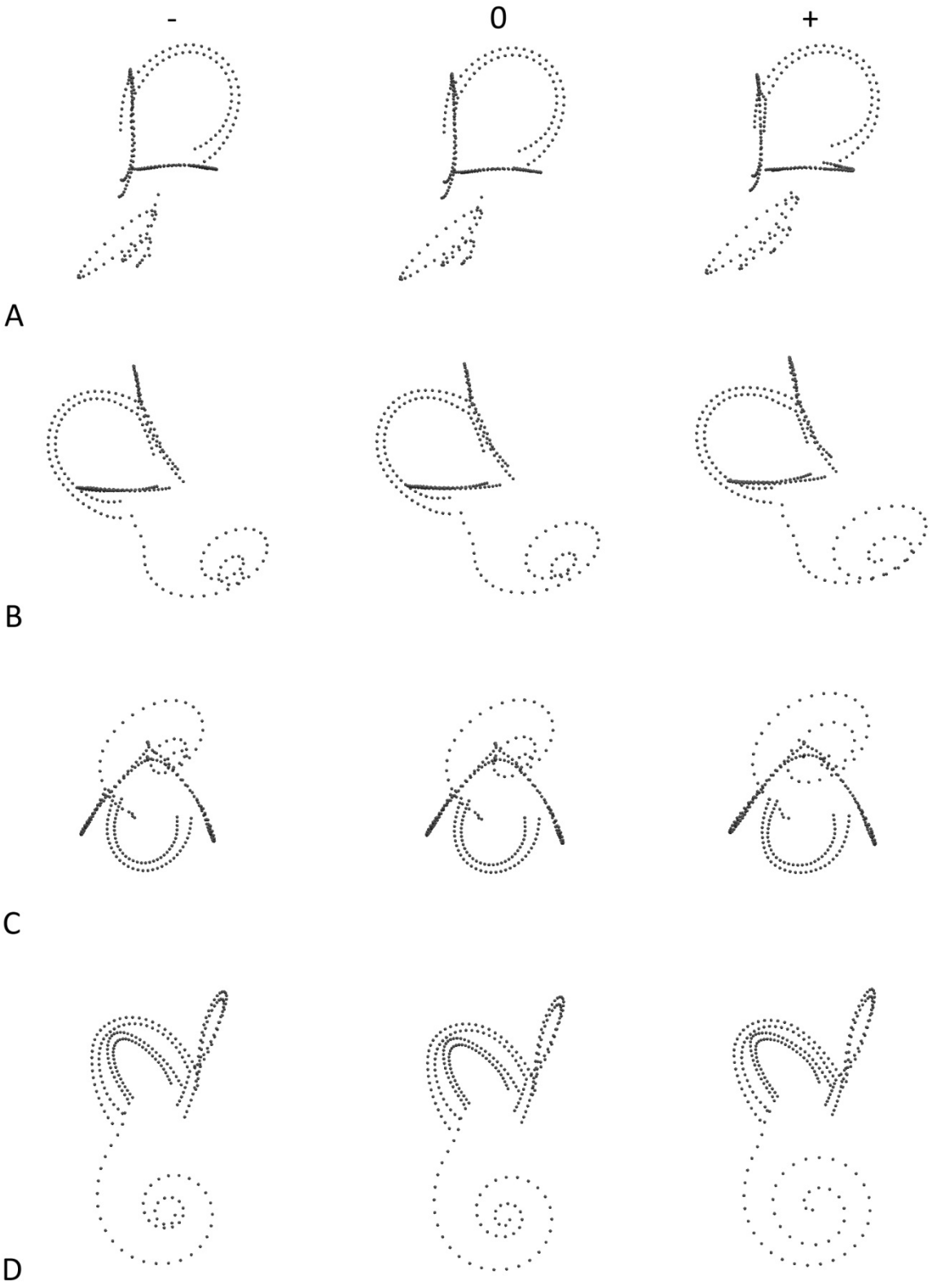

Figure IV.11 : Deformations along the third axis of the analysis (PC3, 11%) restricted to Proboscidea (P1) in the view showing the plane of the anterior (A), posterior (B) and lateral (C) canals and the cochlea (D). "-" represents the extreme shape towards the negative extremity of the axis, "+" the extreme shape towards the positive extremity of the axis and "0" the mean shape on this axis.

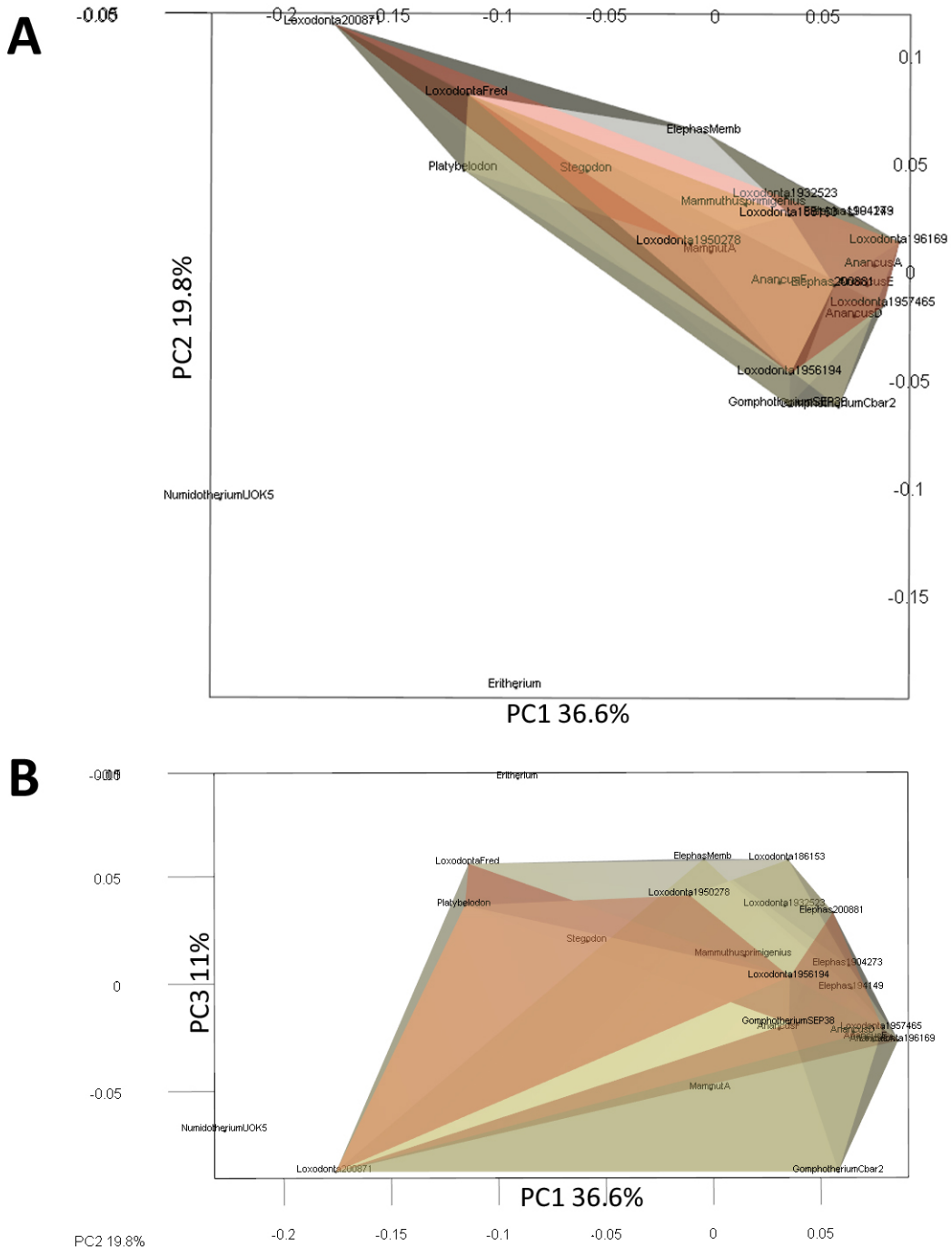

Figure IV.12 : Shape differentiation of the whole labyrinth of proboscideans (analysis **P1**). A) Principal components 1 and 2 and B) principal components 1 and 3. **Grey cluster:** Elephantimorpha. **Red cluster**: Elephantidae. Early proboscideans are not represented in a cluster since they are only two of them in this analysis.

3.2.2. Analysis P2 restricted to the semicircular canals

Results of the PCA performed only on the semicircular canals are given in Fig IV.16. The first three axes of the PCA explain 57.7% (PC1: 32.4%, PC2: 15.4%, PC3: 9.9%) of the total variation of the labyrinth morphology.

Deformations

PC1 (32.4%)

The deformations of the bony labyrinth along the first axis (PC1 which explains 32.4% of the total variation) are given in Fig IV.13 in several views.

The observed deformations along the first axis in this analysis restricted to semicircular canals of proboscideans (P2) are different from the deformations seen in the analysis including the afrotherians (A2). However, some similarities are met. First, towards the negative values of the first axis, the semicircular canals are more slender and the *crus commune* is more elongated. The lateral canal is larger and it extends towards the posterior canal but without crossing the plane defined by it. Only the angle between the anterior and posterior canals increases towards the negative values of this axis. By contrast to the analysis A2 (semicircular canals of afrotherians), the posterior and anterior canals shape does not change drastically. The point of entry of the lateral canal into the vestibule is higher with respect to the posterior ampulla towards negative values of the first PC.

When the analysis is restricted to the semicircular canals of proboscideans, the specimens with positive values along the first axis do not show major deformations explained by the first axis. There is a trend to exhibit thicker semicircular canals and a shorter crus commune.

PC2 (15.4%)

The deformations of the bony labyrinth along the second axis (PC2 which explains 15.4% of the total variation) are given in Fig IV.14 in several views.

The deformations along this axis and towards the negative values are very similar to those observed in the analysis that includes other afrotherians (see A2, section PC2).

There are a few differences with A2 in the deformations towards the positive values. The lateral canal is not much smaller in P2. The undulations of the anterior and posterior canals are less marked. The angle between the anterior and lateral canals and the angle between the posterior and lateral canals still tend

to decrease but less than in A2. However, the point of entry of the lateral canal into the vestibule still tends to be located higher.

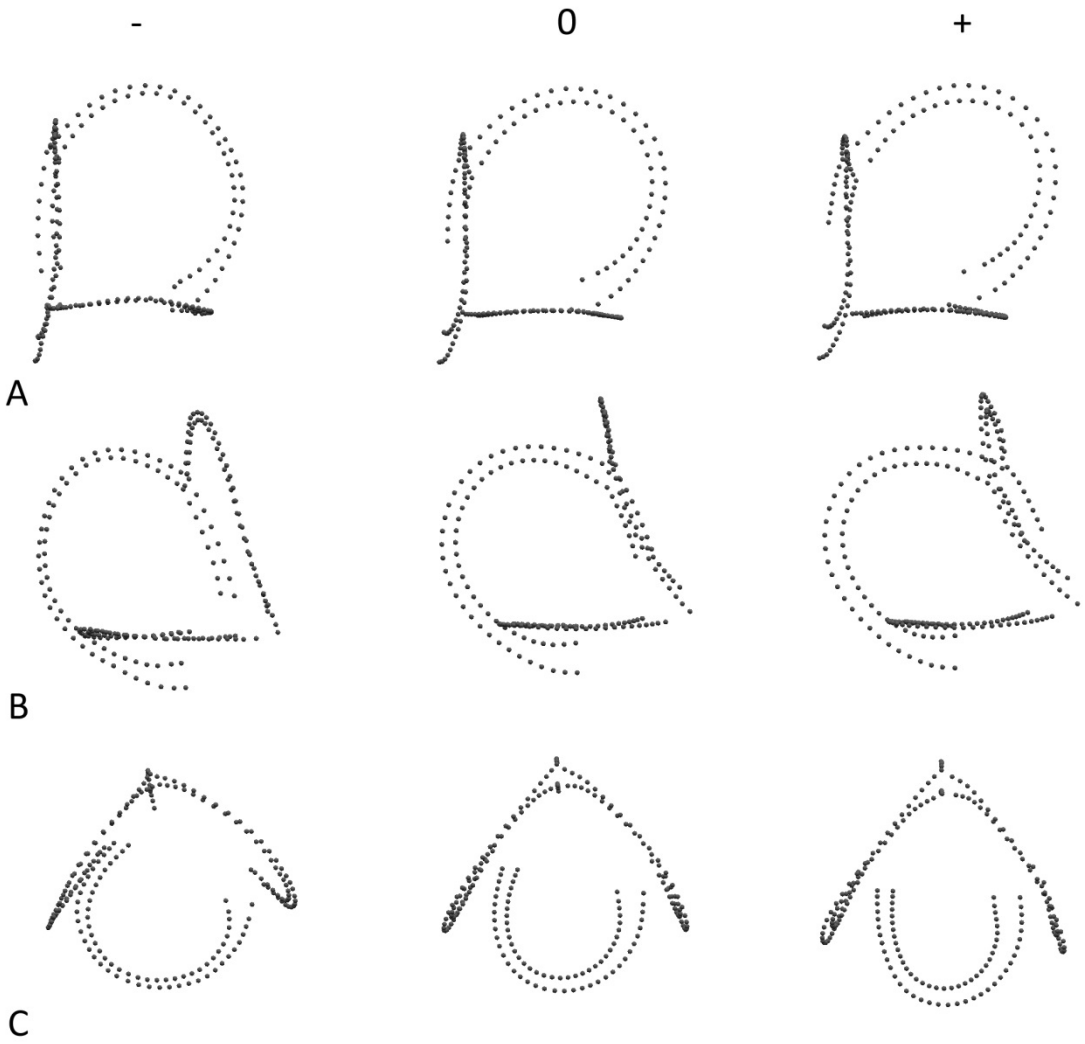

Figure IV.13 : Deformations along the first axis of the analysis (PC1, 32.4%) restricted to the semicircular canals of Proboscidea (P2) in the view showing the plane of the anterior (A), posterior (B) and lateral (C) canals. "-" represents the extreme shape towards the negative extremity of the axis, "+" the extreme shape towards the positive extremity of the axis and "0" the mean shape on this axis.

PC3 (9.9%)

The deformations of the bony labyrinth along the third axis (PC3 which explains 9.9% of the total variation) are given in Fig IV.15 in several views.

Towards the negative values, the specimens exhibit a rounder anterior canal. The angle between the anterior and posterior canals canal decreases.

Towards the positive values, the specimens display a slightly rounder posterior semicircular canal while the angle between the anterior and posterior canals increases.

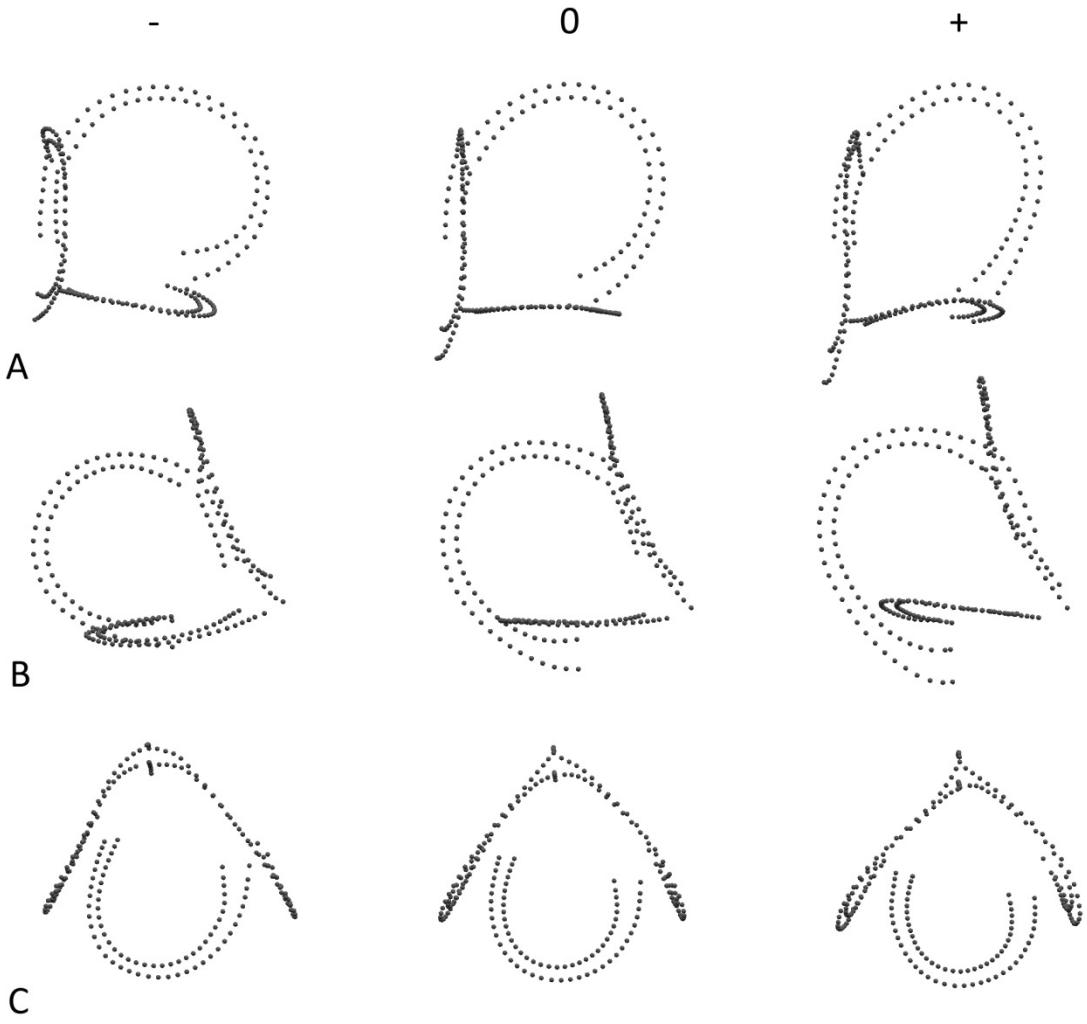

Figure IV.14 : Deformations along the second axis of the analysis (PC2, 15.4%) restricted to the semicircular canals of Proboscidea (P2) in the view showing the plane of the anterior (A), posterior (B) and lateral (C) canals. "-" represents the extreme shape towards the negative extremity of the axis, "+" the extreme shape towards the positive extremity of the axis and "0" the mean shape on this axis.

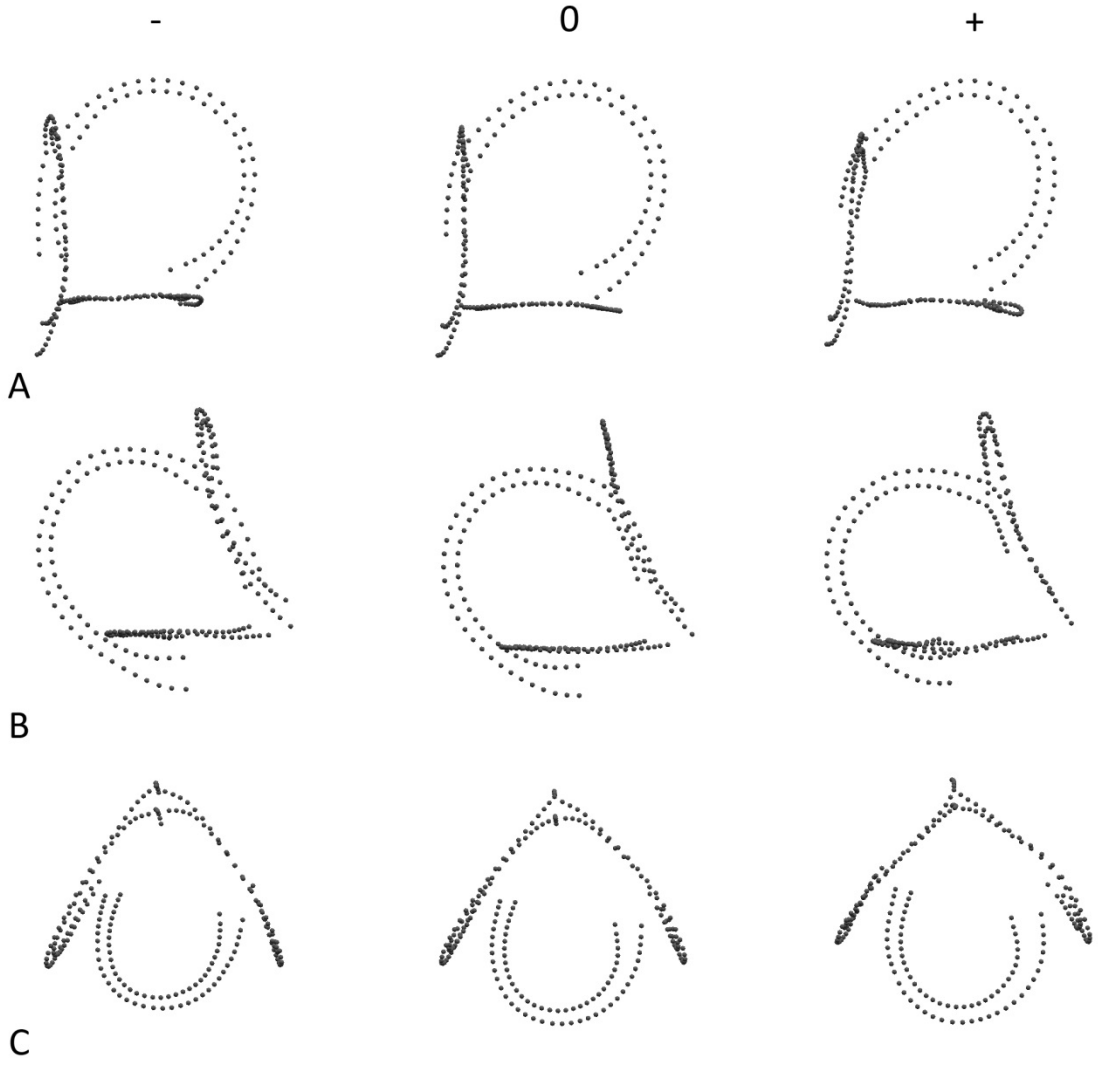

Figure IV.15 : Deformations along the third axis of the analysis (PC3, 9.9%) restricted to the semicircular canals of Proboscidea (P2) in the view showing the plane of the anterior (A), posterior (B) and lateral (C) canals. "-" represents the extreme shape towards the negative extremity of the axis, "+" the extreme shape towards the positive extremity of the axis and "0" the mean shape on this axis.

Clusters

Results of the PCA restricted on the semicircular canals of the Proboscidea are given in Fig IV.16 below.

Elephantimorphs

First, the results show that it is possible to separate the elephantimorph taxa from non-elephantimorph taxa using semicircular canals 3D landmarks. There is clearly an elephantimorph cluster that can be discriminated from the non-elephantimorph cluster (containing *Eritherium*, *Phosphatherium*, *Numidotherium* and *Prodeinotherium*). The separation is mostly explained by a

combination of the first two components (PC1 and PC2) that represent respectively 32.4% and 15.4% of the total variation. *Prodeinotherium* displays a somewhat intermediary morphology as it is closer to the elephantimorphs than to the early proboscideans along both axes. Early proboscideans exhibit markedly negative values along PC1 and PC2 which correlates - amongst others - with more slender canals, a more elongated *crus commune* and a relatively larger lateral canal. By contrast, the elephantimorphs display more positive values along these two axes. This correlates with thicker semicircular canals, smaller lateral canals, a stockier *crus commune* and a higher location of the point of entry of the lateral canal into the vestibule.

Elephantidae

Within the elephantimorph cluster, the Elephantidae (*Loxodonta*, *Elephas*, *Palaeoloxodon*, *Mammuthus*) forms a well distinct cluster. Its separation from other elephantimorphs is explained by a combination of - at least - the first three PCs (especially PC1 and PC2). The Elephantidae display more positive values along PC1 than the other elephantimorphs. This is probably due to their higher degree of semicircular canals thickness (the mean of the average thickness ratio is 3.98 in Elephantidae and 3.54 in other elephantimorphs) and their trend to display a stockier *crus commune*. On the other hand, members of the Elephantidae family have more negative values than other elephantimorphs along PC2.

Platybelodon

One peculiar detail is the location of the Amebelodontidae family member *Platybelodon* within the morphospace. Although not included into the Elephantidae cluster, it displays a very close morphology to this family with very negative PC2 values and very positive PC1 values.

Anancus genus

It is noted that the seven specimens of *Anancus* form a distinct cluster explained mostly by PC2 (positive) and PC3 (negative). This correlates with acute angles between the semicircular canals in general.

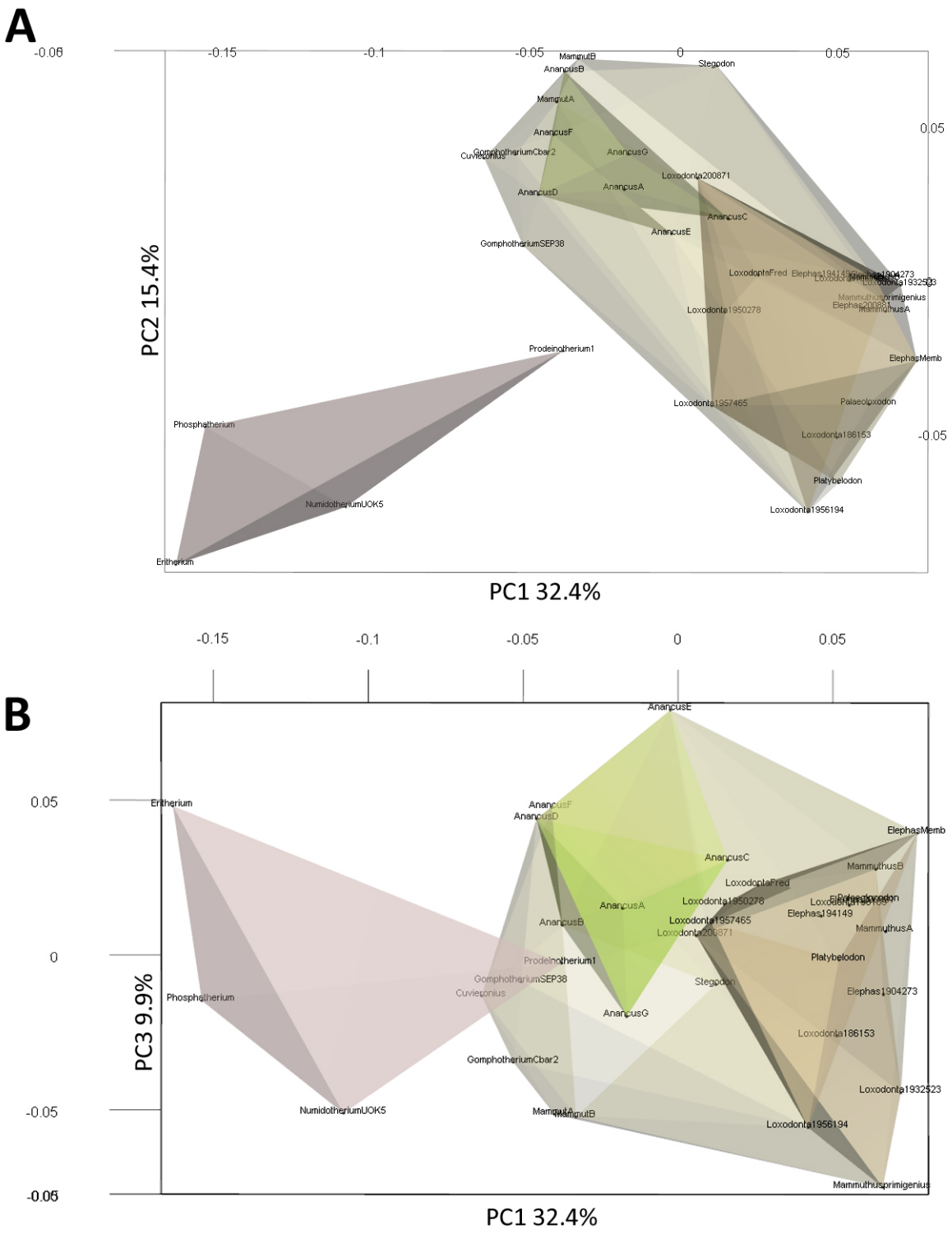

Figure IV.16 : Shape differentiation of the semicircular canals of proboscideans (analysis **P2**). A) Principal components 1 and 2 and B) principal components 1 and 3. **Grey cluster:** Elephantimorpha. **Green cluster**: genus *Anancus*. **Brown cluster:** Elephantidae. **Violet cluster:** non-elephantimorphs. Early proboscideans are not represented in a cluster since they are only two of them in this analysis.

3.3. Analysis of extant elephants

3.3.1. Analysis E1 of the whole labyrinth

Results of the PCA performed on the whole labyrinth are given in Fig IV.20. The first three axes of the PCA explain 79% (PC1: 52.2%, PC2: 14.8%, PC3: 12%) of the total variation of the labyrinth morphology.

Deformations

PC1 (52.2%)

The deformations of the bony labyrinth along the first axis (PC1 which explains 52.2% of the total variation) are given in Fig IV.17 in several views.

The first axis is almost entirely controlled by the cochlea morphology. Towards negative values, specimens tend to display a cochlea with less turns. By contrast, towards the middle and positive end of this axis, the specimens have a cochlea with more turns. On the other hand, the coiling of the second turn of the cochlea seems to be controlled by this axis. Indeed, towards positive values, the second turn is less tightly coiled.

PC2 (14.8%)

The deformations of the bony labyrinth along the second axis (PC2 which explains 14.8% of the total variation) are given in Fig IV.18 in several views.

There again, the cochlea morphology explains most of the variation. More exactly, the coiling of the cochlea is very tight towards negative values while it is looser towards positive values. The axis of rotation of the second turn is different than the axis of rotation of the first turn towards negative values.

PC3 (12%)

The deformations of the bony labyrinth along the second axis (PC3 which explains 12% of the total variation) are given in Fig IV.19 in several views.

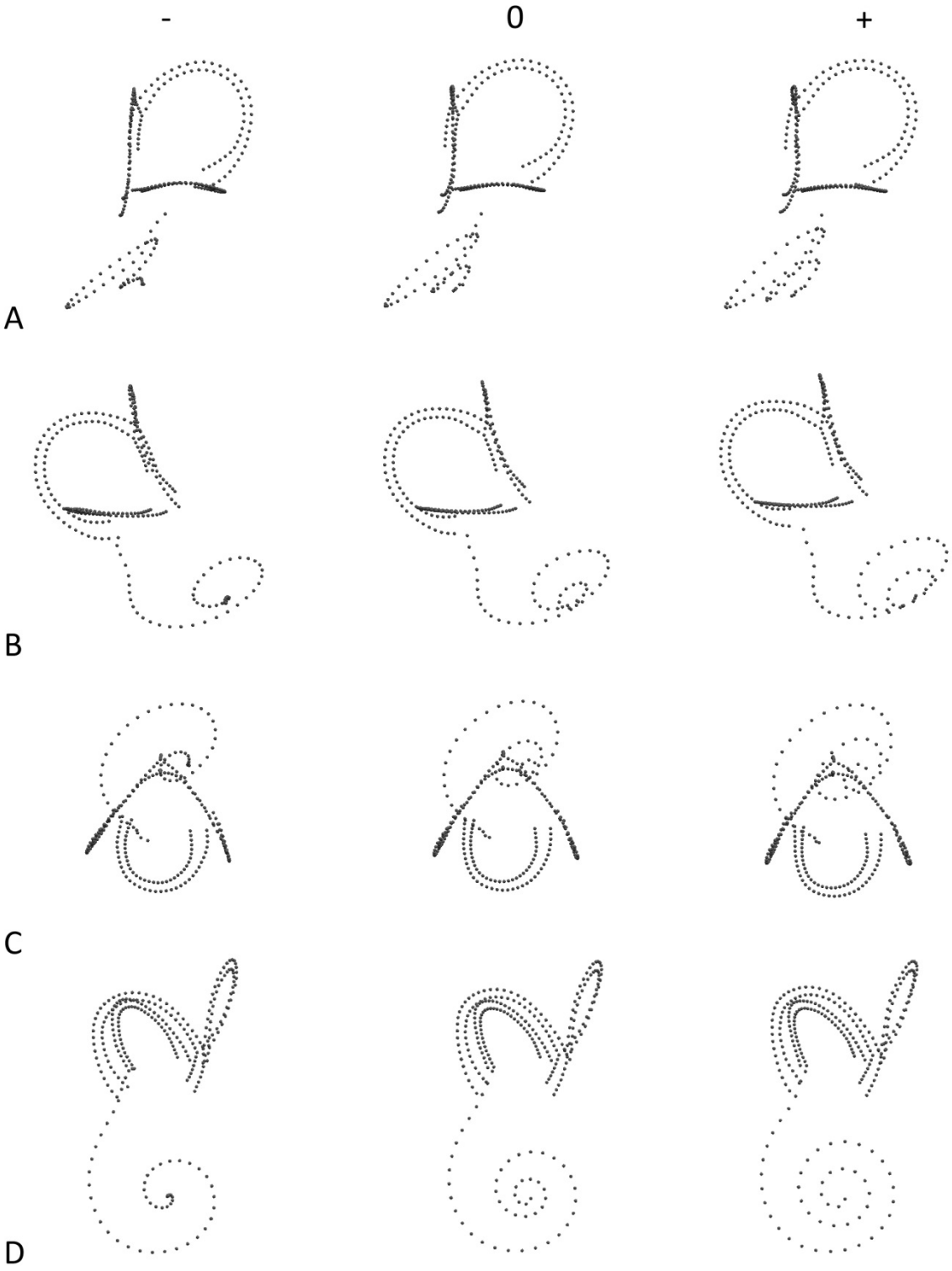

Figure IV.17 : Deformations along the first axis (PC1, 52.2%) of the analysis on the whole labyrinth of extant elephants (E1) in the view showing the plane of the anterior (A), posterior (B) and lateral (C) canals. "-" represents the extreme shape towards the negative extremity of the axis, "+" the extreme shape towards the positive extremity of the axis and "0" the mean shape on this axis.

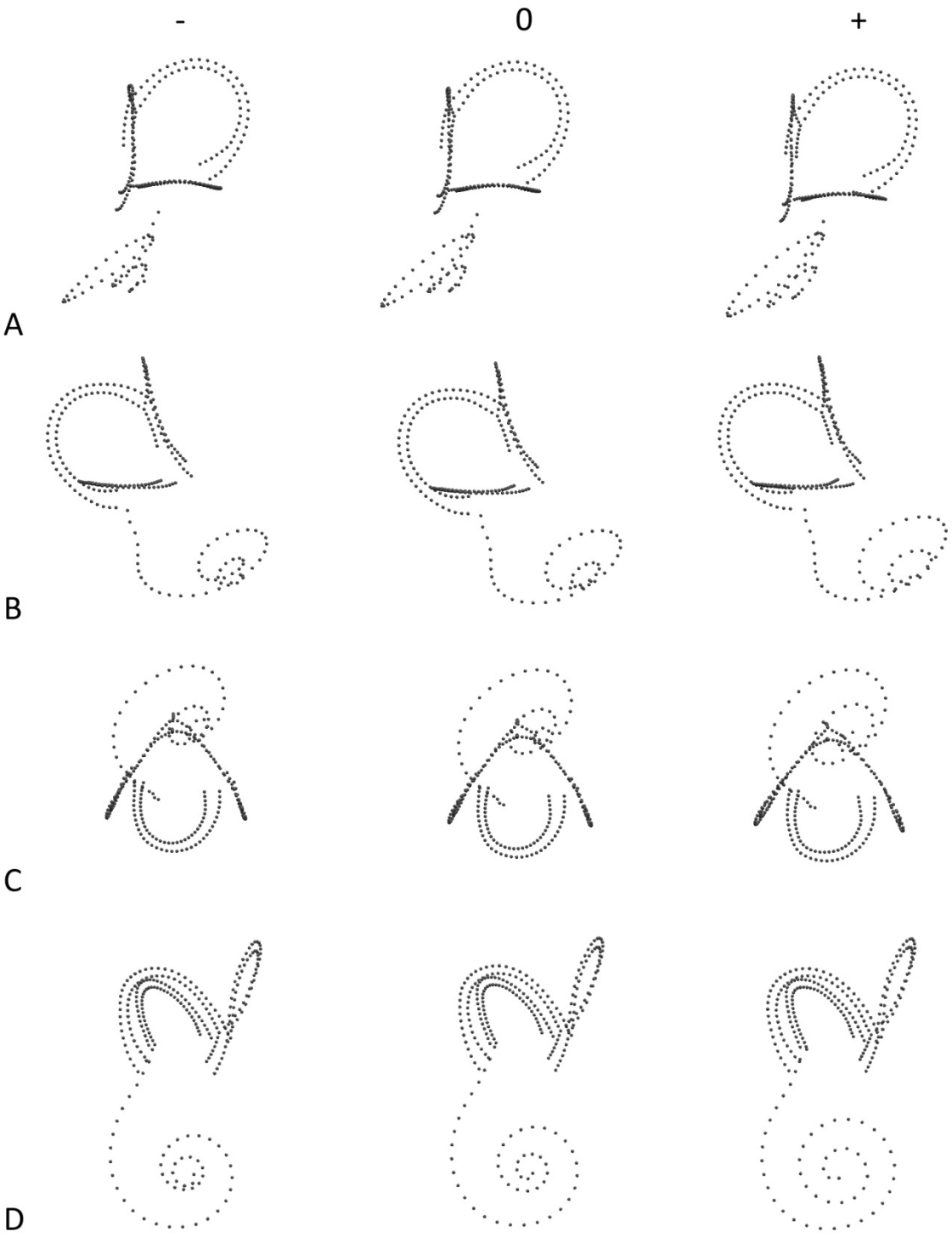

Figure IV.18 : Deformations along the second axis (PC2, 14.8%) of the analysis on the whole labyrinth of extant elephants (E1) in the view showing the plane of the anterior (A), posterior (B) and lateral (C) canals. "-" represents the extreme shape towards the negative extremity of the axis, "+" the extreme shape towards the positive extremity of the axis and "0" the mean shape on this axis.

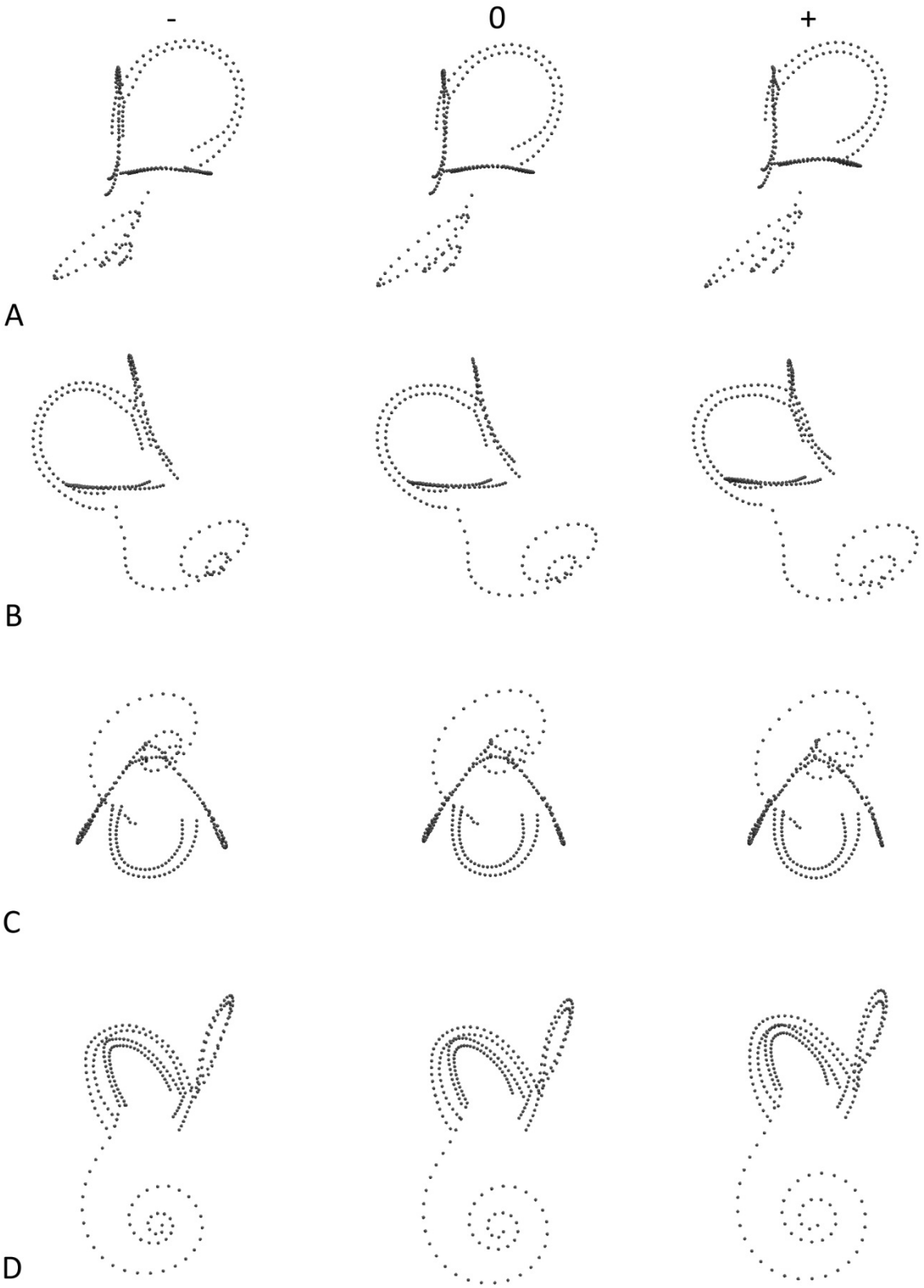

Figure IV.19 : Deformations along the third axis (PC3, 12%) of the analysis on the whole labyrinth of extant elephants (E1) in the view showing the plane of the anterior (A), posterior (B) and lateral (C) canals. "-" represents the extreme shape towards the negative extremity of the axis, "+" the extreme shape towards the positive extremity of the axis and "0" the mean shape on this axis.

Clusters

The *Elephas* and the *Loxodonta* clusters almost do not intersect within the morphospace (Fig IV.20). Actually, no *Elephas* specimens are contained within the *Loxodonta* cluster and *vice versa*. In any case, both genera are not well distinct based on the entire bony labyrinth morphology. The *Loxodonta* specimens have a wide distribution along at least the three first axes. This means that they display variable morphologies. This is very probably due to the high difference of number of turns between the specimens. This feature explains the majority of the variation (PC1: 52.2%). The negative values correlate with a lower number of turns and the most negative specimen along this axis is indeed MNHN.AC.ZM.2008-71 that displays only 1.625 turns. CEB130168 is also located towards the negative values of this axis (cochlea with two turns). Other *Loxodonta* specimens that display a greater number of turns are located at the positive extremity. *Loxodonta* specimens also display a great disparity along the second axis (PC2: 14.8%) which correlates with the degree of coiling of the cochlea. The most extreme specimen towards the positive values is CEB130168 and it exhibits a very loose coiling of the cochlea to the point of having an apical lacuna. The *Elephas* specimens seem to display smaller morphological variability than in African elephants. They are mostly limited to the positive extremity of the first three axes which correlates with loose cochlea displaying a great number of turns. *Loxodonta* specimen MNHN.AC.ZM.1932-523 shares a very close morphology with *Elephas* specimens since it is located very close to their cluster within the morphospace.

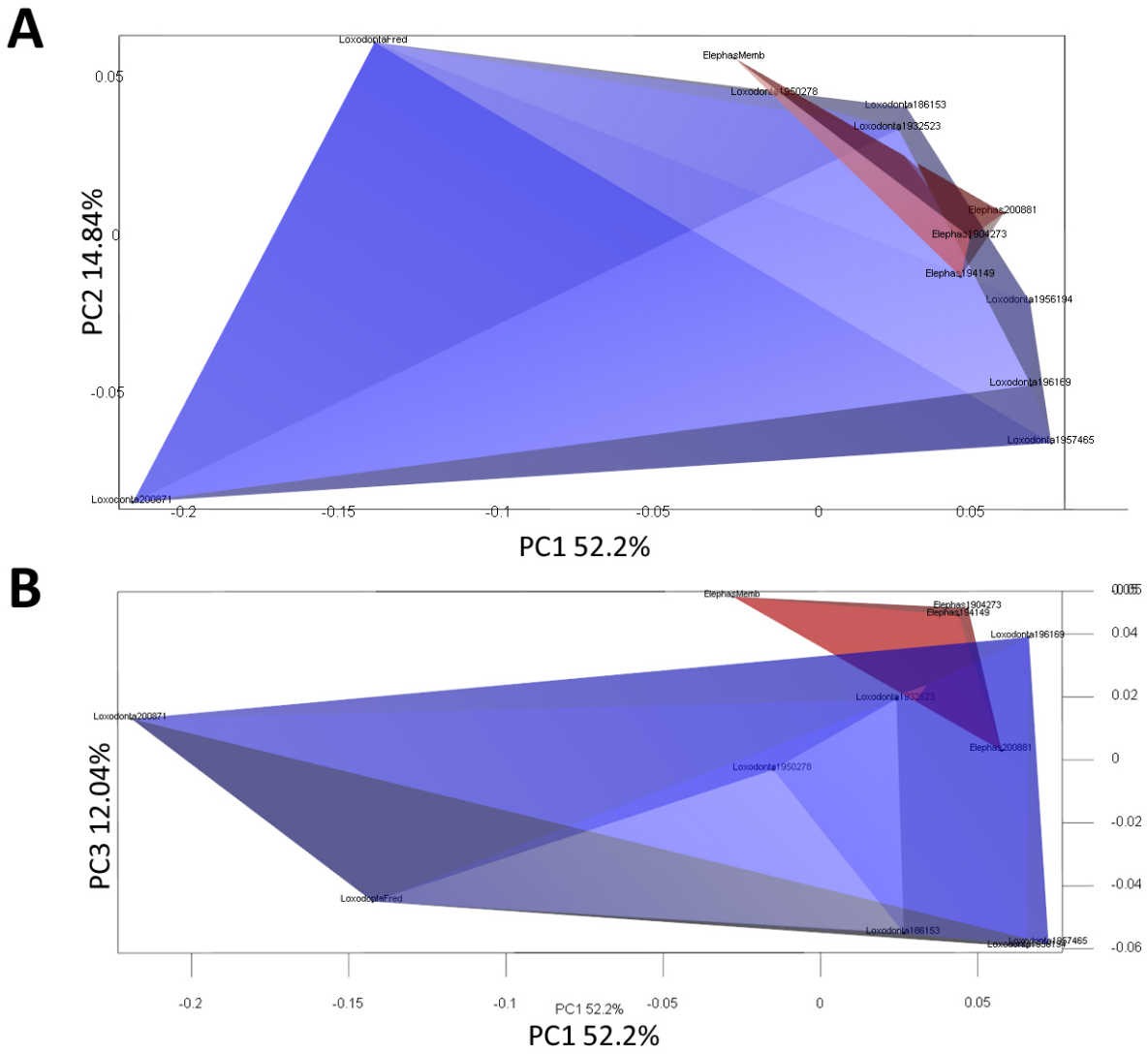

Figure IV.20 : Shape differentiation of the whole labyrinth of extant elephants (analysis **E1**). A) Principal components 1 and 2 and B) principal components 1 and 3. **Blue cluster:** Loxodonta. **Red cluster**: *Elephas*.

3.3.2. Analysis E2 restricted to the semicircular canals

Results of the PCA restricted to the semicircular canals of extant elephants are given in Fig IV.24. The first three axes of the PCA explain 66.1% (PC1: 36.2%, PC2: 17.1%, PC3: 12.8%) of the total variation of the labyrinth morphology.

Deformations

PC1 (36.2%)

The deformations of the bony labyrinth along the first axis (PC1 which explains 36.2% of the total variation) are given in Fig IV.21 in several views.

Towards the negative values, the semicircular canals are more slender along the first axis. The meeting point of the anterior and posterior semicircular canals is located lower. The anterior semicircular tends to be rounder.

Towards the positive values, the semicircular canals tend to be thicker. The meeting point of the anterior and posterior canals tends to be located higher.

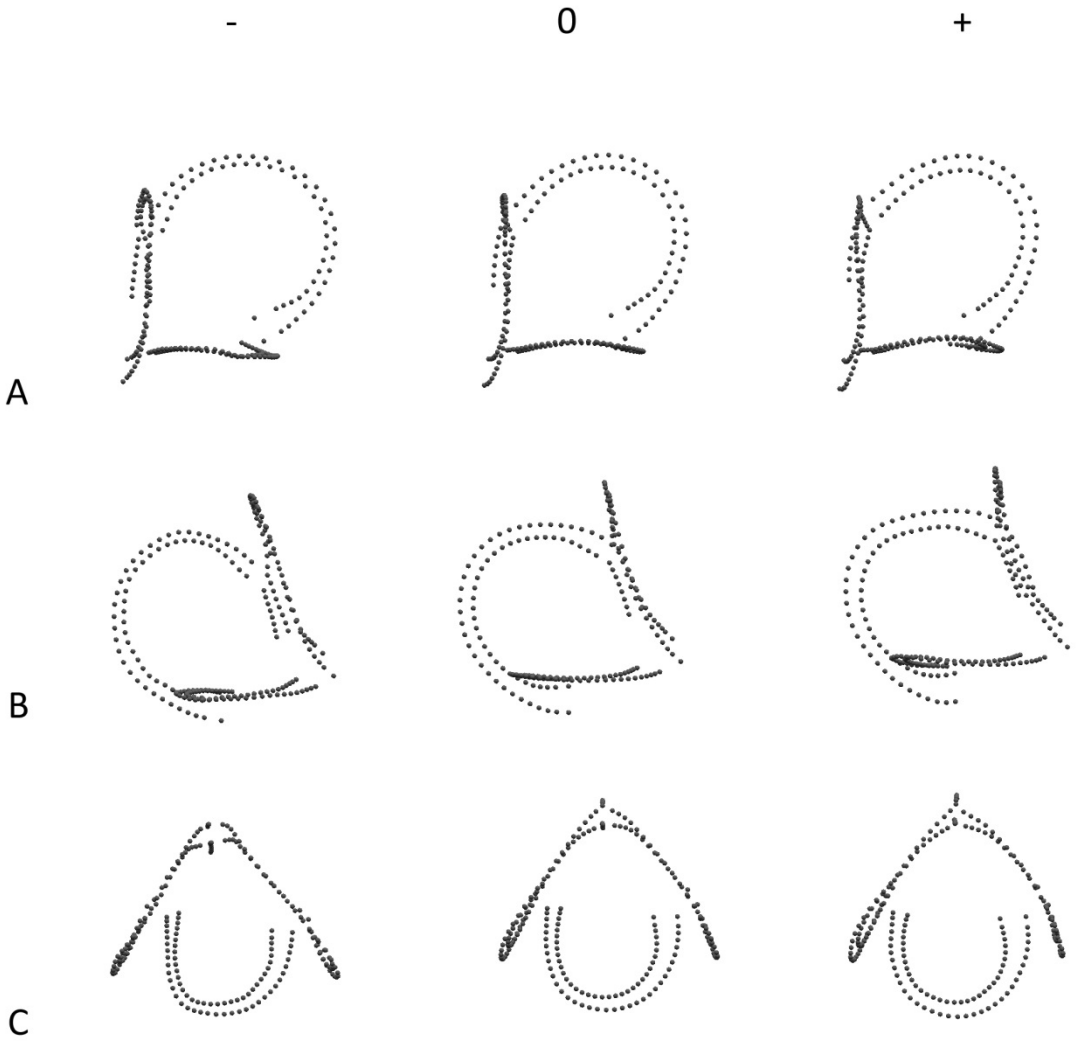

Figure IV.21 : Deformations along the first axis (PC1, 36.2%) of the analysis restricted to the semicircular canals of extant elephants (E2) in the view showing the plane of the anterior (A), posterior (B) and lateral (C) canals. "-" represents the extreme shape towards the negative extremity of the axis, "+" the extreme shape towards the positive extremity of the axis and "0" the mean shape on this axis.

PC2 (17.1%)

The deformations of the bony labyrinth along the second axis (PC2 which explains 17.1% of the total variation) are given in Fig IV.22 in several views.

Towards the negative values, the *crus commune* is shorter and stockier. The angle between the anterior and posterior canals is more obtuse. The lateral canal is slightly larger as well.

Conversely, towards the positive values, the *crus commune* is more elongated and the angle between the anterior and posterior canals is more acute.

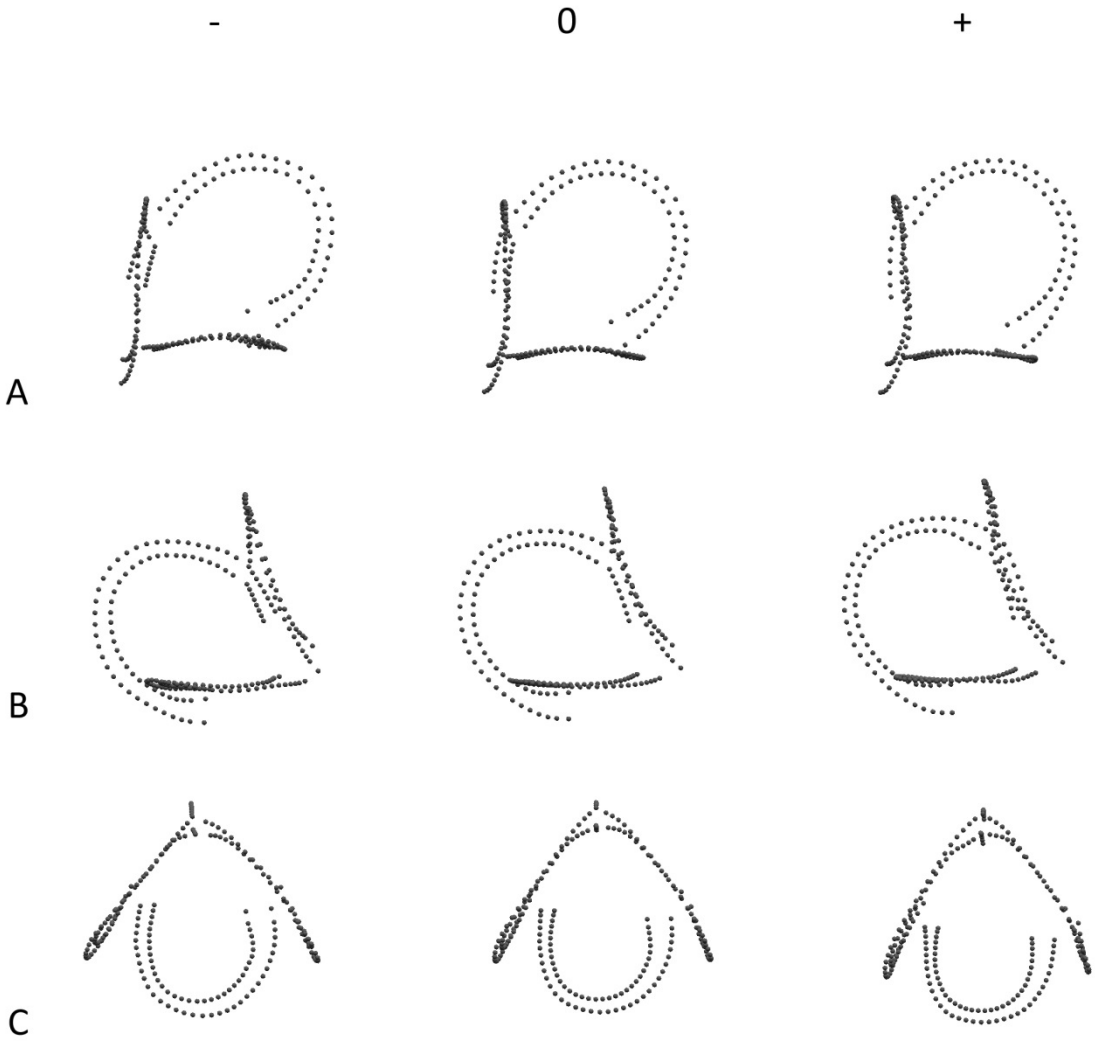

Figure IV.22 : Deformations along the second axis (PC2, 17.1%) of the analysis restricted to the semicircular canals of extant elephants (E2) in the view showing the plane of the anterior (A), posterior (B) and lateral (C) canals. "-" represents the extreme shape towards the negative extremity of the axis, "+" the extreme shape towards the positive extremity of the axis and "0" the mean shape on this axis.

PC3 (12.8%)

The deformations of the bony labyrinth along the third axis (PC3 which explains 12.8% of the total variation) are given in Fig IV.23 in several views.

Towards the negative values, the anterior canal is slightly larger and rounder. The lateral canal is thicker and the posterior canal slightly smaller, rounder and more undulated.

Towards the positive values, the anterior canal is slightly more oval. The angle between the anterior and posterior canals is more acute.

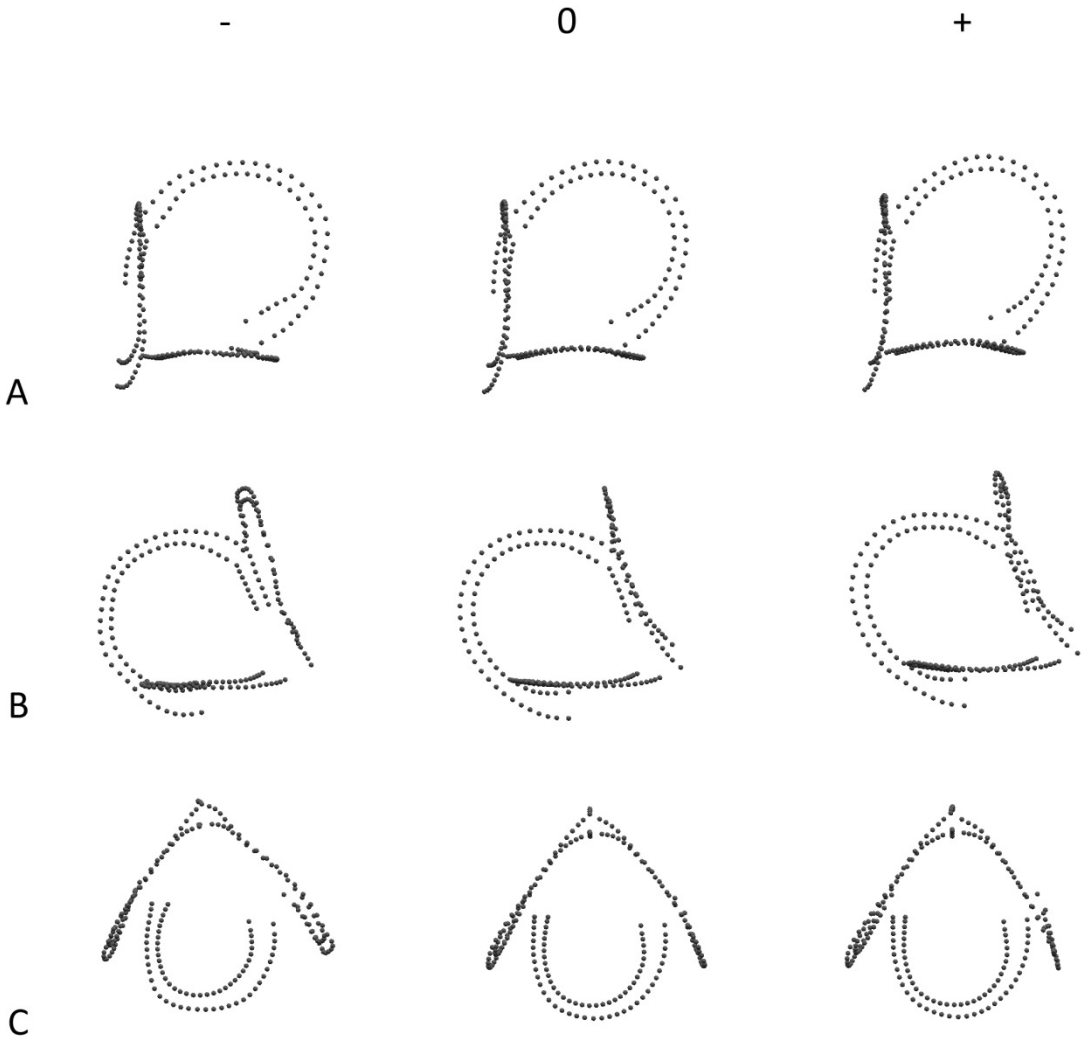

Figure IV.23 : Deformations along the third axis (PC3, 12.8%) of the analysis restricted to the semicircular canals of extant elephants (E2) in the view showing the plane of the anterior (A), posterior (B) and lateral (C) canals. "-" represents the extreme shape towards the negative extremity of the axis, "+" the extreme shape towards the positive extremity of the axis and "0" the mean shape on this axis.

Clusters

Apparently, the semicircular canals morphology only does discriminate well the African elephants from Asian elephants: the African elephant cluster and the Asian elephants cluster are not well separated within the morphospace (Fig IV.24). However, we can notice that the Asian elephants display particularly positive values along the first axis (PC1, 36.2%) which correlates with thicker canals and a higher meeting point of the anterior and posterior canals. Indeed, the general average thickness ratio of the semicircular canal is higher in *Elephas* (mean: 4.29) than in *Loxodonta* (mean: 3.62). Moreover, the *Elephas* specimens display positive values along PC3 (12.8%) which correlates with a more acute angle between the anterior and posterior canals. The mean of this angle is indeed lower in *Elephas* (76.1°) than in *Loxodonta* (78.5°), although the difference is slight. Moreover, this character is subject to variability in both genera. The *Elephas* specimens have a broad distribution along the PC2 axis which means that they exhibit a range of variability for the features that control this axis; these features are the aspect of the *crus commune* and the angle between the anterior and posterior canals. In contrast, the *Loxodonta* specimens have a broad distribution along at least the first three axes and they exhibit a significant morphological variability, although this is less marked than in the analysis including the cochlea.

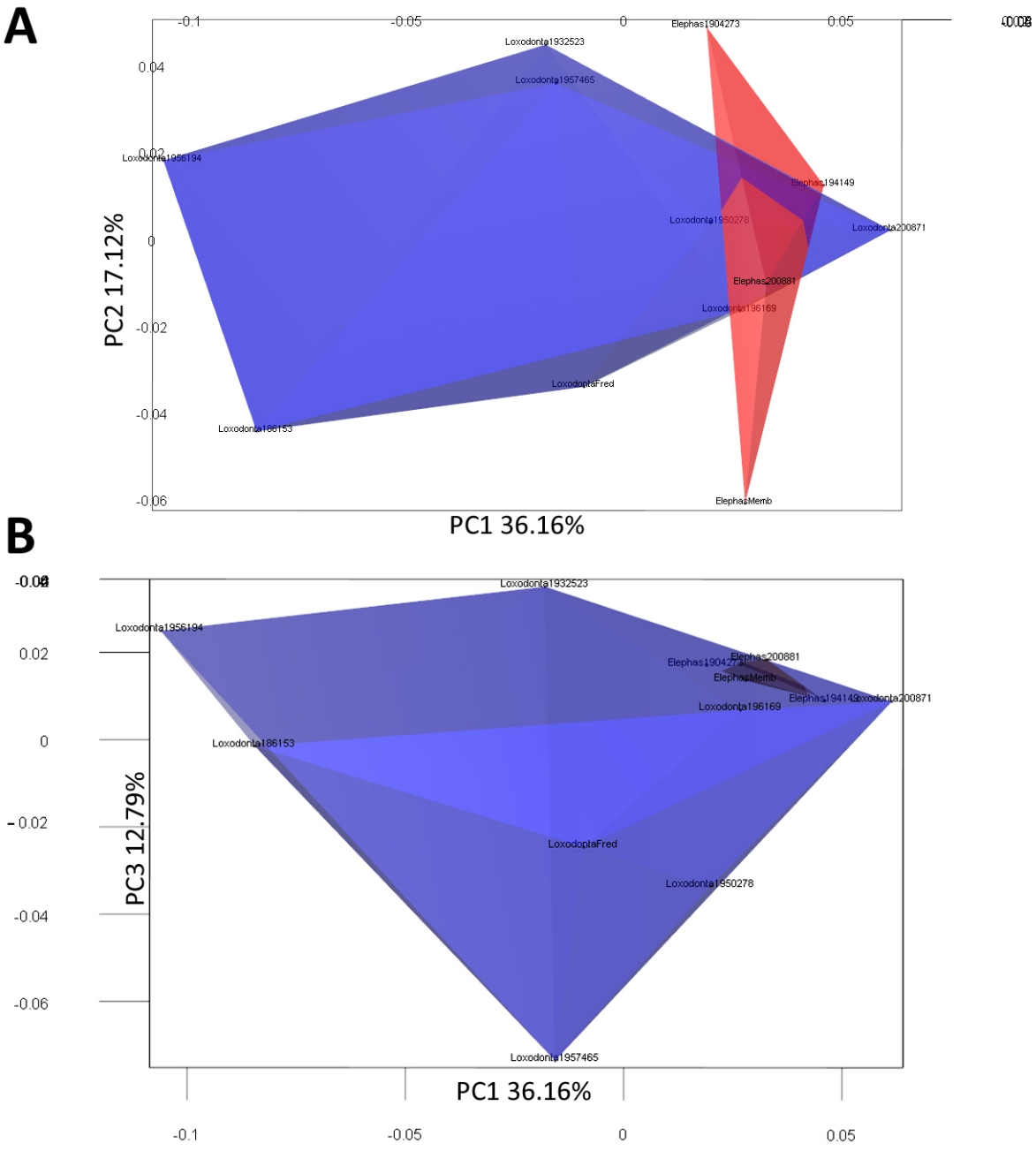

Figure IV.24 : Shape differentiation of the semicircular canals of extant elephants (analysis **E2**). A) Principal components 1 and 2 and B) principal components 1 and 3. **Blue cluster:** Loxodonta. **Red cluster**: *Elephas*.

4. Discussion

4.1. Impact of the addition of cochlear landmarks

The analysis restricted to semicircular canals permits to include a larger number of specimens into the analysis. On the other hand, the comparison of the results found in the two analyses permits to discuss about the importance of the cochlear morphology in the comparative anatomy of the afrotherian bony labyrinths. There are significant differences between the two sets of analyses: the principal components do not explain the same amount of the total variation (see Table IV.2) and some clusters are better defined in one analysis, while they are less defined in the other. These changes are greatly influenced by the presence/absence of the cochlea in the analysis but this can also be influenced by the additional taxa analyses restricted to the canals. Hence, we will first compare the two analyses performed on extant elephants. Indeed, while the first analysis (E1) includes the cochlea, the second (E2) is performed only on semicircular canals. However, the taxonomic sample is the same between the two analyses; hence the differences observed between the results are only due to the addition of cochlear landmarks into the dataset.

Table IV.2 : Relative participation of the principal components (PCs) in the different analyses (in % of the total variation)

	PC1	PC2	PC3	PC4	PC5	PC6
Afrotheria – Whole labyrinth (A1)	31.8	23.5	12.5	9.2	5	3.7
Afrotheria – Canals only (A2)	40.6	15.5	8.5	6.2	5.3	4.7
Proboscidea – Whole labyrinth (P1)	36.6	19.8	11	8.3	5.8	3.9
Proboscidea – Canals only (P2)	32.4	15.4	9.9	9.5	6.3	4.5
Extant elephants – Whole labyrinth (E1)	52.2	14.8	12	6.7	4.1	2.9
Extant elephants – Canals only (E2)	36.2	17.1	12.8	10.5	6.6	5.4

Extant elephants (E1 and E2)

In both analyses E1 and E2, the clusters of the African and Asian elephants overlap. However, we can note that the first PC explains a larger part (52.2%) of the total variation in the analysis including

the cochlea (E1). In fact, this axis in E1 is totally controlled by the cochlear morphology while the second and third axes are controlled by a combination of both cochlea and canals. The morphology of the cochlea has clearly a huge impact on the results. Indeed, the cochlea displays a great variability among extant elephants (Chapter II). The addition of the cochlea to the analysis results in a different repartition of the specimens within the morphospace. In E1, the most extreme taxa are *Loxodonta* MNHN.AC.ZM.2008-71 and CEB130168 which is easily explained by the particularly low number of turns of the cochlea they exhibit. On the other hand, the most extreme taxa are *Loxodonta* MNHN.AC.ZM.1861-53 and 1956-194 along PC1, and 1957-465 along PC2 in the E2 analysis. Clearly, the number of turns of the cochlea and its degree of coiling play a major role in the repartition of the specimens within the morphospace. Unfortunately, the intraspecific and even intra-individual variability of these features (see Chapter II) also adds noise and contribute to prevent the full discrimination of both genera.

Afrotheria (A1 and A2)

In both the analyses A1 and A2**,** the proboscidean and afrotherian clusters overlap. However, in both analyses, the elephantimorphs form a distinct cluster. Elephantimorphs are better discriminated in the analysis restricted to semicircular canals (A2) than in the analysis that includes the cochlea (A1). The first PC in A2 (analysis restricted to semicircular canals) explains more of the total variation than the first PC in A1 (analysis on the whole labyrinth). The cochlea explains a great part of the variability along the first PCs of A1. *Procavia* exhibits an extreme morphology in both A1 and A2 but it is more marked in A2 (analysis restricted to the semicircular canals). This means that the semicircular canals of *Procavia* are very different, in addition to its cochlea (which displays 3.5 turns). Indeed, the zone of insertion of the lateral canal into the vestibule is very high and close to the *crus commune* and the lateral canal crosses the plane defined by the posterior canal. Those features are seen in other Procaviidae (Benoit, 2013) that were not included in our analysis. In both analyses, the early proboscideans *Eritherium, Phosphatherium, Numidotherium* tend to group with the non-proboscideans afrotherians. This means that neither the

whole labyrinth morphology, nor the semicircular canals morphology allow to discriminate these taxa at the ordinal proboscidean level, at least based on the features measured with our landmark protocol. This suggests a high level of plesiomorphy in early proboscideans. This has yet to be tested with a phylogenetic analysis (see Chapter V) but we can assume based on these results that early proboscideans retains many characters from the ancestral morphotype of Afrotheria. Conversely, the elephantimorphs and *Prodeinotherium* display the modern proboscideans - probably derived - morphology. The major difference seen between analyses A1 and A2 is the possibility to discriminate the Elephantidae from other elephantimorphs when restricting the analysis to the semicircular canals (see discussion on P1 and P2 analyses in next paragraph).

Proboscidea (P1 and P2)

The comparison of the results found in P1 and P2 shows that the addition of the cochlear landmarks has significant influence on the analysis. In the analysis P1 with the cochlea, the Elephantidae does not form an exclusive cluster. The different specimens of *Anancus* are close to each other within the morphospace, but so are also other specimens of *Loxodonta*. By contrast, the analysis P2 restricted to the semicircular canals shows well distinct clusters. The early proboscideans form a cluster distinct from elephantimorphs. *Prodeinotherium* is located in a somewhat intermediary position between the two clusters. Within the Elephantimorpha, the Elephantidae forms a distinct cluster as well as all the *Anancus* specimens. Although some specimens are located closely to specimens from a different cluster (e.g., *Platybelodon* and the Elephantidae), there is no overlap of these clusters within the morphospace. This highlights the potential perturbation generated by the cochlear morphology. Within this particular taxa sample, it seems that the semicircular canals are more discriminant than the whole labyrinths. This is certainly due to the high level of intraspecific (and even intra-individual) cochlear variability observed in chapter II.

4.2. *Procavia capensis*, a derived afrotherian

As previously said, the elephantimorphs display a quite derived bony labyrinth morphology which is well distinctive from other afrotherians. However, early proboscideans display a

more generalized morphology significantly closer to non-proboscidean taxa. In fact most non-proboscidean afrotherians included in this analysis seems to share some resemblance as they are grouped together. They retain noticeable plesiomorphic conditions and are much closer to the ancestral morphotype of Afrotheria. However, *Procavia capensis* displays a very specialized morphology in our two analyses of the Afrotheria. This is explained mostly by the shape of its lateral canal. It expands posteriorly to the extent of crossing the plane defined by the posterior canals. Moreover, its insertion into the vestibule is located very high and close to the *crus commune*. This suggests that *Procavia capensis* is a peculiarly derived afrotherian which acquired many autapomorphies during evolution. Together with the other known procaviid species (Benoit, 2013), it indicates that the entire Procaviidae family is extremely derived, by contrast to the general postcranial construction, but in accordance with the morphology of the feet and hands (Gheerbrant et al, 2007). *Tenrec* and *Elephantulus* probably display labyrinths closer to the hypothetical ancestral morphotype of the Afrotheria. Only fossil species of sirenians are included in our analyses. Their peculiar labyrinth morphology (Benoit, 2013) makes it likely that the modern sirenians would exhibit similar levels of specialization, as observed in *Procavia*. This hypothesis remains to be checked with the inclusion of the modern sirenians in the analysis.

4.3. Differences between the bony labyrinth of *Arsinoitherium* and elephants

A surprising result of the analysis A2 restricted to the semicircular canals of Afrotheria is the location of *Arsinoitherium* within the morphospace. It is located towards the non-proboscidean afrotherians, not far from the new embrithopod (PM53) from the Ypresian of Morocco. Therefore, the semicircular canals of *Arsinoitherium* are morphologically closer to the ancestral morphotype of afrotherians than to the derived morphotype of elephantimorphs. This contrasts with previous conclusions that the ear region of *Arsinoitherium* is very similar to the ear of extant elephants. Such convergences were observed in the petrosal anatomy (Court, 1990) and in the bony labyrinth (Benoit et al. 2013b). In the latter study, *Arsinoitherium* is even found as the sister group of the clade (Moeritherium-Elephantimorpha) based on one homoplastic synapomorphy - the

stocky aspect of the semicircular canals - and four non-homoplastic synapomorphies (including the flattened cross-section of the semicircular canals). However, our results suggest that the shape of *Arsinoitherium* semicircular canals differs from the shape of elephantimorphs semicircular canals. It is closer to *Numidotherium* and to the new early embrithopod PM53. The axis PC1 best discriminates *Arsinoitherium* from the elephantimorphs. It is controlled by several features that can explain the difference between *Arsinoitherium* and elephantimorphs. First, the shape of the anterior semicircular canal tends to be modified along this axis. Indeed, the specimens located towards negative values display a rounder anterior semicircular canal while specimens located towards positive values display a more oval anterior canal. The angle between the major axis of this canal and the *crus commune* tends to be positive towards the positive values. The anterior semicircular canal of all studied elephantimorphs displays this morphology – oval, with a positive angle – with the exception of one *Gomphotherium* specimen (CBar coll. V2) which exhibits a round anterior canal. Noteworthy, the anterior canal of *Palaeoloxodon* displays a remarkably large angle between its major axis and the *crus commune*. On the other hand, all other studied afrotherians (including *Arsinoitherium*) display a round anterior canal. Another different trait is the aspect of the *crus commune* which is also controlled by axis PC1. It is thicker in elephantimorphs while it is more slender in other afrotherians. *Arsinoitherium* exhibits a relatively slender *crus commune* which explains its grouping with other afrotherians. The relative size of the lateral semicircular canal is also controlled by PC1 axis. The non-elephantimorph afrotherians tend to display relatively larger semicircular canals than the elephantimorphs. The lateral canal of *Arsinoitherium* is not particularly large (radius of curvature = 3.58) but compared to the vertical canals, it is relatively larger than in other elephantimorphs (except for two *Elephas* specimens, see Appendix 13). Finally, the location of the point of entry of the lateral canal into the vestibule is also controlled by PC1 axis. In *Arsinoitherium* and non-elephantimorphs it is high and close to the posterior ampulla, while it tends to be located lower in modern elephants. All these features contribute to make *Arsinoitherium* closer to non-elephantimorphs and suggest that it might be likely to separate them from

proboscideans in cladistic analyses based on semicircular canals characters (see chapter V).

4.4. *Loxodonta cyclotis* VS *Loxodonta africana*

At that time, we were not able to convincingly discriminate the African bush elephants (*Loxodonta africana*) from the African forest elephants (*Loxodonta cyclotis*). This is not surprising as the *Elephas* specimens could not be discriminated from those of *Loxodonta* as well. The great level of variability found in the number of turns of the cochlea of *Loxodonta* explains the wide distribution of the specimens within the morphospace in E1. However, there is also significant variability in the semicircular canals because the analysis restricted to canals (E2) failed to discriminate *Loxodonta* from *Elephas* and also known *Loxodonta cyclotis* from known *Loxodonta africana*. In PCA, the variation measured by the axes corresponds to the most variable morphologies and not to the morphologies that discriminates best the specimens. In perspective, a between group analysis should be performed in the future to see if it allows completely discriminating African elephants from Asian elephants.

4.5. Effect of the size

While the analyses presented in this chapter were performed on the bony labyrinth shape, which is supposedly free of size, size can still influence the results via allometry. To investigate allometry, phylogenetic generalized least squared regressions were performed. Details about the method are given in the 'Material and Methods' section of this chapter (§ 2.2.).

Regression parameters are given in Appendix 22 whereas adjusted R-squared and p-values are given in Table IV.3. To determine if size significantly influences values obtained on the principal components, one must look at the p-values of the regression. If the p-value is inferior to 0.05, then the effect of size is significant (it means that the chances that size does not influence the principal component are less than 5%). The adjusted R-squared value gives an indication of how much of the variation is explained by the regression. In A1, the first PC is not significantly influenced by the size of the organisms (p-value = 0.6429), suggesting that morphological variation depicted by this principal component (see 'Results' section) rather reflect taxonomical variation than size differences. Conversely, size appears to slightly influence morphological variation

depicted by PC2 and PC3 with R-squares of respectively 25% and 32%. In A2, only the first PC is significantly influenced by size, with an R-square of 38%. In P1, morphological variation along the first PC is not influenced significantly by size contrary to PC2 and PC3. In PC2, size drives almost all morphological variation with a R-square of 94%, while the effect is lower in PC3 (R-square of 48%). Finally, in P2, morphological variation along the PCs is influenced significantly by size. Size greatly influences the morphological variation along PC2 (R-square of 69%) and more moderately along PC1 (R- square of 42%) and PC3 (R-square of 25%).

Table IV.3 : Results of the phylogenetic generalized least-squared regressions performed on the first three PCs of analyses A1 (whole labyrinth of Afrotheria), A2 (semicircular canals of Afrotheria), P1 (whole labyrinth of Proboscidea) and P2 (semicircular canals of Proboscidea). Bold p-values are for principal components significantly influenced by the size.

		p-value	Adjusted R-square
A1	PC1	0.6429	-0.05858
	PC2	**0.03247**	0.2525
	PC3	**0.01584**	0.3232
A2	PC1	**0.001288**	0.3823
	PC2	0.637	-0.03808
	PC3	0.3785	-0.009078
P1	PC1	0.6636	-0.09704
	PC2	**2.74E-06**	0.9371
	PC3	**0.01549**	0.4824
P2	PC1	**0.005409**	0.4191
	PC2	**7.14E-05**	0.6932
	PC3	**0.03208**	0.2538

5. Conclusion

Our geometric morphometric analyses based on 3D landmarks of the labyrinth of proboscideans and other afrotherians help to answer to the three main questions investigated in this chapter.

1. We find some overlap between some proboscideans and afrotherians. The early proboscideans (*Eritherium, Phosphatherium, Numidotherium*) display a morphology more similar to other afrotherians. This is indicated by our two sets of analysis (with or without the cochlea) showing that the cochlea and the semicircular canals of early proboscideans are both morphologically more similar to other afrotherians than to other proboscideans, as the result of retained symplesiomorphies. Conversely, the proboscidean clade containing the Elephantimorpha and the Deinotheriidae is discriminated from other afrotherians in both analyses (although the discrimination is more marked in the analysis restricted to the semicircular canals).

2. It is possible to discriminate several groups of proboscideans using the 3D landmarks-based geometric morphometrics. First, the elephantimorphs clearly show a distinct morphology from early proboscideans in the two analyses restricted to proboscideans (with or without the cochlea). The deinotheriid *Prodeinotherium* is located at an intermediate position between the early proboscideans and the elephantimorphs, but closer to the latter. This shows a significant morphological similarity between the members of the clade containing Elephantimorpha and Deinotheriidae. Members of this clade are located preferably towards the positive extremity of PC1 and PC2. Based on the observation of the deformations along the axes we identified the morphological trend of the members of this clade. They tend to display cochlea with more turns and that forms a larger angle with respect to the lateral canal plane. The axis of rotation of the apical turn of the cochlea tends to be offset with respect to the axis rotation of the basal turn. The area enclosed by the lateral canal is smaller and the semicircular canal is thicker in general. The *crus commune* tends to be shorter and thicker as well. The anterior and posterior canals are more oval and tend to display apical extensions. The angles between the lateral canals and the angle

between the posterior and lateral canals tend to decrease. Finally, the point of entry of the lateral canal into the vestibule is located higher with respect to the posterior ampulla. On the other hand, it was also possible to discriminate within the elephantimorphs the Elephantidae family in the analysis restricted to semicircular canals, but not in the analysis on the whole labyrinth. This suggests that only the semicircular canals characters are significant to characterize the elephantid family. Compared to the other elephantimorphs, the elephantids are located preferably towards the positive end of PC1 and the negative end of PC2. Therefore, the elephantids display thicker canals than in the other elephantimorphs, a lateral canal even smaller and a stockier *crus commune*. Moreover, they exhibit a point of entry of the lateral canal located lower with respect to the posterior ampulla.

3. It was not possible using classic PCA analyses to fully discriminate the Asian elephants from the African elephants. Even though the Asian elephants form a limited cluster in both analyses, it always overlaps with the large cluster of the African elephants, highlighting the greater morphological variability of *Loxodonta*. Unexpectedly, this greater variability is not the result of the presence of two species within this genus, as the *Loxodonta cyclotis* specimens do not form a distinct group from *Loxodonta africana* in our analyses.

The regressions showed that the majority of the typical elephant morphology is not influenced by size. This is particularly true for the whole labyrinth. However, the morphology of the canals only displays a stronger (though moderate) influence of size.

To conclude, we were able to discriminate the morphology of the labyrinth of several proboscideans groups, mostly for the clade (elephantimorphs-deinotheriids) and for the elephantid family. Our geometric morphometric analyses evidence the morphological trend of these groups. The identified morphological trends corroborate our anatomic observations described in previous Chapters II and III. They help to define the phylogenetic characters used in our cladistic analysis of the proboscideans petrosal morphology (chapter V). They especially help to establish the primary homologies of the labyrinth characters.

CHAPTER V

Evolution of the ear region characters within the Proboscidea and the Afrotheria

1. Introduction

Previous chapters provide a comprehensive study of the bony labyrinth and petrosal anatomy of proboscideans. Even though these studies highlight a significant level of intraspecific variation in the proboscidean order, many features are constant at the species level and are therefore interesting to study in a phylogenetic perspective. The main objective of this chapter is to investigate the evolution of the inner ear and petrosal characters within the Proboscidea. To do so, a cladistic analysis is performed on the features that were defined in previous chapters. Phylogenetic analyses restricted on a narrow anatomical region are not appropriate to reconstruct phylogenetic relationships. Hence, we do not intend to review the proboscidean tree here. However, our study provides the opportunity to test the phylogenetic signal carried by the ear region of proboscideans. Except for the preliminary analysis of Schmitt & Gheerbrant (2016) on very few proboscidean taxa (Chapter I), this is the first detailed phylogenetic study of the petrosal characters of the proboscideans. A previous study (Benoit et al. 2013b) focused on the ear region of the Tethytheria, but only four proboscidean taxa are included in this work; these include the early representatives *Phosphatherium*, *Numidotherium* and *Moeritherium,* and a general Elephantimorpha taxon. Moreover, the inner ear anatomy of *Eritherium* was still unknown at the time. The cladistic analysis performed in Chapter V is substantially more exhaustive. It includes the inner ear anatomy of early taxa *Eritherium* and *Phosphatherium*, the deinotheriid *Prodeinotherium,* and 11 elephantimorph genera. Additionally, it includes newly defined characters and it takes into account the intraspecific variation. This chapter also extends the analysis at the larger scale of the afrotherians in order to evaluate the significance of the new petrosal characters identified in this work. The phylogenetic message carried by the ear region in this group has been thoroughly investigated before (Benoit, 2013). We only explore here the impact of new characters and several new or recently described afrotherian taxa (the Moroccan embrithopod, *Ocepeia*, proboscideans) in the evolutionary hypotheses about the ear region.

2. Material and methods

As previously said, two sets of analyses were performed, one restricted to the Proboscidea and one extended to the Afrotheria. Taxa samples and methods for each of these two sets are detailed in this section.

2.1. Taxon sampling

2.1.1. Proboscidea

The characters studied in our cladistic analysis were defined and the matrix was constructed thanks to the observations made in chapters I to IV. Most of the information comes from the anatomical observations made on extinct and extant proboscideans during the thesis. Complementary information was found in the literature. The taxa sample of the first cladistic analysis is restricted to Proboscidea. The stem paenungulate *Ocepeia* (Gheerbrant et al. 2014, 2016, and further observations made in the thesis) and the early placental *Protungulatum* (O'Leary, 2010; Orliac & O'Leary, 2016) were defined as outgroups. The ingroup comprises proboscidean taxa described in chapters I to III. *Eritherium* and *Phosphatherium* are the earliest-known proboscideans and information about their ear region anatomy have been described in Schmitt & Gheerbrant (2016) (chapter I). *Numidotherium* and *Moeritherium* were described in Court & Jaeger (1991), Court (1992), Court (1994) and Benoit et al. (2013b). New specimens of these two taxa were studied here and used to fill the matrix. There was some information about the petrosal of *Gomphotherium angustidens* in Tassy (2013), but most of the phylogenetic characters were coded thanks to specimens newly studied during the thesis. The other taxa included in the analysis (*Prodeinotherium*, *Mammut*, *Platybelodon*, *Mammuthus columbi*, *Mammuthus primigenius*, *Palaeoloxodon*, *Elephas*, *Loxodonta*, *Anancus*, *Stegodon*, *Cuvieronius* and *Stegomastodon*) were all coded using new observations made in chapters II and III which brings the number of taxa to a total of 19 taxa (including outgroups).

2.1.2. Afrotheria

The second set of analyses extends to Afrotheria. It is composed with the same 19 taxa used in the analyses focused on the Proboscidea to which 11 taxa have been added, bringing the total number of taxa to 30 (including outgroups). The

embrithopods are represented by *Arsinoitherium* (Court, 1990; Benoit et al. 2013b; new observations from Chapter III) and by the unpublished petrosal of a new Moroccan embrithopod (new observations from Chapter III). The sirenians are represented by *Prorastomus* and the isolated sirenian petrosal from Chambi (Benoit et al. 2013a; new observations from Chapter III). The hyracoids are represented by *Seggeurius* (Benoit et al. 2016), *Helioseus* (Benoit, 2013) and *Titanohyrax* (Benoit, 2013). The macroscelids are represented by *Chambius* (Benoit et al. 2013c). The Bibymalagasia is represented by *Plesiorycteropus* (Benoit et al. 2015). The unknown elephantimorph labyrinth described in Ekdale (2011) has also been coded and included in the analysis for identification. Finally, the late Cretaceous zalambdalestid *Kulbeckia* (Ekdale et al. 2004; Ekdale, 2013) was included as the outgroup taxon. We chose to add only fossil taxa to the analysis. Hence, while the Paenungulata is well represented in the taxa sample, only a few non-paenungulate afrotherians are represented. Representatives of the Afrosoricida and the Tubulidentata are not included in the analysis (although Plesiorycteropus is believed to be included in Tubulidentata by some authors).

2.2. Methods

2.2.1. Cladistic analysis performed on the Proboscidea

The cladistic analysis performed on Proboscidea was carried out using the software PAUP 3.3.1 (Swofford, 1991). The analysis is based on 32 ear region characters: 12 petrosal characters and 20 bony labyrinth characters. The complete list of characters is given in Appendix 23. Details about the characters are given in the following section of this chapter (section 3, 'Characters'). In this section, the states of the characters are given as well as illustrations of each state. Details about the coding method and choices are also given as well as the distribution of the characters states within Proboscidea. Among the 32 characters, six have more than two states. These multi-state characters were all treated as ordered, as we consider them to correspond to morphological clines. In the analysis restricted to the Proboscidea, eight characters are not informative (4, 6, 8, 14, 25, 26, 27 and 30). *Ocepeia* and *Protungulatum* are used as outgroups. We performed a heuristic search and all characters were equally weighted. The matrix is given in Appendix 24.

2.2.2. Character cartography performed on the Proboscidea

Introducing characters of the ear region in the published matrices of Proboscidea (e.g. Delmer, 2005) yields a set of problems. Although the total evidence approach (Kluge, 1989) has been widely accepted it sometimes brings undesirable ambiguities or noise (i.e. Lecointre & Deleporte, 2000), especially when the taxonomic samples are too different in terms of both taxa and characters. On the one hand several terminal taxa used in the present analyses have not been coded in previously published analyses. On the other hand, many terminal taxa in previously published analyses do not bear ear-region information. The combination of these two difficulties can only bring the inflation of missing data (an undesirable result in respect to total evidence) unless a careful revision and recoding of all known proboscidean characters used by previous authors is done, which is beyond the scope of this study. Sometimes more is less. Hence the decision was taken to 1) compare the result of the characters of the ear region to the presently accepted phylogeny of Proboscidea, and 2) map the ear region characters on the presently accepted phylogeny of Proboscidea, so that both congruence and incongruence in distributions of characters between the two resulting analyses can be discussed and explained. The consensual tree used to map the characters is a synthesis of Tassy (1994), Tassy (1996), Kalb et al. (1996), Shoshani (1996) and Shoshani et al. (1998).

2.2.3. Cladistic analysis performed on the Afrotheria

Two cladistic analyses were performed on the Afrotheria, using the software TNT (Goloboff et al. 2008). The analyses are based on the same 32 ear region characters used in the Proboscidea analysis. The multi-state characters were treated as ordered as well, as we consider them to be morphological clines. In the analyses extended to Afrotheria, three characters remain not informative (8, 25 and 27). *Kulbeckia* is defined as the outgroup. A first analysis was carried out with all the characters equally weighted and using a traditional search (10 random seeds and 100 replicates). The second analysis was carried out using implied weighting, in order to minimize the weight of very homoplastic characters. A traditional search was held as well (10 random seeds and 100 replicates). The matrix is given in Appendix 25.

3. Characters

1. Subarcuate fossa: (0) deep; (1) shallow; (2) absent

This character was used by Benoit et al. (2013b; character 23), but its states are modified here. The subarcuate fossa is a depression located on the cerebellar surface of the petrosal. It houses the paraflocculus of the cerebellum in life. Most mammals display a deep subarcuate fossa (0). A deep fossa can be spherical (e.g. *Eritherium*) or more conical (e.g. *Ocepeia*), but these states related to its shape are not discriminated in our study. Several afrotherians (e.g. *Phosphatherium*) display a more superficial fossa (1). In this state (1), the fossa depth is clearly more moderate than in state (0), but the outlines of the fossa remain well distinct by contrast to state (2). In state (2) the subarcuate fossa is more superficial with no a clear outline or is even not distinct at all. The character states of the subarcuate fossa are illustrated in Fig V.1.

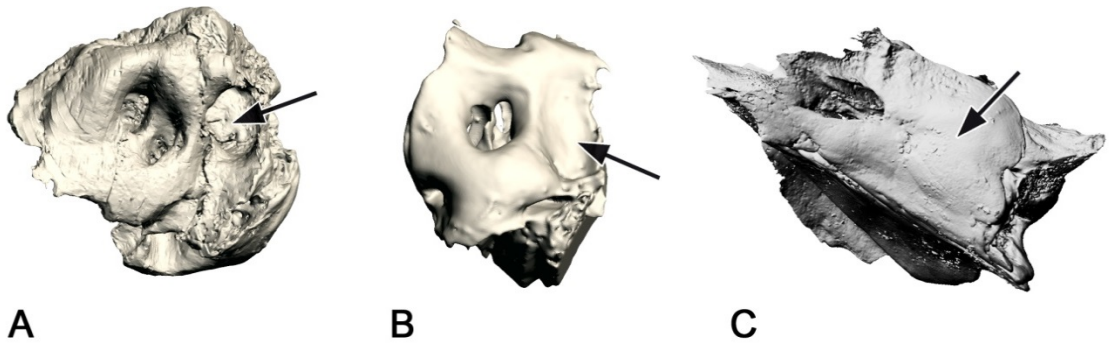

Figure V.1 : Character 1, depth of the subarcuate fossa (cerebellar view), 3 states. A : state 0 (*Eritherium azzouzorum*); B: state 1 (*Phosphatherium escuilliei*, mirrored); C: state 2 (*Elephas maximus,* mirrored).

Ocepeia	*Protungulatum*	*Eritherium*	*Phosphatherium*	*Numidotherium*	*Moeritherium*	*Prodeinotherium*	*Mammut*	*Platybelodon*	*Gomphotherium*	*Cuvieronius*	*Stegomastodon*	*Stegodon*	*Anancus*	*Loxodonta*	*Palaeoloxodon*	*Elephas*	*M. columbi*	*M. primigenius*
0	0	0	1	2	2	2	2	2	2	2	2	2	2	2	2	2	2	2

2. Internal auditory meatus: (0) opens perpendicular to the cerebellar surface, (1) is oriented antero-posteriorly

The internal auditory meatus consists of an opening on the cerebellar surface of the petrosal. It is composed of the *foramen acusticum inferior* and the *foramen acusticum superior* that convey the cranial nerves VIII and VII respectively. Two different orientations of the meatus have been observed. In state (0) most mammals display a meatus with foramens that convey the nerves dorsally, hence perpendicular to the cerebellar surface. In state (1), some proboscideans exhibit a meatus with foramens that convey the nerves anteriorly, hence parallel to the cerebellar surface. Both states are illustrated in Fig. V.2. This character is best seen with the petrosal oriented with the cerebellar surface parallel to the screen (observer). If the foramens of the meatus are clearly visible, the character is coded 0. Conversely, if the foramens of the meatus are not distinct in this view but clearly observable in anterior view, then the character must be coded 1. To our knowledge, this is an original character that has not been used in previous cladistic analyses of proboscideans and afrotherians.

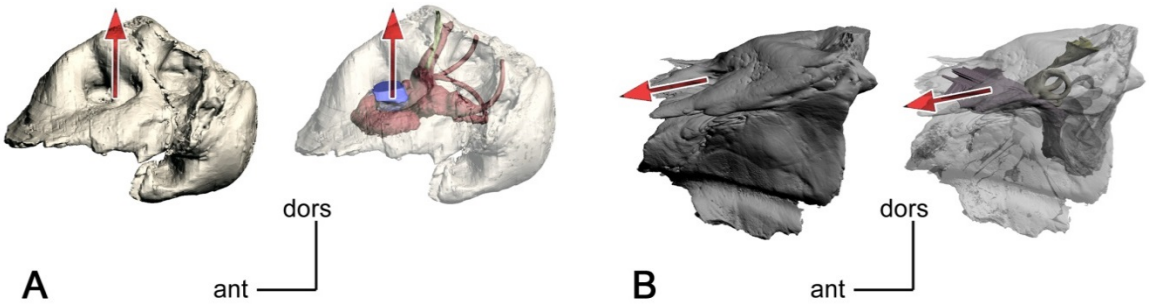

Figure V.2 : Character 2, internal auditory meatus orientation, 2 states. A: state 0 (*Eritherium azzouzorum*); B: state 1 (*Elephas maximus*).

Ocepeia	*Protungulatum*	*Eritherium*	*Phosphatherium*	*Numidotherium*	*Moeritherium*	*Prodeinotherium*	*Mammut*	*Platybelodon*	*Gomphotherium*	*Cuvieronius*	*Stegomastodon*	*Stegodon*	*Anancus*	*Loxodonta*	*Palaeoloxodon*	*Elephas*	*M. columbi*	*M. primigenius*
0	0	0	0	0	0	1	1	?	1	1	1	1	1	1	1	1	1	1

3. Perilymphatic foramen: (0) divided into the *fenestra cochleae* and the *aquaeductus* cochleae during ontogeny, (1) retained in adults

This character was used in previous analyses (Court, 1990; Benoit et al. 2013b: character 16). The *aquaeductus cochleae* houses the perilymphatic sac. The *fenestra cochlea* is an opening of the petrosal at the level of the *scala tympani*. In the early stages ontogeny, these two openings are not separated but instead form a unique perilymphatic foramen. This foramen generally divides into the *aquaeductus cochleae* and the *fenestra cochleae* later during ontogeny (state 0). However, some taxa retain the perilymphatic foramen in adult life (state 1). Illustrations of the character states are given in Fig V.3 below. The presence of the *aquaeductus cochleae* in the jugular fossa of the petrosal with a trumpet like shape in 3D models of the bony labyrinth clearly corresponds to state 0. A unique perilymphatic foramen is located near the *crista interfenestralis* (under the *promontorium*) and looks like a very large and elongated *fenestra cochleae* in 3D models of the bony labyrinth. The character was coded 0 in *Eritherium* based on the presence of a foramen in the jugular fossa that is very likely for the *aquaeductus cochleae*.

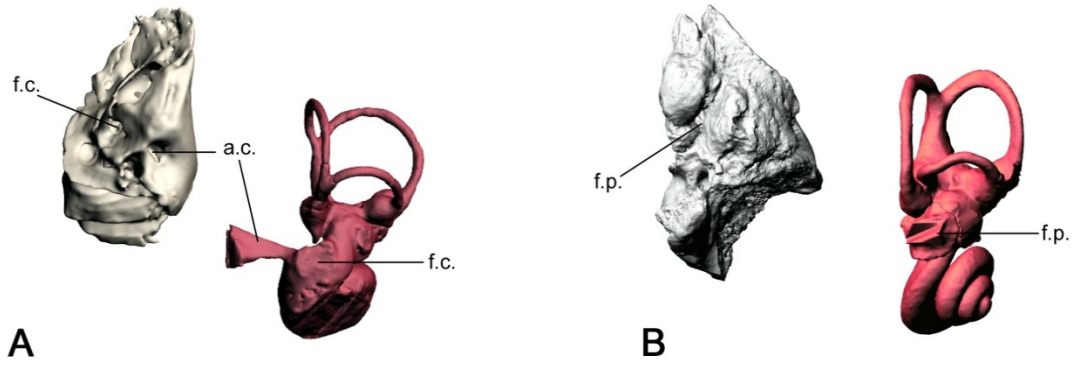

Figure V.3 : Character 3, perilymphatic foramen, 2 states. A: state 0 (*Phosphatherium escuilliei*) ; B : state 1 (*Gomphotherium angustidens*). Caption: **a.c.** *aquaeductus cochleae,* **f.c.** *fenestra cochleae*, **f.p.** unique perilymphatic foramen.

Ocepeia	*Protungulatum*	*Eritherium*	*Phosphatherium*	*Numidotherium*	*Moeritherium*	*Prodeinotherium*	*Mammut*	*Platybelodon*	*Gomphotherium*	*Cuvieronius*	*Stegomastodon*	*Stegodon*	*Anancus*	*Loxodonta*	*Palaeoloxodon*	*Elephas*	*M. columbi*	*M. primigenius*
0	0	0	0	0	0	1	1	?	1	1	1	?	1	1	1	1	1	1

4. Mastoid apophysis: (0) visible on the skull laterally, (1) amastoidy

The mastoid apophysis is a bony prominence that is generally apparent on the skull, at the postero-lateral corner, between the exoccipital and the squamosal (Gheerbrant et al. 2005). Some taxa do not exhibit such prominence and the petrosal is not visible on the lateral part of the skull; this condition is called amastoidy (state 1). Most of the specimens studied during this thesis were isolated petrosals and were therefore not observed in connection with the other skull bones. However, comparisons of the specimens with other amastoid petrosals allow assessing the presence of an amastoidy condition. Paenungulates classically exhibit amastoidy (Gheerbrant et al. 2005). This condition is confirmed in extant elephants (Chapter II). The condition was found in every other studied proboscidean, making this character constant in Proboscidea. However, the absence of a visible mastoid apophysis on the skull laterally is coded unknown in *Eritherium*. However, since the petrosals of *Ocepeia* and *Eritherium* display really similar morphologies, it is likely that the petrosal of *Eritherium* exhibit amastoidy as well.

Ocepeia	*Protungulatum*	*Eritherium*	*Phosphatherium*	*Numidotherium*	*Moeritherium*	*Prodeinotherium*	*Mammut*	*Platybelodon*	*Gomphotherium*	*Cuvieronius*	*Stegomastodon*	*Stegodon*	*Anancus*	*Loxodonta*	*Palaeoloxodon*	*Elephas*	*M. columbi*	*M. primigenius*
1	0	?	1	1	1	1	1	1	1	1	1	1	1	1	1	1	1	1

5. Shape of the *tegmen tympani*: (0) poorly developed, (1) prominent and inflated prominent, (2) forming a flat and large cerebral surface

The shape of the *tegmen tympani* was used in previous cladistic analyses such as Benoit et al. (2013b); however, we modified the coding to fit with the character states of the proboscideans. The shape of the *tegmen tympani* differs within mammals. Some taxa display a poorly developed *tegmen tympani* (state 0). In this case, the *tegmen tympani* is a small and uninflated bony structure. Some taxa exhibit a much more prominent *tegmen tympani* (state 1). The structure is inflated and can take different forms (tubular, kidney-shaped…). Finally, most of proboscidean taxa studied here displays a characteristic *tegmen tympani.* It is very prominent but rather flat and forms a large surface of bone on the cerebral surface of the petrosal (state 2). This surface is separated from the cerebellar surface by a more or less sharp ridge called the *crista partis petrosa*. Illustrations of the character states are given in Fig V.4.

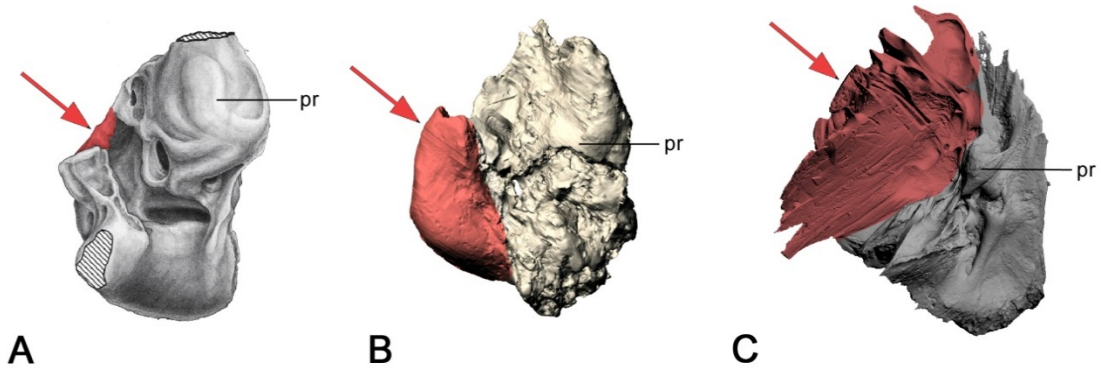

Figure V.4 : Character 5, shape of the *tegmen tympani*, 3 states. A: state 0 (*Protungulatum* ; modified after O'Leary 2010); B: state 1 (*Eritherium azzouzorum*); C: state 2 (*Loxodonta africana*). Caption: **pr**, promontorium.

Ocepeia	*Protungulatum*	*Eritherium*	*Phosphatherium*	*Numidotherium*	*Moeritherium*	*Prodeinotherium*	*Mammut*	*Platybelodon*	*Gomphotherium*	*Cuvieronius*	*Stegomastodon*	*Stegodon*	*Anancus*	*Loxodonta*	*Palaeoloxodon*	*Elephas*	*M. columbi*	*M. primigenius*
1	0	1	?	1	?	2	2	2	2	2	2	2	2	2	2	2	2	2

6. *Hiatus Fallopii*: (0) forms a discrete foramen within the petrosal; (1) forms a notch (fallopian notch)

This character was used in previous cladistic analyses of the petrosal of afrotherians. We used this character from Benoit et al. (2013b, character 18) with unchanged coding. The facial nerve is contained in the fallopian canal (sometimes called facial canal) of the petrosal. It runs close to the *promontorium* and exits the petrosal anteriorly. The exit point of the facial nerve from the petrosal forms either a discrete foramen (state 0), or a notch (state 1). Illustrations of the character states are given in Fig V.5. In state 0 (foramen present), the exit point is entirely enclosed by bony structures. In some specimens such as *Phosphatherium*, the petrosal is broken in this area because the bony roof of the facial canal is fragile. However, the exit point of the facial nerve was clearly entirely outlined by bony structures and hence is coded 0. Conversely, the exit point of the facial nerve can be defined by bony structures that are not fully joined, as observed in *Numidotherium* and *Arsinoitherium* (Benoit et al. 2013b). This structure is called fallopian notch (state 1).

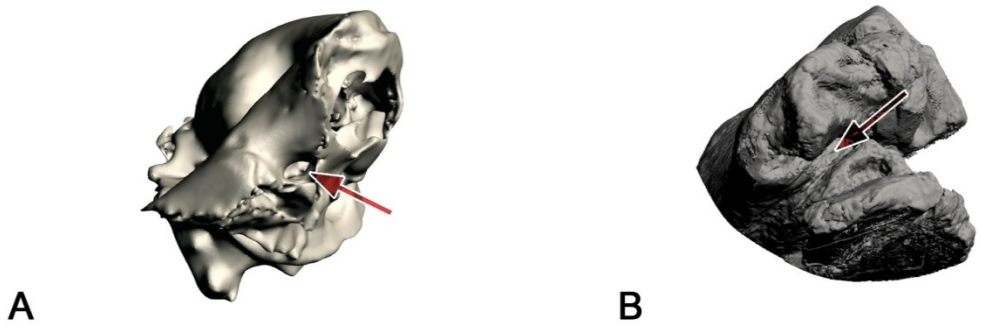

Figure V.5 : Character 6, *hiatus Fallopii*, 2 states. A, state 0 (*Phosphatherium escuilliei*); B: state 1 (*Numidotherium koholense*).

Ocepeia	*Protungulatum*	*Eritherium*	*Phosphatherium*	*Numidotherium*	*Moeritherium*	*Prodeinotherium*	*Mammut*	*Platybelodon*	*Gomphotherium*	*Cuvieronius*	*Stegomastodon*	*Stegodon*	*Anancus*	*Loxodonta*	*Palaeoloxodon*	*Elephas*	*M. columbi*	*M. primigenius*
?	0	?	0	1	?	?	?	?	?	?	?	?	?	0	?	0	?	?

7. Petrosal pneumatization: (0) absent, (1) present

The petrosal of some mammals display bony air cells: this feature is called pneumatization. The role of the pneumatization can be functional (e.g. sound transmission) or to reduce skull weight. For instance, the skull of some large mammals such as elephants is heavily pneumatized in order to lighten its weight. Pneumatic air cells of the petrosal are generally found in the most peripheral layers of bone, the center of the petrosal being generally very dense. Very large pneumatic cells are commonly found in the mastoid region of extant elephants (see chapter II). On the other hand, the inflated *tegmen tympani* usually exhibit pneumatic cells as well (e.g. *Ocepeia* and *Eritherium*). Finally, the pneumatic cells can be quite small and dispersed in the whole petrosal. Here, only the presence of pneumatic air cells is studied in this character. Taxa displaying pneumatization are all coded 1. Conversely, taxa lacking pneumatic cells in the petrosal are coded 0. Illustrations of the character states are given in Fig V.6 below.

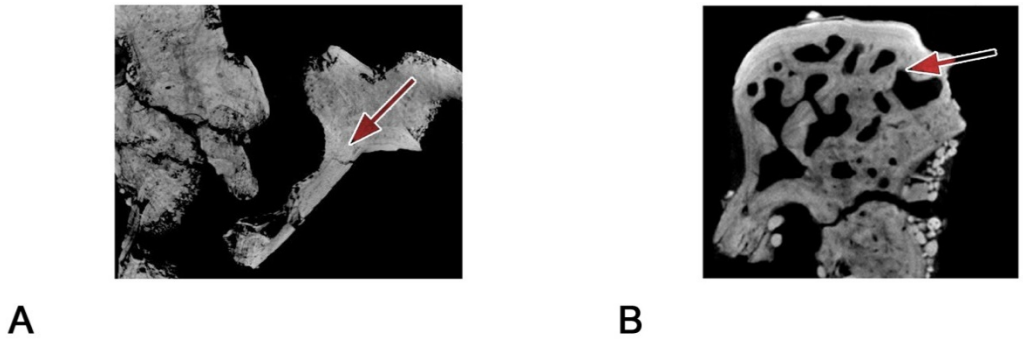

Figure V.6 : Character 7, petrosal pneumatization, 2 states. A: state 0 (*Phosphatherium escuilliei)*; B: state 1 (*Eritherium azzouzorum*).

Ocepeia	*Protungulatum*	*Eritherium*	*Phosphatherium*	*Numidotherium*	*Moeritherium*	*Prodeinotherium*	*Mammut*	*Platybelodon*	*Gomphotherium*	*Cuvieronius*	*Stegomastodon*	*Stegodon*	*Anancus*	*Loxodonta*	*Palaeoloxodon*	*Elephas*	*M. columbi*	*M. primigenius*
1	?	1	0	1	01	0	0	0	0	0	0	0	0	01	0	01	0	1

8. Prootic sinus: (0) absent, (1) present

The prootic sinus is a groove that runs anterolateral to the subarcuate fossa of the petrosal. The presence of this groove (1) is a plesiomorphic trait in Eutheria (Ekdale et al. 2004) and is observed in marsupials (e.g. *Didelphis*) and early eutherians (e.g. the 'Zhelestidae' petrosal described in Ekdale et al. 2004). A sinus running anterolateral to the subarcuate fossa was hypothesized to be the prootic sinus in *Eritherium* (see Chapter I, Schmitt & Gheerbrant, 2016) but further examination does clearly not support this determination, and the state of *Eritherium* is coded unknown. The character is absent in all studied proboscideans (state 0) and therefore is constant within taxa of this order. Hence, this character is more useful in less restricted analyses performed on Afrotheria or even Eutheria. This character comes from Benoit et al. (2013b) and the coding was left unchanged. Illustrations of the character states are given in Fig V.7 below.

Figure V.7 : Character 8, prootic sinus (cerebellar view), 2 states. A: state 0 (*Loxodonta africana*); B: state 1 ('Zhelestidae' petrosal after Ekdale et al.2004)

Ocepeia	*Protungulatum*	*Eritherium*	*Phosphatherium*	*Numidotherium*	*Moeritherium*	*Prodeinotherium*	*Mammut*	*Platybelodon*	*Gomphotherium*	*Cuvieronius*	*Stegomastodon*	*Stegodon*	*Anancus*	*Loxodonta*	*Palaeoloxodon*	*Elephas*	*M. columbi*	*M. primigenius*
0	0	?	0	0	?	0	0	0	0	0	0	0	0	0	0	0	0	0

9. *Crista falciformis*: (0) thick, (1) thin

This character was used in previous cladistic analyses focused on the ear region of mammals. We used the same coding as in Benoit et al. (2013b; character 20). The *crista falciformis* (or *crista transversa*) is the bony ridge that separates the *foramen acusticum inferior* and the *foramen acusticum superior* within the internal auditory meatus. The width of the *crista* varies among mammals. In most afrotherians, the *crista* is thick and separates well the two acoustic foramens (state 0). In this case, the *crista falciformis* is very robust and rarely damaged in fossil specimens. Conversely, most proboscideans display a thin *crista falciformis* (state 1). The structure can be very fragile and is often damaged in fossil specimens and even sometimes in extant specimens. Illustrations of the character states are given in Fig V.8 below.

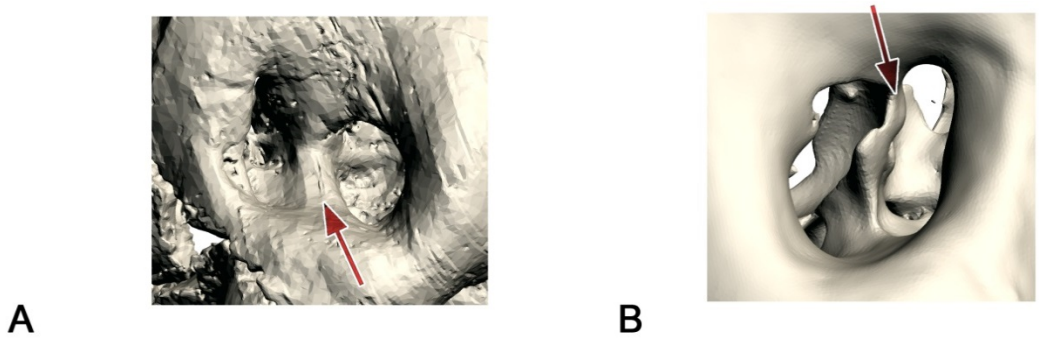

Figure V.8 : Character 9, *crista falciformis,* 2 states. A: state 0 (*Eritherium azzouzorum*); B, state 1 (*Phosphatherium escuilliei*).

Ocepeia	*Protungulatum*	*Eritherium*	*Phosphatherium*	*Numidotherium*	*Moeritherium*	*Prodeinotherium*	*Mammut*	*Platybelodon*	*Gomphotherium*	*Cuvieronius*	*Stegomastodon*	*Stegodon*	*Anancus*	*Loxodonta*	*Palaeoloxodon*	*Elephas*	*M. columbi*	*M. primigenius*
0	0	0	1	1	1	?	?	?	1	?	?	?	1	1	?	1	?	1

10. Petromastoid canal: (0) absent, (1) present

The petromastoid canal is a discrete canal that lies at the bottom of the subarcuate fossa. It carries the subarcuate artery, vein and nerves in humans (Gannon et al. 1988). The absence of this canal is coded 0 while its presence is coded 1. Illustrations of the character states are given in Fig V.9 below. A canal has been observed at the bottom of the subarcuate fossa of *Ocepeia* and *Phosphatherium*. The homology with the petromastoid canal is difficult to establish, however we decided to consider these canals to be homologous with the petromastoid canal based on their locations within the fossa. The presence of the canal in *Phosphatherium* was suggested by Benoit et al. (2013b) based on the observation of a foramen in the external subarcuate fossa. The CT investigation of the petrosal confirms the presence of a bony canal originating from this foramen.

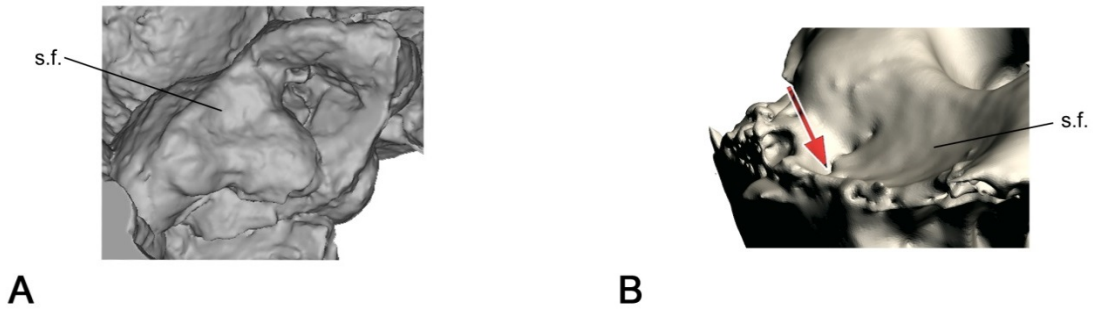

Figure V.9 : Character 10, petromastoid canal, 2 states. A: state 0 (*Moeritherium*) ; B: state 1 (*Phosphatherium escuilliei*). Caption: **s.f.** subarcuate fossa (or emplacement of the subarcuate fossa).

Ocepeia	*Protungulatum*	*Eritherium*	*Phosphatherium*	*Numidotherium*	*Moeritherium*	*Prodeinotherium*	*Mammut*	*Platybelodon*	*Gomphotherium*	*Cuvieronius*	*Stegomastodon*	*Stegodon*	*Anancus*	*Loxodonta*	*Palaeoloxodon*	*Elephas*	*M. columbi*	*M. primigenius*
1	0	0	1	0	0	0	0	0	0	0	0	0	0	0	0	0	0	0

11. Groove for the middle meningeal artery (or internal carotid artery): (0) not visible on the petrosal, (1) large and deep, runs on the cerebral surface of the *tegmen tympani*

The shape of the *tegmen tympani* of proboscideans varies (character 5) and its surface can display one or several grooves. In some specimens, a very large and deep groove excavates the *tegmen tympani* on its cerebral surface (state 1). In others specimens, the feature is absent (state 0). When present, the groove runs generally antero-posteriorly in the axis of the petrosal (and parallel to the *crista partis petrosa*). It can be straight, but most of the time, the groove meanders on the cerebral surface of the *tegmen tympani*. In many fossil elephantimorphs, the *tegmen tympani* is not entirely preserved and broken at the usual location of the groove (e.g. *Cuvieronius*). In this case, the character is coded '?' because the information is missing. Illustrations of the character states are given in Fig V.10 below. To our knowledge, this character has not been used in previous analyses using characters of the ear region of proboscideans and/or afrotherians.

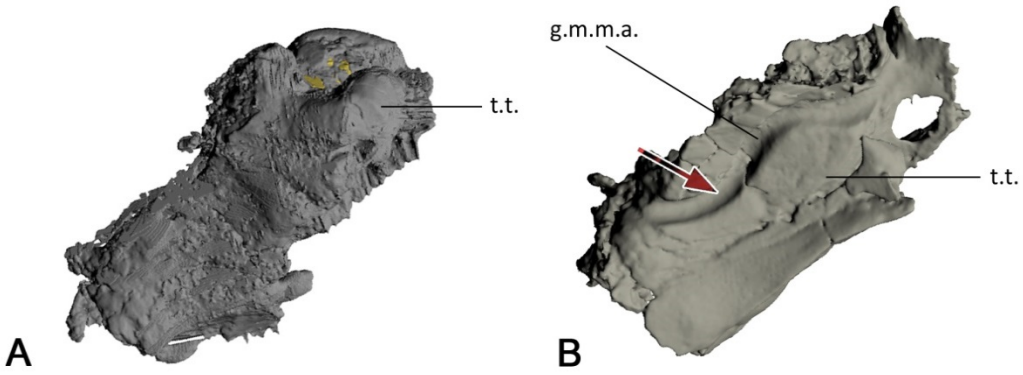

Figure V.10 : Character 11, groove for the middle meningeal artery, 2 states. A: state 0 (*Ocepeia daouiensis*); B: state 1 (*Gomphotherium angustidens*). Caption: **g.m.m.a.** groove for the middle meningeal artery, **t.t.** *tegmen tympani*.

Ocepeia	*Protungulatum*	*Eritherium*	*Phosphatherium*	*Numidotherium*	*Moeritherium*	*Prodeinotherium*	*Mammut*	*Platybelodon*	*Gomphotherium*	*Cuvieronius*	*Stegomastodon*	*Stegodon*	*Anancus*	*Loxodonta*	*Palaeoloxodon*	*Elephas*	*M. columbi*	*M. primigenius*
0	0	0	?	0	?	?	?	1	1	?	1	1	1	1	1	1	?	1

12. Transpromontory sulcus: (0) absent, (1) present

This character directly comes from Benoit et al. (2013b; character 11) and is modified from Wible (1986). The coding is left unchanged from Benoit et al. (2013b). The internal carotid artery generally runs in the petrosal region of mammals (Wible, 1986). In some taxa, the artery runs on the surface of the *promontorium*, leaving a groove called the transpromontory sulcus (state 1). This groove displays an antero-posterior course on the promontorial surface. Conversely, the transpromontory sulcus is absent in other taxa (state 0). Illustrations of the character states are given in Fig V.11. Specimens in which the *promontorium* is entirely broken are coded as missing data. The surface of the *promontorium* is not clearly observable in *Platybelodon* and the character was coded missing data for this taxon as well. The groove observed in *Phosphatherium* is located more medial than in other taxa displaying the transpromontory sulcus. We assume that the sulcus observed in *Phosphatherium* is instead more likely the groove for the inferior petrosal sinus.

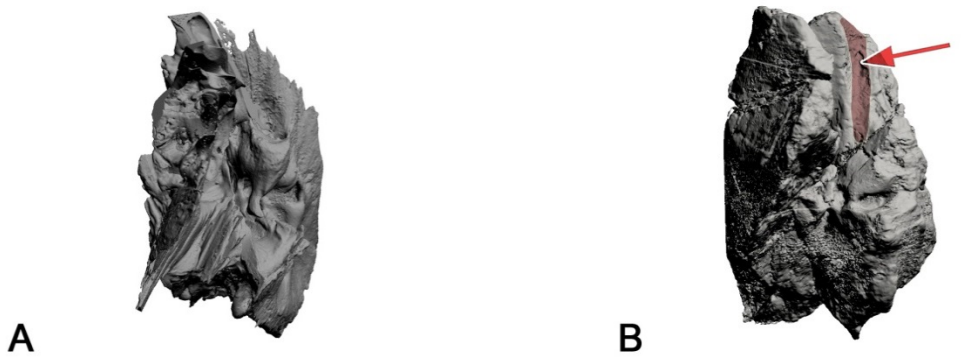

Figure V.11 : Character 12, transpromontory sulcus, 2 states. A: state 0 (*Loxodonta africana*); B: state 1 (*Numidotherium kohlense*).

Ocepeia	*Protungulatum*	*Eritherium*	*Phosphatherium*	*Numidotherium*	*Moeritherium*	*Prodeinotherium*	*Mammut*	*Platybelodon*	*Gomphotherium*	*Cuvieronius*	*Stegomastodon*	*Stegodon*	*Anancus*	*Loxodonta*	*Palaeoloxodon*	*Elephas*	*M. columbi*	*M. primigenius*
0	1	0	0	1	0	0	0	?	0	?	?	0	0	0	?	0	?	0

13. Definition of the ampullae: (0) well-defined and bulbous, (1) poorly defined

The bony ampullae enclose the membranous ampullae of the semicircular ducts in life. In most mammals, the bony ampullae are bulbous and well-defined (state 0). However, the bony ampullae are poorly distinct in modern proboscideans (state 1). Figure V.12 illustrates these two character states. The most important feature for the definition of these character states is the junction of the ampulla and the slender part of the canal. In taxa coded 0, the ampullae are distinctly bulbous apically. The junction of the ampulla and the slender part of the canal is marked by a strong demarcation, with the volume of the bony labyrinth rapidly decreasing from the ampulla to the slender part of the canal. Conversely, in taxa coded 1 the ampullae are not clearly bulbous apically. There is no clear line of demarcation between the ampulla and the slender part of the canal. The volume of the bony labyrinth decreases very progressively from the ampulla to the slender part of the canal in this area, which gives the bony ampullae a poorly defined aspect. To our knowledge, this character is original and has not been used in previous cladistic analyses of proboscideans and afrotherians.

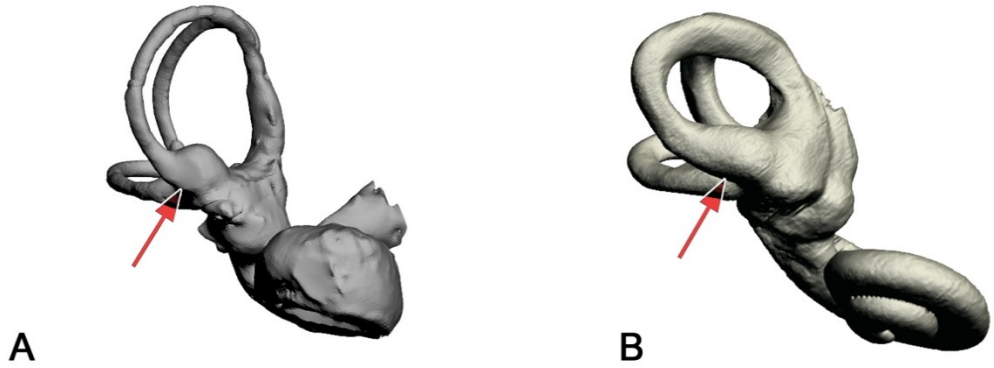

Figure V.12 : Character 13, definition of the ampullae, 2 states. A: state 0 (*Phosphatherium escuilliei)*; B: state 1 *(Elephas maximus)*

Ocepeia	*Protungulatum*	*Eritherium*	*Phosphatherium*	*Numidotherium*	*Moeritherium*	*Prodeinotherium*	*Mammut*	*Platybelodon*	*Gomphotherium*	*Cuvieronius*	*Stegomastodon*	*Stegodon*	*Anancus*	*Loxodonta*	*Palaeoloxodon*	*Elephas*	*M. columbi*	*M. primigenius*
0	0	0	0	0	0	1	1	1	1	1	1	1	1	1	1	1	1	1

14. Basal thickening of the *crus commune*: (0) absent or slight,(1) pyramidal in shape

The bony *crus commune* houses the membranous *crus commune* in life, which is the fusion of the slender part of the anterior and posterior ducts. The membranous *crus commune* is connected basally with the common utricle contained in the bony vestibule. The ossification of the bony *crus commune* varies among taxa. In some specimens, the demarcation between the *crus commune* and the vestibule is well-marked, there is no basal thickening of the crus (state 0). In some specimens, there is a slight basal thickening but this is very variable even intra-specifically. Such specimens are also coded 0. On the other hand, in the two studied specimens of *Gomphotherium*, a very strong basal thickening is observed (state 1). The volume of the *crus commune* increases very progressively from its top to its basis, giving it a characteristic pyramidal shape. Illustrations of the two character states are given in Fig V.13. To our knowledge, this character is original and has not been used in previous cladistic analyses of proboscideans and afrotherians.

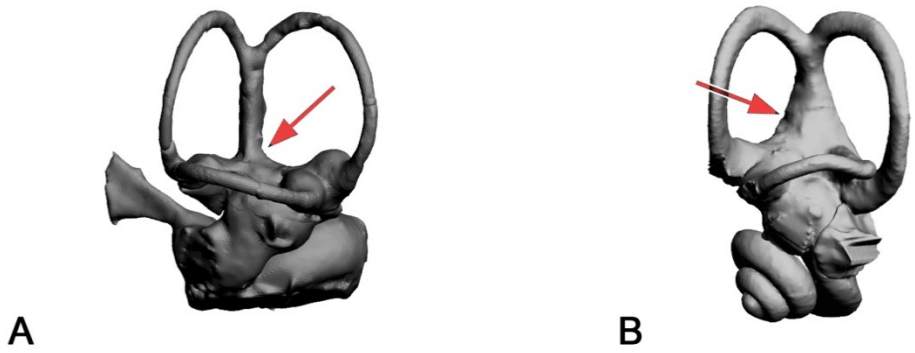

Figure V.13 : States of character 14 (basal thickening of the *crus commune*) illustrated in *Phosphatherium escuilliei* A: state 0 and *Gomphotherium angustidens* B: state 1.

Ocepeia	*Protungulatum*	*Eritherium*	*Phosphatherium*	*Numidotherium*	*Moeritherium*	*Prodeinotherium*	*Mammut*	*Platybelodon*	*Gomphotherium*	*Cuvieronius*	*Stegomastodon*	*Stegodon*	*Anancus*	*Loxodonta*	*Palaeoloxodon*	*Elephas*	*M. columbi*	*M. primigenius*
0	0	0	0	0	0	0	0	0	1	0	0	0	0	0	0	0	0	0

15. Thickness of the *crus commune*: (0) slender, thickness ratio < 15, (1) thick, thickness ratio > 15

The *crus commune* thickness varies among mammals. The definition of the states of a character based on the thickness of a structure is tricky. While it is easy to separate extreme specimens, those with a more average thickness are difficult to class. To address this issue, we used a ratio to categorize the different levels of thickness (see Chapter III). The study of the distribution of this ratio within our sample (see Chapter III, Fig III.39) allowed us to discriminate two groups: those with a slender *crus commune* (ratio < 15, state 0) and those with a thick *crus commune* (ratio > 15, state 1). Illustrations of the character states are given in Fig V.14 below. One disadvantage of this method is that two measurements of the *crus commune* are necessary to calculate the ratio. These values are directly given by the software ARIADNE, but the specimens have to be correctly prepared and landmarked. Hence, the character is only applicable on specimens for which we have a 3D reconstruction of the bony labyrinth. It is not possible to code specimens only illustrated in the literature. To do so, the character would have to be modified and be less precise, not using the thickness ratio. This ratio was previously not used in cladistic analyses.

Figure V.14 : Character 15, thickness of the *crus commune*, 2 states. A: state 0 (*Arsinoitherium zitteli)*; B: state 1 (*Elephas maximus*)

Ocepeia	*Protungulatum*	*Eritherium*	*Phosphatherium*	*Numidotherium*	*Moeritherium*	*Prodeinotherium*	*Mammut*	*Platybelodon*	*Gomphotherium*	*Cuvieronius*	*Stegomastodon*	*Stegodon*	*Anancus*	*Loxodonta*	*Palaeoloxodon*	*Elephas*	*M. columbi*	*M. primigenius*
0	0	0	0	0	?	1	1	1	01	1	1	1	1	1	1	1	1	1

16. Meeting point of the anterior and posterior semicircular canals in the *crus commune*: (0) high, (1) low

The anterior and posterior semicircular bony canals meet at the level of the *crus commune* were they begin to fuse. The position of this meeting point varies among mammals. To estimate the height of the junction of the two canals, one must compare its position with respect to the height of the anterior canal. A meeting point will be considered high if it is situated at least at two thirds of the height of the anterior canals (state 0). A meeting point will be considered low if it is located at mid-height (or less) of the height of the anterior canals (state 1). Illustrations of the character states are given in Fig V.15. This character shows a high level of intraspecific variability. States 0 and 1 are observed in *Mammut*, *Elephas*, *Loxodonta* and *Anancus*. Nevertheless, we included this character in the analysis in order to test its pertinence. To our knowledge, this character is original and has not been used previously in cladistic analyses.

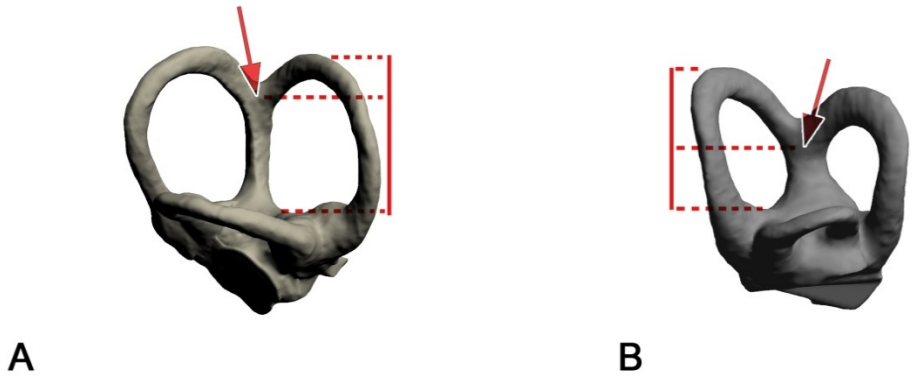

Figure V.15 : Character 16, meeting point of the anterior and posterior canals, 2 states. A: state 0 (*Arsinoitherium zitteli*); B: state 1 (*Mammuthus columbi*)

Ocepeia	*Protungulatum*	*Eritherium*	*Phosphatherium*	*Numidotherium*	*Moeritherium*	*Prodeinotherium*	*Mammut*	*Platybelodon*	*Gomphotherium*	*Cuvieronius*	*Stegomastodon*	*Stegodon*	*Anancus*	*Loxodonta*	*Palaeoloxodon*	*Elephas*	*M. columbi*	*M. primigenius*
0	0	?	0	0	0	0	01	1	0	0	0	0	01	01	0	01	1	1

17. Overall shape of the anterior canal: (0) round, (1) oval

The shape of the anterior semicircular canal varies among mammals. The term shape can hold different meanings but here we mean the shape of the area enclosed by the outline of the anterior canal. In some mammals, the anterior canal is round (state 0). The radii of a round canal measured at different locations are very similar. Some other mammals display anterior canals which outline is oval or elliptical (state 1). In that case, the radii measured at different locations of the canal can display very different values. Given the elliptical nature of the canal, the area possesses a major axis which corresponds to its larger radius. The orientation of this axis can vary between specimens but this is not taken into account in the definition of this character. Illustrations of the character states are given in Fig V.16 below. This character is most usually included cladistic analyses focused on the bony labyrinth. However, it is absent in Benoit et al. (2013b) analysis which only studies the shape of the posterior canal.

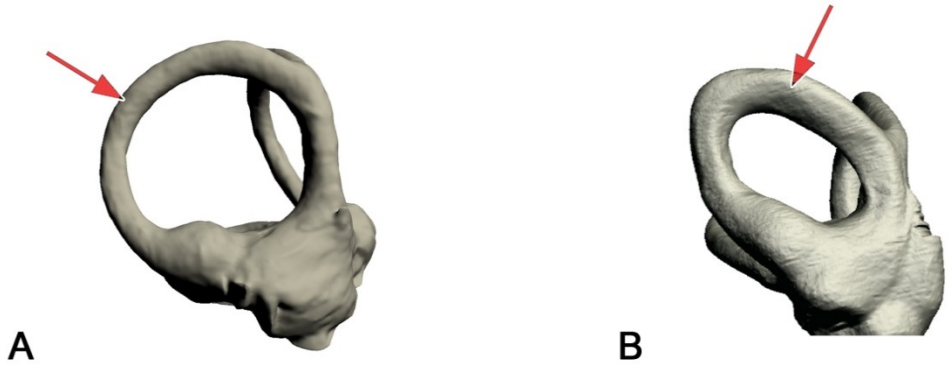

Figure V.16 : Character 17, shape of the anterior canal, 2 states. A: state 0 (*Arsinoitherium zitteli*); B: state 1 (*Elephas maximus)*

Ocepeia	*Protungulatum*	*Eritherium*	*Phosphatherium*	*Numidotherium*	*Moeritherium*	*Prodeinotherium*	*Mammut*	*Platybelodon*	*Gomphotherium*	*Cuvieronius*	*Stegomastodon*	*Stegodon*	*Anancus*	*Loxodonta*	*Palaeoloxodon*	*Elephas*	*M. columbi*	*M. primigenius*
0	0	0	0	0	1	1	1	1	01	1	1	1	1	1	1	1	1	1

18. Overall shape of the posterior canal: (0) round, (1) oval

As for the anterior canal, the shape of the posterior canal varies as well among mammals. The definition and the states are the same as for the anterior semicircular canal. Specimens with a rounded area outlined by the posterior canal are coded 0. Specimens with an elliptical area outlined by the posterior canal are coded 1. Illustrations of the character states are given in Fig V.17 below. This character has been used in Benoit et al. (2013b) as well. It is used here with the same coding.

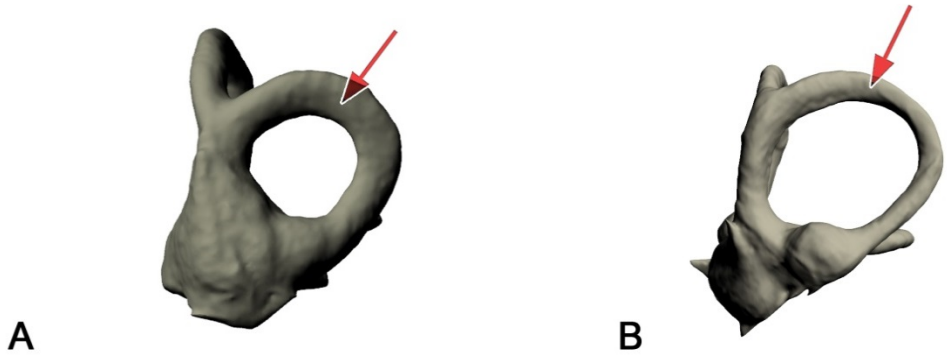

Figure V.17 : Character 18, shape of the posterior canal, 2 states. A: state 0 (*Mammuthus columbi*); B: state 1 (*Arsinoitherium zitteli*)

Ocepeia	*Protungulatum*	*Eritherium*	*Phosphatherium*	*Numidotherium*	*Moeritherium*	*Prodeinotherium*	*Mammut*	*Platybelodon*	*Gomphotherium*	*Cuvieronius*	*Stegomastodon*	*Stegodon*	*Anancus*	*Loxodonta*	*Palaeoloxodon*	*Elephas*	*M. columbi*	*M. primigenius*
0	0	0	0	1	1	0	1	0	1	1	01	1	1	0	0	0	0	1

19. Extension of the anterior canal apex: (0) at the same level than the apex of the posterior canal, (1) higher than the apex of the posterior canal

The apex of a vertical semicircular canal is defined here as its maximum of height when oriented with the *crus commune* vertical (see Fig. V.18 below). In some mammals, the apex of the anterior canal and the apex of the posterior canal extend at the same height (state 0). Some other mammals display an anterior canal apex that extends higher than the posterior canal apex (state 1). A posterior canal higher than the anterior canal has not been observed in our taxa sample. To correctly code this character, the specimen must be oriented in such a way that the *crus commune* is vertical. A virtual horizontal line must be traced from the posterior apex. If the apex of the anterior canal is located along the line, the state is 0. In contrary, if the apex of the anterior canal is above this line, the state is 1. To our knowledge, this is the first time that such a character is used in a cladistic analysis focused on the ear region of afrotherians and/or proboscideans.

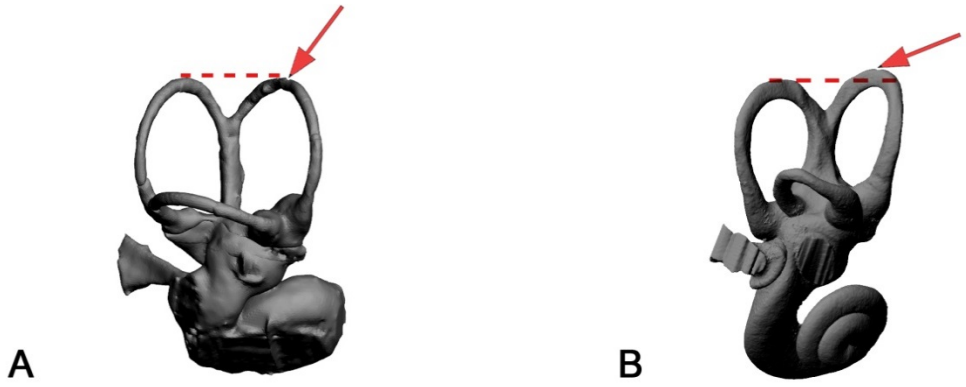

Figure V.18 : Character 19, extension of the anterior canal apex, 2 states. A: state 0 (*Phosphatherium escuilliei*); B: state 1 (*Anancus arvernensis*)

Ocepeia	*Protungulatum*	*Eritherium*	*Phosphatherium*	*Numidotherium*	*Moeritherium*	*Prodeinotherium*	*Mammut*	*Platybelodon*	*Gomphotherium*	*Cuvieronius*	*Stegomastodon*	*Stegodon*	*Anancus*	*Loxodonta*	*Palaeoloxodon*	*Elephas*	*M. columbi*	*M. primigenius*
1	1	?	0	0	01	1	1	1	1	1	0	1	1	1	1	1	1	1

20. Position of the point of entry of the lateral semicircular canal into the vestibule: (0) high and close to the posterior ampulla, (1) high and distant to the posterior ampulla, (2) low

In life, the lateral semicircular duct is connected with the common utricle via the lateral utricle. The beginning of the lateral utricle corresponds more or less with the point of entry of the bony lateral canal into the vestibule. The position of this point of entry varies according to the taxon, however this character is constant intra-specifically. Some mammals display a point of entry of the lateral canal high and close to the posterior ampulla (state 0). In many proboscideans, the point of entry is still high but becomes very distant from the posterior ampulla (state 1). Finally, every Elephantidae displays a point of entry of the lateral canal into the vestibule that is located low with respect to the posterior ampulla (2). Illustrations of this character states are given in Fig V.19. This character is mostly original. While some analyses use the position of the lateral canal as a phylogenetic character (Benoit et al. 2013b; character 28), no study using this character with such coding were previously published.

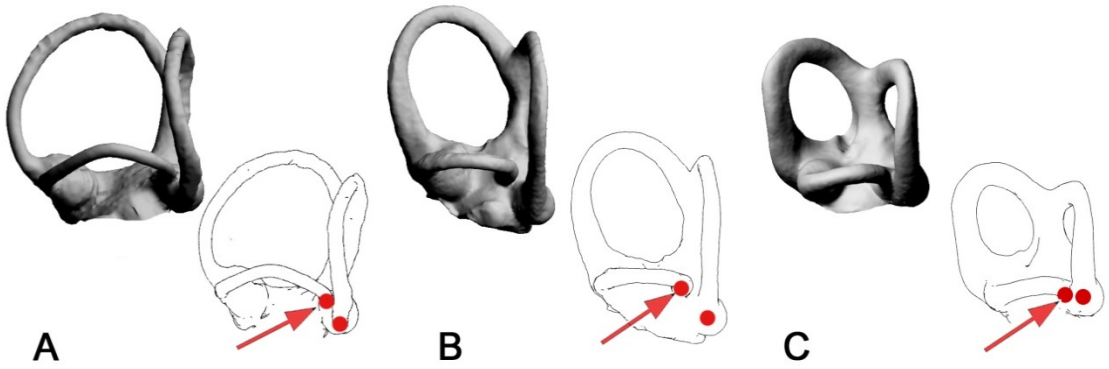

Figure V.19: Character 20, point of entry of the lateral semicircular canal into the vestibule, 3 states. A: state 0 (*Ocepeia daouiensis*); B: state 1 (*Cuvieronius* sp.); C: state 2 (*Elephas maximus*)

Ocepeia	*Protungulatum*	*Eritherium*	*Phosphatherium*	*Numidotherium*	*Moeritherium*	*Prodeinotherium*	*Mammut*	*Platybelodon*	*Gomphotherium*	*Cuvieronius*	*Stegomastodon*	*Stegodon*	*Anancus*	*Loxodonta*	*Palaeoloxodon*	*Elephas*	*M. columbi*	*M. primigenius*
0	0	0	0	0	?	1	0	1	1	1	?	1	1	2	2	2	2	2

21. Shape of the semicircular canals in cross-section: (0) circular, (1) flattened

The outline of the bony semicircular canals shows different forms when viewed in cross-section. In most mammals, the bony canal cross section is circular (state 0). Some mammals have markedly flattened bony semicircular canals (state 1). All the three semicircular canals are not necessarily flattened altogether. Generally, at least the anterior and posterior semicircular canals are flattened. It should be noted that in the studied afrotherians the flattening of the bony canals does not imply the flattening of their membranous ducts (see chapter II). Illustrations of this character states are given in Fig V.20. The coding of this character is quite simple. The state 1 does not require a flattening in all three canals. At least one canal must be markedly flattened. Moreover, the flattening is not necessarily present on the whole length of the canal. This character has been used before, notably in the cladistic analysis performed on Tethytheria in Benoit et al. (2013b) (characters 33) and has been adapted here.

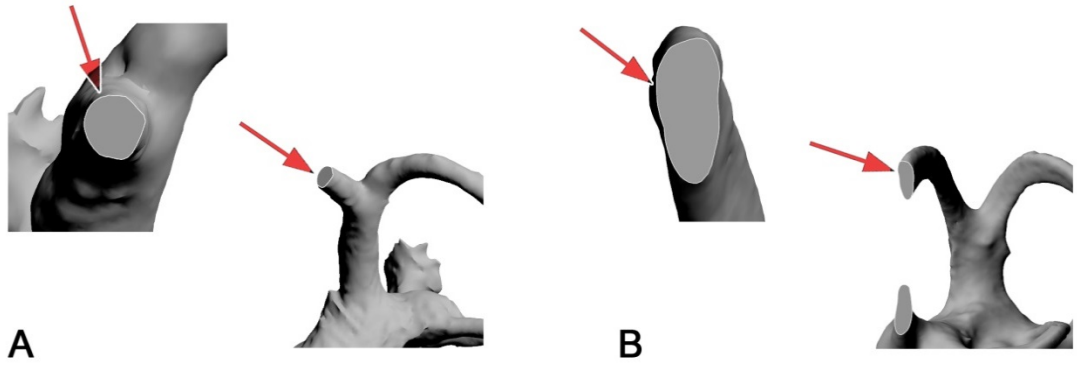

Figure V.20 : Character 21, shape of the cross-section of the canals, 2 states. A: state 0 (*Ocepeia daouiensis*); B: state 1 (*Loxodonta cyclotis*)

Ocepeia	*Protungulatum*	*Eritherium*	*Phosphatherium*	*Numidotherium*	*Moeritherium*	*Prodeinotherium*	*Mammut*	*Platybelodon*	*Gomphotherium*	*Cuvieronius*	*Stegomastodon*	*Stegodon*	*Anancus*	*Loxodonta*	*Palaeoloxodon*	*Elephas*	*M. columbi*	*M. primigenius*
0	0	0	0	0	1	1	1	1	1	1	1	1	1	1	1	1	1	1

22. General thickness of the semicircular canals: (0) slender canals, thickness ratio < 3, (1) thick canals, thickness ratio >3

The thickness of the bony semicircular canals varies among mammals in general, and in particular among proboscideans. As for the *crus commune* thickness (character 15), it can be tricky to evaluate the degree of thickness of the canals and to translate it into a phylogenetic character. Thus we used the same method as for character 15, except that we instead used the general thickness ratio of the canals. This ratio is the mean of the average thickness ratios of each canal, which is the ratio of the average section radius on the central streamline length of the canal. The examination of the distribution of this ratio within our taxa sample (chapter III, Fig III.42) allowed us to determine two states. Specimens that display a thickness ratio lower than 3 are considered to have slender canals (state 0), while specimens with a thickness ratio over 3 are considered to have thick canals (state 1). Illustrations of this character states are given in Fig V.21. As for character 15, the main problem of this character is that it can be determined (with this coding at least) only for specimens for which we know the average section radius and the canal length. Specimens must be prepared according to the David et al. (in press) protocol. A similar character can be found in Benoit et al. (2013b) (character 32) but without using the ratio to define the states.

Figure V.21 : Character 22, thickness of the semicircular canals, 2 states. A: state 0 (*Eritherium azzouzorum*); B: state 1 (*Loxodonta cyclotis*)

Ocepeia	*Protungulatum*	*Eritherium*	*Phosphatherium*	*Numidotherium*	*Moeritherium*	*Prodeinotherium*	*Mammut*	*Platybelodon*	*Gomphotherium*	*Cuvieronius*	*Stegomastodon*	*Stegodon*	*Anancus*	*Loxodonta*	*Palaeoloxodon*	*Elephas*	*M. columbi*	*M. primigenius*
0	?	0	0	0	?	0	1	1	1	1	?	1	01	01	1	1	1	1

23. Relative size of the lateral canal: (0) approximately same size than anterior and posterior canals (lateral canal ratio > 85%), (1) slightly smaller than other canals (72% < lateral canal ratio < 85%), (2) very small (lateral canal ratio < 72%)

There are various manners to estimate the size of a semicircular canal: length, enclosed area, radius of curvature. The latter is the most commonly used in the literature and we used it to determine the size of the canals. The three semicircular canals of the same specimen do not necessarily have the same radius. Generally, the anterior and posterior canals share similar radii, but the relative size of the lateral canal varies. To estimate the relative size of this canal, we defined a lateral canal ratio, which is the radius of the lateral canal on the average radius of the vertical canals. A study of the distribution of this ratio within our taxa sample (chapter III, Fig III.40) allowed us to determine three groups: specimens with lateral canals that are approximately the same size as vertical canals (ratio superior to 85%, state 0), specimens with slightly smaller lateral canals (ratio between 72% and 85%, state 1) and specimen with small lateral canals (ratio inferior to 72%, state 2). Illustrations of this character states are given in Fig V.22 below. A similar character can be found in Benoit et al. (2013b) minus the use of the lateral canal ratio to define character states.

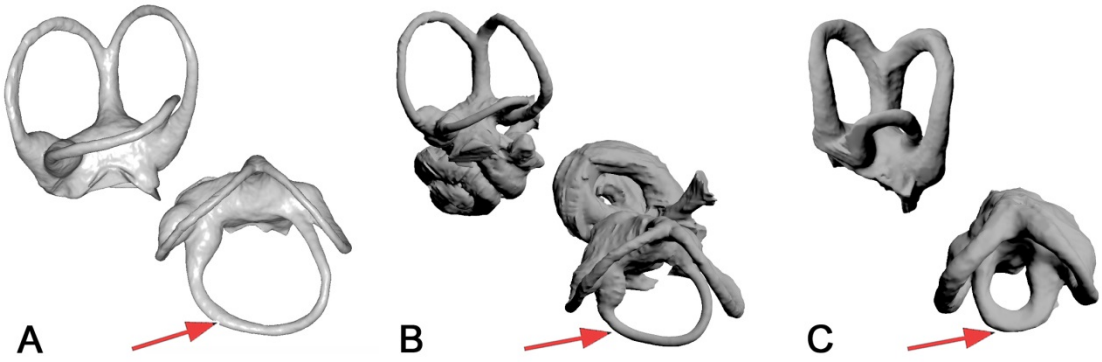

Figure V.22 : Character 23, relative size of the lateral canal, 3 states. A: state 0 (*Tenrec*); B: state 1 (*Ocepeia daouiensis)*; C: state 2 (*Mammut americanum*)

Ocepeia	*Protungulatum*	*Eritherium*	*Phosphatherium*	*Numidotherium*	*Moeritherium*	*Prodeinotherium*	*Mammut*	*Platybelodon*	*Gomphotherium*	*Cuvieronius*	*Stegomastodon*	*Stegodon*	*Anancus*	*Loxodonta*	*Palaeoloxodon*	*Elephas*	*M. columbi*	*M. primigenius*
1	0	1	1	1	?	1	2	2	2	2	?	2	2	2	1	12	2	2

24. Contact between the lateral and posterior canals: (0) the ampulla and the slender part of the posterior canal are fused with the lateral canal, (1) only the posterior ampulla is fused with the lateral canal, (2) the canals are not in contact

Specimens may or may not display a fusion between their lateral and posterior canals. Advanced fusion of these canals is referred to as *crus commune secundaria* in the literature. The use of this term is debatable as a true *crus commune* never occurs between these two canals: the lateral and posterior ducts are never fused even when their bony canals are fused (David, 2011). The *crus commune* between the anterior and posterior canal actually corresponds only to a bony counterpart. Moreover, even when a bony *crus commune secundaria* occurs, the streamline of both canals are always distinguishable. Here, we prefer to use the presence – or absence – of contact between these two canals. Specimens displaying a lateral canal in contact with the posterior canal ampulla as well as its slender part are coded 0. If the contact is only between the lateral canal and the posterior ampulla, they are coded 1. Finally, if there is no contact at all between the canals, the state is 2. Illustrations of this character states are given in Fig V.23 below. This character could be considered an adaptation of character 27 from Benoit et al. (2013b), but with a heavily modified coding.

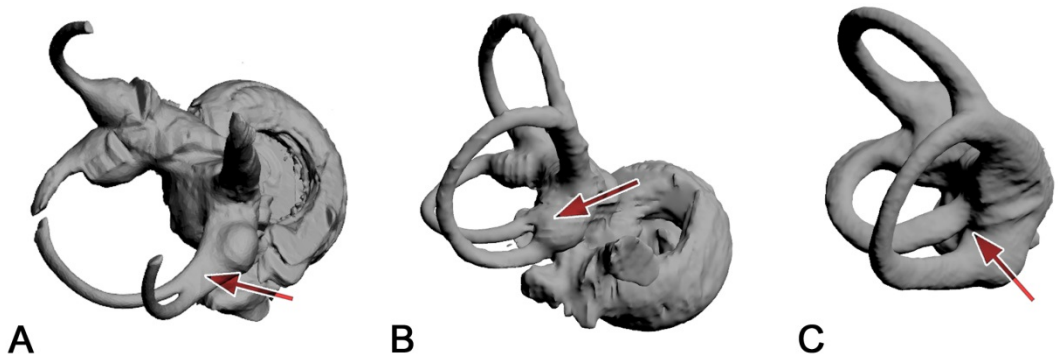

Figure V.23 : Character 24, contact between the lateral and posterior canals, 3 states. A: state 0 (*Eritherium azzouzorum*); B: state 1 (*Ocepeia daouiensis*); C: state 2 (*Cuvieronius sp.*)

Ocepeia	*Protungulatum*	*Eritherium*	*Phosphatherium*	*Numidotherium*	*Moeritherium*	*Prodeinotherium*	*Mammut*	*Platybelodon*	*Gomphotherium*	*Cuvieronius*	*Stegomastodon*	*Stegodon*	*Anancus*	*Loxodonta*	*Palaeoloxodon*	*Elephas*	*M. columbi*	*M. primigenius*
1	0	0	0	0	?	2	1	2	2	2	?	2	2	2	1	1	2	2

25. Posterior expansion of the lateral canal: (0) absent, (1) present, the lateral canal crosses the posterior canal plane

The lateral semicircular canal size of the bony labyrinth varies between mammals. Moreover, its position and conformation with respect to the other semicircular canals can change. In most mammals the lateral canal never crosses the plane of the other two canals (state 0). An alternative remarkable conformation is a posterior expansion of the lateral canal. Some taxa (e.g. *Procavia capensis*) display lateral canals which are extended (on the side of the utricle) accross the plan defined by the posterior canal (state 1). Illustrations of this character states are given in Figure V.24. State 1 is not observed in the studied proboscideans, but it is present some other afrotherians that are included in the matrix. This character is similar to character 28 used in Benoit et al. (2013b).

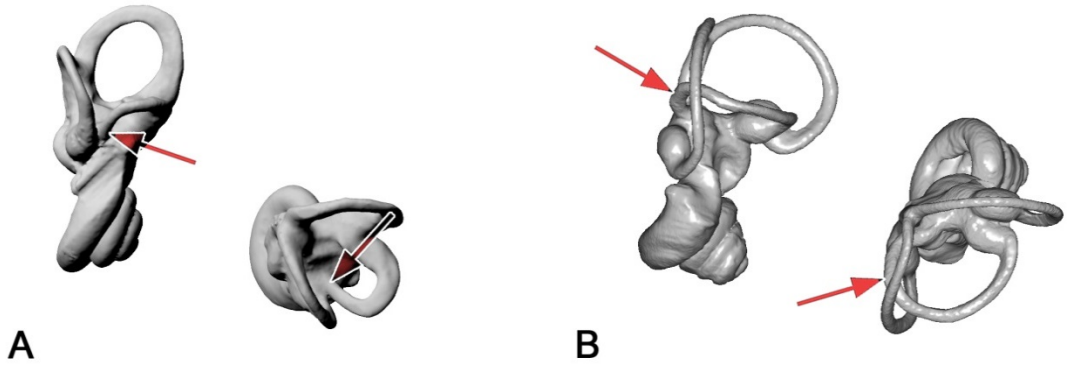

Figure V.24 : Character 25, posterior expansion of the lateral canal, 2 states. A: state 0 (*Loxodonta cyclotis*); B: state 1 (*Procavia capensis*)

Ocepeia	*Protungulatum*	*Eritherium*	*Phosphatherium*	*Numidotherium*	*Moeritherium*	*Prodeinotherium*	*Mammut*	*Platybelodon*	*Gomphotherium*	*Cuvieronius*	*Stegomastodon*	*Stegodon*	*Anancus*	*Loxodonta*	*Palaeoloxodon*	*Elephas*	*M. columbi*	*M. primigenius*
0	0	0	0	0	?	0	0	0	0	0	?	0	0	0	0	0	0	0

26. Aspect ratio of the cochlea: (0) superior to 0.6, (1) inferior to 0.6

When viewed in profile, the cochlea has a rather conical form or a more planispiral aspect. To measure the aspect of the cochlea, the cochlear ratio (or aspect ratio) has been used by previous authors. The method to calculate the ratio is given in the main 'Material and Methods' section of the thesis (§ 2.2.). This character is continuous, and it is delicate to delimit the different states. To be really discriminant, limits should not be defined between two close values. The study of the distribution of this character among our taxa sample (Fig III.45) allowed us to define such limit and to avoid polymorphism. Specimens with a ratio superior to 0.6 tend to display more conical cochleae when viewed in profile (0). In contrary, specimens with a ratio inferior to 0.6 exhibit a more planispiral cochlea (1). Illustrations of the character states are given in Fig V.25 below. This character is commonly used in phylogenetic analyses on the ear region of mammals, notably in Benoit et al. (2013b) (character 24). Their coding is the same used here after study of the character distribution.

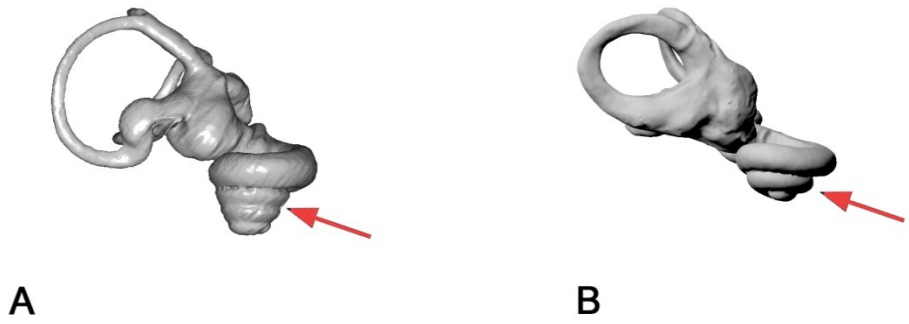

Figure V.25 : Character 26, aspect ratio of the cochlea, 2 states. A: state 0 (*Procavia capensis)*; B: state 1 (*Loxodonta cyclotis*)

Ocepeia	*Protungulatum*	*Eritherium*	*Phosphatherium*	*Numidotherium*	*Moeritherium*	*Prodeinotherium*	*Mammut*	*Platybelodon*	*Gomphotherium*	*Cuvieronius*	*Stegomastodon*	*Stegodon*	*Anancus*	*Loxodonta*	*Palaeoloxodon*	*Elephas*	*M. columbi*	*M. primigenius*
0	1	1	?	1	?	1	1	1	1	?	1	1	1	1	?	1	?	1

27. Number of turns of the cochlea: (0) inferior to 3, (1) superior to 3

While the cochlea of monotremes retains many plesiomorphic structures (absence of coiling, lagena) (Pritchard, 1881), in therians, the cochlea is always coiled. However, the number of turns of the cochlea varies greatly among eutherian mammals. Moreover, the variation of the number of turns of the cochlea has been also observed at intra-specific and even intra-individual levels (see Chapter II). Study of the variation within the *Loxodonta* genus revealed variability than can attain one full turn (1.625 turns to 2.625 turns). Moreover, study of the distribution of the number of turns within our taxa sample (chapter III, Fig III.43) revealed that almost the whole inter-taxa variation was comprised within the variation range of *Loxodonta*. In all cases, the entire variation observed in proboscideans is comprised within the variation range of *Loxodonta*. Therefore, it does not seem pertinent to determine limits within this range. Hence we only separated taxa that display less than three turns of the cochlea (state 0) from taxa display more than three turns (state 1). Illustrations of the two character states are given in Fig. V.26. The character is therefore constant among proboscideans, but other afrotherians such as *Procavia capensis* display more than three turns.

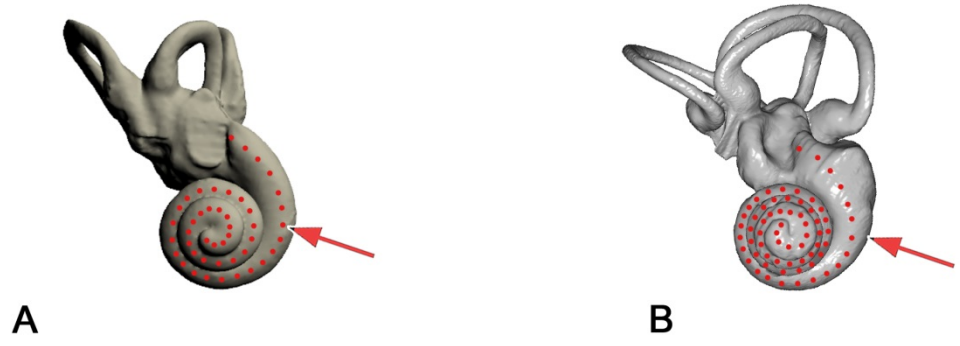

Figure V.26 : Character 27, number of turns of the cochlea, 2 states. A: state 0 (*Loxodonta cyclotis) ;* B: state 1 (*Procavia capensis*)

Ocepeia	*Protungulatum*	*Eritherium*	*Phosphatherium*	*Numidotherium*	*Moeritherium*	*Prodeinotherium*	*Mammut*	*Platybelodon*	*Gomphotherium*	*Cuvieronius*	*Stegomastodon*	*Stegodon*	*Anancus*	*Loxodonta*	*Palaeoloxodon*	*Elephas*	*M. columbi*	*M. primigenius*
0	0	0	0	0	0	0	0	0	0	?	0	0	0	0	?	0	?	0

28. *Lamina secundaria*: (0) present, (1) absent

The basilar membrane is a spiral membranous structure located between the *scala vestibuli* and *scala tympani*. The stiffness of this membrane – which is influenced by its width – plays a large role in the animal capacities of hearing low-frequency sounds. This is discussed with more details in Chapter VII. The basilar membrane is not preserved in fossils; however, some inferences can be made through study of the bony labyrinth. The membrane is located between the primary bony lamina – which runs on the inner part of the spiral cochlea – and the secondary bony lamina (also known as the *lamina secundaria*), which runs on the external part of the spiral cochlea. Most mammals display a furrow for the lamina secundaria on the external surface of their bony labyrinth endocast (state 0). The depth and the number of turns of the cochlea on which the *lamina secundaria* is present can vary, but here we code only the presence of this structure. On the other hand, several taxa lack a lamina secundaria on the external surface of the spiral cochlea (state 1). Illustrations of the character states are given in Fig V.27. This character is usually included in phylogenetic analyses of the ear region of mammals. In Benoit et al. (2013b), the coding of the character (character 26) is reversed with respect to our study.

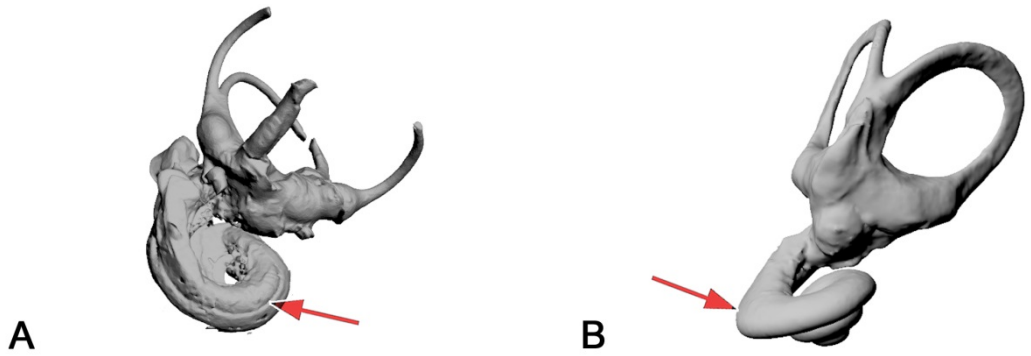

Figure V.27 : Character 28, *lamina secundaria*, 2 states. A: state 0 (*Eritherium azzouzorum*) ; B: state 1 (*Loxodonta cyclotis*)

Ocepeia	*Protungulatum*	*Eritherium*	*Phosphatherium*	*Numidotherium*	*Moeritherium*	*Prodeinotherium*	*Mammut*	*Platybelodon*	*Gomphotherium*	*Cuvieronius*	*Stegomastodon*	*Stegodon*	*Anancus*	*Loxodonta*	*Palaeoloxodon*	*Elephas*	*M. columbi*	*M. primigenius*
0	0	0	0	01	?	1	1	1	1	?	1	1	1	1	?	1	?	1

29. Relative volume of the cochlea: (0) superior to 55% of the total volume of the bony labyrinth, (1) inferior to 55%

The cochlear volume is estimated with respect to the volume of the entire bony labyrinth. The separation of the different parts of the bony labyrinth is performed as a step of the functional protocol (see Material and Methods section of the thesis). The cochlear and total volumes of the labyrinth are given by the software ARIADNE. The relative volume of the cochlea is simply the quotient of the cochlear volume and the total volume. Based on the study of the distribution of the volume values within our taxa sample (see Chapter III, Fig III.44), a limit was defined at 55%. Specimens with a cochlear volume that represents more than 55% of the total bony labyrinth volume are coded 0. In contrary, specimens with a cochlear volume that represents less than 55% of the total bony labyrinth volume are coded 1. Illustrations of the character states are given in Fig V.28. This character is already included in published analysis of the ear region of Tethytheria (Benoit et al. 2013b; character 25); however the coding has been adapted in our analysis. Indeed, the character states as defined by Benoit et al. (2013b) failed to bring information within our taxa sample.

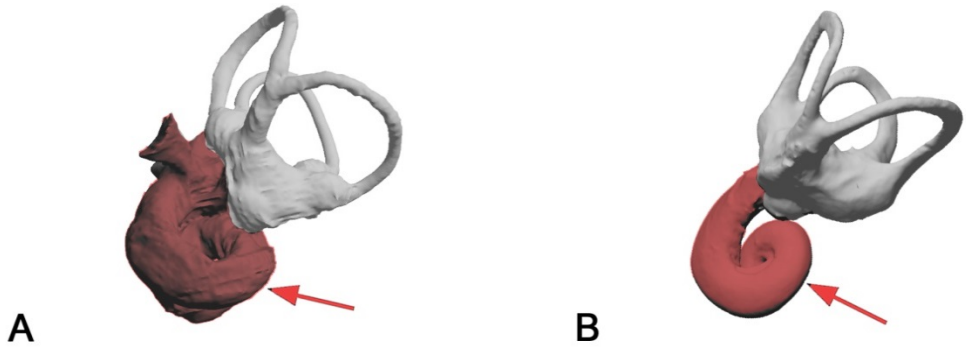

Figure V.28 : Character 29, relative volume of the cochlea, 2 states. A: state 0 (*Ocepeia daouiensis*); B: state 1 (*Loxodonta cyclotis*)

Ocepeia	*Protungulatum*	*Eritherium*	*Phosphatherium*	*Numidotherium*	*Moeritherium*	*Prodeinotherium*	*Mammut*	*Platybelodon*	*Gomphotherium*	*Cuvieronius*	*Stegomastodon*	*Stegodon*	*Anancus*	*Loxodonta*	*Palaeoloxodon*	*Elephas*	*M. columbi*	*M. primigenius*
0	0	1	0	1	?	1	1	1	1	?	?	1	1	1	?	1	?	1

30. Point of entry of the *fenestra cochleae* and the *aquaeductus cochleae* within the *scala tympani*: (0) distant to each other, (1) close to each other or fused

As said in the description of character 3, the fenestra cochleae and the aquaeductus cochleae are openings issued from the division during ontogeny of a unique perilymphatic foramen. Several mammals display a unique perilymphatic foramen even in adults, because of the non-separation of these two foramens. Benoit et al. (2013b) also observed that in some taxa, the point of entry of the *fenestra cochleae* and the *aquaeductus cochleae* within the scala tympani are close to each other. They suggested that this condition precedes the retention of the unique perilymphatic foramen and is probably the ancestral condition of Tethytheria. This character comes from Benoit et al. (2013b) (character 17) and the coding is here left unchanged. Taxa with a point of entry of the *fenestra cochleae* and the *aquaeductus cochleae* distant from another are coded 0. Taxa with close point of entries or fused point of entries (unique perilymphatic foramen) are coded 1. Illustrations of this character states are given in Fig V.29 below.

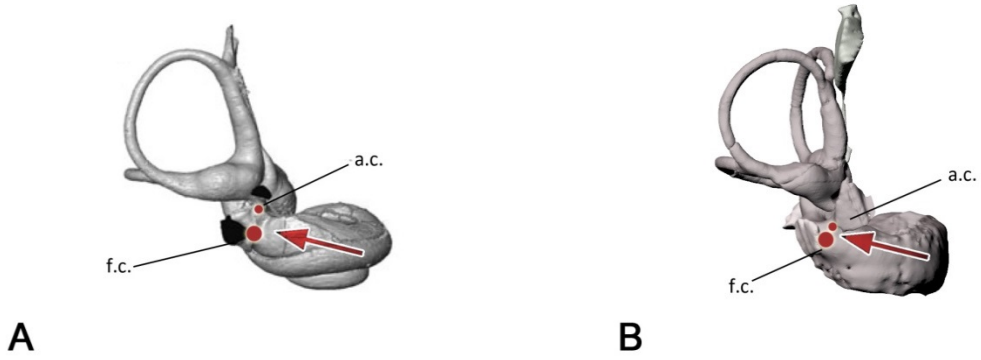

Figure V.29 : Character 30, point of entry of the *fenestra cochleae* and the cochlear canaliculus within the *scala tympani, 2* states. A: state 0 (*Protungulatum* sp., after Orliac & O'Leary, 2016); B: state 1 (*Phosphatherium escuilliei*)

Ocepeia	*Protungulatum*	*Eritherium*	*Phosphatherium*	*Numidotherium*	*Moeritherium*	*Prodeinotherium*	*Mammut*	*Platybelodon*	*Gomphotherium*	*Cuvieronius*	*Stegomastodon*	*Stegodon*	*Anancus*	*Loxodonta*	*Palaeoloxodon*	*Elephas*	*M. columbi*	*M. primigenius*
1	0	?	1	1	?	1	1	1	1	?	?	?	1	1	?	1	?	1

31. Vestibulo-cochlear angle: (0) right or acute angle (≤ 90°), (1) obtuse angle (90° < angle < 142°), (2) very obtuse angle (angle ≥ 142°)

The orientation of the cochlea with respect to the semicircular canals varies in mammals. The vestibulo-cochlear angle measures the angle between the vestibular system and the cochlear system. More exactly, the angle between the axis of the *crus commune* and the plane of the basal turn of the cochlea is measured, following the protocol described in Benoit et al. (2013b). Study of the distribution of this character within our taxa sample allowed us to define three groups (see Chapter III, Fig III.46). Specimens displaying a vestibulo-cochlear angle inferior or equal to 90° are coded 0. Specimens displaying a more obtuse angle (between 90° and 142°) are coded 1. Specimens with a particularly large angle (superior to 142°) are coded 2. Illustrations of the character states are given in Fig V.30. This character is tested here for the first time on proboscideans. In our studied material sample, *Cuvieronius*, *Palaeoloxodon* and *Mammuthus columbi* do not preserve the cochlea; the coding of this character is undetermined for these taxa and for the taxa that we did not segment ourselves (e.g. *Protungulatum*).

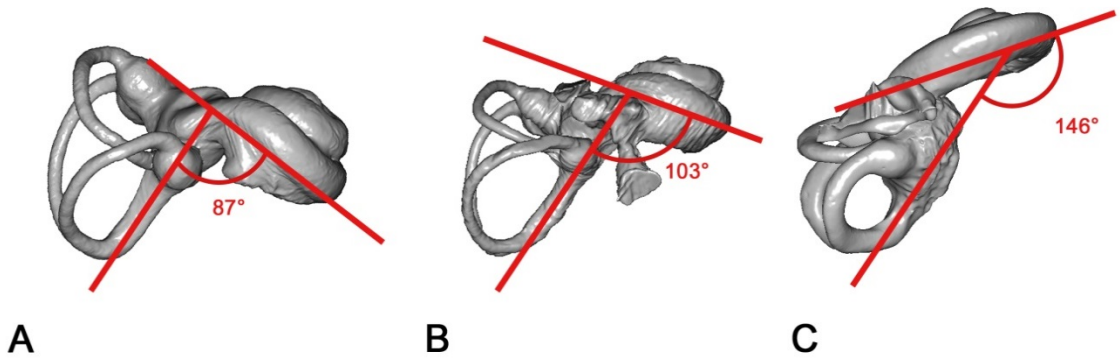

Figure V.30 : Character 31, vestibulo-cochlear angle, 3 states. A: state 0 (*Tenrec*); B: state 1 (*Ocepeia daouiensis*); C: state 2 (*Loxodonta cyclotis*)

Ocepeia	*Protungulatum*	*Eritherium*	*Phosphatherium*	*Numidotherium*	*Moeritherium*	*Prodeinotherium*	*Mammut*	*Platybelodon*	*Gomphotherium*	*Cuvieronius*	*Stegomastodon*	*Stegodon*	*Anancus*	*Loxodonta*	*Palaeoloxodon*	*Elephas*	*M. columbi*	*M. primigenius*
1	?	1	1	1	?	1	1	1	1	?	1	1	2	12	?	2	?	2

32. Axis of rotation of the apical turn of the cochlea with respect to the basal turn: (0) both turns are centered, the axes are the same, (1) the axis of the apical turn is offset

In our taxa sample, the cochlea always consists of several turns, even though the apical turn does not always completes a full turn. The bony modiolus is the axis around which the bony cochlea spirals. Depending on the taxa, the axis of rotation of the basal turn and the axis of rotation of the apical turn can be different. In some taxa, the axis of rotation of the apical turn is the same as the axis of rotation of the basal turn (state 0). In this case, both turns are centered and spiral around the same axis. In other taxa, the axis of rotation of the apical turn is offset compared to the axis of rotation of the basal turn (state 1). In this case, in ventral view, the apical turn is not centered on the basal turn. Illustrations of the character states are given in Fig V.31 below. In the geometric morphometrics analyses performed in Chapter IV, this state is shared by the elephantimorphs and the deinotheriids. However, some members of this group display cochleae with centered axes of rotation. To our knowledge, this is the first attempt to test this character in a phylogenetic analysis of the proboscideans and afrotherians.

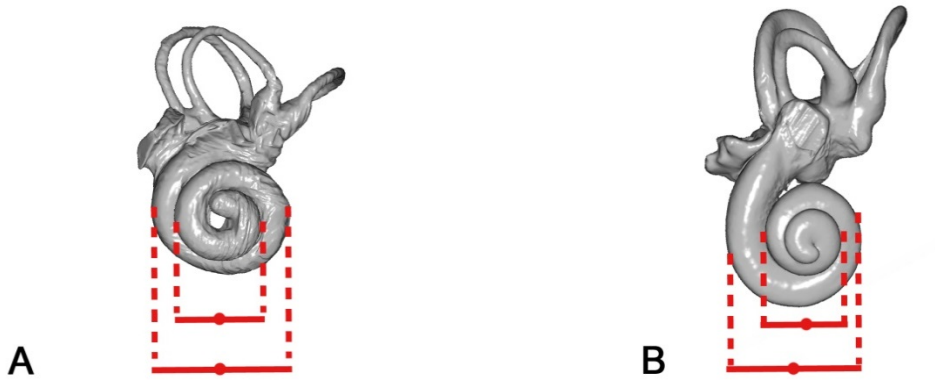

Figure V.31 : Character 32, axis of rotation of the apical turn of the cochlea, 2 states. A: state 0 (*Ocepeia daouiensis*); B: state 1 (*Elephas maximus*)

Ocepeia	*Protungulatum*	*Eritherium*	*Phosphatherium*	*Numidotherium*	*Moeritherium*	*Prodeinotherium*	*Mammut*	*Platybelodon*	*Gomphotherium*	*Cuvieronius*	*Stegomastodon*	*Stegodon*	*Anancus*	*Loxodonta*	*Palaeoloxodon*	*Elephas*	*M. columbi*	*M. primigenius*
0	0	0	?	0	?	1	1	0	1	?	0	0	1	1	?	1	?	1

4. Results & discussion

4.1. Evolution of the petrosal and the bony labyrinth in the Proboscidea

4.1.1. Cladistic analysis

The cladistic analysis performed on the ear region of Proboscidea provided 10,160 most parsimonious trees with a length of 53 steps. The strict consensus of these trees is given in Fig V.32 and displays a length of 69 steps. The consistency index (CI) is 0.493 which is very low and implies a great level of homoplasy. This contrasts with the results obtained in a preliminary analysis performed only in few proboscideans (CI = 0.905) (Chapter I, Schmitt & Gheerbrant, 2016). However, the consistency index is defective and strongly influenced by other factors than the homoplasy (Darlu & Tassy, 1993). For instance, the index tends to be higher in datasets that contains a small number of taxa which partially explains the very high consistency index found in the preliminary analysis conducted in Chapter I. To address that problem, we chose instead to use the retention index in the rest of the chapter as a measurement of the homoplasy. The retention index measures the opposite of the distortion; the higher the index, the lower the homoplasy (RI; Farris, 1989a, 1989b). Here, the index value (RI = 0.628) is higher than the consistency index value. Such a value indicates homoplasy but also shows the presence of information in the tree. While the consistency index found in this analysis (CI = 0.493) is largely lower than in the analysis in Chapter I (CI = 0.905), the difference between the two retention indices is smaller (RI = 0.833 in the analysis of Chapter I and RI = 0.628 here). This highlights the conceptual differences between the two indices. Character indices are summarized in Appendix 26.

In the analysis, the ingroup – Proboscidea – is not found monophyletic. *Ocepeia*, *Protungulatum* and *Eritherium* form a polytomy at the base of the tree (node 1). The locations of the transformations are illustrated in Fig V.32. The locations of the ambiguous transformations were fixed on a case-by-case basis, depending on the nature of the character; optimizations that seemed more plausible were favored. For most characters, the chosen optimization is ACCTRAN. Only four nodes are found in the strict consensus tree.

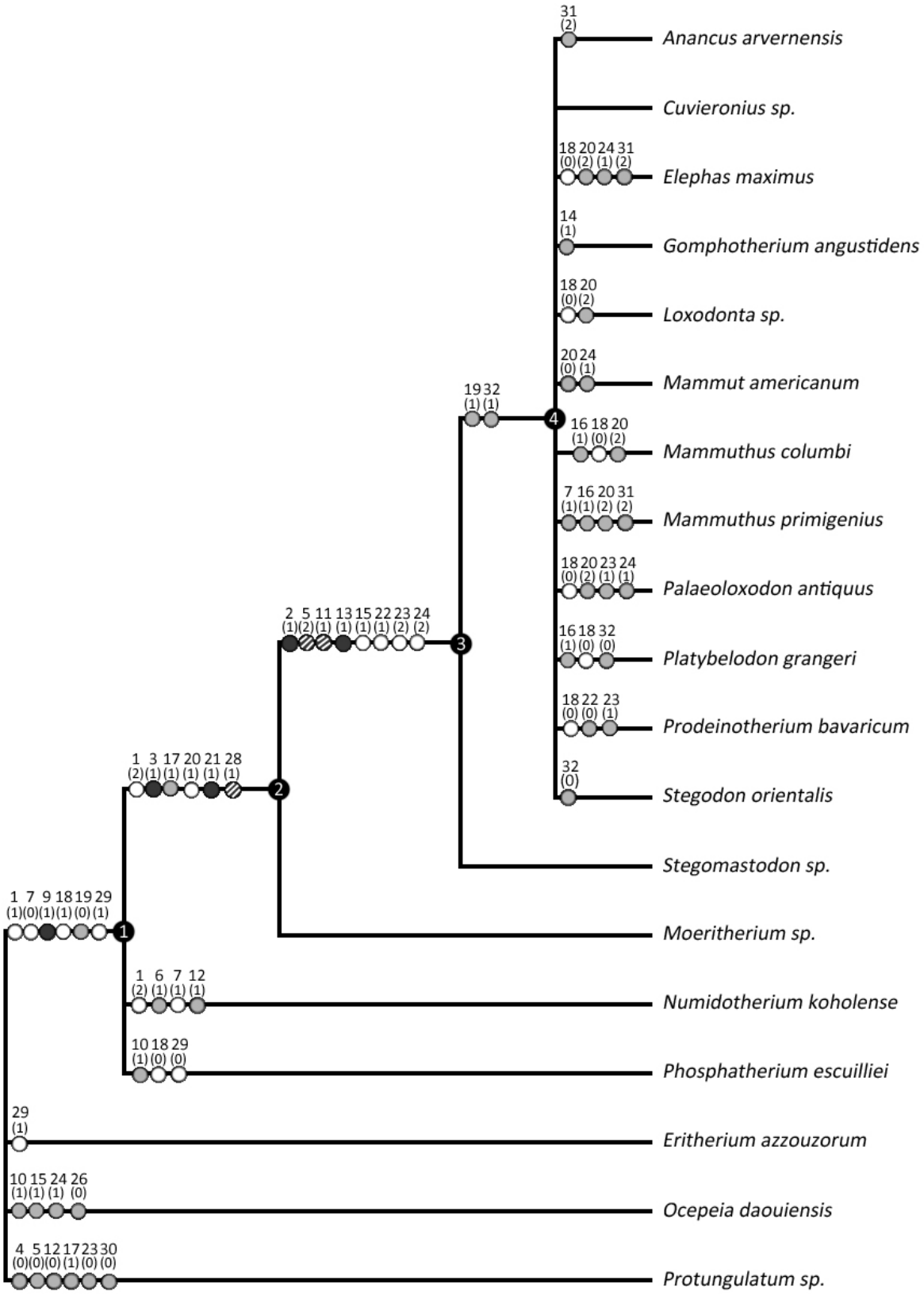

Figure V.32 : Results of the cladistic analysis performed on the ear region characters of Proboscidea. Strict consensus of the 10,160 most parsimonious trees with location of the transformations. **White dots:** ambiguously located transformations. **Grey dots:** unambiguously located transformations. **Black dots:** unambiguously located transformations that display no homoplasy (RI=1). **Black and white striped dots:** ambiguously located transformations that display no homoplasy (RI=1). The upper number is the character number and the number between brackets is the character state.

The node 1 includes all proboscideans at the exception of *Eritherium*. The existence of this clade is commonly found in cladistic analyses performed on Proboscidea (Gheerbrant, 2009; Gheerbrant & Tassy, 2009; Schmitt & Gheerbrant, 2016). This clade is supported by two non-ambiguously located synapomorphies and four ambiguously located transformations. Only one non-ambiguous synapomorphy is non-homoplastic: the transformation from a thick to a thin *crista falciformis* (character 9, 0→1). The other non-ambiguous synapomorphy is homoplastic (RI = 0.500); it is the loss of the apical extension of the anterior canal (reversed in node 4). The four ambiguously located transformations supporting the node 1 are the followings: the evolution of a deep to a moderate subarcuate fossa (character 1, RI = 0.800, 0→1), the loss of the petrosal pneumatization (character 7, RI = 0.333, 1→0), the transformation of a round to an oval posterior canal (character 18, RI = 0, 0→1) and the decrease of the relative cochlear volume (character 29, RI = 0, 0→1). The first character displays very low homoplasy but characters 7, 18 and 29 are highly homoplastic. We chose to optimize character 1 in DELTRAN. Indeed, the ACCTRAN optimization implies that the subarcuate fossa transforms from a very deep fossa to the loss of the fossa (0→2) in this node which takes two steps since the character is ordered. The loss of the fossa would be then reversed in *Phosphatherium* (2→1). This evolutionary hypothesis is highly unlikely and we hence favor the DELTRAN optimization which implies a convergent loss of the fossa in *Numidotherium* and node 2. In addition, in most phylogenetic analyses (i.e. Gheerbrant, 2009, Gheerbrant & Tassy, 2009), *Numidotherium* is contained in node 2. We chose to optimize character 7 in ACCTRAN which implies that the pneumatization of the proboscideans is lost early in proboscideans (node 2) but is then reacquired convergently in *Numidotherium* and *Mammuthus primigenius*. However, given the high level of polymorphism of this character, its evolution remains ambiguous. Character 18 is optimized in ACCTRAN as well in the tree. The optimization here is not important because the ambiguity is caused by the failure to obtain the monophyly of the Proboscidea in the analysis. This transformation would certainly be located at the presently accepted node that includes *Numidotherium* and later proboscideans but this node does not exist in our tree.

Character 29 is optimized in ACCTRAN. This implies that the relatively voluminous cochlea of *Phosphatherium* is an autapomorphy. This hypothesis is plausible as all the other studied proboscideans display a cochlea with a relatively low volume.

The node 2 includes *Moeritherium*, *Prodeinotherium* and all elephantimorphs. This clade was recovered in previous studies (Court, 1995; Delmer, 2005; Gheerbrant & Tassy, 2009; Schmitt & Gheerbrant, 2016). It is supported by three non-ambiguous synapomorphies and three ambiguously located transformations. The three non-ambiguous synapomorphies are: the retention of a unique perilymphatic foramen in adults (character 3, 0→1, RI = 1), the transformation of a round to an oval anterior semicircular canal (character 17, 0→1, RI = 0.667) and the flattening of the semicircular canals in cross-section (character 21, 0→1, RI = 1). Characters 3 and 21 are non-homoplastic and character 17 displays a moderate level of homoplasy. This node is therefore supported by three solid synapomorphies. The three ambiguously located transformations supporting node 2 are: the loss of the subarcuate fossa (character 1, 1→2, RI = 0.800), the transformation of a lateral canal entering into the vestibule at a high and close position to a high and distant position (character 20, 0→1, RI = 0.444) and the loss of the *lamina secundaria* (character 28, 0→1, RI = 1). Character 28 is non-homoplastic and character 1 display very few homoplasy but character 20 is highly homoplastic. The DELTRAN optimization of character 1 was already discussed in the precedent paragraph. The ambiguity of the transformation location of character 20 (0→1) is caused by the missing data in *Moeritherium* and *Stegomastodon*. We chose here to place the transformation at its earliest possible location. The ambiguity of the transformation location of character 28 (0→1) is caused by the missing data in *Moeritherium*. We chose to place the transformation at its earliest possible location because the loss of the *lamina secundaria* seems to happen early in proboscidean evolution. In fact, the lamina is not found in one of the two *Numidotherium* studied cochleae.

The node 3 includes *Prodeinotherium* and the elephantimorphs. This clade was recovered in previous studies (Gheerbrant & Tassy, 2009). It is supported by two non-

ambiguous synapomorphies and six ambiguously located transformations. The two non-ambiguous synapomorphies are: the transformation of a dorsally-oriented to an anteriorly-oriented internal auditory meatus (character 2, 0→1, RI = 1) and the acquisition of poorly-defined bony ampullae (character 13, 0→1, RI = 1). Both characters are non-homoplastic and support this node well. The six ambiguously located transformations supporting the node 2 are: the acquisition of a prominent and flat *tegmen tympani* (character 5, 1→2, RI = 1), the development of a deep groove likely for the middle meningeal artery on the cerebral surface of the *tegmen tympani* (character 11, 0→1, RI = 1), the thickening of both the *crus commune* (character 15, 0→1, RI = 0.500) and the semicircular canals (character 22, 0→1, RI = 0.750), the reduction of the lateral canal (character 23, 1→2, RI = 0.667) and the loss of contact between the posterior and lateral canals (character 24, 0→2, two steps, RI = 0.600). The first two characters (5 and 11) are non-homoplastic, while characters 15, 22, 23 and 24 display relatively moderate homoplasy. The ambiguity of the transformation location of character 5 (1→2) is caused by the missing data in *Moeritherium*. The transformation can be placed at nodes 2 or 3, but we chose to place it at node 3. Indeed, this node groups proboscideans that seem to display globally the same pattern of petrosal anatomy. The petrosal of *Moeritherium* display several features closer to early proboscideans (e.g. orientation of the internal auditory meatus). Hence the transformation is placed later at node 3. The same can be said about character the transformation location of character 11 (0→1). The ambiguity of the transformation location of character 15 (0→1) is also caused by the missing data in *Moeritherium.* The *crus commune* thickness ratio of *Moeritherium* could not be calculated, however, the crus appears elongated and not very thick and *Moeritherium* would be certainly coded 0 if the crus was preserved enough. Hence, the transformation of character 15 is placed at node 3. The ambiguity of the transformation location of character 22 (0→1), 23 (1→2) and 24 (0→2) is caused by the missing data in both *Moeritherium* and *Stegomastodon.* They were not placed at node 4 because the existence of this node is highly improbable. Since *Moeritherium* displays a general anatomy that seems closer to earlier proboscideans than to elephantimorphs, the transformations were placed at node 3.

The node 4 includes all taxa of the node 3 at the exception of *Stegomastodon*. Contrary to the other nodes, the node 4 is unusual as *Stegomastodon* is generally found as a gomphother close to other American genera such as *Cuvieronius* (Mothé et al. 2016a). This clade is only supported by two non-ambiguous synapomorphies that are homoplastic. The first synapomorphy is the re-acquisition of an anterior canal apex (character 19, 0→1, RI = 0.500), a feature lost in node 1 in this tree. The anterior canal apex is indeed absent in both studied ears of *Stegomastodon*. The second synapomorphy is the offset of the axis of rotation of the cochlear apical turn with respect the axis of the basal turn (character 32, 0→1, RI = 0.667) which is lost convergently in *Platybelodon* and *Stegodon*. Both characters display moderate level of homoplasy.

Within the node 4 the elephantimorphs and *Prodeinotherium* form a large polytomy due to a high level of homoplasy. Several synapomorphies of consensual groups are therefore depicted here as convergences. One example is the transformation from a high and distant to a low point of entry of the lateral canal into the vestibule (character 20, 1→2 RI = 0.444). This transformation appears as convergent autapomorphies of *Elephas*, *Loxodonta*, both *Mammuthus* species and *Palaeoloxodon* (5 steps) on the consensus tree. However, these taxa are all Elephantidae which is an undebated clade of proboscideans. If this clade had been found in our analysis, the transformation of character 20 (1→2) would have been one of its synapomorphy.

The moderately high level of homoplasy of our tree prevents from getting a good resolution of the internal topology of the proboscideans and especially of the elephantimorphs. However, the same analysis performed with implied weighting displays a slightly better resolution within early proboscideans (see Appendix 27). The phylogenetic signal carried by the ear region of proboscideans allows the distinction of only three congruent clades in our tree (node 1, 2 and 3). The monophyly of Proboscidea is not obtained and the phylogenetic relationships within elephantimorphs are not solved. Therefore, we cannot discuss the evolution of these characters among the main proboscidean taxa. For this reason, we studied the distribution of the ear characters of our proboscidean sample taxa in a mapped consensual tree (for the method, see § 2.2.2.).

4.1.2. Character cartography on the proboscidean tree

1. Subarcuate fossa

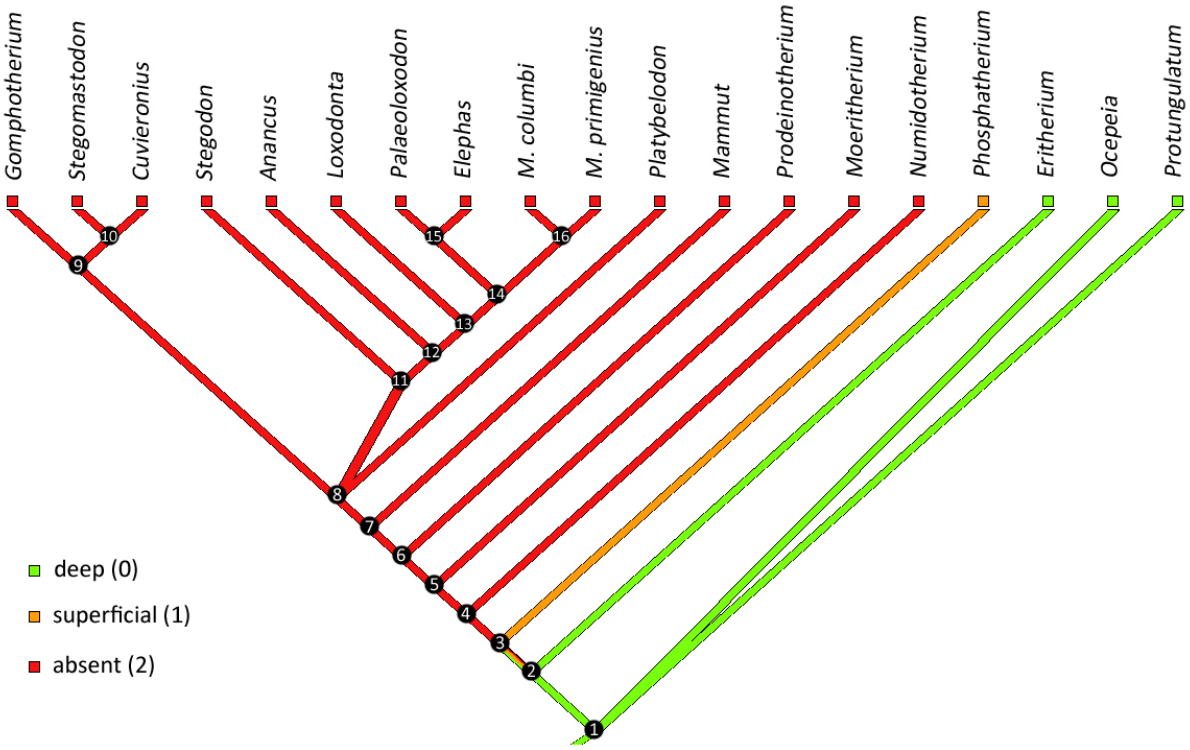

Figure V.33 : Mapping of character 1 (depth of the subarcuate fossa) on the proboscidean tree.

The evolution of the subarcuate fossa depth within Proboscidea appears to be rather simple (Fig V.33). The subarcuate fossa is ancestrally deep. This is a plesiomorphy retained by *Eritherium* which displays a particularly deep and spherical fossa. *Phosphatherium* displays a more moderate and superficial fossa. The transformation from the state deep (0) to the state superficial (1) can be an autapomorphy of *Phosphatherium* but we consider the progressive filling of the fossa to be an ordered character (morphological cline), hence it is more parsimonious to place this transformation at the node representing the ancestor of all proboscideans except *Eritherium* (node 3). The subarcuate fossa is fully filled in later proboscideans (node 4) which all lack a distinct subarcuate fossa on the cerebellar surface of the petrosal.

2. Internal auditory meatus orientation

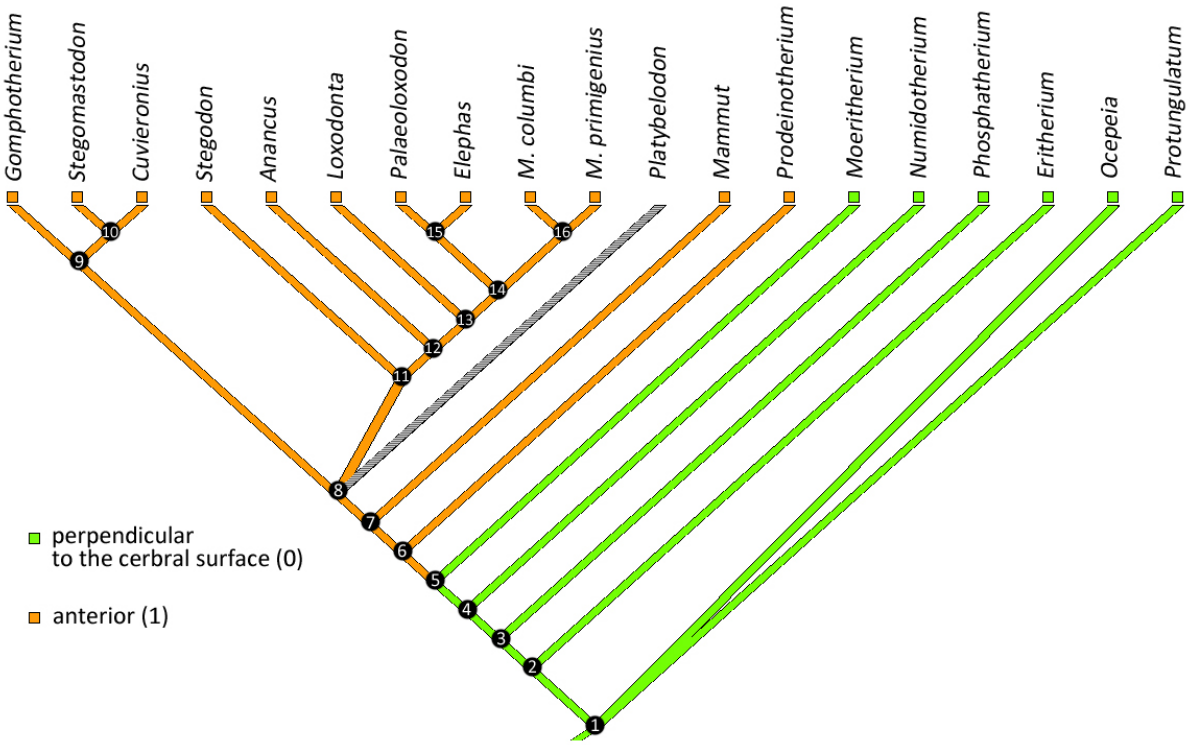

Figure V.34 : Mapping of character 2 (orientation of the internal auditory meatus) on the proboscidean tree.

The evolution of the internal auditory meatus orientation within Proboscidea seems to be simple as well (Fig V.34). The vast majority of mammals display an internal auditory meatus with dorsally-oriented acoustical foramens. Indeed, the cranial nerves VII and VIII exit the meatus with a trajectory that is perpendicular to the cerebellar surface (state 0, see Fig V.2) hence directed dorsally. This plesiomorphy is retained in early proboscideans such as *Eritherium*, *Phosphatherium, Numidotherium* and *Moeritherium*. The orientation of the meatus is modified in the clade that includes the elephantimorphs and the deinotheriids (node 6). The foramens are directed anteriorly and the trajectory of the cranial nerves VII and VIII is parallel to the cerebellar surface of the petrosal (state 1, see Fig V.2). This structure has been observed in all members of this clade except *Platybelodon*, which internal auditory meatus was not clearly observable. However, the character optimization suggests that *Platybelodon* would display an anteriorly oriented meatus as other elephantimorphs and *Prodeinotherium*.

3. Perilymphatic foramen

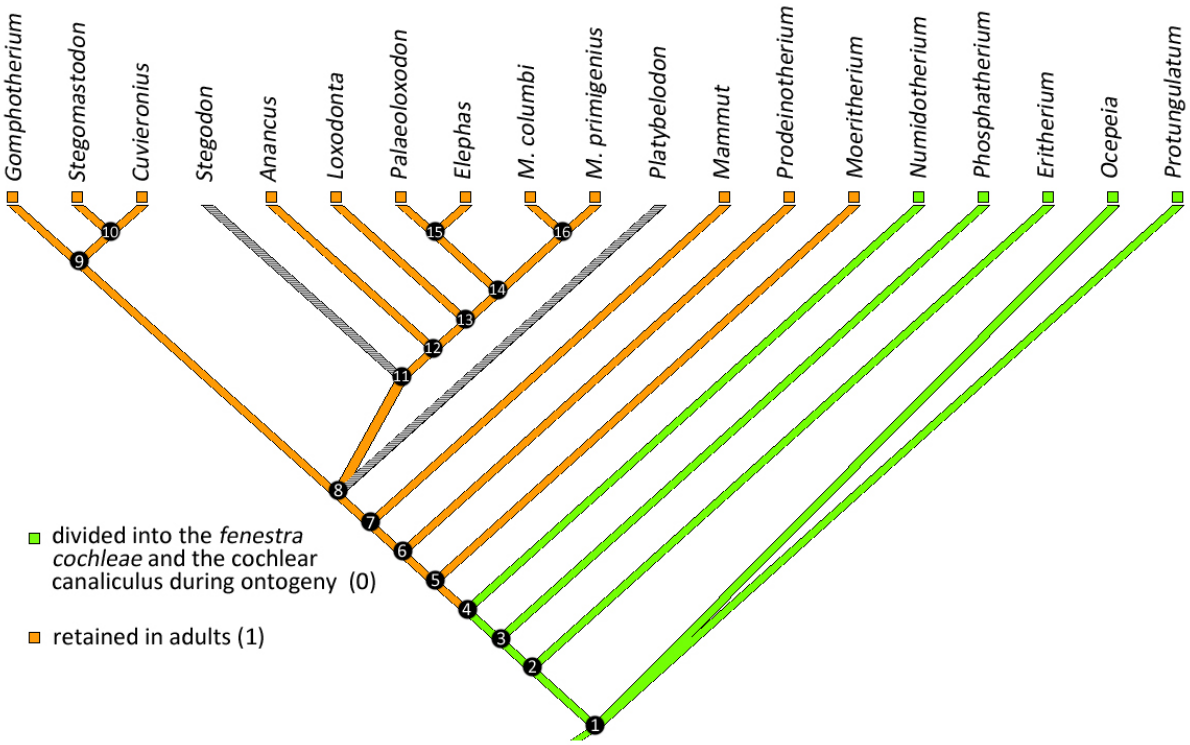

Figure V.35 : Mapping of character 3 (perilymphatic foramen) on the proboscidean tree.

The evolution of the retention of the unique perilymphatic during ontogeny in the Proboscidea is illustrated in Fig V.35. The vast majority of mammals display the two foramens in adult life. This is a plesiomorphy that is retained in early proboscideans (*Eritherium*, *Phosphatherium* and *Numidotherium*). The *aquaeductus cochleae* is not clearly visible in *Eritherium*, however the presence of a broken foramen at the level of the jugular fossa tips the scale in favor of its presence. On the other hand, the other proboscideans retain the perilymphatic foramen during adult life. This paedomorphic character appears to be a synapomorphy of the clade containing *Moeritherium*, deinotheriids and elephantimorphs (node 5). The structure was not clearly observable on several taxa (*Platybelodon, Stegodon*) but the most parsimonious optimization is to consider them having a unique perilymphatic foramen. This is supported by the fact that these taxa display several features that seem characteristic of the elephantimorph morphotype (*tegmen tympani* forming a flat cerebral surface, anterior orientation of the internal auditory meatus…) and all the elephantimorphs studied here display a perilymphatic foramen.

4. Mastoid apophysis

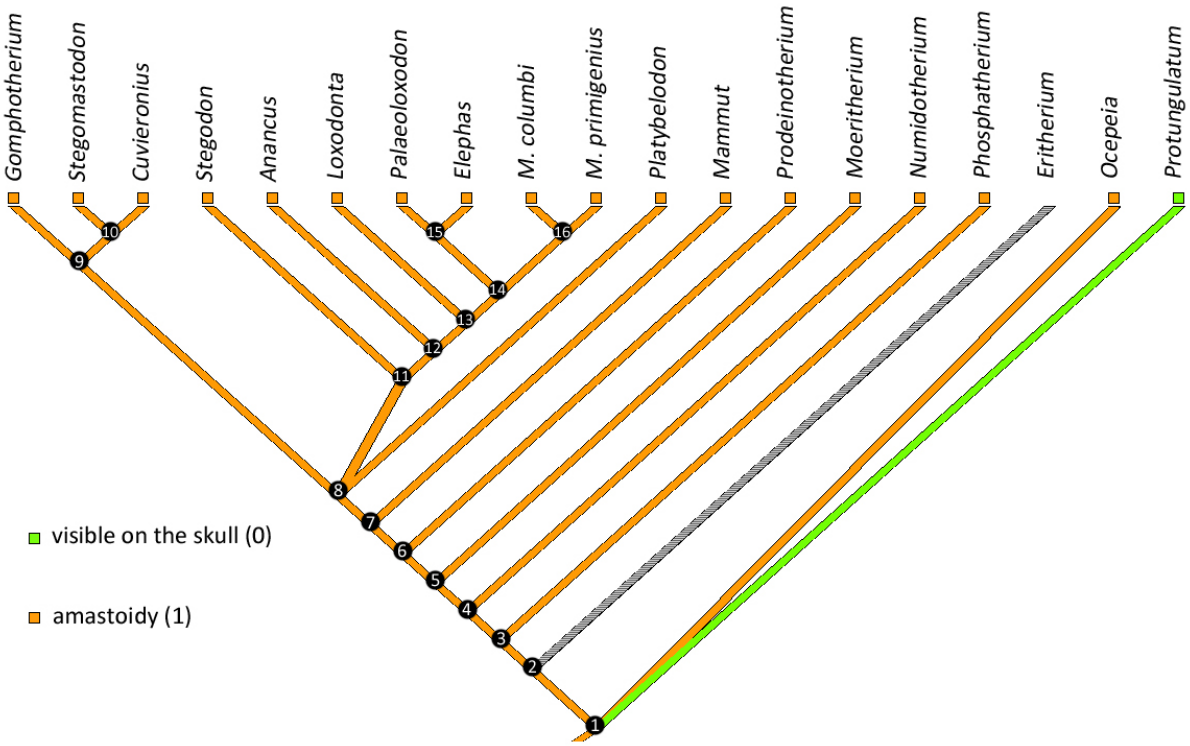

Figure V.36 : Mapping of character 4 (mastoid apophysis) on the proboscidean tree.

The mastoid apophysis is not visible on the skull of extant elephants. This condition is called amastoidy. Evolution of this character within Proboscidea is illustrated in Fig V.36. This character state is constant among Proboscidea, as no representatives of the order display a visible mastoid apophysis. The amastoid condition is also found in *Ocepeia daouiensis* (Gheerbrant et al. 2014). The state "visible" appears as an autapomorphy of *Protungulatum* on the tree but it is actually the generalized condition of eutherian mammals.

5. *Tegmen tympani* shape

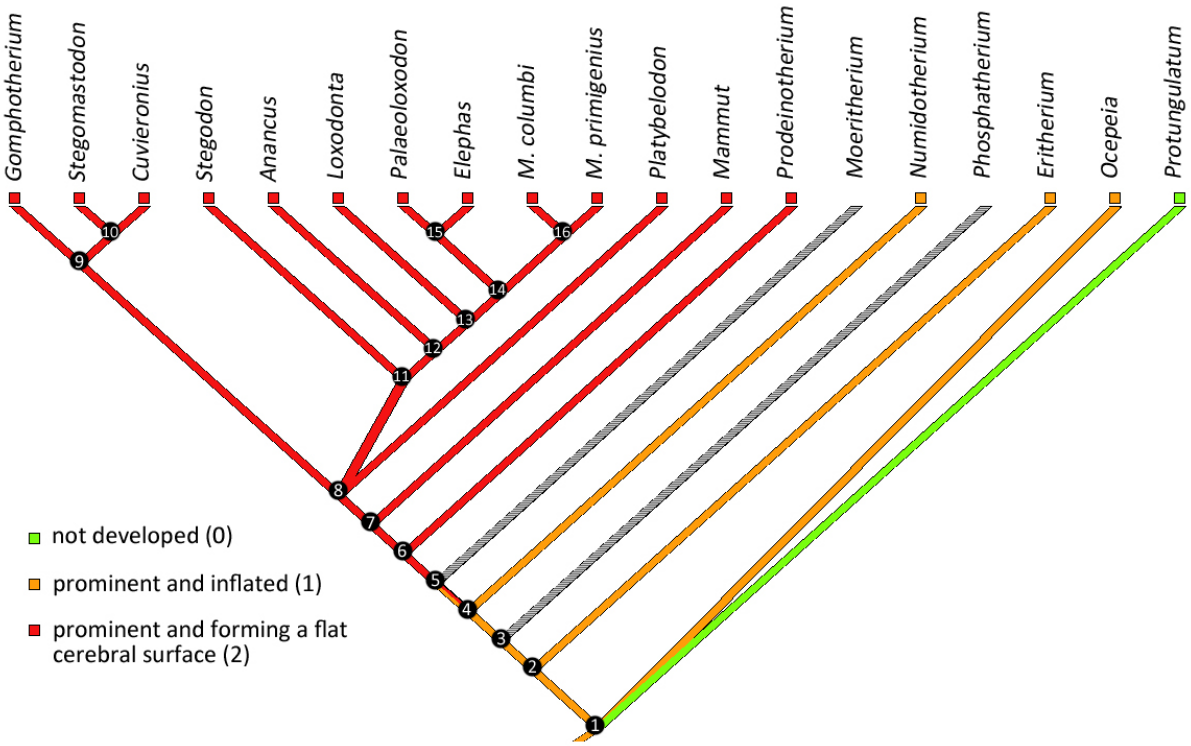

Figure V.37 : Mapping of character 5 (*tegmen tympani* shape) on the proboscidean tree.

Evolution of the *tegmen tympani* shape within Proboscidea is illustrated in Fig V.37. The *tegmen tympani* is primitively prominent and inflated in Proboscidea. Early afrotherian *Ocepeia* also displays such feature, suggesting its larger distribution in paenungulates. The *tegmen tympani* of *Eritherium* is very similar to that of *Ocepeia*, being inflated and having a somewhat tubular shape. In *Numidotherium*, The *tegmen tympani* is not tubular as in *Eritherium* but it is still prominent and inflated. The information is missing in *Phosphatherium* and *Moeritherium*. The prominent *tegmen tympani* that forms a flat cerebral surface is likely a synapomorphy of node 6 (clade that includes elephantimorphs and deinotheriids). Several features of the elephant morphotype actually occur at this node (e.g. anteriorly-oriented internal auditory meatus) which seems indeed to correspond to a key new evolutionary stage in the Proboscidea. A similar morphology in members of this clade is also supported by geometric morphometrics analyses of the inner ear (Chapter IV).

6. *Hiatus Fallopii*

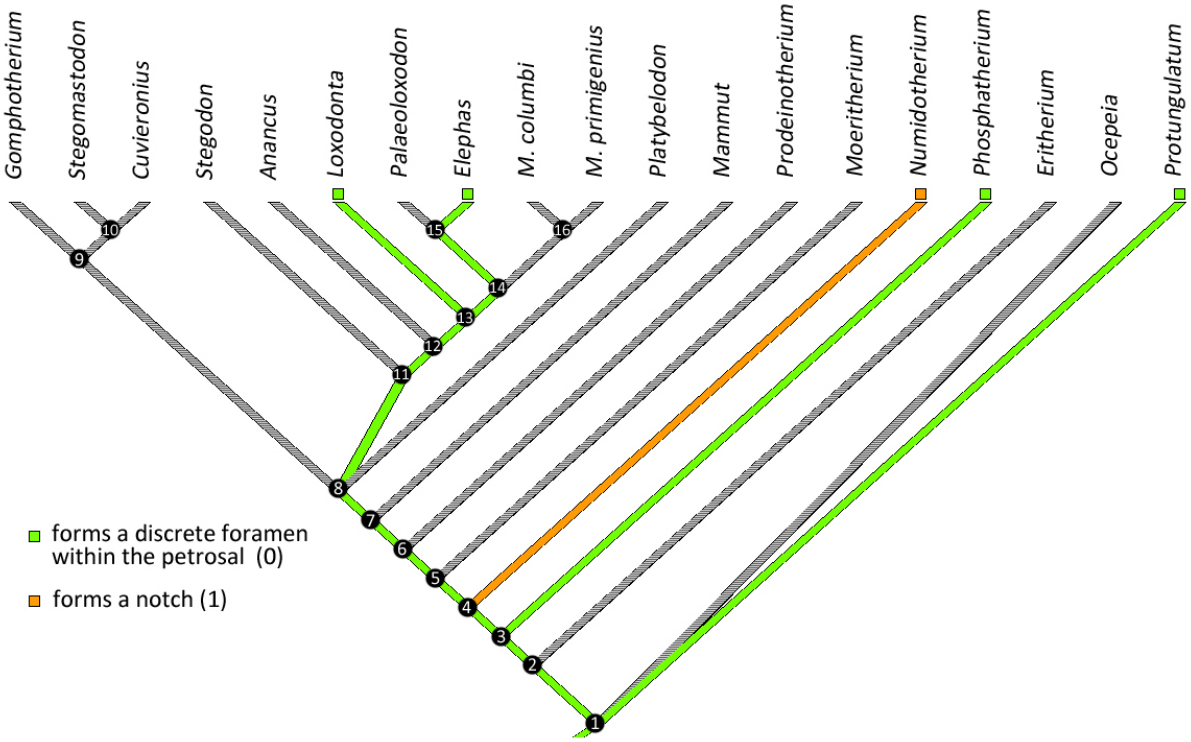

Figure V.38 : Mapping of character 6 (*hiatus fallopii*) on the proboscidean tree.

Evolution of the *hiatus Fallopii* in proboscideans remains mainly unknown (Fig V.38). This character is difficult to observe on fossils, the region carrying this structure being often broken. The *hiatus Fallopii* forms a discrete foramen in *Phosphatherium* and extant elephants. This condition seems to be generalized in proboscideans but the information is missing for the most part. To the best of our knowledge, the notch aspect of the *hiatus Fallopii* is an autapomorphy of *Numidotherium*.

7. Pneumatization of the petrosal

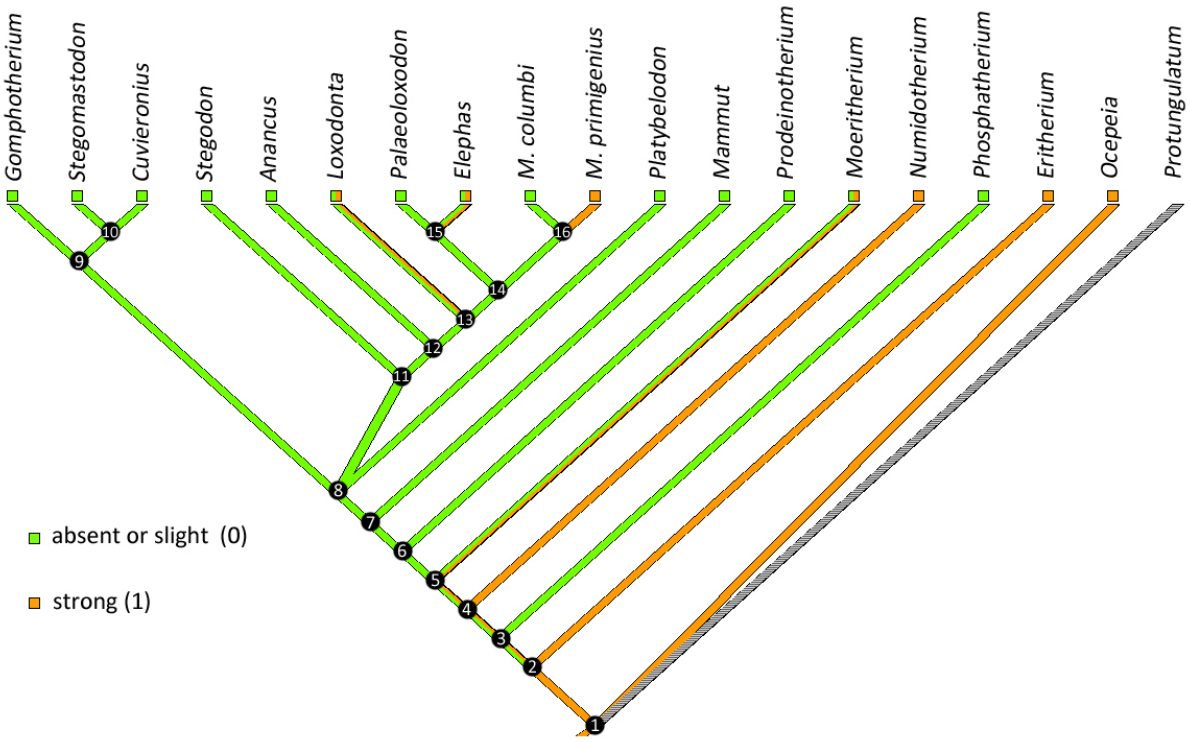

Figure V.39 : Mapping of character 7 (pneumatization of the petrosal) on the proboscidean tree.

Evolution of the petrosal pneumatization in proboscideans is illustrated in Fig V.39. The petrosal appears to be primitively pneumatized in proboscideans. The early paenungulate *Ocepeia* displays a highly pneumatized petrosal, especially in the region of the *tegmen tympani*. The petrosal of *Eritherium* is similar and exhibits numerous osseous cells. The loss of the pneumatization is of ambiguous location within Proboscidea. It could be a convergent loss in *Phosphatherium* and node 5 but the character is polymorphic in *Moeritherium*. In fact, the character is polymorphic in many taxa (*Loxodonta*, *Elephas*, *and Moeritherium*) and seems to be quite variable intra-specifically. In *Loxodonta*, the most pneumatized specimen is MNHN.AC.ZM.1961-69, a very young (15 days) African forest elephant calf. Therefore, this character could be variable during ontogeny. Anyway, this character is highly homoplastic in Proboscidea and its evolutionary history remains ambiguous.

8. Prootic sinus

The prootic sinus is absent in all studied proboscideans. Therefore, the character is constant in this mammal order. This character is only useful in analyses performed on Afrotheria or Eutheria.

9. Crista falciformis

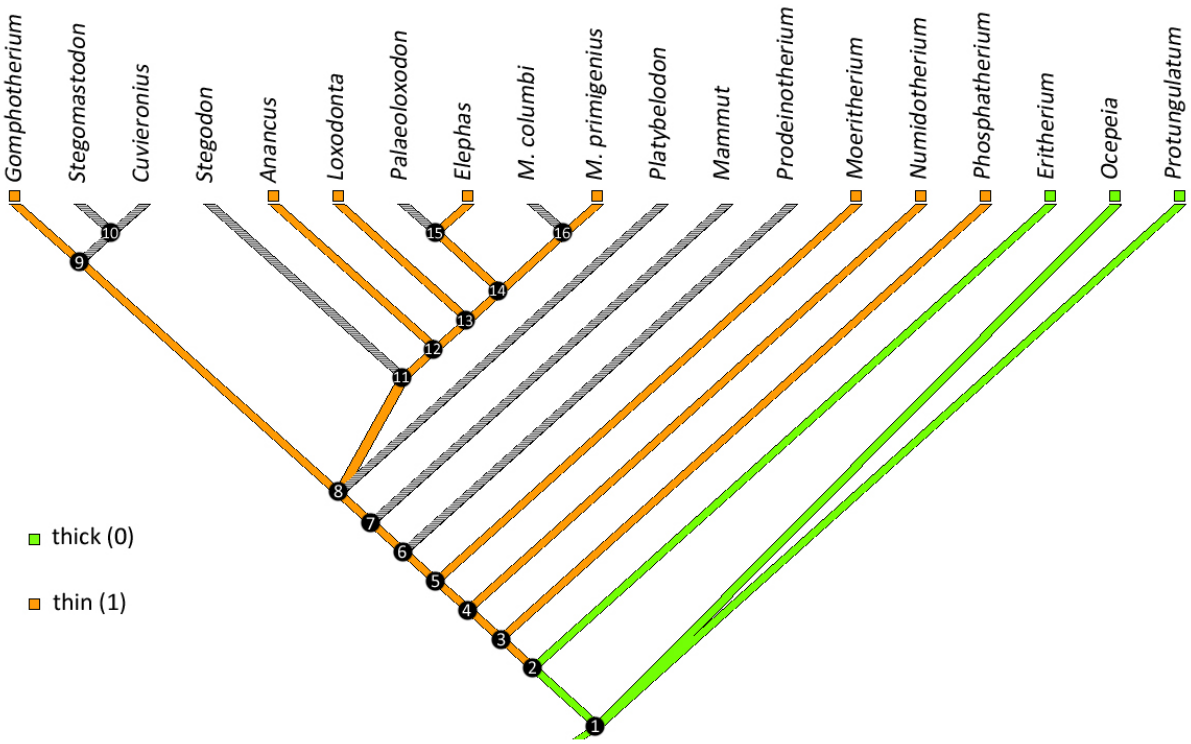

Figure V.40 : Mapping of character 9 (*crista falciformis*) on the proboscidean tree.

Evolution of the thickness of the *crista falciformis* within Proboscidea is illustrated in Fig V.40. The *crista falciformis* is primitively thick in the Proboscidea. Outgroups such as *Protungulatum* and *Ocepeia* exhibit a thick and solid crista. This plesiomorphy is retained in *Eritherium*. A thin *crista falciformis* is a synapomorphy of the node 3 (all proboscideans at the exception of *Eritherium*). The *crista falciformis* remains thin in later proboscideans. For several taxa (*Stegomastodon*, *Cuvieronius*, *Stegodon*, *Palaeoloxodon*, *Platybelodon*, *Mammut* and *Prodeinotherium*), the information is coded missing because the whole region of the internal auditory meatus is broken. However, we assume that the crista is probably thin in these taxa as well.

10. Petromastoid canal

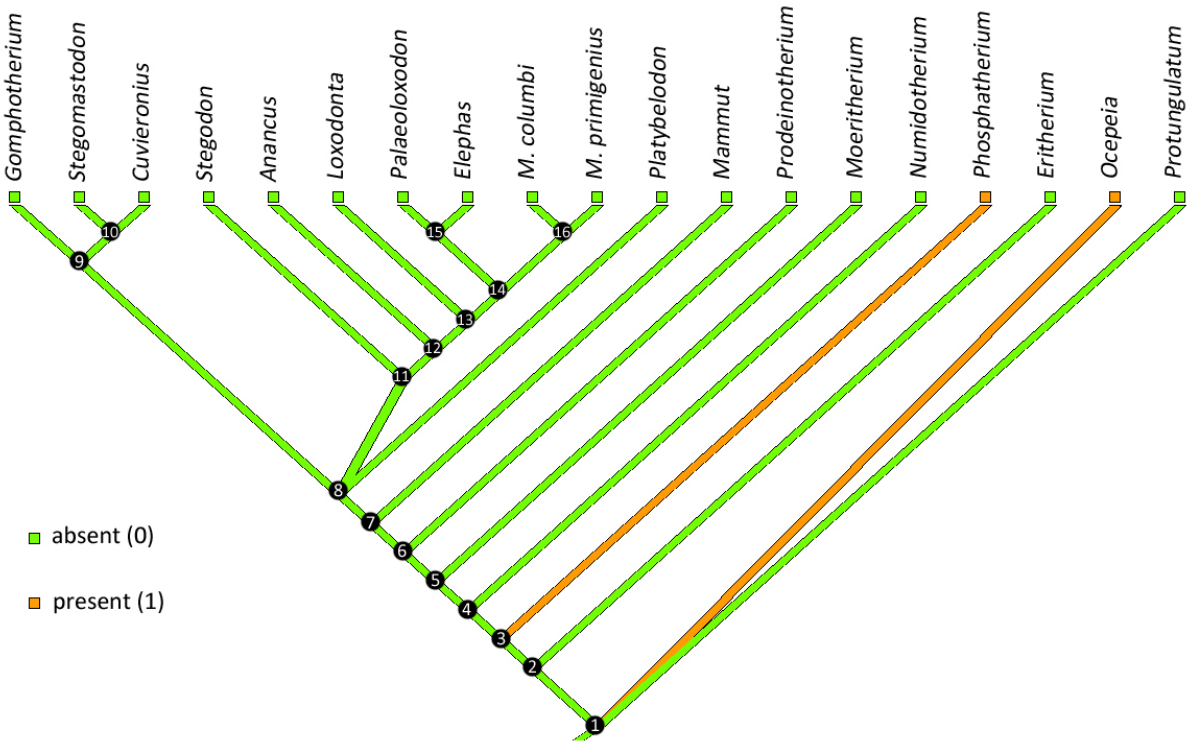

Figure V.41 : Mapping of character 10 (petromastoid canal) on the proboscidean tree.

Evolution of the petromastoid canal within Proboscidea is illustrated in Fig V.41. The petromastoid canal is likely present in outgroup taxon *Ocepeia* but not in *Protungulatum*. This feature seems to be primitively absent in Proboscidea as there is no trace of a petromastoid canal in *Eritherium*. Only *Phosphatherium* seems to display such canal at the bottom of its subarcuate fossa. This implies that this feature is an autapomorphy of *Phosphatherium*. The petromastoid canal is not observed in other proboscidean specimens. The other hypothesis would be the primitive presence of the petromastoid canal in Paenungulata (as suggested in Benoit et al. 2013b) and its convergent reversion in *Eritherium* and node 4. This character is not much informative within Proboscidea and is therefore more interesting to use in analyses performed on afrotherian or eutherian mammals in general.

11. Groove for the middle meningeal artery

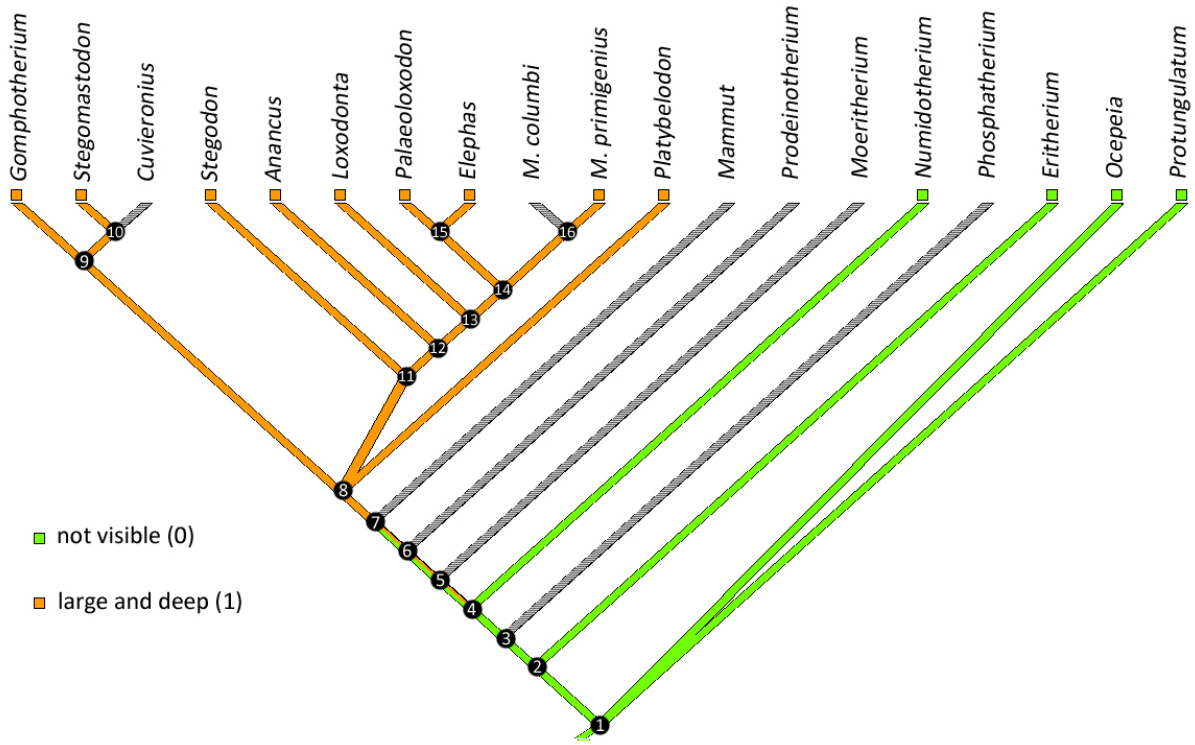

Figure V.42 : Mapping of character 11 (groove for the middle meningeal artery) on the proboscidean tree.

Evolution of the groove for the middle meningeal artery within Proboscidea is illustrated in Fig V.42. When present, the groove is large and deep and located on the cerebral surface of the *tegmen tympani*. The groove seems to be primitively absent in Proboscidea. Outgroups and early proboscideans all lack this feature. The location of the acquisition of the groove in the tree is ambiguous because the *tegmen tympani* is partially broken in *Prodeinotherium* and *Mammut*. The transformation could be a synapomorphy of nodes 5, 6, 7 (Elephantimorpha) or 8. However, given that this character is likely to be linked with the presence of a prominent and flat *tegmen tympani* that forms a cerebral surface, the transformation is probably a synapomorphy of the node 6.

12. Transpromontory sulcus

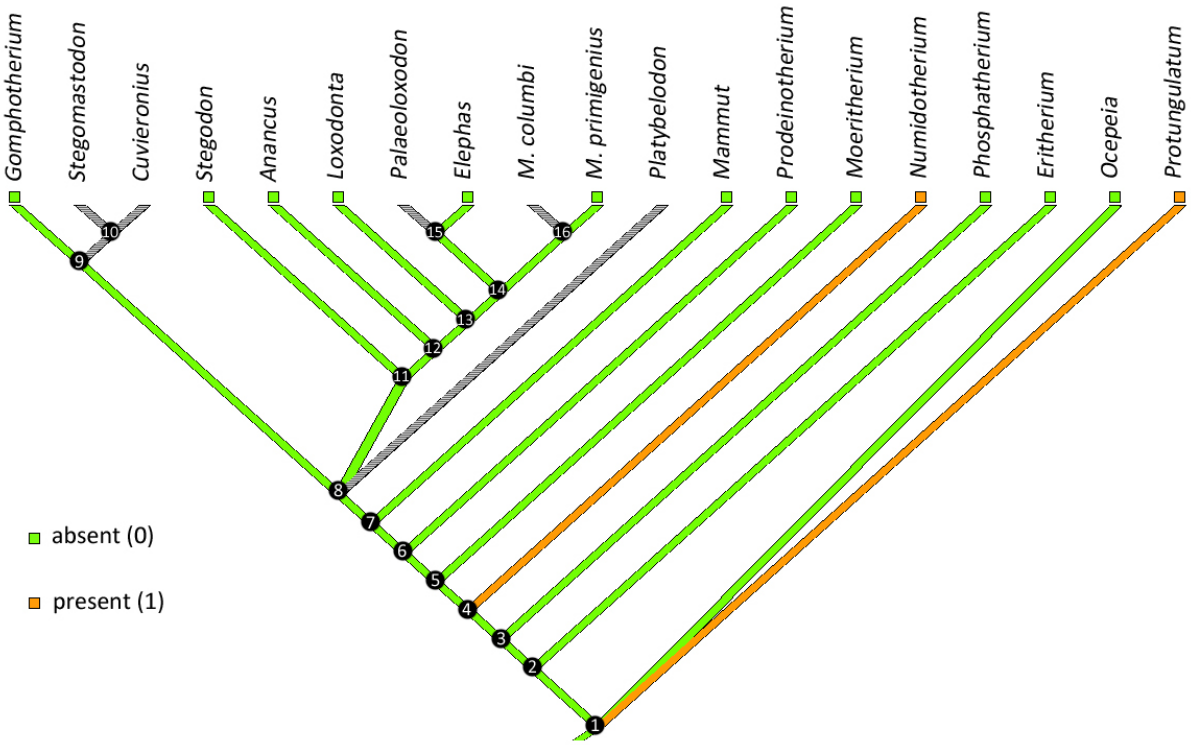

Figure V.43 : Mapping of character 12 (transpromontory sulcus) on the proboscidean tree.

Evolution of the transpromontory sulcus within Proboscidea is illustrated in Fig V.43. This character is primitively absent in proboscideans. The early paenungulate *Ocepeia* and the early proboscideans *Eritherium* and *Phosphatherium* all lack a transpromontory sulcus. However, the *promontorium* of the outgroup taxon *Protungulatum* exhibit such feature. Other proboscideans do not exhibit this sulcus at the exception of *Numidotherium*. Therefore, the acquisition of the transpromontory sulcus is considered an autapomorphy of this taxon. However, it should be noticed that this sulcus is never really deep and that its absence does not necessarily mean that there were no blood vessels running on the *promontorium*, only that these vessels did not excavate the bony surface of the petrosal.

13. Definition of the ampullae

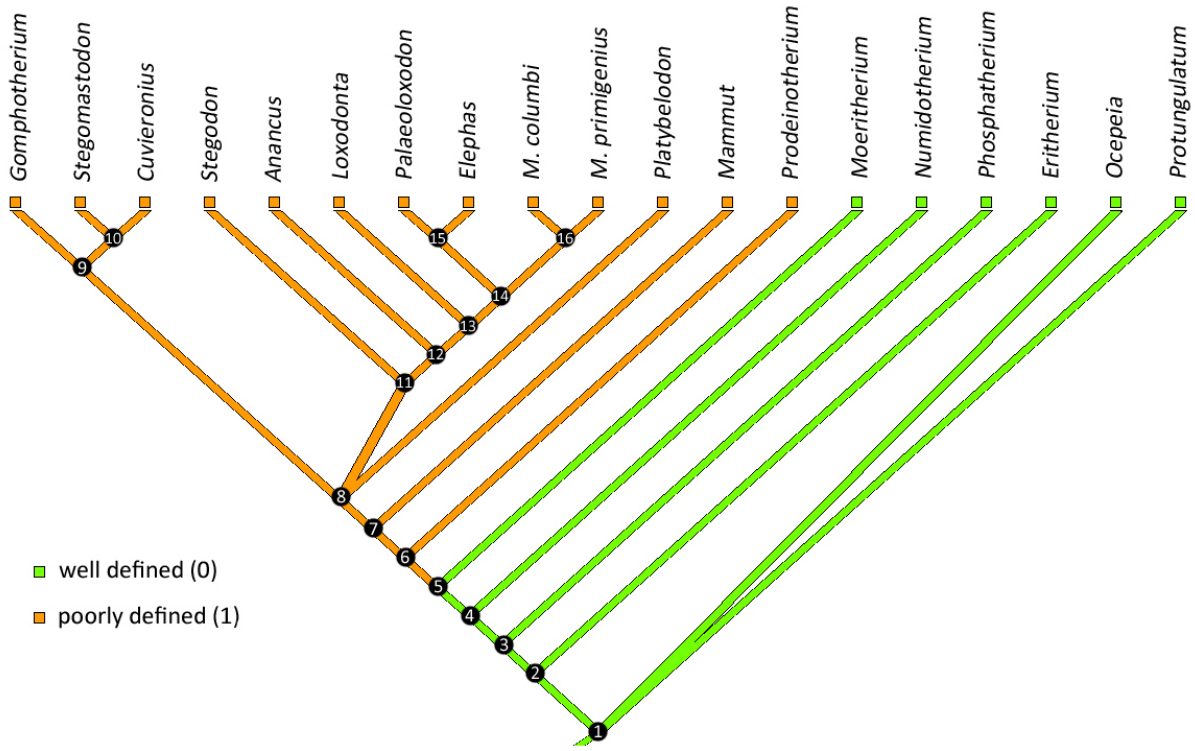

Figure V.44 : Mapping of character 13 (definition of the ampullae) on the proboscidean tree.

The ampullae of the bony semicircular canals are well-defined in most mammals (Fig V.44). In *Protungulatum* and the early afrotherian *Ocepeia*, the ampullae are bulbous and well distinct on the reconstruction. This plesiomorphy is retained in early proboscideans (*Eritherium*, *Phosphatherium*, *Numidotherium* and *Moeritherium*). By contrast, later proboscideans display bony labyrinths in which the ossification does not define distinct ampullae. The ampullae have less distinct limits and are less bulbous than in early proboscideans. This transformation is a synapomorphy of the clade containing the deinotheriids and the elephantimorphs.

14. Basal thickening of the *crus commune*

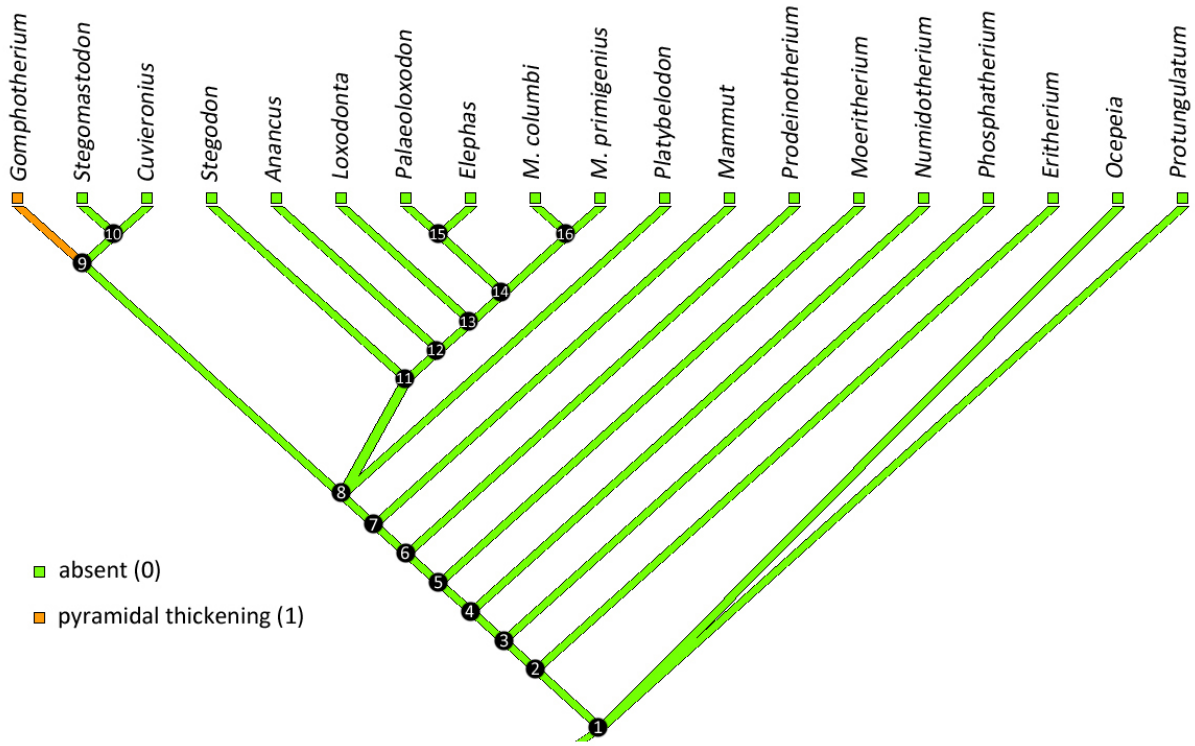

Figure V.45 : Mapping of character 14 (basal thickening of the *crus commune*) on the proboscidean tree.

The *crus commune* in *Protungulatum* and *Ocepeia* is not particularly thickened basally (Fig V.45). This plesiomorph state is retained in almost every studied proboscidean taxa. While several specimens display a *crus commune* with a slight basal thickening (*Cuvieronius*, some specimens of *Anancus*…), both studied specimens of *Gomphotherium* display a characteristic pyramidal-shaped basal thickening. Such a character appears to be autapomorphic in our taxa sample. However, the bony labyrinth of an elephantimorph described in Ekdale (2011) displays a basal thickening similar to what can be observed in *Gomphotherium*.

15. Thickness of the *crus commune*

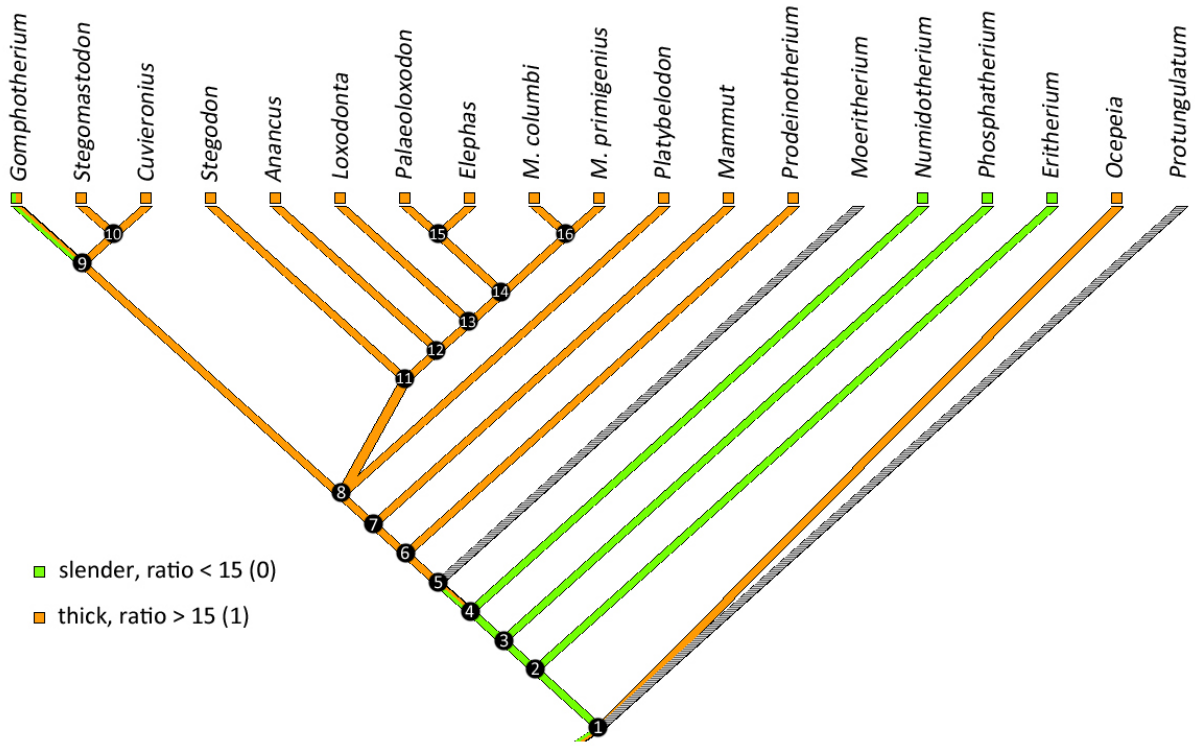

Figure V.46 : Mapping of character 15 (thickness ratio of the *crus commune*) on the proboscidean tree.

The evolution of the *crus commune* thickness ratio within proboscideans is illustrated in Fig V.46. The *crus commune* of *Ocepeia* is considered thick with our coding protocol but its ratio (17.4) is close to the limit between states (15). In the proboscideans, however, the *crus commune* seems to be primitively slender as early taxa display a very small ratio (*Eritherium*, *Phosphatherium*, *Numidotherium*). The thickening of the *crus commune* in later proboscideans is a synapomorphy that appeared either in node 5 or 6 (it was not possible to calculate the ratio in *Moeritherium*). *Gomphotherium* display polymorphism as the CBar coll. V2 specimen ratio is under 15.

16. Meeting point of the anterior and posterior canals into the *crus commune*

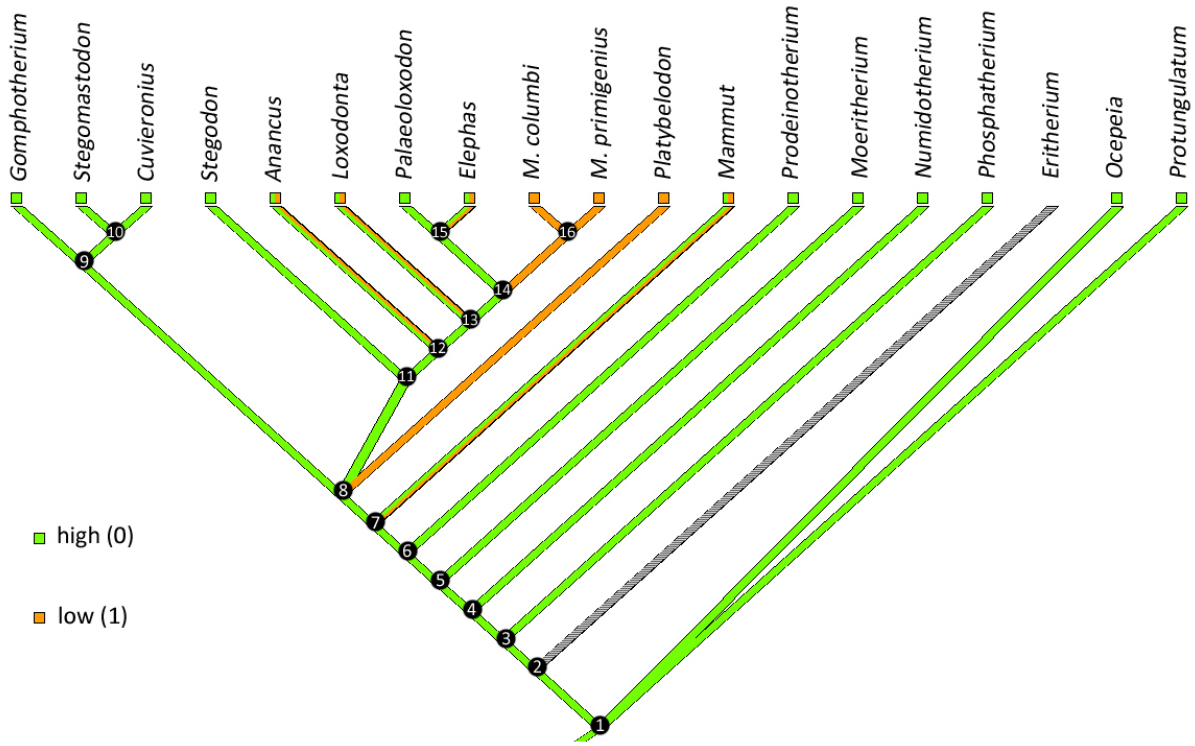

Figure V.47 : Mapping of character 16 (meeting point of the anterior and posterior canals into the *crus commune*) on the proboscidean tree.

The plesiomorphic state of this character is undoubtedly a high meeting point of the anterior and posterior canals into the *crus commune* (Fig V.47). This is observed in *Ocepeia* and Protungulatum as well as in early proboscideans (*Phosphatherium*, *Numidotherium*, *Moeritherium*, *Prodeinotherium* and one specimen on *Mammut*). The apical part of the bony labyrinth is broken in *Eritherium* so this character is missing in this taxon. However, the most parsimonious optimization would be to consider the meeting point of *Eritherium* to be high as well. A low meeting point seems to develop convergently in several groups of proboscideans: it is a synapomorphy of the *Mammuthus* clade and an autapomorphy of *Platybelodon*. On the other hand, a high level of polymorphism was found in *Elephas*, *Mammut*, *Loxodonta* and *Anancus*.

17. Overall shape of the anterior semicircular canal

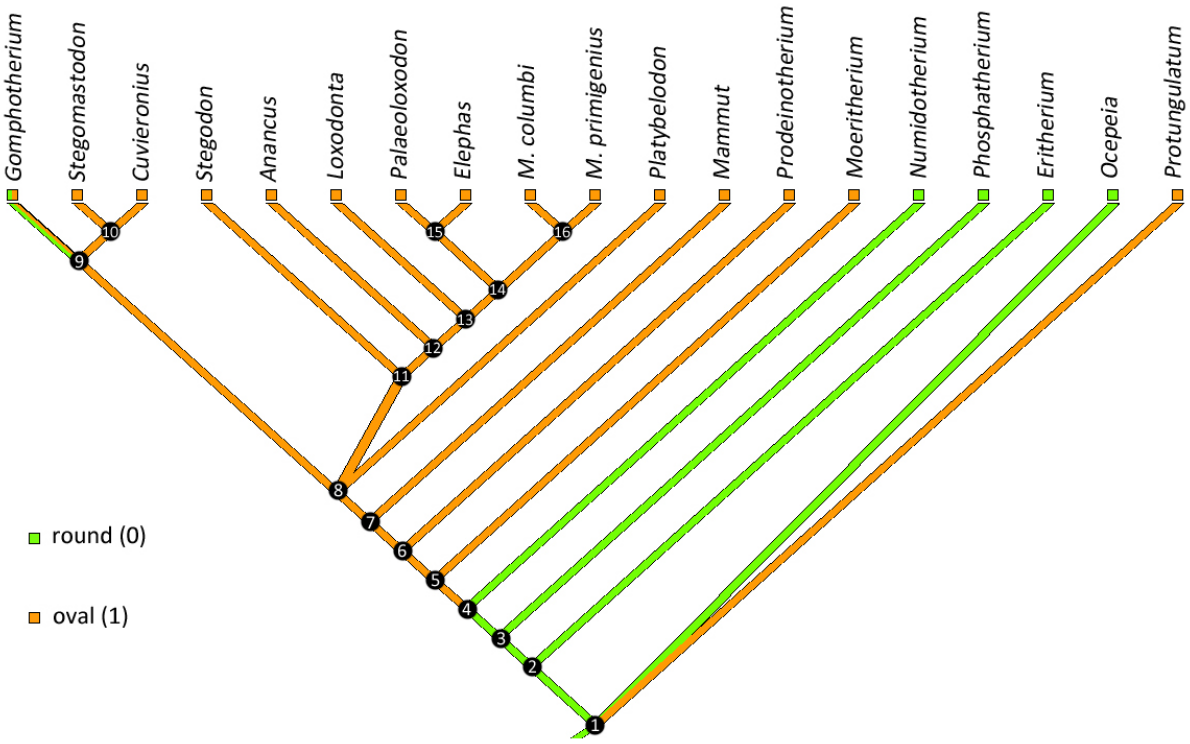

Figure V.48 : Mapping of character 17 (overall shape of the anterior canal) on the proboscidean tree.

The evolution of the anterior semicircular canal shape within Proboscidea is quite simple (Fig V.48). The canal is plesiomorphically round. This plesiomorphy is retained in *Eritherium*, *Phosphatherium* and *Numidotherium*. The shape of the canal becomes oval at node 5 (clade including *Moeritherium*, deinotheriids and elephantimorphs). *Gomphotherium* display some polymorphism; the canal is round in specimen CBar coll. V2 and oval in MNHN.F.SEP38.

18. Overall shape of the posterior semicircular canal

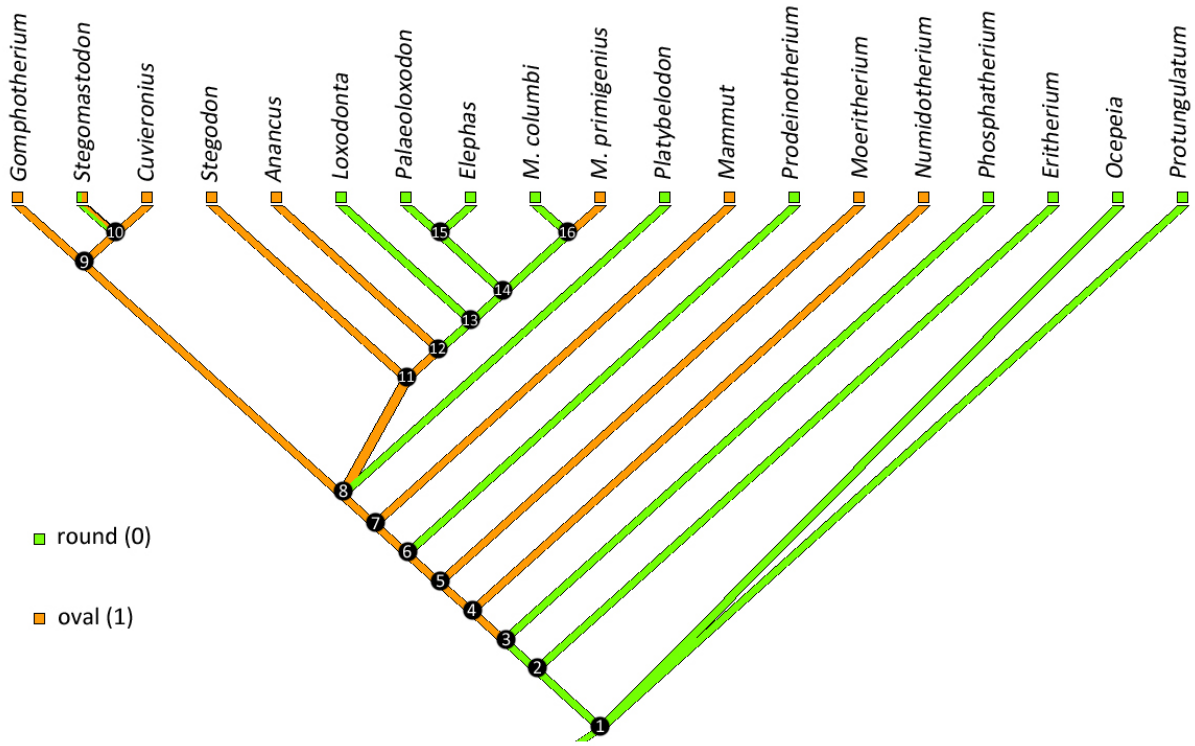

Figure V.49 : Mapping of character 18 (overall shape of the posterior canal) on the proboscidean tree.

The evolution of the posterior semicircular canal shape is more complex than for the anterior semicircular canal shape (Fig V.49). The posterior canal is primitively round (observed in *Ocepeia*, *Protungulatum*). This plesiomorphy is retained in *Eritherium* and *Phosphatherium*. The transformation to an oval posterior canal seems to be a synapomorphy of the clade containing all the other proboscideans with some reversals. Reversals are observed in *Prodeinotherium*, *Platybelodon*. A synapomorphic reversal is also observed in Elephantidae, although a round posterior semicircular canal is present in *Mammuthus columbi*. Finally, the character is polymorphic in *Stegomastodon* but the rounder aspect of FM21807B is to be taken with caution given the uncommon swollen aspect of the canals.

19. Extension of the anterior canal apex

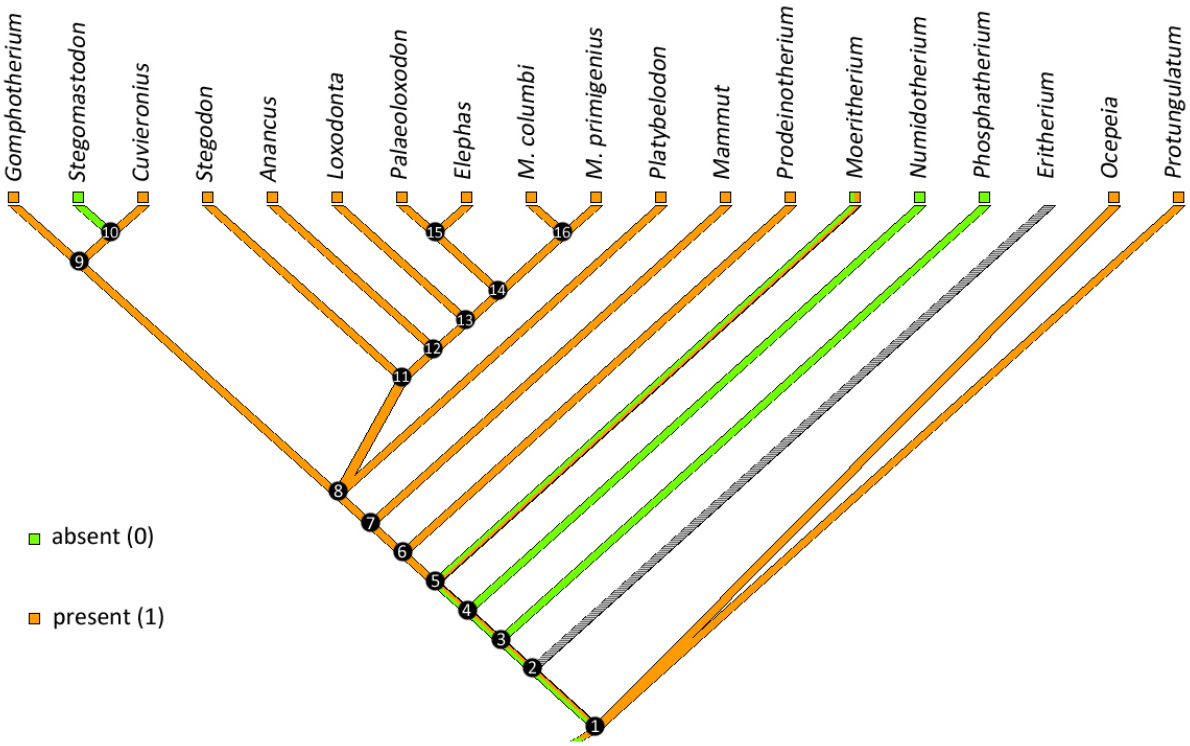

Figure V.50 : Mapping of character 19 (apical extension of the anterior canal apex) on the proboscidean tree.

The apex of the anterior canal seems to be primitively located higher than the apex of the posterior canal as it is observed in both outgroups (*Ocepeia*, *Protungulatum*)(Fig V.50). However, early proboscideans display vertical apices that extend at the same height. The localization of this transformation is ambiguous because the structure is broken and therefore unknown in *Eritherium*. Thus it can be a synapomorphy of the Proboscidea (node 2) or of all proboscideans except *Eritherium* (node 3). In *Moeritherium*, both states were observed. A synapomorphic reversion appears either at node 5 or node 6. Finally, the extension of the anterior canal apex seems to be lost in *Stegomastodon* (observed in both studied specimens).

20. Position of the point of entry of the lateral canal into the vestibule

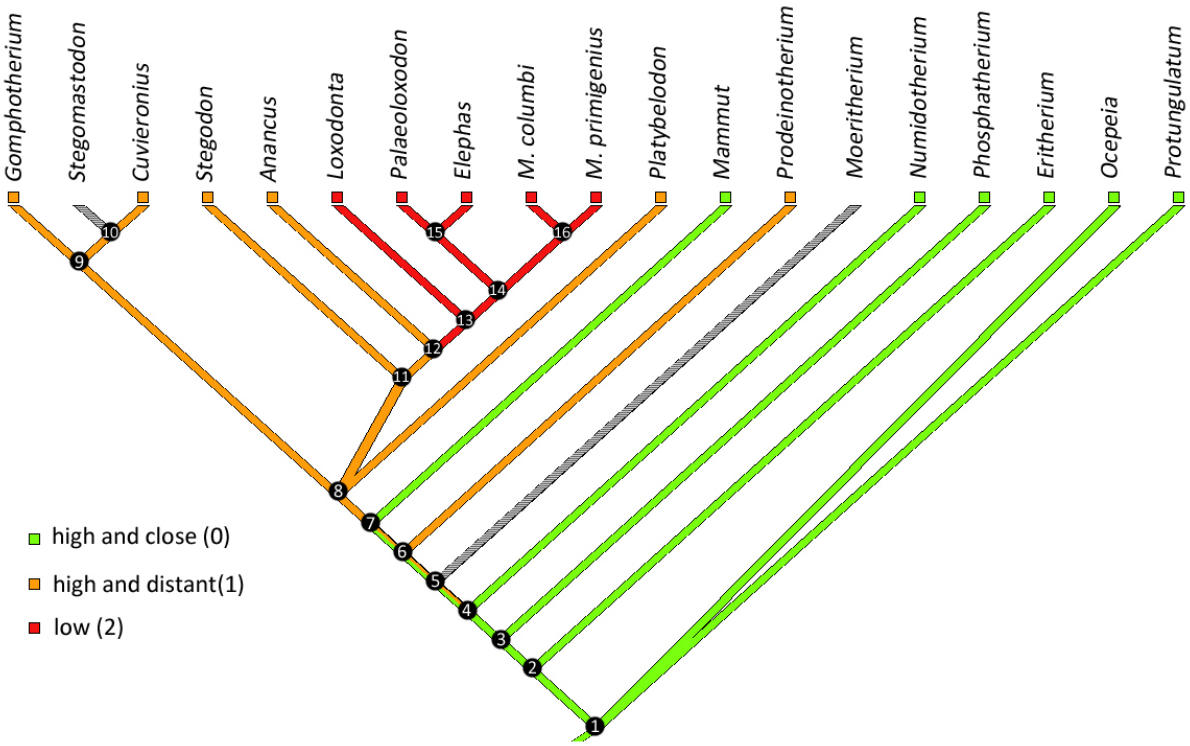

Figure V.51 : Mapping of character 20 (position of the point of entry of the lateral canal intro the vestibule) on the proboscidean tree.

The point of entry of the lateral canal into the vestibule is primitively located high and close to the posterior ampulla (state 0). *Ocepeia* and *Protungulatum* display this feature as well as the early proboscideans *Eritherium*, *Phosphatherium* and *Numidotherium*. The location of the transformation from a high and close point of entry to a high and distant point of entry is ambiguous (Fig V.51). This can be a synapomorphy of node 6 or even node 5 (ACCTRAN optimization) given that the information is missing in *Moeritherium*. In this case, a reversal occurs in *Mammut*. The other optimization would be to consider this transformation a convergence of *Prodeinotherium* and node 8 (DELTRAN optimization). The location of the transformation from a high and distant point of entry to a low point of entry, on the other hand, is an unambiguous synapomorphy of the Elephantidae (node 13).

21. Shape of the semicircular canals in cross-section

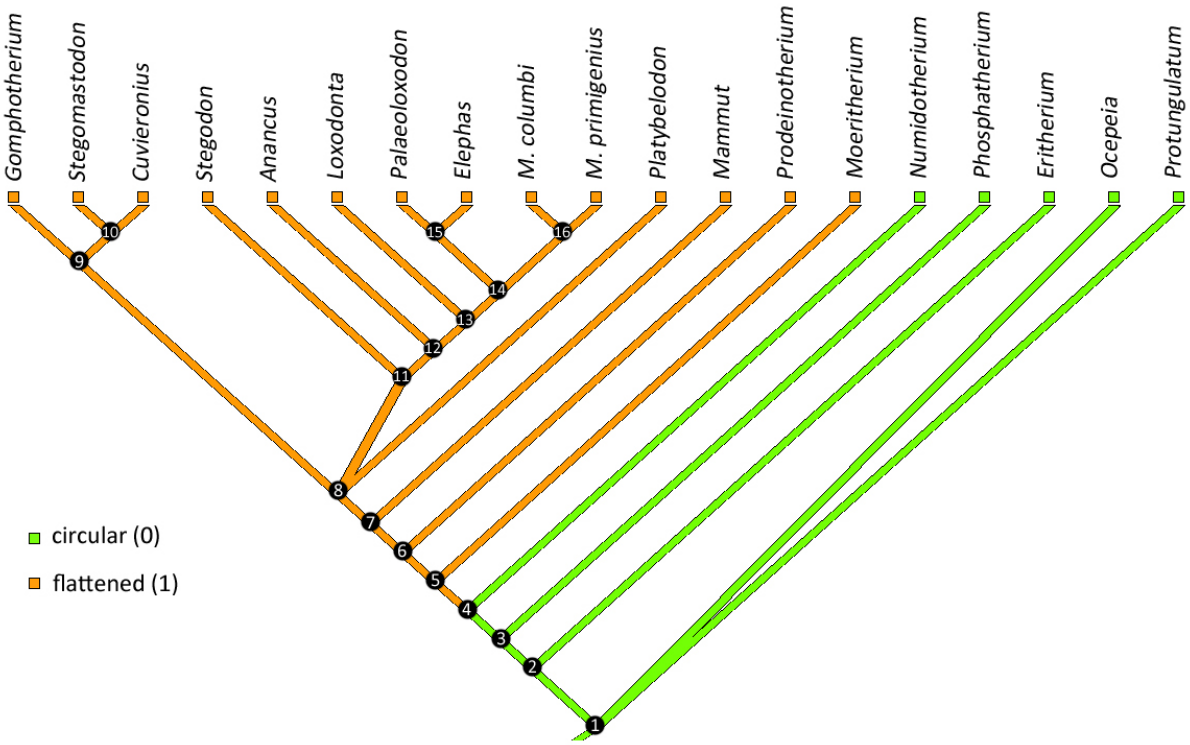

Figure V.52 : Mapping of character 21 (shape of the semicircular canals in cross-section) on the proboscidean tree.

The evolution of the shape of the semicircular canals in cross-section appears to be quite simple within the Proboscidea (Fig V.52). In most mammals, the canals are circular in cross-section. This seems to be the plesiomorphic state in Proboscidea as it is present in the outgroups (*Ocepeia* and *Protungulatum*) and in the early proboscideans representatives *Eritherium*, *Phosphatherium* and *Numidotherium*. The transformation to flattened canals is an unambiguous synapomorphy of the node 5 which is the unnamed clade containing *Moeritherium*, *Prodeinotherium* and the elephantimorphs.

22. General thickness of the semicircular canals

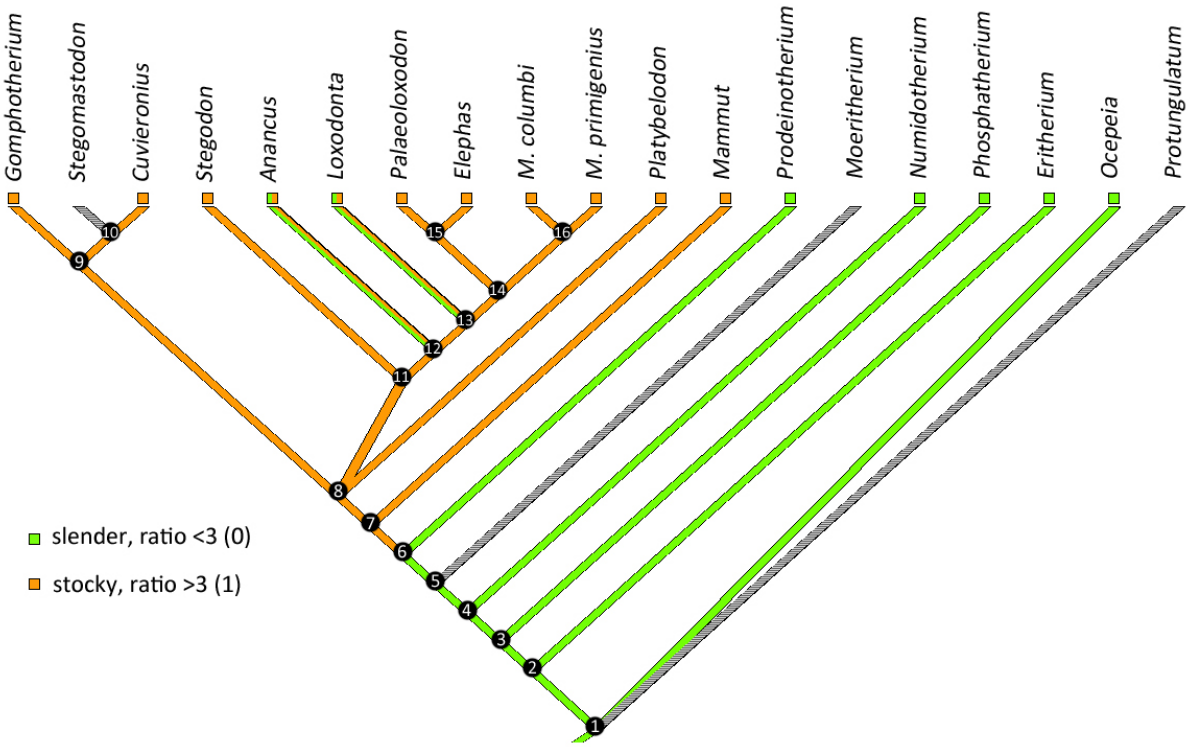

Figure V.53 : Mapping of character 22 (general thickness of the semicircular canals) on the proboscidean tree.

Evolution of the semicircular canals thickness among proboscideans is represented in Fig V.53. Primitively, the semicircular canals are slender. Most mammals display relatively thin semicircular canals (e.g. *Ocepeia*, thickness ratio = 2.15). The thickness ratio of *Protungulatum* could not be calculated but the canals appear to be slender in the 3D reconstruction (Orliac & O'Leary, 2016). The transformation to thicker and stockier canals (thickness ratio > 3) is likely a synapomorphy of elephantimorphs (node 7). The character 22 displays some polymorphism. Indeed, one specimen of *Anancus* (NMNHS.FM2991B) and one specimen of *Loxodonta cyclotis* (MNHN.ZM.AC.1956-194) have semicircular canals with thickness ratios under 3.

23. Relative size of the lateral canal

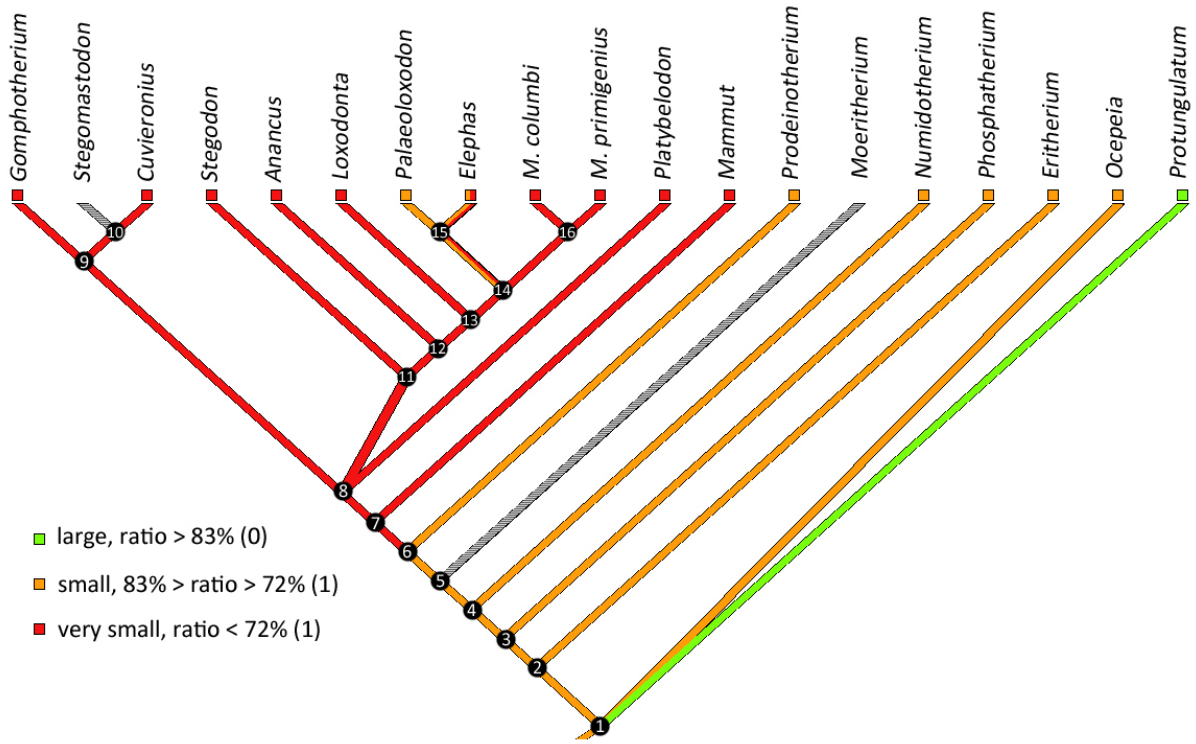

Figure V.54 : Mapping of character 23 (relative size of the lateral canal) on the proboscidean tree.

Evolution of the relative size of the lateral semicircular canal within proboscideans is illustrated in Fig V.54. As explained in the 'Characters' section of this chapter (chapter V, § 3.23), the relative size of the lateral canal was quantified with the lateral canal ratio (quotient of the radius of curvature of the lateral canal and the mean of the radii of curvature of the vertical canals, expressed in percentage). The higher the ratio, the larger the lateral canal with respect to the vertical canals. In this tree, the primitive state appears to be a lateral canal with a ratio between 72% and 83%. This is the condition of *Ocepeia* and early proboscideans. The relatively large lateral canal (ratio > 83%) appears to be an autapomorphy of *Protungulatum*, but this condition is actually found in numerous non-afrotherian mammals. It appears that the lateral canal tends to become relatively smaller in elephantimorphs. Transformation to lateral canals with ratios under 72% is a synapomorphy of elephantimorphs (node 7). The reversion to more average ratios is observed in *Palaeoloxodon* and some *Elephas* specimens.

24. Contact between the lateral and posterior canals

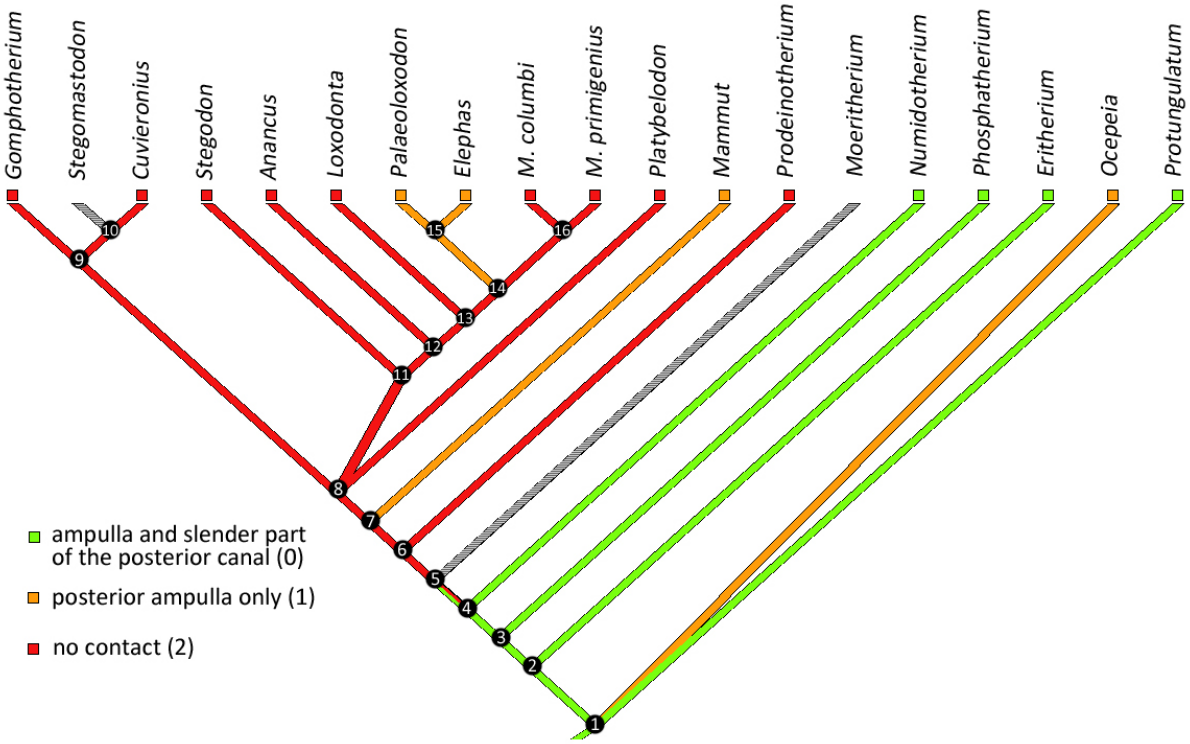

Figure V.55 : Mapping of character 24 (contact between the lateral and posterior canals) on the proboscidean tree.

Evolution of the contact between the lateral and posterior canals is illustrated in Fig V.55. Primitively, the lateral and posterior canals are fused at the level of the ampulla and the slender part of the posterior canal, a condition often referred to as *crus commune secundaria*. Early proboscideans display such feature. While the fusion of the canals in *Numidotherium* and *Phosphatherium* is very advanced to the point of having difficulties to distinguish the streamlines of the two canals, in *Eritherium* the streamline of the lateral canal is distinct and the two canals seem less fused. However, our character coding does not include this difference in the fusion of the two canals. Hence, since the slender part and the ampulla of the posterior canal are in contact with the lateral canal, *Eritherium* is coded 0. The transformation to canals that are not in contact seems to be a synapomorphy of node 5 or 6 (depending on the condition of *Moeritherium* which is unknown). The contact with the posterior ampulla only would be a convergence observed in *Mammut* and the clade containing *Elephas* and *Palaeoloxodon* (node 15).

25. Posterior expansion of the lateral canal

The lateral canal posterior expansion is absent in all studied proboscidean. This character is only useful in analyses performed on Afrotheria or Eutheria.

26. Aspect ratio of the cochlea

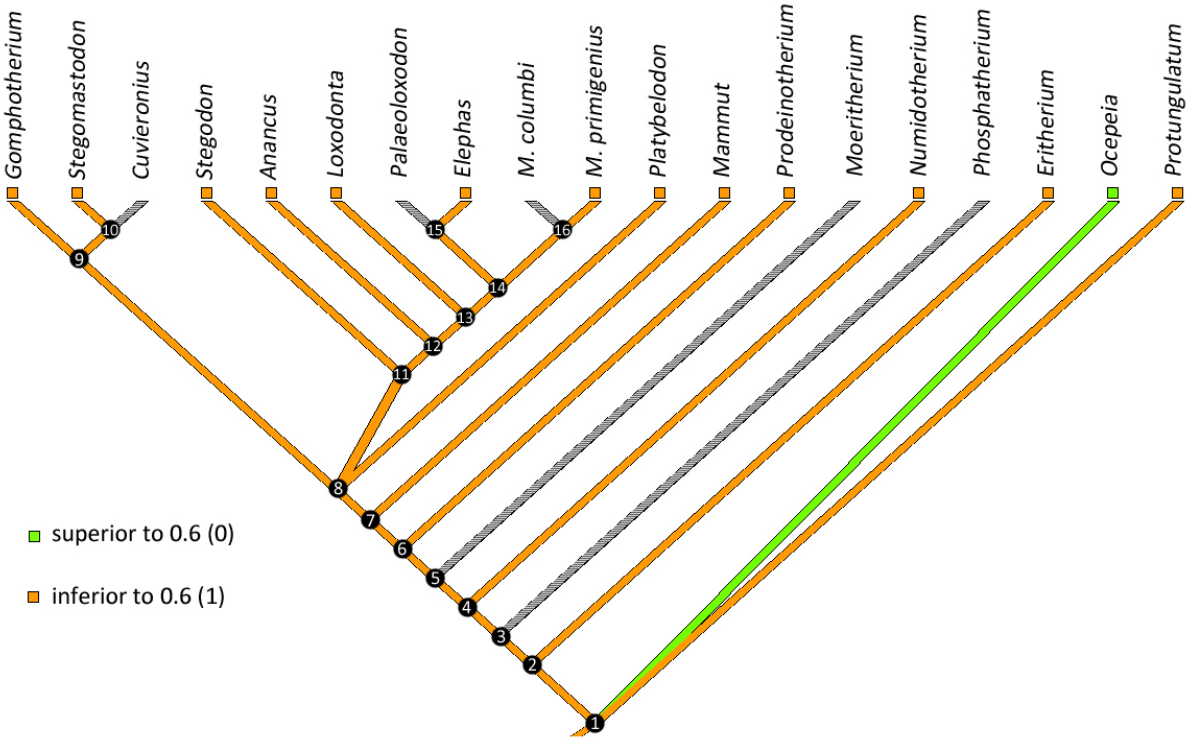

Figure V.56 : Mapping of character 26 (aspect ratio of the cochlea) on the proboscidean tree.

The aspect ratio of the cochlea is inferior to 0.6 in all studied proboscideans. The cochlea is not preserved in studied specimens of *Cuvieronius*, *Palaeoloxodon* and *Mammuthus columbi*. In *Moeritherium*, the cochlea is not sufficiently preserved to calculate a precise aspect ratio. Finally, the roof of the promontorium is damaged in *Phosphatherium* which prevents from calculating the aspect ratio as well. However, given its morphology, the cochlea of *Phosphatherium* is likely to display a ratio superior to 0.6, as *Ocepeia*. The evolution of this character is therefore ambiguous (Fig V.56).

27. Number of turns of the cochlea

This character is constant in proboscideans, at least with the coding that was defined. The character is therefore only useful in analyses performed on Afrotheria or Eutheria.

28. Lamina secundaria

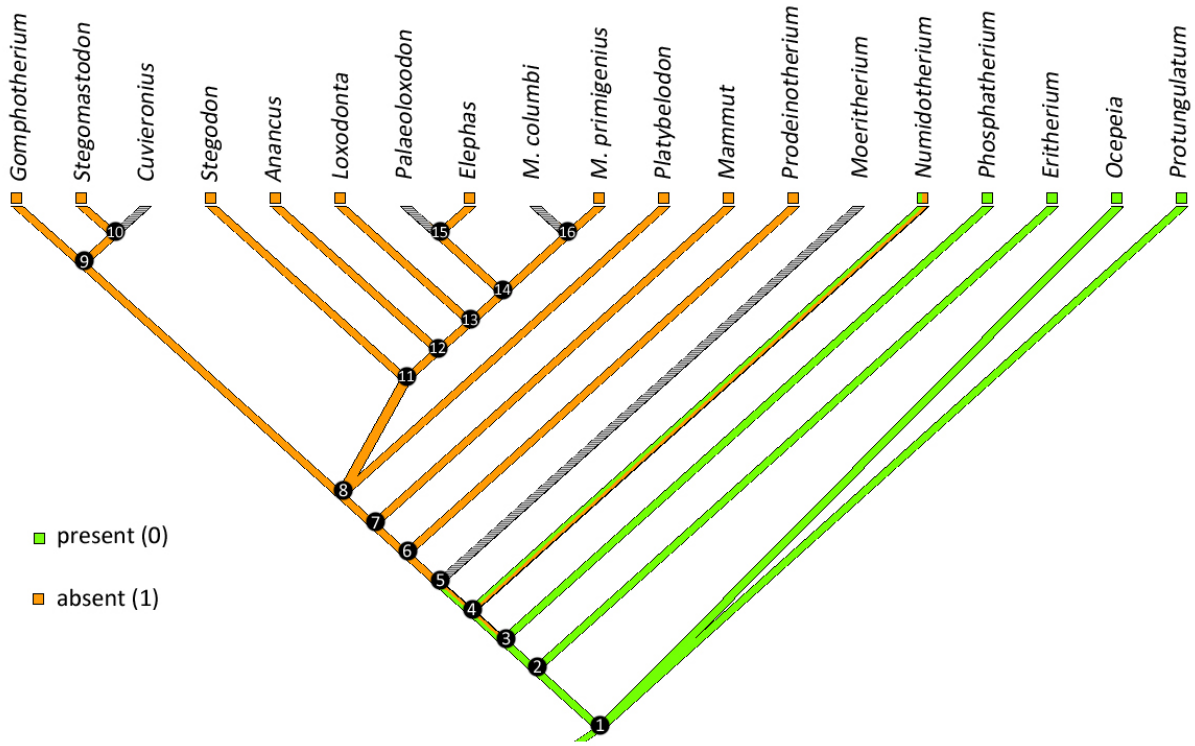

Figure V.57 : Mapping of character 28 (*lamina secundaria*) on the proboscidean tree.

The evolution of the presence of the *lamina secundaria* within Proboscidea is illustrated in Fig V.57. The lamina is primitively present. Most mammals display such feature and it is the case in outgroups *Ocepeia* and *Protungulatum*. Early proboscideans exhibit a *lamina secundaria* as well. In *Eritherium*, the lamina is quite deep and marked. The lamina is weaker in *Phosphatherium* but still present. In *Numidotherium*, it has been observed in some specimens (Court, 1992) but the lamina is absent on others. Moreover, the information is missing in *Moeritherium*. Therefore, the loss of the *lamina secundaria* could be a synapomorphy of node 4, 5 or 6. The structure is absent in all studied elephantimorphs and *Mammut americanum*.

29. Relative volume of the cochlea

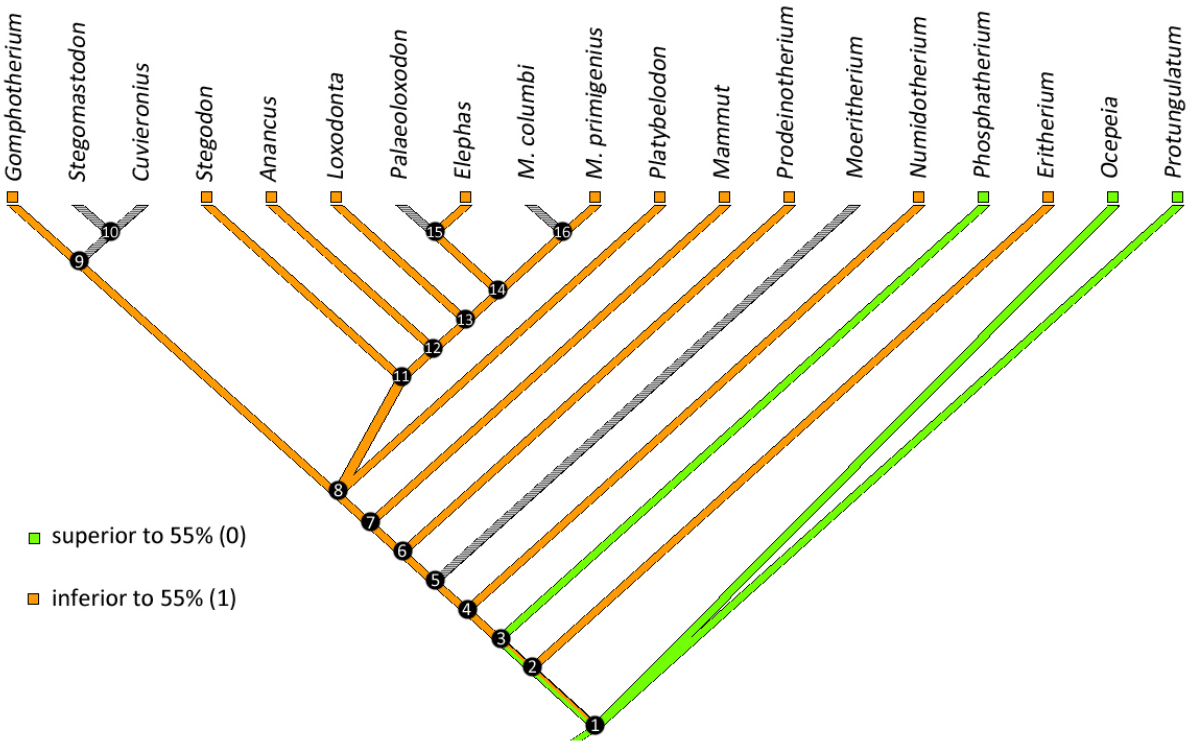

Figure V.58 : Mapping of character 29 (relative volume of the cochlea) on the proboscidean tree.

The evolution of the relative volume of the cochlea within Proboscidea is illustrated in Fig V.58. The cochlear volume is primitively superior to 55% (*Ocepeia*, *Protungulatum*). In *Eritherium*, the volume is inferior to 55% and in *Phosphatherium* the volume is superior. The state of this character in the ancestral morphotype of proboscideans is therefore ambiguous. The transformation from a relatively upper volume of cochlea to a relatively lower volume of cochlea could be a synapomorphy of Proboscidea (the character would be reversed in *Phosphatherium*, ACCTRAN) or a synapomorphy of node 4 (*Eritherium* would have developed a lower volume of cochlea independently, DELTRAN).

30. Point of entry of the *fenestra cochleae* and the cochlear canaliculus

Most proboscideans display a unique perilymphatic foramen (character 3, state 1) which means the *fenestra cochleae* and the cochlear canaliculus are fused. We chose to consider this feature to be an extreme variation of a close point of entry of the *fene*stra cochleae and the cochlear canaliculus. All studied proboscidean taxa that lack a unique perilymphatic foramen display a fenestra cochleae and a cochlear canaliculus which entry points are close to each other, hence this character is constant among Proboscidea.

31. Vestibulo-cochlear angle

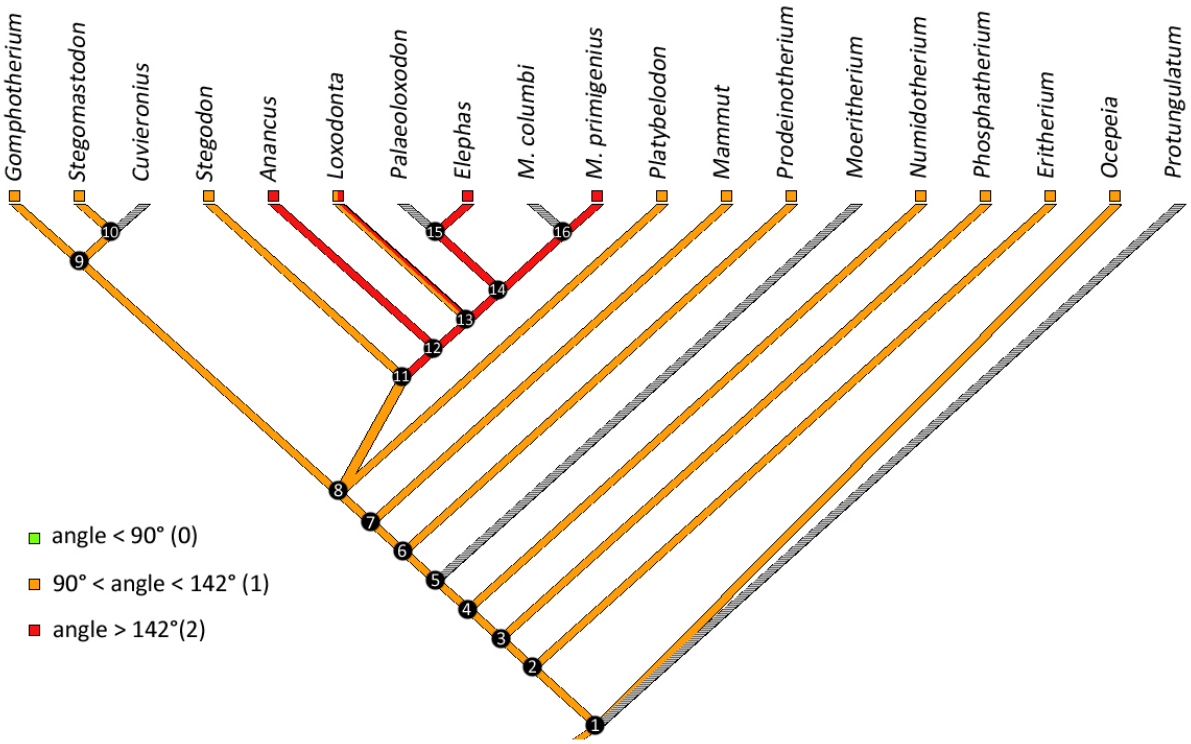

Figure V.59 : Mapping of character 31 (vestibulo-cochlear angle) on the proboscidean tree.

The evolution of the vestibulo-cochlear angle within Proboscidea is illustrated in Fig V.59. The angle is primitively slightly obtuse (comprised between 90° and 142°). This feature is shared by most proboscideans and *Ocepeia*. The acquisition of a larger angle (over 142°) seems to be a synapomorphy of node 12 (clade including *Anancus* and Elephantidae). However, the character is polymorphic in *Loxodonta* and most of the specimens belonging to this genus display an angle under 142°. The information is missing in *Cuvieronius*, *Palaeoloxodon* and *Mammuthus columbi* (the cochlea is not preserved in the studied specimens).

32. Axis of rotation of the apical turn of the cochlea with respect to the basal turn

The evolution of the alignment of the axis of rotation of the apical turn of the cochlea with respect to the basal turn is illustrated in Fig V.60. The axis of rotation of the apical turn is primitively aligned with the axis of rotation of the apical turn in Proboscidea. This feature is found in outgroups (*Ocepeia*, *Protungulatum*) and in early proboscideans (*Eritherium*, *Numidotherium*). In all of these taxa, the apical and basal turns are centered on the bony modiolus.

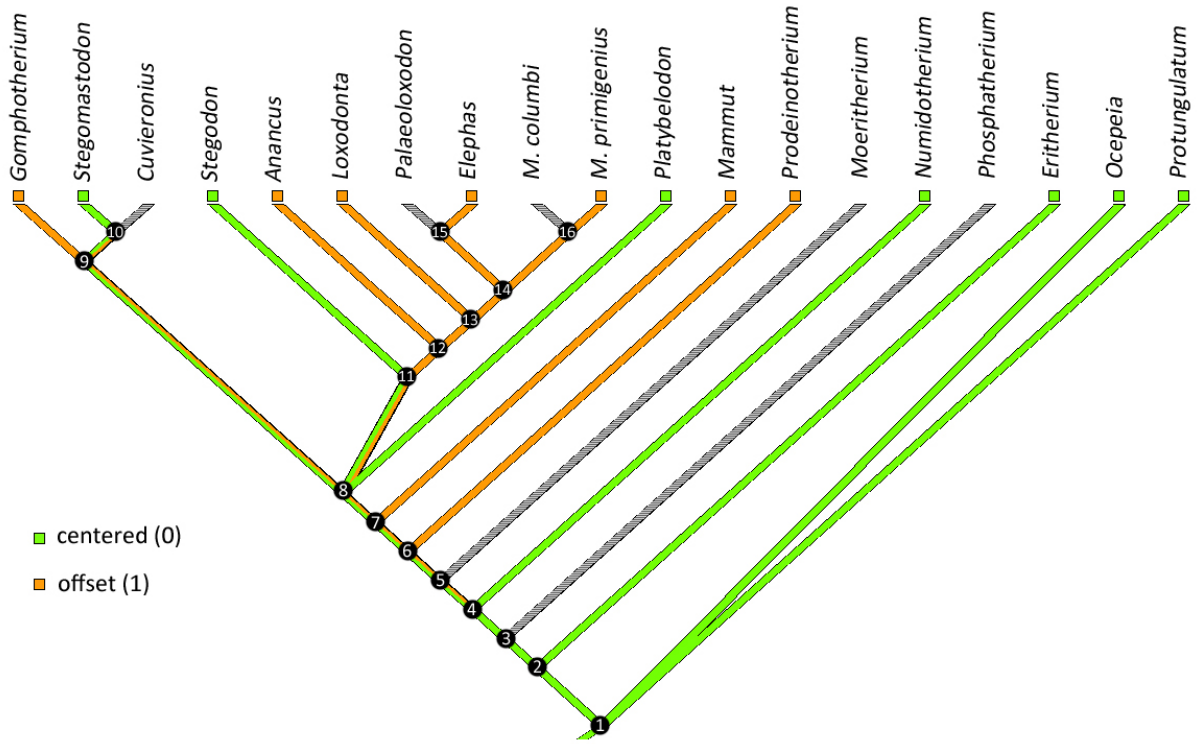

Figure V.60 : Mapping of character 32 (axis of rotation of the apical turn of the cochlea) on the proboscidean tree.

In *Phosphatherium*, the roof of the promontorium is broken, therefore, the apical turn is not entirely preserved and the observation of its center of rotation is not possible. In *Moeritherium*, the cochlea is not preserved enough to code this character in SMNS 47789-90 and it is difficult to evaluate the axis of rotation of the apical turn in the natural cochlear endocast of MNHN.F.LBE1 since it is partially covered by bony structures. The distribution of this character in the rest of proboscideans is ambiguous because of its great degree of homoplasy. The offset of the axis of rotation of the apical turn could be a synapomorphy of node 6 and the feature would be convergently lost in *Platybelodon*, *Stegomastodon* and *Stegodon*. Another optimization would be a synapomorphy in node 6, followed by a synapomorphic loss in node 8 and a convergent re-acquisition in Gomphotherium and node 12. The third optimization would be a convergence in *Mammut*, *Prodeinotherium*, *Gomphotherium* and node 12. It is hard to evaluate which hypothesis makes more sense.

4.2. Analyses extended to Afrotheria

4.2.1. Unweighted analysis

The unweighted cladistic analysis performed on the ear region of Afrotheria provided 30 most parsimonious trees with a length of 78 steps. The strict consensus of these trees is given in Fig V.61 and displays a length of 119 steps. The retention index of the consensus tree (RI = 0.634) is very close to that observed in the analysis on the Proboscidea (RI = 0.628). Such a value indicates significant homoplasy but also shows the presence of information in the tree. The consistency index found in this analysis (CI = 0.286) is very low, but the conceptual limitations of this index have been already addressed in this chapter (§ 4.1.1.). Character indices are summarized in Appendix 28A.

In the analysis, the ingroup – Afrotheria – is not found monophyletic. Indeed, the non-afrotherian *Protungulatum* is not excluded from the polytomy that includes other afrotherians. The locations of the transformations are illustrated in Fig V.61. The locations of the ambiguous transformations are optimized in DELTRAN. Only six nodes are found in the strict consensus tree.

A node containing most tethytheres (node 2) is observed while *Phosphatherium*, *Eritherium*, the Moroccan embrithopod and the sirenian from Chambi are included in a large polytomy with all the other non-tethytheres. The node 2 is supported by seven homoplastic synapomorphies that are all not ambiguously-located: the loss of the subarcuate fossa (character 1, 1→2, RI = 0.71), the inflation of the *tegmen tympani* (character 5, 0→1, RI = 0.86), the development of a fallopian notch (character 6, 0→1, RI = 0.5), the reduction of the *crista falciformis* thickness (character 9, 0→1, RI = 0.75), the posterior canal that becomes oval (character 18, 0→1, RI = 0.3), the loss of the *lamina secundaria* (character 28, 0→1, RI = 0.85) and the decrease of the cochlear volume (character 29, 0→1, RI = 0.6). These transformations exhibit few to moderate homoplasy, at the exception of character 18 which is highly homoplastic.

The node 3 contains all the previous taxa at the exception of *Numidotherium* and *Prorastomus* that form a polytomy at the base of the node. It is supported by five homoplastic synapomorphies and one non-homoplastic synapomorphy.

Figure V.61 : Strict consensus of the 30 most parsimonious trees found in the unweighted analysis extended to the Afrotheria with a DELTRAN optimization. **Length:** 119; **RI:** 0.634. **White dots**: ambiguously located transformations. **Grey dots:** unambiguously located transformations. **Black dots:** unambiguously located transformations that display no homoplasy (RI=1). **Black and white striped dots:** ambiguously located transformations that display no homoplasy (RI=1). The upper number is the character number and the lower number is the character state.

Among the five homoplastic synapomorphies, three are not ambiguously located: the flattening of the canals in cross-section (character 21, 0→1, RI = 0.9), the thickening of the semicircular canals (character 22, 0→1, RI = 0.83) and the reduction of the lateral canal relative size (character 23, 0→1, RI = 0.47). The other two homoplastic synapomorphies are ambiguously located: the amastoid condition of the petrosal (character 4, 0→1, RI = 0) appears either as a convergence of the node 3 with *Numidotherium*, *Helioseus*, *Ocepeia* and *Phosphatherium* (present optimization, DELTRAN) or a synapomorphy of node 1 that is reversed in *Protungulatum*, the sirenian from Chambi, *Prorastomus* and *Seggeurius* (ACCTRAN). We find the DELTRAN optimization figured in Fig V.61 more plausible. The fusion of the lateral canal with the posterior ampulla (character 24, 0→1, RI = 0.37) appears either as a convergence of the node 3 with the Moroccan embrithopod (PM53), *Ocepeia*, *Seggeurius*, *Titanohyrax* and *Prorastomus* (present optimization, DELTRAN) or a synapomorphy of node 1 that is reversed in the sirenian from *Chambi*, *Chambius*, *Eritherium*, *Phosphatherium*, *Protungulatum* and *Numidotherium* (ACCTRAN). This character is also highly homoplastic (RI = 0.37). Finally, the sixth synapomorphy located at the node 3 is non-homoplastic and not ambiguously located. It corresponds to the presence of a unique perilymphatic in adult life (character 3, 0→1, RI = 1). This synapormorphy is strong and characterizes all members of node 3. It has already been described in previous works (Court, 1994).

The node 4 separates *Arsinoitherium* from the remaining members of the node 3. It is similar to the node 2 found in the analysis restricted to the Proboscidea (§ 4.1.1.). It is supported by only one homoplastic synapomorphy that is not ambiguously located: the anterior canal that becomes oval (character 17, 0→1, RI = 0.83). This transformation displays a low level of homoplasy and is a convergence with *Protungulatum* and *Kulbeckia* in the tree.

The node 5 separates *Moeritherium* from the remaining members of the node 4. It is similar to the node 3 found in the analysis restricted to the Proboscidea (§ 4.1.1.). It is the best supported node with three non-homoplastic synapormophies and two homoplastic synapomorphies. Among the non-homoplastic synapomorphies, two

are not ambiguously located: the anteriorly oriented internal auditory meatus (character 2, 0→1, RI = 1) and the poor definition of the bony ampullae (character 13, 0→1, RI = 1). The third non-homoplastic synapomorphy is ambiguously located. It corresponds to the presence of a deep groove for the middle meningeal artery on the *tegmen tympani* (character 11, 0→1, RI = 1). The character is unknown in *Moeritherium* which explains the ambiguity of its location. This transformation is located either at the node 5 (present optimization, DELTRAN) or at the node 4 (ACCTRAN), depending on its actual presence in *Moeritherium* or not. We find the DELTRAN optimization (as illustrated in Fig V.61) more plausible. Indeed, the presence of the groove seems linked to petrosals that display the modern proboscidean morphology (flat and prominent *tegmen tympani*, dorsal surfaces forming a large angle, anteriorly oriented internal auditory meatus). The internal auditory meatus of *Moeritherium* is indeed dorsally oriented and its petrosal morphology differs greatly from that of modern proboscideans. Hence, we here favor the location of this character at node 5 rather than at earlier node 4. The two homoplastic synapormophies that support the clade are ambiguously located. The development of a prominent and flat *tegmen tympani* (character 5, 1→2, RI = 0.86) depends on its location or not in *Moeritherium*. It can be located either at the node 4 (ACCTRAN) or at the node 5 (DELTRAN). For the same reasons as for the character 11, we find the DELTRAN optimization more plausible. The thickening of the *crus commune* (character 15, 0→1, RI = 0.75) also depends of its presence or not in *Moeritherium*. The location of this character has been addressed in the analysis restricted to the Proboscidea (§ 4.1.1.). The node 5 is globally supported by synapomorphies with very low homoplasy (three out of five are non-homoplastic and the other two display a high RI), including two that are not ambiguously located. Hence, this is the strongest node of the tree. It is interesting to note that this clade corresponds to the morphological group found in the geometric morphometrics analyses of Chapter IV. It matches with the morphological group that appears in red in Fig IV.8 illustrating the morphospace of analysis A2 (semicircular canals of afrotherians only).

The most exclusive node (node 6) is similar to the node 4 found in the analysis performed on proboscideans and

separates *Stegomastodon* from the other remaining taxa. As we mentioned in § 4.1.1., this grouping is very unlikely. Indeed, it is poorly supported in this analysis as well. There are six synapomorphies located at this node in DELTRAN optimization. However, none of these transformations are non-homoplastic. Moreover, only two of them are not ambiguously located: the apical extension of the anterior canal (character 19, 0→1, RI = 0.28) and the offset of the cochlear apical turn axis of rotation (character 32, 0→1, RI = 0.57). The character 19 is highly homoplastic and the character 32 displays a moderate level of homoplasy. The other synapomorphies supporting this node are ambiguously located: the *hiatus Fallopii* forms once more a discrete foramen (character 6, 1→0, RI = 0.5), the point of entry of the lateral canal into the vestibule becomes high and distant from the posterior ampulla (character 20, 0→1, RI = 0.66), the lateral canal becomes very small with respect to the vertical canals (character 23, 1→2, RI = 0.47) and the lateral canal is not fused at all with the posterior canal or ampulla (character 24, 1→2, RI = 0.37). The first two display moderate levels of homoplasy while the last two are highly homoplastic. All of these transformations are ambiguous because their states are unknown in *Moeritherium* and *Stegomastodon*. Hence they can be located at the nodes 4, 5 or 6 and appear here at the node 6 because of the DELTRAN optimization. This optimization is not the most plausible because the node 6 is very unlikely. They are more probably located at nodes 4 or 5. Therefore, the node 6 is not well supported. Within node 6, the taxa form a large polytomy.

The unknown elephantimorph bony labyrinth described in Ekdale (2011) is included here in the analysis. The isolated petrosal scanned in 2011 comes from the Pleistocene deposit of Friesenhahn Cave. The only identified proboscideans of the site are *Mammuthus columbi* and *Mammut americanum*, based on the dental anatomy (Graham, 1976), with the majority of the material assigned to *Mammuthus*. Here the elephantimorph is included in the polytomy of node 6. This confirms the assignment to Elephantimorpha but does not provide a more precise determination, conversely to the result found with the implied weighting analysis (next section, § 4.2.2.).

In general, the analysis fails to reconstruct most afrotherian relationships. It is indeed very different to the results found in comprehensive phylogenetic analyses such as Seiffert (2007). In our tree, the Afrotheria is not found monophyletic, there is a Tethytheria clade but some tethytheres (sirenian from Chambi, *Phosphatherium* and *Eritherium*) are not included in this clade. The clade Paenungulata is not found either, because hyracoids are in the large basal polytomy. The Pseudoungulata clade proposed in Seiffert, (2007) is not tested here because no unambiguous representative of Tubulidentata is included. Our poorly resolved topology can be explained by a significantly high level of homoplasy of the tree (RI = 0.634). The addition of other afrotherians do not affect the topology found for the analysis restricted to Proboscidea much (section, § 4.1.1.). Only the location of *Phosphatherium* is modified and it is found in the large basal polytomy here. The character 9 (thin *crista falciformis*) that was a non-homoplastic and not ambiguously located transformation that supported the grouping of *Phosphatherium* with the other proboscideans in § 4.1.1. is found convergent here. On the other hand, *Prorastomus* and *Arsinoitherium* are found in the proboscidean clade. *Prorastomus* is in the polytomy with *Numidotherium* while Arsinoitherium is found basal to the node 4. Not surprisingly, the only non-homoplastic and not ambiguously located transformation that supports the grouping of *Arsinoitherium* with other proboscideans is the presence of the unique perilymphatic foramen (character 3, 0→1, RI = 1). The other not ambiguously located transformations supporting this grouping are homoplastic and are the following: flattened canals in cross-section (character 21 0→1, RI = 0.9), a high thickness ratio for the semicircular canals (character 22, 0→1, RI = 0.83) and the decrease of the lateral canal relative size (character 23, 0→1, RI = 0.47). The grouping of *Arsinoitherium* with proboscideans based on ear region characters is not new (Benoit et al. 2013b). It is interesting to note that most of the characters that groups *Arsinoitherium* with the Proboscidea here are very similar as those in Benoit et al. (2013b).

4.2.2. Implied weighting analysis

A second analysis of the same data set was developed using implied weighting to minimize the weight of the homoplastic characters. The resulting tree (Fig V.62) is

compared with the previous tree (§ 4.2.1.).

The implied weighting cladistic analysis performed on the ear region of Afrotheria provided 290 most parsimonious trees with a length of 80 steps. The strict consensus of these trees is given in Fig V.62 and displays a length of 95 steps which is less than for the unweighted analysis (119 steps). The retention index of the consensus tree (RI = 0.737) is better than for the unweighted analysis (RI = 0.634). This comes as no surprise since the homoplastic characters have less weight with the implied weighting method. Character indices are summarized in Appendix 28B.

The analysis with implied weighting impacts the relationships within Afrotheria and within Proboscidea in the tree. First, the monophyly of the Afrotheria is obtained in the implied weighting analysis (node 2), contrary to the traditional analysis. It is supported by three homoplastic and ambiguously located transformations: a moderate subarcuate fossa (character 1, 0→1, RI = 0.78), a round anterior canal (character 17, 1→0, RI = 0.91) and the contact between the lateral and posterior canals that is only at the level of the posterior ampulla (character 24, 0→1, RI = 0.56).

On the other hand, *Eritherium*, *Phosphatherium*, *Ocepeia* and the early Moroccan embrithopod (PM53) are found closer to the other proboscideans than in the unweighted analysis (node 3). This grouping is supported by six transformations. Three of them are not ambiguously located: the inflation of the *tegmen tympani* (character 5, 0→1, RI = 1), the development of a petrosal pneumatization (character 7, 0→1, RI = 0.2) and the decrease of the lateral canal relative size (character 23, 0→1, RI = 0.7).

Within the Proboscidea, the location of *Mammut* is different between the two analyses. It is not found in the large polytomy anymore but considered more basal (node 8). This grouping is supported by three synapomorphies. The acquisition of the apical extension of the lateral canal (character 19, 0→1, RI = 0.42) and the offset of the cochlear apical turn axis of rotation (character 32, 0→1, RI = 0.57) are not ambiguously located but are homoplastic. The further decrease of the lateral canal relative size (character 23 1→2, RI = 0.7) is ambiguously located because of the missing data in *Stegomastodon* and *Moeritherium*.

With the shift of *Mammut*, the Elephantida is found in the implied weighting tree (node 9). *Stegomastodon* is the only Elephantida excluded from this clade. In addition, the non-Elephantida *Prodeinotherium* is included in this node. The node 9 is supported by three synapomorphies: the *hiatus Fallopii* forms once more a discrete foramen (character 6, 1→0, RI = 0.5), the point of entry of the lateral canal into the vestibule is located high and distant from the posterior ampulla (character 20, 0→1, RI =1) and the lateral canal is not in contact at all with the posterior slender canal nor the posterior ampulla (character 24, 1→2, RI = 0.56). While the character 6 is ambiguously located, the character 20 and 24 are unambiguously located at this node. Moreover, the character 20 is non-homoplastic (RI = 1).

The Elephantidae clade is also found in the implied weighting analysis (node 11). All studied elephantids are included in the clade that contains only elephantids. This node is supported by three not ambiguously located synapomorphies: a round posterior semicircular canal (character 18, 1→0, RI = 0.46), a lateral canal point of entry into the vestibule situated low and close to the posterior ampulla (character 20, 1→2, RI = 1) and a very high angle between the vestibule and the cochlea (character 31, 1→2, RI = 0.5). This node is hence well supported, with three not unambiguous synapomorphies, one of which is non-homoplastic (character 20). Hence, the position of the lateral canal point of entry into the vestibule seems to be a strong character. A point of entry located low and close to the ampulla is therefore a new diagnostic character state of the Elephantidae.

Within the Elephantidae, *Elephas* and *Palaeoloxodon* are found monophyletic (node 12). This comes as no surprise, because *Palaeoloxodon* was considered a subgenus of *Elephas* for a long time. However, recent reappraisals consider *Palaeoloxodon* to be a *bona fide* elephant genus (Shoshani et al. 2007). Here the grouping of *Palaeoloxodon* and *Elephas* is supported by one unambiguously located reversal: the contact between the lateral canal and the posterior ampulla (character 24, 2→1, RI = 0.56).

Figure V.62 : Strict consensus of the 30 most parsimonious trees found in the implied weighting analysis extended to the Afrotheria with a DELTRAN optimization. **White dots**: ambiguously located transformations. **Grey dots:** unambiguously located transformations. **Black dots:** unambiguously located transformations that display no homoplasy (RI=1). **Black and white striped dots:** ambiguously located transformations that display no homoplasy (RI=1). The upper number is the character number and the number between brackets is the character state.

Finally, the implied weighting analysis adds insight into the position of the undetermined elephantimorph labyrinth from Friesenhahn cave (Ekdale, 2011). It is grouped with *Gomphotherium* in the node 10 based on only one unambiguous and non-homoplastic synapomorphy: the presence of a pyramidal basal thickening of the *crus commune* (character 14, 0→1, RI = 1). This is surprising because the cave is known to contain only *Mammut americanum* and *Mammuthus columbi* specimens (Graham, 1976). The basal thickening of the *crus commune* could be an intraspecific character. In any case, the grouping of the elephantimorph with *Gomphotherium* is supported by only one synapomorphy, which is few. However, in the implied weighting analysis, *Mammut* is not contained in the node 9, which makes the undetermined elephantimorph more closely related to *Mammuthus primigenius* than to *Mammut americanum*. The point of entry of the lateral canal into the vestibule of the undetermined elephantimorph is high and distant from the posterior ampulla (character 20, 1), by contrast to *Mammut* which displays a point of entry high and very close to the posterior ampulla (20, 0). However, it is not the same state as in *Mammuthus* either, because the undetermined elephantimorph does not display the characteristic low and close point of entry of Elephantidae (20, 2). Hence, we cannot settle definitively on the taxonomic assignment of this isolated labyrinth. Nevertheless, we can hypothesize that it is more closely related to *Mammuthus primigenius* than to *Mammut americanum*.

5. Conclusion

In this chapter, the evolution of the petrosal and bony labyrinth characters within Proboscidea has been studied using several methods. The cladistic analyses allowed us to test the phylogenetic message carried by the ear region. It highlights some homoplasy of the petrosal and bony labyrinth characters. However, it was possible to discriminate several proboscidean groups using only characters of the auditory region and to identify the ear region characters that support these groupings. On the other hand, the character mapping on a consensual proboscidean tree allowed raising evolutionary hypotheses of morphological evolution on the current phylogenetic tree of the Proboscidea that was not recovered in our analysis. Thanks to these two approaches, we gain more insight into the evolution of the ear region within the Proboscidea. Our main evolutionary hypotheses are summarized in Fig V.63.

The ear region morphotype of the extant elephants has not been acquired gradually during the evolutionary history of Proboscidea. Most of the key ear characters that define the elephant morphotype were already acquired by earlier clades than the Elephantimorpha (node G).

Some nodes represent key evolutionary stages in the Proboscidea. While *Eritherium* exhibits a generalized morphology similar to Paenungulata, Afrotheria and Eutheria, *Phosphatherium* already displays a few proboscidean features: in the unnamed node C, the *crista falciformis* becomes thinner and the subarcuate fossa becomes less deep before becoming completely shallow in the following node (node D).

The higher node E, which contains *Moeritherium*, *Prodeinotherium* and Elephantimorpha, bears several transformations of the ear region as well. The major acquisition is the undivided perilymphatic foramen, which is a crucial feature that defines the modern elephant morphotype. This node is also characterized by the flattened semicircular canals and the oval shape of the anterior semicircular canal.

The next node F is probably the most important in terms of evolution of the ear region. It bears five major synapomorphies.

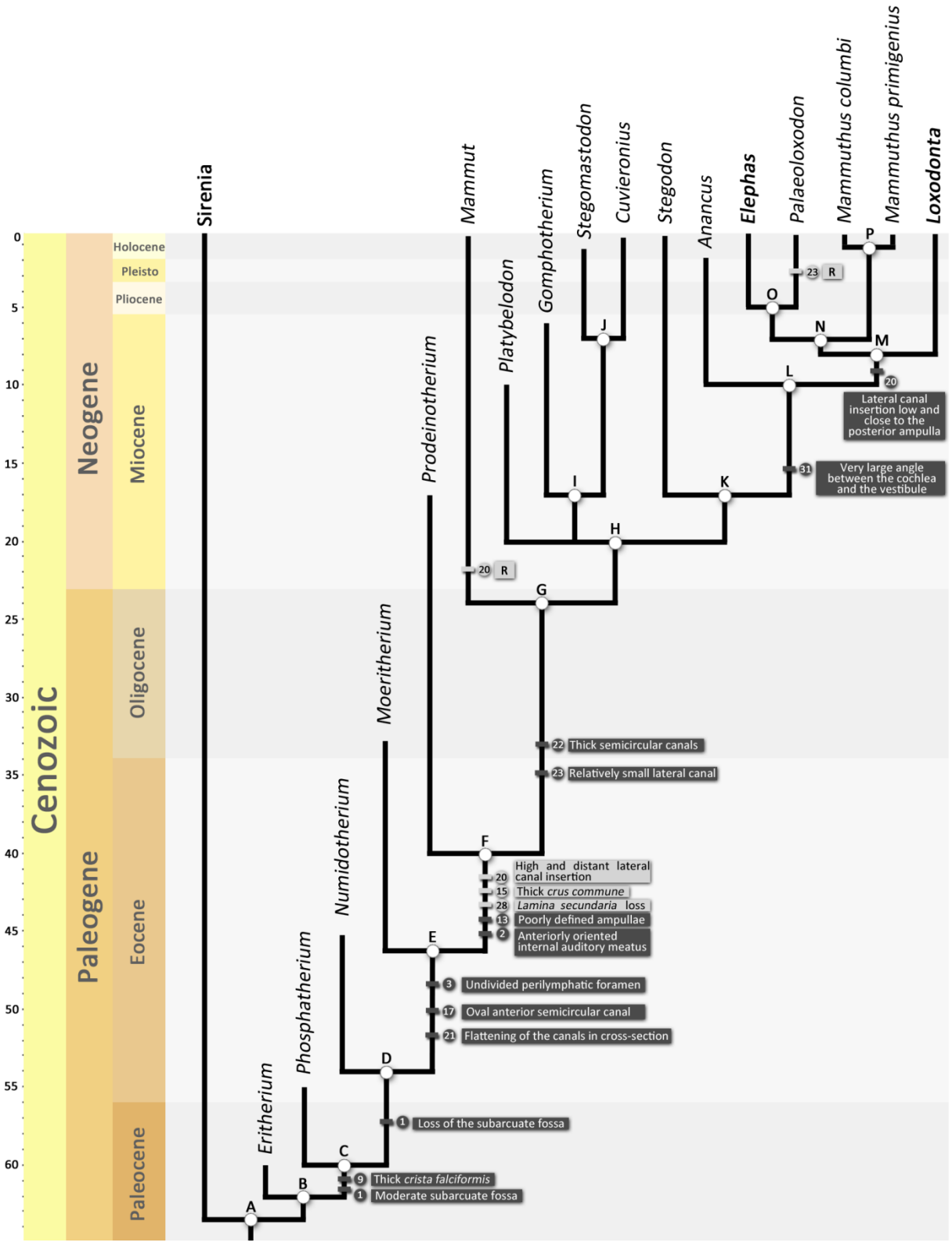

Figure V.63 : Summary of the principal evolutionary hypotheses on the ear region of Proboscidea. Divergence dates and time ranges are approximated. The order of the transformations at a same node is not relevant. Only taxa studied in this work are represented. **In dark grey:** unambiguously located transformations. **In light grey:** ambiguously located transformations. **R** is for reversal. **Clades: A)** Tethytheria, **B)** Proboscidea, **C,D,E,F)** Unnamed clades, **G)** Elephantimorpha, **H)** Elephantida, **I,J,K,L)** Unnamed clades **M)** Elephantidae, **N)** Elephantini, **O)** Unnamed clade, **P)** *Mammuthus* genus.

Even though three of them are ambiguously located, their hypothetical placement at this node makes the most sense. This is the node where the modern proboscidean morphology of the petrosal is most probably acquired. The anterior orientation of the internal auditory meatus appears here. This feature seems to be linked with the typical proboscidean morphology of the petrosal (petrosal forming two very angular surfaces separated by the *crista partis petrosa* in dorsal view). All studied proboscideans belonging to this clade display this morphology (*Prodeinotherium* and *Mammut* included), while earlier proboscideans retain a general morphology closer to the eutherian morphotype (dorsally oriented internal auditory meatus, no angular surfaces in dorsal view). All studied proboscideans belonging to this node also exhibit the typical poorly defined ampullae of the bony labyrinth. This is also probably the node of apparition of the thick crus commune, the loss of *the lamina secundaria* and the displacement of the lateral canal point of entry into the vestibule (it moves away from the posterior ampulla). These transformations are ambiguously located in our analysis, mainly because of the missing data in *Moeritherium*. In the following node (node G, Elephantimorpha), the bony labyrinth shows other typical features: a general high degree of thickness of the semicircular canals and a relatively small lateral canal with respect to the vertical canals. Although the lateral canal is already primitively relatively small in the Proboscidea (compared to other afrotherians), it becomes even smaller in the Elephantimorpha. Most apomorphies are thus already acquired in the Elephantimorpha. There are only a few apomorphies that appears within the Elephantimorpha. The vestibulo-cochlear angle increases in the node L including *Anancus* and the Elephantidae. On the other hand, the insertion of the lateral canal into the vestibule becomes low and close to the posterior ampulla in the Elephantidae (node M). This is a new diagnostic character of the Elephantidae.

In conclusion, key evolutionary stages of the proboscidean evolution were brought to light, and especially at node C, node E and node F that display key transformations. They define the modern proboscidean morphotype of the ear region that is definitely acquired in the Elephantimorpha.

CHAPTER VI

The semicircular duct system of the Proboscidea and the Afrotheria: functional capacities and inferences on the inner ear of extinct taxa

1. Introduction

In a morpho-functional perspective, the membranous labyrinth can be divided into three parts: the cochlear duct, which encodes sounds, the otolithic organs, which encodes linear accelerations and tilt, and the semicircular ducts, which encodes angular velocity (i.e. rotations of the head). The saccule, utricle and semicircular ducts form the peripheral organ of the vestibular system. This chapter investigates the capacities of proboscideans (and to a lesser extent afrotherian) to detect rotations and therefore only focuses on the semicircular duct system.

Semicircular duct anatomy

The semicircular ducts are contained in the bony semicircular canals of the labyrinth. They consist of three slender ducts filled with a fluid called endolymph and delimited by endolymphatic membranes. Each duct displays an ampulla at one end, which corresponds to an inflated region containing the cupula and the *crista ampullaris*. The anterior and posterior ducts are connected through the *crus commune*. All three semicircular ducts are connected to the utricular part of the semicircular duct system. The semicircular duct system of *Elephas* is illustrated in Fig. VI.1.

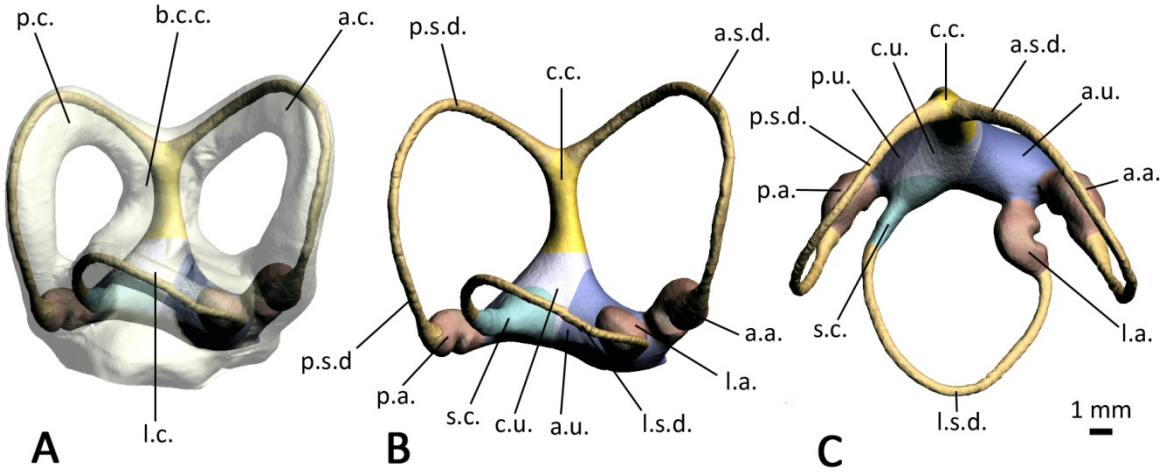

Figure VI.1 : Semicircular duct system of *Elephas maximus* CEB150009, viewed in transparency within the bony labyrinth (A), in frontal view (B) and viewed in the plane of the lateral duct (C). Legends: **a.a.** anterior ampulla, **a.c.** anterior bony canal, **a.s.d.** anterior semicircular duct, **a.u.** anterior utricle, **b.c.c.** bony *crus commune*, **c.c.** *crus commune*, **c.u.** common utricle, **l.a.** lateral ampulla, **l.c.** lateral bony canal, **l.s.d.** lateral semicircular duct, **l.u.** lateral utricle, **p.a.** posterior ampulla, **p.c.** posterior bony canal, **p.s.d.** posterior semicircular duct, **p.u.** posterior utricle, **s.c.** simple crus.

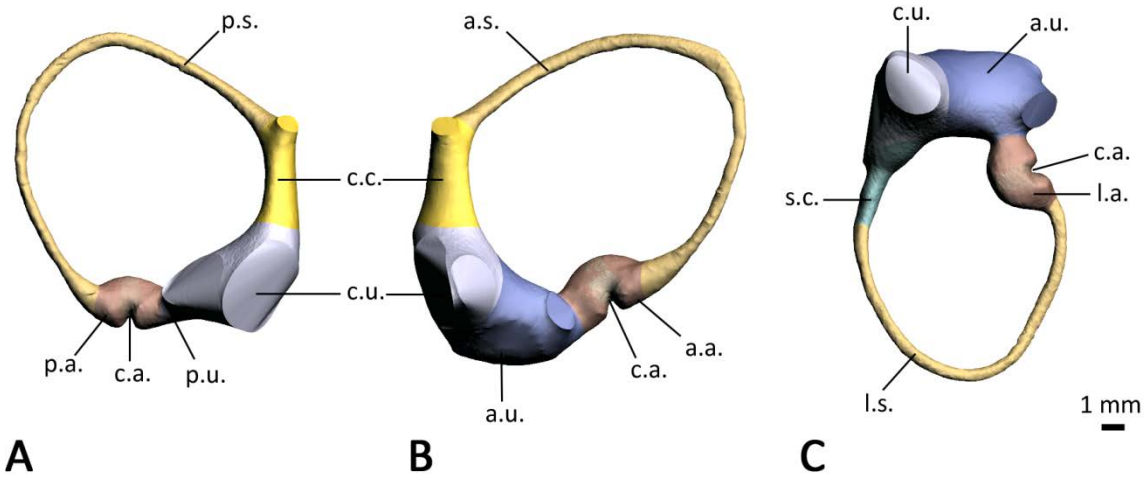

Figure VI.2 : Different parts involved in the endolymphatic trajectories of the posterior (A), anterior (B) and lateral (C) membranous semicircular ducts of *Elephas maximus*. Legends: **a.a.** anterior ampulla, **a.s.** anterior slender duct, **a.u.** anterior utricle, **c.a.** *crista ampullaris*, **c.c.** *crus commune*, **c.u.** common utricle, **l.a.** lateral ampulla, **l.s.** lateral slender duct, **p.a.** posterior ampulla, **p.s.** posterior slender duct, **p.u.** posterior utricle, **s.c.** simple crus.

Endolymphatic trajectory of the posterior duct

The posterior semicircular duct can be divided into five different parts illustrated in Fig. VI.2A. The ampulla communicates with the slender part of the duct, which represents about half the length of the duct streamline. The slender part connects with the *crus commune,* which is shared with the anterior duct. The *crus commune* leads to the common utricle. This region is the only part of the membranous labyrinth where all the ducts share a common trajectory. The common utricle communicates with the posterior utricle which is connected to the ampulla.

Endolymphatic trajectory of the anterior duct

The anterior semicircular duct can be divided into five different parts as well, (Fig. VI.2B). As for the posterior duct, the ampulla communicates with the slender part of the duct, which represents about half the length of the duct streamline. The slender part then connects with the *crus commune,* which is shared with the anterior duct. The *crus commune* leads to the common utricle. Contrary to the posterior duct, the trajectory of the anterior duct then continues to the anterior utricle, which is shared with the lateral duct. This utricle communicates with the anterior ampulla.

Endolymphatic trajectory of the lateral duct

The lateral semicircular duct can be divided into five different parts as well, which are illustrated in Fig VII.2C. As for the other ducts, the ampulla communicates with the slender part of the duct, which represents about half the length of the duct streamline. The slender part then leads to the simple crus, which is connected to the common utricle. As for the anterior duct, the trajectory of the lateral duct then continues to the anterior utricle, which communicates with the lateral ampulla.

Crista ampullaris

The *crista ampullaris* is a ridge located at the center of each ampulla. It has the shape of a semi-catenoid when viewed from the top. The *crista ampullaris* concentrates hair cells whose ciliae are embed in a gel-like structure called the cupula. The cupula consists of a hydrogel delimited by two fibrous membranes that are produced by supporting cells of the crista (Rabbitt et al. 2004). Rotations (i.e. angular accelerations) of the head trigger an endolymphatic flow that induces deformations of the cupula and consequently deflections of the hair bundle of the crista hair cells (Fig VI.3A-B).

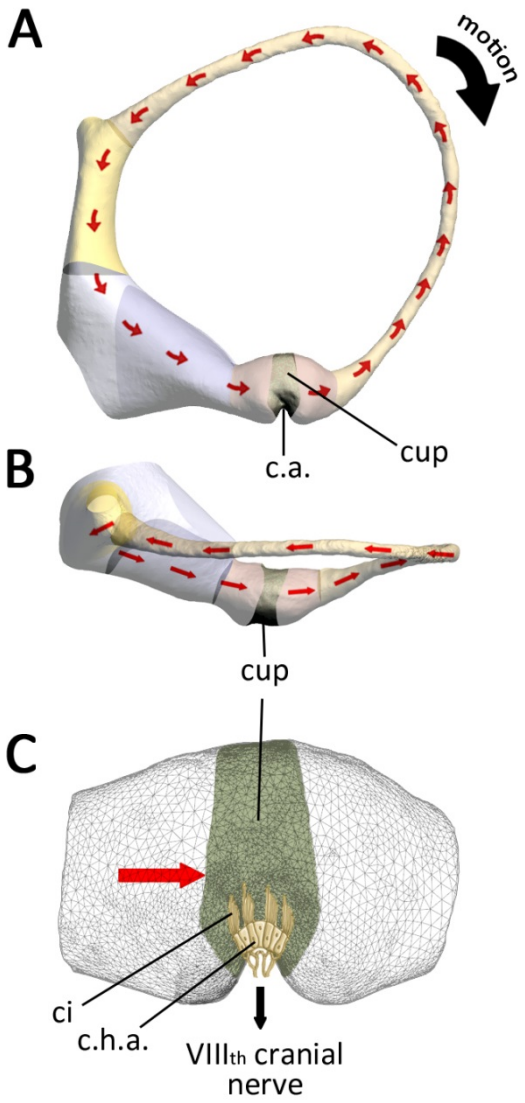

Figure VI.3 : Schematic representations of the endolymphatic flow (in red) in the anterior duct in views parallel (A) and perpendicular (B) to the duct, with a focus on the ampulla (C). The size of hair cells in panel C is exaggerated. Legends: **c.a.** *crista ampullaris*, **c.h.a.** *crista* hair cells, **ci** ciliae, **cup** cupula.

The deflection of the ciliae triggers action potentials which are carried by the VIIIth cranial nerve to the brain (Fig VI.3C). The integration of nervous messages transmitted by the six semicircular ducts allows the brain to interpret the direction and amplitude of head rotations.

Semicircular ducts biomechanics

Biomechanics of the semicircular ducts can be compared to that of a torsion pendulum. Hence the mechanics of this system can be summarized with this equation:

$$\frac{d^2Q_k(t)}{dt^2} * M_k + \frac{dQ_k(t)}{dt} * C_k + Q_k(t) * K_k = \overrightarrow{G_k} \cdot \frac{d^2\vec{\Omega}(t)}{dt^2}$$

In this equation, $\frac{d^2Q_k(t)}{dt^2}$, $\frac{dQ_k(t)}{dt}$ and $Q_k(t)$ respectively correspond to volume acceleration, velocity and displacement of the endolymph at time t. M_k is the mass parameter of the semicircular duct k. C_k is the damping parameter of the semicircular duct k. K_k is the stiffness parameter of the cupula k. $\overrightarrow{G_k}$ corresponds to a vector representing, by its direction, the axis of rotation that optimally displaces endolymph contained in the semicircular duct and by its magnitude, the inertial forcing parameter of the semicircular duct k. $\frac{d^2\vec{\Omega}(t)}{dt^2}$ is the vector of head angular acceleration at time t.

$\overrightarrow{G_k} \cdot \frac{d^2\vec{\Omega}(t)}{dt^2}$ corresponds to the differential of pressure exerted onto both sides of the cupula. If this scalar product equals 0, it thus means that no endolymphathic displacement is generated in the duct during head motion. Rotation axes leading to such values are contained in a plane called the null plane. Conversely, a rotation of the head around the axis defined by the vector $\overrightarrow{G_k}$ will induce a maximal response of the duct.

Mass parameter (M_k)

To calculate the mass parameter, the equation is (following Rabbitt et al. 2004):

$$M_k = \sum_0^i \rho \int_0^{sk,i} \frac{1}{a_{k,i}} d_{sk,i}$$

In this equation, ρ represents the endolymph density (which is close to that of water), a_k is the average cross-sectional area of the i-th part of the semicircular duct k and d_{sk} is the length of the streamline s.

Damping parameter (C_k)

To calculate the damping parameter, the equation is (following Rabbitt et al. 2004):

$$C_k = \sum_0^i \mu_e(T°C) \int_0^{sk,i} \lambda_{\mu k,i} \frac{1}{a_{k,i}^2} d_{sk,i}$$

In this equation, μ_e represents the endolymph viscosity which depends of the body temperature of the animal. However, since the viscosity does not vary very significantly within the range of mammal body temperature, the temperature of humans is used here to define the viscosity. λ_μ represents the wall shape drag factor, which is influenced by the shape of the ducts in cross-section.

Cupula stiffness parameter (K_k)

To calculate this parameter, the equation is (following Rabbitt et al. 2004):

$$K_K = \frac{\lambda_{\gamma k} \cdot \gamma \cdot t_k}{A c_k^2}$$

In this equation, $\lambda_{\gamma k}$ represents the cupula deformation factor, γ represents the shear stress factor, which is a physiological parameter affecting the deformation profile of the cupula, t_k represents the average thickness of the cupula and Ac represents the average section area of the cupula.

Inertial forcing parameter ($\overrightarrow{G_k}$)

To calculate this parameter, the equation is (following Rabbitt et al. 2004):

$$\overrightarrow{G_k} = 2\rho\vec{\Lambda}$$

In this equation, $\vec{\Lambda}$ corresponds to the area enclosed by the duct torus, as projected into the maximal response plane.

Functional parameters

Semicircular ducts are governed by several functional parameters. In this chapter, we will focus on three parameters that are useful to define vestibular capacities of animals (following Rabbitt et al. 2004; David et al. in press):

- the short time constant (T_2), which represents the time taken by the cupula to attain the maximal deflection induced by the stimulus

- the natural frequency (ω_0), which is the frequency for which the deflection of the cupula is in phase with angular velocity

- the sensitivity (or velocity gain, $\overrightarrow{VGs_k}$), which corresponds to the degree of deflection of the ciliae per degree per second of head rotation.

Short time constant (T_2)

The short-time constant represents the time taken by the cupula to be maximally displaced after the stimulus. The lower the short-time constant, the faster the head rotation is encoded. It can be calculated with this equation:

$$\overrightarrow{T_{2k}} = \frac{M_k}{C_k}$$

Now, as we said earlier, M_k is influenced by the inverse of the average cross-sectional area of the duct a_k. C_k is even more influenced by the inverse of this measurement, because it is squared in the equation. Since most other morphological parameters get canceled in this equation, the short time constant is then only driven by the average cross-sectional area of the duct. This highlights the importance of applying these calculations on measurements taken on the membranous ducts instead of the bony canals. Indeed, the average cross-sectional area of the ducts can be very different than that of the bony canals, especially in large animals such as *Elephas maximus* (see Chapter II).

Natural frequency (ω_0)

The natural frequency (ω_0) is the frequency for which the deflection of the cupula is in phase with angular velocity. The higher the natural frequency, the higher the tendency of the animal to experience frequent head motion. It can be calculated with this equation:

$$\omega_{0k} = \frac{1}{2\pi} * \sqrt{\frac{K_k}{M_k}}$$

K_k is a parameter defined by the cupula which is a membranous feature that cannot be inferred using the bony labyrinth only. As previously said, M_k is greatly influenced by the average cross-sectional area of the duct. Hence, meticulously-segmented membranous labyrinth 3D models are crucial to calculate this parameter.

Sensitivity (or velocity gain, $\overrightarrow{VGs_k}$)

The sensitivity (or velocity gain, $\overrightarrow{VGs_k}$), corresponds to the degree of deflection of the ciliae per degree per second of head rotation. The higher the sensitivity, the more rotations are accurately detected, but the less the system can sustain high angular velocities

without saturating (David, 2011). It can be calculated with this equation:

$$\overrightarrow{VGs_k} = \frac{\varepsilon * \overrightarrow{G_k}}{C_k}$$

In this equation, ε corresponds to the transfer factor for endolymph volume displacement to cilia deflection. ε is computed through finite element analysis in ARIADNE (David et al. in press), using a 3D model of the cupula inferred from the the membranous *crista ampullaris*. On the other hand, C_k is extremely influenced by the average cross-sectional area of the ducts. Studying the membranous labyrinth is therefore crucial to the investigation of the sensitivity in mammals.

Axes of rotation

The vertical semicircular ducts do not detect the same types of rotation than the lateral duct. This is due to the differences of orientation of the ducts and therefore, the difference of orientation of their null plane. The anterior and posterior ducts detect head motions in pitch and roll rotations (Fig. VI.4A and VI.4C) while the lateral duct detects head motions in yaw rotations (Fig. VI.4B). Differences between the lateral and vertical canals capacities are taken into account in this chapter.

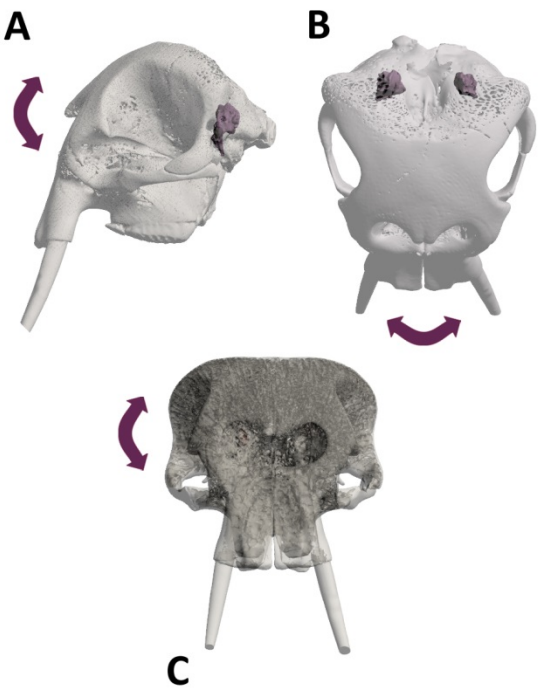

Figure VI.4 : Natural rotations of the head: pitch (A), yaw (B) and roll (C) in the skull of an elephant, with the petrosals seen in transparency.

Objectives

The first goal of this chapter is to calculate these functional parameters in several extant afrotherians. These calculations allow discussing the functional differences between species that display very different locomotor behaviors. The second objective is to infer the same functional parameters in extinct proboscideans (and to a lesser extent afrotherians) and to investigate its evolution within the group.

2. Material and methods

2.1. Taxa sample

Three extant specimens preserving the membranous labyrinth were sampled (*Procavia*, *Elephantulus* and *Elephas*), in a view to segment the membranous ducts in 3D. The reconstructions are used, amongst other things, in order to infer the membranous features of extinct taxa. On the other hand, the bony labyrinths of proboscideans that were segmented during the thesis were prepared in order to infer their functional capacities. Only specimens preserving all three semicircular canals are analyzed here (Table VI.1).

2.2. Preparation of the membranous specimens

2.2.1. Dissection and stain protocol

The membranous labyrinth of *Elephantulus* was sampled on a specimen conserved in formaldehyde from the collections of the MNHN (MNHN.AC.ZM.1930-92). Given the very small size of *Elephantulus* specimens, the whole head was severed and the petrosals were not detached from the skull. The membranous labyrinth of *Procavia capensis* has been sampled on a fresh cadaver from the Leipzig zoo. Here, the back of the head was severed and the petrosals were not isolated. The sampling was made less than 48 hours after the death to assure a good preservation of the structures.

Table VI.1 : Summary of the taxa sample used in this chapter with information on the number of specimens used (number) and among them the number of specimens that preserves the membranous labyrinth (soft) and the number of specimens that preserves the bony labyrinth (bony).

Taxa	Number	Soft	Bony
Tenrec	1	0	1
Elephantulus	1	1	1
Ocepeia	1	0	1
Procavia	1	1	1
Embrithopoda PM53	1	0	1
Arsinoitherium	1	0	1
Prorastomus	1	0	1
Chambi sirenian	1	0	1
Eritherium	1	0	1
Phosphatherium	1	0	1
Numidotherium	1	0	1
Prodeinotherium	1	0	1
Mammut	2	0	2
Stegodon	1	0	1
Loxodonta sp	2	0	2
Loxodonta africana	2	0	2
Loxodonta cyclotis	4	0	4
Palaeoloxodon	1	0	1
Elephas	4	1	4
Mammuthus columbi	1	0	1
M. primigenius	1	0	1
Anancus	7	0	7
Gomphotherium	2	0	2
Cuvieronius	1	0	1
Platybelodon	1	0	1

Finally, the membranous labyrinth of *Elephas maximus* was sampled on a dead newborn elephant from Leipzig zoo, less than 48h after its death. The head was severed and then put in Bouin solution for fixation for several weeks. The ear region was later carefully removed to improve the staining of the inner ear.

The three specimens were then dehydrated and stained following the protocol of David et al. (in press) and explained in Chapter II (§ 2.2). While *Elephantulus* and *Procavia* specimens only needed one stain bath, it took several baths to properly stain the *Elephas* specimen (given its larger size).

2.2.2. CT acquisition

The membranous specimens were scanned at the Max Planck Institute for Evolutionary Anthropology (MPI-EVA) in Leipzig, using a SkyScan1173. The scanning resolution is 8.94 µm for *Elephas* CEB150009, 8.22 µm for *Procavia* CEB150012 and 7.86 µm for *Elephantulus* MNHN.ZM.AC.1930-92.

2.2.3. Segmentation

Segmentations of the membranous labyrinths were conducted with AVIZO 7.1 (*Procavia capensis*) and Materialise MIMICS 16 and 17 (*Elephas maximus, Elephantulus*). Only the endolymph is selected in the microtomographic slices; the membrane of the membranous labyrinth is not included in the selection. The segmentation has to be very precise in order to prevent miscalculations of the endolymphatic volumes. A crucial step of the segmentation is to select areas around the *crista ampullaris*. The cupula is often shrunk in sampled membranous labyrinths, therefore it is modeled in a later step. The shrunk cupula and the subcupular spaces (including the sterociliae/kinociliae layers) were included in the segmentation.

2.2.4. Labyrinth preparation

After segmentation of the membranous ducts, a raw 3D model is exported. We then applied the data preparation protocol of David et al. (in press.), which permits to apply the same decimation and smoothing parameters to all specimens. The different anatomical regions of the membranous labyrinth were then manually separated following the David et al. (in press) protocol. At the end, the labyrinth is divided into eleven individual meshes illustrated in Fig. VI.5.

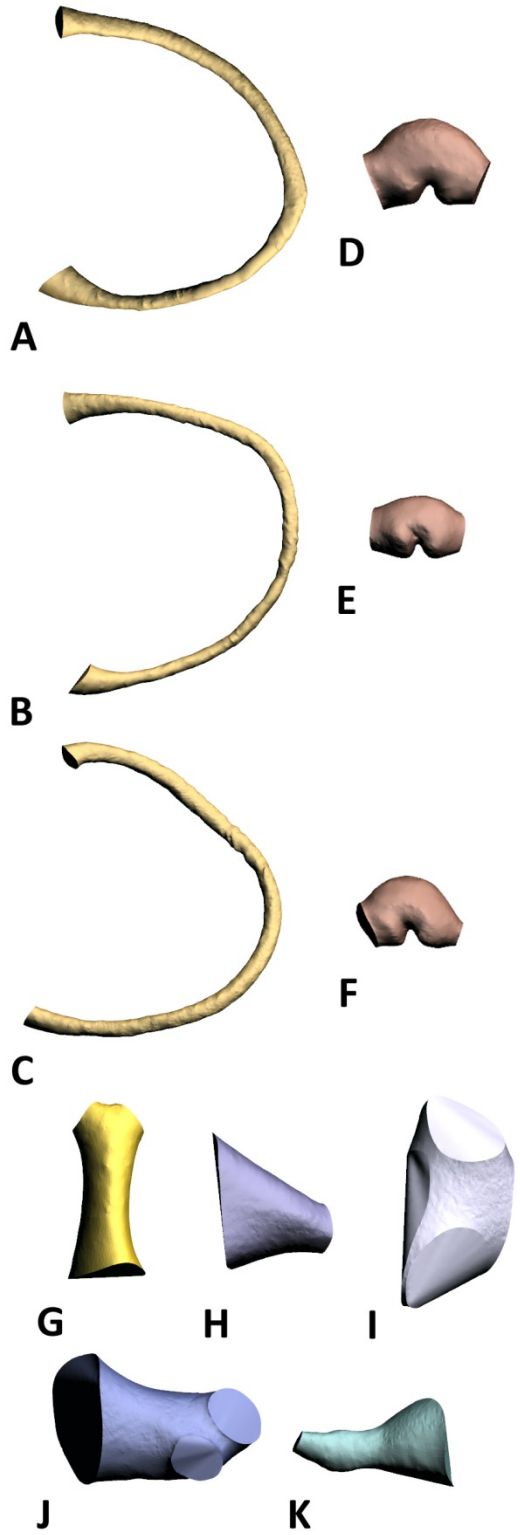

Figure VI.5 : Volume meshes of *Elephas* obtained at the end of the preparation protocol; Anterior (A), posterior (B) and lateral (C) slender ducts, anterior (D), posterior (E) and lateral (F) ampullae, *crus commune* (G), posterior utricle (H), common utricle (I), anterior utricle (J) and simple crus (K).

2.2.5. Landmark protocol

Landmarks were then placed on the membranous labyrinths of *Procavia*, *Elephas* and *Elephantulus* following the protocol of David et al. (in press) and using AVIZO 7.1. Contrary to the bony labyrinth protocol (see 'Introduction' section of the thesis, § 2.2.), all the placed landmarks are internal here.

A set of landmarks is placed along the central streamline of each semicircular duct (Fig. VI.6, orange sets). For the vertical ducts, the first landmark is placed at the intersection between the ampulla and the slender duct and the last landmark is placed at the intersection between the duct and the *crus commune*. For the lateral duct, the first landmark is placed at the intersection between the ampulla and the duct as well, but the last landmark is placed at the intersection between the duct and the simple crus.

A set of landmarks is then placed along the streamline of the ampulla of each duct. The first landmark is placed at the intersection between the anterior utricle and the ampulla. The last landmark is placed at the intersection between the ampulla and the duct (Fig. VI.6, pale yellow sets).

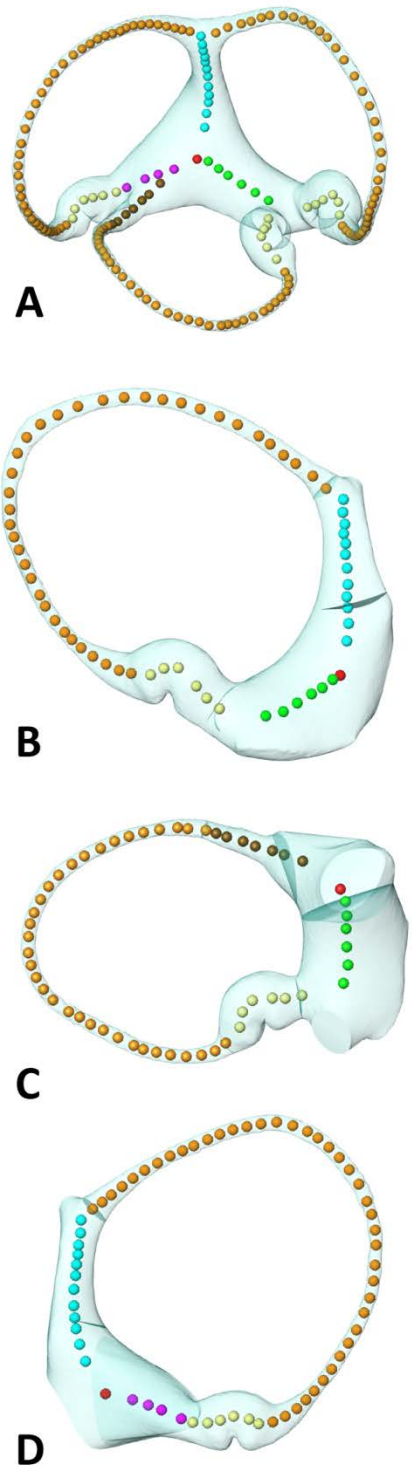

Figure VI.6 : Landmarks sets of the membranous labyrinth of *Elephas* in general (A), posterior (B), lateral (C) and anterior (D) views. In **orange**, landmarks of the slender ducts; in **pale yellow**, ampullae landmarks; in **blue**; *crus commune* landmarks; in **brown**, simple crus landmarks; in **green**, anterior utricle landmarks; in **purple**, posterior utricle landmarks; in **red**, common utricle landmark.

A set of landmarks is placed along the *crus commune*. The first landmark is placed at the junction of the streamlines of the anterior and posterior slender duct and of the *crus commune*, while the last landmark is placed at the intersection between the central streamline and the common utricle side of the *crus commune* (Fig. VI.6, blue set).

A set of landmarks is placed along the streamline of each utricular part of the vestibule. The first set begins at the intersection between the common and anterior utricles and ends at the junction of the central streamlines of the anterior and lateral ampullae and of the anterior utricle (Fig. VI.6, green set). The second set begins at the intersection between the common and posterior utricles and ends at the intersection between the posterior ampulla and the posterior utricle (Fig. VI.6, purple set). The third set begins at the intersection between the lateral duct and the simple crus and ends shortly before the intersection of the central streamline and the common utricle side of the simple crus (Fig. VI.6, brown set). Finally, the last set consists of a single landmark placed at the junction of the trajectories of the central streamlines of the anterior and posterior utricles, of the *crus commune*

and of the simple crus (Fig. VI.6, red landmark).

2.2.6. Cupula modelling

A 3D baseline tridimensional model of the cupulae of each duct is then built using GEOMAGICS Studio 2012 (Fig VI.7A). This 3D model is then used by ARIADNE (David et al. in press) in order to calculate the cupula stiffness parameter (K_k, §1).

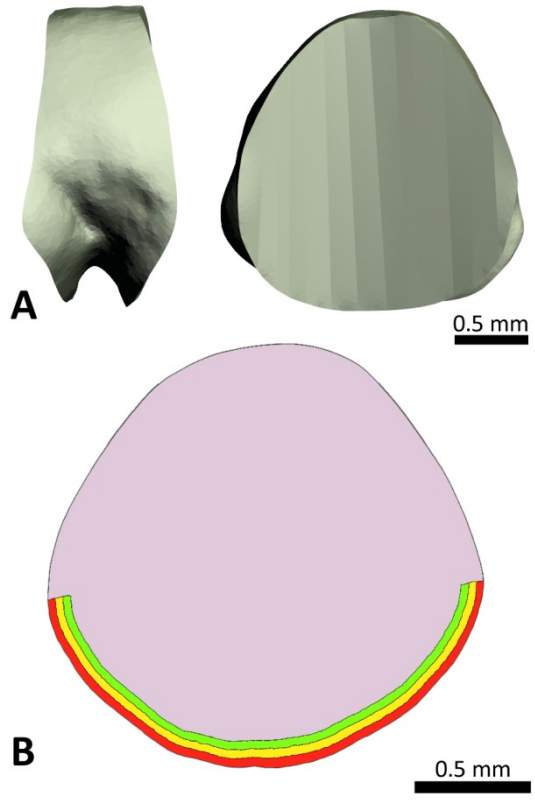

Figure VI.7 : 3D baseline tridimensional model of the posterior cupula of *Elephas maximus* CEB150009 (A). 3D model of the middle cross-section of the posterior ampulla with the different stereociliae/kinociliae areas (B). In **red**, 0-30 µm, in **yellow**, 30-60 µm and in **green**, 60-90 µm.

Since the cupula of the specimens is shrunk (a commonly-seen post-mortem feature of the membranous labyrinth, pers. comm. Romain David, 2014), a 3D model has to be inferred.

The cupula is thought to be secreted by the supporting cells of the *crista ampullaris*, hence the best way to do this is to perform an extrusion of the shape of the *crista ampullaris* towards the ampulla roof. The calculated thickness is adapted for biomechanical analyses depending on the assumed value for stereociliae length (Fig VI.7B). Finally, the cupula deflection is analyzed using the finite elements method.

2.2.7. Analysis in ARIADNE

The 3D volumes, surfaces and landmarks sets are then inputted in ARIADNE (David et al. in press), which automatically calculates the functional parameters of the membranous specimens. We assumed the endolymph viscosity to be similar as humans. Since no shrinkage of the semicircular ducts was observed, we did not apply shrinkage correction. Finally, we assumed the sterociliae length of the *crista ampullaris* hair cells to be comprised between 30 and 60 µm (Fig VI.7B, yellow area).

2.2.8. Regressions

Raw values of the functional parameters are effective values that define the vestibular capacities of animals. However, these parameters are strongly influenced by the size (and/or body mass) of the animals. Hence, we calculated the same values but without the effect of size.

To do so, we used phylogenetic generalized least square regressions of the logarithm of functional parameters onto the logarithm of body mass, based on semicircular duct systems of 30 mammal species, belonging to various clades, showing various behaviors and covering a large range of body sizes (pers. comm. Romain David, list of taxa and phylogenetic tree used in regressions in Appendix 29). We used these regressions in order to compute residuals for the logarithm of each functional parameter. We then calculated estimated values for the logarithm of the functional parameters of the three afrotherian species, as if they weighted the same mass (50 kg), to which we added the previously computed residuals, and we finally raised 10 to the power of the obtained value to get body mass-free functional parameters. Functional parameters of an estimated mammalian ancestral morphotype, based on these 30 mammal species, are used as a comparison.

2.3. Functional inferences on the bony specimens

To infer the functional capacities of the fossil taxa, the corresponding bony labyrinths have been segmented and a similar preparation protocol was applied for each specimen (decimation, smoothing) in order to standardize the data. 3D models were landmarked following the protocol of Gunz et al. (2012) (see 'Material and Methods' section of the thesis, § 4.2.). A custom software (developed by Romain David) was then used to compute the lengths of the semicircular canals, the *crus commune* and the enclosed area for the midline and external landmark sets.

The raw functional parameters have been inferred using regressions with the same data set given in Appendix 29, to which are added the three extant afrotherians (*Elephas*, *Elephantulus* and *Procavia*) that we studied. In this set, measurements of both the bony and membranous labyrinth are available. We calculated the log of the functional parameters of the membranous labyrinths and the log of the area and length parameters for the specimens of this set.

A PCA was performed on the morphological parameters of the bony labyrinth. Phylogenetic regressions were then performed between the log of the functional parameters and the PCs of the bony labyrinth parameters that displayed the lowest Aikaike information criterion. Regressions were performed using R with the function 'PGLS' and the package 'caper'. We also used a consensual mammal tree (see Appendix 29). Residuals are inferred for the node 'Afrotheria' calculated with the function fastAnc of the 'phytools' package. We used these regressions to predict fitted functional parameters values of the data set for which we only have the bony labyrinth (extant and extinct afrotherians and proboscideans). The fitted values were calculated with a confidence interval of 95%. The script used to perform these calculations is given in Appendix 30.

The raw values were then freed from the effect of body-mass using the same method explained in § 2.2.8.

3. Results

3.1. Functional capacities of extant afrotherians

Comparisons of the functional parameters of the semicircular duct system of three afrotherian mammals (*Elephas maximus*, *Procavia capensis* and *Elephantulus*) allow us to discuss differences in the context of variation in animal size and ecology.

3.1.1. Raw values

Raw – or effective – values of the functional parameters calculated with the software ARIADNE are given in Table VI.2. Among these values, we will discuss three major functional parameters: the short-time constant (T_2), the natural frequency (ω_0) and the sensitivity (or velocity gain, VGs).

Short time constant (T_2)

The short-time constant is particularly low in *Elephantulus* with little to no difference between its ducts (1.2 ms in vertical ducts and 1.3 ms in the lateral duct). In comparison, *Procavia* displays an approximately 1.5 times higher short-time constant with still no particular differences between ducts (1.9 ms in the anterior duct, 2.1 ms in the posterior duct and 2.0 ms in the lateral duct).

Table VI.2 : Raw functional parameters of extant afrotherians.

	Elephantulus	*Elephas*	*Procavia*
Short time constant (T_2) of the anterior duct, in ms	1.2	14.2	1.9
Short time constant (T_2) of the posterior duct, in ms	1.2	11.8	2.1
Short time constant (T_2) of the lateral duct, in ms	1.3	8.6	2.0
Natural frequency (ω_0) of the anterior duct, in Hz	4.3	0.7	2.4
Natural frequency (ω_0) of the posterior duct, in Hz	5.7	0.9	2.4
Natural frequency (ω_0) of the lateral duct, in Hz	4.3	0.7	3.2
Sensitivity (velocity gain VGs) of the anterior duct, in mdeg/deg.s^{-1}	0.0036	0.0339	0.0058
Sensitivity (velocity gain VGs) of the posterior duct, in mdeg/deg.s^{-1}	0.0037	0.0393	0.0060
Sensitivity (velocity gain VGs) of the lateral duct, in mdeg/deg.s^{-1}	0.0030	0.0123	0.0055
Sensitivity V/L ratio	0.85	2.10	0.76

This means that responses within the semicircular duct system are approximately 1.5 times faster in *Elephantulus* than in *Procavia*. In contrast, *Elephas* exhibits extremely high short-time constants. Its vertical short-time constants are more than ten times higher than in *Elephantulus* while its lateral short-time constant is almost eight times higher than in *Elephantulus*. This implies that the vestibular system of Elephas responds to angular rotations much more slowly than in *Elephantulus* and *Procavia*. This is probably due to the particularly large size and body mass of *Elephas* but this does not change the fact that the vestibular system of *Elephas* is slower to respond to the excitation than the two other studied afrotherians. On the other hand, *Elephas* also displays significant differences between values of vertical and lateral ducts. Vertical ducts (and especially the anterior duct) display higher short-time constants and therefore respond more slowly to angular rotations than the lateral duct. This means that elephants are capable to respond more rapidly to yaw motion than to pitch or roll motion.

Natural frequency (ω_0)

Elephas exhibits particularly low values for the natural frequency. This implies that elephants do not tend to display high frequency motion of the head. The values are similar in all three semicircular ducts, hence this tendency is constant in pitch, roll and yaw motion. *Elephantulus*, on the other hand, displays higher values of the natural frequency which means it is capable to move its head more often. The value is even higher for the posterior duct, meaning that *Elephantulus* is capable of particularly frequent head motion along pitch and/or roll axes. *Procavia* displays somewhat average values compared to the other two afrotherians. However, given its higher natural frequency in the lateral duct, it is capable of higher frequency motion in yaw than in pitch and roll.

Sensitivity (or velocity gain, VGs)

Elephas displays the highest sensitivity values of the three studied afrotherians. The sensitivity of its vertical ducts is approximately ten times higher than in *Elephantulus* and approximately six times higher than in *Procavia*. This means that the minimal change in vertical

head angular rotation *Elephas* is able to detect is ten times smaller than in *Elephantulus* and six times smaller than in *Procavia*. This also means that the maximal angular velocities that *Elephas* is able to experiment in pitch and roll are ten times less important than in *Elephantulus* and six times less important than in *Procavia*. Regarding the lateral duct, the difference is less marked with *Elephas* exhibiting a sensitivity four times higher than *Elephantulus* and two times higher than *Procavia*.

To better compare vertical and lateral values of the sensitivity within the same individual, an ideal inclination of the vertical ducts with the coronal plane (45°) has to be taken into account. Hence the values for the vertical ducts have to be multiplied by 0.707 (cos(45°)). A ratio of vertical/lateral values (that we will call the V/L ratio in this work) is calculated to express differences between lateral and vertical values and is given in Table VI.3.

The equation to calculate the V/L ratio is:

$$(\text{VGs ant} + \text{VGs post}) * \frac{0.707}{2 * \text{VGs lat}}$$

In *Elephantulus* and *Procavia*, the ratio is close to 1, which means that sensitivity values are not significantly different for lateral and vertical motion. This implies that the angular velocities these two animals experiment in yaw are of the same order of magnitude as the angular velocities they experiment in roll and pitch. In contrary, *Elephas* exhibits a ratio that equals two, meaning that the sensitivity of its lateral duct is two times lower than the sensitivity of its vertical ducts. This implies that the angular velocities the elephant is able to experiment in pitch and roll are two times less important that in yaw. In contrary, the vestibular system of *Elephas* is two times more precise to discriminate angular rotations in pitch and roll than in yaw. In other terms, *Elephas* is capable of faster movements in yaw than in pitch and roll but can detect more precisely movements of its head in pitch and roll than in yaw.

3.1.2. Adaptations and effect of the size

Raw values previously discussed are effective functional values that define the vestibular capacities of animals. However, these parameters are strongly influenced by the size (and/or body mass) of the animals. Large labyrinths tend to display higher short-time constants and sensitivities as well as lower natural

frequencies. In short, large animals tend to be less agile and display semicircular duct systems that respond more slowly to stimuli. Raw values remain interesting to discuss because they reflect real vestibular capacities of animals. However, to truly study adaptations of the semicircular duct system, we must suppress the effect of size. To do so, we used phylogenetic generalized least square regressions. They are presented in the 'Material and Methods' section (§ 2.2.8). Body-mass free values of our specimens and of the mammalian morphotype are given in Table VI.3.

Short time constant (T_2)

The short time constant of the mammalian ancestral morphotype is more or less constant between anterior and posterior ducts. It is slightly lower for the lateral duct, meaning that the semicircular duct system generally responds slightly faster in yaw than in pitch and roll in mammals.

The short time constant of the vertical ducts of *Elephantulus* are similar to the mammalian ancestral morphotype although slightly higher. This implies that when the effect of the size is eliminated, the response speed of the semicircular duct system of *Elephantulus* is in the mammalian middle range but slightly slower. The particularly low effective short time constants (effective functional parameters given in Table VI.2) are thus principally caused by the small size of the animal. Values for the lateral duct are similar to that of the vertical duct in *Elephantulus*; the slight reduction of the short time constant observed in the mammalian ancestral morphotype is not observed in *Elephantulus*. Hence, the lateral duct short time constant of *Elephantulus* is higher than the mammalian ancestral morphotype. *Elephantulus* therefore would display slower semicircular duct response speed than the mammalian ancestral morphotype in yaw movements if all mammals had the same size.

Table VI.3 : Body mass-free functional parameters of the semicircular duct system of afrotherians

	Elephantulus	*Elephas*	*Procavia*	Mammalian ancestral morphotype
Short time constant (T_2) of the anterior duct, in ms	4.2	6.4	3.1	3.7
Short time constant (T_2) of the posterior duct, in ms	4.6	5.0	3.5	4.0
Short time constant (T_2) of the lateral duct, in ms	4.7	3.9	3.2	3.1
Natural frequency (ω_0) of the anterior duct, in Hz	1.9	1.5	1.7	1.4
Natural frequency (ω_0) of the posterior duct, in Hz	2.4	1.6	1.8	1.7
Natural frequency (ω_0) of the lateral duct, in Hz	2.0	1.1	2.4	1.7
Sensitivity (velocity gain VGs) of the anterior duct, in mdeg/deg.s^{-1}	0.0157	0.0132	0.0101	0.0098
Sensitivity (velocity gain VGs) of the posterior duct, in mdeg/deg.s^{-1}	0.0175	0.0145	0.0109	0.0095
Sensitivity (velocity gain VGs) of the lateral duct, in mdeg/deg.s^{-1}	0.0133	0.0048	0.0096	0.0075
Sensitivity V/L ratio	0.88	2.04	0.77	0.91

The short time constants of *Procavia* are similar between ducts. At equal body mass, they are slightly lower than the mammalian ancestral morphotype for the vertical ducts and similar to the mammalian ancestral morphotype for the lateral duct. *Procavia* therefore displays semicircular duct response speed within the same range of the mammalian ancestral morphotype. Thus, the low effective short time constants (Table VI.2) are mostly influenced by the small size of the animal.

In *Elephas*, the short time constant values are different according to the ducts. The anterior duct exhibits the higher constant (6.4 ms) followed by the posterior duct constant (5.0 ms). The constant of the lateral duct is the lowest (3.9 ms). These values are high compared to the mammalian ancestral morphotype especially for the anterior duct (almost

twice as high). The difference is slighter for the lateral duct. This shows that the very large size of *Elephas* is not the only factor that influences the particularly slow response speed of its semicircular duct system. At equal body mass, the vestibular system of *Elephas* displays particularly slow response speed to angular rotations compared to the mammalian ancestral morphotype. This is more pronounced in pitch and roll motion than in yaw.

Natural frequency (ω_0)

The natural frequency of the mammalian ancestral morphotype is rather similar between all its ducts, which means that, in general, mammals tend to display similar frequencies of head motion in all axes.

The natural frequency of *Elephantulus* is slightly higher than that of the mammalian ancestral morphotype if we eliminate the effect of the size, especially compared to the mammalian ancestral morphotype vertical ducts. This implies a slight size-independent adaptation to exhibit high frequencies of head motion in pitch and roll. *Elephas* displays vertical natural frequencies similar to the mammalian ancestral morphotype. However, the lateral duct frequency of *Elephas* is significantly lower than in the mammalian ancestral morphotype. This implies that, independently to the size of the animal, *Elephas* tends to exhibit lower frequencies of head motion than the mammalian ancestral morphotypes in yaw movements. Body mass-free natural frequency values of the vertical ducts of *Procavia* are very similar to that of the mammalian ancestral morphotype. The lateral duct, however, display a particularly high natural frequency (2.4 Hz) compared to other afrotherians and even the mammalian ancestral morphotype. This suggests that the tendency of *Procavia* to exhibit higher frequencies of yaw head motion observed in its effective functional parameters (Table VI.2) is not only due to its size. Its lateral duct is adapted to high frequencies of yaw head motion.

Sensitivity (or velocity gain, VGs)

The V/L ratio of the mammalian ancestral morphotype is very close to 1 (0.91) which means it displays a very similar sensitivity in all three ducts. Hence the angular velocities the mammalian ancestral morphotype experiments in yaw

are of the same order of magnitude as the velocities it experiments in roll and pitch.

In *Elephantulus*, the V/L ratio is also close to 1 (0.88) hence the difference between the vertical and lateral ducts sensitivities is not important. As for the mammalian ancestral morphotype, *Elephantulus* experiments similar angular velocities for pitch, roll and yaw motion. However, its body mass-free sensitivity values are 1.5 to 2 times higher than for the mammalian ancestral morphotype, which implies that if we eliminate the effect of the size, *Elephantulus* is less capable of experimenting rapid direction changes than the mammalian ancestral morphotype (i.e. *Elephantulus* would be less agile).

Elephas displays sensitivity values similar – although slightly lower – as those of *Elephantulus* for the vertical ducts. This means that, even if we eliminate the effect of size, elephants experiment lower angular velocities than the mammalian ancestral morphotype for pitch and roll motion. In contrary, the lateral duct body mass-free sensitivity is lower than that of the mammalian ancestral morphotype. This implies that elephants display an adaptation to lower sensitivities in the lateral duct. Hence, at equal size, elephants would be able to experience higher angular velocities than the mammalian ancestral morphotype in yaw. This is also supported by the V/L ratio (2.04) that shows that the sensitivity of the vertical ducts is two times higher than the sensitivity of the lateral duct in elephants (hence experienced angular velocities are two times higher in yaw).

Body mass-free sensitivity values of the vertical ducts are slightly lower in *Procavia* than in the two other afrotherians. They are quite similar to the mammalian ancestral morphotype. This implies that, at equal size, *Procavia* experience slightly higher angular velocities in pitch and roll than *Elephas* and *Elephantulus* but in the range of values of the mammalian ancestral morphotype. On the other hand, the lateral duct sensitivity value of *Procavia* is higher than *Elephas* and than the mammalian ancestral morphotype. Hence *Procavia* displays poor levels of angular velocity in yaw motion. This means that the relatively low effective sensitivity of *Procavia* for the lateral duct is actually due to its small size.

3.2. Functional inferences on fossil proboscideans and afrotherians

3.2.1. Raw estimated functional parameters

As previously said, size have a high impact on functional parameters. Species with a large size (and body mass) display very low values for the natural frequency and particularly high values for the short time constant and the sensitivity. Hence, the distribution of raw estimated functional parameters mainly reflects the size of the taxa. The raw values are therefore not discussed. However, phylogenetically generalized least-square regressions were performed on the results to discuss the functional parameters free of the effect of size.

3.2.2. Body-mass free estimated functional parameters

Inferred estimated functional parameters free of the effect of size are presented in this section. In each graph, the fitted value is represented with a triangle and the confidence interval is represented with arrows. The value of the functional parameter is contained in the confidence interval but its most probable value is the fitted value. Hence one must be careful when comparing two fitted values of different specimens when their confidence intervals strongly overlap.

Short time constant (T_2)

Body-mass free inferred short time constants of the lateral duct of Afrotheria are given in Fig VI.8A. *Eritherium* and *Phosphatherium* exhibit particularly low constants for the lateral duct, which implies that, even if we eliminate the effect of size, their semicircular duct system responds rapidly to excitation during yaw motion. The fitted value of the constant is lower in *Eritherium* than in *Phosphatherium* hence *Eritherium* probably displays a faster response speed. However, the confidence intervals of both specimens strongly overlap. The constants of both specimens appear to be even lower than that of smaller afrotherians such as *Elephantulus* or *Tenrec*. This implies that *Eritherium* and *Phosphatherium* had probably vestibular systems well adapted to respond rapidly to excitation during yaw head motion compared to other proboscideans and even afrotherians. The fitted value of the constant of *Numidotherium* is higher which means that its semicircular duct system probably took more time to respond to excitations during yaw

movements than in *Eritherium* and *Phosphatherium*. The abilities of *Numidotherium* for the lateral duct are very similar to those of *Ocepeia*, *Tenrec* and *Prorastomus*. *Prodeinotherium* and *Arsinoitherium* display similar short time constants, which fitted values are higher than previously cited afrotherians, which means that they probably respond more slowly to yaw head motion. Another functional group contains *Procavia*, Embrithopoda PM53, *Palaeoloxodon*, *Elephantulus* and *Platybelodon*. These five afrotherians display similar fitted values for this functional parameter, which are higher than in previously mentioned afrotherians. It is noted that the unpublished embrithopod – which is older and smaller than *Arsinoitherium* – probably displays slower response speed than the very large *Arsinoitherium*. This suggests an adaptation in *Arsinoitherium* to faster response speed of the semicircular duct system to excitations in yaw motion. Finally, the remaining elephantimorphs display even higher fitted values for the lateral short time constants and form a group with more or less similar values. An interesting detail is the difference between *Loxodonta cyclotis* and *Loxodonta africana*. *Loxodonta africana* (the African bush elephant) displays a lower fitted value for the short time constant in its lateral duct, meaning that its semicircular duct system is probably faster to respond to yaw head motion than *Loxodonta cyclotis* (the African forest elephant). The latter seems to be functionally more similar to *Elephas maximus* (the Asian elephant) for this parameter. This similarity could be explained by the more similar environment they live in (they both live mostly in forests).

Body-mass free inferred short time constants of the vertical ducts of Afrotheria are given in Fig VI.8B. In general, values for the vertical ducts are always smaller than for the lateral duct in the same taxon, which suggests that the semicircular duct system tends to be faster to respond to excitation in pitch and roll head motion than in yaw motion in Afrotheria. The distribution of this parameter is very similar to the distribution observed for the lateral duct, with a few exceptions. Values of *Ocepeia* for the vertical ducts are closer to *Eritherium* and *Phosphatherium*. *Prodeinotherium* and *Prorastomus* have very similar values. The probable functional differences between

Arsinoitherium and the unpublished embrithopod for the lateral duct are verified for the vertical ducts. Contrary to the lateral values, the vertical values of *Mammuthus columbi* and *Mammuthus primigenius* are significantly different, *M. primigenius* displaying faster response speed of the semicircular duct system in pitch and roll head motion than *M. columbi*. The functional differences between *Loxodonta cyclotis* and *Loxodonta africana* and the similarity between *L. cyclotis* and *Elephas maximus* observed for the lateral duct are observed in the vertical ducts as well and are even more marked.

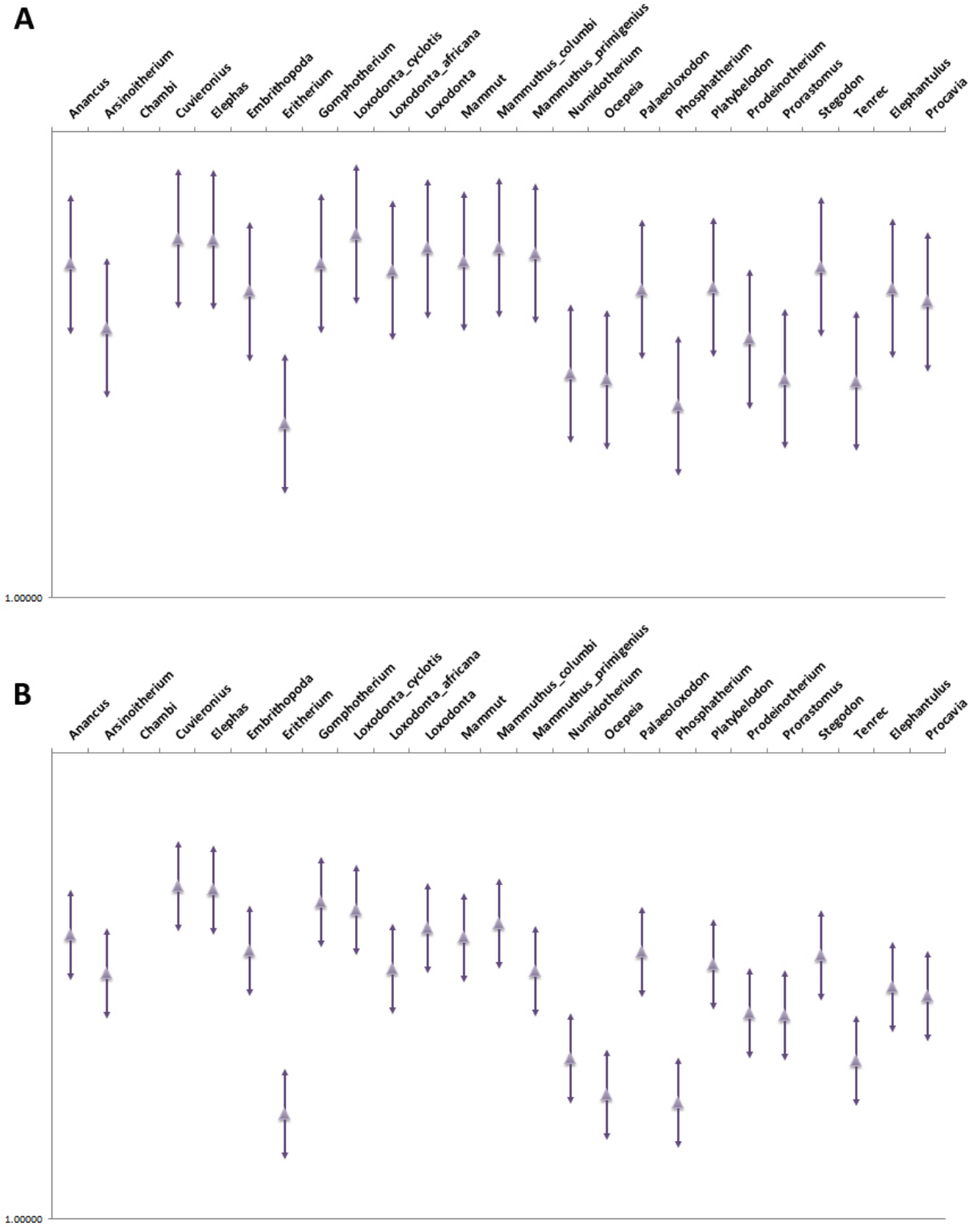

Figure VI.8 : Body mass-free inferred short time constant (T_2) of afrotherians for the lateral duct (A) and vertical ducts (B). Values are in ms.

Natural frequency (ω_0)

Body-mass free inferred natural frequencies of the lateral duct of Afrotheria are given in Fig VI.9A. This estimated parameter is particularly low in *Prorastomus* which exhibits the lowest frequency of all sampled afrotherians. This implies that *Prorastomus* did not tend to exhibit high frequencies of head motion in yaw. *Loxodonta africana* displays a poor natural frequency for the lateral duct as well, at least probably lower than that of *Loxodonta cyclotis* which is closer to that of *Elephas maximus*. The remaining elephantimorphs form more or less two functional groups for this parameter. The first group contains *Anancus*, *Platybelodon* and *Palaeoloxodon*. They display similar values as *Elephas* and *L. cyclotis* but also *Procavia*, *Prodeinotherium* and the early embrithopod. The second group includes *Mammut*, *Stegodon*, *Gomphotherium*, *Cuvieronius* and both *Mammuthus* species. They display values similar to *Arsinoitherium* and *Elephantulus*. It is interesting that, at equal size, very large taxa such as *Arsinoitherium* or *Cuvieronius* display natural frequencies similar to that of *Elephantulus*. On the other hand, *Arsinoitherium* probably exhibits a higher tendency to display high frequencies of head motion compared to the earlier and much smaller embrithopod. Early taxa (*Numidotherium*, *Phosphatherium* and *Eritherium*) display the highest values in Proboscidea. While *Numidotherium* seems to be functionally closer to elephantimorphs for this parameter, *Eritherium* and *Phosphatherium* exhibit natural frequencies probably more similar to *Ocepeia* and *Tenrec*.

Body-mass free inferred natural frequencies of the vertical ducts of Afrotheria are given in Fig VI.9B. In general, values for the vertical ducts are always smaller than for the lateral duct in the same taxon which suggests that afrotherians have greater tendencies to exhibit high frequencies of head motion in yaw than in pitch and roll movements. The distribution of this parameter for the vertical ducts is very similar to that of the lateral duct with one noteworthy exception. Indeed, *Prorastomus* exhibits a relatively higher natural frequency for its vertical ducts than for its lateral duct, making it functionally more similar to *Prodeinotherium* or *Palaeoloxodon*. This suggests that *Prorastomus* is somewhat more adapted to experiment high frequencies of head motion in pitch and roll than in yaw.

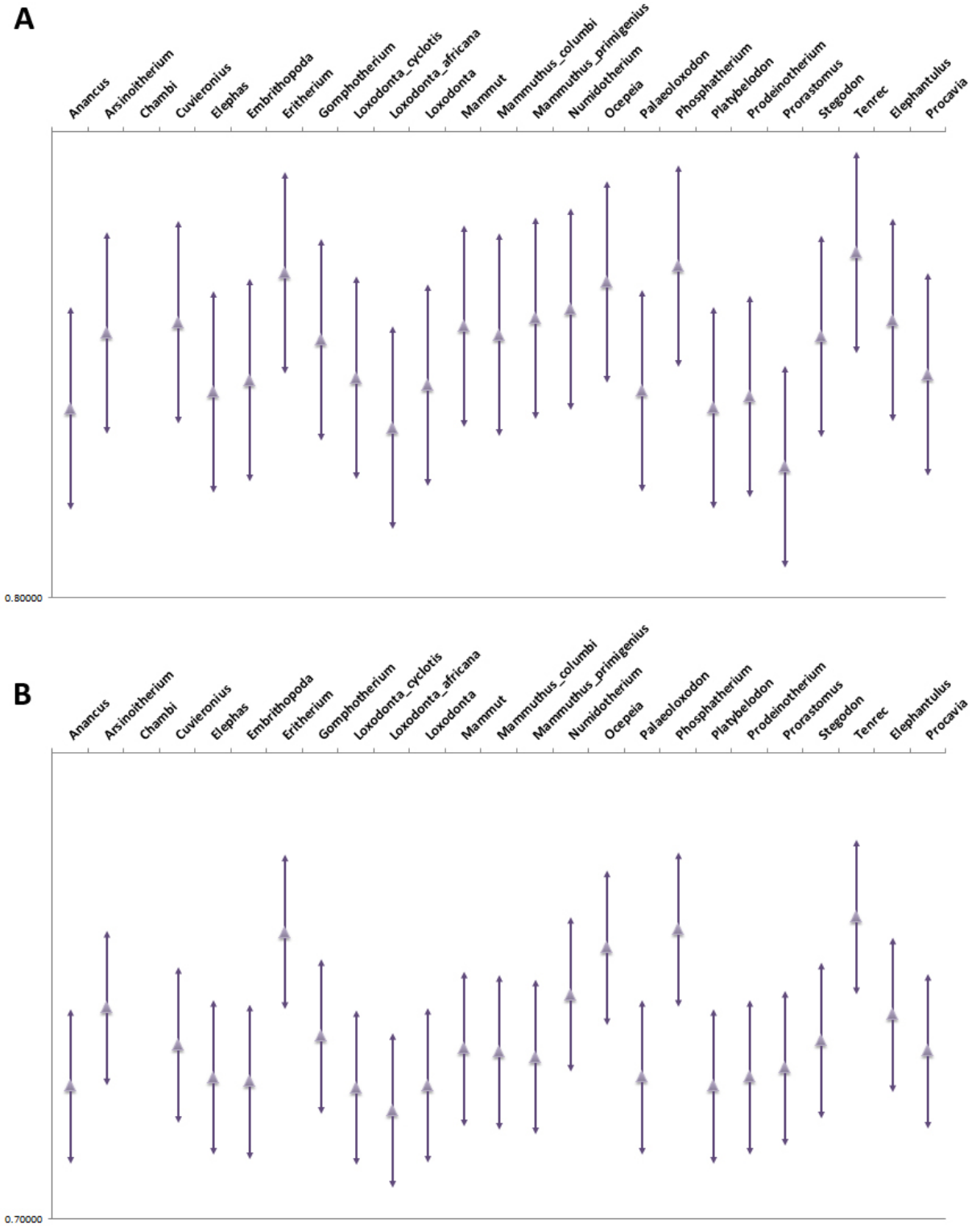

Figure VI.9 : Body mass-free inferred natural frequency (ω_0) of afrotherians for the lateral duct (A) and vertical ducts (B). Values are in Hz.

Sensitivity (or velocity gain, VGs)

Body mass-free sensitivity values for the lateral duct are very similar within studied proboscideans and afrotherians (Fig VI.10A). All proboscideans form a functional group with *Tenrec*, *Ocepeia* and *Arsinoitherium*. They display a relatively low sensitivity compared to the other afrotherians (the early embrithopod, *Prorastomus*, *Procavia* and *Elephantulus*). This suggests that, if we eliminate the effect of size, they experience relatively higher angular velocities for yaw rotations. Hence we can assume that either proboscideans display adaptations of the lateral duct to compensate their large size, or that the lateral ducts of *Prorastomus*, *Procavia*, *Elephantulus* and the early embrithopod are poorly adapted to experience relatively high angular velocities for yaw rotations. Within the Proboscidea, *Mammuthus columbi* and *Stegodon* display slightly lower sensitivity values, probably making them the taxa experiencing the higher angular velocities for yaw rotation of our sample, if the effect of size is eliminated. On the other hand, *Elephantulus* displays the highest body mass-free sensitivity.

The distribution of body-mass free sensitivity values for the vertical ducts is different than for the lateral duct (Fig VI.10B). Early proboscideans (*Eritherium* and *Phosphatherium*) and *Ocepeia* display the lowest body mass-free fitted sensitivities of the sample which means that they are probably experiencing the highest angular velocities in pitch and roll motion when the effect of size is eliminated. A second functional group is composed of *Prorastomus*, *Prodeinotherium*, *Tenrec*, *Numidotherium* and *Loxodonta africana*. They display higher fitted sensitivities hence probably experience lower angular velocities in pitch and roll. *Platybelodon* is slightly less sensitive for these types of motion and similar to *Procavia*. *Palaeoloxodon*, *Mammuthus primigenius*, *Arsinoitherium*, *Anancus* and *Stegodon* display body mass-free values similar to *Elephantulus* and higher than previous taxa. The other proboscideans all display even higher sensitivity values which means that even without the influence of size, they are experiencing lower angular velocities during pitch and roll motion than the other afrotherians.

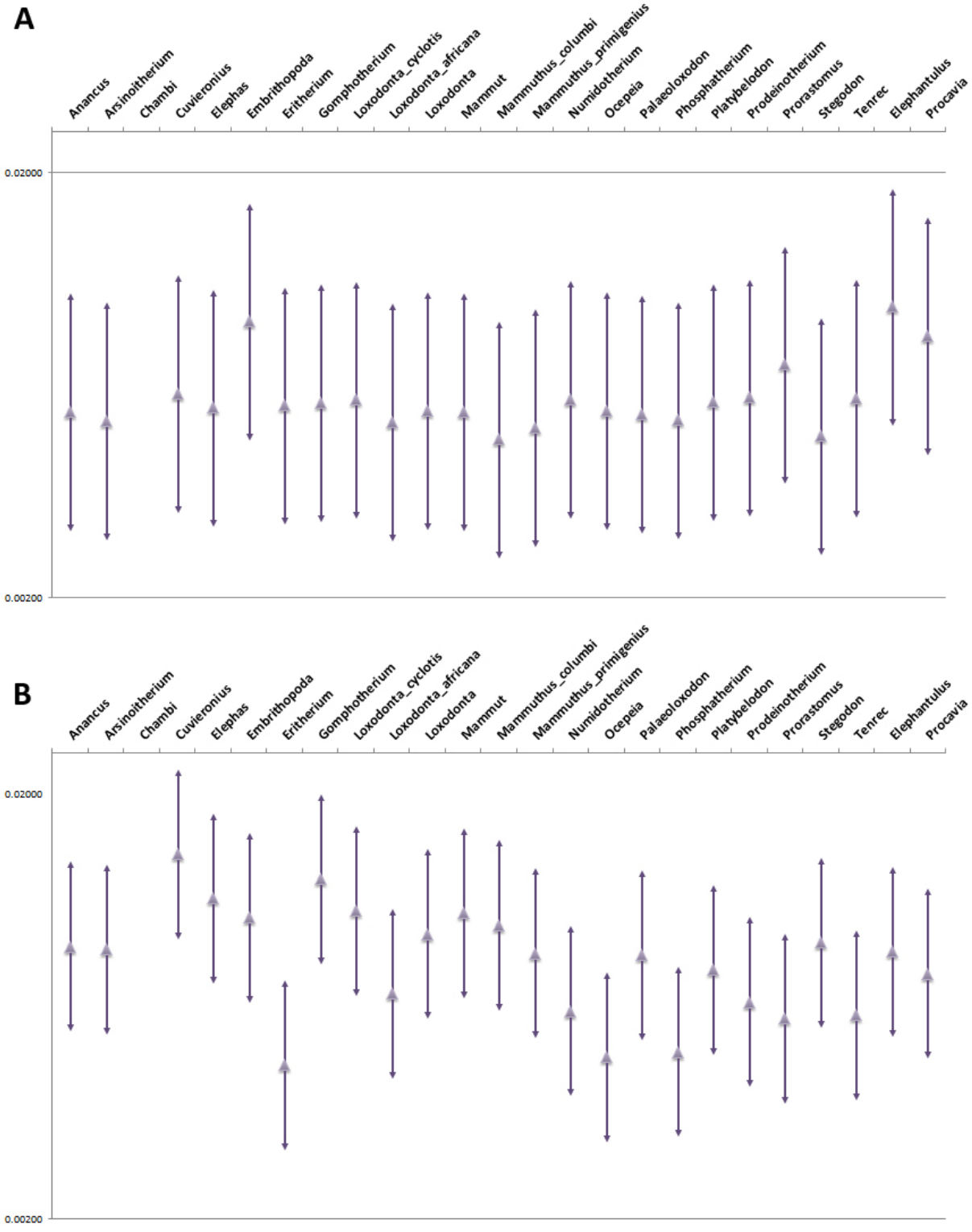

Figure VI.10 : Body mass-free inferred sensitivity (VGs) of afrotherians for the lateral duct (A) and vertical ducts (B). Values are in mdeg/deg.s^{-1}.

4. Discussion

Agility

Agility can be defined as the capacity to rapidly change directions (David, 2011). This is controlled by angular velocity during head motion, which is detected by the semicircular ducts. Hence, the information given by the morphology of semicircular ducts (inferred from that of the canals) provides insights on the agility of extinct mammals. Agility is inversely proportional to the sensitivity (VGs). Indeed, the more an animal is sensitive, the faster its ciliae attain their maximum of deflection, which leads to saturation of the system (David, 2011). On the other hand, the more an animal is sensitive, the more precise it is to detect small angular velocities. Therefore, adaptation of the sensitivity in mammals is a trade-off. If the system is adapted to high sensitivities (VGs), the animal will be able to detect precise small angular velocities. However, the semicircular duct system will be saturated more rapidly and the animal will not be able to change directions rapidly (i.e. the animal will not be very agile). Conversely, if the system is adapted to low sensitivities (VGs), the animal will be very agile but will not be able to detect small angular velocities. To evaluate the agility of terrestrial vertebrates, the most interesting sensitivity values are that of the lateral duct. Indeed, terrestrial vertebrates move predominantly in two (horizontal) dimensions contrary to flying vertebrates which move in three dimensions (Cox & Jeffery, 2010).

It has been pointed out that *Elephantulus* displays a very low effective sensitivity for the lateral duct, which means that it is very agile. However, its body-mass free lateral duct sensitivity is particularly elevated compared to other afrotherians and even the mammalian morphotype (Table VI.3). This suggests that the morphology of the *Elephantulus* lateral duct is not particularly adapted to agility if the effect of size is eliminated. This could be easily explained by the lack of predators that have a similar size as *Elephantulus*. The very small size of *Elephantulus* (it weighs only 56.5 g) already naturally confers it a great agility (hence the very low effective sensitivity). Therefore, there must thus be less selection pressure onto the vestibular system of *Elephantulus* to decrease its sensitivity because its predators already have the disadvantage to be larger (and thus naturally less agile) while

Elephantulus has already the advantage to be smaller (and thus more agile).

On the other hand, the effective value for the lateral duct sensitivity is particularly elevated in *Elephas* (ten times higher than that of *Elephantulus*), which suggests that elephants are not capable of changing directions rapidly (i.e. they are not agile). However, its body-mass free lateral duct sensitivity is particularly low compared to other afrotherians and even the mammalian morphotype (Table VI.3). This suggests that the morphology of the elephant lateral duct is very much adapted to agility if the effect of size is eliminated. Hence, the morphology of the lateral duct of elephants probably partially compensates for their very large size. In chapter II and III, we pointed out that the radius of the lateral canal of elephants is relatively very small compared to other mammals (the lateral canal ratio of elephants is very small). It is possible that the reduction of the lateral canal in elephants is an adaptation to compensate the large size of the animal. Moreover, the values for the lateral duct in *Elephas* are much lower than for the vertical ducts (V/L ratio = 2), which confirms the singularity of the lateral duct.

Evolution of the functional parameters in the Afrotheria

The inferred body-mass free functional values of extant and fossil proboscideans and afrotherians show different patterns depending on the parameter. To study these patterns in an evolutionary perspective, the body-mass free parameter values were discretized and mapped on a cladogram. The topology used here is the same one used for the phylogenetic generalized least squared regressions in Chapter IV (Appendix 20). It is important to point out that the distribution of the functional parameters within the Afrotheria is not tested with a cladistic analysis here, only mapped on the tree to discuss its repartition.

Evolution of the short time constant (T_2) in the Afrotheria

The body mass-free short time constant of the lateral duct appears to primitively display fitted values between 2.40 and 2.60 ms (Fig VI.11A) which is quite low. Hence, the last common ancestor of Afrotheria (node 1) was probably adapted to display fast response speed of the semicircular duct system for yaw motion if the effect of size is eliminated.

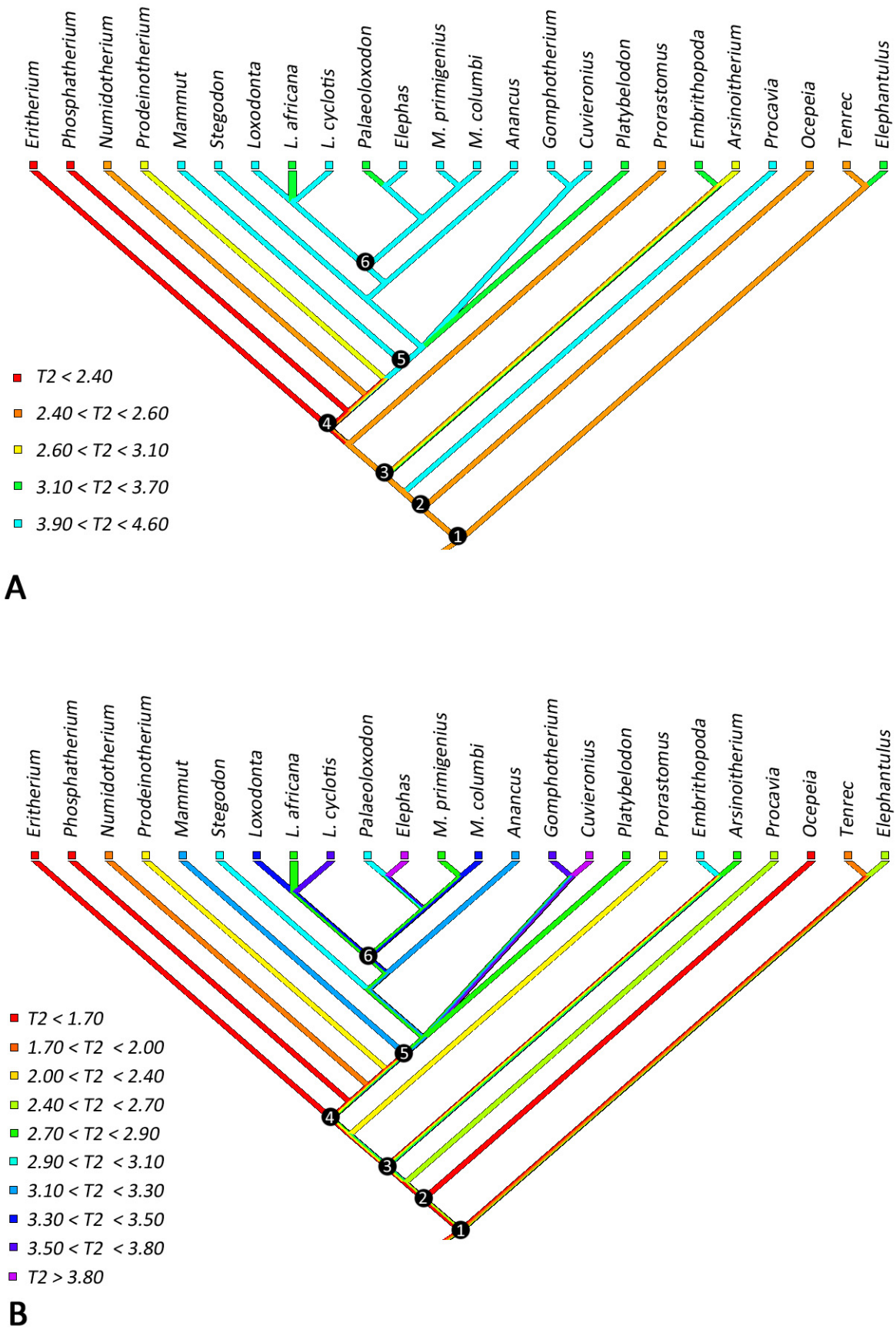

Figure VI.11 : Mapping of the fitted short time constant (T2) of the lateral duct (A) and the vertical ducts (B) on the afrotherian tree. Values are in ms.

In *Elephantulus*, however, the semicircular duct system is less adapted to exhibit fast response speed in yaw, probably for the reasons discussed in previous paragraph ('Agility'). The ancestral morphotype of Paenungulata (node 2) is also linked with relatively fast response speed of the system in yaw. However, the semicircular duct system convergently loses its adaptation to respond rapidly to yaw head motion in Hyracoidea (*Procavia*) and Embrithopoda (*Arsinoitherium* and the early embrithopod). Proboscideans seem to display primitively lower body mass-free short time constants for the lateral duct than any other afrotherian (node 4). Indeed, the fitted values for *Eritherium* and *Phosphatherium* are the lowest (<2.40). Hence their semicircular duct system was probably adapted to respond rapidly to excitation during yaw head motion. A progressive slowdown of the semicircular duct response speed seems to have occurred in later proboscideans (*Numidotherium* and *Prodeinotherium*). The ancestral morphotype of Elephantimorpha (node 5) exhibits very slow response speed of the semicircular duct system to yaw motion, a feature generalized in the entire clade and seen in extant elephants.

The body mass-free short time constant of the vertical ducts exhibit a similar pattern in Proboscidea (Fig VI.11B). Early proboscideans *Eritherium* and *Phosphatherium* display fast response speed of the semicircular duct system in pitch and roll motion if the effect of size is eliminated. The response speed slows down progressively in later proboscideans *Numidotherium* and *Prodeinotherium*. There is a clear pattern of even slower response speed in Elephantimorpha in pitch and roll, the members of this clade all exhibiting body mass-free short time constants over 2.70 ms. The clade (*Gomphotherium-Cuvieronius*) displays particularly high short time constants and hence slow response speed of the semicircular duct system in pitch and roll. On the other hand, Elephantidae display various short time constants, with taxa that exhibit really slow semicircular duct response speed (e.g. Elephas) and other that exhibit more average short time constant values (e.g. *Loxodonta africana* and *Palaeoloxodon*). Concerning other afrotherians, the representatives of the different orders exhibit very different short time constants and the evolution of this parameter is ambiguous.

Evolution of the natural frequency (ω_0) in the Afrotheria

The last common ancestor of the Afrotheria (node 1) displays a high body mass-free natural frequency for the lateral duct (Fig VI.12A). This suggests that the ancestor of Afrotheria was probably capable of experiencing a high frequency of head motion in yaw if the effect of the size is eliminated. This condition is apparently retained in *Tenrec*, while *Elephantulus* developed relatively lower frequencies of yaw head motion at equal size. The last common ancestor of Paenungulata (node 2) probably displayed adaptations to high frequencies of yaw head motion, a condition retained in *Ocepeia*. Hyracoidea, Embrithopoda and Sirenia probably developed convergent decreases of high frequency yaw motion capacities, sirenians being the afrotherians exhibiting the lowest natural frequencies for the lateral duct of our taxa sample. The ancestral condition of Proboscidea (node 4) is similar to that of Afrotheria and Paenungulata (high natural frequency). While *Eritherium* and *Phosphatherium* retain high frequency capacities of head motion in yaw, this condition is lost in *Numidotherium* and later proboscideans. Elephantidae (node 6) seem to have developed even lower capacities of high frequency yaw motions, at the exception of both *Mammuthus* species.

The body mass-free natural frequency for the vertical ducts displayed by the last common ancestor of the Afrotheria (node 1) is ambiguous (Fig VI.12B). *Tenrec* displays the highest natural frequency of our taxa sample while *Elephantulus* is more average compared to other afrotherians. The natural frequency of the ancestor of Paenungulata (node 2) is also ambiguous. *Ocepeia* displays a relatively high value. The body mass-free natural frequency for the vertical ducts displayed by the last common ancestor of Proboscidea (node 4) is also ambiguous but probably high, as in *Eritherium* and *Phosphatherium*. This parameter appears to decrease in *Numidotherium* and even more in the (Elephantimorpha - Prodeinotherium) clade, which members all exhibit body mass-free natural frequencies under 1.30 Hz. Hyracoidea and Sirenia display similar values but we cannot tell if this is due to either convergences or symplesimorphies. The particularly low natural frequency of *Loxodonta africana* (under 1.00 Hz) seems to be an autapomorphy.

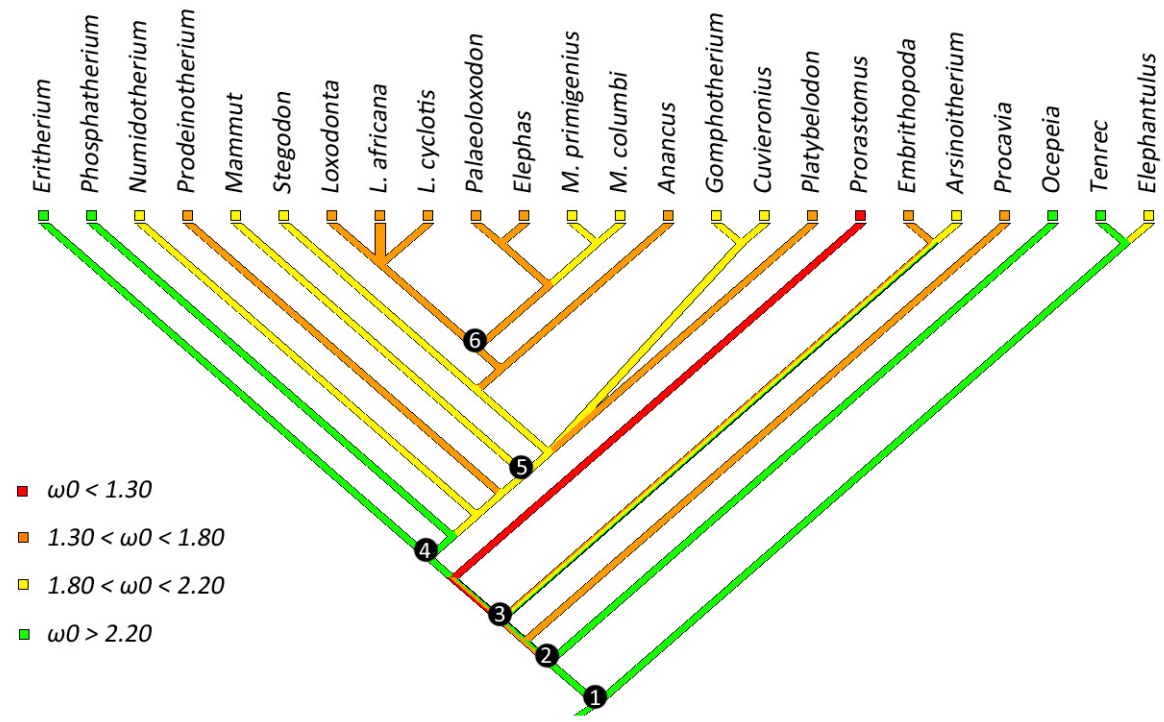

A

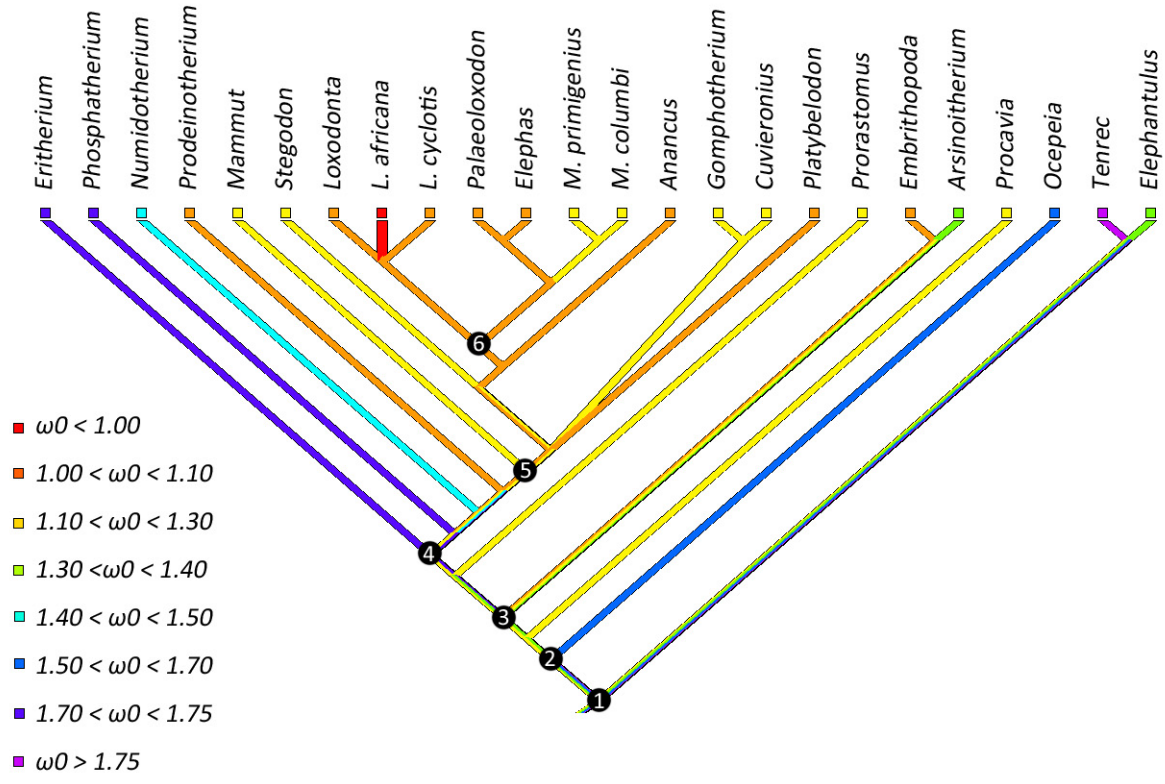

B

Figure VI.12 : Mapping of the fitted natural frequency (ω0) of the lateral duct (A) and the vertical ducts (B) on the afrotherian tree. Values are in Hz.

Evolution of the sensitivity (VGs) in the Afrotheria

As previously said in the 'Results' section, the body mass-free sensitivity values of the lateral duct are very similar within afrotherians. The reconstructed ancestral condition (sensitivity between 0.005 and 0.006 mdeg/deg.s^{-1}) is generalized in the Afrotheria with a few exceptions (Fig VI.13A). *Elephantulus* seems to have developed a particularly high sensitivity in the lateral duct which means that, at equal size, *Elephantulus* experience lower angular velocities for yaw motion than the other afrotherians. Similar decreases in experienced angular velocities (when the effect of size is eliminated) appear convergently in Hyracoidea (*Procavia*), the early embrithopod and Sirenia (*Prorastomus*), but to a lesser extent. Conversely, increases of adaptations to experience higher angular velocities in yaw motion seem to have appeared convergently in *Stegodon* and *Mammuthus columbi*.

The evolution of the body mass-free sensitivity of the vertical ducts within Afrotheria is not clear (Fig VI.13B). The last common ancestor of the group (node 1) displayed an either low or average sensitivity. This suggests that the ancestral condition of Afrotheria is able to experience a good level of angular velocities in pitch and roll. The same can be said about Paenungulata (node 2). The evolution of this condition is more ambiguous in the ancestor of Tethytheria (node 3). Embrithopods seem to have evolved lower levels of experience angular velocities in pitch and roll even without the effect of size. The ancestral condition of Proboscidea (node 4) is a very low sensitivity (hence relatively high experienced angular velocities) in pitch and roll, a feature retained in *Eritherium* and *Phosphatherium*. *Numidotherium* and *Prodeinotherium* exhibit slightly lower levels of experience angular velocities. An important decrease of experienced angular velocities appears to be a characteristic developed in Elephantimorpha (node 5), the most extreme group being the clade (*Gomphotherium-Cuvieronius*).

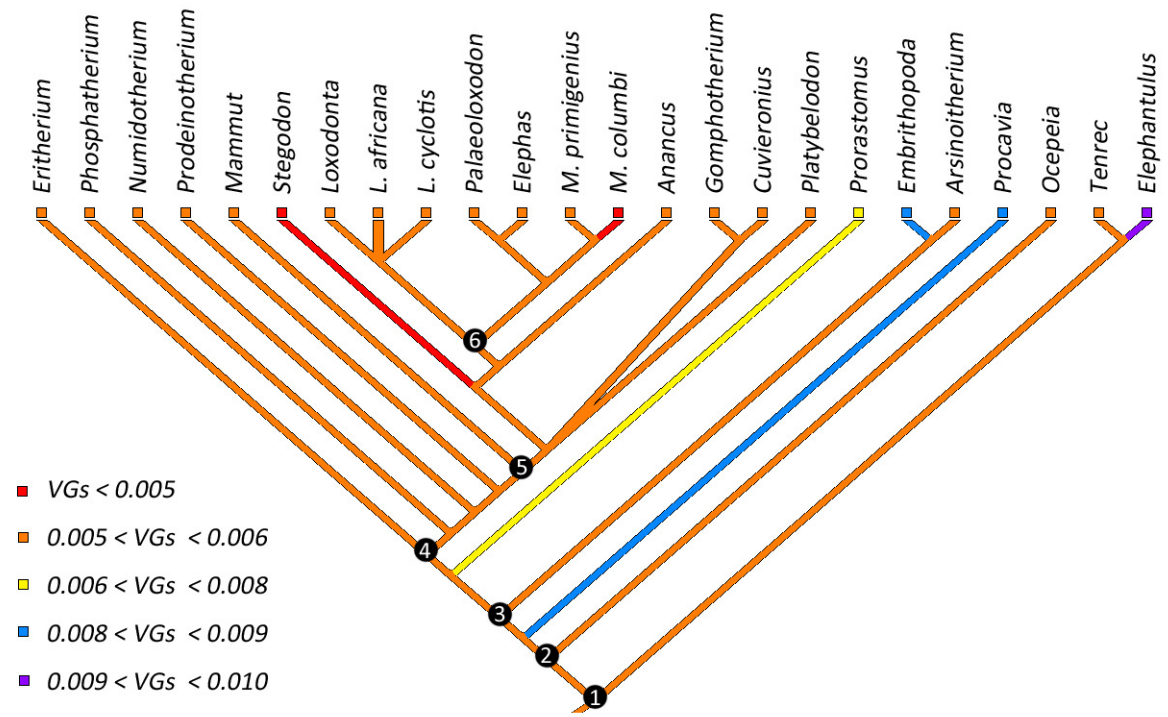

A

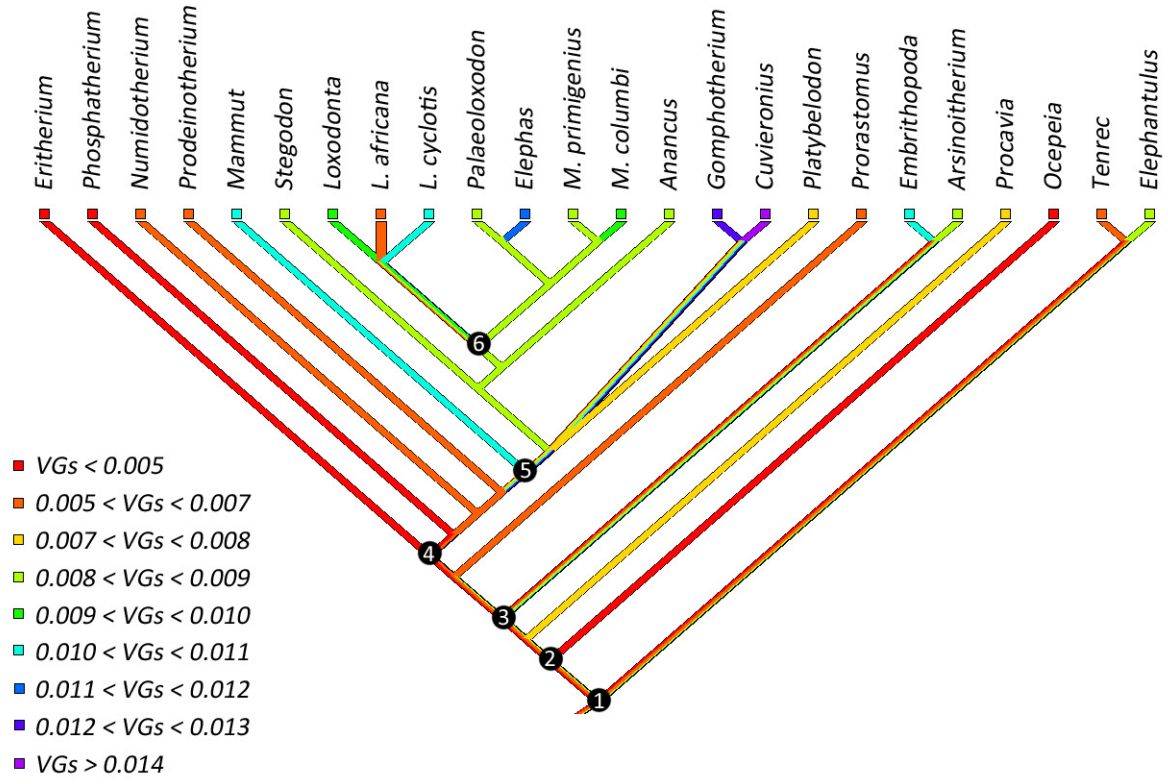

B

Figure VI.13 : Mapping of the fitted sensitivity (VGs) of the lateral duct (A) and the vertical ducts (B) on the afrotherian tree

5. Conclusion

The semicircular duct system functional capacities of extinct proboscideans have been appraised here for the first time. On the other hand, the values of several functional parameters have been calculated in three extant afrotherians using measurements based on the anatomy of their membranous labyrinth. One of the most striking observations is that extant elephants display body mass-free sensitivities very much lower than what we would have expected based on their size. Hence, despite raw sensitivity values that suggests a poor agility in elephants, the semicircular duct system of *Elephas* is adapted to agility. Elephants seem to compensate their large size with their labyrinth morphology. In Chapter II, we pointed out that the semicircular ducts of *Elephas* are particularly thin with respect to the bony canals. Indeed, the membranous (endolymphatic) volume appears to be much lower than the bony labyrinth volume. This contrasts with the labyrinths of *Procavia* and *Elephantulus*, which display more or less similar membranous and bony labyrinth volumes. A reduction of the endolymphatic volume could be an adaptation to prevent from rapid saturation and therefore to increase agility.

On the other hand, the lateral duct of elephants seems to be particularly adapted and displays values very different from that of the vertical ducts. The very small relative size of the lateral canal in elephants hence could be an adaptation in order to increase agility capacities. This morphological character is generalized in elephantimorphs, it could therefore be an adaptation shared by the members of this clade. However, body-mass free inferred sensitivities for the lateral duct are not strikingly different in Elephantimorpha compared to other proboscideans. This question hence deserves further investigation.

Finally, the study of the evolution of the inferred body-mass free functional capacities shows that there is a key functional evolutionary stage in the Elephantimorpha and sometimes even the clade containing Elephantimorpha and deinotheriids. This corroborates the results found in the phylogenetic studies. This also suggests that the evolution of the bony canal morphological characters and the evolution of the semicircular duct capacities are somehow linked.

CHAPTER VII

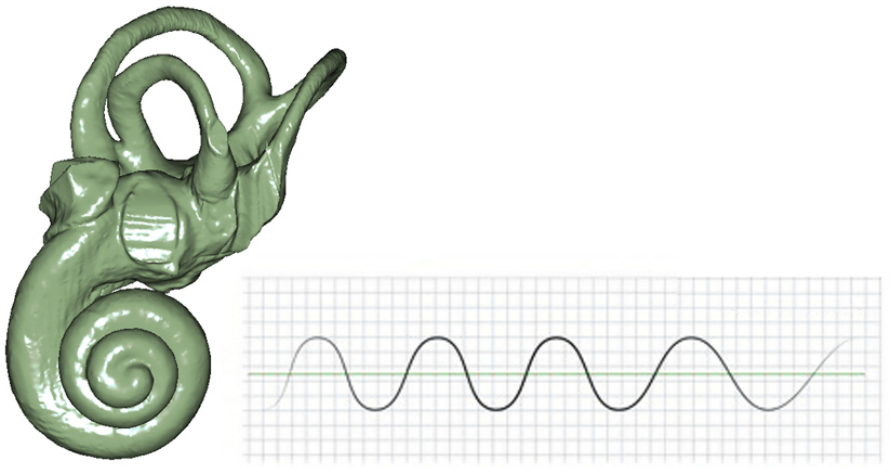

Preliminary considerations on the auditory capacities of proboscideans

1. Introduction

Extant elephants display very specialized auditory capacities. They are low-frequency specialists (Heffner & Heffner, 1982) and it was documented that they are able to produce sounds below the human auditory range (i.e. infrasounds, inferior to 20 Hz; Payne et al. 1986). The infrasound vocalization has been related to spatial coordination and mating (Poole et al. 1988) and allows the elephant to communicate at long distances (Langbauer et al. 1991). The distance range in which the calls can be perceived by elephants (i.e. calling area) depends on topographic and atmospheric factors; hence, the calling area varies during the day and between seasons (Larom et al. 1997a; 1997b). The infra-sounds can be perceived at 2.5 km but vocal recognition of family and bond group members is usually achieved in smaller distances (McComb et al. 2003). It has been demonstrated that elephant vocalizations produce Rayleigh waves, a type of ground surface wave (O'Connell et al. 1997). The ossicular chain morphology of elephants is suitable for sensing ground vibrations (Reuter & Nummela, 1998). Moreover, O'Connell-Rodwell et al. (2001) suggest that elephants may use bone conduction in order to hear low-frequency sounds. All of these considerations imply that long-range infrasound callings are transmitted via ground surface waves. This is confirmed by O'Connell-Rodwell et al. (2006) and reviewed in O'Connell-Rodwell (2007). The low frequency sounds are produced thanks to flow-induced vocal fold vibrations (Herbst et al. 2012; 2013).

While extant elephants are clearly low-frequency hearing specialists, extinct taxa do not necessary display the same pattern. Indeed, Court (1992) suggests that *Numidotherium* was not able to hear low-frequency sounds, based on the morphology of its cochlea. The objective here is to conduct a preliminary study of the auditory capacities of extinct proboscideans based on their bony labyrinth morphology. These considerations are helpful to make hypotheses on the evolution of low-frequency hearing within the Proboscidea.

2. Material and methods

2.1. Taxa sample

Within our proboscidean sample, some specimens do not preserve the cochlea, hence it is not possible to infer their auditory capacities. A table summarizing the afrotherian taxa for which at least one labyrinth preserving the cochlea has been segmented during this thesis is given (Table VII.1 below). Only one of these taxa is not a proboscidean (*Ocepeia*). Early proboscideans are well represented even though the cochleae of *Phosphatherium* and *Moeritherium* are incomplete. Cochleae of deinotheriids and gomphotheriids have also been sampled, as well as several cochleae of elephantids.

Table VII.1 : Afrotherian taxa segmented during the thesis for which at least one labyrinth preserves the cochlea. The first number refers to the number of specimens and the number in bracket refers to the number of labyrinths. Numbers in italics are for incomplete labyrinths.

Genus	Species	Specimens (ears)
Ocepeia	*daouiensis*	1(2)
Eritherium	*azzouzorum*	1(1)
Phosphatherium	*escuilliei*	1(*2*)
Numidotherium	*koholense*	1(1)
Moeritherium	*lyonsi*	1(*1*)
Prodeinotherium	*bavaricum*	1(*1*)
Mammut	*americanum*	1(*1*)
Platybelodon	*grangeri*	1(*1*)
Gomphotherium	*angustidens*	2(3)
Stegomastodon	*sp.*	1(1)
Stegodon	*orientalis*	1(2)
Anancus	*arvernensis*	6(6)
Loxodonta	*sp.*	2(3)
Loxodonta	*africana*	2(2)
Loxodonta	*cyclotis*	4(4)
Mammuthus	*primigenius*	1(1)
Elephas	*maximus*	4(4)

2.2. Features observed to infer auditory capacities

There are several features of the cochlea that can inform us about the auditory capacities of fossil species. Observations of these characters can give some clues about the tendency of the animal capacity to hear high-frequency

sounds or low-frequency sounds. Most of these considerations are qualitative and therefore not very precise but they are useful to provide an overall picture of the auditory capacities of fossil mammals.

2.2.1. Coiling of the cochlea

It has been demonstrated that the shape of the cochlea influences greatly the auditory capacities of mammals. Indeed, the cochlear spiral graded curvature enhances sensitivity to low frequencies (Manoussaki et al. 2006; 2008). The radii ratio (ratio between the radius of the basal turn and the radius of the apical turn of the cochlea) therefore correlates with the low-frequency limit of the animal. Using the equations given in Manoussaki et al. (2008), it is possible to infer the low-frequency limit of extinct proboscideans. Measurements of the radius of the apical turn and the radius of the basal turn are necessary to calculate the radii ratio ρ. These measurements are part of the protocol of Manoussaki et al. (2008). The low-frequency limit of hearing f is then calculated with this equation:

$$f = 1.507 \exp[-0.578(\rho - 1)]$$

However, it should be noted that these calculations are just estimates. First, this method is normally applied on the basilar membrane. This membranous structure is obviously not preserved in fossils; however, the method has already been applied on the bony cochlea of fossils (Orliac et al. 2012, Macrini et al. 2013). On the other hand, the correlations used in Manoussaki et al. (2008) are based only on 13 specimens, which is quite small. Estimates calculated with this method therefore must be taken with caution.

Finally, the protocol given in Manoussaki et al. (2008) is not very detailed, to the point that we failed to apply the protocol to our data sample. The method is indeed difficult to reproduce and is therefore not used by several authors anymore (pers. comm. Maeva Orliac, 2016). Hence, we finally chose not to infer frequency ranges of fossil proboscideans with this method.

2.2.2. Cochlear length and number of turns

The length of the cochlea and its number of turns influence the hearing capacities of mammals. In West (1985), the author succeeds in correlating these two parameters with the low- and high-frequency limits of hearing. Using the product of the absolute bony cochlear

length and the number of turns is a proxy to estimate approximately the hearing capacities of fossil taxa. Indeed, the higher this product, the higher the sensibility of the animal to low frequencies (Ekdale, 2016, Manoussaki et al. 2008). The method has been tested here to approximately estimate auditory tendencies of extinct proboscideans. The length of the cochlea is given by the ARIADNE add-on currently developed by Romain David and based on cochlear landmarks (for more details, see the main 'Material and Methods' section of the thesis). The numbers of turns has been calculated with the protocol of West (1985).

On other hand, estimations of the low-frequency limits at 60 dB SPL have then been calculated using the equation given in West (1985):

$$1.76 - 1.66 * \log(basilar\ membrane\ length * number\ of\ turns)$$

However, the method requires measuring the basilar membrane which is not preserved in fossils. The low-frequency limits were therefore calculated using the length of the cochlear canal which is an approximation of the basilar membrane length. Hence, the limits found with this method can be slightly overestimated.

2.2.3. Basilar membrane and secondary bony lamina

Another feature that can inform us about the hearing capacities of mammals is the basilar membrane. The thickness and stiffness of the basilar membrane correlates with the frequency range of animals (Wever et al. 1971; Pye, 1979; Ekdale, 2016). Mammals with a thick and stiff basilar membrane generally display better sensibilities to high frequency sounds (von Békésy, 1970). However, the basilar membrane is not preserved in fossils. To estimate its degree of stiffness and thickness, we must find a proxy capable of estimating the width of the membrane. Generally, authors use the laminar gap, which is the distance between the primary and secondary bony laminae (Geisler & Luo, 1996). However, given the fragile nature of the laminae, the estimation of the basilar membrane width using the laminar gap is very imprecise (Ketten, 2000). Therefore, we did not use the laminar gap in our study. Instead, we only noted the absence (or presence) of the secondary bony lamina on the cochlea of our specimens. The absence of a

secondary bony lamina implies a larger and softer basilar membrane, thus a preferential sensibility to low frequencies.

2.2.4. Perilymphatic foramen

The perilymphatic foramen is found only in the earlier stages of development in metatherian and eutherian mammals (Fischer, 1990). Its separation into the *fenestra cochleae* (opening at the level of the the *scala tympani*) and the *aquaeductus cochleae* (which conducts the perilymphatic duct) occurs during the morphogenesis of the ear (Kuhn, 1971; Zeller, 1985). However, a few eutherian mammals exhibit an undivided perilymphatic foramen in adults: several extant and fossil sirenians, extant (and some extinct) proboscideans, the embrithopod *Arsinoitherium* and some cetaceans (Fischer, 1990; Court, 1990; Court & Jaeger, 1991; Court, 1994; Geisler & Luo, 1996; Ekdale et al. 2011). Even though the persistence of a unique perilymphatic foramen is found in early non-therian mammals as well (Zeller, 1985, 1989; Wible, 1990), its occurrence in some eutherian lineages is considered a derived trait (Fischer, 1990). Previous studies suggest that the persistence of the perilymphatic foramen is to be linked with an adaptation to low-frequency hearing. Early non-therian mammals exhibiting an undivided perilymphatic foramen are considered low-frequency hearing animals (Luo & Ketten, 1991). Court (1994) suggests that the persistence of the perilymphatic foramen in extant elephants permits to reduce stiffness within the auditory system which enhances the capacities of the animal to hear low frequencies. The presence of an undivided perilymphatic foramen in an extinct mammal is another hint at its capacities of hearing low frequency sounds. The distribution of the perilymphatic foramen among proboscideans is therefore studied here to discuss the evolution of hearing within Proboscidea.

3. Results & discussion

3.1. Length and number of turns

As previously said, the product of the absolute cochlear length and the number of turns of the cochlea is a proxy to estimate the hearing capacities of fossil mammals. This product correlates positively with low-frequency hearing capacities (Ekdale, 2016). However, this method is imprecise and found products should not be compared with too much detail. This only allows us to grossly estimate which proboscideans tend to hear low-frequency sounds and which are less adapted to low-frequency hearing. Results are given in the form of histograms in Fig. VII.1. The number of turns, cochlear length and product are summarized in Appendix 31.

Values for early proboscideans (*Eritherium*, *Numidotherium*) and *Ocepeia* are very low which implies that they are not adapted to low-frequency hearing (see Appendix 31). The restriction of *Numidotherium koholense* to high frequency hearing has already been hypothesized in Court (1992); however, this is the first attempt to deduce the auditory abilities of *Ocepeia daouiensis* and *Eritherium azzouzorum*. The early proboscideans *Phosphatherium* and *Moeritherium* were not tested here because we could not apply the same measurement methods to these taxa; none of the studied *Phosphatherium* bony labyrinths preserves the cochlea entirely and we could not segment a *Moeritherium* cochlea precisely enough to apply the landmark protocol. Later proboscideans display greater values (at least two times the values of early proboscideans) which means they tend to display better abilities to hear low-frequency sounds. Values progressively increase within our sample, hence we cannot discriminate functional groups other than early proboscideans and the clade including deinotheriids and elephantimorphs. Moreover, as we previously said, these values are just tendencies and are to be taken with caution. Nevertheless, we can highlight some interesting details. The certainly pathological *Loxodonta* specimen (MNHN.AC.ZM.2008-71) – which displays a very different right and left cochleae – exhibits different values. Its right ear, which has only 1.625 turns, has a value 1.5 times smaller than its left ear.

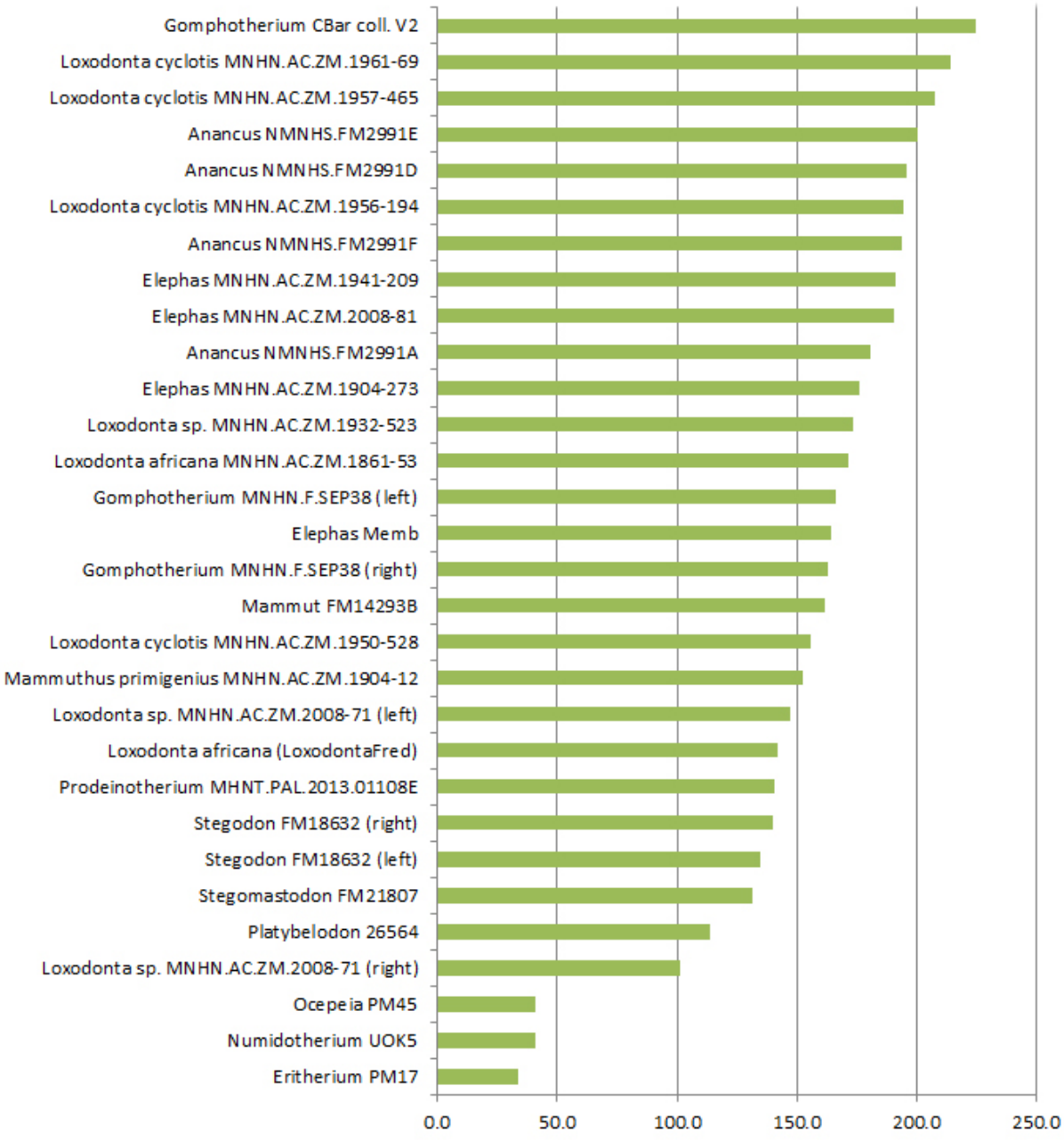

Figure VII.1 : Products of the number of turns of the cochlea and the absolute cochlear length in proboscideans and *Ocepeia*

This means that it was probably more capable of hearing low frequencies with its left ear than with its right ear. *Platybelodon* displays a relatively small value compared to other proboscideans but it falls in the group supposedly adapted to hear low-frequency sounds. *Prodeinotherium*, *Stegomastodon* and *Stegodon* exhibit slightly higher values. *Mammut* and *Mammuthus* exhibit rather average values. The two specimens of *Gomphotherium* display relatively different products, MNHN.F.SEP38 being relatively average and CBar coll. V2 displaying the higher value observed in proboscideans (236). *Anancus* specimens, as well as *Elephas*, tend to display relative high values. *Loxodonta cyclotis* tends to display greater values than *L. africana* even though one *L. cyclotis* specimen is rather in the middle range (MNHN.AC.ZM.1950-523). However, except for the probably pathological ear of MNHN.AC.ZM.2008-71, *Loxodonta* specimens exhibit a great variety of values (142 to 214) which covers almost the entire sample. The values used here reflect the relatively high level of cochlear variability among extant elephants – and probably proboscideans in general – highlighted in Chapter II. The mechanisms of low-frequency hearing in elephants remain poorly understood and certainly are multifactorial. The negative influence of a shorter cochlea displaying less turns on low-frequency hearing could be compensated by variations of other ear features such as the ossicular chain or the spiral ganglion.

Estimates of the low-frequency limits using the equations of West (1985) are proportional to the values discussed above and given in Fig. VII.2 (see also Appendix 31). As said in the 'Material and Methods' section (§ 2.2.2.), the results obtained here are approximated and should only be discussed in terms of tendencies. It appears that *Ocepeia* and early proboscideans *Eritherium* and *Numidotherium* have a low frequency limit superior to 100 Hz. They definitely do not display the adaptations to low-frequency hearing observed in extant elephants. The estimated low-frequency limit of *Eritherium* is the highest of the sample (ca. 168 Hz) which means that is even less adapted to low-frequency hearing than *Ocepeia* and *Numidotherium*. Finally, the elephantimorphs and deinotheriids all display very low low-frequency limits (between 6.6 and 27.1 Hz).

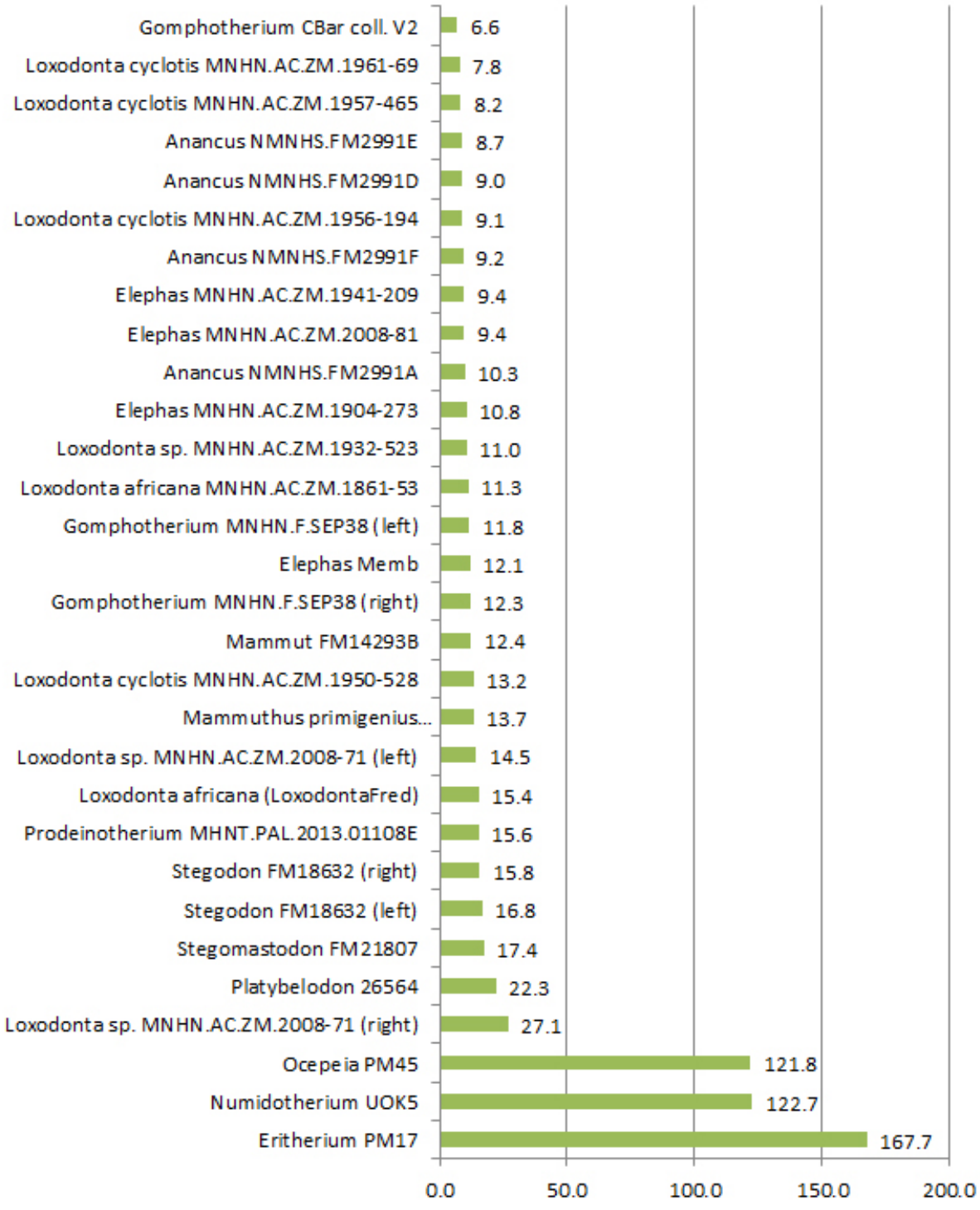

Figure VII.2 : Low-frequency limits estimations (Hz) based on the protocol of West (1985).

Given the approximated values and the high level of intraspecific variability observed here, the differences among this functional will not be thoroughly discussed. However, a few singularities can be pointed out. First, as previously discussed, there is a significant difference between the values found in the right and left ears of *Loxodonta* specimen MNHN.ZM.AC.2008-71. While the low-frequency limit of the left ear is estimated to be 14.5 Hz, the low-frequency limit of the right is 27.1 Hz. This suggests that this specimen was able to hear infra-sounds only with its left ear. However, the values are too approximated to really discuss about infra-sound hearing in this functional group. The only proboscidean taxa that are unable to hear infra-sounds according to our results are *Eritherium*, *Numidotherium* and *Platybelodon*. While *Eritherium* and *Numidotherium* seem undoubtedly unable to hear infra-sounds (low-frequency limits of 167.7 Hz and 127.7 Hz respectively), the approximation of our results prevent us from drawing conclusions about Platybelodon (low-frequency limit of 22.3 Hz).

On the other hand, we observed that proboscideans that display the highest estimated low-frequency limits in our sample exhibit a cochlea which apical turn axis of rotation is not offset with respect to that of the basal turn (character 32 in the phylogenetic analysis). Indeed, *Eritherium*, *Numidotherium*, *Stegomastodon*, *Stegodon* and *Platybelodon* all exhibit this character and appear to be the proboscideans that display the highest low-frequency limits. Hence, this morphological feature could potentially be an adaptation to low-frequency hearing.

3.2. Secondary bony lamina

The secondary bony lamina (or *lamina secundaria*) is primitively present in eutherian mammals and even in afrotherians. *Ocepeia* displays a *lamina secundaria*. The loss of this spiral lamina is present in almost every studied proboscidean. Only *Eritherium* and *Phosphatherium* unarguably exhibit a secondary bony lamina. The information is missing concerning *Moeritherium* and the presence of a *lamina secundaria* in *Numidotherium* appears to be variable. It is absent in the unlabeled specimen segmented by Benoit et al. (2013b) and in UOK5 (described here). However, a *lamina secundaria* is visible on the natural endocast described in Court (1992). As previously said (in the ‘Material and

Methods' section of this chapter), the loss of the secondary bony lamina probably correlates with low-frequency hearing. This suggests that early proboscideans *Eritherium* and *Phosphatherium* were very likely not adapted to hear low frequencies. The presence of the lamina in the specimen of *Numidotherium* described by Court (1992) is congruent with the assumed high-frequency capacities of this mammal. The absence of the lamina in the UOK5 specimen could hint to lower frequencies abilities but this is not congruent with the results found with the other methods that all point out that *Numidotherium* is rather adapted to high-frequency hearing. The loss of the secondary bony lamina appears at the latest in the clade that includes the deinotheriids and the elephantimorphs, which suggests that these taxa display adaptations to low-frequency hearing.

3.3. Perilymphatic foramen

As previously discussed (section 'Material and Methods' of this chapter), the presence of a perilymphatic foramen in proboscideans is very likely linked to the ability of hearing low frequencies (Court, 1994). This feature is generalized in most proboscideans and it is – to our current knowledge – a synapomorphy of the clade that includes *Moeritherium*, the deinotheriids and the elephantimorphs (see Fig V.35, Chapter V). On the other hand, early proboscideans *Eritherium*, *Phosphatherium* and *Numidotherium* do not display such feature. This anatomical feature provides another hint that suggests that early proboscideans were not low-frequency hearing mammals. The adaptation to low-frequency would thus appear in the clade that includes Moeritherium, the deinotheriids and the elephantimorphs.

4. Conclusion

The auditory capacities of proboscideans have been briefly investigated. The evolutionary hypotheses proposed here are summarized in Fig. VII.3. The information given by the three different proxies appears to be congruent. The estimated low-frequency limits suggest that early proboscideans were not able to hear low frequencies (Fig. VII.3A). Conversely, all elephantimorphs and deinotheriids seem to be adapted to low-frequency hearing. The apparition of this adaptation is ambiguous and is therefore a synapomorphy of the clade (deinotheriids-elephantimorphs) or the clade that includes *Moeritherium*, deinotheriids and elephantimorphs. Similar conclusions are suggested by the distribution of the *lamina secundaria* among elephantimorphs (Fig VII.3B). However, it should be noted that the presence of the *lamina secundaria* has been documented only in one *Numidotherium* specimen. Finally, the distribution of the perilymphatic foramen suggests an adaptation to low-frequency hearing that would appear in the clade containing *Moeritherium*, the deinotheriids and the elephantimorphs (Fig VII.3C).

These observations confirm the results of the previous chapters. The modern elephantine morphotype of the ear region seems to have been already acquired in *Prodeinotherium* (and maybe even *Moeritherium*) and is generalized in elephantimorphs. Such hypotheses are also supported by the geometric morphometrics analysis and the functional study of the semicircular canals. In this case, the modern morphotype seems to be linked with low-frequency hearing, which is a condition that is probably generalized in elephantimorphs, in *Prodeinotherium* and maybe even in *Moeritherium*.

However, it should be noted that the considerations made in this chapter are only preliminary. The singular auditory capacities of extant elephants (infra-sound hearing abilities) deserve a further study. The evolution of this striking feature remains poorly investigated here, because of too approximated low-frequency limit calculations. On the other hand, the hearing capacities depend on more features than those studied here. Further investigations of the ossicular chain of extant and extinct proboscideans would be of great interest to complete the preliminary work presented here.

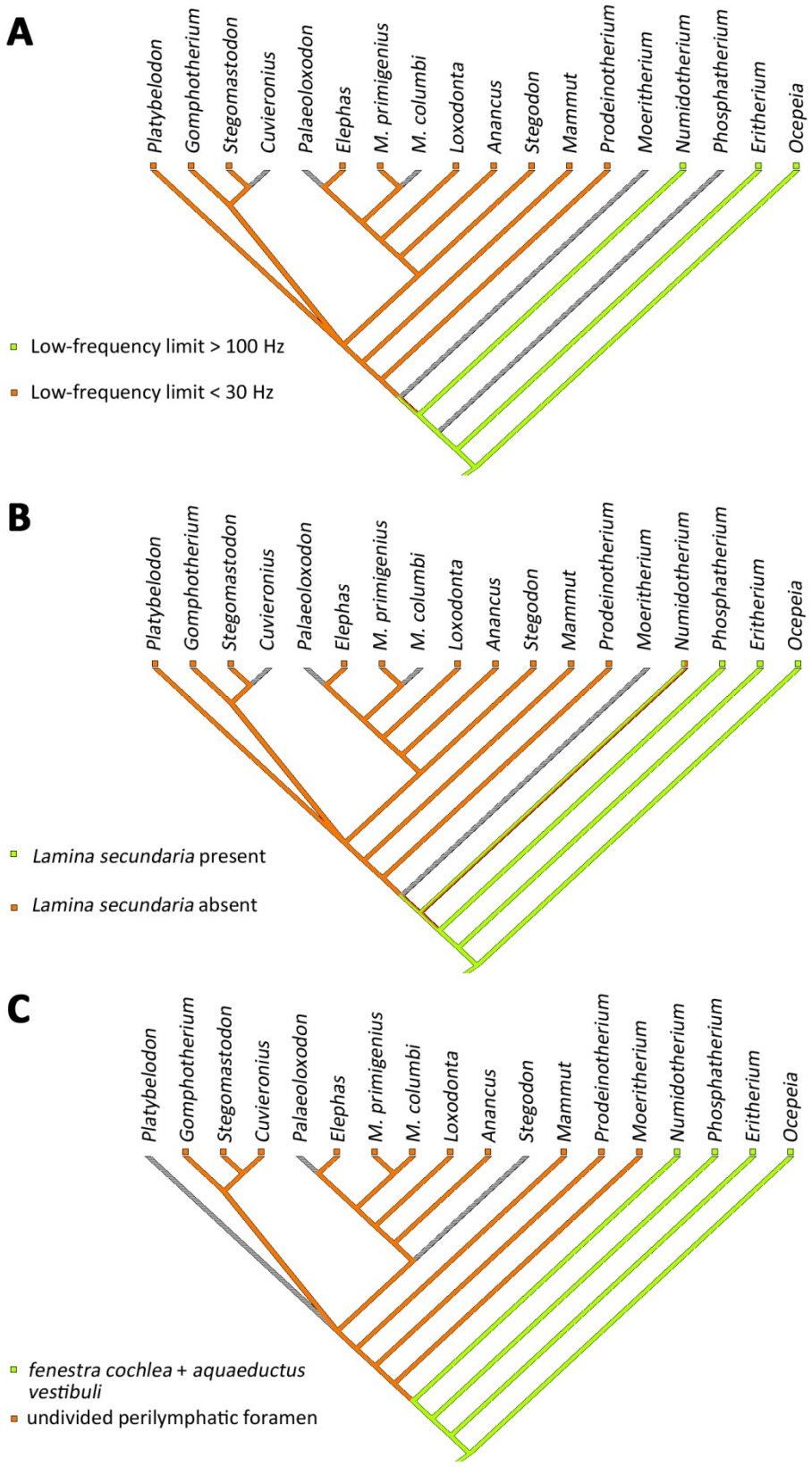

Figure VII.3 : Summary of the hypotheses on the evolution of audition in the Proboscidea. A) Estimated low-frequency limits. B) *Lamina secundaria*. C) Perilymphatic foramen. Orange states suggest adaptations to low-frequency hearing while green states suggest more generalized auditory capacities.

GENERAL CONCLUSIONS AND PERSPECTIVES

The ear region is a key anatomical complex useful for anatomical, evolutionary and functional studies. Its peculiar but poorly known morphology in proboscideans deserves the detailed investigation developed in this work.

The study of the petrosal and inner ear of earliest-known proboscideans *Eritherium azzouzorum* and *Phosphatherium escuilliei* provides key data about the ancestral morphotype of the Proboscidea. It shows that the ancestral state of the proboscidean ear region was not specialized but was rather generalized and close to the morphology of other paenungulates and afrotherians.

The petrosal of extant elephants is solidly fused in the skull and therefore difficult to access. While this region has already been described in the past, the ancient studies fail to provide most of the anatomical considerations taken into account in recent studies of the petrosal and inner ear of mammals. Our anatomical description of the ear region of extant elephants using modern investigation technical tools such as the CT scan provides the first comprehensive study of this structure in one of the most emblematic mammals. The petrosal and bony labyrinth of the three extant elephant species are illustrated and compared, but no striking specific features could be discriminated. The comparison of several specimens of the same species shows some level of intra-specific variability in both the petrosal and the bony labyrinth. Moreover, the segmentation of the right and left ears of the same specimen of an African elephant shows a singular case of intra-individual variability that is likely pathological: the number of turns of the cochlea displays a difference of half a turn between the right and left ears. The intra-specific variability of extant elephants evidenced in this work allows refining the description of extinct proboscidean taxa and the definition of the phylogenetic characters of the petrosal.

This study is the first to document the morphological diversity of the petrosal and inner ear of extinct proboscidean taxa. The region is described in sixteen genera (including extant ones), covering most major proboscidean groups. Comparisons with other afrotherians and considerations about the intra-specific variation help to identify some problematic phylogenetic characters and to define a pertinent coding. On the other hand, several new phylogenetic characters

are proposed here, such as the definition of the bony ampullae, the position of the lateral canal insertion with respect to the posterior ampulla, the orientation of the internal auditory meatus, and quantitative ratios are used to define characters measuring the thickness and relative size.

Our geometric morphometrics study shows that the morphology of the bony labyrinth discriminates most proboscideans from other afrotherians. However, early proboscideans exhibit a morphology closer to the other afrotherians than to modern proboscideans, which corroborates the observations made in the first chapter. On the other hand, the PCA shows that it is possible to discriminate the Elephantimorpha and the Elephantidae within proboscideans and almost *Elephas* from *Loxodonta* (the two clusters overlap). Phylogenetic generalized least-squared regressions show that size does not significantly influence these results when the entire labyrinth is investigated. Conversely, size influences the results of the PC analyses that focus on the semicircular canals; however, the influence is moderate.

The phylogenetic message carried by the ear region allows recovering three consensual groups of proboscideans: the clade that includes all the proboscideans except *Eritherium*, the clade that includes *Moeritherium*, the deinotheriids and the Elephantimorpha and the clade that includes deinotheriids and the Elephantimorpha. The study of the character distribution on a consensual tree of the Proboscidea shows that the modern morphotype exhibited in extant elephants is acquired gradually in the first stages of proboscidean evolution but generalized in the clade that includes deinotheriids and Elephantiformes. The definition of new phylogenetic characters allows defining new synapomorphies of emblematic groups of proboscideans (e.g. a lateral canal insertion located low and close to the posterior ampulla appears to be a synapomorphy of the Elephantidae).

Thanks to an original method (David et al. in press), we were able to study the functional capacities of the vestibular system of proboscideans. Extant elephants display a poor level of agility, especially compared to other afrotherians such as *Elephantulus*. However, the semicircular duct capacities are dependent of size. When the effect of size is eliminated, *Elephas* actually displays better functional capacities than

predicted. We suggest that extant elephants compensate their large size with the morphology of their semicircular duct. Reductions of the duct volume and of the lateral duct radius seem to be adaptations allowing *Elephas* to compensate the disadvantage due to its large size. On the other hand, inferences on the semicircular canals of extinct proboscideans confirm the existence of a key evolutionary stage of the ear region in this group. Indeed, the functional capacities exhibited in extant elephants appear to have been already acquired in *Prodeinotherium* and generalized in elephantimorphs.

A preliminary study of the evolution of auditory capacities in proboscideans suggests that early proboscideans were not adapted to low-frequency hearing. Conversely, the ability to hear low frequencies seems to be already present in *Prodeinotherium* and generalized in elephantimorphs.

The existence of this evolutionary stage is confirmed by geometric morphometrics, phylogenetics and functional analyses of the locomotor and auditory capacities of proboscideans. The congruence of these data strongly supports the idea that the modern morphotype exhibited in extant elephants was already acquired in *Prodeinotherium* and generalized in elephantimorphs and that those features were selected for their functional implications.

Several areas of work need further studies. Given the difficulty to scan large skulls of elephants, the study of the intra-specific variation in extant species remains based on a low number of specimens. The sample expansion would allow testing the variability with statistical methods and making considerations on the ontogenetic variability of the inner ear and petrosal characters. On the other hand, several membranous features of the labyrinth (cochlear duct, perilymphatic compartments, nerves, muscles…) were not described here and deserve further investigations. The ear region of several key taxa of proboscideans such as the early Elephantiformes *Phiomia* and *Palaeomastodon*, and the early proboscideans *Barytherium*, *Arcanotherium* and *Moeritherium* remains unknown or partially known and should be studied in the future. Geometric morphometrics analyses using between-groups methods should be tested to see if it allows discriminating *Elephas* from *Loxodonta*, and even *Loxodonta cyclotis* from *Loxodonta africana*. The

segmentation of the membranous labyrinths of other afrotherians such as the sirenians would allow us to calibrate the functional inferences even more and to make assumptions on the controversial lifestyle of early proboscideans. Finally, the preliminary study of the audition in the Proboscidea should be expanded. Indeed, a complete and connected ossicular chain is preserved in one of the studied extant specimens as well as isolated ossicles in *Anancus* and other extant elephants. A morpho-functional study of the ossicles is therefore envisaged in the future. The study of the preserved membranous cochlear duct in one specimen of *Elephas* should allow us to draw more precise conclusions on the audition of extant elephants and to infer the morphology of the duct in extinct species. Hopefully, these considerations would shed new lights on the evolution of audition in the Proboscidea and specifically on the development of low-frequency hearing in this emblematic modern order of mammals.

BIBLIOGRAPHICAL REFERENCES

Andrews CW (1901) Über das Vorkommen von Proboscidiern in untertertiären Ablagerungen Aegypten. *Tageblatt des V Internationalen Zoologischen-Kongresses, Berlin* (6), 4–5.

Andrews CW (1906) A descriptive catalogue of the Tertiary Vertebrata of the Fayûm, Egypt. *British Museum (Natural History), London*, xxxvii + 324 pp.

Andrews CW, Beadnell, HJL (1902) A preliminary note on some new mammals from the Upper Eocene of Egypt. *National Printing Department*, Public Works, Ministry, Cairo, 1-9.

Arambourg C, Magnier P (1961) Gisements de vertébrés dans le Bassin Tertiaire de Syrte (Libye). *Comptes Rendus de l'Académie des Sciences de Pari*s 233, 68-70.

Aymard A (1855) *Anancus* Aymard. *Anancus macroplus* Aymard. In Dorlhac, M.J, (ed.), Notice géologique sur le cratère de Coupet et sur son gisement de gemmes et d'ossements fossiles. *Annales de la Societé d'Agriculture, Sciences, Arts et Commerce du Puy*, 19: 497-517.

Barbour EH (1927) Preliminary notice on a new proboscidean *Amebelodon fricki* g. et sp nov. *Nebraska State Museum Bulletin* 13, 3, 131-134.

Benoit J (2013) Evolution des caractères crâniens et endocrâniens chez les Afrotheria (Mammalia) et phylogénie du groupe. Ph.D. dissertation, University of Montpellier II, Montpellier, France, 468 pp.

Benoit J, Adnet S, El Mabrouk E, et al. (2013a) Cranial remain from Tunisia provides new clues for the origin and evolution of Sirenia (Mammalia, Afrotheria) in Africa. *PLoS ONE* 8, e54307.

Benoit J, Crochet JY, Mahboubi M, et al. (2016) New material of *Seggeurius amourensis* (Paenungulata, Hyracoidea), including a partial skull with intact basicranium. *Journal of Vertebrate Paleontology* 36 (1), e1034358.

Benoit J, Orliac M, Tabuce R (2013b) Homoplasy in the ear region of Tethytheria and the systematic position of Embrithopoda (Mammalia, Afrotheria). *Geobios* 46, 357–370.

Benoit J, Orliac M, Tabuce R (2013c) The petrosal of the earliest elephant-shrew *Chambius* (Macroscelidea: Afrotheria) from the Eocene of Djebel Chambi (Tunisia) and the evolution of middle and inner ear of elephant-shrews. *Journal* of *Systematic Paleontology* 11, 907–923.

Benoit J, Lehmann T, Vatter M, et al. (2015) Comparative anatomy and three-dimensional geometric-morphometric study of the bony labyrinth of Bibymalagasia (Mammalia, Afrotheria). *Journal* of *Vertebrate Paleontology* 35, 1–14.

Billet G, Hautier L, Lebrun R (2015) Morphological diversity of the bony labyrinth (inner ear) in extant xenarthrans and its relation to phylogeny. *Journal* of *Mammalogy* 96 (4), 658–672.

Blair P (1710–1712a) *Osteographia elephantina*: Or, a full and exact description of all the bones of an elephant, which died near Dundee, April the 27th, 1706. With their several dimensions. Communicated in a letter to Dr. Hans Sloane, R. S. Secr. By Mr. Patrick Blair, *Philos Trans* (27), 53–116.

Blair P (1710–1712b) A continuation of the osteographia elephantina: Or, a description of the bones of an elephant, which died near Dundee, April the 27th, 1706. By Mr. Patrick Blair. *Philos Trans* (27), 117–168.

Blair P (1717-1719) A description of the organ of hearing in the elephant, with the figures and situation of the ossicles, labyrinth and cochlea, in the ear of that large animal. *Philosophical transactions of the Royal Society of London* 30, 885-899.

Blumenbach JF (1797) Handbuch der Naturegeschichte. J. C. Dietrich, Göttingen, 5th ed., [I]-XVIII, 714 p., 2 pls.

Borissiak AA (1928) On a new mastodon from the Chokrak Beds (middle Miocene) of the Kuban region. Platybelodon danovi n. gen. n. sp. *Ann. Soc. Paleont. Russie*, P1. viii, 105-120.

Brookes J (1828) A catalogue of the anatomical and zoological museum of Joshua Brookes. London (Taylor), Part I, 70 p.

Buck AH (1888) A contribution to the anatomy of the elephant's ear. *Transactions of the American Otological Society*, 240-253.

Buck AH (1890) A revised description of the anatomy of the elephant's ear. *Transactions of the American Otological Society*, 3-15

Burmeister H (1837) Handbuch der Naturgeschichte. Zum Gebrauch bei Vorlesungen. 2. Abt. Zoologie . T.C.F. Enslin, Berlin, 858 p.

Butler PM (1956) The skull of Ictops and the classification of the Insectivora. *Proceedings of the Zoological Society of London*, 126 (1956), pp. 453–481.

Cifelli R (1982) The petrosal structure of *Hyopsodus* with respect to that of some other ungulates, and its phylogenetic implications. *Journal* of *Paleontology* 56, 795–805.

Claudius (1865) Das Gehörlabyrinth von Dinotherium giganteum nebst Bemerkungen über den Werth der Labyrinthformen für die Systematik der Säugethiere. *Palaeontographica* Bd XIII, 65-74.

Court N (1990) Periotic anatomy of *Arsinoitherium* (Mammalia, Embrithopoda) and its phylogenetic implications. *Journal* of *Vertebrate Paleontology* 10, 170–182.

Court N (1992) Cochlea anatomy of *Numidotherium koholense* : auditory acuity in the oldest known proboscidean. *Lethaia* 25, 211-215.

Court N (1994) The periotic of *Moeritherium* (Mammalia, Proboscidea) : homology or homoplasy in the ear region of Tethytheria McKenna, 1975 ? *Zoological Journal of the Linnean Society* 112, 13-28.

Court N (1995) A new species of *Numidotherium* (Mammalia : Proboscidea) from the Eocene of Libya and the early phylogeny of the Proboscidea. *Journal of Vertebrate Paleontology* 15(3), 650-671.

Court N, Jaeger J-J (1991) Anatomy of the periotic bone in the Eocene Proboscidean *Numidotherium koholense* : An example of parallel evolution in the inner ear of tethytheres. *Comptes Rendus de l'Académie des Sciences de Paris* 312, ser. II, 559-565.

Cox PG, Jeffery N (2010) Semicircular canals and agility: the influence of size and shape measures. *Journal of Anatomy* 216 (1), 37-47.

Croizet JB, Jobert A (1828) Recherches sur les ossements fossiles du Département du Puy-de-Dôme – 226 pp.

Darlu P, Tassy P (1993) La reconstruction phylogénétique. Concepts et méthodes. Paris, France, Masson.

David R, Stoessel A, Berthoz A, Spoor F, Bennequin D (in press.) Assessing morphology and function of the semicircular duct system: introducing new in-situ visualization and software toolbox. *Scientific Reports* (in press.)

David R (2011) Le système des canaux semi-circulaires des archosaures : anatomie, morphométrie, morphologie fonctionnelle, évolution. *Paris. Thèse Muséum National d'Histoire Naturelle de Paris.*

De Jong WW, Zweers A, Goodman M (1981) Relationship of aardvark to elephants, hyraxes and sea cows from a-crystallin sequences. *Nature* 292, 538–540.

Debruyne R, Van Holt A, Barriel V, Tassy P (2003) Status of the so-called African pygmy elephant (*Loxodonta pumilio* (NOACK 1906)): phylogeny of cytochrome b and mitochondrial control region sequences. *C.R. Biologies* 326, 687-697.

Delmer C (2005) Les premières phases de différenciation des proboscidiens (Tethytheria, Mammalia): le rôle du *Barytherium grave* de Libye. *Paris. Thèse Muséum National d'Histoire Naturelle de Paris.*

Delmer C (2009) Reassessment of the generic attribution of *Numidotherium savagei* and the homologies of lower incisors in proboscideans. *Acta Palaeontologica Polonica* 54, 561–580.

Dercum F (1879) On the morphology of the semicircular canals. *Am Nat 13*, 366–374.

Eales NB (1926) XI.—The Anatomy of the Head of a Fœtal African Elephant, *Elephas africanus* (*Loxodonta africana*). *Transactions of the Royal Society of Edinburgh* 54 (03), 491-551.

Éhik J, Szalay T (1930). *Prodinotherium hungaricum* ng, n. sp. *Geologica Hungarica, Series Paleontologica* 6, 1-24.

Ekdale EG (2011) Morphological variation in the ear region of Pleistocene Elephantimorpha (Mammalia, Proboscidea) from Central Texas. *Journal of Morphology* 272, 452–464.

Ekdale EG (2013) Comparative anatomy of the bony labyrinth (inner ear) of placental mammals. *PLoS ONE 8*, e66624.

Ekdale EG (2016) Form and function of the mammalian inner ear. *Journal of anatomy* 228 (2), 324-337.

Ekdale EG, Archibald J, Averianov A (2004) Petrosal bones of placental mammals from the Late Cretaceous of Uzbekistan. *Acta Palaeontologica Polonica* 49, 161–176.

Ekdale EG, Rowe T (2011) Morphology and variation within the bony labyrinth of zhelestids (Mammalia, Eutheria) and other therian mammals. *Journal* of *Vertebrate Paleontology* 31, 658–675.

Falconer H, Cautley PT (1847) *Fauna Antiqua Sivalensis*, Being the Fossil Zoology of the Siwalik Hills, in the North India, Atlas. Smith, Lender and Co., London, plates, 25-80.

Falconer H (1857) On the Species of Mastodon and Elephant occurring in the fossil state in Great Britain. Part I. Mastodon. *Quarterly Journal of the Geological Society* 13 (1-2), 307-360.

Farris, JS (1989) The retention index and the rescaled consistency index. *Cladistics* 5 (4), 417-419.

Farris, JS (1989a) The retention index and homoplasy excess. *Systematic Biology* 38 (4), 406-407.

Fick L (1844) Über das Labyrinth des Elephanten. *Archiv für Anatomie, Physiologie und wissenschaftliche Medizin*, 431-432.

Fischer MS (1990) Un trait unique de l'oreille des éléphants et des siréniens (Mammalia) : un paradoxe phylogénétique. *Comptes Rendus de l'Académie des Sciences*. 311 Série III, 157-162.

Fischer MS, Tassy P (1993) The interrelation between Proboscidea, Sirenia, Hyracoidea, and Mesaxonia: the morphological evidence. In: Szalay FS, Novacek MJ, McKenna MC (Eds.), Mammal Phylogeny: Placentals. Springer, New York, pp. 217–234.

Flower WH (1885) An introduction to the osetology of the Mammalia. 3rd edition, Macmillan, London, 258 p. (reprinted by A. Asher and Co, Amsterdam, 1966)

Frade F (1955) Ordre des proboscidiens (Proboscidea Illiger, 1811). In : Traite de Zoologie (ed. P.-P. Grasse). Paris: Masson & Cie. pp. 715–875.

Gaeth AP, Short RV, Renfree MB (1999) The developing renal, reproductive, and respiratory systems of the African elephant suggest an aquatic ancestry. *Proceedings of the National Academy of Sciences* 96 (10), 5555-5558.

Gannon PJ, Eden AR, Laitman JT (1988) The subarcuate fossa and cerebellum of extant primates: Comparative study of a skull-brain interface. *American journal of physical anthropology* 77 (2), 143-164.

Geisler JH, Luo Z (1996) The petrosal and inner ear of *Herpetocetus* sp. (Mammalia: Cetacea) and their implications for the phylogeny and hearing of archaic mysticetes. *Journal of Paleontology,* 1045-1066.

Gheerbrant E (2009) Paleocene emergence of elephant relatives and the rapid radiation of African ungulates. *Proceedings of the National Academy of Sciences* 106 (26), 10717-10721.

Gheerbrant E, Amaghzaz M, Bouya B, et al. (2014) *Ocepeia* (Middle Paleocene of Morocco): the oldest skull of an afrotherian mammal. *PLoS ONE* 9, e89739.

Gheerbrant E, Bouya B, Amaghzaz M (2012) Dental and cranial anatomy of *Eritherium azzouzorum* from the Paleocene of Morocco, earliest known proboscidean mammal. *Palaeontographica* Abt A, 297, 151–183.

Gheerbrant E, Filippo A, Schmitt A (2016) Convergence of Afrotherian and Laurasiatherian Ungulate-Like Mammals: First Morphological Evidence from the Paleocene of Morocco. *PloS one* 11 (7), e0157556.

Gheerbrant E, Peigné S, Thomas H (2007) Première description du squelette d'un hyracoïde paléogène: *Saghatherium antiquum* de l'Oligocène inférieur de Jebel al Hasawnah, Libye. *Palaeontographica Abteilung A*, 93-145.

Gheerbrant E, Sudre J, Iarochene M, Moumni A (2001) First ascertained African "condylarth" mammals (primitive ungulates: cf. Bulbulodentata and cf. Phenacodonta) from the earliest Ypresian of the Ouled Abdoun Basin, Morocco. *Journal of Vertebrate Paleontology* 21 (1), 107-118.

Gheerbrant E, Sudre J, Cappetta H (1996) A Paleocene proboscidean from Morocco. *Nature* 383, 68 - 70.

Gheerbrant E, Sudre J, Cappetta H, Bignot G (1998) *Phosphatherium escuilliei* du Thanétien du bassin des Ouled Abdoun (Maroc), plus ancien proboscidien (Mammalia) d'Afrique. *Geobios* 30, 247–269.

Gheerbrant E, Sudre J, Cappetta H, et al. (2003) Les localités à mammifères des carrières de Grand Daoui, bassin des Ouled Abdoun, Maroc, Yprésien: premier état des lieux. *Bull Soc Geol France* 174, 279–293.

Gheerbrant E, Sudre J, Cappetta H, et al. (2002) A new large mammal from the Ypresian of Morocco: Evidence of a surprising diversity of early proboscideans. *Act. Pal. Pol.* 47, 493–506.

Gheerbrant E, Sudre J, Tassy P, et al. (2005) Nouvelles données sur *Phosphatherium escuilliei* (Mammalia, Proboscidea) de l'Eocène inférieur du Maroc, apports à la phylogénie des Proboscidea et des ongulés lophodontes. *Geodiversitas* 27(2), 239-333.

Gheerbrant E, Tassy P (2009) L'origine et l'évolution des éléphants. *Comptes Rendus Palevol* 8, 281–294.

Goloboff PA, Farris JS, Nixon KC (2008) TNT, a free program for phylogenetic analysis. *Cladistics* 24 (5), 774-786.

Graham RW (1976) Pleistocene and Holocene mammals, taphonomy, and paleoecology of the Friesenhahn Cave local fauna, Bexar County, Texas [PhD dissertation]. *Austin, TX: The University of Texas at Austin.* 233 p.

Gray JE (1821) On the natural arrangement of vertebrose animals. *London Med. Reposit*., 15(1):296-310

Gray AA (1907) The Labyrinth of Animals. Volume 2. J & A Churchill, London.

Gray AA (1908) The Labyrinth of Animals. J & A Churchill, London.

Gunz P, Ramsier M, Kuhrig M, et al. (2012) The mammalian bony labyrinth reconsidered, introducing a comprehensive geometric morphometric approach. *Journal of Anatomy* 220 (6), 529-543.

Hay OP (1922) Further observations on some extinct elephants. *Proceedings of the Biological Society of Washington* 35 (9).

Heffner RS, Heffner HE (1982) Hearing in the elephant (Elephas maximus): Absolute sensitivity, frequency discrimination, and sound localization. *Journal of Comparative and Physiological Psychology* 96 (6), 926.

Herbst CT, Stoeger AS, Frey R, et al. (2012) How low can you go? Physical production mechanism of elephant infrasonic vocalizations. *Science* 337 (6094), 595-599.

Herbst CT, Švec JG, Lohscheller J, et al. (2013) Complex vibratory patterns in an elephant larynx. *Journal of Experimental Biology* 216 (21), 4054-4064.

Huxley TH (1869) An introduction to the classification of animals. London J. Churchill & sons. 147.

Huxley TH (1872). A manual anatomy of the vertebrated animals. New York DF Appelton and Co, 431 p.

Hyrtl J (1845) Vergleichend-anatomische Untersuchungen über das innere Gehörorgan des Menschen und der Säugethiere. F. Ehrlich, Prag.

Igarashi M, Yoshinobu T (1966) Comparative observations of the *eminentia cruciata* in birds and mammals. *The Anatomical Record* 155 (2), 269-277.

Illiger CW (1811) *Prodomus systematis mammalium et avium additis terminis zoographicis utriusque classis, eorumque versione germanica*. Salfeld, Berlin.

Kalb JE, Froelich DJ, Bell GL (1996) Palaeobiogeography of late Neogene African and Eurasian Elephantoidea. In J. Shoshani and P. Tassy (Eds.). The Proboscidea: evolution and palaeoecology of elephants and their relatives, Oxford University Press. 101–116.

Kaup JJ (1829): Neues Säugethier, *Deinotherium* : *Deinotherium giganteum . Isis* 22 /4: 401-404.

Kerr R (1792) Class I. Mammalia: containing a complete Systematic Description, Arrangement, and Nomenclature, of all the known Species and Varieties of the Mammalia, or Animals which give suck to their young. Anim. Kingdom. A Strahan, T. Cadell, W Creech (eds), London and Edinburgh, p. 1-400.

Ketten DR (2000) Cetacean ears. In Hearing by whales and dolphins (pp. 43-108). Springer New York.

Kluge AG (1989) A concern for evidence and a phylogenetic hypothesis of relationships among *Epicrates* (Boidae, Serpentes). *Systematic Biology* 38 (1), 7-25.

Kocsis L, Gheerbrant E, Mouflih M, et al. (2014) Comprehensive stable isotope investigation of marine biogenic apatite from the late Cretaceous–early Eocene phosphate series of Morocco. *Palaeogeogr Palaeoclimatol Palaeoecol* 394, 74–88.

Köstlin O (1844) Der Bau des knöchernen Kopfes in den vier Klassen der Wirbelthiere.Stuttgart, pp. 1-506.

Kuhn HJ (1971) Die Entwicklung und Morphologie des Schädels von Tachyglossus aculeatus. *Abh Senckenberg Naturforsch Ges* 528, 1–224.

Ladevèze S, Missiaen P, Smith T (2010) First skull of *Orthaspidotherium edwardsi* (Mammalia, 'Condylarthra') from the late Paleocene of Berru (France) and phylogenetic affinities of the enigmatic European family Pleuraspidotheriidae. *Journal* of *Vertebrate Paleontology* 30, 1559–1578.

Langbauer WR, Payne KB, Charif RA, et al. (1991) African elephants respond to distant playbacks of low-frequency conspecific calls. *Journal of Experimental Biology* 157 (1), 35-46.

Larom D, Garstang M, Lindeque M, et al. (1997a) Meteorology and elephant infrasound at Etosha National Park, Namibia. *The Journal of the Acoustical Society of America* 101 (3), 1710-1717.

Larom D, Garstang M, Payne K, et al. (1997b) The influence of surface atmospheric conditions on the range and area reached by animal vocalizations. *Journal of experimental biology* 200 (3), 421-431.

Larramendi A (in press.) Shoulder height, body mass and shape of proboscideans. *Acta Palaeontol. Pol*. in press. doi, 10.

Lebrun R (2008) Evolution and development of the strepsirrhine primate skull. Ph.D. dissertation, University Montpellier II, Montpellier, France, and University of Zürich, Zürich, Switzerland.

Lebrun R, Ponce de León MS, Tafforeau P, Zollikofer CPE (2010) Deep evolutionary roots of strepsirrhine primate labyrinthine morphology. *Journal of Anatomy* 216, 368–380.

Lecointre G, Deleporte P (2000) Le principe du "total evidence" requiert l'exclusion de données trompeuses. *Biosystema* 18, 129-151.

Linnaeus C (1758) Systema naturae per regna tria naturae : secundum classes, ordines, genera, species cum characteribus, differentiis, synonymis, locis (in Latin). 10th ed., Stockholm: Laurentius Salvius, 828 p.

Liu AG, Seiffert ER, Simons EL (2008) Stable isotope evidence for an amphibious phase in early proboscidean evolution. *Proceedings of the National Academy of Sciences* 105 (15), 5786-5791.

Luo Z, Ketten DR (1991) CT scanning and computerized reconstructions of the inner ear of multituberculate mammals. *Journal of Vertebrate Paleontology* 11 (2), 220-228.

MacIntyre GT (1972) The trisulcate petrosal pattern of mammals. In: Evolutionary Biology, vol. 6 (eds Dobzhansky T, Hecht KM, Steere WC), pp. 275–303, New York: Appleton Century-Crofts.

Macrini T, Flynn J, Croft D, et al. (2010) Inner ear of a notoungulate placental mammal: anatomical description and examination of potentially phylogenetically informative characters. *Journal of Anatomy* 216, 600–610.

Macrini T, Flynn J, Ni X, et al. (2013) Comparative study of notoungulate (Placentalia, Mammalia) bony labyrinths and new phylogenetically informative inner ear characters. *Journal of anatomy* 223 (5), 442-461.

Mahboubi M, Ameur R, Crochet J-Y, Jaeger J-J (1986) El Kohol (Saharan Atlas, Algeria): a new Eocene mammal locality in Northwestern Africa. *Palaeontographica* 192 (1/3): 15-49.

Mahboubi S, Bocherens H, Scheffler M, et al. (2014) Was the Early Eocene proboscidean *Numidotherium koholense* semi-aquatic or terrestrial? Evidence from stable isotopes and bone histology. *Comptes Rendus Palevol* 13 (6), 501-509.

Manoussaki D, Dimitriadis EK, Chadwick RS (2006) Cochlea's graded curvature effect on low frequency waves. *Physical review letters* 96 (8), 088701.

Manoussaki D, Chadwick RS, Ketten DR, et al. (2008) The influence of cochlear shape on low-frequency hearing. *Proceedings of the National Academy of* Sciences 105 (16), 6162-6166.

Maseko B.C., Patzke N, Fuxe K, Manger PR (2013) Architectural Organization of the African Elephant Diencephalon and Brainstem. Brain Behav Evol 82, 83–128.

Matschie P (1900) Uber geographische Albatern des Afrikanischen elephantens. *Sitzber. Ges. Naturforsch Fr, Berlin 8: 189-197.*

Matsumoto H (1924) A revision of *Palaeomastodon*: dividing it into two genera, and with descriptions of two new species. O*rder of the Trustees, the American Museum of Natural History*.

McComb K, Reby D, Baker L, Moss C, Sayialel S (2003) Long-distance communication of acoustic cues to social identity in African elephants. *Animal Behaviour* 65 (2), 317-329.

McKenna, MC (1975) Toward a phylogenetic classification of the Mammalia. In: Luckett, W.P., Szalay, F.S. (Eds.), Phylogeny of the Primates: A Multidisciplinary Approach. Plenum Press, New York, pp. 21–46.

Meng J, Fox R (1995) Osseous inner ear structures and hearing in early marsupials and placentals. *Zool* J *Linn Soc* 115, 47–71.

Mothé D, Avilla LS, Zhao D, Xie G, Sun B (2016b) A new Mammutidae (Proboscidea, Mammalia) from the late Miocene of Gansu Province, China. *Anais da Academia Brasileira de Ciências* 88(1), 65-74.

Mothé D, Ferretti MP, Avilla LS (2016a) The Dance of Tusks: Rediscovery of Lower Incisors in the Pan-American Proboscidean *Cuvieronius hyodon* Revises Incisor Evolution in Elephantimorpha. *PloS one* 11 (1), e0147009.

O'Connell-Rodwell CE (2007) Keeping an "ear" to the ground: seismic communication in elephants. *Physiology* 22 (4), 287-294.

O'Connell CE, Arnason BT, Hart LA (1997) Seismic transmission of elephant vocalizations and movement. *The Journal of the Acoustical Society of America* 102 (5), 3124-3124.

O'Connell-Rodwell CE, Hart LA, Arnason BT (2001) Exploring the potential use of seismic waves as a communication channel by elephants and other large mammals. *American Zoologist* 41 (5), 1157-1170.

O'Connell-Rodwell CE, Wood JD, Rodwell TC, et al. (2006) Wild elephant (Loxodonta africana) breeding herds respond to artificially transmitted seismic stimuli. *Behavioral Ecology and Sociobiology 59* (6), 842-850.

O'Leary MA (2010) An anatomical and phylogenetic study of the osteology of the petrosal of extant and extinct artiodactylans (Mammalia) and relatives. *Bull Am Mus Nat Hist*, 335, 1–206.

Orliac M, Benoit J, O'Leary M (2012) The inner ear of *Diacodexis*, the oldest artiodactyl mammal. *Journal of Anatomy* 221, 417–426.

Orliac M, O'Leary M (2014) Comparative anatomy of the petrosal bone of Dichobunoids, early members of Artiodactylamorpha (Mammalia). *Journal of Mammalian Evolution* 21, 299–320.

Orliac M, O'Leary MA (2016) The inner ear of *Protungulatum* (Pan-Euungulata, Mammalia) J Mammal Evol doi:10.1007/s10914-016-9327-z

Osborn HF (1918) Equidae of the Oligocene, Miocene, and Pliocene of North America, iconographic type revision*. Memoirs of the American Museum of Natural History*, New Serie 2(1), 1-330.

Osborn HF (1923) New subfamily, generic, and specific stages in the evolution of the proboscidea. *American Museum Novitates* 99, 1–4

Osborn HF (1929). New Eurasiatic and American proboscideans. *American Museum of Natural History.*

Owen R (1870) On fossil remains of mammals found in China. *Quarterly Journal of the Geological Society* 26 (1-2), 417-436.

Payne KB, Langbauer Jr WR, Thomas EM (1986) Infrasonic calls of the Asian elephant (Elephas *maximus*). *Behavioral Ecology and Sociobiology* 18 (4), 297-301.

Pohlig H (1888): Dentition und Kraniologie des *Elephas antiquus* Falc. mit Beiträgen über *Elephas primigenius* Blum. und *Elephas meridionalis* Nesti. *Nova Acta der K. Leop.-Carol. Deutschen Akademie der Naturf. Halle*, 53, 1, 1-279 .

Pohlig H (1912) Sur une vieille mandibule de" *Tetracaulodon ohioticum*" Blum., avec défense in situ. *Bulletin de la Société Belge de Géologie* 26, 187-193.

Poole JH, Payne K, Langbauer Jr WR, Moss, CJ (1988) The social contexts of some very low frequency calls of African elephants. *Behavioral Ecology and Sociobiology* 22(6), 385-392.

Pritchard U (1881) The cochlea of the *Ornithorhynchus platypus* compared with that of the ordinary mammals and of birds. *Philosophical transactions of the Royal Society of London* 172, 267-282.

Provatidis CG, Theodorou EG, Theodorou GE (2011) Computed tomography and CAD/CAE methods for the study of the osseus inner Ear bone of Greek quaternary endemic mammals. *Mediterranean Archaeology and Archaeometry* 11 (2), 121-127.

Pye A (1979) The structure of the cochlea in some mammals. *Journal of Zoology* 187 (1), 39-53.

Rabbitt RD, Damiano ER, Grant JW (2004) Biomechanics of the semicircular canals and otolith organs. In *The vestibular system* (pp. 153-201). Springer New York.

Rasmussen DT, Gutierrez M (2009) A mammalian fauna from the late Oligocene of northwestern Kenya. *Palaeontographica Abteilung A*, 1-52.

Reuter T, Nummela S, Hemilä S (1998) Elephant hearing. *The Journal of the Acoustical Society of America* 104 (2), 1122-1123.

Richards (1890) A further report on the anatomy of the elephant's ear. *Transactions of the American Otological Society* 4, 587-604.

Ruf I, Luo Z, Wible J, et al. (2009) Petrosal anatomy and inner ear structures of the late Jurassic *Henkelotherium* (Mammalia, Cladotheria, Dryolestoidea): insight into the early evolution of the ear region in cladotherian mammals. *Journal of Anatomy* 214, 679–693.

Sanders WJ, Kappelman J, Rasmussen DT (2004) New large-bodied mammals from the late Oligocene site of Chilga, Ethiopia. *Acta Palaeontologica Polonica* 49 (3).

Schlesinger G (1917) Die Mastodonten des KK Naturhistorischen Hofmuseums. *Denkschriften der K. K. Naturhistorischen Hofmuseurns 1, Geologisch-Palåontologische Reihe*, l, 1—230.

Schmitt A, Gheerbrant E (2016) The ear region of earliest known elephant relatives: new light on the ancestral morphotype of proboscideans and afrotherians. *Journal of Anatomy* 228, 137-152.

Segall W (1970) Morphological parallelisms of the bulla and auditory ossicles in some insectivores and marsupials. *Fieldiana Zoology* 51:169–205.

Seiffert ER (2007) A new estimate of afrotherian phylogeny based on simultaneous analysis of genomic, morphological, and fossil evidence. *BMC Evolutionary Biology* 7 (1), 1.

Seiffert ER, Nasir S, Al-Harthy A, et al. (2012) Diversity in the later Paleogene proboscidean radiation: a small barytheriid from the Oligocene of Dhofar Governorate, Sultanate of Oman. *Naturwissenschaften* 99(2), 133-141.

Shoshani J (1996) Para-or monophyly of the gomphotheres and their position within Proboscidea. The Proboscidea: Evolution and palaeoecology of elephants and their relatives. Oxford University Press, Oxford, 149-177.

Shoshani J, Ferretti P, Lister A.M., et al. (2007) Relationships within the Elephantinae using hyoid characters. *Quaternary International* 169, 174-185.

Shoshani J, Golenberg EM, Yang H (1998) Elephantidae phylogeny: morphological versus molecular results. *Acta Theriologica* Suppl. 5: 89-122.

Sikes SK (1971) Natural history of the African elephant. Part 1. Weidenfeld and Nicholson, London, pp. 1-184

Simpson GG (1945) The principles of classification and a classification of mammals. *Bull. Amer. Museum Nat. History,* 85, 1-350.

Specht M (2007) Spherical surface parameterization and its application to geometric morphometric analysis of the braincase. Ph.D. dissertation, University of Zürich Irchel, Zürich, Switzerland.

Specht M, Lebrun R, Zollikofer CPE (2007) Visualizing shape transformation between chimpanzee and human braincases. *The Visual Computer* 23, 743–751.

Spoor F, Garland T, Krovitz G, Ryan TM, Silcox MT, Walker A (2007) The primate semicircular canal system and locomotion. *PNAS* 104 (26), 10808-10812.

Spoor F, Zonneveld F (1998) Comparative review of the human bony labyrinth. *Yearbook* of *Physical Anthropology* 41, 211– 251.

Springer MS, Stanhope MJ, Madsen O, de Jong WW (2004) Molecules consolidate the placental mammal tree. *Trends in Ecology & Evolution* 19 (8), 430-438.

Stanhope MJ, Waddell VG, Madsen O, et al. (1998) Molecular evidence for multiple origins of Insectivora and for a new order of endemic African insectivore mammals. *Proceedings of the National Academy of* Sciences 95 (17), 9967-9972.

Swofford DL (1991) PAUP: Phylogenetic Analysis Using Parsimony, Version 3.1 Illinois Natural History Survey, Champaign, Illinois.

Tassy P (1981) Le crâne de *Moeritherium* (Proboscidea, Mammalia) de l'Eocène de Dor El Talha (Libye) et le problème de la classification phylogénétique du genre dans les Tethytheria McKenna, 1975*. Bulletin du Museum national d'Histoire naturelle* C 3, 87–147.

Tassy P (1994) Gaps, parsimony, and early Miocene elephantoids (Mammalia), with a re-evaluation of *Gomphotherium annectens* (Matsumoto, 1925). *Zoological Journal of the Linnean Society* 112 (1-2), 101-117

Tassy P (1996) Who is who among the Proboscidea? In J. Shoshani and P. Tassy (eds.), *The Proboscidea: Evolution and Palaeoecology of Elephants and Their Relatives*. Oxford University Press, Oxford. pp. 39–48

Tassy P (2013) L'anatomie cranio-mandibulaire de *Gomphotherium angustidens* (Cuvier, 1817) (Proboscidea, Mammalia) : données issues du gisement d'En Péjouan (Miocène moyen du Gers, France). *Geodiversitas* 35 (2), 377-445.

Tassy P, Pickford M (1983) Un nouveau mastodonte zygolophodonte (Proboscidea, Mammalia) dans le Miocène inférieur d'Afrique orientale: Systématique et paléoenvironnement. *Geobios* 16 (1), 53-77.

Vacek M (1877) Über österreichische Mastodonten und ihre Beziehungen zu den Mastodonarten Europas (etc.). na.

Van der Merwe NJ, Bezuidenhout AJ, Seegers CD (1995) The skull and mandible of the African elephant (*Loxodonta africana*). Onderstepoort *Journal of Veterinary Research* 62 (4), 245-260.

Von Békésy G (1970) Travelling waves as frequency analysers in the cochlea. *Nature* 225, 1207-1209.

Watson M (1874) Contributions to the Anatomy of the Indian Elephant: Part IV. Muscles and Blood-Vessels of the Face and Head. *Journal of anatomy and physiology* 9 (Pt 1), 1-118.

West CD (1985) The relationship of the spiral turns of the cochlea and the length of the basilar membrane to the range of audible frequencies in ground dwelling mammals. *Journal of the Acoustical Society of America* 77, 1091–1101.

Wever EG, McCormick JG, Palin J, Ridgway, SH (1971) The cochlea of the dolphin, *Tursiops truncatus*: hair cells and ganglion cells. *Proceedings of the National Academy of Sciences* 68 (12), 2908-2912.

Wible JR (1983) The internal carotid artery in early eutherians. *Acta Palaeontologica Polonica* 28, 281–293.

Wible JR (1986) Transformations in the extracranial course of the internal carotid artery in mammalian phylogeny. *Journal of Vertebrate Paleontology* 6 (4), 313-325.

Wible JR (1990) Petrosals of Late Cretaceous marsupials from North America, and a cladistic analysis of the petrosal in therian mammals. *Journal of Vertebrate Paleontology* 10 (2), 183-205.

Wible JR (2010) Petrosal anatomy of the nine-banded armadillo, *Dasypus novemcinctus* Linnaeus, 1758 (Mammalia, Xenarthra, Dasypodidae). *Ann Carnegie Mus* 79, 1–28.

Wible JR, Novacek M, Rougier G (2004) New data on the skull and dentition in the Mongolian late Cretaceous eutherian mammal *Zalambdalestes*. *Bull Am Mus Nat Hist* 281, 1–144.

Wible JR, Rougier G, Novacek M, et al. (2001) Earliest eutherian ear region: a petrosal referred to *Prokennalestes* from the early cretaceous of Mongolia. *Am Mus Novit* 3322, 1–44.

Wible JR, Rougier G, Novacek M, et al. (2009) The Eutherian Mammal *Maelestes gobiensis* from the late Cretaceous of Mongolia and the phylogeny of Cretaceous eutherian. *Bull Am Mus Nat Hist* 327, 1–123.

Wight AWR (1980) Paleogene vertebrate fauna and regressive sediments of Dur at Talhah, southern Sirt Basin, Libya; pp. 309–325 in M. J. Salem and M. T. Busrewil (eds.), *The Geology of Libya, vol. 1. Academic Press, London*

Yans J, Amaghzaz M, Bouya B, et al. (2014) First carbon isotope chemostratigraphy of the Ouled Abdoun Phosphate Basin, Morocco; implications for dating and evolution of earliest African placental mammals. *Gondwana Research* 25, 257–269.

Zeller U (1985) The morphogenesis of the fenestra rotunda in mammals. *Fortschritte der Zoologie* 30, 153-157.

Zeller U (1989) Die Enwicklung und Morphologie des Schädels von Ornithorhynchus anatinus (Mammalia: Prototheria: Monotremata). *Abhandlungen der Senckenbergischen Naturforschenden Gesellschaft* 545, 1–188.

Chapter cover illustrations

Chapter I

Reconstitution of *Phosphatherium escuilliei* (illustration by Dominique Visset) with the skull seen in transparency and with a focus on the petrosal and the labyrinth.

Chapter II

Skull of an African forest elephant with the petrosal seen in transparency. Illustration of the petrosal of an African forest elephant (Charlène Letenneur, CR2P-MNHN). 3D reconstruction of the bony labyrinth and the ossicular chain of an African elephant.

Chapter III

3D reconstruction of the petrosal of *Stegomastodon* sp., with the natural cast of the bony labyrinth visible at the surface, with the bony labyrinth seen in transparency, and with the labyrinth only.

Chapter IV

Bony labyrinth of an elephant with the landmarks sets used in the thesis seen in transparency.

Chapter V

Bony labyrinths of extinct and extant proboscideans (from the smallest to the largest: *Eritherium*, *Phosphatherium*, *Numidotherium*, *Mammut*, *Platybelodon*, *Stegomastodon*, *Gomphotherium*, *Stegodon*, *Anancus*, *Elephas* and *Loxodonta*). The figure is not in scale.

Chapter VI

Membranous semicircular ducts seen in transparency in the bony labyrinth of *Procavia*, *Elephantulus* and *Elephas.* The membranous saccule and cochlear duct are not represented.

Chapter VII

Bony labyrinth of *Gomphotherium angustidens* and schematic representation of infrasound waves.

APPENDICES

Appendix 1 – List of characters of the preliminary cladistic analysis performed on proboscideans

1. *Fossa subarcuata* (Benoit et al. 2013a **[21]** / Benoit et al. 2013b **[38]** / Wible et al. 2009 **[330]** / **modified**):
   very deep (0); moderate (1); superficial or absent (2)
2. Fusion of the *fenestra cochleae* and the cochlear canaliculus forming a unique perilymphatic foramen (Benoit et al. 2013a **[4]**):
   absent (0); present (1)
3. Shape of the *fenestra vestibuli* (Benoit et al. 2013a **[5]** / Wible et al. 2009 **[275]** / **modified**):
   oval with a stapedial ratio superior to 1.7 (0) ; round with a stapedial ratio inferior to 1.7 (1)
4. Size of the *fenestra vestibuli*:
   large (0); small (1)
5. Shape of the *promontorium* (Wible et al. 2009 **[278]** / **modified**):
   clearly bulging (0) ; slightly bulging or flat (1)
6. Inflation of the *tegmen tympani* (O'Leary 2010 **[9]** / Wible et al. 2009 **[287]** / **modified**):
   absent (0); strong (1)
7. Stapedial sulcus on the *promontorium* (Benoit et al. 2013a **[9]** / Benoit et al. 2013b **[16]** / Wible et al. 2009 **[274]** / **modified**):
   present (0); absent (1)
8. Transpromontorial sulcus (Benoit et al, 2013a **[8]** / **modifié**) :
   absent (0); present (1)
9. Ramus superior of the stapedial artery (Benoit et al. 2013b **[22]**):
   not visible or contained in a groove (0); contained in an ossified canal (1)
10. Prootic sinus (Benoit et al. 2013b **[24]** ; Benoit et al. 2013c **[19]**) :
    present (0); absent (1)
11. Pneumatization of the petrosal (Benoit et al. 2013a **[3]** / **modified**):
    absent (0); present (1)
12. Cross-section of the semicircular canals (Benoit et al. 2013a **[27]** / **modified**):
    circular (0); flattened (1)
13. Fusion of the posterior and lateral semicircular canals (Benoit et al. 2013a **[24]** / Benoit et al. 2013b **[51]** / **modified**):
    fusion of the lumen of the canals forming a true *crus commune secundaria* (0); partial fusion (1); absent (2)
14. Thickness of the semicircular canals (Benoit et al. 2013c **[32]**):
    slender (0); stocky (1)
15. Position of the lateral semicircular canal (Benoit et al. 2013c **[28]**):
    high (0); low (1)
16. Shape of the cochlea (Benoit et al. 2013a **[22]** / Benoit et al. 2013b **[41]**)
    planispiral, aspect ratio <0.65 (0); conical, aspect ratio >0.65 (1)
17. Number of turns of the cochlea (Benoit et al. 2013b **[39]**) :
    inferior to 1.5 (0); superior to 1.5 (1)
18. *Lamina secundaria* (Benoit et al. 2013b **[43]** / **modified**):
    present (0); absent (1)

Appendix 2 – Illustrations of the phylogenetic characters used in the preliminary cladistic analysis performed on proboscideans. ASC = Anterior semicircular canal ; LSC = Lateral semicircular canal ; PSC = Posterior semicircular canal (3 pages).

(1) *Fossa subarcuata*

Eritherium : very deep (0)

Phosphatherium : moderate (1)

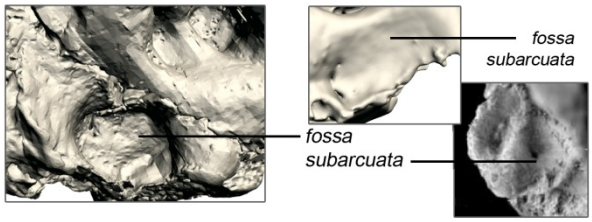

(2) Fusion of the *fenestra cochleae* and the cochlear canaliculus forming a unique perilymphatic foramen

Eritherium : absent (0)

Phosphatherium : absent (0)

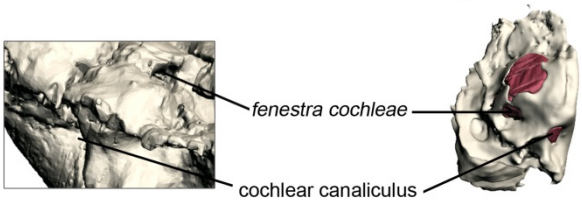

(3) Shape of the *fenestra vestibuli*

Eritherium : round (1)

Phosphatherium : round (1)

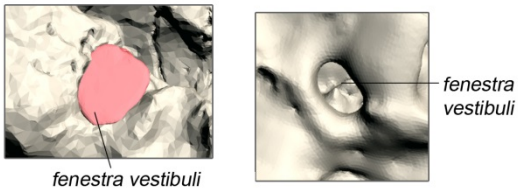

(4) Size of the *fenestra vestibuli*

Eritherium : large (0)

Phosphatherium : small (1)

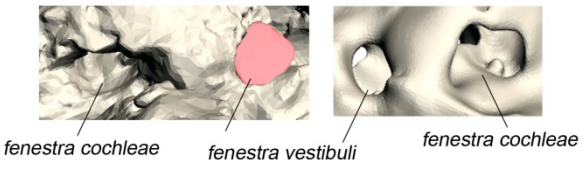

(5) Shape of the *promontorium*

Eritherium : slightly bulging (1)

Phosphatherium : clearly bulging (0)

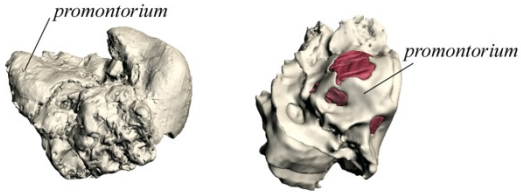

(6) Inflation of the *tegmen tympani*

Eritherium : strong (1)

Phosphatherium : absent (0)

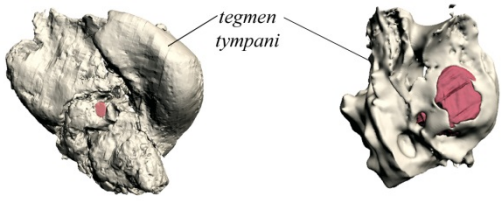

(7) Stapedial sulcus on the *promontorium*

Eritherium : absent (1)

Phosphatherium : absent (1)

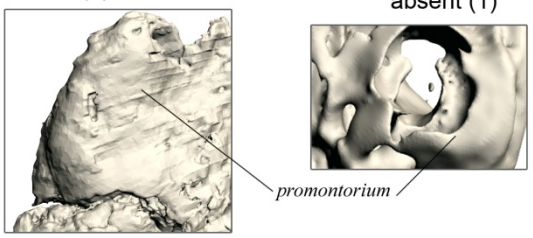

(8) Transpromontorial sulcus

Eritherium : absent (0)

Phosphatherium : absent (0)

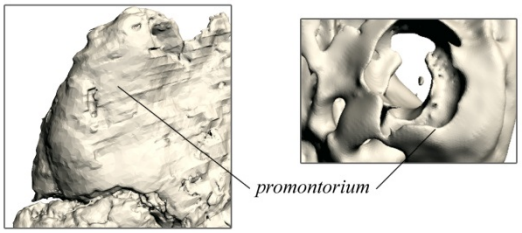

(9) Ramus superior of the stapedial artery

Eritherium :
contained in an ossified canal (1)

Phosphatherium :
not visible (0)

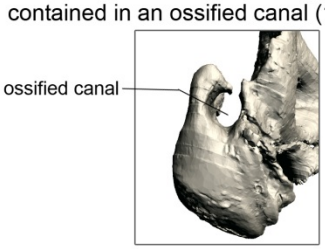

(10) Prootic sinus

Eritherium :
present (0)

Phosphatherium :
absent (1)

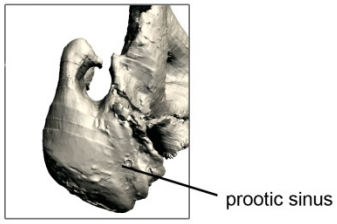

(11) Pneumatization of the petrosal

Eritherium :
present (0)

Phosphatherium :
absent (1)

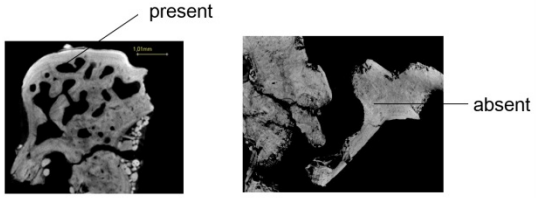

(12) Cross-section of the semicircular canals

Eritherium :
circular (0)

Phosphatherium :
circular (0)

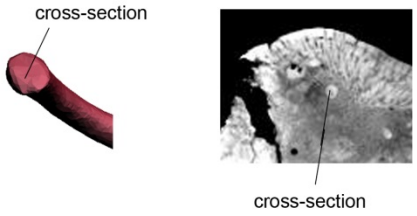

(13) Fusion of the posterior and lateral semicircular canals

Eritherium :
partial fusion (1)

Phosphatherium :
total fusion (0)

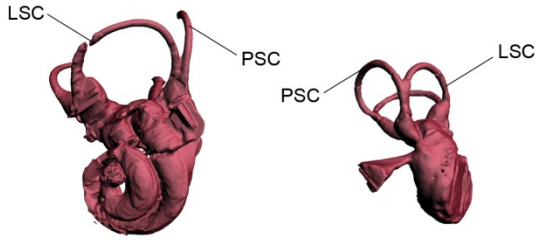

(14) Thickness of the semicircular canals

Eritherium :
slender (0)

Phosphatherium :
slender (0)

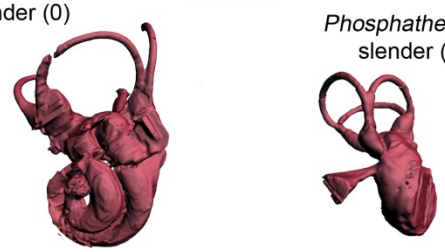

(15) Position of the lateral semicircular canal

Eritherium :
high (0)

Phosphatherium
high (0)

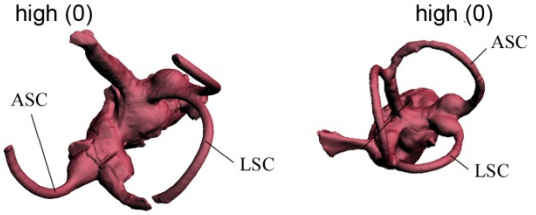

(16) Shape of the cochlea

Eritherium :
planispiral,
aspect ratio <0.65 (0);

Phosphatherium :
incomplete (?)

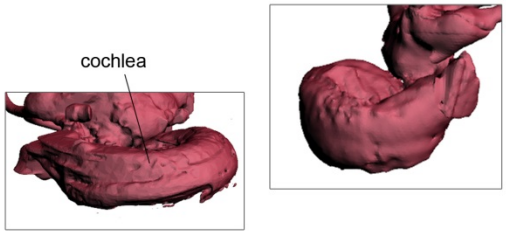

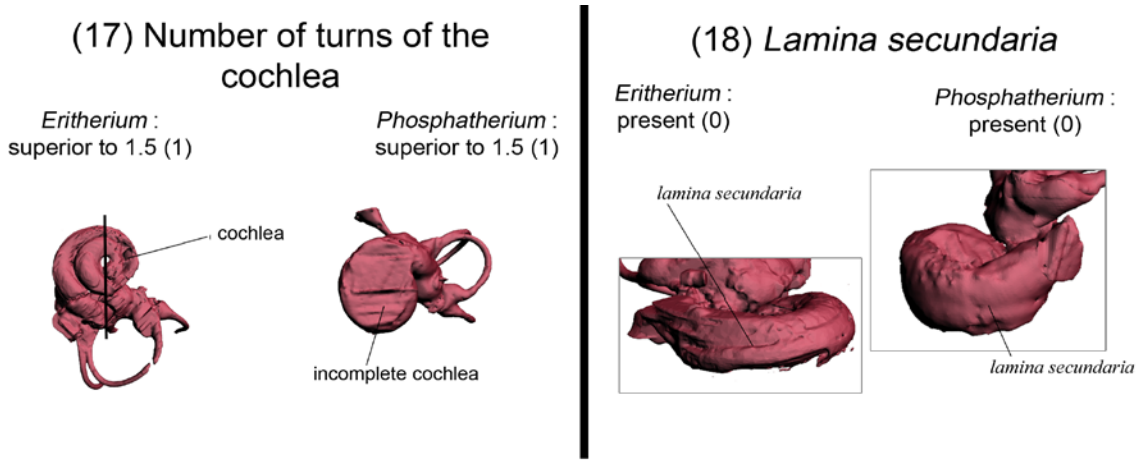

Appendix 3 – Matrix used in the preliminary cladistic analysis performed on proboscideans.

	1	2	3	4	5	6	7	8	9	10	11	12	13	14	15	16	17	18
Zhelestid	0	0	(01)	0	0	0	1	1	0	0	0	0	0	0	0	0	0	0
Henkelotherium	0	0	?	?	1	?	?	1	0	0	?	?	0	?	?	0	0	0
Eritherium	0	0	1	0	1	1	1	0	1	0	1	0	1	0	0	0	1	0
Phosphatherium	1	0	1	1	0	0	1	0	0	1	0	0	0	0	0	?	?	0
Numidotherium	1	0	0	1	0	0	1	1	?	1	0	0	0	0	?	0	1	0
Moeritherium	1	1	1	?	0	?	1	0	?	1	?	?	?	?	?	1	?	?
Gomphotherium	2	1	?	0	0	0	1	0	0	1	?	?	?	?	?	?	?	?
Elephantidae	2	1	1	?	0	0	1	0	0	1	0	1	2	1	1	0	1	1

Appendix 4 – Cladogram obtained in the analysis extended to the Afrotheria with its associated matrix.

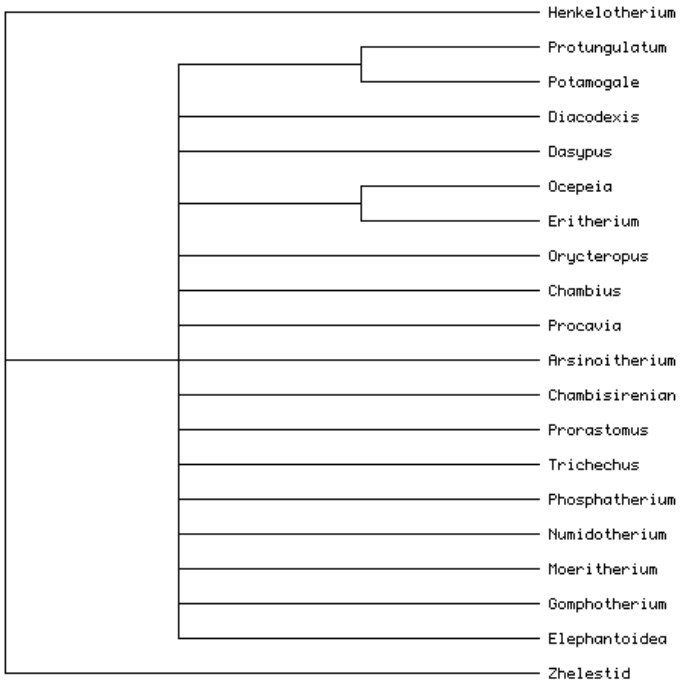

	1	2	3	4	5	6	7	8	9	10	11	12	13	14	15	16	17	18
Henkelotherium	0	0	?	?	1	?	?	1	0	0	?	?	0	?	?	0	0	0
Zhelestids	0	0	(01)	0	0	0	1	1	0	0	0	0	0	0	0	0	0	0
Protungulatum	0	0	0	0	1	0	0	1	?	1	?	?	?	?	?	?	?	?
Diacodexis	0	0	0	1	?	0	?	?	0	?	0	0	0	0	1	0	1	0
Dasypus	1	0	0	0	0	0	1	1	0	1	?	0	2	0	0	0	1	0
Ocepeia	0	0	0	0	0	1	1	0	1	?	1	0	1	0	0	0	1	0
Orycteropus	1	0	1	?	0	1	0	1	0	1	0	0	0	0	?	0	1	0
Chambius	0	0	0	0	0	1	0	1	0	1	0	0	0	0	?	1	1	0
Potamogale	0	0	1	0	1	0	0	1	0	1	?	0	2	0	0	1	1	0
Procavia	1	0	0	0	1	0	1	0	?	1	1	1	2	0	0	1	1	0
Arsinoitherium	2	1	1	?	0	0	1	0	0	1	0	1	0	1	1	0	1	0
Chambi sirenian	?	?	0	0	0	1	1	0	0	1	1	0	0	0	?	1	1	1
Prorastomus	2	0	1	?	0	1	1	0	0	1	1	0	2	0	1	0	1	0
Trichechus	2	1	1	?	?	?	1	0	?	1	1	0	2	0	1	0	0	1
Eritherium	0	0	1	0	1	1	1	0	1	0	1	0	1	0	0	0	1	0
Phosphatherium	1	0	1	1	0	0	1	0	0	1	0	0	0	0	0	?	?	0
Numidotherium	1	0	0	1	0	0	1	1	?	1	0	0	0	0	?	0	1	0
Moeritherium	1	1	1	?	0	?	1	0	?	?	?	?	?	?	?	1	?	?
Gomphotherium	2	1	?	0	0	0	1	0	0	1	?	?	?	?	?	?	?	?
Elephantoidea	2	1	1	?	0	0	1	0	0	1	0	1	2	1	1	0	1	1

Henkelotherium and zhelestids were defined as outgroups. Characters are unordered. This topology was found after a heuristic search with PAUP 3.1.1. Length: 79 steps; CI: 0.253; HI: 0.747; RI: 0.157.

Appendix 5 – Comparative chart of the semicircular canals of studied proboscideans and afrotherians in a view parallel to the anterior canal plane

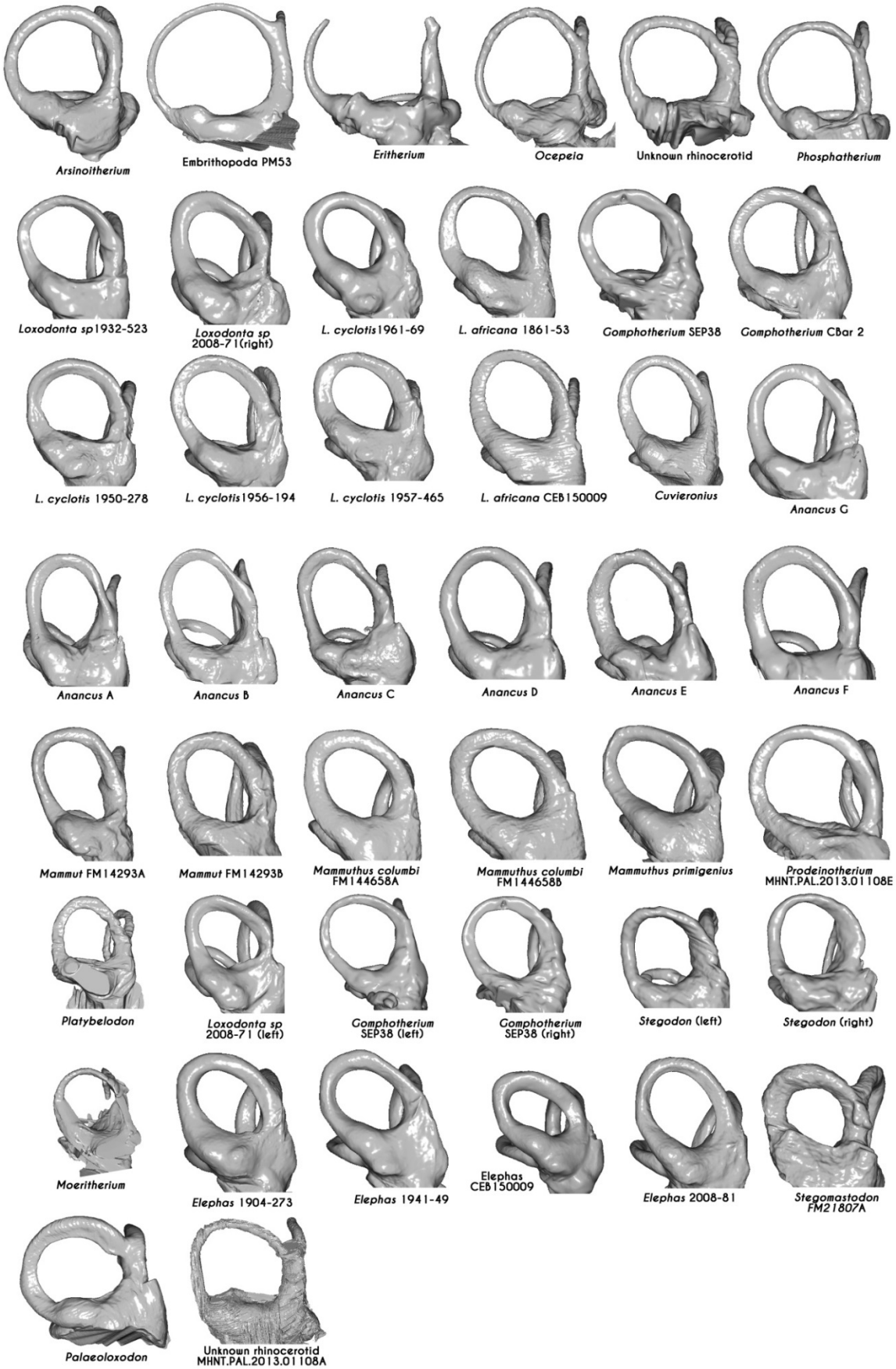

Appendix 6 – Comparative chart of the semicircular canals of studied proboscideans and afrotherians in a view parallel to the posterior canal plane

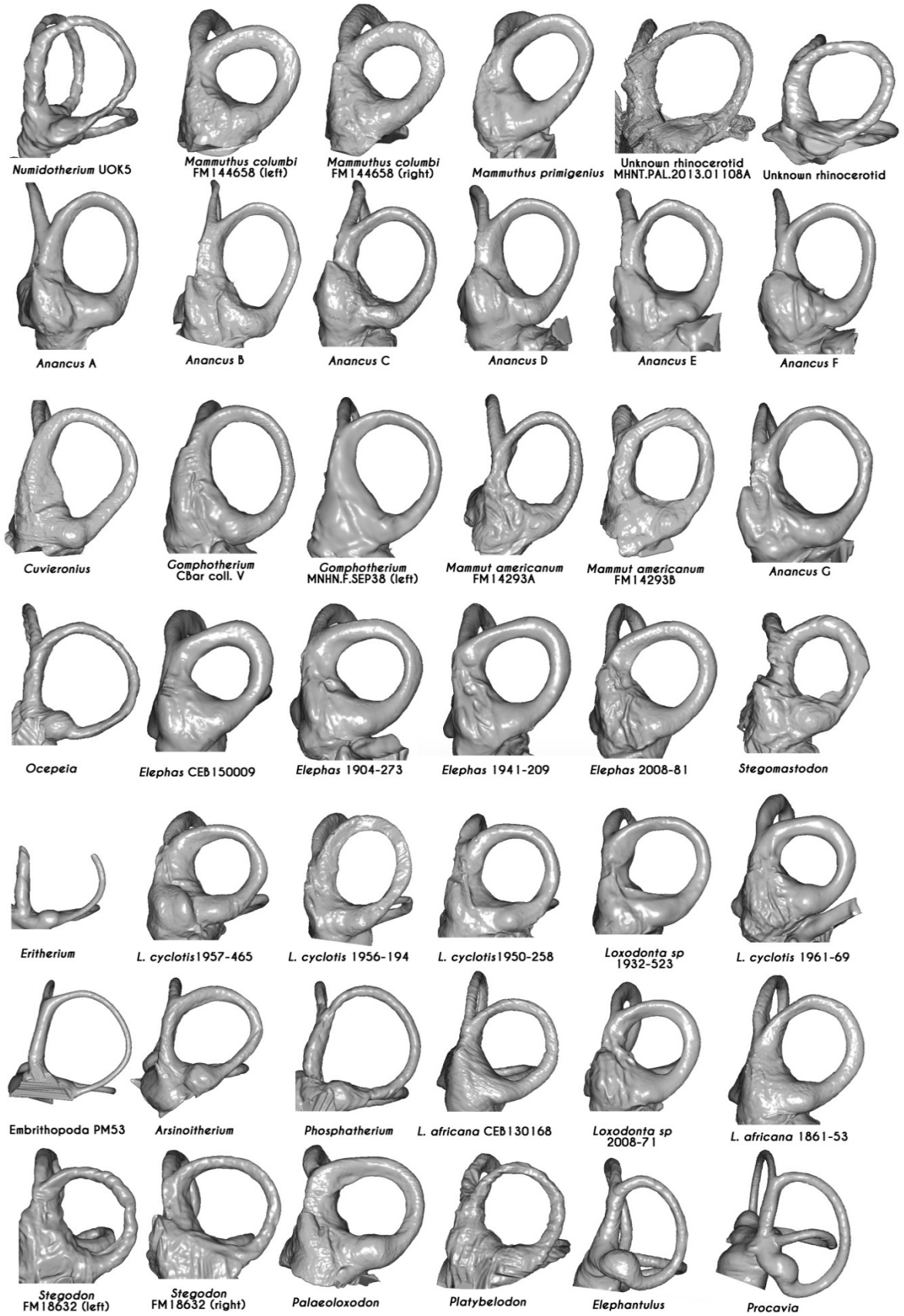

Appendix 7 – Comparative chart of the semicircular canals of studied proboscideans and afrotherians in a view parallel to the lateral canal plane

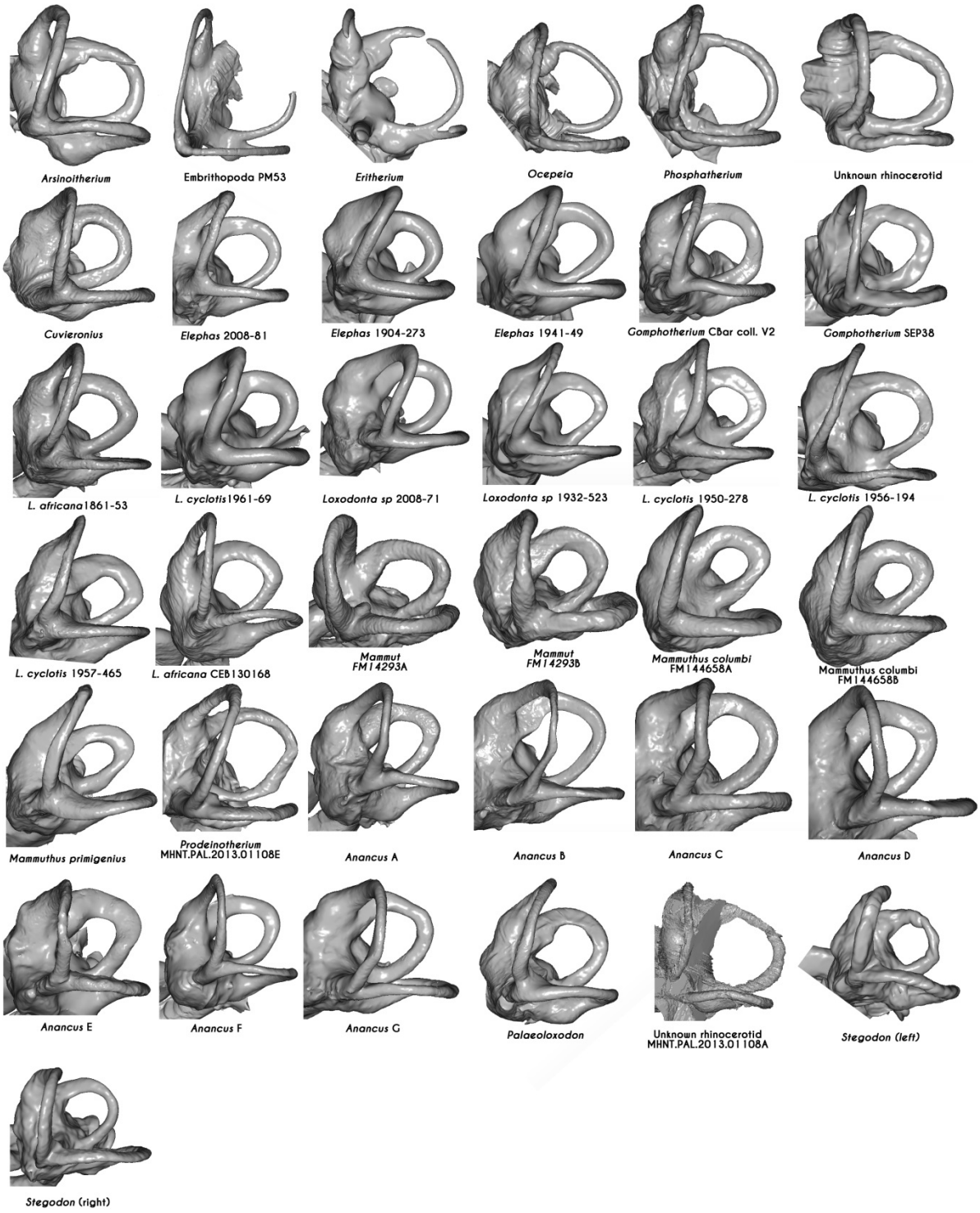

Appendix 8 – Comparative chart of the semicircular canals of studied proboscideans and afrotherians in a view illustrating best the insertion of the lateral canal into the vestibule

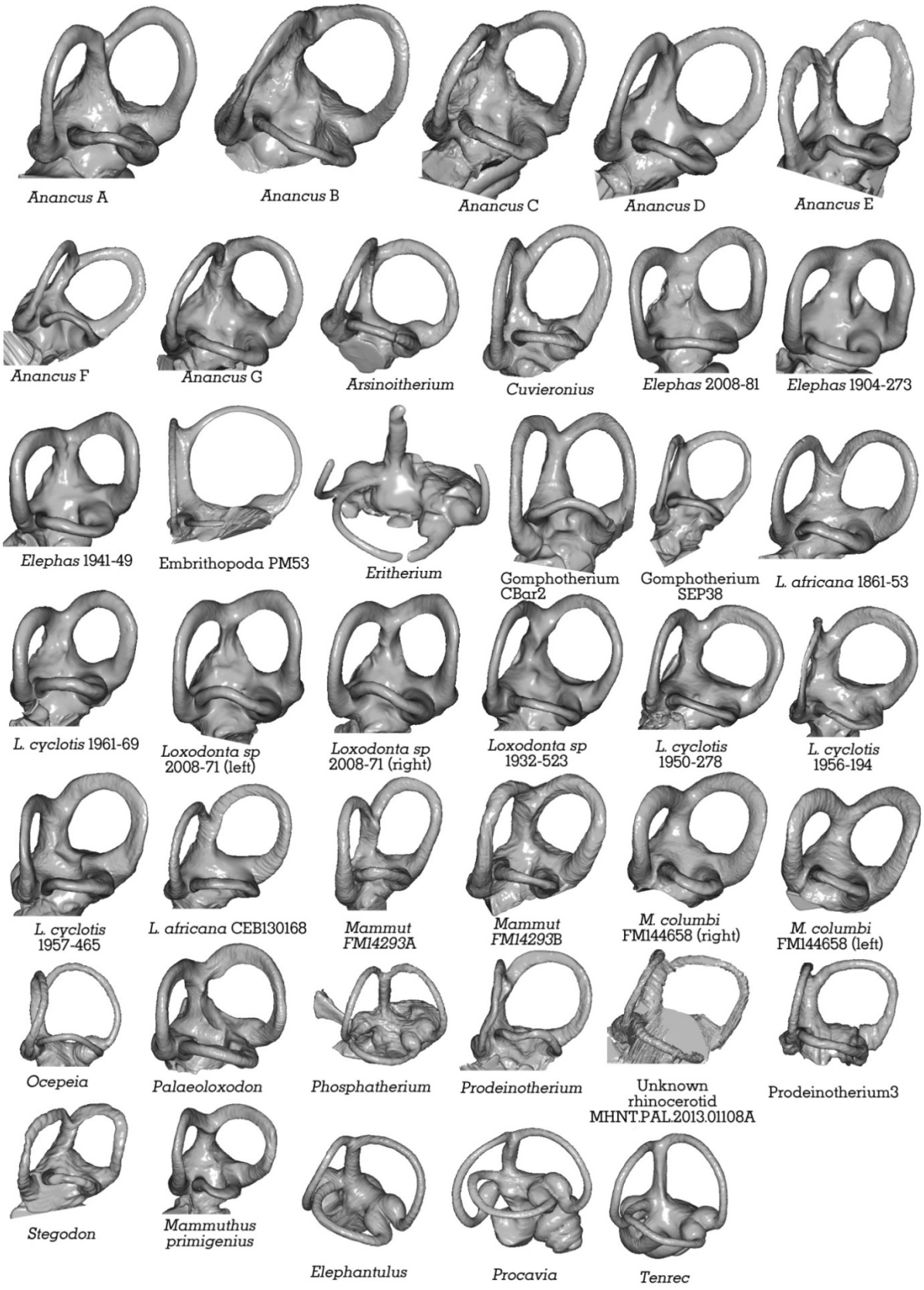

Appendix 9 – Comparative chart of the bony labyrinths of studied proboscideans and afrotherians in a view illustrating best the vestibulo-cochlear angle

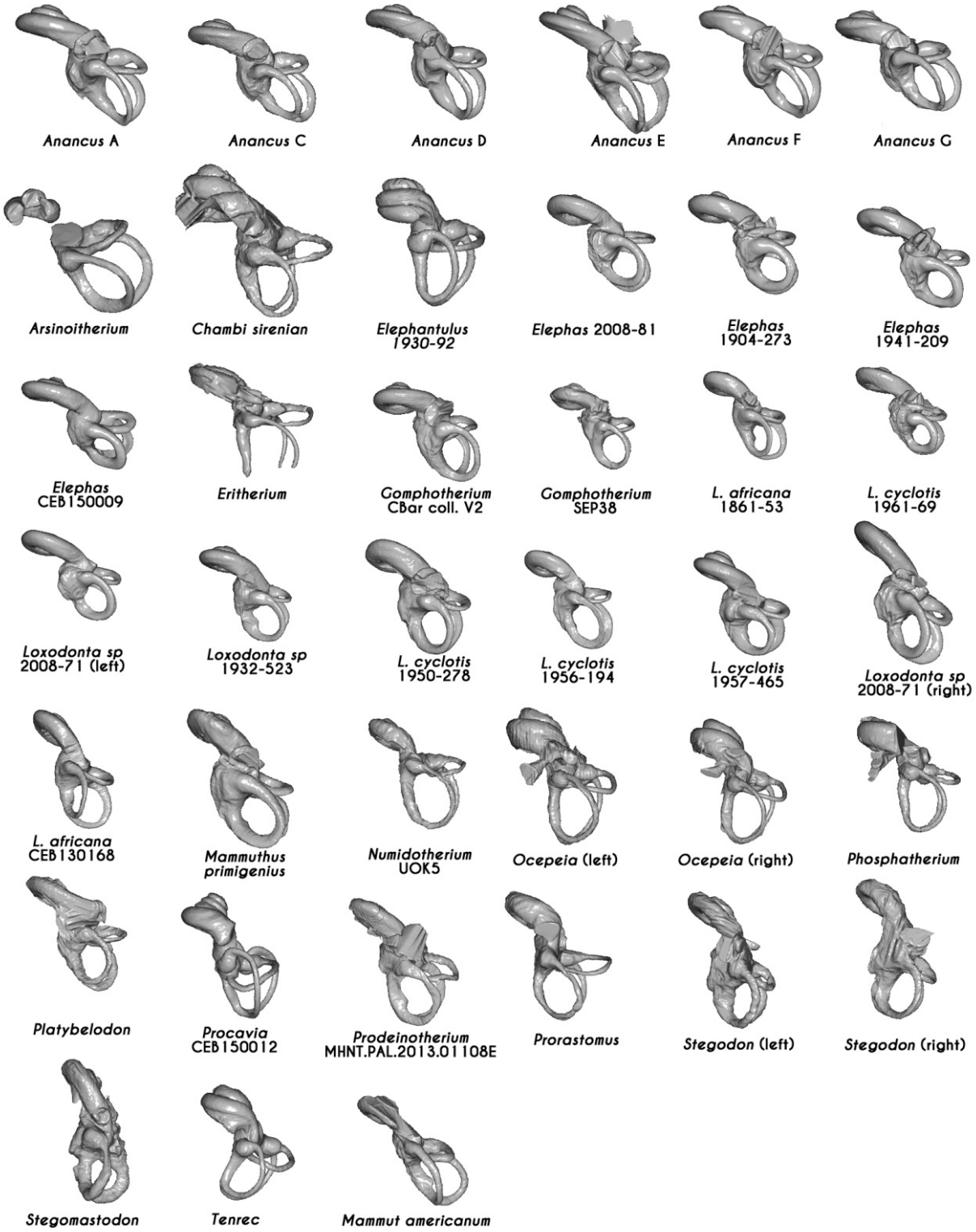

Appendix 10 – Comparative chart of the bony labyrinths of studied proboscideans and afrotherians in a view illustrating best the morphology of the cochlea

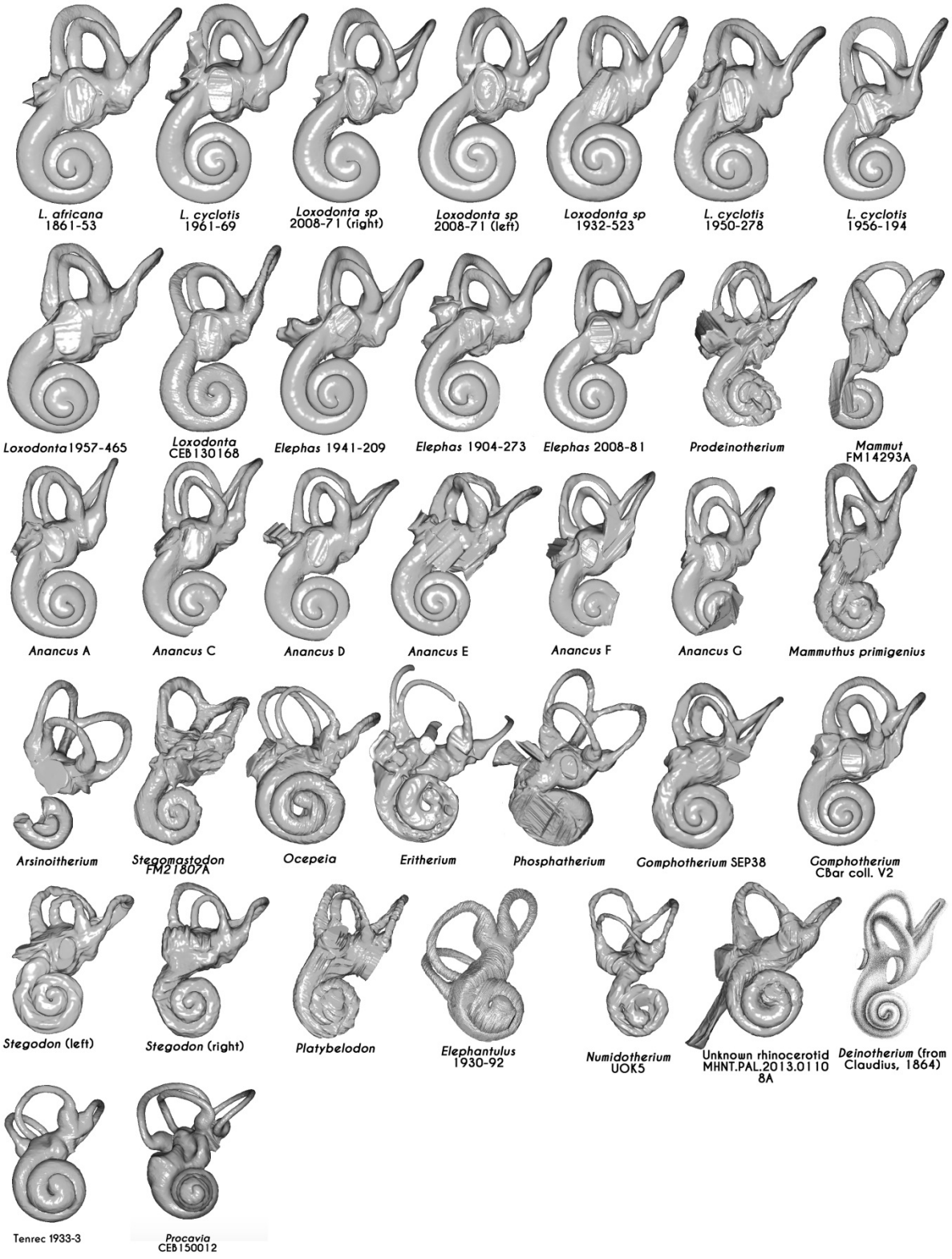

Appendix 11 – Comparisons of the stapedial ratio values in proboscideans and other mammals

	Stapedial ratio
Amphiorycteropus (Benoit et al., 2015; average)	1.18
Anancus NMNHS.FM2991A	1.66
Anancus NMNHS.FM2991C	1.64
Anancus NMNHS.FM2991D	1.73
Anancus NMNHS.FM2991E	1.65
Anancus NMNHS.FM2991F	1.76
Anancus NMNHS.FM2991G	1.58
Arsinoitherium BMNH 8800	1.60
Chambi sirenian	1.95
Chambius (Benoit et al., 2013c)	1.72
Chrysochloris (Benoit et al., 2015; average)	2.26
Chrysochloris (Ekdale, 2013)	2.80
Dendrohyrax (Benoit, 2013)	2.07
Elephantimorpha (Ekdale, 2011)	1.60
Elephantulus (Benoit, 2013)	1.65
Elephas CEB150009	1.52
Elephas MNHN.AC.ZM.1904-273	1.83
Elephas MNHN.AC.ZM.1941-209	1.65
Elephas MNHN.AC.ZM.2008-81	1.63
Eritherium PM88	1.57
Gomphotherium Cbar coll. V2	1.52
Gomphotherium MNHN.F.SEP38	1.48
Helioseus (Benoit, 2013)	1.55
Hemicentetes (Ekdale, 2013)	1.60
Heterohyrax (Benoit, 2013)	1.74
Hyopsodus (Ravel & Orliac, 2015)	1.44
Kulbeckia (Ekdale, 2013)	2.00
Loxodonta africana CEB130168	1.70
Loxodonta africana MNHN.AC.ZM.1861-53	1.58
Loxodonta cyclotis MNHN.AC.ZM.1950-278	1.76
Loxodonta cyclotis MNHN.AC.ZM.1957-465	1.74
Loxodonta cyclotis MNHN.AC.ZM.1961-69	1.69
Loxodonta sp MNHN.AC.ZM.1932-523	1.72
Loxodonta sp MNHN.AC.ZM.2008-71 (left)	1.65
Loxodonta sp MNHN.AC.ZM.2008-71 (right)	1.74
Macroscelides (Benoit et al., 2013)	1.78
Macroscelides (Ekdale, 2013)	1.90
Numidotherium unlabeled (Benoit et al., 2013b)	1.81
Orycteropus (Benoit et al., 2015; average)	1.80
Petrodromus (Benoit, 2013)	1.50
Phosphatherium PM17	1.62
Plesiorycteropus (Benoit et al., 2015; average)	1.42
Potamogale (Benoit et al., 2015; average)	1.61
Procavia (Benoit et al., 2013b)	1.84
Procavia (Ekdale, 2013)	2.10
Prorastomus	1.54
Rhynchocyon (Benoit, 2013)	1.70
Seggeurius (Benoit et al., 2016)	1.79
Tenrec (Benoit et al., 2015; average)	1.45
Trichechus (Ekdale, 2013)	1.60
Zalambdalestes (Ekdale, 2013)	1.70

Appendix 12 – Comparisons of the *crus commune* thickness ratio values in proboscideans and other mammals

	Thickness ratio (*crus commune*)
Anancus NMNHS.FM2991A	20.81
Anancus NMNHS.FM2991B	20.05
Anancus NMNHS.FM2991C	40.37
Anancus NMNHS.FM2991D	35.82
Anancus NMNHS.FM2991E	21.65
Anancus NMNHS.FM2991F	18.42
Anancus NMNHS.FM2991G	20.33
Arsinoitherium BMNH 8800	14.55
Cuvieronius FM103247	17.39
Elephantulus MNHN.AC.ZM.1930-92	19.33
Elephas CEB150009	49.20
Elephas MNHN.AC.ZM.1904-273	21.19
Elephas MNHN.AC.ZM.1941-209	21.53
Elephas MNHN.AC.ZM.2008-81	22.62
Embrithopoda PM53	13.63
Eritherium PM88	11.46
Gomphotherium Cbar coll. V2	14.25
Gomphotherium MNHN.F.SEP38	18.66
Loxodonta africana CEB130168	37.23
Loxodonta africana MNHN.AC.ZM.1861-53	27.27
Loxodonta cyclotis MNHN.AC.ZM.1950-278	27.87
Loxodonta cyclotis MNHN.AC.ZM.1956-194	29.20
Loxodonta cyclotis MNHN.AC.ZM.1957-465	40.15
Loxodonta cyclotis MNHN.AC.ZM.1961-69	31.33
Loxodonta sp MNHN.AC.ZM.1932-523	25.26
Loxodonta sp MNHN.AC.ZM.2008-71	20.09
Mammut FM14293A	21.55
Mammuthus columbi FM144658 (left)	24.52
Mammuthus columbi FM144658 (right)	29.57
Mammuthus primigenius MNHN.F.1904-12	25.45
Numidotherium UOK5	14.96
Ocepeia PM45	17.35
Palaeoloxodon M82706	22.24
Phosphatherium PM17	12.45
Platybelodon 26564 (824+)	27.92
Prodeinotherium MHNT.PAL.2013.01108E	21.37
Sirenian from Chambi	21.83
Stegodon FM18632	25.72
Stegomastodon FM21807	19.35
Unknown rhinocerotid	24.91
Unknown rhinocerotid MHNT.PAL.2013.01108E	27.77

Appendix 13 – Comparisons of the relative size of the lateral canal in proboscideans and other mammals (page 1/3)

	Anterior radius of curvature	Posterior radius of curvature	Mean radius of the vertical canals	Lateral radius of curvature	Lateral canal ratio (%)
Amphiorycteropus (Benoit et al., 2015)	3.26	2.83	3.05	3.3	108.4
Anancus NMNHS.FM2991A	5.01	4.79	4.9	3.19	65
Anancus NMNHS.FM2991B	5.91	5.63	5.77	4.06	70.4
Anancus NMNHS.FM2991C	5.15	4.89	5.02	3.39	67.6
Anancus NMNHS.FM2991D	5.24	5.39	5.32	3.43	64.5
Anancus NMNHS.FM2991E	5.52	5.37	5.45	3.54	65.1
Anancus NMNHS.FM2991F	5.68	5.67	5.68	3.92	69.1
Anancus NMNHS.FM2991G	5.21	5.69	5.45	3.64	66.8
Arsinoitherium BMNH 8800	4.5	4.34	4.42	3.3	74.7
Chambius (Benoit et al., 2013c)	0.8	0.71	0.76	0.65	86.1
Chrysochloris (Benoit et al., 2015)	0.86	0.68	0.77	0.61	79.2
Chrysochloris (Benoit et al., 2015)	0.98	0.68	0.83	0.66	79.5
Cuvieronius FM103247	6.18	6.06	6.12	3.58	58.5
Dendrohyrax (Benoit, 2013)	2.3	2.38	2.34	1.97	84.2
Didelphis (Ekdale, 2013)	1.46	1.23	1.35	0.88	65.4
Dugong (Benoit et al., 2013b)	2.85	2.57	2.71	2.41	88.9
Elephantimorph (Ekdale, 2011)	5	5.5	5.25	2.7	51.4
Elephantulus (Benoit et al., 2013c)	1.4	1.24	1.32	1.05	79.5
Elephas CEB150009	5.04	4.65	4.85	3.65	75.3
Elephas MNHN.AC.ZM.1904-273	5.23	5.2	5.22	3.16	60.5
Elephas MNHN.AC.ZM.1941-209	5.27	5.21	5.24	3.52	67.1
Elephas MNHN.AC.ZM.2008-81	4.97	5.64	5.31	4.06	76.5
Embrithopoda PM53	3.26	3.13	3.2	2.29	71.7
Eritherium PM88	1.74	1.83	1.78	1.38	77.5
Gomphotherium Cbar coll. V2	5.25	5.99	5.62	3.71	66
Gomphotherium MNHN.F.SEP38	5.45	5.12	5.28	3.36	63.7
Helioseus (Benoit, 2013)	1.42	1.27	1.35	1.24	92.2

Appendix 13 – Comparisons of the relative size of the lateral canal in proboscideans and other mammals (page 2/3)

	Anterior radius of curvature	Posterior radius of curvature	Mean radius of the vertical canals	Lateral radius of curvature	Lateral canal ratio (%)
Hemicentetes (Benoit et al., 2015)	1.1	0.89	1	0.68	68.3
Heterohyrax (Benoit, 2013)	4.43	4.11	4.27	3.39	79.4
Hyopsodus (Ravel & Orliac, 2015)	1.48	1.19	1.34	1.12	83.9
Kulbeckia (Ekdale, 2013)	1.19	0.96	1.08	0.92	85.6
Loxodonta africana CEB130168	5.8	5.56	5.68	3.72	65.4
Loxodonta africana MNHN.AC.ZM.1861-53	6.1	5.2	5.65	3.54	62.7
Loxodonta cyclotis MNHN.AC.ZM.1950-278	5.37	4.91	5.14	3.35	65.1
Loxodonta cyclotis MNHN.AC.ZM.1956-194	6.86	6.25	6.55	4.09	62.3
Loxodonta cyclotis MNHN.AC.ZM.1957-465	5.46	4.96	5.21	3.17	60.8
Loxodonta cyclotis MNHN.AC.ZM.1961-69	5.08	4.8	4.94	3.37	68.3
Loxodonta sp MNHN.AC.ZM.1932-523	5.65	5.35	5.5	3.21	58.3
Loxodonta sp MNHN.AC.ZM.2008-71	5.17	5.13	5.15	3.56	69.2
Macroscelides (Benoit et al., 2013c)	1.27	1.08	1.18	1.02	86.8
Mammut FM14293A	6.33	6.09	6.21	3.84	61.8
Mammut FM14293B	5.63	5.62	5.62	2.96	52.7
Mammuthus columbi FM144658 (left)	5.71	4.84	5.28	3.08	58.4
Mammuthus columbi FM144658 (right)	5.68	4.81	5.24	3.24	61.8
Mammuthus primigenius MNHN.F.1904-12	5.8	5.52	5.66	2.92	51.6
Numidotherium unlabelled (Benoit et al., 2013b)	3.27	3.21	3.24	2.46	75.9
Numidotherium UOK5	3.7	3.29	3.49	2.56	73.3
Ocepeia PM45	1.64	1.55	1.59	1.25	78.5
Orycteropus (Benoit et al., 2015)	3.37	3.14	3.26	3.42	105.1
Palaeoloxodon M82706	5.87	5.14	5.51	3.99	72.4
Petrodromus (Benoit, 2013)	1.52	1.23	1.38	1.32	96
Phosphatherium PM17	1.91	1.88	1.9	1.49	78.5

Appendix 13 – Comparisons of the relative size of the lateral canal in proboscideans and other mammals (page 3/3)

	Anterior radius of curvature	Posterior radius of curvature	Mean radius of the vertical canals	Lateral radius of curvature	Lateral canal ratio (%)
Platybelodon 26564 (824+)	5.37	4.81	5.09	3.55	69.7
Plesiorycteropus (Benoit et al., 2015)	2.31	1.89	2.1	2.14	101.9
Potamogale (Benoit et al., 2015)	1.61	1.37	1.49	1.49	100
Procavia (Benoit et al., 2013b)	2.12	1.66	1.89	1.97	104.2
Prodeinotherium MHNT.PAL.2013.01108E	5.6	5.01	5.31	3.98	75
Prorastomus	2.84	3.01	2.93	2.96	101.2
Protungulatum (Orliac & O'Leary, 2016)	1.18	1.02	1.1	0.94	85.5
Rhynchocyon (Benoit, 2013)	2	1.77	1.89	1.45	76.9
Seggeurius (Benoit et al., 2016)	1.52	1.54	1.53	1.28	83.7
Sirenian from Chambi	2.21	2.14	2.18	1.95	89.6
Stegodon FM18632	5.36	7.48	6.42	3.27	51
Tenrec (Benoit et al., 2015)	1.19	1.11	1.15	1.12	97.4
Titanohyrax (Benoit, 2013)	2.42	2.34	2.38	2.15	90.3
Trichechus (Benoit et al., 2013c)	4.3	4.46	4.38	3.54	80.8
Unknown rhinocerotid	4.19	3.94	4.06	3.26	80.3
Unknown rhinocerotid MHNT.PAL.2013.01108A	4.13	3.98	4.06	3.44	84.9
Zalambdalestes (Ekdale, 2013)	1.46	1.2	1.33	1.21	91

Appendix 14 – Comparisons of the angles between the semicircular canals in proboscideans and other mammals

	Angle Ant-Post (°)	Angle Ant-Lat (°)	Angle Post-Lat (°)
Anancus NMNHS.FM2991A	90.5	58.2	77.6
Anancus NMNHS.FM2991B	81	58.9	78
Anancus NMNHS.FM2991C	79.8	63.8	81.3
Anancus NMNHS.FM2991D	92.4	70.4	81.2
Anancus NMNHS.FM2991E	87.5	70.4	87.9
Anancus NMNHS.FM2991F	88.6	68.9	80.5
Anancus NMNHS.FM2991G	78.5	64.6	79.7
Arsinoitherium BMNH 8800	85.3	71.1	83.9
Cuvieronius FM103247	82.1	77.4	85.5
Elephantulus MNHN.AC.ZM.1930-92	87.6	84	90.4
Elephas CEB150009	78.9	67.9	85.7
Elephas MNHN.AC.ZM.1904-273	72.6	75.7	88.8
Elephas MNHN.AC.ZM.1941-209	76.5	74.2	83.2
Elephas MNHN.AC.ZM.2008-81	76.6	75	85.8
Embrithopoda PM53	86	83.4	98.6
Eritherium PM88	93.8	83.5	91.4
Gomphotherium CBar coll. V2	79.2	67.8	85.3
Gomphotherium MNHN.F.SEP38	85.7	72.8	91.1
Loxodonta africana CEB130168	84.8	72.7	78
Loxodonta africana MNHN.AC.ZM.1861-53	81.1	73.8	82.2
Loxodonta cyclotis MNHN.AC.ZM.1950-278	83.3	72.3	88.5
Loxodonta cyclotis MNHN.AC.ZM.1956-194	76.7	72.9	93.8
Loxodonta cyclotis MNHN.AC.ZM.1957-465	74.7	80	85
Loxodonta cyclotis MNHN.AC.ZM.1961-69	80.9	68.1	80.6
Loxodonta sp MNHN.AC.ZM.1932-523	70.9	72.4	85.8
Loxodonta sp MNHN.AC.ZM.2008-71	75.9	59.8	83.5
Mammut FM14293A	86.5	68.8	81.4
Mammut FM14293B	80.5	65.1	80.9
Mammuthus columbi FM144658 (left)	77.5	71.9	89
Mammuthus columbi FM144658 (right)	75.7	74.7	85.4
Mammuthus primigenius MNHN.F.1904-12	68.6	71.4	88
Numidotherium UOK5	78	75.5	96.1
Ocepeia PM45	91.5	80.1	87.8
Palaeoloxodon M82706	77.1	76.2	92.6
Phosphatherium PM17	85.6	77.1	89.7
Platybelodon 26564 (824+)	73.9	67.4	98.8
Prodeinotherium MHNT.PAL.2013.01108E	77.2	67.6	90.7
Sirenian from Chambi	88.1	80.5	95.8
Stegodon FM18632	107.6	74.9	94
Stegomastodon FM21807	96.6	?	?
Unknown rhinocerotid	91	73.9	95
Unknown rhinocerotid MHNT.PAL.2013.01108A	94.4	76.1	98.9

Appendix 15 – Comparisons of the average thickness ratio values for the semicircular canals

	Average thickness ratio of the semicircular canals
Anancus NMNHS.FM2991A	3.36
Anancus NMNHS.FM2991B	2.56
Anancus NMNHS.FM2991C	3.40
Anancus NMNHS.FM2991D	3.54
Anancus NMNHS.FM2991E	4.20
Anancus NMNHS.FM2991F	3.33
Anancus NMNHS.FM2991G	3.21
Arsinoitherium BMNH 8800	3.42
Cuvieronius FM103247	3.65
Elephantulus MNHN.AC.ZM.1930-92	2.79
Elephas CEB150009	4.86
Elephas MNHN.AC.ZM.1904-273	4.64
Elephas MNHN.AC.ZM.1941-209	4.13
Elephas MNHN.AC.ZM.2008-81	3.52
Embrithopoda PM53	1.46
Eritherium PM88	1.08
Gomphotherium Cbar coll. V2	3.51
Gomphotherium MNHN.F.SEP38	3.40
Loxodonta africana CEB130168	3.28
Loxodonta africana MNHN.AC.ZM.1861-53	3.57
Loxodonta cyclotis MNHN.AC.ZM.1950-278	3.69
Loxodonta cyclotis MNHN.AC.ZM.1956-194	2.74
Loxodonta cyclotis MNHN.AC.ZM.1957-465	4.01
Loxodonta cyclotis MNHN.AC.ZM.1961-69	4.77
Loxodonta sp MNHN.AC.ZM.1932-523	3.02
Loxodonta sp MNHN.AC.ZM.2008-71	3.90
Mammut FM14293A	3.61
Mammut FM14293B	4.47
Mammuthus columbi FM144658 (left)	4.86
Mammuthus columbi FM144658 (right)	4.83
Mammuthus primigenius MNHN.F.1904-12	3.99
Numidotherium UOK5	2.16
Ocepeia PM45	2.15
Palaeoloxodon M82706	3.82
Phosphatherium PM17	2.24
Platybelodon 26564 (824+)	3.25
Prodeinotherium MHNT.PAL.2013.01108E	2.82
Sirenian from Chambi	2.18
Stegodon FM18632	4.04
Unknown rhinocerotid	3.17
Unknown rhinocerotid MHNT.PAL.2013.01108A	2.37

Appendix 16 – Comparisons of the number of turns of the cochlea in mammals

	Turns
Amphiorycteropus (Benoit et al., 2015)	1.714
Anancus NMNHS.FM2991A	2.500
Anancus NMNHS.FM2991C	2.500
Anancus NMNHS.FM2991D	2.500
Anancus NMNHS.FM2991E	2.500
Anancus NMNHS.FM2991F	2.500
Arsinoitherium BMNH 8800	2.000
Chambius (Benoit et al., 2013c)	2.000
Chrysochloris (Benoit et al., 2015)	3.332
Deinotherium (Claudius, 1865)	2.250
Dendrohyrax (Benoit, 2013)	3.669
Dugong (Benoit et al., 2013a)	1.428
Elephantimorpha (Ekdale, 2011)	2.125
Elephantulus (Benoit et al., 2013c)	1.844
Elephantulus MNHN.AC.ZM.1930-92	1.875
Elephas CEB150009	2.250
Elephas MNHN.AC.ZM.1904-273	2.375
Elephas MNHN.AC.ZM.1941-209	2.375
Elephas MNHN.AC.ZM.2008-81	2.375
Eritherium PM88	2.000
Gomphotherium Cbar coll. V2	2.625
Gomphotherium MNHN.F.SEP38	2.375
Helioseus (Benoit, 2013)	1.643
Hemicentetes (Benoit et al., 2015)	1.500
Heterohyrax (Benoit, 2013)	3.681
Hyopsodus (Ravel & Orliac, 2015)	2.250
Kulbeckia (Ekdale, 2013)	1.280
Loxodonta africana CEB130168	2.000
Loxodonta africana MNHN.AC.ZM.1861-53	2.375
Loxodonta cyclotis MNHN.AC.ZM.1950-278	2.250
Loxodonta cyclotis MNHN.AC.ZM.1956-194	2.625
Loxodonta cyclotis MNHN.AC.ZM.1957-465	2.625
Loxodonta cyclotis MNHN.AC.ZM.1961-69	2.625
Loxodonta sp	2.250
MNHN.AC.ZM.1932-523	
Loxodonta sp MNHN.AC.ZM.2008-71 (left)	2.000
Loxodonta sp MNHN.AC.ZM.2008-71 (right)	1.625
Macroscelides (Benoit et al., 2013)	2.056
Mammut FM14293A	2.375
Mammuthus primigenius MNHN.F.1904-12	2.250
Microgale (Benoit et al., 2015)	1.889
Moeritherium (Benoit et al., 2013)	2.250
Numidotherium (Court, 1992)	1.500
Numidotherium unlabelled (Benoit et al., 2013b)	1.620
Numidotherium UOK5	1.500
Ocepeia PM45	2.125
Orycteropus (Benoit et al., 2015)	1.843
Petrodromus (Benoit, 2013)	2.264
Platybelodon 26564 (824+)	2.000
Plesiortycteropus (Benoit et al., 2015)	1.829
Potamogale (Benoit et al., 2015)	2.093
Procavia (Benoit et al., 2013b)	3.428
Procavia CEB150012	3.500
Prodeinotherium MHNT.PAL.2013.01108E	2.250
Prorastomus (Benoit et al., 2013a)	1.530
Rhynchocyon (Benoit, 2013)	2.119
Seggeurius (Benoit et al., 2016)	1.910
Sirenian from Chambi (Benoit et al., 2013a)	2.500
Stegodon FM18632	2.000
Stegomastodon FM21807	2.000
Tenrec (Benoit et al., 2015)	1.767
Tenrec MNHN.AC.ZM.1933-3	1.875
Titanohyrax (Benoit, 2013)	1.919
Trichechus (Benoit et al., 2013b)	1.131
Unknown rhinocerotid MHNT.PAL.2013.01108A	2.000
Zalambdalestes (Ekdake, 2012)	1.022

Appendix 17 – Comparisons of the relative volume of the cochlea in proboscideans and other mammals

	Volume of the cochlea (mm^3)	Bony labyrinth volume (mm^3)	Relative volume of the cochlea (%)
Anancus NMNHS.FM2991A	468.32	934.63	50
Anancus NMNHS.FM2991C	442.19	957.51	46
Anancus NMNHS.FM2991D	539.30	1150.75	47
Anancus NMNHS.FM2991E	701.81	1440.54	49
Chrysochloris (Ekdale, 2013)	2.93	4.11	71
Elephantimorph (Ekdale, 2013)	351.00	1145.00	31
Elephas CEB150009	518.66	1180.15	44
Elephas MNHN.AC.ZM.1904-273	606.16	1273.83	48
Elephas MNHN.AC.ZM.1941-209	622.82	1251.01	50
Elephas MNHN.AC.ZM.2008-81	641.31	1295.32	50
Eritherium PM88	5.91	11.22	53
Gomphotherium Cbar coll. V2	497.03	988.32	50
Gomphotherium MNHN.F.SEP38	400.16	814.39	49
Hemicentetes (Ekdale, 2013)	1.39	2.78	50
Kulbeckia (Ekdale)	2.59	5.37	48
Loxodonta africana CEB130168	514.30	1078.76	48
Loxodonta africana MNHN.AC.ZM.1861-53	506.73	1078.15	47
Loxodonta cyclotis MNHN.AC.ZM.1950-278	542.46	1074.12	51
Loxodonta cyclotis MNHN.AC.ZM.1956-194	441.99	1118.89	40
Loxodonta cyclotis MNHN.AC.ZM.1957-465	524.03	1208.55	43
Loxodonta cyclotis MNHN.AC.ZM.1961-69	626.21	1295.64	48
Loxodonta sp MNHN.AC.ZM.1932-523	585.55	1138.08	51
Loxodonta sp MNHN.AC.ZM.2008-71	557.41	1167.69	48
Macroscelides (Ekdale, 2013)	6.59	9.19	72
Mammut FM14293A	343.09	936.25	37
Mammuthus primigenius MNHN.F.1904-12	480.12	1131.01	42
Numidotherium UOK5	35.06	84.39	42
Ocepeia PM45	11.65	17.53	66
Orycteropus (Ekdale, 2013)	59.30	107.00	55
Phosphatherium PM17	22.38	32.54	69
Platybelodon 26564 (824+)	373.76	854.52	44
Procavia (Ekdale, 2013)	9.24	19.40	48
Prodeinotherium MHNT.PAL.2013.01108E	322.08	674.35	48
Sirenian from Chambi	45.47	74.60	61
Stegodon FM18632	507.85	1117.53	46
Trichechus (Ekdale, 2013)	442.00	621.00	71
Unknown rhinocerotid MHNT.PAL.2013.01108A	229.25	401.26	57
Zalambdalestes (Ekdale, 2013)	2.91	6.07	48

Appendix 18 – Comparisons of the aspect ratio of the cochlea in proboscideans and other mammals

	Aspect ratio
Amphiorycteropus (Benoit et al., 2015; average)	0.49
Anancus NMNHS.FM2991A	0.43
Anancus NMNHS.FM2991C	0.41
Anancus NMNHS.FM2991D	0.37
Anancus NMNHS.FM2991E	0.37
Anancus NMNHS.FM2991F	0.47
Anancus NMNHS.FM2991G	0.45
Arsinoitherium BMNH 8800	0.45
Chambius (Benoit et al., 2013c)	0.74
Chrysochloris (Benoit et al., 2015; average)	0.68
Dendrohyrax (Benoit, 2013)	0.81
Dugong (Benoit et al., 2013a)	0.57
Elephantimorpha (Ekdale, 2011)	0.42
Elephantulus (Benoit, 2013)	0.84
Elephantulus MNHN.AC.ZM.1930-92	0.79
Elephas CEB150009	0.38
Elephas MNHN.AC.ZM.1904-273	0.38
Elephas MNHN.AC.ZM.1941-209	0.38
Elephas MNHN.AC.ZM.2008-81	0.43
Eritherium PM88	0.35
Gomphotherium Cbar coll. V2	0.47
Gomphotherium MNHN.F.SEP38	0.47
Hemicentetes (Benoit et al., 2015; average)	0.38
Heterohyrax (Benoit, 2013)	0.88
Hyopsodus (Ravel & Orliac, 2015)	0.77
Loxodonta africana CEB130168	0.37
Loxodonta africana MNHN.AC.ZM.1861-53	0.45
Loxodonta cyclotis MNHN.AC.ZM.1950-278	0.40
Loxodonta cyclotis MNHN.AC.ZM.1956-194	0.40
Loxodonta cyclotis MNHN.AC.ZM.1957-465	0.44
Loxodonta cyclotis MNHN.AC.ZM.1961-69	0.44
Loxodonta sp MNHN.AC.ZM.1932-523	0.41
Loxodonta sp MNHN.AC.ZM.2008-71	0.30
Macroscelides (Benoit et al., 2013c)	0.85
Mammut FM14293A	0.44
Mammuthus primigenius MNHN.F.1904-12	0.46
Microgale (Benoit et al., 2015; average)	0.74
Numidotherium (Court, 1992)	0.52
Numidotherium unlabelled (Benoit et al., 2013b)	0.51
Numidotherium UOK5	0.48
Ocepeia PM45	0.72
Orycteropus (Benoit et al., 2015; average)	0.52
Petrodromus (Benoit, 2013)	0.97
Platybelodon 26564 (824+)	0.41
Plesiorycteropus (Benoit et al., 2015; average)	0.64
Potamogale (Benoit et al., 2015; average)	0.66
Procavia (Benoit et al., 2013b)	0.75
Procavia CEB150012	0.64
Prodeinotherium MHNT.PAL.2013.01108E	0.29
Prorastomus	0.34
Rhynchocyon (Benoit, 2013)	0.71
Seggeurius (Benoit et al., 2016)	0.48
Sirenian from Chambi	0.67
Stegodon FM18632	0.50
Stegomastodon FM21807	0.45
Tenrec (Benoit et al., 2015; average)	0.64
Tenrec MNHN.AC.ZM.1933-3	0.64
Trichechus (Benoit et al., 2013a)	0.55
Unknown rhinocerotid MHNT.PAL.2013.01108A	0.33

Appendix 19 – Comparisons of the vestibulo-cochlear angle among mammals

	Vestibulo-cochlear angle (°)
Anancus NMNHS.FM2991A	150
Anancus NMNHS.FM2991C	166
Anancus NMNHS.FM2991D	154
Anancus NMNHS.FM2991E	145
Anancus NMNHS.FM2991F	150
Anancus NMNHS.FM2991G	147
Arsinoitherium BMNH 8800	124
Dugong (Benoit, 2013)	128
Elephantulus MNHN.AC.ZM.1930-92	90
Elephas CEB150009	144
Elephas MNHN.AC.ZM.1904-273	155
Elephas MNHN.AC.ZM.1941-209	166
Elephas MNHN.AC.ZM.2008-81	156
Eritherium PM88	117
Gomphotherium Cbar coll. V2	132
Gomphotherium MNHN.F.SEP38 (left)	120
Gomphotherium MNHN.F.SEP38 (right)	120
Helioseus (Benoit, 2013)	107
Loxodonta africana CEB130168	132
Loxodonta africana MNHN.AC.ZM.1861-53	124
Loxodonta cyclotis MNHN.AC.ZM.1950-278	132
Loxodonta cyclotis MNHN.AC.ZM.1956-194	137
Loxodonta cyclotis MNHN.AC.ZM.1957-465	136
Loxodonta cyclotis MNHN.AC.ZM.1961-69	146
Loxodonta sp MNHN.AC.ZM.1932-523	131
Loxodonta sp MNHN.AC.ZM.2008-71 (left)	140
Loxodonta sp MNHN.AC.ZM.2008-71 (right)	144
Mammut FM14293A	153
Mammuthus primigenius MNHN.F.1904-12	148
Numidotherium UOK5	128
Ocepeia PM45 (left)	103
Ocepeia PM45 (right)	101
Phosphatherium PM17	102
Platybelodon 26564 (824+)	132
Procavia (Benoit, 2013)	128
Procavia CEB150012	127
Prodeinotherium MHNT.PAL.2013.01108E	132
Prorastomus	110
Seggeurius (Benoit, 2013)	107
Sirenian from Chambi	113
Stegodon FM18632 (left)	126
Stegodon FM18632 (right)	117
Stegomastodon FM21807	139
Tenrec MNHN.AC.ZM.1933-3	87

Appendix 20 – Phylogenetic tree used in the phylogenetic generalized least-squared regressions between the PCs and the body mass (pers. comm. Pascal Tassy, 2016). Divergence dates are figured on the tree.

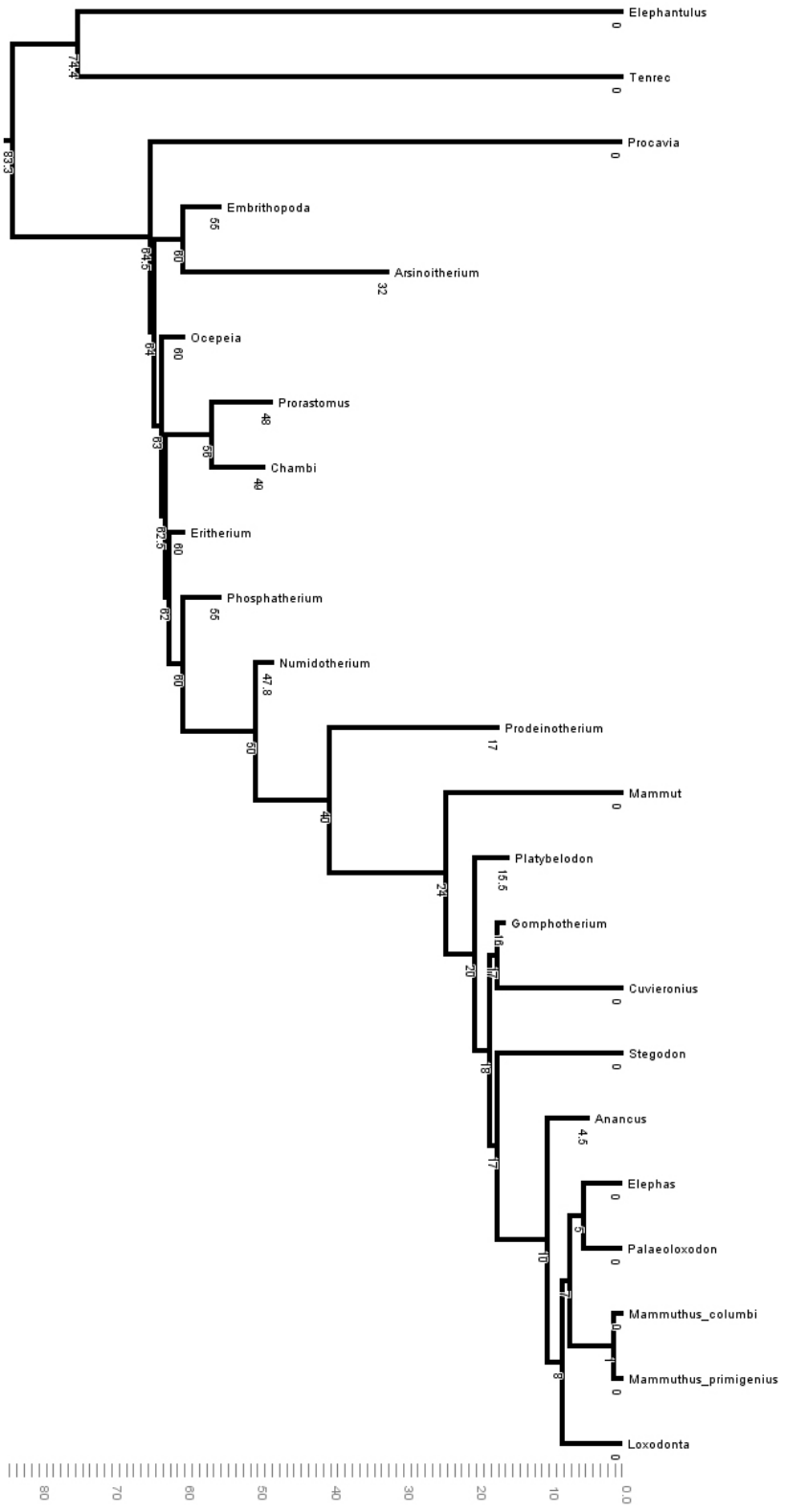

Appendix 21 – Body masses used in the phylogenetic generalized least-squared regressions

	Body mass (g)	Body mass reference	Method
Anancus arvernensis	3750000	Taken as similar as *Elephas*	
Arsinoitherium zitteli	2200000	Taken as similar to white rhino	
Chambi sirenian	?	Not used in the regression	Not used in the regression
Cuvieronius sp	6213000	Christiansen P. (2004)	Average of best regressions, complete or partial skeletons
Elephas maximus	3750000	Shoshani (1992)	Direct measurement
Embrithopoda PM53	85000	Pers. comm. Gheerbrant (2016)	
Eritherium azzouzorum	4500	Gheerbrant (2009)	Allometric regressions of tooth size
Gomphotherium angustidens	3969000	Christiansen (2004)	Forelimb best measurement
Loxodonta africana	5500000	Shoshani (1992)	Direct measurement
Loxodonta cyclotis	3250000	Shoshani (1992)	Direct measurement
Loxodonta	4093750	Average *africana/cyclotis*	Average *africana/cyclotis*
Mammut americanum	7035500	Christiansen P., (2004)	Average of best regressions, complete or partial skeletons
Mammuthus columbi	7220166	Christiansen P., (2004)	Weighted average of individual bone regressions based on the reciprocal of the SEE
Mammuthus primigenius	6000000	Larramendi, (in press.)	
Numidotherium koholense	275000	Larramendi, (in press.)	
Ocepeia daouiensis	3500	Gheerbrant et al. (2014)	Estimates on tooth size and skull length
Palaeoloxodon antiquus	6041871	Christiansen P., (2004)	Weighted average of individual bone regressions based on the reciprocal of the SEE
Phosphatherium escuilliei	15000	Saarinen et al. (2014)	
Platybelodon grangeri	2200000	Pascal Tassy pers. Comm. 2016 (also similar to white rhino)	
Prodeinotherium bavaricum	3700000	Larramendi, (in press.)	Mean of body masses
Prorastomus sirenoides	98155.5	Benoit et al. (2013)	
Stegodon orientalis	7220166	Similar to *M. columbi*	
Tenrec ecaudatus	852	Kaufman et al. (2013)	Direct measurement
Elephantulus sp	56.5	Eisenberg, (1981)	
Procavia capensis	3800	Nowak et Paradisio, (1983)	Direct measurement

Appendix 22 – Parameters of the phylogenetic generalized least-squared regressions performed on the first three PCs of analyses A1, A2, P1 and P2 (4 pages)

A1 analysis (full labyrinth of afrotherians)

> summary(PGLS_PC1_A1)

```
Call:
pgls(formula = PC1_A1 ~ BM, data =
comparative.data(TREE, PGLS_SET,
   Taxa), lambda = "ML")

Residuals:
     Min       1Q   Median       3Q      Max
-0.02117 -0.00226  0.00846  0.01429  0.01625

Branch length transformations:

kappa  [Fix]  : 1.000
lambda [ ML]  : 1.000
  lower bound : 0.000, p = 0.010859
  upper bound : 1.000, p = 1
  95.0% CI   : (0.675, NA)
delta  [Fix]  : 1.000

Coefficients:
             Estimate Std. Error t value Pr(>|t|)
(Intercept) -0.1663697  0.0783798 -2.1226
0.05357 .
BM           0.0087699  0.0184779  0.4746  0.64294
---
Signif. codes:  0 '***' 0.001 '**' 0.01 '*' 0.05 '.' 0.1 '
' 1

Residual standard error: 0.01258 on 13 degrees of
freedom
Multiple R-squared: 0.01703,    Adjusted R-
squared: -0.05858
F-statistic: 0.2253 on 1 and 13 DF,  p-value: 0.6429
```

> summary(PGLS_PC2_A1)

```
Call:
pgls(formula = PC2_A1 ~ BM, data =
comparative.data(TREE, PGLS_SET,
   Taxa), lambda = "ML")

Residuals:
     Min       1Q   Median       3Q      Max
-0.016876 -0.005652  0.001287  0.007808
0.017547

Branch length transformations:

kappa  [Fix]  : 1.000
lambda [ ML]  : 0.000
  lower bound : 0.000, p = 1
  upper bound : 1.000, p = 0.006909
  95.0% CI   : (NA, 0.938)
delta  [Fix]  : 1.000

Coefficients:
             Estimate Std. Error t value Pr(>|t|)
(Intercept)  0.157767   0.069174  2.2807  0.04007 *
BM          -0.032125   0.013421 -2.3937  0.03247 *
---
Signif. codes:  0 '***' 0.001 '**' 0.01 '*' 0.05 '.' 0.1 '
' 1

Residual standard error: 0.01084 on 13 degrees of
freedom
Multiple R-squared: 0.3059,    Adjusted R-squared:
0.2525
F-statistic:  5.73 on 1 and 13 DF,  p-value: 0.03247
```

> summary(PGLS_PC3_A1)

```
Call:
pgls(formula = PC3_A1 ~ BM, data =
comparative.data(TREE, PGLS_SET,
   Taxa), lambda = "ML")

Residuals:
     Min       1Q   Median       3Q      Max
-0.020744 -0.005315  0.003951  0.010588
0.022654

Branch length transformations:

kappa  [Fix]  : 1.000
lambda [ ML]  : 0.972
  lower bound : 0.000, p = 0.047336
  upper bound : 1.000, p = 0.61073
  95.0% CI   : (0.407, NA)
delta  [Fix]  : 1.000

Coefficients:
             Estimate Std. Error t value Pr(>|t|)
(Intercept) -0.260763   0.083945 -3.1064 0.008344
**
BM           0.054994   0.019836  2.7725 0.015842 *
---
Signif. codes:  0 '***' 0.001 '**' 0.01 '*' 0.05 '.' 0.1 '
' 1
```

Residual standard error: 0.01327 on 13 degrees of freedom
Multiple R-squared: 0.3716, Adjusted R-squared: 0.3232
F-statistic: 7.687 on 1 and 13 DF, p-value: 0.01584

A2 analysis (semicircular canals of afrotherians)

> summary(PGLS_PC1_A2)

Call:
pgls(formula = PC1_A2 ~ BM, data = comparative.data(TREE, PGLS_SET, Taxa), lambda = "ML")

Residuals:
Min 1Q Median 3Q Max
-0.014685 -0.004700 0.002381 0.005561 0.013766

Branch length transformations:

kappa [Fix] : 1.000
lambda [ML] : 0.843
lower bound : 0.000, p = 0.0093742
upper bound : 1.000, p = 0.037623
95.0% CI : (0.323, 0.997)
delta [Fix] : 1.000

Coefficients:
Estimate Std. Error t value Pr(>|t|)
(Intercept) -0.2665909 0.0468186 -5.6941 1.425e-05 ***
BM 0.0373230 0.0099763 3.7412 0.001288 **

Signif. codes: 0 '***' 0.001 '**' 0.01 '*' 0.05 '.' 0.1 ' ' 1

Residual standard error: 0.007866 on 20 degrees of freedom
Multiple R-squared: 0.4117, Adjusted R-squared: 0.3823
F-statistic: 14 on 1 and 20 DF, p-value: 0.001288

> summary(PGLS_PC2_A2)

Call:
pgls(formula = PC2_A2 ~ BM, data = comparative.data(TREE, PGLS_SET, Taxa), lambda = "ML")

Residuals:
Min 1Q Median 3Q Max
-0.010424 -0.002994 0.003655 0.011908 0.029060

Branch length transformations:

kappa [Fix] : 1.000
lambda [ML] : 0.966
lower bound : 0.000, p = 0.012502
upper bound : 1.000, p = 0.38069
95.0% CI : (0.506, NA)
delta [Fix] : 1.000

Coefficients:
Estimate Std. Error t value Pr(>|t|)
(Intercept) -0.0033227 0.0694863 -0.0478 0.9623
BM -0.0069617 0.0145268 -0.4792 0.6370

Residual standard error: 0.0122 on 20 degrees of freedom
Multiple R-squared: 0.01135, Adjusted R-squared: -0.03808
F-statistic: 0.2297 on 1 and 20 DF, p-value: 0.637

> summary(PGLS_PC3_A2)

Call:
pgls(formula = PC3_A2 ~ BM, data = comparative.data(TREE, PGLS_SET, Taxa), lambda = "ML")

Residuals:
Min 1Q Median 3Q Max
-0.008039 -0.003331 -0.001045 0.003225 0.011791

Branch length transformations:

kappa [Fix] : 1.000
lambda [ML] : 0.000
lower bound : 0.000, p = 1
upper bound : 1.000, p = 0.0015414
95.0% CI : (NA, 0.961)
delta [Fix] : 1.000

Coefficients:
Estimate Std. Error t value Pr(>|t|)
(Intercept) 0.0254082 0.0310538 0.8182 0.4229
BM -0.0052361 0.0058141 -0.9006 0.3785

Residual standard error: 0.00539 on 20 degrees of freedom
Multiple R-squared: 0.03897, Adjusted R-squared: -0.009078
F-statistic: 0.8111 on 1 and 20 DF, p-value: 0.3785

P1 analysis (full labyrinth of proboscideans)

> summary(PGLS_PC1_P1)

```
Call:
pgls(formula = PC1_P1 ~ BM, data =
comparative.data(TREE, PGLS_SET,
   Taxa), lambda = "ML")

Residuals:
     Min       1Q   Median       3Q      Max
-0.024605 -0.015154 -0.006615  0.013204
0.035892

Branch length transformations:

kappa  [Fix]  : 1.000
lambda [ ML]  : 0.881
  lower bound : 0.000, p = 0.054834
  upper bound : 1.000, p = 0.30621
  95.0% CI   : (NA, NA)
delta  [Fix]  : 1.000

Coefficients:
            Estimate Std. Error t value Pr(>|t|)
(Intercept) -0.037624   0.150292 -0.2503   0.8086
BM          -0.017006   0.037664 -0.4515   0.6636

Residual standard error: 0.02114 on 8 degrees of
freedom
Multiple R-squared: 0.02485,    Adjusted R-
squared: -0.09704
F-statistic: 0.2039 on 1 and 8 DF,  p-value: 0.6636
```

> summary(PGLS_PC2_P1)

```
Call:
pgls(formula = PC2_P1 ~ BM, data =
comparative.data(TREE, PGLS_SET,
   Taxa), lambda = "ML")

Residuals:
     Min       1Q   Median       3Q      Max
-0.009156 -0.002379  0.001740  0.003318
0.009297

Branch length transformations:

kappa  [Fix]  : 1.000
lambda [ ML]  : 0.000
  lower bound : 0.000, p = 1
  upper bound : 1.000, p = 0.0011126
  95.0% CI   : (NA, 0.732)
delta  [Fix]  : 1.000

Coefficients:
            Estimate Std. Error t value  Pr(>|t|)
(Intercept) -0.4369699  0.0261694 -16.698 1.674e-
07 ***
BM           0.0662886  0.0057045  11.620 2.738e-06
***
---
Signif. codes:  0 ‘***’ 0.001 ‘**’ 0.01 ‘*’ 0.05 ‘.’ 0.1 ‘
’ 1

Residual standard error: 0.005883 on 8 degrees of
freedom
Multiple R-squared: 0.9441,     Adjusted R-squared:
0.9371
F-statistic:   135 on 1 and 8 DF,  p-value: 2.738e-06
```

> summary(PGLS_PC3_P1)

```
Call:
pgls(formula = PC3_P1 ~ BM, data =
comparative.data(TREE, PGLS_SET,
   Taxa), lambda = "ML")

Residuals:
     Min       1Q   Median       3Q      Max
-0.006125 -0.002075  0.001503  0.012584
0.020044

Branch length transformations:

kappa  [Fix]  : 1.000
lambda [ ML]  : 0.889
  lower bound : 0.000, p = 0.04705
  upper bound : 1.000, p = 0.33126
  95.0% CI   : (0.055, NA)
delta  [Fix]  : 1.000

Coefficients:
            Estimate Std. Error t value Pr(>|t|)
(Intercept)  0.323546   0.082575  3.9182  0.00443
**
BM          -0.063424   0.020700 -3.0640  0.01549 *
---
Signif. codes:  0 ‘***’ 0.001 ‘**’ 0.01 ‘*’ 0.05 ‘.’ 0.1 ‘
’ 1

Residual standard error: 0.0116 on 8 degrees of
freedom
Multiple R-squared: 0.5399,     Adjusted R-squared:
0.4824
F-statistic: 9.388 on 1 and 8 DF,  p-value: 0.01549
```

P2 analysis (semicircular canals or proboscideans)

> summary(PGLS_PC1_P2)

```
Call:
pgls(formula = PC1_P2 ~ BM, data =
comparative.data(TREE, PGLS_SET,
   Taxa), lambda = "ML")

Residuals:
      Min        1Q    Median        3Q       Max
-0.0130665 -0.0048281 -0.0003642  0.0035023
0.0157722

Branch length transformations:

kappa  [Fix]  : 1.000
lambda [ ML]  : 0.605
  lower bound : 0.000, p = 0.32693
  upper bound : 1.000, p = 0.11213
  95.0% CI   : (NA, NA)
delta  [Fix]  : 1.000

Coefficients:
            Estimate Std. Error t value  Pr(>|t|)
(Intercept) -0.324942   0.052791 -6.1553 3.458e-05
***
BM           0.043345   0.013010  3.3315  0.005409 **
---
Signif. codes:  0 ‘***’ 0.001 ‘**’ 0.01 ‘*’ 0.05 ‘.’ 0.1 ‘
’ 1

Residual standard error: 0.008443 on 13 degrees of
freedom
Multiple R-squared: 0.4606,     Adjusted R-squared:
0.4191
F-statistic:  11.1 on 1 and 13 DF,  p-value: 0.005409
```

> summary(PGLS_PC2_P2)

```
Call:
pgls(formula = PC2_P2 ~ BM, data =
comparative.data(TREE, PGLS_SET,
   Taxa), lambda = "ML")

Residuals:
     Min       1Q   Median       3Q      Max
-0.011725 -0.002827  0.002372  0.003692
0.011986

Branch length transformations:

kappa  [Fix]  : 1.000
lambda [ ML]  : 0.000
  lower bound : 0.000, p = 1
  upper bound : 1.000, p = 0.10516
  95.0% CI   : (NA, NA)
delta  [Fix]  : 1.000

Coefficients:
            Estimate Std. Error t value  Pr(>|t|)
(Intercept) -0.1973687  0.0245369 -8.0438 2.106e-
06 ***
BM           0.0296548  0.0051908  5.7130 7.137e-05
***
---
Signif. codes:  0 ‘***’ 0.001 ‘**’ 0.01 ‘*’ 0.05 ‘.’ 0.1 ‘
’ 1

Residual standard error: 0.006214 on 13 degrees of
freedom
Multiple R-squared: 0.7152,     Adjusted R-squared:
0.6932
F-statistic: 32.64 on 1 and 13 DF,  p-value: 7.137e-
05
```

> summary(PGLS_PC3_P2)

```
Call:
pgls(formula = PC3_P2 ~ BM, data =
comparative.data(TREE, PGLS_SET,
   Taxa), lambda = "ML")

Residuals:
     Min       1Q   Median       3Q      Max
-0.010280 -0.008040 -0.005321  0.004053
0.016030

Branch length transformations:

kappa  [Fix]  : 1.000
lambda [ ML]  : 0.741
  lower bound : 0.000, p = 0.048564
  upper bound : 1.000, p = 3.8919e-05
  95.0% CI   : (0.018, 0.941)
delta  [Fix]  : 1.000

Coefficients:
            Estimate Std. Error t value Pr(>|t|)
(Intercept)  0.155418   0.053955  2.8805  0.01288 *
BM          -0.032176   0.013406 -2.4002  0.03208 *
---
Signif. codes:  0 ‘***’ 0.001 ‘**’ 0.01 ‘*’ 0.05 ‘.’ 0.1 ‘
’ 1

Residual standard error: 0.008275 on 13 degrees of
freedom
Multiple R-squared: 0.3071,     Adjusted R-squared:
0.2538
F-statistic: 5.761 on 1 and 13 DF,  p-value: 0.03208
```

Appendix 23 – List of the characters used in the phylogenetic analyses of Chapter V

1. **Subarcuate fossa:** (0) deep; (1) shallow; (2) absent
2. **Internal auditory meatus:** (0) opens perpendicular to the cerebellar surface, (1) is oriented antero-posteriorly
3. **Perilymphatic foramen:** (0) divided into the *fenestra cochleae* and the *aquaeductus* cochleae during ontogeny, (1) retained in adults
4. **Mastoid apophysis:** (0) visible on the skull laterally, (1) amastoidy
5. **Shape of the *tegmen tympani*:** (0) poorly developed, (1) prominent and inflated prominent, (2) forming a flat and large cerebral surface
6. ***Hiatus Fallopii*:** (0) forms a discrete foramen within the petrosal; (1) forms a notch (fallopian notch)
7. **Petrosal pneumatization:** (0) absent, (1) present
8. **Prootic sinus:** (0) absent, (1) present
9. ***Crista falciformis*:** (0) thick, (1) thin
10. **Petromastoid canal:** (0) absent, (1) present
11. **Groove for the middle meningeal artery (or internal carotid artery**): (0) not visible on the petrosal, (1) large and deep, runs on the cerebral surface of the *tegmen tympani*
12. **Transpromontory sulcus**: (0) absent, (1) present
13. **Definition of the ampullae:** (0) well-defined and bulbous, (1) poorly defined
14. **Basal thickening of the *crus commune*:** (0) absent or slight,(1) pyramidal in shape
15. **Thickness of the *crus commune*:** (0) slender, thickness ratio < 15, (1) thick, thickness ratio > 15
16. **Meeting point of the anterior and posterior semicircular canals in the *crus commune*:** (0) high, (1) low
17. **Overall shape of the anterior canal:** (0) round, (1) oval
18. **Overall shape of the posterior canal:** (0) round, (1) oval
19. **Extension of the anterior canal apex:** (0) at the same level than the apex of the posterior canal, (1) higher than the apex of the posterior canal
20. **Position of the point of entry of the lateral semicircular canal into the vestibule:** (0) high and close to the posterior ampulla, (1) high and distant to the posterior ampulla, (2) low
21. **Shape of the semicircular canals in cross-section:** (0) circular, (1) flattened
22. **General thickness of the semicircular canals**: (0) slender canals, thickness ratio < 3, (1) thick canals, thickness ratio >3
23. **Relative size of the lateral canal:** (0) approximately same size than anterior and posterior canals (lateral canal ratio > 85%), (1) slightly smaller than other canals (72% < lateral canal ratio < 85%), (2) very small (lateral canal ratio < 72%)
24. **Contact between the lateral and posterior canals: (**0) the ampulla and the slender part of the posterior canal are fused with the lateral canal, (1) only the posterior ampulla is fused with the lateral canal, (2) the canals are not in contact
25. **Posterior expansion of the lateral canal:** (0) absent, (1) present, the lateral canal crosses the posterior canal plane
26. **Aspect ratio of the cochlea:** (0) superior to 0.6, (1) inferior to 0.6
27. **Number of turns of the cochlea:** (0) inferior to 3, (1) superior to 3
28. ***Lamina secundaria*:** (0) present, (1) absent
29. **Relative volume of the cochlea:** (0) superior to 55% of the total volume of the bony labyrinth, (1) inferior to 55%
30. **Point of entry of the *fenestra cochleae* and the *aquaeductus cochleae* within the *scala tympani*:** (0) distant to each other, (1) close to each other or fused
31. **Vestibulo-cochlear angle:** (0) right or acute angle (≤ 90°), (1) obtuse angle (90° < angle < 142°), (2) very obtuse angle (angle ≥ 142°)
32. **Axis of rotation of the apical turn of the cochlea with respect to the basal turn:** (0) both turns are centered, the axes are the same, (1) the axis of the apical turn is offset

Appendix 24 – Matrix used in the phylogenetic analysis of Chapter V focused on proboscideans

	1	2	3	4	5	6	7	8	9	10	11	12	13	14	15	16
Anancus	2	1	1	1	2	?	0	0	1	0	1	0	1	0	1	(01)
Cuvieronius	2	1	1	1	2	?	0	0	?	0	?	?	1	0	1	0
Elephas	2	1	1	1	2	0	(01)	0	1	0	1	0	1	0	1	(01)
Eritherium	0	0	0	?	1	?	1	?	0	0	0	0	0	0	0	?
Gomphotherium	2	1	1	1	2	?	0	0	1	0	1	0	1	1	(01)	0
Loxodonta	2	1	1	1	2	0	(01)	0	1	0	1	0	1	0	1	(01)
Mammut	2	1	1	1	2	?	0	0	?	0	?	0	1	0	1	(01)
Mammuthus columbi	2	1	1	1	2	?	0	0	?	0	?	?	1	0	1	1
Mammuthus primigenius	2	1	1	1	2	?	1	0	1	0	1	0	1	0	1	1
Moeritherium	2	0	1	1	?	?	(01)	?	1	0	?	0	0	0	?	0
Numidotherium	2	0	0	1	1	1	1	0	1	0	0	1	0	0	0	0
Ocepeia	0	0	0	1	1	?	1	0	0	1	0	0	0	0	1	0
Palaeoloxodon	2	1	1	1	2	?	0	0	?	0	1	?	1	0	1	0
Phosphatherium	1	0	0	1	?	0	0	0	1	1	?	0	0	0	0	0
Platybelodon	2	?	?	1	2	?	0	0	?	0	1	?	1	0	1	1
Prodeinotherium	2	1	1	1	2	?	0	0	?	0	?	0	1	0	1	0
Protungulatum	0	0	0	0	0	0	?	0	0	0	0	1	0	0	?	0
Stegodon	2	1	?	1	2	?	0	0	?	0	1	0	1	0	1	0
Stegomastodon	2	1	1	1	2	?	0	0	?	0	1	?	1	0	1	0

	17	18	19	20	21	22	23	24	25	26	27	28	29	30	31	32
Anancus	1	1	1	1	1	(01)	2	2	0	1	0	1	1	1	2	1
Cuvieronius	1	1	1	1	1	1	2	2	0	?	?	?	?	?	?	?
Elephas	1	0	1	2	1	1	(12)	1	0	1	0	1	1	1	2	1
Eritherium	0	0	?	0	0	0	1	0	0	1	0	0	1	?	1	0
Gomphotherium	(01)	1	1	1	1	1	2	2	0	1	0	1	1	1	1	1
Loxodonta	1	0	1	2	1	(01)	2	2	0	1	0	1	1	1	(12)	1
Mammut	1	1	1	0	1	1	2	1	0	1	0	1	1	1	1	1
Mammuthus columbi	1	0	1	2	1	1	2	2	0	?	?	?	?	?	?	?
Mammuthus primigenius	1	1	1	2	1	1	2	2	0	1	0	1	1	1	2	1
Moeritherium	1	1	(01)	?	1	?	?	?	?	?	0	?	?	?	?	?
Numidotherium	0	1	0	0	0	0	1	0	0	1	0	(01)	1	1	1	0
Ocepeia	0	0	1	0	0	0	1	1	0	0	0	0	0	1	1	0
Palaeoloxodon	1	0	1	2	1	1	1	1	0	?	?	?	?	?	?	?
Phosphatherium	0	0	0	0	0	0	1	0	0	?	0	0	0	1	1	?
Platybelodon	1	0	1	1	1	1	2	2	0	1	0	1	1	1	1	0
Prodeinotherium	1	0	1	1	1	0	1	2	0	1	0	1	1	1	1	1
Protungulatum	1	0	1	0	0	?	0	0	0	1	0	0	0	0	?	0
Stegodon	1	1	1	1	1	1	2	2	0	1	0	1	1	?	1	0
Stegomastodon	1	(01)	0	?	1	?	?	?	?	1	0	1	?	?	1	0

Appendix 25 – Matrix used in the phylogenetic analysis of Chapter V extended to afrotherians (page 1/2)

	1	2	3	4	5	6	7	8	9	10	11	12	13	14	15	16
Anancus	2	1	1	1	2	?	0	0	1	0	1	0	1	0	1	(01)
Arsinoitherium	2	0	1	1	1	1	1	0	1	0	0	0	0	0	0	0
Chambi sirenian	?	0	0	0	0	0	0	0	0	0	0	0	0	0	?	0
Chambius	0	0	0	?	?	0	?	0	0	?	0	1	0	0	?	0
Cuvieronius	2	1	1	1	2	?	0	0	?	0	?	?	1	0	1	0
Elephantimorpha Ekdale 2011	2	1	1	1	2	0	?	0	1	0	?	0	1	1	?	1
Elephas	2	1	1	1	2	0	(01)	0	1	0	1	0	1	0	1	(01)
Embrithopoda PM53	1	0	?	?	?	?	1	?	?	1	?	?	0	0	0	0
Eritherium	0	0	0	?	1	?	1	?	0	0	0	0	0	0	0	?
Gomphotherium	2	1	1	1	2	?	0	0	1	0	1	0	1	1	(01)	0
Helioseus	1	0	0	1	0	?	?	?	0	0	0	0	0	0	?	0
Kulbeckia	0	0	0	0	0	0	?	1	1	?	0	0	0	0	?	0
Loxodonta	2	1	1	1	2	0	(01)	0	1	0	1	0	1	0	1	(01)
Mammut	2	1	1	1	2	?	0	0	?	0	?	0	1	0	1	(01)
Mammuthus columbi	2	1	1	1	2	?	0	0	?	0	?	?	1	0	1	1
Mammuthus primigenius	2	1	1	1	2	?	1	0	1	0	1	0	1	0	1	1
Moeritherium	2	0	1	1	?	?	(01)	?	1	0	?	0	0	0	?	0
Numidotherium	2	0	0	1	1	1	1	0	1	0	0	1	0	0	0	0
Ocepeia	0	0	0	1	1	?	1	0	0	1	0	0	0	0	1	0
Palaeoloxodon	2	1	1	1	2	?	0	0	?	0	1	?	1	0	1	0
Phosphatherium	1	0	0	1	?	0	0	0	1	1	?	0	0	0	0	0
Platybelodon	2	?	?	1	2	?	0	0	?	0	1	?	1	0	1	1
Plesiorycteropus	1	0	0	?	?	?	?	?	0	0	0	?	0	0	?	1
Prodeinotherium	2	1	1	1	2	?	0	0	?	0	?	0	1	0	1	0
Prorastomus	2	0	0	0	1	1	0	0	1	?	0	0	0	0	?	0
Protungulatum	0	0	0	0	0	0	?	0	0	0	0	1	0	0	?	0
Seggeurius	1	0	0	0	0	?	0	0	0	1	0	1	0	0	?	0
Stegodon	2	1	?	1	2	?	0	0	?	0	1	0	1	0	1	0
Stegomastodon	2	1	1	1	2	?	0	0	?	0	1	?	1	0	1	0
Titanohyrax	1	0	0	?	0	?	?	?	0	?	0	0	0	0	?	0

Appendix 25 – Matrix used in the phylogenetic analysis of Chapter V extended to afrotherians (page 2/2)

	17	18	19	20	21	22	23	24	25	26	27	28	29	30	31	32
Anancus	1	1	1	1	1	(01)	2	2	0	1	0	1	1	1	2	1
Arsinoitherium	0	1	0	0	1	1	1	1	0	1	0	1	?	?	1	0
Chambi sirenian	0	0	0	0	0	0	0	0	0	0	0	1	0	?	1	0
Chambius	0	1	?	0	0	?	0	0	0	0	0	0	0	0	?	0
Cuvieronius	1	1	1	1	1	1	2	2	0	?	?	?	?	?	?	?
Elephantimorpha	?	1	1	1	1	?	2	2	0	1	0	1	?	1	?	?
Elephas	1	0	1	2	1	1	(12)	1	0	1	0	1	1	1	2	1
Embrithopoda PM53	0	0	0	0	0	0	2	1	0	?	?	0	?	?	?	?
Eritherium	0	0	?	0	0	0	1	0	0	1	0	0	1	?	1	0
Gomphotherium	(01)	1	1	1	1	1	2	2	0	1	0	1	1	1	1	1
Helioseus	0	1	1	0	0	?	0	2	0	1	0	?	?	?	1	?
Kulbeckia	1	?	1	0	0	?	0	0	0	1	0	0	1	?	?	?
Loxodonta	1	0	1	2	1	(01)	2	2	0	1	0	1	1	1	(12)	1
Mammut	1	1	1	0	1	1	2	1	0	1	0	1	1	1	1	1
M. columbi	1	0	1	2	1	1	2	2	0	?	?	?	?	?	?	?
M. primigenius	1	1	1	2	1	1	2	2	0	1	0	1	1	1	2	1
Moeritherium	1	1	(01)	?	1	?	?	?	?	?	0	?	?	?	?	?
Numidotherium	0	1	0	0	0	0	1	0	0	1	0	(01)	1	1	1	0
Ocepeia	0	0	1	0	0	0	1	1	0	0	0	0	0	1	1	0
Palaeoloxodon	1	0	1	2	1	1	1	1	0	?	?	?	?	?	?	?
Phosphatherium	0	0	0	0	0	0	1	0	0	?	0	0	0	1	1	?
Platybelodon	1	0	1	1	1	1	2	2	0	1	0	1	1	1	1	0
Plesiorycteropus	0	0	(01)	0	0	?	0	(01)	0	0	0	0	?	?	?	0
Prodeinotherium	1	0	1	1	1	0	1	2	0	1	0	1	1	1	1	1
Prorastomus	0	1	0	0	0	?	0	1	0	1	0	1	1	1	1	0
Protungulatum	1	0	1	0	0	?	0	0	0	1	0	0	0	0	?	0
Seggeurius	0	1	1	0	1	?	1	1	0	1	0	0	0	1	1	1
Stegodon	1	1	1	1	1	1	2	2	0	1	0	1	1	?	1	0
Stegomastodon	1	(01)	0	?	1	?	?	?	?	1	0	1	?	?	1	0
Titanohyrax	0	0	0	0	?	?	0	1	0	0	0	?	?	?	1	0

Appendix 26 – Parameters of the phylogenetic characters used in the analysis focused on the Proboscidea. 'NI' is for not informative.

Character	Steps	CI	RI
1	3	0.667	0.800
2	1	1	1.000
3	1	1	1.000
4	1	NI	NI
5	2	1	1.000
6	1	1	NI
7	3	0.333	0.333
8	0	NI	NI
9	1	1	1.000
10	2	0.5	0.000
11	1	1	1.000
12	2	0.5	0.000
13	1	1	1.000
14	1	NI	NI
15	2	0.5	0.500
16	3	0.333	0.000
17	2	0.5	0.667
18	8	0.125	0.000
19	2	0.5	0.500
20	7	0.286	0.444
21	1	1	1.000
22	2	0.5	0.750
23	4	0.5	0.667
24	6	0.333	0.600
25	0	NI	NI
26	1	NI	NI
27	0	NI	NI
28	1	1	1.000
29	3	0.333	0.000
30	1	NI	NI
31	3	0.333	0.000
32	3	0.333	0.667

Appendix 27 – Strict consensus of the 18 most parsimonious trees obtained for the implied weighting analysis performed on proboscideans. Length = 66; CI = 0.579; RI = 0.922. Except for the implied weighting, the parameters of the analysis are the same as the unweighted analysis presented in Chapter V. The software TNT was used instead of PAUP. The multi-state characters are ordered.

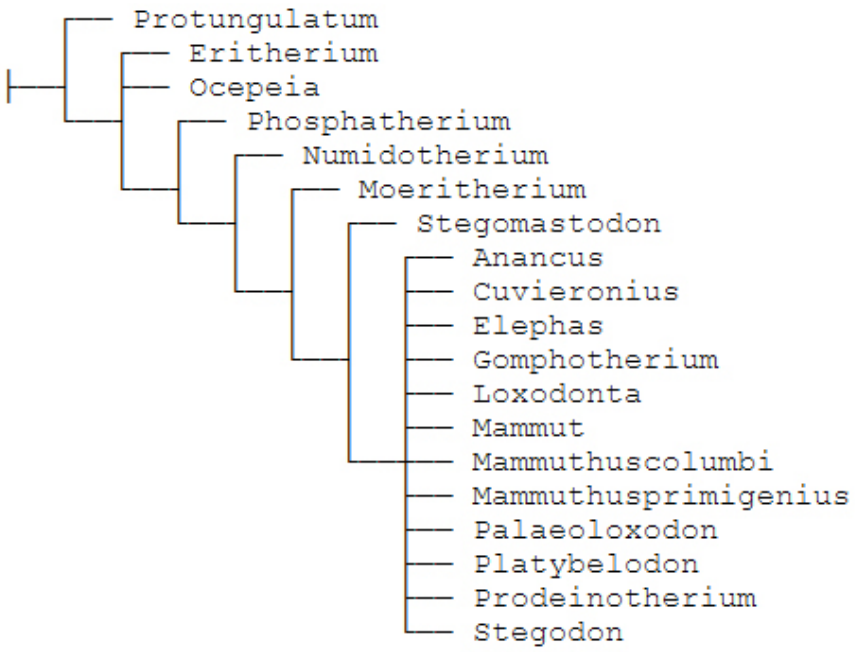

Appendix 28A – Parameters of the phylogenetic characters used in the unweighted analysis extended to the Afrotheria. 'NI' is for not informative.

Character	Steps	CI	RI
1	6	0	0.71
2	1	1	1
3	1	1	1
4	5	0	0
5	4	1	0.86
6	2	1	0.5
7	6	0	0
8	1	NI	NI
9	3	0	0.75
10	4	0	0
11	1	1	1
12	4	0	0
13	1	1	1
14	2	1	0
15	2	1	0.75
16	5	0	0
17	3	0	0.83
18	10	0	0.3
19	6	0	0.28
20	7	0	0.66
21	2	1	0.9
22	2	1	0.83
23	11	0	0.47
24	12	0	0.37
25	0	NI	NI
26	5	0	0
27	0	NI	NI
28	2	1	0.85
29	3	0	0.6
30	2	1	0
31	3	0	0
32	4	0	0.57

Appendix 28B – Parameters of the phylogenetic characters used in the implied weighting analysis extended to the Afrotheria. 'NI' is for not informative.

Character	Steps	CI	RI
1	5	0	0.78
2	1	1	1
3	1	1	1
4	3	0	0.5
5	2	1	1
6	2	1	0.5
7	5	0	0.2
8	1	NI	NI
9	3	0	0.75
10	4	0	0
11	1	1	1
12	4	0	0
13	1	1	1
14	1	1	1
15	2	1	0.75
16	5	0	0
17	2	1	0.91
18	8	0	0.46
19	5	0	0.42
20	2	1	1
21	2	1	0.9
22	2	1	0.83
23	7	0	0.7
24	9	0	0.56
25	0	NI	NI
26	5	0	0
27	0	NI	NI
28	2	1	0.87
29	3	0	0.6
30	2	1	0
31	2	1	0.5
32	4	0	0.57

Appendix 29 – Phylogenetic tree used to infer the functional capacities of extinct and extant afrotherians and proboscideans

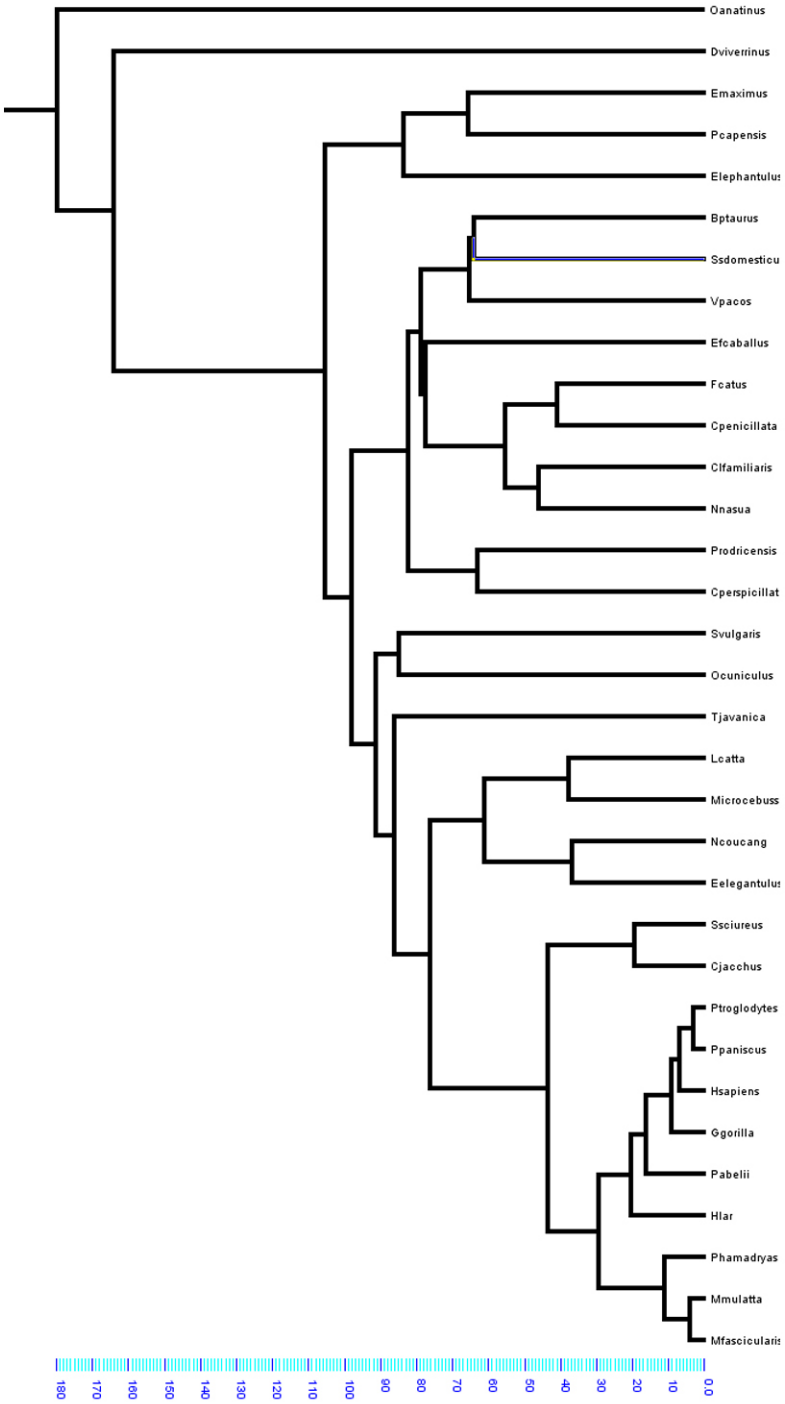

Appendix 30 – Script used to infer the functional capacities of extinct and extant proboscideans and afrotherians with R (7 pages)

```
################### Loading libraries ###################


library(phytools)
library(caper)
library(geiger)
library(rgl)
library(calibrate)
library(MASS)
library(geometry)


################### Loading functions ###################


joint.lambda<-function(tree,X){
  result<-optimize(f=likMlambda,X=X,C=vcv(tree),interval=c(0,1),     maximum=TRUE)
  return(list(lambda=result$maximum,logL=result$objective[1]))
}


################### Loading raw datasets ###################


DATA_AVERAGE = read.table("Path_to/RData_BonyMemb_Arnaud.txt", header = TRUE)
DATA_BONY = read.table("Path_to/RData_BonyEstimation_Arnaud.txt", header = TRUE)
TREE = read.nexus("Path_to/MammalTreeComplete.nex")


################### Check for missing specimens in tree/datasets ###################


TEST = name.check(TREE, data.names = DATA_AVERAGE[,1])
TREE = drop.tip(TREE, TEST$tree_not_data)


################### Preparing sub datasets ###################


Names_AVERAGE = DATA_AVERAGE[,1, drop=FALSE]
Morpho_AVERAGE = DATA_AVERAGE[,2:15]
Function_AVERAGE = DATA_AVERAGE[,16:30]

Function_Subset_AVERAGE =
cbind(Function_AVERAGE[,3],rowMeans(Function_AVERAGE[,1:2]),rowMeans(Function_AVERAGE[,1:3]),Functi
on_AVERAGE[,6],rowMeans(Function_AVERAGE[,4:5]),
rowMeans(Function_AVERAGE[,4:6]),Function_AVERAGE[,9],rowMeans(Function_AVERAGE[,7:8]),rowMeans(F
unction_AVERAGE[,7:9]),Function_AVERAGE[,12],rowMeans(Function_AVERAGE[,10:11]),rowMeans(Function_
AVERAGE[,10:12]),
Function_AVERAGE[,15],rowMeans(Function_AVERAGE[,13:14]),rowMeans(Function_AVERAGE[,13:15]))

colnames(Function_Subset_AVERAGE)=c("T1_H", "T1_V", "T1_M", "T2_H", "T2_V", "T2_M", "w0_H", "w0_V",
"w0_M", "VG_H", "VG_V", "VG_M", "AG_H", "AG_V", "AG_M")
```

```
Names_BONY = DATA_BONY[,1, drop=FALSE]
Morpho_BONY = DATA_BONY[,2:15]


################### Log transformation of some datasets ####################


Morpho_AVERAGE_LOG = log10(Morpho_AVERAGE)
Morpho_BONY_LOG = log10(Morpho_BONY)

Function_Subset_AVERAGE_LOG = log10(Function_Subset_AVERAGE)


################### PCA on "bony" morphology of CEB specimens ####################


joint.lambda(TREE,as.matrix(Morpho_AVERAGE_LOG)) # If Lambda is close to 0, a classic PCA is doable, if not use phyl.pca

PCA_Morpho_AVERAGE_LOG = prcomp(Morpho_AVERAGE_LOG,scale.=TRUE)
#summary(PCA_Morpho_AVERAGE_LOG)
#PCA_Morpho_AVERAGE_LOG

PCA_Morpho_BONY_LOG_x = predict(PCA_Morpho_AVERAGE_LOG, Morpho_BONY_LOG)


############## Phylogenetic regression of membranous parameters onto "bony" morphology ##############


PGLS_SET = cbind(Names_AVERAGE,Function_Subset_AVERAGE_LOG, Morpho_AVERAGE_LOG,
PCA_Morpho_AVERAGE_LOG$x[,1:5])

PGLS_T1_H = pgls(T1_H~PC1+PC2+PC3+PC4,comparative.data(TREE,PGLS_SET,B_Taxa),lambda = "ML")
PGLS_T1_V = pgls(T1_V~PC1+PC2,comparative.data(TREE,PGLS_SET,B_Taxa),lambda = "ML")
PGLS_T1_M = pgls(T1_M~PC1+PC2,comparative.data(TREE,PGLS_SET,B_Taxa),lambda = "ML")
PGLS_T2_H = pgls(T2_H~PC1+PC2+PC3+PC4+PC5,comparative.data(TREE,PGLS_SET,B_Taxa),lambda = "ML")
PGLS_T2_V = pgls(T2_V~PC1+PC2+PC3+PC4+PC5,comparative.data(TREE,PGLS_SET,B_Taxa),lambda = "ML")
PGLS_T2_M = pgls(T2_M~PC1+PC2+PC3+PC4+PC5,comparative.data(TREE,PGLS_SET,B_Taxa),lambda = "ML")
PGLS_w0_H = pgls(w0_H~PC1+PC2+PC3,comparative.data(TREE,PGLS_SET,B_Taxa),lambda = "ML")
PGLS_w0_V = pgls(w0_V~PC1+PC2,comparative.data(TREE,PGLS_SET,B_Taxa),lambda = "ML")
PGLS_w0_M = pgls(w0_M~PC1+PC2+PC3,comparative.data(TREE,PGLS_SET,B_Taxa),lambda = "ML")
PGLS_VG_H = pgls(VG_H~PC1,comparative.data(TREE,PGLS_SET,B_Taxa),lambda = "ML")
PGLS_VG_V = pgls(VG_V~PC1+PC2+PC3+PC4+PC5,comparative.data(TREE,PGLS_SET,B_Taxa),lambda = "ML")
PGLS_VG_M = pgls(VG_M~PC1+PC2+PC3+PC4+PC5,comparative.data(TREE,PGLS_SET,B_Taxa),lambda = "ML")
PGLS_AG_H = pgls(AG_H~PC1+PC2+PC3,comparative.data(TREE,PGLS_SET,B_Taxa),lambda = "ML")
PGLS_AG_V = pgls(AG_V~PC1+PC2+PC3+PC4+PC5,comparative.data(TREE,PGLS_SET,B_Taxa),lambda = "ML")
PGLS_AG_M = pgls(AG_M~PC1+PC2+PC3+PC4+PC5,comparative.data(TREE,PGLS_SET,B_Taxa),lambda = "ML")

PGLS_T1_H$aicc
PGLS_T1_V$aicc
PGLS_T1_M$aicc
PGLS_T2_H$aicc
PGLS_T2_V$aicc
PGLS_T2_M$aicc
PGLS_w0_H$aicc
PGLS_w0_V$aicc
```

```
PGLS_w0_M$aicc
PGLS_VG_H$aicc
PGLS_VG_V$aicc
PGLS_VG_M$aicc
PGLS_AG_H$aicc
PGLS_AG_V$aicc
PGLS_AG_M$aicc

summary(PGLS_T1_H)
summary(PGLS_T1_V)
summary(PGLS_T1_M)
summary(PGLS_T2_H)
summary(PGLS_T2_V)
summary(PGLS_T2_M)
summary(PGLS_w0_H)
summary(PGLS_w0_V)
summary(PGLS_w0_M)
summary(PGLS_VG_H)
summary(PGLS_VG_V)
summary(PGLS_VG_M)
summary(PGLS_AG_H)
summary(PGLS_AG_V)
summary(PGLS_AG_M)


################## Computation of fitted function parameters for BONY specimens ####################

plot(TREE)
nodelabels()

Fitted_Function_BONY_LOG =
 cbind((predict(PGLS_T1_H,
as.data.frame(PCA_Morpho_BONY_LOG_x[,1:4]))+fastAnc(TREE,PGLS_T1_H$residuals,CI=TRUE)$ace[4]),
(predict(PGLS_T1_V,
as.data.frame(PCA_Morpho_BONY_LOG_x[,1:2]))+fastAnc(TREE,PGLS_T1_V$residuals,CI=TRUE)$ace[4]),
(predict(PGLS_T1_M,
as.data.frame(PCA_Morpho_BONY_LOG_x[,1:2]))+fastAnc(TREE,PGLS_T1_M$residuals,CI=TRUE)$ace[4]),
 (predict(PGLS_T2_H,
as.data.frame(PCA_Morpho_BONY_LOG_x[,1:5]))+fastAnc(TREE,PGLS_T2_H$residuals,CI=TRUE)$ace[4]),
predict(PGLS_T2_V,
as.data.frame(PCA_Morpho_BONY_LOG_x[,1:5]))+fastAnc(TREE,PGLS_T2_V$residuals,CI=TRUE)$ace[4]),
predict(PGLS_T2_M,
as.data.frame(PCA_Morpho_BONY_LOG_x[,1:5]))+fastAnc(TREE,PGLS_T2_M$residuals,CI=TRUE)$ace[4]),
(predict(PGLS_w0_H,
as.data.frame(PCA_Morpho_BONY_LOG_x[,1:3]))+fastAnc(TREE,PGLS_w0_H$residuals,CI=TRUE)$ace[4]),
(predict(PGLS_w0_V,
as.data.frame(PCA_Morpho_BONY_LOG_x[,1:2]))+fastAnc(TREE,PGLS_w0_V$residuals,CI=TRUE)$ace[4]),
(predict(PGLS_w0_M,
as.data.frame(PCA_Morpho_BONY_LOG_x[,1:3]))+fastAnc(TREE,PGLS_w0_M$residuals,CI=TRUE)$ace[4]),
(predict(PGLS_VG_H, as.data.frame(PCA_Morpho_BONY_LOG_x[,1,
drop=FALSE]))+fastAnc(TREE,PGLS_VG_H$residuals,CI=TRUE)$ace[4]),
(predict(PGLS_VG_V,
as.data.frame(PCA_Morpho_BONY_LOG_x[,1:5]))+fastAnc(TREE,PGLS_VG_V$residuals,CI=TRUE)$ace[4]),
(predict(PGLS_VG_M,
as.data.frame(PCA_Morpho_BONY_LOG_x[,1:5]))+fastAnc(TREE,PGLS_VG_M$residuals,CI=TRUE)$ace[4]),
 (predict(PGLS_AG_H,
as.data.frame(PCA_Morpho_BONY_LOG_x[,1:3]))+fastAnc(TREE,PGLS_AG_H$residuals,CI=TRUE)$ace[4]),
```

```
 (predict(PGLS_AG_V,
as.data.frame(PCA_Morpho_BONY_LOG_x[,1:5]))+fastAnc(TREE,PGLS_AG_V$residuals,CI=TRUE)$ace[4]),
(predict(PGLS_AG_M,
as.data.frame(PCA_Morpho_BONY_LOG_x[,1:5]))+fastAnc(TREE,PGLS_AG_M$residuals,CI=TRUE)$ace[4]))

fastAnc(TREE,PGLS_T1_H$residuals,CI=TRUE)$CI95[4,1] fastAnc(TREE,PGLS_T1_H$residuals,CI=TRUE)$CI95[4,2]
fastAnc(TREE,PGLS_T1_H$residuals,CI=TRUE)$ace[4]

Fitted_Function_BONY = 10^(Fitted_Function_BONY_LOG)

Fitted_Function_AVERAGE_LOG = cbind((predict(PGLS_T1_H,
as.data.frame(PCA_Morpho_AVERAGE_LOG$x[,1:4]))+fastAnc(TREE,PGLS_T1_H$residuals,CI=TRUE)$ace[4]),
predict(PGLS_T1_V,
as.data.frame(PCA_Morpho_AVERAGE_LOG$x[,1:2]))+fastAnc(TREE,PGLS_T1_V$residuals,CI=TRUE)$ace[4]),
 (predict(PGLS_T1_M,
as.data.frame(PCA_Morpho_AVERAGE_LOG$x[,1:2]))+fastAnc(TREE,PGLS_T1_M$residuals,CI=TRUE)$ace[4]),
 (predict(PGLS_T2_H,
as.data.frame(PCA_Morpho_AVERAGE_LOG$x[,1:5]))+fastAnc(TREE,PGLS_T2_H$residuals,CI=TRUE)$ace[4]),
 (predict(PGLS_T2_V,
as.data.frame(PCA_Morpho_AVERAGE_LOG$x[,1:5]))+fastAnc(TREE,PGLS_T2_V$residuals,CI=TRUE)$ace[4]),
(predict(PGLS_T2_M,
as.data.frame(PCA_Morpho_AVERAGE_LOG$x[,1:5]))+fastAnc(TREE,PGLS_T2_M$residuals,CI=TRUE)$ace[4]),
(predict(PGLS_w0_H,
as.data.frame(PCA_Morpho_AVERAGE_LOG$x[,1:3]))+fastAnc(TREE,PGLS_w0_H$residuals,CI=TRUE)$ace[4]),
 (predict(PGLS_w0_V,
as.data.frame(PCA_Morpho_AVERAGE_LOG$x[,1:2]))+fastAnc(TREE,PGLS_w0_V$residuals,CI=TRUE)$ace[4]),
(predict(PGLS_w0_M,
as.data.frame(PCA_Morpho_AVERAGE_LOG$x[,1:3]))+fastAnc(TREE,PGLS_w0_M$residuals,CI=TRUE)$ace[4]),
 (predict(PGLS_VG_H, as.data.frame(PCA_Morpho_AVERAGE_LOG$x[,1,
drop=FALSE]))+fastAnc(TREE,PGLS_VG_H$residuals,CI=TRUE)$ace[4]),
(predict(PGLS_VG_V,
as.data.frame(PCA_Morpho_AVERAGE_LOG$x[,1:5]))+fastAnc(TREE,PGLS_VG_V$residuals,CI=TRUE)$ace[4]),
(predict(PGLS_VG_M,
as.data.frame(PCA_Morpho_AVERAGE_LOG$x[,1:5]))+fastAnc(TREE,PGLS_VG_M$residuals,CI=TRUE)$ace[4]),
 (predict(PGLS_AG_H,
as.data.frame(PCA_Morpho_AVERAGE_LOG$x[,1:3]))+fastAnc(TREE,PGLS_AG_H$residuals,CI=TRUE)$ace[4]),
(predict(PGLS_AG_V,
as.data.frame(PCA_Morpho_AVERAGE_LOG$x[,1:5]))+fastAnc(TREE,PGLS_AG_V$residuals,CI=TRUE)$ace[4]),
 (predict(PGLS_AG_M,
as.data.frame(PCA_Morpho_AVERAGE_LOG$x[,1:5]))+fastAnc(TREE,PGLS_AG_M$residuals,CI=TRUE)$ace[4]))


Fitted_Function_AVERAGE = 10^(Fitted_Function_AVERAGE_LOG)

Lower_Function_BONY_LOG = cbind((predict(PGLS_T1_H,
as.data.frame(PCA_Morpho_BONY_LOG_x[,1:4]))+fastAnc(TREE,PGLS_T1_H$residuals,CI=TRUE)$CI95[4,1]),
 (predict(PGLS_T1_V,
as.data.frame(PCA_Morpho_BONY_LOG_x[,1:2]))+fastAnc(TREE,PGLS_T1_V$residuals,CI=TRUE)$CI95[4,1]),
(predict(PGLS_T1_M,
as.data.frame(PCA_Morpho_BONY_LOG_x[,1:2]))+fastAnc(TREE,PGLS_T1_M$residuals,CI=TRUE)$CI95[4,1]),
 (predict(PGLS_T2_H,
as.data.frame(PCA_Morpho_BONY_LOG_x[,1:5]))+fastAnc(TREE,PGLS_T2_H$residuals,CI=TRUE)$CI95[4,1]),
(predict(PGLS_T2_V,
as.data.frame(PCA_Morpho_BONY_LOG_x[,1:5]))+fastAnc(TREE,PGLS_T2_V$residuals,CI=TRUE)$CI95[4,1]),
(predict(PGLS_T2_M,
as.data.frame(PCA_Morpho_BONY_LOG_x[,1:5]))+fastAnc(TREE,PGLS_T2_M$residuals,CI=TRUE)$CI95[4,1]),
```

```
(predict(PGLS_w0_H,
as.data.frame(PCA_Morpho_BONY_LOG_x[,1:3]))+fastAnc(TREE,PGLS_w0_H$residuals,CI=TRUE)$CI95[4,1]),
(predict(PGLS_w0_V,
as.data.frame(PCA_Morpho_BONY_LOG_x[,1:2]))+fastAnc(TREE,PGLS_w0_V$residuals,CI=TRUE)$CI95[4,1]),
(predict(PGLS_w0_M,
as.data.frame(PCA_Morpho_BONY_LOG_x[,1:3]))+fastAnc(TREE,PGLS_w0_M$residuals,CI=TRUE)$CI95[4,1]),
 (predict(PGLS_VG_H, as.data.frame(PCA_Morpho_BONY_LOG_x[,1,
drop=FALSE]))+fastAnc(TREE,PGLS_VG_H$residuals,CI=TRUE)$CI95[4,1]),
(predict(PGLS_VG_V,
as.data.frame(PCA_Morpho_BONY_LOG_x[,1:5]))+fastAnc(TREE,PGLS_VG_V$residuals,CI=TRUE)$CI95[4,1]),
 (predict(PGLS_VG_M,
as.data.frame(PCA_Morpho_BONY_LOG_x[,1:5]))+fastAnc(TREE,PGLS_VG_M$residuals,CI=TRUE)$CI95[4,1]),
 (predict(PGLS_AG_H,
as.data.frame(PCA_Morpho_BONY_LOG_x[,1:3]))+fastAnc(TREE,PGLS_AG_H$residuals,CI=TRUE)$CI95[4,1]),
 (predict(PGLS_AG_V,
as.data.frame(PCA_Morpho_BONY_LOG_x[,1:5]))+fastAnc(TREE,PGLS_AG_V$residuals,CI=TRUE)$CI95[4,1]),
(predict(PGLS_AG_M,
as.data.frame(PCA_Morpho_BONY_LOG_x[,1:5]))+fastAnc(TREE,PGLS_AG_M$residuals,CI=TRUE)$CI95[4,1]))

Lower_Function_BONY = 10^(Lower_Function_BONY_LOG)

Lower_Function_AVERAGE_LOG = cbind((predict(PGLS_T1_H,
as.data.frame(PCA_Morpho_AVERAGE_LOG$x[,1:4]))+fastAnc(TREE,PGLS_T1_H$residuals,CI=TRUE)$CI95[4,1]),
 (predict(PGLS_T1_V,
as.data.frame(PCA_Morpho_AVERAGE_LOG$x[,1:2]))+fastAnc(TREE,PGLS_T1_V$residuals,CI=TRUE)$CI95[4,1]),
(predict(PGLS_T1_M,
as.data.frame(PCA_Morpho_AVERAGE_LOG$x[,1:2]))+fastAnc(TREE,PGLS_T1_M$residuals,CI=TRUE)$CI95[4,1])
,
 (predict(PGLS_T2_H,
as.data.frame(PCA_Morpho_AVERAGE_LOG$x[,1:5]))+fastAnc(TREE,PGLS_T2_H$residuals,CI=TRUE)$CI95[4,1]),
predict(PGLS_T2_V,
as.data.frame(PCA_Morpho_AVERAGE_LOG$x[,1:5]))+fastAnc(TREE,PGLS_T2_V$residuals,CI=TRUE)$CI95[4,1]),
(predict(PGLS_T2_M,
as.data.frame(PCA_Morpho_AVERAGE_LOG$x[,1:5]))+fastAnc(TREE,PGLS_T2_M$residuals,CI=TRUE)$CI95[4,1])
,
(predict(PGLS_w0_H,
as.data.frame(PCA_Morpho_AVERAGE_LOG$x[,1:3]))+fastAnc(TREE,PGLS_w0_H$residuals,CI=TRUE)$CI95[4,1])
,
(predict(PGLS_w0_V,
as.data.frame(PCA_Morpho_AVERAGE_LOG$x[,1:2]))+fastAnc(TREE,PGLS_w0_V$residuals,CI=TRUE)$CI95[4,1])
,
 (predict(PGLS_w0_M,
as.data.frame(PCA_Morpho_AVERAGE_LOG$x[,1:3]))+fastAnc(TREE,PGLS_w0_M$residuals,CI=TRUE)$CI95[4,1]
),
 (predict(PGLS_VG_H, as.data.frame(PCA_Morpho_AVERAGE_LOG$x[,1,
drop=FALSE]))+fastAnc(TREE,PGLS_VG_H$residuals,CI=TRUE)$CI95[4,1]),
 (predict(PGLS_VG_V,
as.data.frame(PCA_Morpho_AVERAGE_LOG$x[,1:5]))+fastAnc(TREE,PGLS_VG_V$residuals,CI=TRUE)$CI95[4,1])
,
(predict(PGLS_VG_M,
as.data.frame(PCA_Morpho_AVERAGE_LOG$x[,1:5]))+fastAnc(TREE,PGLS_VG_M$residuals,CI=TRUE)$CI95[4,1]
),
 (predict(PGLS_AG_H,
as.data.frame(PCA_Morpho_AVERAGE_LOG$x[,1:3]))+fastAnc(TREE,PGLS_AG_H$residuals,CI=TRUE)$CI95[4,1])
,
```

```
(predict(PGLS_AG_V,
as.data.frame(PCA_Morpho_AVERAGE_LOG$x[,1:5]))+fastAnc(TREE,PGLS_AG_V$residuals,CI=TRUE)$CI95[4,1])
,
(predict(PGLS_AG_M,
as.data.frame(PCA_Morpho_AVERAGE_LOG$x[,1:5]))+fastAnc(TREE,PGLS_AG_M$residuals,CI=TRUE)$CI95[4,1]
))

Lower_Function_AVERAGE = 10^(Lower_Function_AVERAGE_LOG)

Upper_Function_BONY_LOG = cbind((predict(PGLS_T1_H,
as.data.frame(PCA_Morpho_BONY_LOG_x[,1:4]))+fastAnc(TREE,PGLS_T1_H$residuals,CI=TRUE)$CI95[4,2]),
 (predict(PGLS_T1_V,
as.data.frame(PCA_Morpho_BONY_LOG_x[,1:2]))+fastAnc(TREE,PGLS_T1_V$residuals,CI=TRUE)$CI95[4,2]),
(predict(PGLS_T1_M,
as.data.frame(PCA_Morpho_BONY_LOG_x[,1:2]))+fastAnc(TREE,PGLS_T1_M$residuals,CI=TRUE)$CI95[4,2]),
 (predict(PGLS_T2_H,
as.data.frame(PCA_Morpho_BONY_LOG_x[,1:5]))+fastAnc(TREE,PGLS_T2_H$residuals,CI=TRUE)$CI95[4,2]),
 (predict(PGLS_T2_V,
as.data.frame(PCA_Morpho_BONY_LOG_x[,1:5]))+fastAnc(TREE,PGLS_T2_V$residuals,CI=TRUE)$CI95[4,2]),
(predict(PGLS_T2_M,
as.data.frame(PCA_Morpho_BONY_LOG_x[,1:5]))+fastAnc(TREE,PGLS_T2_M$residuals,CI=TRUE)$CI95[4,2]),
 (predict(PGLS_w0_H,
as.data.frame(PCA_Morpho_BONY_LOG_x[,1:3]))+fastAnc(TREE,PGLS_w0_H$residuals,CI=TRUE)$CI95[4,2]),
(predict(PGLS_w0_V,
as.data.frame(PCA_Morpho_BONY_LOG_x[,1:2]))+fastAnc(TREE,PGLS_w0_V$residuals,CI=TRUE)$CI95[4,2]),
(predict(PGLS_w0_M,
as.data.frame(PCA_Morpho_BONY_LOG_x[,1:3]))+fastAnc(TREE,PGLS_w0_M$residuals,CI=TRUE)$CI95[4,2]),
 (predict(PGLS_VG_H, as.data.frame(PCA_Morpho_BONY_LOG_x[,1,
drop=FALSE]))+fastAnc(TREE,PGLS_VG_H$residuals,CI=TRUE)$CI95[4,2]),
 (predict(PGLS_VG_V,
as.data.frame(PCA_Morpho_BONY_LOG_x[,1:5]))+fastAnc(TREE,PGLS_VG_V$residuals,CI=TRUE)$CI95[4,2]),
(predict(PGLS_VG_M,
as.data.frame(PCA_Morpho_BONY_LOG_x[,1:5]))+fastAnc(TREE,PGLS_VG_M$residuals,CI=TRUE)$CI95[4,2]),
 (predict(PGLS_AG_H,
as.data.frame(PCA_Morpho_BONY_LOG_x[,1:3]))+fastAnc(TREE,PGLS_AG_H$residuals,CI=TRUE)$CI95[4,2]),
 (predict(PGLS_AG_V,
as.data.frame(PCA_Morpho_BONY_LOG_x[,1:5]))+fastAnc(TREE,PGLS_AG_V$residuals,CI=TRUE)$CI95[4,2]),
(predict(PGLS_AG_M,
as.data.frame(PCA_Morpho_BONY_LOG_x[,1:5]))+fastAnc(TREE,PGLS_AG_M$residuals,CI=TRUE)$CI95[4,2]))

Upper_Function_BONY = 10^(Upper_Function_BONY_LOG)

Upper_Function_AVERAGE_LOG = cbind((predict(PGLS_T1_H,
as.data.frame(PCA_Morpho_AVERAGE_LOG$x[,1:4]))+fastAnc(TREE,PGLS_T1_H$residuals,CI=TRUE)$CI95[4,2]),
 (predict(PGLS_T1_V,
as.data.frame(PCA_Morpho_AVERAGE_LOG$x[,1:2]))+fastAnc(TREE,PGLS_T1_V$residuals,CI=TRUE)$CI95[4,2]),
 (predict(PGLS_T1_M,
as.data.frame(PCA_Morpho_AVERAGE_LOG$x[,1:2]))+fastAnc(TREE,PGLS_T1_M$residuals,CI=TRUE)$CI95[4,2])
,
 (predict(PGLS_T2_H,
as.data.frame(PCA_Morpho_AVERAGE_LOG$x[,1:5]))+fastAnc(TREE,PGLS_T2_H$residuals,CI=TRUE)$CI95[4,2]),
 (predict(PGLS_T2_V,
as.data.frame(PCA_Morpho_AVERAGE_LOG$x[,1:5]))+fastAnc(TREE,PGLS_T2_V$residuals,CI=TRUE)$CI95[4,2]),
(predict(PGLS_T2_M,
as.data.frame(PCA_Morpho_AVERAGE_LOG$x[,1:5]))+fastAnc(TREE,PGLS_T2_M$residuals,CI=TRUE)$CI95[4,2])
,
```

```
(predict(PGLS_w0_H,
as.data.frame(PCA_Morpho_AVERAGE_LOG$x[,1:3]))+fastAnc(TREE,PGLS_w0_H$residuals,CI=TRUE)$CI95[4,2])
,
(predict(PGLS_w0_V,
as.data.frame(PCA_Morpho_AVERAGE_LOG$x[,1:2]))+fastAnc(TREE,PGLS_w0_V$residuals,CI=TRUE)$CI95[4,2])
,
(predict(PGLS_w0_M,
as.data.frame(PCA_Morpho_AVERAGE_LOG$x[,1:3]))+fastAnc(TREE,PGLS_w0_M$residuals,CI=TRUE)$CI95[4,2]
),
(predict(PGLS_VG_H, as.data.frame(PCA_Morpho_AVERAGE_LOG$x[,1,
drop=FALSE]))+fastAnc(TREE,PGLS_VG_H$residuals,CI=TRUE)$CI95[4,2]),
(predict(PGLS_VG_V,
as.data.frame(PCA_Morpho_AVERAGE_LOG$x[,1:5]))+fastAnc(TREE,PGLS_VG_V$residuals,CI=TRUE)$CI95[4,2])
,
 (predict(PGLS_VG_M,
as.data.frame(PCA_Morpho_AVERAGE_LOG$x[,1:5]))+fastAnc(TREE,PGLS_VG_M$residuals,CI=TRUE)$CI95[4,2]
),
 (predict(PGLS_AG_H,
as.data.frame(PCA_Morpho_AVERAGE_LOG$x[,1:3]))+fastAnc(TREE,PGLS_AG_H$residuals,CI=TRUE)$CI95[4,2])
,
 (predict(PGLS_AG_V,
as.data.frame(PCA_Morpho_AVERAGE_LOG$x[,1:5]))+fastAnc(TREE,PGLS_AG_V$residuals,CI=TRUE)$CI95[4,2])
,
(predict(PGLS_AG_M,
as.data.frame(PCA_Morpho_AVERAGE_LOG$x[,1:5]))+fastAnc(TREE,PGLS_AG_M$residuals,CI=TRUE)$CI95[4,2]
))

Upper_Function_AVERAGE = 10^(Upper_Function_AVERAGE_LOG)

#############################################################################################
```

Appendix 31 – Calculation of the low-frequency limit estimates in proboscideans using the equations of West, (1985)

	Length (mm)	Nb turns	Product	Low-frequency limit (Hz)
Anancus NMNHS.FM2991A	72.33	2.5	180.8	10.3
Anancus NMNHS.FM2991D	78.34	2.5	195.9	9.0
Anancus NMNHS.FM2991E	80.08	2.5	200.2	8.7
Anancus NMNHS.FM2991F	77.54	2.5	193.9	9.2
Elephas CEB150009	73.11	2.25	164.5	12.1
Elephas MNHN.AC.ZM.1904-273	74.13	2.375	176.1	10.8
Elephas MNHN.AC.ZM.1941-209	80.46	2.375	191.1	9.4
Elephas MNHN.AC.ZM.2008-81	80.28	2.375	190.7	9.4
Eritherium PM17	16.84	2	33.7	167.7
Gomphotherium CBar coll. V2	90.06	2.625	236.4	6.6
Gomphotherium MNHN.F.SEP38 (left)	70.11	2.375	166.5	11.8
Gomphotherium MNHN.F.SEP38 (right)	68.53	2.375	162.8	12.3
Loxodonta africana CEB130168	70.84	2	141.7	15.4
Loxodonta africana MNHN.AC.ZM.1861-53	72.18	2.375	171.4	11.3
Loxodonta cyclotis MNHN.AC.ZM.1950-528	69.16	2.25	155.6	13.2
Loxodonta cyclotis MNHN.AC.ZM.1956-194	74.16	2.625	194.7	9.1
Loxodonta cyclotis MNHN.AC.ZM.1957-465	79.03	2.625	207.5	8.2
Loxodonta cyclotis MNHN.AC.ZM.1961-69	81.55	2.625	214.1	7.8
Loxodonta sp. MNHN.AC.ZM.1932-523	77.13	2.25	173.5	11.0
Loxodonta sp. MNHN.AC.ZM.2008-71 (left)	73.67	2	147.3	14.5
Loxodonta sp. MNHN.AC.ZM.2008-71 (right)	62.18	1.625	101.0	27.1
Mammut FM14293B	68.03	2.375	161.6	12.4
Mammuthus primigenius MNHN.AC.ZM.1904-12	67.64	2.25	152.2	13.7
Numidotherium UOK5	27.10	1.5	40.7	122.7
Ocepeia PM45	19.22	2.125	40.8	121.8
Platybelodon 26564	56.78	2	113.6	22.3
Prodeinotherium MHNT.PAL.2013.01108E	62.66	2.25	141.0	15.6
Stegodon FM18632 (left)	67.40	2	134.8	16.8
Stegodon FM18632 (right)	69.91	2	139.8	15.8
Stegomastodon FM21807	65.83	2	131.7	17.4

Bibliographical references found in the appendices only

Christiansen P (2004) Body size in proboscideans, with notes on elephant metabolism. *Zoological Journal of the Linnean Society* 140 (4), 523-549.

Eisenberg JF, Eisenberg JF (1981) The mammalian radiations: An analysis of trends in evolution, adaptation, and behaviour (No. 591.5: 599 EIS).

Ekdale EG (2013) Comparative anatomy of the bony labyrinth (inner ear) of placental mammals. *PLoS One* 8 (6), e66624.

Kaufman JA, Turner GH, Holroyd PA, Rovero F, Grossman A (2013) Brain volume of the newly-discovered species rhynchocyon udzungwensis (mammalia: afrotheria: macroscelidea): implications for encephalization in sengis. *PloS one* 8 (3), e58667.

Nowak JL, Paradiso JL (1983) Walker's mammals of the world. Johns Hopkins Universty Press, Baltimore (USA).

Ravel A, Orliac MJ (2015) The inner ear morphology of the 'condylarthran' *Hyopsodus lepidus*. *Historical Biology* 27 (8), 957-969.

Saarinen JJ, Boyer AG, Brown JH, et al. (2014) Patterns of maximum body size evolution in Cenozoic land mammals: eco-evolutionary processes and abiotic forcing. *Proceedings of the Royal Society of London B: Biological Sciences* 281 (1784), 2013-2049.

Shoshani J (1992) The African Elephant and its Environment. Elephant: The Animal and Its Ivory in African Culture, 43-59.

La région de l'oreille osseuse chez les Proboscidea (Afrotheria, Mammalia) : anatomie, fonction, évolution

Résumé

Les éléphants font partie des rares mammifères capables d'entendre les infrasons et leur comportement locomoteur est unique. Ces singularités correspondent à des spécialisations de leurs organes sensoriels contenus dans l'oreille interne : la cochlée (audition) et le système vestibulaire (locomotion). Alors que la diversité actuelle des proboscidiens est très faible (trois espèces), ce groupe a été bien plus diversifié pendant les 60 millions d'années qui composent son histoire. Cette thèse étudie pour la première fois de façon complète la morphologie et la fonction de la région de l'oreille (périotique, labyrinthes osseux et membraneux) d'éléphants actuels grâce aux techniques CT scan 3D. De plus, les périotiques de quatorze genres de proboscidiens fossiles sont décrits afin de documenter l'évolution de ce complexe anatomique au sein de cet ordre de mammifères. Les résultats montrent que certains caractères de l'oreille sont très variables au niveau spécifique. Notre analyse inclut les plus anciens proboscidiens connus et suggère que la morphologie de la région otique a évolué graduellement pendant la première moitié de l'histoire évolutive du groupe et que le morphotype moderne éléphantin est déjà acquis chez les Deinotheriidae et généralisé chez les éléphantimorphes. Les inférences sur la locomotion et l'audition des taxons fossiles confirment ces observations. Ce travail permet ainsi de lever le voile sur l'évolution d'une région anatomique majeure, jusque-là méconnue chez un groupe emblématique de mammifères.

Mots clés : périotique, labyrinthe, Proboscidea, éléphant, anatomie, phylogénie, analyse fonctionnelle

The ear region of the Proboscidea (Afrotheria, Mammalia): anatomy, function, evolution

Abstract

Elephants are among the few mammals able to hear infra-sounds, and they display a unique locomotor behavior. It corresponds to specializations of their sensory organs contained in the inner ear: the cochlea (audition) and the vestibular system (spatial orientation). While only three species are living today, they were a much more diverse group found in five continents and with a 60 Ma-long history. We provide here the first comprehensive morphological and functional study of the ear region (petrosal, bony and membranous labyrinths) of extant elephants using 3D CT scan techniques. Additionally, we describe and compare the petrosals of fourteen extinct proboscidean genera in order to shed light on the evolution of this anatomical complex in the Proboscidea. The results show that some features of the petrosal and bony labyrinth of extant elephants - such as the number of turns of the cochlea – display a noticeable level of intra-specific variability. Our analysis includes the earliest-known proboscideans and suggests that the petrosal and bony labyrinth morphology evolved gradually during the first half of the proboscidean evolutionary history, but also that the modern morphotype exhibited in elephants was probably already acquired in deinotheriids and generalized in elephantimorphs. Functional inferences on the locomotor behavior and the audition of extinct proboscideans confirm these observations. This work hence provides new insights on the evolution of a major anatomical region hitherto poorly known in an emblematic group of mammals.

Keywords: petrosal, labyrinth, Proboscidea, elephant, anatomy, phylogeny, functional analysis

UMR 7207 - CR2P, Centre de recherche sur la paléobiodiversité et les paléoenvironnements Muséum National d'Histoire Naturelle, Département Histoire de la Terre, CP 38 - 8, rue Buffon 75005 Paris